N° /__/__/__/__/__/__/__/__/__/__/

PhD THESIS

for the degree of

Doctor

of

the Institut des Sciences et Industries du Vivant et de l'Environnement (Agro Paris Tech)

the Universidade de São Paulo, Escola Superior de Agricultura Luiz de Queiroz

Area: Forest Sciences

by

Valérie MAQUERE

defended on

DYNAMICS OF MINERAL ELEMENTS UNDER A FAST-GROWING *EUCALYPTUS* PLANTATION IN BRAZIL. IMPLICATIONS FOR SOIL SUSTAINABILITY.

Thesis Director France: ***Jacques RANGER***
Thesis Diretor Brazil: ***José Leonardo de Moraes GONCALVES***
Supervisor: ***Jean-Paul LACLAU***

INRA Unité Biogéochimie des Ecosystèmes Forestiers, Champenoux, France
CIRAD UPR Fonctionnement et pilotage des écosystèmes de plantations, Montpellier, France
ESALQ Departamento de Ciências Florestais, Piracicaba, Brasil

Jury:

Mr Bruno Delvaux, Professor, **Catholic University of Louvain**, Belgium .....Reviewer
Mr Alex Vladimir Krushe, Researcher, **CENA/USP**, Brazil.....Reviewer
Mr Marc Voltz, Research Director, **INRA**, France..... Reviewer
Mr Bruno Ferry, Lecturer, **ENGREF**, France .....Examinor
Mr Julien Tournebize, Researcher, **CEMAGREF**, France .....Examinor
Mr José Leonardo de Moraes Gonçalves, Professor Doctor, **ESALQ/USP**, Brazil .....Director
Mr Jacques Ranger, Research Director, **INRA**, France .....Director
Mr Jean-Paul Laclau, Researcher, **CIRAD/USP**, Brazil .....Supervisor

ACKNOWLEDGEMENTS

L'absent

Ce frère brutal mais dont la parole était sûre, patient au sacrifice, diamant et sanglier, ingénieux et secourable, se tenait au centre de tous les malentendus tel un arbre de résine dans le froid inalliable. Au bestiaire de mensonges qui le tourmentait de ses gobelins et de ses trombes il opposait son dos perdu dans le temps. Il venait à vous par des sentiers invisibles, favorisait l'audace écarlate, ne vous contrariait pas, savait sourire. Comme l'abeille quitte le verger pour le fruit déjà noir, les femmes soutenaient sans le trahir le paradoxe de ce visage qui n'avait pas des traits d'otage.

J'ai essayé de vous decrire ce compère indélébile que nous sommes quelques-uns à avoir fréquenté. Nous dormirons dans l'espérance, nous dormirons en son absence, puisque la raison ne soupçonne pas que ce qu'elle nomme, à la légère, absence, occupe le fourneau dans l'unité.

René Char, *Seuls demeurent,* 1938-1944

Merci à ceux qui ont été là
A l'occasion d'un geste, d'une amitié
partagée ou d'une vie passée
Cette thèse est la vôtre.

Saravá !

Many thanks to those who participated in this project:

For thesis direction:
Jacques Ranger, José Leonardo de Moraes Gonçalves and Jean-Paul Laclau

For institutional supervision:
Bruno Ferry

For their scientific advises:
Marie-Pierre Turpault, Frédéric Gérard, Bruno Delvaux
Bénédicte Augeard, Thomas Delfosse, Bernard Longdoz, Jean Pétard

For funding:

- French Ministry of Agriculture and Fishing (GREF) (salary)
- CIRAD and INRA (thesis funding and technical assistance)
- USP/COFECUB (No. 2003.1.10895.1.3) (experimental project funding)
- FAPESP (No. 2002/11827-9) (experimental project funding)
- French Ministry of Foreign Affairs (experimental project funding)
- European Ultra Low CO2 Steelmaking project (ULCOS - Contract n°515960) (experimental project funding)

Main laboratories:

- INRA Unité Biogéochimie des Ecosystèmes Forestiers, France: Director Etienne Dambrine. Pascal Bonnaud and all staff.
- CIRAD UPR Fonctionnement et pilotage des écosystèmes de plantations, France: Coordinator Jean-Pierre Bouillet and all staff.
- ESALQ Departamento de Ciências Florestais, Brasil: Prof. Dr. José Leonardo de Moraes Gonçalves and all staff.

Experimental station

- ESALQ Departamento de Ciências Florestais Estação Experimental de Ciências Florestais de Itatinga, Brasil: Rildo Moreira e Moreira and all staff.

Partner laboratories: Brazil

- CENA Laboratório de Biogeoquímica Ambiental. Carlos C. Cerri Marisa de Cássia Piccolo and all staff.
- CENA Laboratorio de Ecologia Isotópica. Prf Dr Reynaldo L. Victória, Alex Vladimir Krusche and all staff.
- CENA Laboratório de Química Analítica. Prf Dr Maria Fernanda Giné Rosías, Aparecida de Fátima Patreze.
- CENA Laboratório de Tratamento de Resíduos. Glauco Arnold Tavares, Juliana Graciela Giovannini.

- ESALQ Departamento de Ciências Florestais Laboratorio de Ecologia Aplicada. Coordinator Alba Valéria Masetto and all staff.
- ESALQ Departamento de Ciências Florestais Laboratório de Química, Celulose e Energia, Prf Dr Francides Gomes da Silva Júnior.
- ESALQ, Departamento de Ciências do solo, Laboratórios de Análises Químicas – Pesquisa, Coordinator Prof.Dr. Luís Reynaldo F. Alleoni. Luis Antonio Silva Junior.
- ESALQ, Departamento de Ciências do solo, Laboratório de Tecidos Vegetais. Coordinator Prof.Dr. Francisco Antonio Monteiro, Lurdes Aparecida D. Gonzáles.
- ESALQ, Departamento de Engenharia Rural, Laboratório de Física de Solos. Gilmar Batista Grigolon.

Partner laboratories: France

- CIRAD Unité Opérationelle Sols et Eaux, Montpellier France. Marc Szwarc.
- CRPG/CNRS, Service d'Analyse des Roches et des Minéraux. J. Carignan.
- INRA, Unité mixte de recherche Écologie et écophysiologie forestières. Jacqueline Marchand.
- Université de Poitiers, UMR 6532 HYDRASA. Laurent Caner.

Many thanks to all the students who study at night and work at day:
Aline, Claudia, David, Gustavo, Leonardo, Mariana, Robson, Tamara, Tiago, …

And to those who shared pit digging experiences in Itatinga:
Selma, Julio, Junior, Marcello, Matthieu, Juan, Eduardo.

Many thanks to the PTSM and to the nursery for sharing their working space with me, and to the Laclau's family for its warm welcome in Brazil.

Many thanks to the jury who accepted to review this thesis.

ABSTRACT

Each year the area of fast-growing tree plantations in the world expands by around one million hectares and concerns are rising regarding their influence on soil fertility and water resources. A comprehensive approach is currently being conducted at the University of São Paulo to study the biogeochemical cycles of nutrients in *Eucalyptus* grandis plantations. As part of this study, the present thesis focuses on the interactions between the soil matrix and the soil solutions during the first two years of growth of the stand to (i) identify the determinisms driving the chemistry of the soil solution, (ii) quantify the water and nutrient fluxes leaving the ecosystem by deep drainage and thus rule on the risks of groundwater pollution, and (iii) prepare reactive transport modeling using the MIN3P model already tested at the INRA-BEF laboratory.

It is shown that (i) a large uptake of water by the *Eucalyptus* trees occurred as soon as six months after planting, the water drainage was thus largely reduced at a depth of 3 m after one year of growth, (ii) almost no nutrient was leached below a depth of 3 m, (iii) large amounts of nutrients were released in the upper soil layers and leached down to a depth of 1 m (65-100 kg ha^{-1} of $N\text{-}NO_3$) following clear cutting and fertilizing, acidification occurred in the upper soil layers but in these ferralsols, the soil Al reserve and buffering capacity are still large, (iv) part of the fertilizers was taken up by the fast growing *Eucalyptus* trees without appearing in soil solution, (v) S present in the nitrogen fertilizers increased Ca, Mg and P mobilities, and decreased the H and Al release in soil solution, (vi) large quantities of S were adsorbed on the soil surface constituents where sewage sludge or ammonium sulphate was applied, if this sulphate happens to be desorbed, greater soil acidification is to be expected.

It is suggested that the amount of N brought by the fertilizers after one year of growth can be reduced without altering the productivity of the stand but the study of the organic part of the ecosystem seems essential to rule on this point. Long-term monitoring of the ecosystem is needed to assess changes in nutrient dynamics throughout the stand rotation. Isotopic labelling coupled to reactive transport modelling would be useful tools to help understanding the ecosystem functioning.

TABLE OF CONTENTS

FIGURE LIST

TABLE LIST

“Je suis allé faire parler le cuir usé d’une valise
entreposée sous la poussière terre d’une vieille remise

../..

GENERAL INTRODUCTION

Each year the area of fast-growing tree plantations in the world expands by around one million hectares as a result of the population growth and the steady increase in the per capit consumption of wood and wood-based products (paper, wood-fibre panels, …) (FAO, 2006). Fast-wood plantations are intensively managed commercial plantations, set in blocks of a single species, which produce industrial round wood at high growth rates (mean annual increment of no less than 15 m^3 per hectare) and which are harvested in less than 20 years. These can be large-scale estates owned by companies or a concentration of a large number of small- to medium-scale commercial woodlots owned by smallholders (Cossalter and Pye-Smith, 2003). *Eucalyptus* is the most widely planted tree genus in the tropics, *E. grandis*, *E. saligna* and *E urophylla* are the main planted species in tropical and subtropical climate (FAO, 2006).

Some 30 years ago, Brazil became the first country in South America to establish large fast-wood plantations. Plantations represent 5.74 millions ha out of the 477.7 millions ha of Brazilian forests, of which 28.3 % are concentrated in the states of Minas Gerais and São Paulo. *Eucalyptus* count 3.55 millions ha and *Pinus* 1.82 millions ha. Planted forests account for 4.33 millions employs (SBS, 2007). *Eucalyptus* plantations mainly supply the pulp and metallurgical industries with wood and charcoal. The rotation length is classically 7 years, 2 or 3 successive rotations are generally performed before the stand is reformed. The yields are among the best in the world and reach classically 40 to 50 m^3 ha^{-1} $year^{-1}$ (Goncalves et al., 2004).

The planting of large areas of eucalypts, acacias, pines and poplars has sparked off bitter controversy, especially in the developing world. For plantations propronents, these have countless virtues: they regulate water cycle, convert sunlight and carbon dioxide into wood and oxygen, stabilise steep slopes against erosion, constitute habitat for animals and micro-organisms, and provide employment to local communities together with timber, firewood, resins and other products. On the other hand, the opponents to fast-wood plantations argue that they are replacing natural forests, that they are threat to biodiversity, to water resources and to soil fertility, that genetically modified tree crops will lead to problems in the future, and that they cause land tenure and conflict with local communities (Cossalter and Pye-Smith, 2003). Fast-wood plantation companies are under increasing pressure from non governmental organizations so that nowadays in Brasil, most of them

are willing to assess the ecological and social impacts of their activity. About 2.25 millions ha of Brazilian plantations are certified FSC (Forest Stewardship Council) and outgrower or joint-venture schemes are being developed in most Brazilian states (SBS, 2007).

In terms of soil sustainability, one major concern regards soil fertility since most of these plantations are managed in short rotations and large amounts of nutrients contained in boles are removed from soils on each harvest (Cossalter and Pye-Smith, 2003; Nambiar et al., 2004). In terms of nutrient cycling, fast-wood plantations behave like most agricultural crops, in that they remove minerals from the soil. As they are frequently established on low fertility soils, fast-wood crops nearly always require applications of fertilizer if they are to sustain high biomass productions. Most of these are mineral fertilizers but increasing production of sewage sludge from wastewater treatment plants of urbanized areas has encouraged the use of sewage sludge as fertilizers. The stakes are for industrials to optimize these fertilizations to supply the stand requirements at minimal cost and for environmentalists to guaranty that they are adapted to maintain soil fertility without polluting underground waters.

Eucalyptus response to P, K and B fertilizations has been widely studied in Brazil (IPEF, 2004) but less attention was put on N fertilizers although they are applicated in industrial plantations (from 100 to 200 kg ha^{-1} for each rotation). It was already observed in the Congo that long-term silviculture of *Eucalyptus* led to imbalanced N budgets (Laclau et al., 2005a), which may result in soil organic nitrogen impoverishment. A strong response to N fertilizers was also observed in Australia and since a few years in Brazil (Corbeels et al., 2005; Goncalves et al., 2004). More precise knowledge of the nitrogen cycle in *Eucalyptus* plantations is required to (i) maintain high yields of production at reduced cost without impoverishing the soils, and (ii) to prevent water pollution with nitrates.

Water consumption of large fast-wood plantations has been widely discussed. These plantations reduce annual water yields, especially when they replace grasslands and farmland, thus leaving less water available to other users, and often reduce stream flow during the dry season. However, where there is abundant rainfall, their effect on water yields may be insignificant (Cossalter and Pye-Smith, 2003). The influence of *Eucalyptus* plantations on the water resource has been intensively studied at the catchment scale in particular in Brazil (Camara and Lima, 1999; Lima, 1996; Lima et al., 1996) and in South Africa (Bosch and Smith, 1989; LeMaitre and Versfeld, 1997; Prinsloo and Scott, 1999;

Scott and Smith, 1997). The *Eucalyptus* consumption in water was also studied at the tree scale by ecophysiological monitoring (Benyon, 1999; Bevilacqua et al., 1997; David et al., 1997b; Dye, 1996; Kallarackal and Somen, 1997; Stape et al., 2004), but less information is available regarding the water dynamics in soils and the chemistry of soil solutions.

The problems related to plantations are often site-specific, and the way in which they are planned and managed is of paramount importance. The impact of plantations is generally a function of the characteristics of (i) the land-use they replace, (ii) the soil and climate of the site, (iii) the size of the planted area, (iv) the silvicultural practices (soil preparation, stocking density, fertilization, length of rotation,…), and (v) the species composition (Cossalter and Pye-Smith, 2003). Site-specific studies are thus needed to identify local determinisms of plantation dynamics which may serve as basis for further generalisation. From a scientific point of view, fast-wood monospecific plantations form simplified and highly homogeneous systems observable at a short time scale (7 years for a whole rotation in Brazil for example). They are thus particularly well adapted for model building, parameterization and validation.

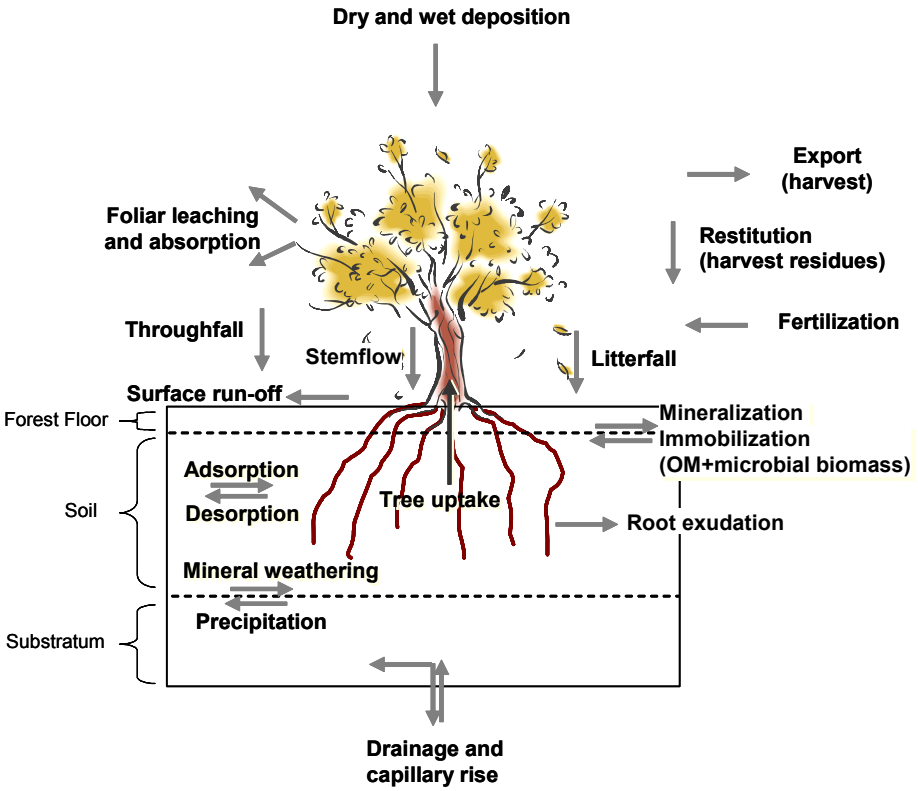

Figure 1 Processes of nutrient transfers occurring within forest ecosystems.

A comprehensive approach is currently being conducted at the University of São Paulo to study the biogeochemical cycles of nutrients in *Eucalyptus* grandis plantations. This

project is developed at the ecosystem level in an experimental stand representative of large areas of plantations in Brazil. The overall aim of the study is to assess the consequences of silviculture, and more particular of different N fertilizer inputs, on water quality and long-term soil fertility by measuring water and nutrient fluxes throughout the ecosystem (Figure 1) and establishing the input-output budgets of nutrients in the soil for the whole rotation (Ranger et al., 2002).

As part of this study, the present thesis focused on the interactions between the soil matrix and the soil solutions during the first two years of growth of the *Eucalyptus* stand.

The main objective was to study the dynamics of the soil and forest floor solutions (system D of Figure 2) and to set hypotheses on the main fluxes driving its chemical composition (fluxes of system D on Figure 2). The underlying hypotheses were that in these deep weathered tropical soils, the reactions of adsorption/desorption on the soil surface are key controls of the dynamics of soil solution, but that the weathering of the mineral phase contributes little to nutrient release in soil solution. The thesis thus aimed at:

- identifying the determinisms driving the chemistry of the soil solution,
- quantifying the water and nutrient fluxes leaving the ecosystem by deep drainage and thus rule on the risks of groundwater pollution,
- preparing reactive transport modeling and assess its feasibility, using the model already in use at the INRA-BEF laboratory, MIN3P (Gerard et al., 2004; Mayer et al., 2002).

The study was organized in different parts which settled the structure of the present dissertation:

- the fertilization experiment is presented in part A, together with the dynamics of the vegetation over the studied period, which was not part of this thesis but helps to understand the dynamics of the soil solution,
- the potential interactions between the soil solid phase and the soil solution were then studied (potential fluxes of mineral weathering and adsorption/desorption indicated in Figure 2) (part B),
- the water fluxes in soils were modelled (part C),

- the chemistry of the soil solution was studied and the nutrient fluxes leaving the soil system by deep drainage were calculated (part D),
- finally, the mass budgets of nutrients within the ecosystem (system A of Figure 2) were assessed to check the validity of the hypotheses formulated in parts B, C and D on the drivers of the soil solution chemistry (part E).

The thesis focuses on the mineral forms of the elements brought by the fertilizers (in particular for N, P, K, Ca, Mg); the organic part of the systems was not presently studied but was discussed in part E.

Since most fluxes of system D (especially those occurring in soils) are difficult to measure experimentally, the hypotheses formulated in parts A, B, C and D were not directly checked by measuring the corresponding fluxes. In part E, we checked by simple mass budget wether these hypotheses were consistant with the main transfers occurring during the experimental period among storage compartments. Mass budgets were performed on system A of Figure 2, for which the main fluxes entering or leaving the system were experimentally available. Part E does not establish nutrient fertility budgets of the experiment.

Throughout the thesis, soil surface represents the contact area between soil constituents and soil solution. For practical purposes, the name “fertilizer” represents mineral fertilizer and sewage sludge applications

Each part of the thesis is self-consistant. A detailed introduction presents, for each one of them, the main questions at stakes. Specific material and methods, results and discussions, and conclusions are developed within each part.

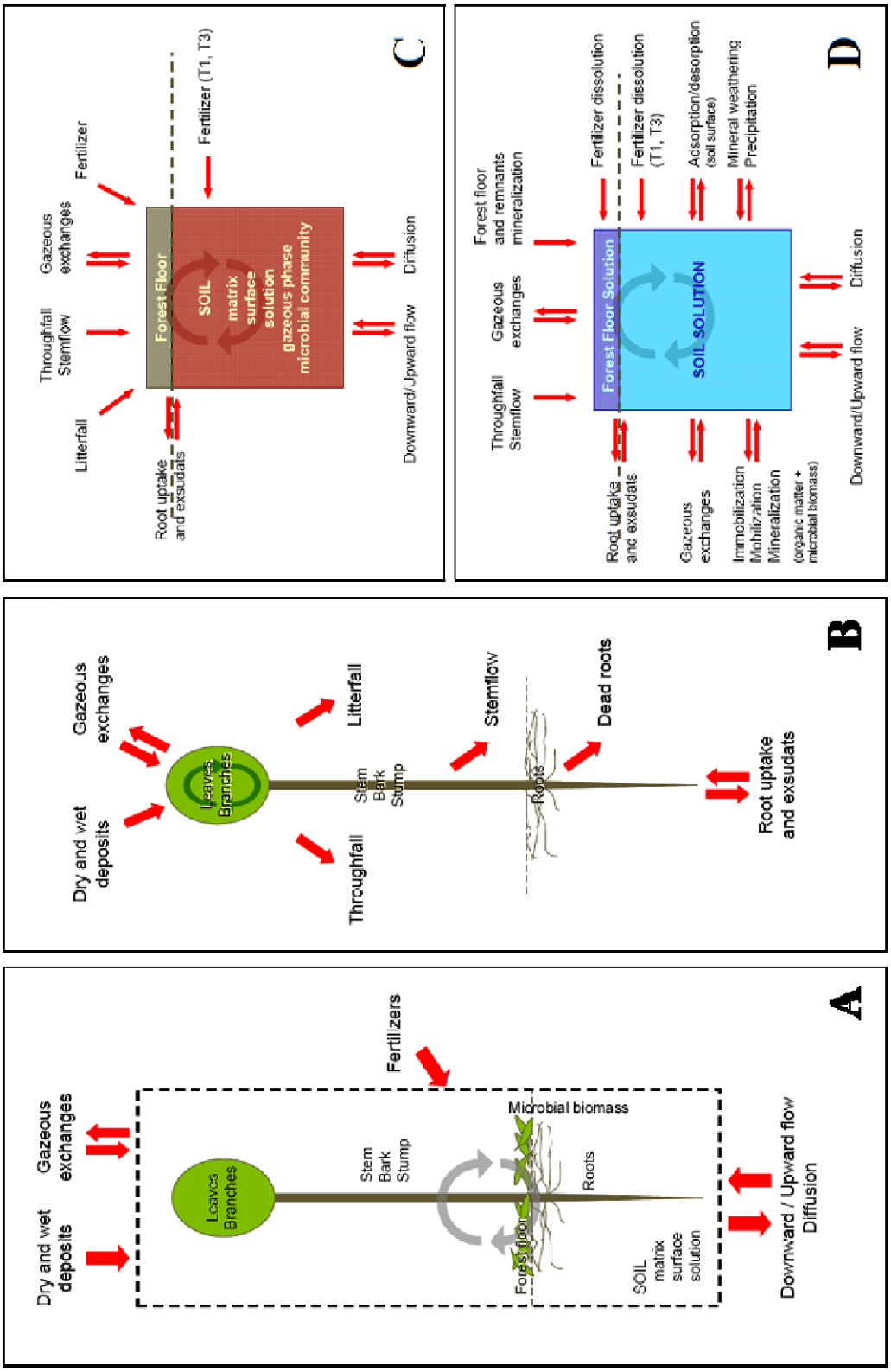

Figure 2 Schematic mass budgets for different sub-systems as part of the ecosystem: system "tree+ forest floor+soil+soil solution" (A), system "tree" (B), system "forest floor+soil+soil solutions" (C), system "forest floor solutions and soil solutions" (D). Fluxes entering or leaving each system are represented in red arrows. The thesis focuses on the dynamics of system D. Mass budgets were performed for system A. Systems A and C are equivalent once the root uptake is calculated as the sum of litterfall plus nutrient accumulation in trees.

PART A PREAMBLE

THE EXPERIMENT:

SITE CHARACTERISTICS

EXPERIMENTAL DESIGN

DYNAMICS OF BIOMASS AND NUTRIENT ACCUMULATION

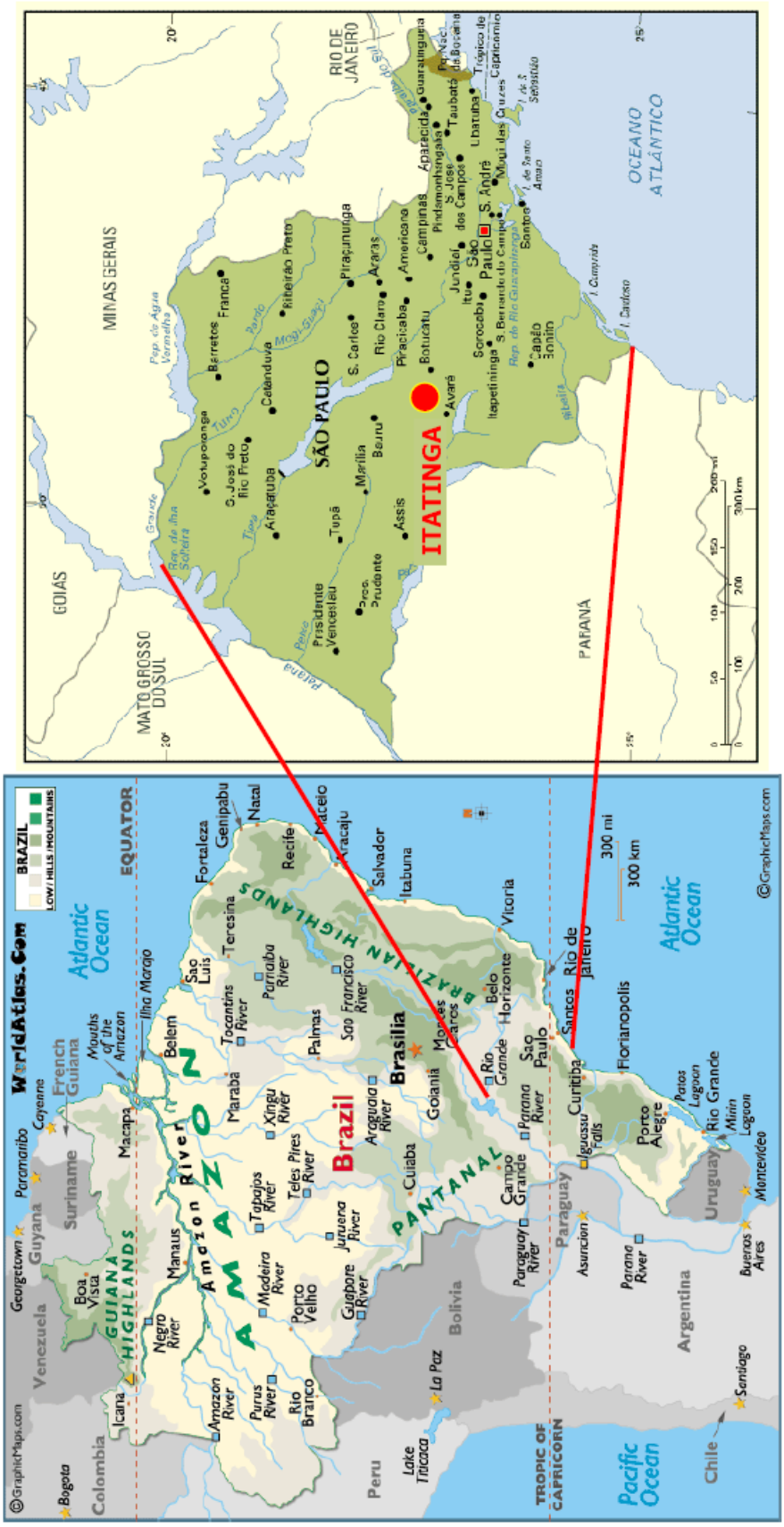

Figure 3 Localization of the experimental station of Itatinga (São Paulo state, Brazil) where the fertilization experiment was established.

A.1 SITE CHARACTERISTICS

The study was conducted at the ESALQ/USP experimental station of Itatinga (23°02'S, 48°38'W) (Figure 3). The climate is *Cfa* according to the Köppen classification. The average annual precipitation from 1990 to 2004 was 1370 mm and the average annual temperature was 19.2°C. The relief is typical of the São Paulo Western Plateau, with topography varying from flat to hilly (FAO, 1977) (slopes ≤ 3%). The maximum altitude is 860 m.

The Itatinga experimental station has been covered for 60 years with *Eucalyptus saligna* Smith plantations. These stands were first planted in 1945 on pasture and have been managed in short rotation coppices for fire wood production since then. The experimental design was implemented in 2003 in a 6 ha coppice harvested in 1997, and planted in 1998 with *Eucalyptus saligna*. Tree spacing was 2 m x 3 m and only a NPK (10:20:10) starter fertilization of 300 kg ha^{-1} had been applied. Soil characteristics are detailed in part B.

A.2 THE EXPERIMENT

A lysimetric design was installed at the beginning of 2003 in the 5.5-year-old *E. saligna* stand. Lysimeters were positioned appropriately for the fertilization experiment planned on the same site after the harvest (Figure 4). A 3-months period was left for soil stabilization, and then nutrient fluxes were monitored over a 9-months period prior to the harvest of the stand (from July 2003 to February 2004). In February 2004, the stand was clear felled and the stumps killed using glyphosate. A half-sib family of *E. grandis* seedlings was planted on the same planting rows at half-distance between the stumps, without any soil preparation. The seeds were produced by the genetic improvement program of the Suzano Company (Brazil). The previous stocking density was maintained (2 m x 3 m spacing).

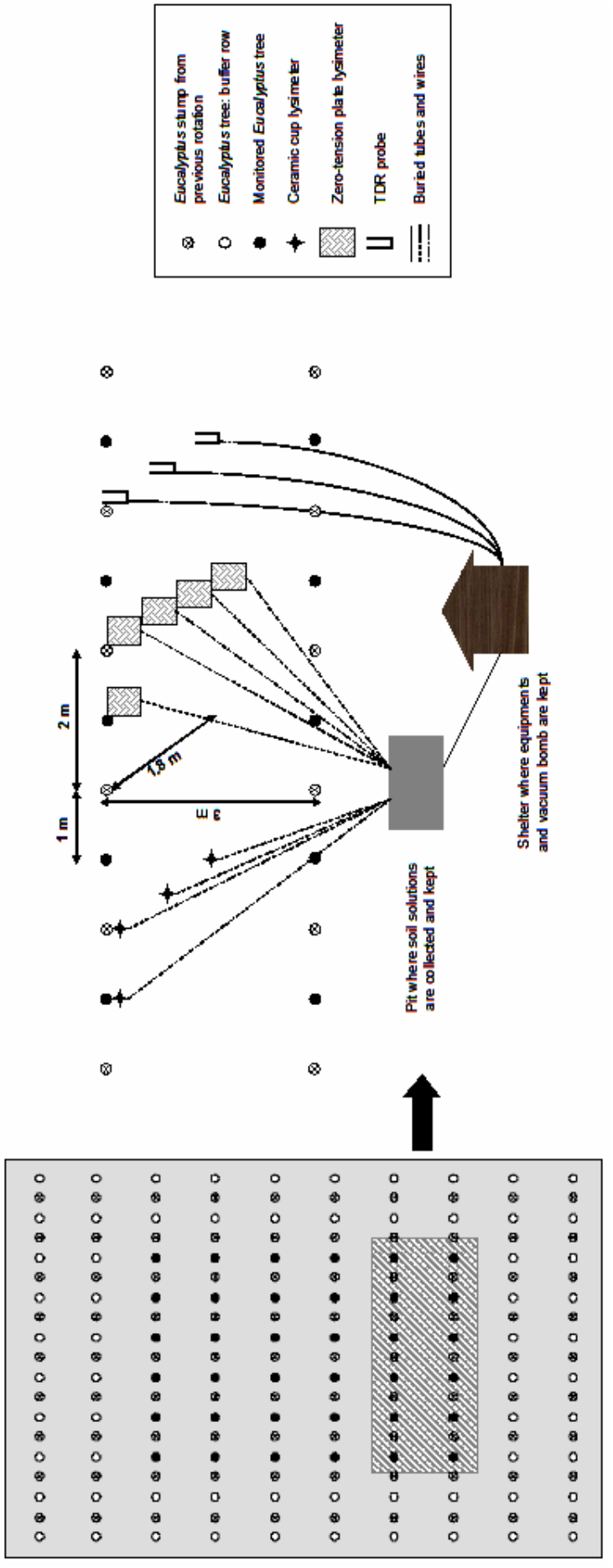

Figure 4 Schematic map of each plot of treatments 1, 3 and 5 in blocks 1, 2 and 3 (10 x 10 trees per plot but growth measurements performed on 6 x 6 trees per plot).

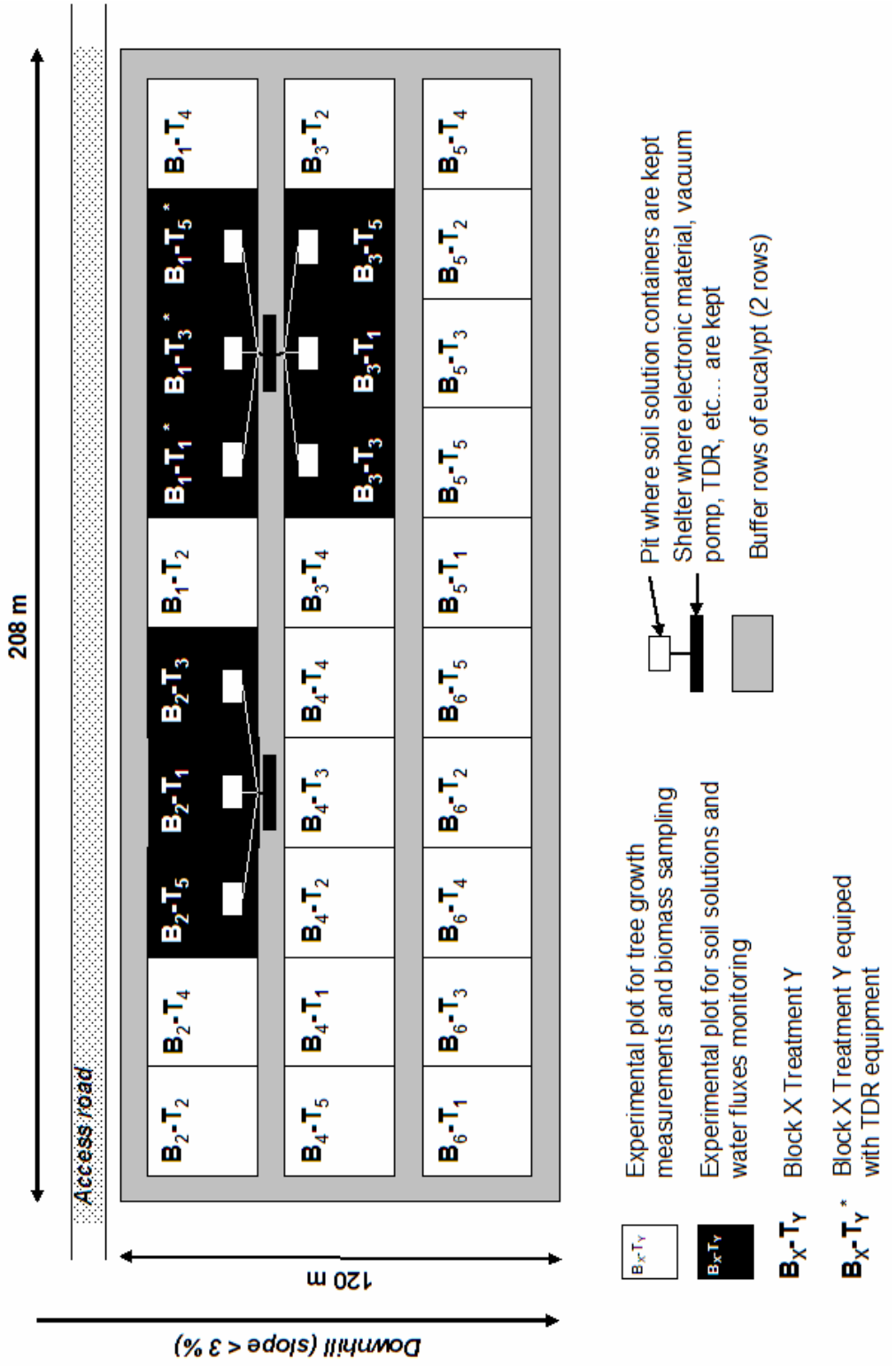

Figure 5 Experimental design.

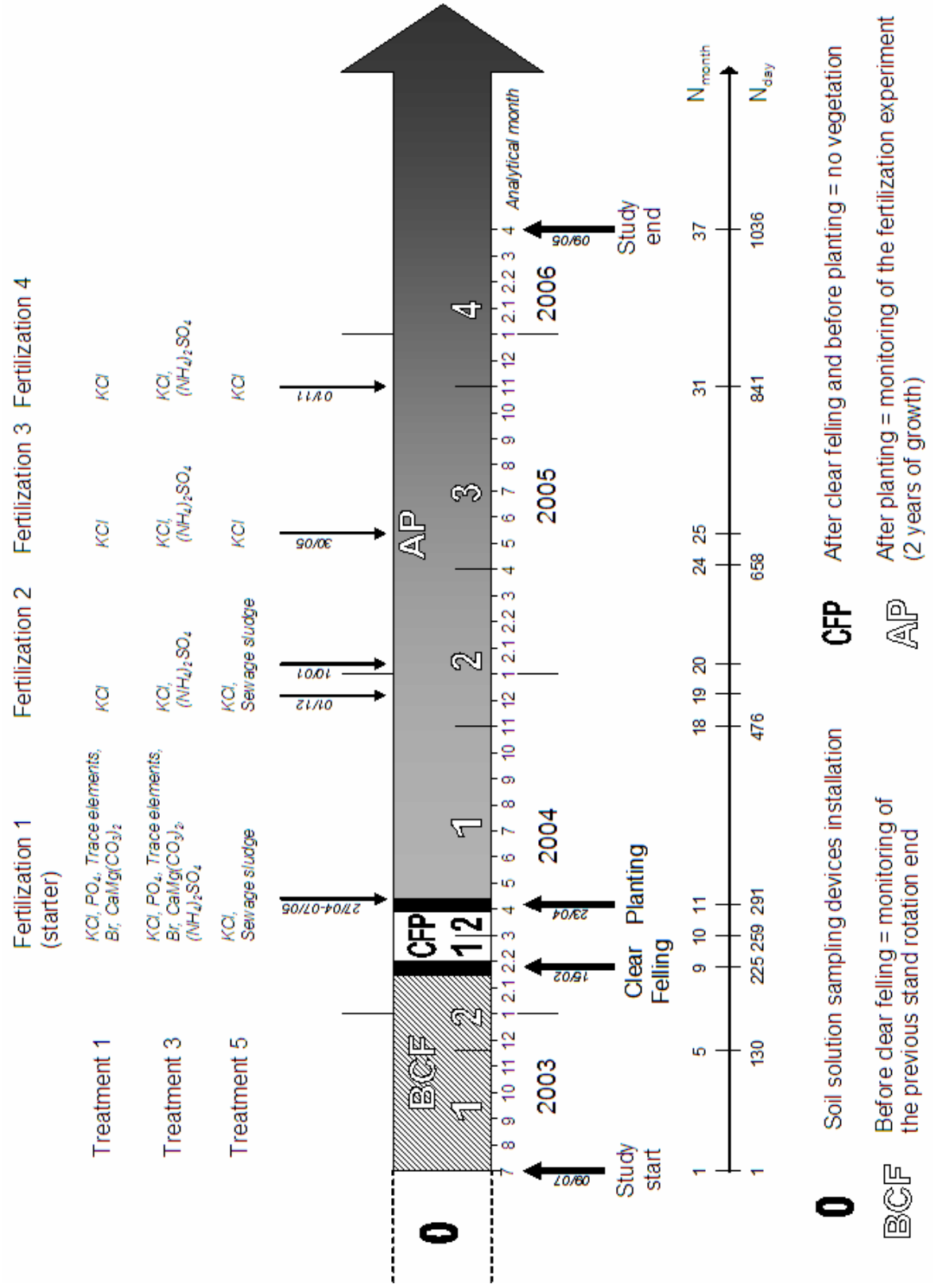

Figure 6 Chronology of the experiment.

A nitrogen fertilization experiment was then initiated using a complete randomized block design, with 6 blocks, 5 treatments and 100 trees per plot (Figure 5). The fertilizations applied in each treatment are presented in Table 1 and the corresponding amounts of nutrients in Table 2. Nutrient fluxes were measured in three treatments (T_1, T_3, T_5) in blocks 1, 2 and 3. Blocks 4, 5 and 6 were installed to sample trees at various ages without disturbing the lysimetry design. T_2 and T_4 treatments were installed to establish a response curve to N inputs and will not be studied in the present thesis. The water and nutrient flux monitoring designs are presented in part C and D, respectively.

The N mineral fertilization (ammonium sulphate) and the KCl fertilization were split in 4 applications, according to the regional silviculture: 25 % of the total dose at planting, 25 % at age 6 months, 25 % at age 1 year and 25 % at age 1.5 year (Table 1 & Figure 6). Other fertilizers were applied in once at planting. The starter fertilization was buried at a depth of about 10 cm at both sides of each *Eucalyptus* seedling (half dose uphill, half dose downhill). Subsequent fertilizations were applied at the soil surface upstream each tree.

Sewage sludge came from Barueri, the major plant of South America in the suburbs of the São Paulo city (SP, Brasil). It was applied in two rows on each side of the planting row (industrial application technique). The total amount was split in two applications: 5 t ha^{-1} at planting and 5 t ha^{-1} at 8 months-old, in dry mass. Treatment 5 did not receive any mineral fertilization but KCl which was applied to meet total K input of the other treatments (sewage sludge was poor in K and eucalypt growth is highly sensitive to K availability).

Total chemical analyses were performed for each applied fertilizer. Dolomitic limestone, potassium chloride and superphosphate were analysed at the CRPG laboratory (Nancy, France) for total elements, oligo elements, bromide and ammonium sulphate were analysed in the CIRAD laboratory (Montpellier, France), and sewage sludge in the IAC laboratory (Campinas, SP, Brasil) (ANNEX 1). The corresponding doses of nutrients received by each treatment are calculated in Table 2.

The four weeks frequency of chemical analysis divided the year in 13 months. The 13th month was reported in February so that February 1 and 2 will be encountered in figures and tables. The number of analytical months or days elapsed since the beginning of the study ($N_{month,}$ N_{day}) will be frequently used to simplify data analysis (Figure 6).

Experimental plots are part of an experimental catchment planted with *Eucalyptus* where stream flow has been monitored for more than 10 years.

Table 1 Experimental treatments and fertilization regimes.

Fertilizer	Date	Fertilization treatments T1	T3	T5
Triple Superphosphate 45% P_2O_5	27/04/2004	167 kg/ha (100 g/plant)		0
Trace elements FTEBR12		45 kg/ha (27 g/plant)		0
Bore Borogran		45 kg/ha (27 g/plant)		0
Dolomitic limestone	30/04/03	2 t/ha		0
KCl 60% K_2O	27/04/2004		*50 kg/ha*	*50 kg/ha*
	1 et 2/12/2004		*50 kg/ha*	*38 kg/ha*
	30/05/2005		*50 kg/ha*	*38 kg/ha*
	01/11/2005		*50 kg/ha*	*50 kg/ha*
	Total		**200 kg/ha (120 g/plant)**	**176 kg/ha (106 g/plant)**
Sewage sludge	06 et 07/05/2004			*5 t/ha*
	10/01/2005			*5 t/ha*
	Total	**0**	**0**	**10 t/ha**
Ammonium sulphate 21% N	27/04/2004		*30 kg N/ha*	
	1 et 2/12/2004		*30 kg N/ha*	
	30/05/2005		*30 kg N/ha*	
	01/11/2005		*30 kg N/ha*	
	Total	**0**	**120 kg N/ha (344 g/plant)**	**0**

Table 2 Total amounts of nutrients applied with each fertilizer.

Fertilizer	Treatment	Fe	Ca	Mg	K	Na	Al	S	P	N	Cl	Si
							kg/ha					
Trace elements	T1, T3	10	2	1	1	0	1	1	0	na	na	na
Borogran	T1, T3	1	6	1	0	0	0	1	0	na	na	na
Dolomitic limestone	T1, T3	7	366	221	3	2	11	na	0	na	na	111
Triple superphosphate	T1, T3	3	24	1	0	0	0	na	35	na	na	1
Ammonium sulphate	T3	0	1	0	1	0	0	138	0	121	na	na
KCl	T1, T3	0	0	0	103	2	0	0	0	na	95	na
	T5	0	0	0	91	2	0	0	0	na	84	na
Sewage sludge	T5	226	191	36	11	9	171	77	138	360	na	na
Total	**T1**	**21**	**398**	**224**	**107**	**5**	**12**	**2**	**35**	**0**	**95**	**112**
	T3	**21**	**399**	**224**	**107**	**5**	**12**	**141**	**35**	**121**	**95**	**112**
	T5	**226**	**191**	**36**	**102**	**10**	**171**	**77**	**138**	**360**	**84**	**na**

A.3 TREE DEVELOPMENT OVER THE STUDIED PERIOD

Tree development in the experiment was studied by other students and researchers but was not part of this thesis. The main results are briefly summarized from Laclau *et al.* (2004b; 2005b; 2007). The experimental methods used to study tree development are briefly presented here because some of these data will be used in part C as inputs in MIN3P simulations and in part E to compute nutrient budgets. A more detailed description of the methods used can be found in Laclau *et al.* (2008). The main conclusions of the vegetation monitoring will help discussing the results presented in part E.

A.3.1 Experimental methods

A.3.1.1 Stand inventories

Stand inventories were performed before clear felling in January and December 2003, and 4, 7, 9, 12, 18, 24, 30 and 36 months after planting. Before clear felling, circumference at breast height (CBH) was measured in all blocks (1-6) of all treatments (1-5), and tree height in block 1 of all treatments. After planting, tree height and CBH were measured in the inner plot (36 trees, excluding 2 buffer rows in each plot) for all blocks of all treatments.

A.3.1.2 Stand biomass and nutrient contents

Given the stand inventories, 14 trees representative of the whole stand were sampled before clear felling, then 10 trees per treatment (T1, T3 and T5) in blocks 5 and 6 were sampled 6, 12, 24 and 36 months after planting. The trees were separated into leaves, living branches, dead branches, stemwood and stembark. The weight of each tree component was measured in the field. A subsample of each component was next dried at 65°C to constant weight and its composition in K, Ca, Mg and P analyzed. Biomass and nutrient content regressions were established for each component and were applied to the inventories to estimate biomasses and nutrient contents on a hectare basis.

Figure 7 Stand vegetal cover over the experimental period: *E saligna* stand at age 6.5 years before clear felling (BCF period) (A); the stand after it was clear felled (CFP period) (B); the *E. grandis* seedling fertilized by mineral fertilizers buried at its stem in T1 and T3 (1) or by sewage slugde spread on the forest floor (2) (C); the *E. grandis* stand at age 6 months (D) and at age 18 months (E) (AP period).

For all trees sampled, 30 leaves in each third of the canopy were randomly sampled. They were scanned immediately after collection to measure their area and dried at 65°C to constant weight to assess the specific leaf area. The area of leaves was calculated for each sampled tree summing the leaf area in each third of the canopy (biomass of leaves x specific leaf area). A regression was then established for each treatment and age to predict the leaf area from the tree characteristics (CBH and H). The leaf area index (LAI) was finally estimated applying the allometric equations to the stand inventories.

The stump and coarse roots biomasses were measured from destructive sampling of 8 stumps representative of the stand before clear felling, then of 5 stumps per treatment 12, 25 and 36 months after planting. Stump and roots were weighted in the field. Subsamples were subsequently dried and analyzed for nutrient contents. Allometric equations (linear and non-linear regressions) were established and applied to the inventories to estimate stump and coarse root biomasses and nutrient contents on a hectare basis.

Fine roots were sampled at 6 distances from an average tree (4 trees sampled) before clear felling, then at 4 distances from one average tree in blocks 4, 5 and 6 of treatments 1, 3 and 5, 4, 6, 12 and 24 months after planting. Soil cores were sampled with a steel corer (internal diameter of 4.5 cm) driven into the soil by a sledgehammer at 0-15 cm, 15-50 cm, 50-100 cm, 100-150 cm, 150-200 cm, 200-250 cm and 250-300 cm. The biomass of living roots (< 1 mm and 1-3 mm in diameter) was measured. Mean root densities in each soil layer were multiplied by the volume of the layer. The whole soil volume of each sub-area down to a depth of 1 m was next destructively sampled and roots of diameter 3-10 mm were separated and weighted. Sub-samples were taken, dried and analyzed for nutrient contents. Average biomasses and nutrient contents were used to estimate root biomasses and nutrient contents on a hectare basis.

A.3.1.3 Litterfall

Leaves, flowers and fruits were collected every 4 weeks from 10 litter traps (52 cm x 52 cm) before clear felling, then from 5 litter traps in blocks 1, 2 and 3 of treatments 1, 3 and 5 (15 litter traps per treatment). The amounts of bark and branches were collected in 6 m^2 areas before clear felling and were negligible until age 3 years after planting. The samples were dried and analyzed for nutrient contents.

A.3.1.4 Forest floor and harvest residues

The forest floor mass was measured before clear felling from 15 samples collected with a metal-ring of diameter 30 cm. After clear felling, a 300 m^2 area was left free from harvest residues. Nylon nets (mesh 2 mm) were installed at different distances from the trees to prevent from mixing the litter produced by the previous stand to the litterfall of the newly planted stand. Fifteen samples were taken with a 30 cm-diameter metal-ring 1, 3, 6, 9, 12, 15, 18, 21 and 24 months after planting to asses the decomposition rate of the forest floor from the clear-felled stand. After planting, the forest floor was measured 1, 2 and 3 years after planting from 5 samples (50 cm x 50 cm) in blocks 1, 2, 3 and 4 of treatments 1, 3 and 5.

The decay rate of harvest residues was estimated from nylon mesh bags (mesh size 2 mm) containing 10 g of dry matter of leaves, twigs, branches of diameter > 2 cm, or roots (fine and coarse) (60 bags per compartment). Mesh bags containing leaves, twigs and branches were placed on the soil surface whereas those containing roots were buried at a depth of 10 cm. Five to six bags of each type of harvest residue were destructively sampled every 3 months for 2 years. After drying and weighting, their nutrient contents were analyzed.

A.3.2 Main results obtained before clear felling

Historically, the stand was managed as a *Eucalyptus* coppice (6 to 10 year-long rotation) without fertilizer application from 1944 to 1997. It was harvested and replanted in 1998 with *Eucalyptus Saligna* Smith at a stocking density of 1667 trees ha^{-1} (tree spacing 3 m x 2 m) and fertilized at planting (300 kg ha^{-1} NPK 10:20:10). Chemical weeding (glyphosate) was performed the first year after planting.

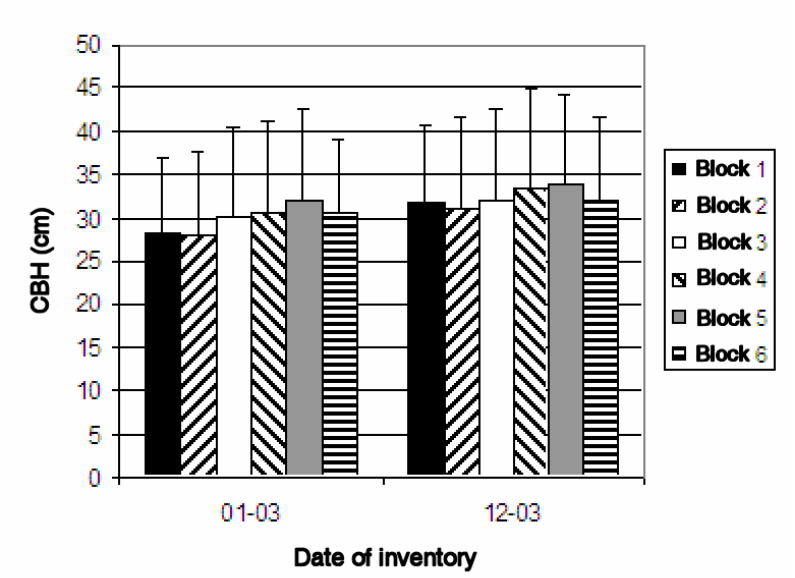

Figure 8 *E. saligna* stand BCF: average and standard deviation of the circumference at breast height (CBH) of the trees located in the area of the fertilization experiment to be installed after clear felling.

The stand inventories at ages 5.5 and 6.5 years showed that the *E. saligna* stand was highly heterogeneous (CV≈30%) which may be explained by the lack of genetic improvement of the seeds. Few differences were observed among the blocks sampled (Figure 8). Tree growth (volume over bark) was estimated from age 5.5 years to age 6.5 years at 27 m^3 ha^{-1}, which was low compared to the mean productivity of commercial plantations in the region (about 40-45 m^3 ha^{-1} $year^{-1}$).

The annual accumulation of nutrients in trees was low at the end of the stand rotation: 39 kg N ha^{-1}, 6 kg P ha^{-1}, 15 kg K ha^{-1}, 16 kg Ca ha^{-1} and 5 kg Mg ha^{-1}, which suggested that nutrients were poorly available in soils after successive rotations of *Eucalyptus* coppices without fertilizer application.

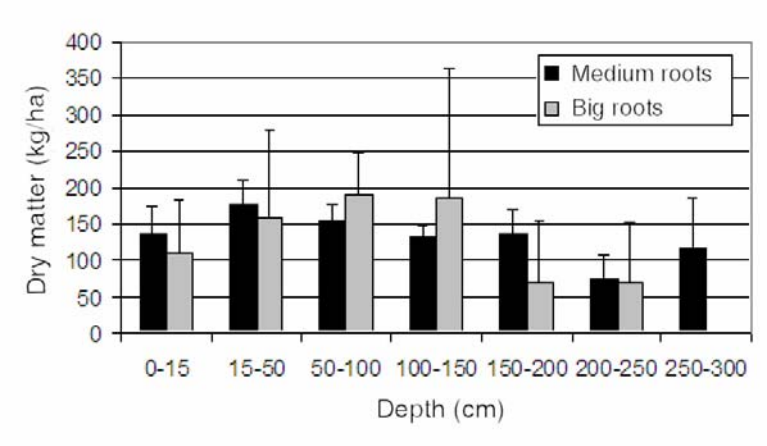

Figure 9 *E. saligna* stand BCF: coarse and medium roots down to a depth of 3 m. The average and standard deviation are represented (n=4).

Stump biomass was estimated at 4032 kg ha^{-1} and 5600 kg ha^{-1} in January and December 2003, respectively. Mean biomasses of coarse and medium-size roots were 930 kg ha^{-1} and 784 kg ha^{-1} in January and December 2003, respectively. Coarse roots were not found below a depth of 2.5 m but medium roots were found deeper than 3 m (Figure 9).

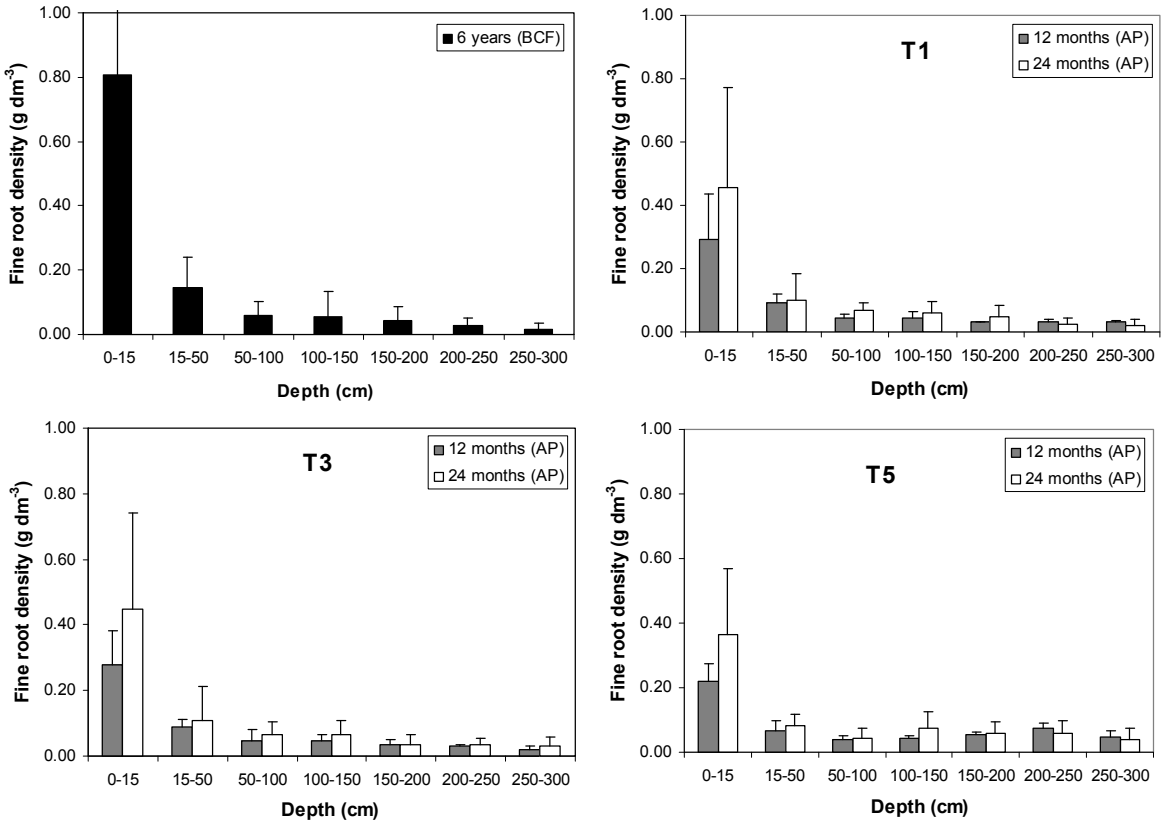

Figure 10 Fine root density (diameter < 1 mm) at the end of the stand rotation (*E. saligna* stand BCF) and 12 and 24 months after planting (AP) in treatments 1, 3 and 5. The average and standard deviations are given (BCF: n=24; AP: n=12).

High densities of fine roots were found in the upper soil layer (0-15 cm) where their spatial heterogeneity was greatest. Their density decreased sharply in deeper soil layers, as classically observed for forest plantations (Figure 10). Fine roots were found down to a depth of 3 m, and even if they were scarce, this pattern suggests that *Eucalyptus* trees may take up soil water deeply if needed.

Litter fall amounted to 6267 kg dry matter ha^{-1} from age 5.5 years to age 6.5 years. The dry masses of leaves, branches and bark were 2865, 1872 and 1470 kg ha^{-1} respectively.

In February 2004, the *E. saligna* stand was clear felled (age 6.5 years) and the stumps were killed using glyphosate.

A.3.3 Growth of the newly planted stand: fertilization experiment

Two months after clear felling, a half-sib family of *E. grandis* seedlings was planted on the same planting rows at half-distance between the stumps, without any soil preparation. The seeds were produced by the genetic improvement program of the Suzano Company. The previous stocking density was kept (2 m x 3 m spacing).

A.3.3.1 Stand growth

A strong tree response to the N-fertilizer applications was observed the first year after planting (Table 3). Tree growth was slower in the control treatment (T1) than in the treatment which received the commercial N-fertilization (T3) (Figure 11). Tree growth was also slower in T5 (sewage sludge application) compared to T3. However, tree height was equivalent in all treatments 30 months after planting.

Table 3 Growth in diameter at breast height and height of the *Eucalyptus* trees before clear felling (BCF) and after planting (AP). Standard errors are given in parenthesis.

Stand	**Age**	**Diameter at breast height**			**Height**		
	months	*cm*			*m*		
BCF	**54**	9.5 *(3.2)*			13.1 *(3.1)*		
	66	10.3 *(3.2)*			14.8 *(2.7)*		
		T1	T3	T5	T1	T3	T5
AP	**4**				0.6 *(0.1)*	0.7 *(0.1)*	0.5 *(0.1)*
	7				1.0 *(0.2)*	1.2 *(0.2)*	1.0 *(0.2)*
	9.5	1.8 *(0.5)*	2.4 *(0.6)*	2.0 *(0.6)*	2.9 *(0.5)*	3.3 *(0.5)*	3.0 *(0.5)*
	11.5	2.9 *(0.7)*	3.6 *(0.7)*	3.2 *(0.8)*	3.8 *(0.7)*	4.4 *(0.6)*	4.2 *(0.8)*
	18.5	6.4 *(1.0)*	6.9 *(1.3)*	6.8 *(1.5)*	7.3 *(0.9)*	7.9 *(1.1)*	8.1 *(1.8)*
	23.5	8.3 *(1.3)*	8.8 *(1.5)*	8.5 *(1.7)*	10.7 *(1.0)*	11.1 *(1.3)*	11.2 *(1.5)*

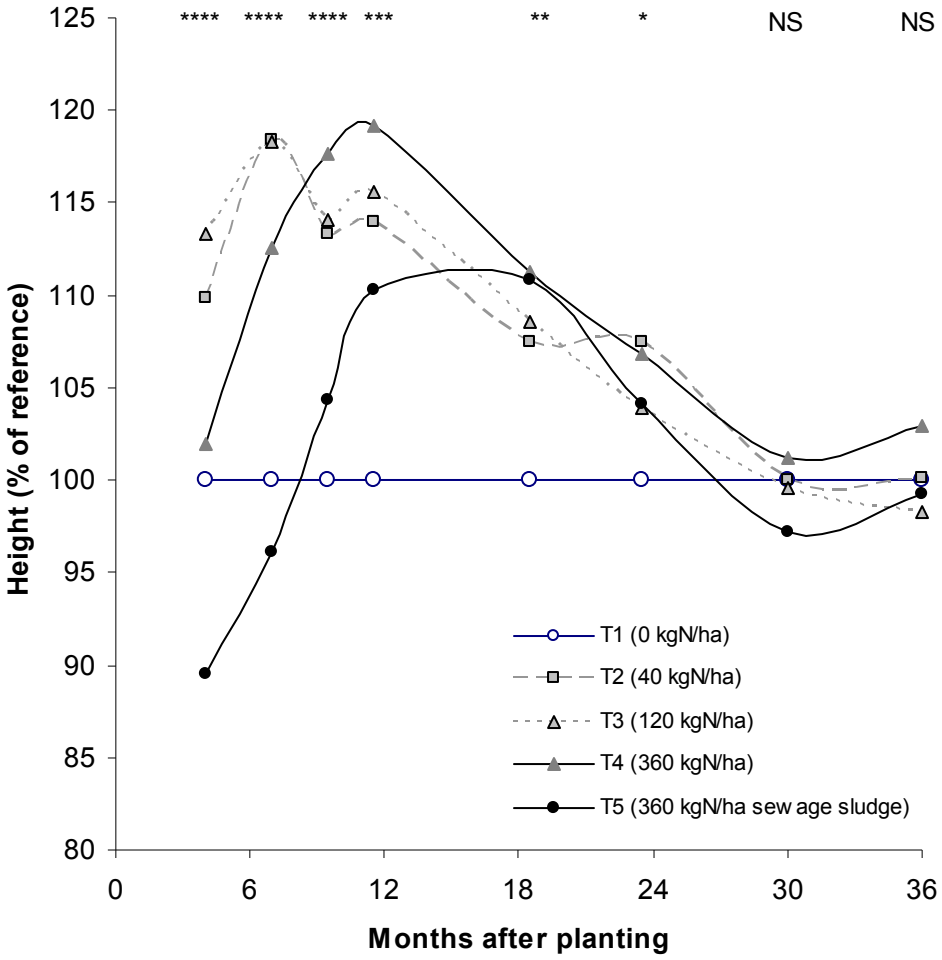

Figure 11 *E. grandis* stand (AP): average tree height in each treatment as a percentage of tree height in the control treatment (T1) Significant differences among treatments at levels of 5%, 1%, 0.1% and 0.01% are indicated by *, **, ***, and ****, respectively. NS indicates non significant differences at 5%.

A.3.3.2 Biomass production

Tree response to N-fertilization was also observed for aboveground biomass up to 24 months after planting (Figure 12 & Figure 13). After the canopy closure one year after planting, leaf biomass was reduced of 30 % in the 3 studied treatments, as classically observed in *Eucalyptus* stands (Reis et al., 1985; Saint-Andre et al., 2005).

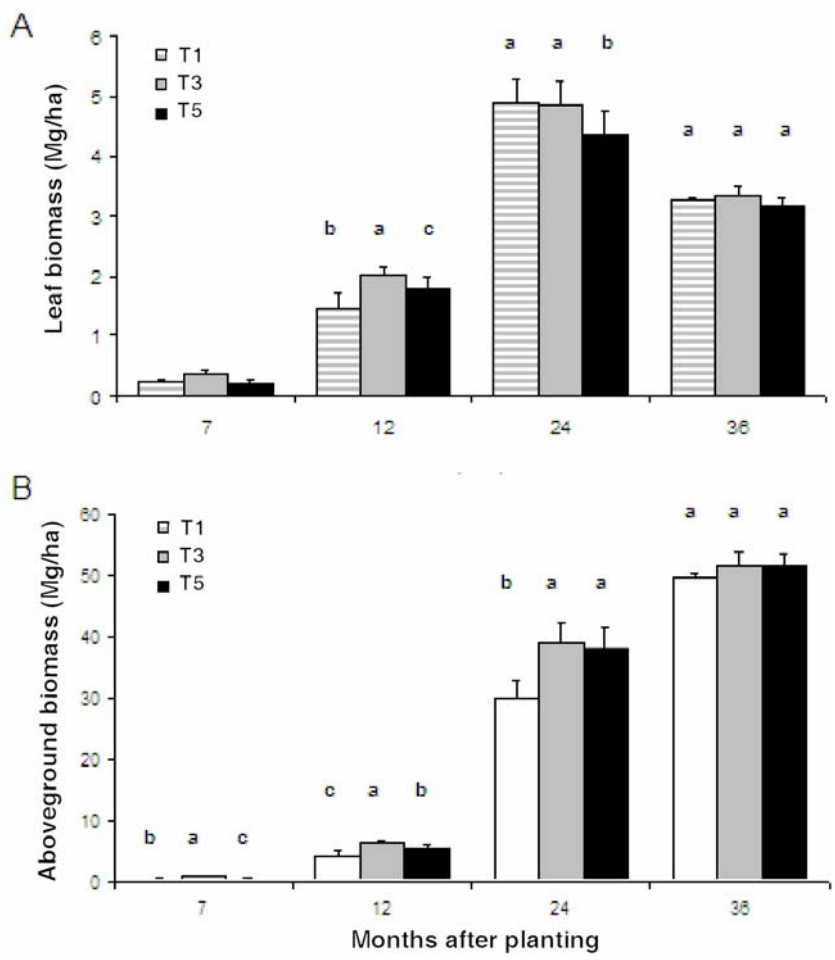

Figure 12 *E. grandis* stand (AP): time course of foliar biomass (A) and aboveground biomass (B) in treatments 1, 3 and 5. Different letters indicate significant differences at $P<0.05$.

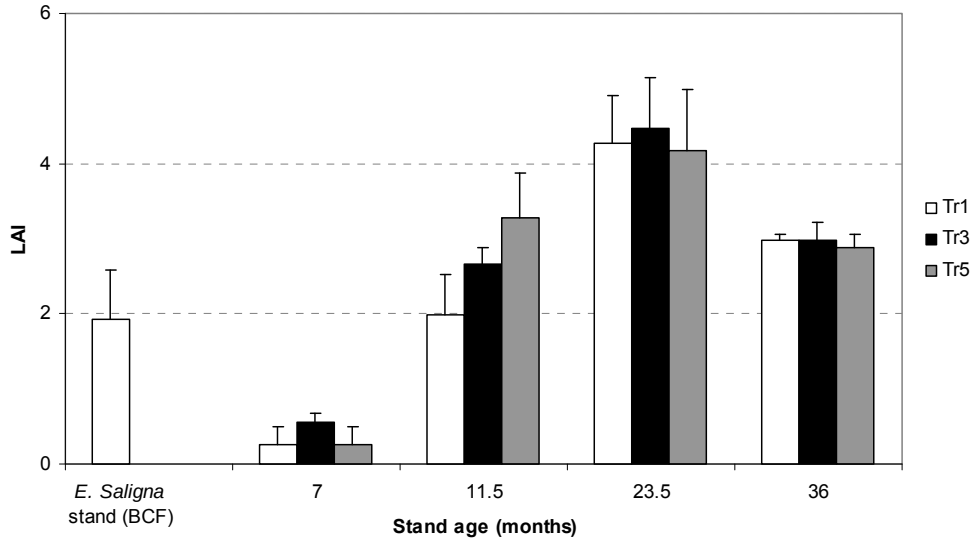

Figure 13 Time course of leaf area index (LAI) before clear felling and after planting in treatments 1, 3 and 5. Mean and standard deviations (n=4) are represented.

On the contrary, fine root biomasses were not influenced by the fertilization treatments throughout the first two years of growth. This pattern was already observed in *Eucalyptus* plantations and confirms the ability of eucalypts to increase the proportion of biomass allocated to the root system under water or nutritional stress. *Eucalyptus* root system develops quickly down to deep soil layers (Figure 10). Complementary studies performed on adjacent stands showed the presence of fine roots down to the depths of 6, 8, and 12 m 12, 24 and 40 months after planting, respectively.

A.3.3.3 Nutrient accumulation in trees

During the first year of growth, the nutrient accumulation in trees was greater of 42%, 58%, 19%, 33% and 18% for N, P, K, Ca and Mg respectively in treatment 3 (mineral N fertilizer) than in treatment 1 (no N fertilizer). In all treatments, the amount of nutrients accumulated was 2 to 3 times greater during the 2nd year of growth than during the first one (ANNEX 2). Differences among treatments were < 30 % except for Mg which was 15 % greater in T3 than in T1, and twice as less in T5 than in T3.

For all treatments, the greatest nutrient accumulation occurred in leaves and amounted to about 50 % and from 25 to 50 % of the total accumulation 12 months and 24 months after planting, respectively. Nutrients accumulated in roots varied little from 12 to 24 months after planting. Nutrient contents were of the same order of magnitude than reported in other intensively managed *Eucalyptus* plantations in Brazil established on soils without water deficiency.

A.3.3.4 Litterfall

Litterfall was 3 to 5 times greater during the 2nd year of growth than during the 1st year after planting (Table 4). The delay observed in crown development in T1 and T5 might be responsible for the delay in litterfall observed in T1 and T5 compared to T3. Nitrogen and P contents in litterfall were larger in T5 than in T1, and Mg content was less in T5 than in T1 and T3. This pattern might be explained by greater N and P availabilities in T5 than in T1 which was not N fertilized, and by a greater Mg availability in T1 and T3 than in T5, where dolomitic limestone was not applied.

Table 4 *E. grandis* stand (AP): dry mass and nutrient content in litterfall during the first and second years of growth in treatments 1, 3 and 5.

Stand age *(months)*		Mass	N	P	K	Ca	Mg
				(kg ha^{-1})			
0-12	T_1	906	9.2	0.2	2.2	10.1	2.6
	T_3	1338	12.9	0.3	3.0	15.2	3.7
	T_5	915	13.4	0.5	2.6	10.8	1.6
12-24	T_1	4456	44.1	1.5	7.9	29.5	10.7
	T_3	5389	50.8	1.7	8.9	35.5	13.1
	T_5	4931	55.6	2.1	8.5	33.1	8.5

A.3.3.5 Decomposition of the forest floor and of the harvest residues after clear felling the E. saligna *stand (BCF)*

About half of the forest floor mass at the harvest of the *E. saligna* stand was decomposed within one year after clear-felling. The nutrient release was of about 80, 2 and 2 kg ha^{-1} of N, P and K respectively. The greatest rates of decomposition occurred during the first 3 months. About 20, 1 and 3 kg ha^{-1} of N, P and K were mineralized during the 2nd year, respectively.

In addition to the amount of nutrients released by the decomposition of the forest floor of the previous stand, harvest residues decay also released nutrients. About 50 % of the harvest residues and of the roots of the previous stand were decomposed within one year, except for branches and coarse roots for which 70 and 60 % of dry matter still remained after two years (ANNEX 2).

A.3.3.6 Absorption of nutrients from the soil

Table 5 *E. grandis* stand (AP): estimation of the amount of nutrients taken up from the soil in T_1, T_3 and T_5.

	Nutrient	N		P		K		Ca		Mg	
	Growth period (year)	0-1	1-2	0-1	1-2	0-1	1-2	0-1	1-2	0-1	1-2
		kg ha^{-1} an^{-1}									
T1	Accumulation in biomass	66.8	106.1	3.1	8.3	28.7	54.3	29.5	54.4	11.0	23.2
	Litterfall	9.2	44.1	0.2	1.5	2.2	7.9	10.1	29.5	2.6	10.7
	Foliar leaching	-0.3	-2.1	0.0	0.0	0.5	1.4	-0.1	0.4	0.1	0.2
	Total uptake	**75.7**	**148.1**	**3.3**	**9.8**	**31.4**	**63.6**	**39.5**	**84.3**	**13.7**	**34.1**
T3	Accumulation in biomass	94.8	116.0	4.9	7.8	33.9	60.0	39.4	60.5	13.0	26.8
	Litterfall	12.9	50.8	0.3	1.7	3.0	8.9	15.2	35.5	3.7	13.1
	Foliar leaching	-0.3	-3.0	0.0	-0.1	0.5	1.3	-0.1	-0.3	0.1	0.0
	Total uptake	**107.4**	**163.8**	**5.2**	**9.4**	**37.4**	**70.2**	**54.5**	**95.7**	**16.8**	**39.9**
T5	Accumulation in biomass	87.6	117.3	7.1	8.6	29.0	59.7	34.8	58.5	9.8	13.1
	Litterfall	13.4	55.6	0.5	2.1	2.6	8.5	10.8	33.1	1.6	8.5
	Foliar leaching	-0.3	-3.3	0.0	0.1	0.5	4.6	-0.1	0.0	0.1	-0.1
	Total uptake	**100.7**	**169.6**	**7.6**	**10.8**	**32.1**	**72.8**	**45.5**	**91.6**	**11.5**	**21.5**

The nutrient uptake increased sharply during the 2nd year after planting (Table 5). Less than 5 and 10 % of the P and K uptake respectively returned to the soil by litterfall during the 1st year of growth. Litterfall represented about 20 and 30 % of Ca and Mg absorption whatever the treatment, respectively. N uptake was 40 to 60 % greater in T3 than in T1 over the first 2 years after planting.

During the 2nd year of growth, K and Ca absorptions doubled in all treatments. The same trend was observed for Mg in T1 and T3. Mg was less accumulated in trees in T5 than in T1 and T3, probably as a result of the lower availability of Mg in T5 (no dolomitic limestone applied). About 50 % of the N, Ca and Mg taken up during the 2nd year of growth returned to the soil surface by litterfall. On the other hand, the proportion of P and K taken up by the trees which returned to soil by litterfall was very low.

A.3.3.7 Amounts of nutrients released by the forest floor and by the harvest residues mineralization: comparison with the amounts taken up by the trees.

Table 6 *E. grandis* stand (AP): nutrients taken up and mineralized from the forest floor or from the harvest residues during the first year of growth.

Element	N			P			K		
Age (months)	0-6	6-12	12-24	0-6	6-12	12-24	0-6	6-12	12-24
	kg ha^{-1}								
Forest floor mineralization	48	37	20	1	1	1	2	0	3
Harvest residues mineralization	2	46	47	3	3	1	13	6	0
Total uptake in T_1	27	51	148	1	2	10	8	23	64
Total uptake in T_3	25	91	164	1	4	9	7	30	70
Total uptake in T_5	38	79	170	2	6	11	9	23	73

The amount of N released by the mineralization of the forest floor and of the harvest residues were (i) larger than stand uptake during the first six months of growth, (ii) of the same order of magnitude during the six months following, and (iii) far less than the stand uptake during the 2nd year of growth (Table 6). K release was about 60 % of the stand uptake the 1st year after planting but was almost null thereafter.

These results show that the decomposition of the forest floor and of the harvest residues has a great influence on the N availability throughout the first 2 years of growth, as already observed in the CIFOR experimental network. Most of the N released issued from the forest floor during the 1st year and from the harvest residues during the 2nd year.

A.3.3.8 Nutrient retranslocations

Table 7 *E. grandis* (AP): retranslocations of nutrients during leaf senescence (kg ha^{-1}). The percentage of total annual requirements of the stand is indicated in parenthesis.

		Retranslocation in leaves									
Stand age	Treatment	N		P		K		Ca		Mg	
months		*kg ha^{-1}*									
0-12	T1	14.5	(16%)	1.1	(25%)	3.4	(10%)	-4.5	(-11%)	-0.1	(-1%)
	T3	26.1	(20%)	1.8	(26%)	8.0	(18%)	-6.0	(-11%)	0.1	(1%)
	T5	13.6	(12%)	1.2	(14%)	5.2	(14%)	-3.6	(-8%)	0.9	(8%)
12-24	T1	55.3	(27%)	4.5	(31%)	20.2	(24%)	1.0	(1%)	2.8	(8%)
	T3	81.8	(33%)	6.1	(39%)	28.3	(29%)	2.9	(3%)	4.7	(11%)
	T5	75.8	(31%)	7.3	(40%)	19.9	(21%)	4.7	(5%)	3.8	(15%)

Negative values indicate accumulation in leaves during senescence.

Nutrient retranslocations started 8 months after planting in T1, T3 and T5 when the leaves began to fall. In T1 and T3, they represented about 25 % of the tree requirements in P and about 10-20 % of the tree requirements in N and K during the 1st year of growth (Table 7). The leaf production was less in T5 than in T1 and T3 during the 1st year of growth, which explains the limited retranslocations observed. During the 2nd year of growth, retranslocations of N, P, and K represented about one third of the tree requirements in all treatments.

Contrary to N, P and K, Ca was not translocated. Such behavior was already observed for others tree species and suggests that the trees depend on Ca availability in soils. Mg translocation represented less than 15 % of the tree requirements, and was less in T5 than in T1 and T3.

PART B

THE SOILS OF THE EXPERIMENT:

CHARACTERIZATION,

MINERALOGY,

AND SURFACE REACTIVITY

INTRODUCTION

The soil compartment holds a major role in the global biogeocycle of nutrients within forest ecosystems, in particular through its dynamic interactions with soil solutions. It acts as a source of nutrients through mobilization and mineralization of organic matter by microorganisms, desorption of the soil surface, and mineral weathering (alteration and dissolution) and as a sink of nutrients through immobilization in soil organic matter and micro-organisms, adsorption on soil surfaces and precipitation of mineral phases. Nutrients may also leave the soil system by volatilization, immobilization in the vegetation biomass and leaching in soil solution, and enter the soil system by wet and dry atmospheric deposits, symbiotic and non-symbiotic nitrogen fixation, litter falls, forest floor mineralization and anthropogenic inputs (fertilizers) (Ranger and Turpault, 1999). Each process occurs with different controls and kinetics and is dependant upon soil type, hydrological regime, physico-chemical and biological parameters, and local dynamic equilibrium conditions between outputs (watershed) and inputs (deposits and fertilizers).

Mineral weathering is reported to be a potential important source of nutrients in temperate ecosystems where 2:1 phylosillicates and primary minerals may release K, Mg or Ca and this flux must be taken into account while establishing nutrient budgets for the ecosystem (Ezzaim, 1997; Fichter, 1997). However, in the tropics ferralsols are highly weathered and may not contain such minerals anymore (Segalen, 1995). In the experimental station where the experiment was conducted, the soils have developed from a Cretaceous sandstone belonging to the Marília formation and the Bauru group (Gonçalves, 2003; IPT, 1981) and are called “Latosolos Vermelhos Amarelos distróficos típicos A” (Dystrophic Red-Yellow Latosol), according to the Brazilian classification (EMBRAPA, 1999), Ferralsols, according to the FAO classification (FAO, 1998), and Typic Hapludox (USDA, 1999). These soils have been widely studied and are highly weathered soils containing kaolinite, quartz, goethite, hematite, gibbsite and traces of magnetite and/or ilmenite (Costa et al., 2004; Fontes and Weed, 1991; Marques et al., 2004). Their weathering may only release Fe, Al and Si. Nevertheless, authors reported the residual presence of 2:1 phyllosilicates (Barnhisel and Bertsch, 1989; Costa et al., 2004; Furian et al., 2002; Rahnemaie et al., 2007a; Soares et al., 2005; Van Ranst et al., 1998) which was identified as an interlayered Al vermiculite (also called pseudo-chlorite). The existence and

the resilience of such a mineral must be checked since 2:1 minerals are susceptible to release nutrients in soil solution by weathering and may contribute largely to the CEC.

Adsorption reactions are reported to be kinetically fast and to be the first step to other sink processes such as occlusion, precipitation or immobilization in soil organic matter and micro-organisms (Axe and Anderson, 1999; Barrow, 1983; Bolan et al., 1999; Cornell and Schwertmann, 2003; Delfosse et al., 2005; Edwards, 1998). Adsorption is thus of central importance in the study of the soil system and is a potential sink for mineral fertilizers dissolved in soil solutions. The studied soils are reported to be variable charge minerals (also called constant surface-potential minerals) for which the surface charge is created by the adsorption of potential-determining ions (classically H^+ and OH^-) onto the surface and are thus dependant upon the soil pH and the soil solution status (ionic strength, chemical composition) (Stumm and Morgan, 1996; Uehara and Gillman, 1981). They are opposed to permanent charge minerals for which the charge results from an excess of positive or negative charge caused by substitutions in the lattice structure of crystals which leads to the permanent higher cation exchange capacity (CEC) observed in temperate ecosystems. Kaolinite, quartz and organic matter present variable negative charges which classically lead in ferralsols to low CEC mainly occupied by aluminium at soil pH (below 5), which means a low capacity to retain cations. On the other hand, Fe and Al oxides and oxihydroxides present positive charges and may retain anions by adsorption. CEC and anion exchange capacity (AEC) < 1 cmolc kg^{-1} at soil pH have been reported for our soil type (Alves and Lavorenti, 2004; Marcano-Martinez and McBride, 1989; Soares et al., 2005; Van Raij and Peech, 1972). Amorphous Al and Fe in particular may lead to high AEC (Cornell and Schwertmann, 2003; Schaefer et al., 2004; Uehara and Gillman, 1981). The presence of the 2:1 interlayered vermiculite may be of central importance since such minerals even in little quantity may lead to high permanent charges. For our soil type, permanent charges from -0.5 to -1.5 cmolc kg^{-1} have already been reported (Chorover and Sposito, 1995; Gillman and Sumner, 1987; Marcano-Martinez and McBride, 1989). The anion and cation exchange capacities must be checked together with their evolution with pH since silvicultural practices are likely to modify soil pH (clear felling and liming in particular).

Besides this non specific adsorption of cations and anions governed by CEC and AEC and the laws of electrostatic, specific adsorptions are classically reported for Ca^{2+}, SO_4^{2-} and $H_2PO_4^-$ (Uehara and Gillman, 1981). K^+ and NH_4^+ may also be specifically adsorbed in the interlayer spaces of 2:1 phillosilicates (Dixon and Weed, 1989), but this pattern has

never been reported for our soil type. Specific adsorption partially transfers the charge of the adsorbed specie to the soil surface and thus increases CEC (in case of specifically adsorbed anion) or AEC (in case of specifically adsorbed cation) (Couto et al., 1979; Gillman, 1984; Hiemstra and Van Riemsdijk, 2006; Hingston et al., 1967; Rahnemaie et al., 2007b; Uehara and Gillman, 1981). This type of adsorption may be quite important for our study since large amounts of Ca^{2+}, SO_4^{2-} and $H_2PO_4^-$ are brought by fertilizers and since the soils are expected to exhibit a weak capacity to retain cations and anions on their AEC and CEC.

The competition for exchange sites on soil surface classically leads to greater adsorption of trivalent (mainly Al at low pH) and divalent cations over monovalent cations (for non specific adsorption) (Stumm and Morgan, 1996). For anions, $H_2PO_4^-$ is specifically adsorbed whereas SO_4^{2-} may show features of both specific and non specific adsorptions. Cl^- and NO_3^- are non-specifically adsorbed. The competition between anions is reported to lead, in the order of greater adsorptions, to $H_2PO_4^- > SO_4^{2-} > Cl^- > NO_3^-$ (Delmelle et al., 2003; Edwards, 1998; Geelhoed et al., 1997; Rietra et al., 1999). Organic matter and DOC may also compete for anionic adsorption sites (Cornell and Schwertmann, 2003; Fuller et al., 1985; Kaiser and Zech, 1996). But co-adsorption (also called ternary adsorption) are also reported for Ca and Al with SO_4 and PO_4 (Cornell and Schwertmann, 2003; Curtin and Syers, 1990b; Gillman and Sumner, 1987; Rasiah et al., 2004; Rietra et al., 2001; Stoop, 1980; Uehara and Gillman, 1981). Such interactions may be of central importance in understanding the retention of fertilizers and nutrients all along the soil profile.

Adsorption and desorption processes are highly dependant upon the contact between soil surface and soil solution (Edwards, 1998). In tropical ferralsols, most of the clay particles < 2 μm, consisting predominantly of kaolinite, are aggregated by organic matter and oxides coatings into secondary particles about 5-300 μm in size, acting as silt particles. The aggregation status of tropical soils has been widely discussed (Balbino et al., 2002; Bartoli et al., 1991; Cambier and Prost, 1981; Neufeldt et al., 1999; Pinheiro-Dick and Schwertmann, 1996; Schaefer et al., 2004; Volland-Tuduri et al., 2005). These aggregates are extremely stable under mechanical stress and consist of mixtures of goethite and hematite, with iron oxide content ranging from 50 to 200 g kg^{-1} (Cornell and Schwertmann, 2003; Meunier, 2003). Such coatings may influence soil adsorption properties: Fe and Al coatings may enhance anion retention whereas OM coatings may passive adsorption sites and/or promote cation adsorption. Adsorption actually affects the electrostatic properties of

suspended particles and colloids, which, in turn, influences their tendency to aggregate and attach (coagulation, settling, filtration), hence aggregation is reversible and sensitive to pH and electrolyte type and concentration (Nimmo and Perkins, 2002; Stumm and Morgan, 1996). Such behaviour may greatly influence analyses classically performed for soil study especially for particle-size analysis and soil fractionation for mineralogical study and great care must be taken to soil pH and ionic strength conditions in the analyses performed.

Sources and sinks of nutrients in soils are thus dependant upon the local status and composition of soil and soil solution which may be spatially heterogeneous. Heterogeneity of the soil constitution may result from the soil mineral composition. In the experimental station of Forest Sciences of Itatinga, geomorphological studies showed that soils were organized according to altitude and slopes. The fertilization experiment located above 800 m of altitude and presenting slopes < 5% corresponds to Dystropic Red-Yellow Latosol as already mentioned (Gonçalves, 2003; IPT, 1981). This soil type differs from the other soil types of the experimental station by its clay content and its colour (EMBRAPA, 1999). The homogeneity of the soil origin may then be easily checked by simple particle-size analysis and X-ray diffractions. The studied soils are reported to be highly homogeneous, with most of their heterogeneity associated to the organic matter of the upper soil layer (0-5 cm) (Maquere et al., 2008). The degree of heterogeneity of the soils of the experiment is important in order to assess whether (i) different kind of responses may be expected depending on the spatial localization, (ii) changes observed during the fertilization experiment may be attributed to changes induced by the experiment or to spatial heterogeneity of the studied variable.

The main goals of the soil study were thus to:

- characterize the pedological soil type of the experiment,
- estimate the spatial heterogeneity of some major characteristics (CEC, pH, organic matter (OM), and particle-size distribution),
- check the mineralogy of the soils of the experiment with a special interest in the 2:1 phyllosilicates,
- assess the soil potential in terms of non specific adsorption (CEC and AEC) depending on soil pH, and specific adsorption for SO_4^{2-} and $H_2PO_4^{2-}$ at average soil pH,

- finally, set hypotheses on the soil system response to silvicultural practices tested in the fertilization treatments (clear felling plus fertilization).

The underlying hypotheses are:

- The spatial heterogeneity does not result from deep mineralogical heterogeneities but from heterogeneities in the upper soil layer (0-5 cm) at the tree scale. The differences in the studied variables may be attributed to the fertilization regimes if greater than this variability.
- The weathering of soil minerals may only produce Al, Fe and Si. The nutrient release by weathering can be neglected.
- The permanent charge of the soil is weak and the soil surfaces behave as a variable charge system which is dependant upon soil solution pH and composition.
- Specific adsorption may occur for sulphate and phosphate with a different intensity in layers dominated by organic matter (upper soil layer) compared to deeper layers.

A reminder on the theories of soil surface reactivity is given in preambule to help further discussions.

THEORETICAL REMINDERS ON SURFACE CHARGE

Adsorption is the result of intermolecular interactions between solute and solid phases occurring at different physical and chemical strengths such as Wan der Waals interactions, proton fixation, hydrogen, hydrophobic and electrostatic bonds, coordination reactions and ligand exchange (which is a particular case of coordination). The process in which chemicals become associated with solid phases is often referred to as sorption (adsorption onto a two-dimensional surface, or absorption into a three-dimensional matrix) (Stumm and Morgan, 1996; Uehara and Gillman, 1981).

Three groups of adsorption status are often differentiated depending on the intensity and/or on the specificity of the association between the molecule or ion and the solid surface: (i) “inner-sphere complex” (or specific adsorption) which is the close complexation between adsorbed specie and surface functional groups by covalent bound without water inserted, (ii) “outer-sphere complex”, which is the adsorption of an ion with its hydration sphere at the surface by electrostatic bond, and (iii) “diffuse-ion” which is an hydrated ion separated from the surface by solubilized ions of contrary sign to the surface (diffuse layer), as a result of the equilibrium between electrostatic attraction and thermal agitation.

Minerals can be separated into two general types with respect to the origin of their surface charge: (i) the constant surface-charge minerals for which the charge results from an excess of positive or negative charge caused by substitution in the lattice structure of crystals compensated for by the accumulation of oppositely charged ions (counterions) at the crystal surfaces; (ii) the constant surface-potential minerals (often called variable charge minerals) for which the surface charge is created by the adsorption of ions onto the surface (potential-determining ions, classically H^+ and OH^-).

The laws of electrical neutrality dictate that an equal amount of charge of the opposite sign will accumulate in the liquid phase near the charged surface. Diffusion forces, however, tend to draw them back toward the equilibrium solution where their concentration would be diminished. The charged surface and the redistribution counterions constitute the electrical double layer. Based on such a model, a simple theory developed by Gouy and independently by Chapman, related the density of charge on the surface to the electrical potential across the double layer. The Gouy-Chapman equation is:

$$\sigma_0 = \left(\frac{2n\varepsilon kT}{\pi} \right)^{1/2} \sinh\left(\frac{ze}{2kT} \Phi_0 \right) \quad (1)$$

where σ_0 is the surface charge density [esu cm^{-2}] (esu=electrostatic unit of charge), n is the counterion concentration in the equilibrium solution [ion cm^{-3}], ε is the dielectric constant (esu^2 $dyne^{-1}$ cm^2), k is the Boltzmann constant (ergs $degree^{-1}$), T is the absolute temperature, z is the counterion valence, e is the charge of an electron (esu), and Φ_0 is the surface potential (esu).

The charge on the particle surface is thus dependent upon the potential difference across the electrical double layer, the electrolyte concentration, the valence of the counterion, the dielectric constant of the medium and the temperature. For constant surface charge, σ_0 is constant. For constant surface potential, the surface potential is controlled by the adsorption of potential determining ions, which in turn depends on the activity of those ions in the equilibrium solution. When H^+ and OH^- are the potential determining ions, the potential is governed by the pH and thanks to the Nernst equation:

$$\sigma_0 = \left(\frac{2n\varepsilon kT}{\pi} \right)^{1/2} \sinh\left(1.15 \cdot z \cdot \left(pH_0 - pH \right)\right) \quad (2)$$

where pH_0 is the pH at which the surface potential is zero, that is, corresponds to a point of maximum chemical stability.

The stern theory takes into account the actual size of the counterions and allows the ions to approach the surface to within a certain minimum distance (a few angstroms). Thus there is a counterion-free, uncharged space (of width d) between the surface and the first layer of adsorbed counterions, and the electrical potential drops linearly from Φ_0 to Φ_d. The remainder of double layer consists of a diffuse layer of counterions, as described in the Gouy-Chapman theory, in which the potential decays exponentially from Φ_d to zero. It includes a specific adsorption potential Φ_s which is the energy required for some ions to be adsorbed into the compact layer by forces other than those that are purely electrostatics. Specific adsorption may be of high-affinity (chemical coordination to the surface) or low-affinity type (adsorption in the Stern layer). Low-affinity specific adsorption of an anion would induce additional positive charge in the surface by OH^- desorption or H^+ sorption, whereas high-affinity specific adsorption would transfer the negative charge of the adsorbed anion (which is now part of the surface) to the solid.

The net total particle surface-charge density σ_0 is the sum of four components (Bolan et al., 1999; Chorover and Sposito, 1995):

$$\sigma_0 = \sigma_P + \sigma_H + \sigma_{IS} + \sigma_{OS} \quad (3)$$

where σ_P is the net permanent structural surface-charge density (isomorphic substitutions in soil minerals), σ_H is the net proton surface-charge density, σ_{IS} is the net inner-sphere complex surface-charge density (net total charge of ions, other than H^+ and OH^- which are bound into inner-sphere surface coordination), and σ_{OS} is the net outer-sphere complex surface-charge density (bound into outer-sphere surface coordination).

If σ_0 is non-zero, it must be balanced by the diffuse layers surface-charge density σ_D and

$$\sigma_0 = -\sigma_D \quad (4)$$

The net adsorbed ion charge is given by:

$$(q_+ - q_-) = \sigma_{IS} + \sigma_{OS} + \sigma_D = -(\sigma_P + \sigma_H) \quad (5)$$

where q refers to adsorbed cation (+) or anion (-) charge.

Different points of zero charge (PZC) can then be defined: the point of zero net charge (PZNC) corresponds to $(q_+ - q_-)=0$, the point of zero net proton charge (PZNPC) corresponds to $\sigma_H=0$ and the point of zero salt effect (PZSE) corresponds to the non-influence of the ionic strength on σ_D.

The maximum number of exchangeable cations (or anions) present in the electrical double layer per unit weight of exchanger under a given set of solution conditions is the cation exchange capacity CEC (or anion exchange capacity AEC) of the system:

$$CEC\left[\text{meq g}^{-1}\right] = S\left[\text{cm}^2\text{g}^{-1}\right] \cdot q_+\left[\text{meq cm}^2\right] \quad (6)$$

where S is the specific surface of the exchanger and q_+ the total charge of the cations adsorbed.

Table 8 Point of zero charge (PZC) for some major soil constituents (taken from Zelany *et al.* (1996))

	Quartz	Kaolinite	Goethite, hematite	Gibbsite	Montmorillonite
PZC	2.3	4.8	7.5-9.5	8.5	2.5

B.1 MATERIAL AND METHODS

B.1.1 Soil general characteristics

B.1.1.1 Pedological description and soil sampling

A complete pedological description was performed for one soil pit excavated in 2003 (before clear felling the 7-year-old *Eucalyptus* stand) down to a depth of 1 m.

Soils were sampled in 2003 at the depths of 0-5 cm, 5-15 cm, 15-50 cm, 50-100 cm, 100-200 cm, 200-300 cm, 300-400 cm, 400-500 cm and 500-600 cm in each one of the nine pits where the lysimeters were to be installed for the fertilization experiment coming next, in April 2004 (data set $SOIL_{BCF}$-1). Each one of the nine pits was localized before clear felling in a plot corresponding to one block (1, 2 and 3) of one treatment (1, 3 and 5) of the fertilization experiment coming next. As most of the soil heterogeneity was located in the upper soil layer, 9 samples each one composite of 4 sub-samples were collected in the 0-5 layer in blocks 1, 2 and 3 of treatment 1 (Figure 14) to study the soil spatial heterogeneity (data set $SOIL_{BCF}$-2).

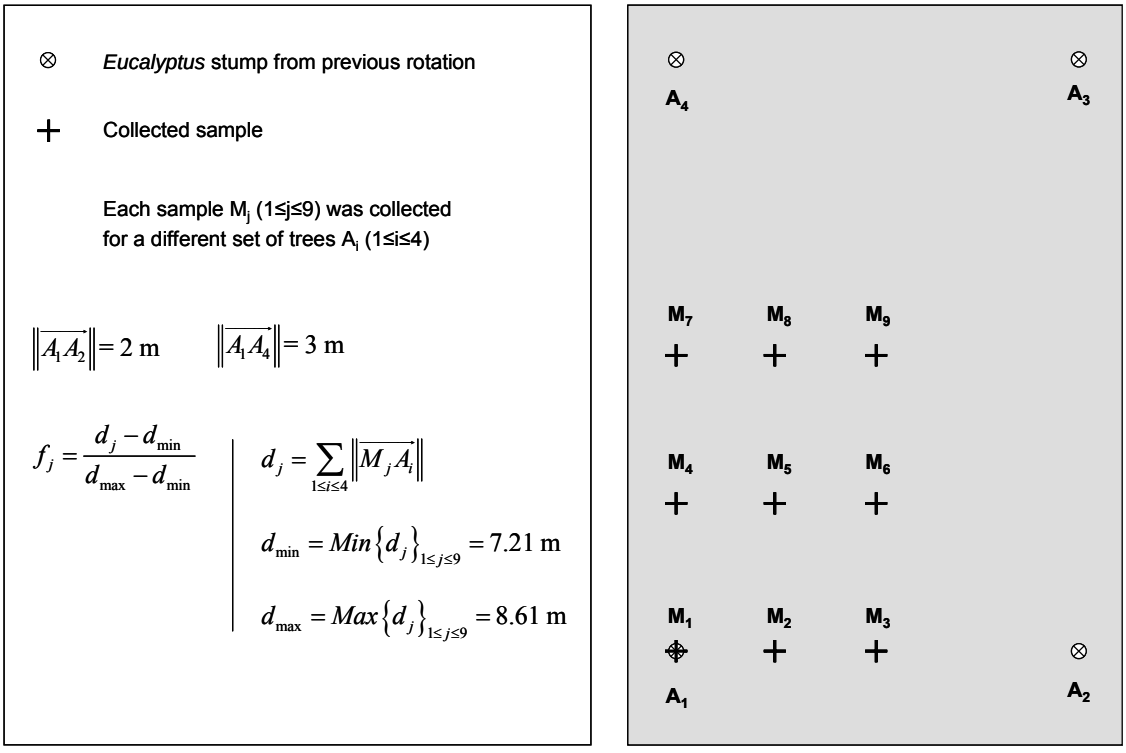

Figure 14 Sampled locations for data set $SOIL_{BCF}$-2 and calculation of a factor f relating a sample to its distance to the nearest trees. The subscript j ($1 \le j \le 9$) and the letter M identify the samples. The subscript i ($1 \le i \le 4$) and the letter A identify the nearest trees.

B.1.1.2 Sample preparation and analysis performed

Unless mentioned, all soils were passed through a 2 mm sieve and oven dried at 40°C. The fraction > 2 mm was made of roots and vegetal matter with no mineral matter and was thus discarded.

Soil residual humidity at 105°C was measured for each soil sample. Bulk densities were measured thanks to a 93 cm^3 cylinder, for three replicates in each soil layer of the nine pits excavated in 2003 down to a depth of 3 m. An aliquot was ground to 150 µm for organic carbon and nitrogen determination (INRA, UMR Écologie et écophysiologie forestières) for all samples down to a depth of 1 m. Granulometry using hexametaphosphate as a dispersant (da Silva et al., 1999) was performed for all samples of data set $SOIL_{BCF}$-1 down to a depth of 3 m and for one composite per block from a depth of 3 to 6 meter (ESALQ, Departamento de Ciências Florestais, Laboratorio de Ecologia Aplicada). Size fractions were separated according to the classical following limits: 50 µm < sands < 2 mm, 2 µm < silts < 50 µm and clays < 2 µm. No size differentiation was made into sand and silt classes. The soil pH in water and KCl 1 mol L^{-1} (5 g of soil in 25 mL of solution) and the effective cation exchange capacity at soil pH (Rouiller et al., 1980) were measured for all samples. Exchangeable cations were extracted with KCl 1 mol L^{-1} (5 g of soil in 2x50 mL of KCl). KCl was replaced by NH_4Cl for the determination of the exchangeable K. After centrifugation and filtration, Ca, Mg, Na, Mn and Fe were measured by inductively coupled plasma (ICP), and H and Al by titration. The saturation in alkaline earth cations was calculated as the sum of exchangeable Ca^{2+}, Mg^{2+}, K^+ and Na^+ and the exchangeable acidity as the sum of Al^{3+} and H^+ measured in the soil extracts. pH and CEC measurements were performed at INRA BEF.

B.1.1.3 Spatial heterogeneity

The studied variables were: bulk density, organic C and N content, pH_{water}, pH_{KCl}, CEC, saturation, acidity, sand, silt and clay contents for data set $SOIL_{BCF}$-1; organic C and N content, pH_{water}, pH_{KCl}, CEC, saturation and acidity for data set $SOIL_{BCF}$-2. As most of the variability was localized in the upper soil layer, data set $SOIL_{BCF}$-1 was divided into 2 sub data sets $SOIL_{BCF}$-1a (samples of the 0-5 cm layer of data set $SOIL_{BCF}$-1) and $SOIL_{BCF}$-1b (data set $SOIL_{BCF}$-1 but the 0-5 cm layer).

Correlations among the measured variables were studied using the CORR procedure of SAS software (www.sas.com) for data sets $SOIL_{BCF}$-1a and $SOIL_{BCF}$-1b. When the

variables were correlated, the linear regressions relating these variables were established using the GLM procedure of SAS Software.

Analyses of variance were performed per soil layer on data set $SOIL_{BCF}$-1 to study the effect of the plot location grouped by block or by treatment (fertilization experiment to be installed in 2004) using the GLM procedure of SAS Software. The purpose of this study was to verify that there existed no clear spatial heterogeneity among the sampled plots so that the differences observed later in the fertilization experiment could be attributed to the fertilization treatments and not to a pre-existing difference among plots.

For data set $SOIL_{BCF}$-2, the influence of the distance of a soil sample to the nearest trees was analyzed through a factor f defined in Figure 14. The maximum influence of the trees corresponded to f=0, the minimum influence to f=1. Linear interactions of f with the measured variables were tested thanks to the GLM procedure of SAS software.

B.1.2 Soil mineralogy

The main objectives of the mineralogical studies were to identify and quantify the minerals constituting the bulk soil of the experiment to (i) verify the hypothesis that in these highly weathered tropical soils, there remains no mineral which may participate significantly to nutrient release in soil solution during the weathering process, and (ii) to estimate their expectable dynamics in terms of surface adsorption. This meant identifying and quantifying roughly the main soil mineralogical constituents on the < 2 mm bulk soil. The soil fractions (mainly the clay fraction < 2 µm) were also study to help identifying and quantifying bulk soil minerals.

B.1.2.1 Studied samples

A new soil sampling was performed in March 2005, in order to have soil material enough to perform all analysis, and to have a thinner division of the 15-50 cm layer. Soils were sampled in 4 pits located in treatment 1, blocks 1, 2, 3 and 4 at depths 0-5 cm, 5-15 cm, 15-30 cm, 30-50 cm, 50-100 cm, 100-200 cm and 200-300 cm (data set $SOIL_{AP11}$). Samples were also collected every meter by augering down to a depth of 15 m (1-1.10 m, 2-2.10 m, …, 15-15.10 m) at the stand edge (data set $SOIL_{15m}$) to check whether nutrients may be retained in deeper soil layers in case they were leached out of the studied soil profile (deep of 3 m).

B.1.2.2 Aggregation

Ferralsols are particularly difficult to disperse and pre-treatment of the sample to enhance the separation or dispersion of aggregates is a key step for mineralogical analysis. Depending on the method of chemical treatment and physical dispersion used, the clay content measured for an individual soil sample can vary by factors of four or more (Gee and Bauder, 1986). The separation and/or dispersion of aggregates may be performed from different ways. Cementing, binding and flocculating agents, such as organic matter or Fe oxides (hematite and goethite) may be chemically removed. Physical treatments may also be used to separate aggregates. Soil particles might also be chemically dispersed. Changing soil surface status (mainly pH) may also help dispersing soil aggregates especially for tropical soils presenting mainly variable charges minerals (Uehara and Gillman, 1981). Nevertheless, chemical treatments may pollute the treated sample and dissolve or damage

soil minerals and physical treatments such as mechanical or ultrasonic dispersions may fragment the individual particles into further subunits.

The particle-size analysis classically used and performed in §B.1.1.2 is performed by chemical dispersion using a dilute alkaline solution of sodium polyphosphate. The 2005 sampling was used to evaluate the degree of aggregation in our soil samples as a preambule of soil fraction preparation for mineralogical analysis. Particle-size analysis in sodium hexametaphosphate was compared to particle-size analysis performed in water for pit 3 of data set $SOIL_{AP11}$. Size fractions were separated according to the same limits than in §B.1.1.2. When the amount of soil material was sufficient, the particle-size analysis was repeated up to four times for a given soil sample to estimate the analytical variability.

B.1.2.3 General strategy

A qualitative determination of the soil mineralogy was performed for all samples of data set $SOIL_{AP11}$ by analyzing by X-ray diffraction their bulk soil and their soil fractions separated after organic matter removal. Quantitative determinations were performed only for pit 3 of data set $SOIL_{AP11}$. The 30-50 and 100-200 cm layers were not studied since they were transition layers without specific mineralogical features. For all studied samples, total analysis, thermo gravimetric and thermo differential analysis, and specific Al and Fe extractions were performed on the sand and clay fractions. The silt fraction consisted of too little material to be analyzed. Each one of the analysis performed is detailed thereafter.

B.1.2.4 Preparation of soil fractions for mineralogical analysis

The methodologies were chosen to maximize soil aggregates dispersion while minimizing the risks of pollution and destruction of the mineral phase. Organic matter was first removed by a mild oxidation using diluted H_2O_2 (20 vol.) at 40°C. The sand fraction (> 50 µm) was separated by sieving under a slight flux of deionised water and gentle manual agitation. The remaining < 50 µm fraction was then saturated and dispersed with Na saturated resin (sol/resin fraction of about 1/10) using gentle agitation during 16 hours. Resins were chosen for their well known efficiency to disperse aggregates in soils rich in oxides (Bartoli et al., 1991; Bartoli et al., 1992a; Bartoli et al., 1992b; Churchman, 1997; Feller, 1991). After resin removal by sieving, the soil suspension was transferred to a 1 L-test tube. The clay fraction (< 2 µm) was then removed by successive sedimentations and

siphoning according to Stockes' law. When needed, drops of NaOH 1N were added to the suspension to ensure soil dispersion. All soil fractions were finally saturated with $MgCl_2$.

B.1.2.5 Identification of soil minerals: X-ray diffraction

X-ray diffraction was used both to identify unknown mineral phases and to determine crystal structures. The X-ray diffractometer was a Siemens D5000 equipped with a Cu anticathode and a graphite monochromator (30 mA and 40 KeV) (INRA BEF). The rotation speed was 0.02°/s. The diffractograms were performed on powder made from the whole soil and from soil fractions saturated with Mg. They were also performed for the clay fraction on oriented deposit to reinforce the 001 reflection for phyllosilicates, before and after deferrification treatments and various other treatments to investigate the interlayer space.

Table 9 Influence of the analytical treatment of a mineralogical clay (saturation with Mg or K, heating, swelling by Ethylene Glycol, destruction of interlayered Al by tricitrate treatment) on the location of its main peak (nm) on the X-ray chart. The shift of the main peak enables the differentiation and the identification of mineralogical clays. Bold and underlined numbers correspond to key steps in the identification. From Mareschal (2008).

	Air-dried	Ethylene Glycol		Air-dried		Heated (550°C)
Saturation	Mg	Mg		K		K
Tricitrate [a]	-	Before	After	Before	After	-
Chlorite	1.4	1.4				**<u>1.4</u>**
Vermiculite	1.4	1.4		**<u>1.0</u>**		1.0
Smectite	1.4	**<u>1.7</u>**		1.4		1.0
HIS [b]	1.4	1.4	**<u>1.7</u>**	1.4	1.0-1.4	1.0
HIV [c]	1.4	1.4		1.4	**<u>1.0</u>**	1.0
Kaolinite	0.715	0.715				**<u>(-)</u>**

[a] Tamura, 1958 ; [b] HIS = Hydroxy interlayered smectite ; [c] HIV = Hydroxy interlayered vermiculite

Clay minerals were identified according to Table 9. Briefly, K saturation was used to collapse interlayer spaces, the tricitrate extraction (Tamura, 1958) was used to remove the aluminium of the interlayer space, ethylene glycol (EG) was used to expand swelling clays, and heatings served to collapse interlayer spaces of intergrades minerals. Diffractograms were performed from 1.5 to 31°2θ or from 1.5 to 20° 2θ for oriented deposits and from 1.5 to 70°2θ for raw powders.

B.1.2.6 Quantification of the minerals

B.1.2.6.1 Selective dissolutions of iron and aluminium

Table 10 Reactant efficiency for aluminium and iron dissolution on different forms of Al and Fe (organic, organo-minerals or minerals). Adapted from Jeanroy (1983) and Soon (1993).

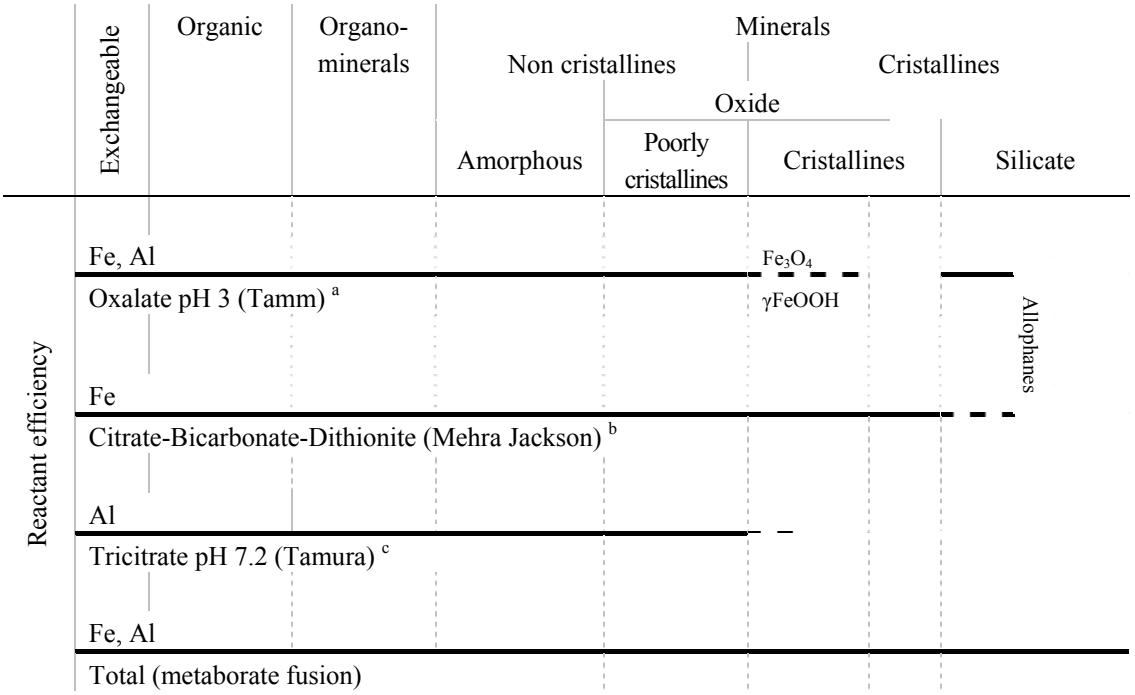

[a] (Tamm, 1922) ; [b] (Mehra and Jackson, 1960) ; [c] (Tamura, 1958).

Various selective dissolutions can be used to extract and thus quantify iron and aluminium in different solid-phase forms (Table 10). The extraction Tamm (1922) is well known to extract exchangeable, organically bound, and amorphous iron and Al oxides (also called "active" or short-range ordered or poorly crystalline oxides). The dissolution is performed by ammonium oxalate at 20°C, pH=3 and in darkness. The extraction Mehra Jackson (1960) extracts exchangeable and organically bound Fe, and iron oxides such as hematite, goethite, lepidocrocite and ferrihydrite. The reaction is a reductive dissolution by dithionite at 80° C. Citrate is used to chelate dissolved Fe and Al. $NaHCO_3$ is used to buffer the solution near pH 7. The Tamura extraction (1958) extracts amorphous forms of Al and Fe and part of interlayer Al from the hydroxyl-interlayered minerals. Three consecutive extractions with sodium tricitrate 1 mol L^{-1} are performed at 95°C and pH=7.3. The elements extracted (Al, Fe, Si) are quantified by inductively coupled plasma emission spectrometry (ICP. Jobin Yvon J-Y 38 PLUS).

Ammonium oxalate (Tamm) and DCB (Mehra Jackson) extractions were performed on bulk soil samples. Ammonium oxalate, DCB and sodium tricitrate (Tamura) extractions were performed on soil fractions. A tricitrate extraction (Tamura) following DCB extraction (Mehra Jackson) was also performed to dissolve interlayered Al (Tamura) inside the aggregates formed by Fe and Al coatings. Analysis were performed for bulk soil at ESALQ (Departamento de Ciências do Solo, Laboratorio de Análises Químicas Pesquisa, and Laboratorio de Tecidos Vegetais). Soil fractions analyses were performed at INRA BEF.

B.1.2.6.2 Total analyses

Total chemical analyses were performed at the CRPG laboratory in Nancy on total soil and on clay fractions saturated with strontium and dried at 105°C. Since the soil contained traces of strontium, total strontium after Sr saturation of the soil sample corresponded to the cation exchange capacity of the sample. Fusion was performed with $LiBO_2$ and dissolution by HNO_3. Total amounts of Sr, SiO_2, Al_2O_3, Fe_2O_3, MnO, MgO, CaO, Na_2O, K_2O, TiO_2 and P_2O_5 in extracts were quantified by ICP. Loss on ignition from 110°C to 1000°C was also measured.

B.1.2.6.3 Differential thermal analysis (DTA) and thermal gravimetric analysis (TGA)

The commonly used methods for thermoanalysis are thermal gravimetric (TGA) and differential thermal analysis (DTA). Gravimetric thermograms provide information about the temperature-dependent weight loss of a sample associated with dehydration and dehydroxylation. Differential thermoanalysis involves recording heat release (resp. absorption) occurring when exothermic (resp. endothermic) reactions such as dehydration, or dehydroxylation (resp. recrystallisation, combustion …) take place. The temperature at which such reactions occur as well as their quantitative water or hydroxyl losses are mineral specifics, so that DTA and TGA allow a qualitative and quantitative estimation of certain minerals.

This complementary analysis was performed to help quantifying kaolinite, gibbsite, and goethite on clay samples of pit 3. The percentage of those minerals in the studied sample can be estimated thanks to its recorded weight loss in a given temperature interval. Between 220 and 320°C, the weight loss can be attributed to gibbsite and goethite which lose 34.6 and 10 % of their weight respectively. Between 450 and 600°C, the sample weight loss can be attributed to kaolinite which loses 14 % of its weight (Bish and Duffy,

1990; Dejou et al., 1977). Samples were analyzed at the Poitiers University (UMR 6532, HYDRASA).

B.1.2.6.4 Normative calculation

The quantitative determination of soil constituents was calculated from the total analysis of the bulk soil and of the soil fractions. The following hypotheses are based on the results of the qualitative mineralogical study presented in the result section (X-ray analysis of § B.2.2.3) and on Fe and Al specific extractions of § B.2.2.4. For methodological purposes, they are presented in the material and method section, even if they ensued from the mineralogical results. Hypotheses are given together with their mathematical translation. Calculations are given in moles (abbreviation n) considering a sample of 1 kg. Each constituent mass (abbreviation m) can be obtained by multiplying the molar quantity by the molar mass of the constituent.

- Fe, Al and Si extracted by the oxalate treatment (Tamm) were considered either amorphous or originating from the organic matter and were systematically subtracted from the total Fe_2O_3, Al_2O_3, and SiO_2 contents before further calculations.

$$n_{SiO_2}^{bulksoil,clay,sand} = n_{SiO_2}^{total}(bulksoil, clay, sand) - n_{SiO_2}^{Tamm}(bulksoil, clay, sand) \quad (7)$$

$$n_{Fe_2O_3}^{bulksoil,clay,sand} = n_{Fe_2O_3}^{total}(bulksoil, clay, sand) - n_{Fe_2O_3}^{Tamm}(bulksoil, clay, sand) \quad (8)$$

$$n_{Al_2O_3}^{bulksoil,clay,sand} = n_{Al_2O_3}^{total}(bulksoil, clay, sand) - n_{Al_2O_3}^{Tamm}(bulksoil, clay, sand) \quad (9)$$

- Bulk soil was constituted of quartz, kaolinite, gibbsite, goethite and hematite. Other minerals present in less quantity and potentially containing Fe or Al were kept as pure oxides (TiO_2, MnO etc…) and were considered negligible in Fe and Al calculations.

  Total organic matter content was roughly estimated as twice the organic C content (Nelson and Sommers, 1996).

$$1 - m_{SiO_2,Al_2O_3,Fe_2O_3}^{Tamm} = m_{quartz}^{bulksoil} + m_{kaolinite}^{bulksoil} + m_{gibbsite}^{bulksoil} + m_{goethite}^{bulksoil} + m_{hematite}^{bulksoil} + m_{TiO_2}^{bulksoil} + ... + 2m_{organicC}^{bulksoil} \quad (10)$$

  Equation (10) served as calculation control at the end of the calculation, once all the masses were calculated.

- The composition of the minerals were the basic theoretical ones, that is, SiO_2 for quartz, $Si_2Al_2O_5(OH)_4$ for kaolinite, $Al(OH)_3$ for gibbsite, Fe_2O_3 for hematite and FeOOH for goethite.

- Fe was considered to be included in iron oxides only (hematite and goethite), so that their quantity was estimated from total Fe_2O_3 and not from the DCB extracts (which only extracted part of Fe oxides, see results section).

$$n_{SiO_2}^{bulksoil} = n_{SiO_2}^{quartz} + n_{SiO_2}^{kaolinite} = n_{quartz}^{bulksoil} + 2n_{kaolinite}^{bulksoil} \quad (11)$$

$$n_{Fe_2O_3}^{bulksoil} = n_{Fe_2O_3}^{hematite} + n_{Fe_2O_3}^{goethite} = n_{hematite}^{bulksoil} + 0.5n_{goethite}^{bulksoil} \quad (12)$$

$$n_{Al_2O_3}^{bulksoil} = n_{Al_2O_3}^{kaolinite} + n_{Al_2O_3}^{gibbsite} = n_{kaolinite}^{bulksoil} + 0.5n_{gibbsite}^{bulksoil} \quad (13)$$

- All the quartz of the bulk soil was supposed to be included in the sand fraction since no significant amount of quartz was observed by X-ray analysis in the other fractions.

$$m_{sand} = m_{quartz}^{sand} + m_{gibbsite}^{sand} + m_{goethite}^{sand} + m_{hematite}^{sand} + m_{TiO_2}^{sand} + ... + 2m_{organicC}^{sand} \quad (14)$$

$$n_{SiO_2}^{sand} = n_{SiO_2}^{quartz} = n_{quartz}^{sand} \quad (15)$$

$$n_{quartz}^{sand} = n_{quartz}^{bulksoil} \quad (16)$$

where m_{sand} is the mass of sand for 1kg of bulk soil.

- All the silica of the clay fraction was attributed to kaolinite since no quartz was detected in the clay fraction.

- All the kaolinite of the bulk soil was supposed to be included in the clay fraction.

$$m_{clay} = m_{kaolinite}^{clay} + m_{gibbsite}^{clay} + m_{goethite}^{clay} + m_{hematite}^{clay} + m_{TiO_2}^{clay} + ... + 2m_{organicC}^{clay} \quad (17)$$

$$n_{SiO_2}^{clay} = n_{SiO_2}^{kaolinite} = 2n_{kaolinite}^{clay} \quad (18)$$

$$n_{kaolinite}^{clay} = n_{kaolinite}^{bulksoil} \quad (19)$$

where m_{clay} is the mass of clay for 1kg of bulk soil.

- Goethite/(hematite+goethite) ratio (R_{gh}) was roughly estimated from the literature on tropical soil yellowing which relates this ratio to the soil hue (Munsell chart). It was taken as R_{gh}=1 for the 0-5 cm layer (7.5 YR ¾), R_{gh}=0.6 from 5 cm down to a depth of 30 cm (5 YR ¾), and R_{gh}=0.3 beyond a depth of 30 cm (2.5 YR 3/6)

(Cornell and Schwertmann, 2003; Torrent et al., 1983). Hue values were taken from Maquère (2004). Hematite and goethite contents thus obtained must be handled cautiously since they were not calculated from direct measurements of these minerals.

$$R_{gh} = \frac{n_{goethite}^{bulksoil}}{n_{goethite}^{bulksoil} + n_{hematite}^{bulksoil}} \tag{20}$$

Amounts of quartz were finally calculated from the total analysis of the sand fraction and the particle size distribution using eq. (15) and (16):

$$n_{quartz}^{bulksoil} = n_{SiO_2}^{sand} \tag{21}$$

Kaolinite and gibbsite were calculated from the particle-size distribution and from the total analysis of the bulk soil, and of the clay and sand fractions, using eq. (18) and (19) , eq. (12) (kaolinite) and (13) (gibbsite):

$$n_{kaolinite}^{bulksoil} = n_{SiO_2}^{sand} + n_{SiO_2}^{clay} \tag{22}$$

$$n_{gibbsite}^{bulksoil} = 2\left(n_{Al_2O_3}^{bulksoil} - n_{SiO_2}^{clay}\right) \tag{23}$$

Goethite and hematite were estimated from total analysis of the bulk soil using (12) and (20):

$$n_{hematite}^{bulksoil} = n_{Fe_2O_3}^{bulksoil} \frac{1 - R_{gh}}{1 - 0.5R_{gh}} \tag{24}$$

$$n_{goethite}^{bulksoil} = n_{Fe_2O_3}^{bulksoil} \frac{1 - R_{gh}}{1 - 0.5R_{gh}} \frac{R_{gh}}{1 - R_{gh}} \tag{25}$$

Equations(10), (14) and (17), as well as losses on ignition for bulk soil and soil fractions were used to check the calculations.

B.1.3 Surface reactivity

B.1.3.1 CEC & AEC as a function of soil pH

The changes in CEC and AEC as a function of pH were measured for pit 3 of data set $SOIL_{AP11}$ for which mineralogical measurements were performed, following the protocol of Gillman (1984). The experiment was performed at INRA BEF. Two grams of soil were saturated by 1h shaking in 20 mL of $CaCl_2$ 0.1 mol L^{-1}. The sample was then washed three times with 20 mL of $CaCl_2$ 0.002 mol L^{-1}, and re-suspended in 10 mL of $CaCl_2$ 0.002 mol L^{-1} (ionic strength approximating field conditions) with H^+ or OH^- to cover a range of pH from 3 to 7. The soil solution suspension was then equilibrated during a six-days shaking at a constant temperature of 25°C. The pH was measured and Ca, Al and Cl in the equilibrium solution were quantified. The index cation (Ca) and anion (Cl) were desorbed using 3 washings of 30 mL NH_4NO_3 1 mol L^{-1} (1 h shaking). Ca, Cl, Al and H were measured in the extract.

Total CEC was calculated as the sum of Al, H and Ca desorbed by NH_4NO_3, basic CEC (CEC_b) was calculated as the amount of Ca desorbed by NH_4NO_3 and total AEC as the amount of Cl desorbed by NH_4NO_3. pH_0 was calculated as the point for which AEC equaled total CEC (Al and H included) which corresponded to the point of zero net charge defined in the introduction of this chapter.

B.1.3.2 Adsorption isotherms for NO_3^-, SO_4^{2-} and $H_2PO_4^-$

Specific adsorption was measured for nitrate, sulphate and phosphate for layers 0-5 cm and 200-300 cm of pit 3 to differentiate soil samples influenced by organic matter from deeper soil layers.

The chosen pH was 4 which corresponded to the average pH of the 0-5 cm layer and to the average minimum pH measured in situ for soil solutions. The pH was adjusted with KOH 1 mol L^{-1} or HCl 1 mol L^{-1}. Ionic strength was set to 10^{-1} mol L^{-1} and maintained thanks to KCl. The average ionic strength for soil solutions was of 10^{-3} mol L^{-1} with minima around 10^{-5} mol L^{-1} and maxima of 3.10^{-2} mol L^{-1}. Fixing the ionic strength at 10^{-2} or 10^{-3} mol L^{-1} would have been a better approximation of field conditions but maintaining this value constant during the whole experiment would have been experimentally tedious. 10^{-1} mol L^{-1} was a good compromise between experimental requirements and field

conditions. This meant that the isotherms measured are maximum adsorption isotherms for our field conditions. K was used preferentially to Ca since interactions between calcium and phosphate or sulphate are reported in the literature (Cornell and Schwertmann, 2003; Curtin and Syers, 1990b; Gillman and Sumner, 1987; Rasiah et al., 2004; Rietra et al., 2001; Stoop, 1980).

Isotherms were realized using solutions of KNO_3 for nitrate, K_2SO_4 for sulphate and KH_2PO_4 for phosphate. For each element, 7 points were measured for concentrations in N, S or P of 0, 0.05, 0.1, 0.5, 1, 2 and 3.5 mmol L^{-1}. Each point was performed in triplicate.

The ration soil/solution was of 1/10 using 2 g of soil in 20 mL of solution. The time of agitation and contact was set to 1h since it is reported to be sufficient a time to reach the equilibrium between soil surface and soil solution, anions adsorbed during longer contact times corresponding to occlusion (Cornell and Schwertmann, 2003; Delfosse, 2005). After one-hour equilibrium at constant pH, ionic strength and temperature, P, S or NO_3 were analyzed in the soil extracts by ICP for S and P and by colourimetry for NO_3.

Langmuir and Freundlich isotherms were fitted on experimental data thanks to proc NLIN of SAS Software (www.sas.com). The Langmuir equation was:

$$q_{ads} = q_{ads}^{\max} \frac{Kc_{solution}}{1 + Kc_{solution}} \tag{26}$$

where q_{ads} is the quantity of N, S or P adsorbed on the soil surface (mg/100g), $c_{solution}$ is the concentration of N, S or P in the contact solution (mg L^{-1}) and $q_{ads}^{\max}$ (mg/100g) and K(L mol^{-1}) are the parameters to be fitted. $q_{ads}^{\max}$ corresponds to the maximum adsorbed N, S or P on soil surface ($\lim_{c_{solution} \to \infty} (q_{ads})$) and 1/K equals the concentration for which $q_{ads} = \frac{q_{ads}^{\max}}{2}$.

The Freundlich formalism is often used when Langmuir equation fails to model experimental data:

$$q_{ads} = k_f c_{solution}^{1/n_f} \tag{27}$$

where k_f and n_f are parameters to be fitted.

B.2 RESULTS AND DISCUSSION

B.2.1 General characteristics

B.2.1.1 Pedological description

Figure 15 Description of the soil pit excavated in 2003 in the 7-year old *Eucalyptus* stand before clear felling. The colour of the different soil layers are given on the right of the depth axis according to Munsell chart.

The main colour was red with yellower hues close to the soil upper limit (from 2.5YR3/6 beyond 50 cm to 7.5YR3/4 in surface). The main structure was blocky subangular and the porosity was high, homogeneously localized in the soil matrix from small pores to 1mm-sized pores, with no fracture. Termit mounds, ant ills, worm piles, and spider nests were frequently encountered in the upper 50 cm of the soil profile.

No clear limit between soil layers was observed. Two gradients defined progressive and continuous transitions from the soil surface down to a depth of 1 m: a gradient of organic matter (grey/yellow colour) increasing from the bottom of the profile and maximum above a depth of 30 cm, and an inverse gradient of clay increasing from a sandy

texture in the upper soil layer to a sandy loam at the bottom of the profile (Figure 15). Soil layers were differentiated by their colour, texture, bulk density and root density as:

- 0-5 cm: dark organo-mineral layer with an intense biological activity and a dense root system (especially fine roots). Charcoals were frequently encountered.
- 5-15 cm: same characteristics as the 0-5 cm layer with fewer roots.
- 15-30 cm: same characteristics as the 5-15 cm layer. Denser soil layer.
- 30-50 cm: transition layer.
- 50-100 cm: transition layer between upper soil layer influenced by organic matter and deeper layers redder, more humid and clayey. The root density decreased (less fine roots, mainly roots of diameter >3mm), the colour changed from yellow to red and the clay content increased.
- Deeper than 100 cm: loamy sand, redder, less roots (mainly roots of diameter > 1 cm).

A dense root material that adhered to decomposed OM developed at the interface between the fresh litter layer and the mineral soil. Its thickness was < 5 mm. Such a litter structure had already been observed in Congolese *Eucalyptus* plantations (Laclau et al., 2004a) and in the experimental station of Itatinga under other vegetation types (Maquère et al., 2008).

B.2.1.2 Particle-size distribution

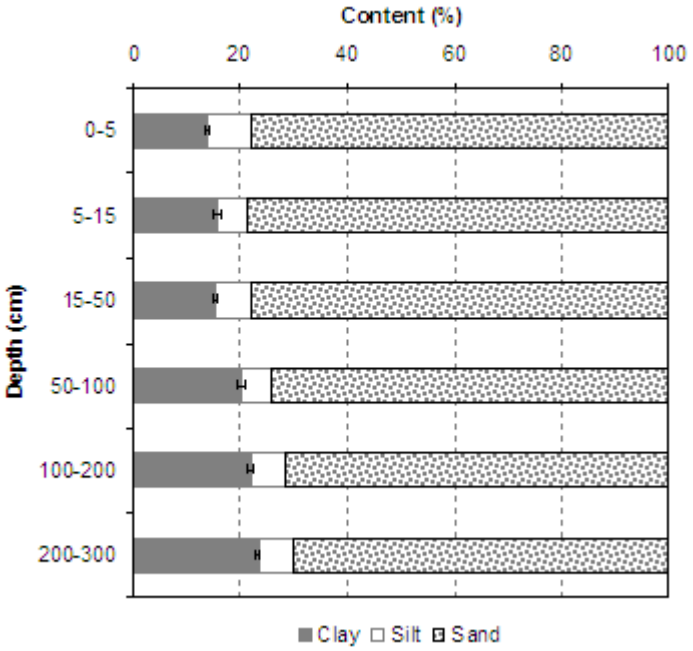

Figure 16 Particle-size distribution performed in hexametaphosphate (da Silva et al., 1999) for each layer of the soils of the experiment (2003 sampling, data set $SOIL_{BCF}$-1). Standard errors are represented for the clay fraction (n=9). Sand fraction from 50 µm to 2 mm, silt fraction from 2 to 50 µm and clay fraction < 2 µm.

Particle-size distribution confirmed the pedological descriptions. Clay content increased with depth from 16 % in the 0-5 cm layer to 24 % below a depth of 1 m. The 50-100 cm layer was a transitory layer with clay contents of about 20 % (Figure 16). Silt content was more or less constant at about 6 %. Sand contents represented 70 % of the bulk soil for the 200-300 cm and up to 79 % for the 0-5 cm and the 5-15 cm layers. Standard errors were <1%.

B.2.1.3 Soil pH

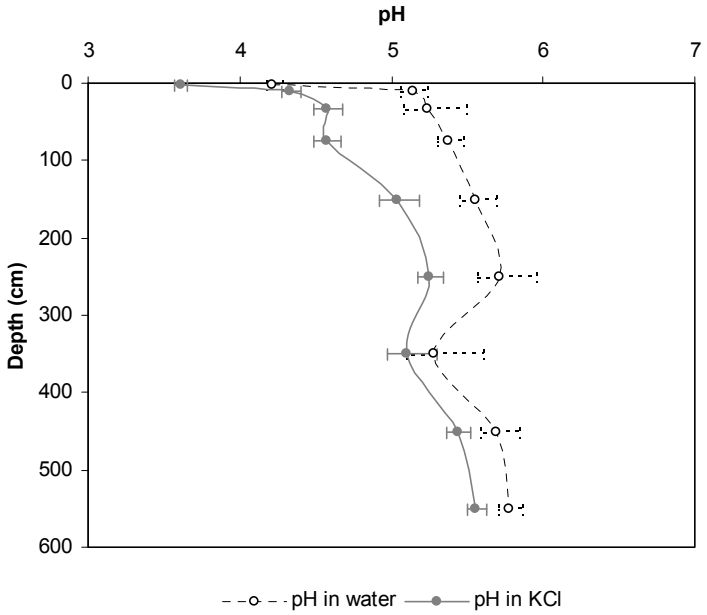

Figure 17 pH measured in water and in KCl 1 mol L^{-1} for each soil layer in the experiment (2003 sampling, data sets $SOIL_{BCF}$-1 & 2). Standard errors calculated from H^+ concentrations are represented (n=36 for the 0-5 cm layer, n=9 otherwise).

Soil pH were more acidic for the upper soil layer (4.2 in water 3.6 in KCl) compared to deeper soil layers (about 5.2 in water and 4.5 in KCl from a depth of 15 cm down to 1 m, and about 5.6 and 5.3 deeper). Standard errors calculated on H^+ concentrations lead to pH ranges of less than 0.5 pH unit (Figure 17).

pH in water was about 0.7 unit pH more basic than pH in KCl down to a depth of 1 m, about 0.5 from a depth of 1m down to a depth of 3m, and about 0.2 below a depth of 3 m.

B.2.1.4 CEC

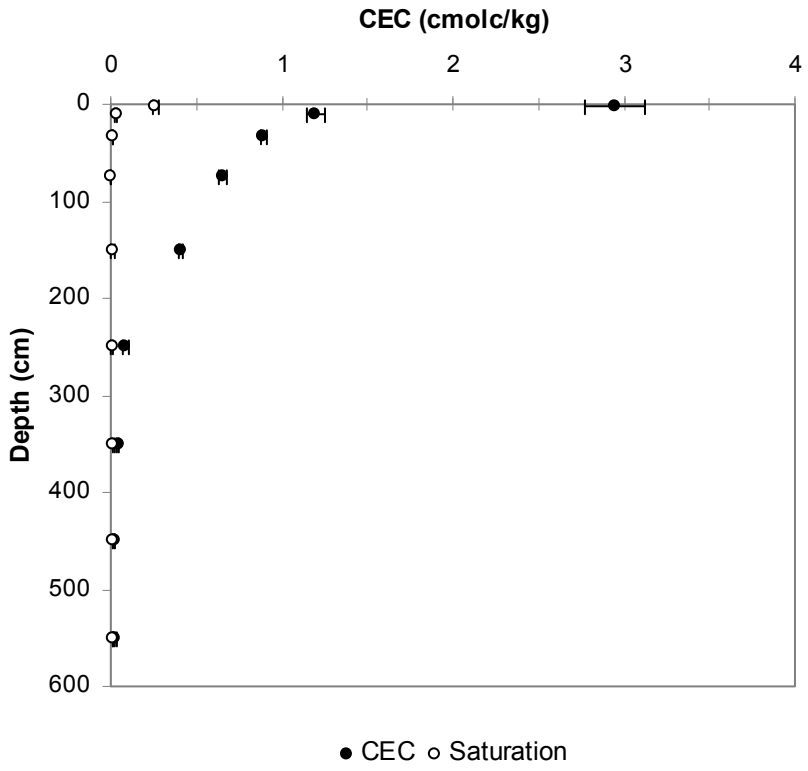

Figure 18 Effective CEC (Rouiller et al., 1980) and saturation in alkaline earths cations for each layer of the soils of the experiment (2003 sampling, data sets $SOIL_{BCF}$-1 & 2). Standard errors are represented (n=36 for the 0-5 cm layer, n=9 otherwise).

The CEC decreased exponentially from 2.95 cmolc kg^{-1} in the 0-5 cm layer down to less than 0.10 cmolc kg^{-1} below a depth of 2 m. Saturation in alkaline earth cations was < 0.30 cmolc kg^{-1} in the 0-5 cm layer and < 0.03 cmolc kg^{-1} deeper, which corresponded to more than 90 % of the CEC saturated with acid cations (Al and H) (Figure 18).

The soils were highly homogeneous regarding their CEC with standard errors < 0.052 cmolc kg^{-1} (n=9), except for the 0-5 cm layer for which the standard error was of 0.173 cmolc kg^{-1} (n=27).

B.2.1.5 Bulk density, organic C and N

Bulk densities ranged from 1.12 kg dm^{-3} for the 0-5 cm layer to about 1.40 kg dm^{-3} at a depth of 3 m. The standard error was of 0.027 kg dm^{-3} for the 0-5 cm layer and < 0.010 kg dm^{-3} below a depth of 5 cm. A slight increase in the bulk density at a depth of 40 cm was confirmed (ANNEX 3), as suggested by the pedological description and by Maquère *et al.* (2008).

Carbon and nitrogen contents decreased with depth from 3.57 % (C) and 0.19 % (N) in the 0-5 cm layer to less than 0.5 % (C) and 0.03 % (N) beyond a depth of 50 cm. The heterogeneity was greatest for the upper soil layer with standard errors of 0.318 % (C) and 0.016 % (N) (n=36), and decreased below a depth of 15 cm with standard errors < 0.020 % (C) and 0.005 % (N) (ANNEX 3).

Table 11 C, N and bulk density models and fitted parameters for data sets $SOIL_{BCF}$-1 & 2 compared to Maquère *et al.* (2008).

			Data sets $SOIL_{BCF}$-1 & 2	**Maquère *et al.* 2008**
C / % as a function of depth / cm *Model 1* [a]	Fitted parameters	a	0.4703	0.4150
		c_{VT}	0.2958	0.0850
	Input variables	$\overline{f_{VT}(x<5)}$	3.5674	1.7361
		$\overline{(x<5)}$	2.5	2.5
N % as a function of depth / cm *Model 1* [a]	Fitted parameters	a	0.0330	0.0227
		$\underline{c}_{VT}$	0.2345	0.0511
	Input variables	$\overline{f_{VT}(x<5)}$	0.1900	0.0796
		$\overline{(x<5)}$	2.5	2.5
Bulk density / g cm^{-3} as a function of depth / cm *Model 2* [b]	Fitted parameters	α_{VT}	1.0719	1.2313
		γ_{VT}	0.0259	0.0176
		δ	1.3186	1.3909

[a] Model 1: $f_{VT}(x) = a + b_{VT}\exp(-c_{VT}x)$; $b_{VT} = \dfrac{a - \overline{f_{VT}(x<5)}}{\exp\left(-\overline{(x<5)}\, c_{VT}\right)}$; f_{VT} is C (resp. N) concentration in %, x is the depth in cm, $\overline{f_{VT}(x<5)}$ is the average $f_{VT}(x)$ value for x<5; $\overline{(x<5)}$ is the average depth for x<5,

[b] Model 2: $d_{VT}(x) = \alpha_{VT} + \beta_{VT}x - \gamma_{VT}{}^2 x^2$, if $x < 40$ cm ; $d_{VT}(x) = \delta$, if $x \geq 40$ cm ; d_{VT} is the bulk density in g m^{-3}; $\beta_{VT} = \dfrac{\delta - \alpha_{VT}}{40} + 40\ \gamma_{VT}{}^2$.

For C, N and bulk density, the evolution with depth can be modelled according to Maquère *et al.* (2008). The equations used and the parameters fitted are reported in Table

11. It confirmed the limit parameters in depth (a and δ) which were considered constants within the studied area for the studied soil type. The c and α parameters slightly differed as a result of spatial heterogeneity. The large number of measurements performed for surface samples (n=36) allowed a more accurate estimation of the parameters controlling C and N concentrations and bulk density at the soil upper limit ($\overline{f_{VT}(x<5)}$, $\overline{(x<5)}$ and α_{VT}) than in Maquère et al. (2008).

B.2.1.6 Variability between plots

Table 12 Pearson coefficients of correlations calculated for the variables of data sets $SOIL_{BCF}$-1a and $SOIL_{BCF}$-1b (P<0.05). The matrix for each data set was symmetric so that only half matrixes are represented.

	$SOIL_{BCF}$-1b (5-600 cm)							**$SOIL_{BCF}$-1a (0-5 cm)**					
	C	**N**	**H_{KCl}**	**CEC**	**Clay**	**Sand**		**C**	**N**	**H_{KCl}**	**CEC**	**Silt**	**Sand**
C	1						**C**	1					
N	0.96	1					**N**	0.99	1				
H_{KCl}	0.74	0.72	1				**H_{KCl}**	0.73	0.75	1			
CEC	0.99	0.94	0.80	1			**CEC**	0.95	0.95	0.77	1		
Clay	-0.71	-0.71	-0.48	-0.81	1		**Silt**	0.94	0.96	0.77	0.98	1	
Sand	0.74	0.77	0.55	0.84	-0.93	1	**Sand**	-0.87	-0.91	-0.75	-0.96	-0.96	1

Table 13 Linear regressions calculated for the correlated variables of data set $SOIL_{BCF}$-1a and $SOIL_{BCF}$-1b. The R-square, the F value and its corresponding probability (Pr>F) are indicated, together with the number of observations (n) and the intercept and slope calculated for the regression. Unless mentioned, intercept and slopes were significantly different from 0 (P < 0.05).

Dependant variable	Regressor	R-square	F value	Pr > F	n	*Intercept*	*Slope*
$SOIL_{BCF}$-1a							
N (%)	C (%)	0.97	262	<.0001	9	*0.01**	*0.05*
H_{KCl} (mmol L^{-1})	C (%)	0.53	8	0.0253		*-0.05**	*0.07*
CEC (cmolc kg^{-1})	C (%)	0.89	59	0.0001		*0.98*	*0.54*
Sand (%)	C (%)	0.76	22	0.0021		*84*	*-2.20*
Acidity (cmolc kg^{-1})	CEC (cmolc kg^{-1})	1.00	9532	<.0001		*0.05**	*0.93*
Silt (%)	Sand (%)	0.92	76	<.0001		*84*	*-0.98*
$SOIL_{BCF}$-1b							
N (%)	C (%)	0.93	468	<.0001	40	*0.00*	*0.08*
H_{KCl} (mmol L^{-1})	C (%)	0.54	44		39	*0.00**	*0.06*
CEC (cmolc kg^{-1})	C (%)	0.97	1325		41	*-0.18*	*1.76*
Sand (%)	C (%)	0.54	35		32	*69*	*12.07*
Acidity (cmolc kg^{-1})	CEC (cmolc kg^{-1}))	1.00	71253		72	*-0.01*	*0.99*
Clay (%)	Sand (%)	0.86	261		45	*84*	*-0.87*

* probability > 0.05.

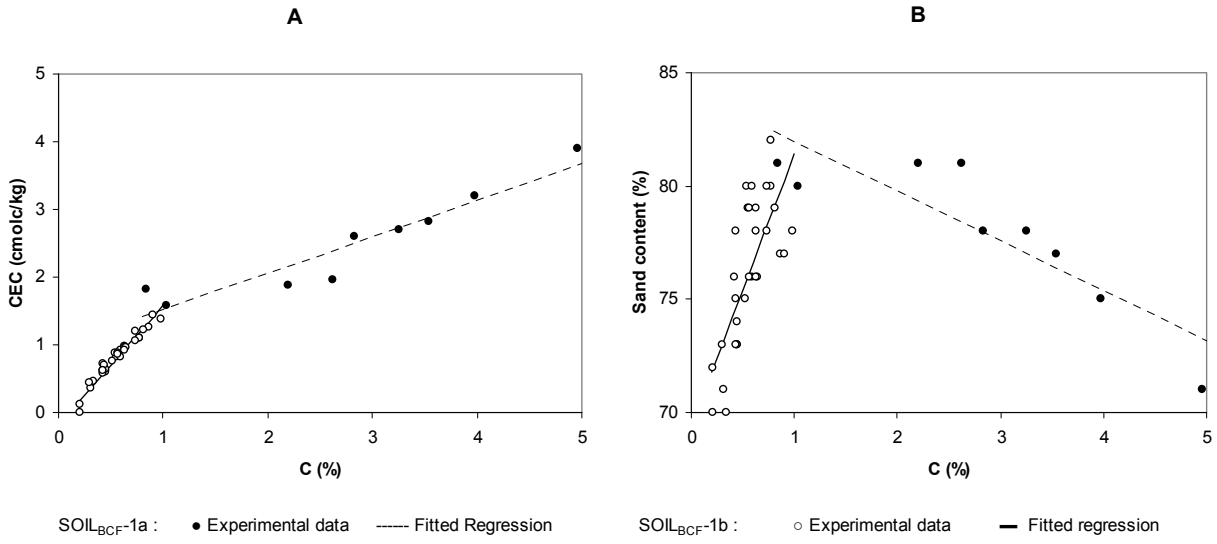

Figure 19 Cation exchange capacity (CEC in cmolc kg^{-1}) (A) and sand content (%) (B) as a function of the organic carbon (C) content (%) for data sets SOIL$_{BCF}$-1a and SOIL$_{BCF}$-1b. The measured data and the corresponding linear regressions from Table 13 are represented.

For data sets SOIL$_{BCF}$-1a and SOIL$_{BCF}$-1b, N content, bulk density, H_{KCl}, H_{water} and CEC were positively and linearly correlated to organic C content (Table 12). The intercepts and slopes of the linear regressions presented different values for data set SOIL$_{BCF}$-1a and SOIL$_{BCF}$-1b (Table 13). For the 0-5 cm layer (data set SOIL$_{BCF}$-1a), the sand content was linearly and negatively correlated to the silt content and to the organic C content. For data set SOIL$_{BCF}$-1b, the clay content was linearly and negatively correlated to the sand content and to the organic C content (Figure 19).

Table 14 One-way ANOVAS performed on the variables of data set $SOIL_{BCF}$-1. The effect of block and treatment are tested independently on each soil layer (n=9).

Regressor	**Layer**	**Dependant variable**													
		Bulk density		C		H_{KCl}		CEC		Clay		Silt		Sand	
	(cm)	*F*	*Pr>F*	*F*	*Pr>F*	*F*	*Pr>F*	*F*	*Pr>F*	*F*	*Pr>F*	*F*	*Pr>F*	*F*	*Pr>F*
Block	0-5	4.26	*0.07*	0.68	*0.54*	1.75	*0.25*	0.48	*0.64*	1.50	*0.30*	0.53	*0.62*	0.49	*0.63*
	5-15	2.00	*0.22*	2.18	*0.19*	2.50	*0.16*	1.46	*0.30*	9.25	*0.01*	7.80	*0.02*	2.53	*0.16*
	15-50	1.63	*0.27*	2.18	*0.19*	4.87	*0.06*	1.60	*0.28*	-	-	1.79	*0.25*	0.83	*0.48*
	50-150	1.03	*0.41*	1.26	*0.35*	0.53	*0.62*	22.73	*0.00*	28.00	*0.00*	1.05	*0.41*	1.54	*0.29*
	200-300	1.52	*0.29*			0.48	*0.64*	0.52	*0.62*	6.00	*0.04*	0.17	*0.84*	2.74	*0.14*
	300-400	2.25	*0.19*			0.11	*0.89*	3.21	*0.11*	6.00	*0.04*	1.91	*0.23*	1.97	*0.22*
Treatment	0-5	0.44	*0.66*	0.17	*0.85*	0.42	*0.67*	0.55	*0.61*	-	-	0.38	*0.70*	0.40	*0.68*
	5-15	0.33	*0.73*	2.36	*0.18*	0.68	*0.54*	2.64	*0.15*	0.50	*0.63*	0.60	*0.58*	2.53	*0.16*
	15-50	0.04	*0.96*	1.97	*0.22*	0.48	*0.64*	4.71	*0.06*	1.50	*0.30*	1.79	*0.25*	4.19	*0.07*
	50-150	0.93	*0.44*	1.09	*0.39*	3.44	*0.14*	0.03	*0.97*	0.10	*0.91*	1.50	*0.30*	2.45	*0.17*
	200-300	1.44	*0.31*			0.75	*0.51*	0.08	*0.92*	-	-	0.04	*0.96*	0.03	*0.97*
	300-400	1.25	*0.35*			0.24	*0.80*	0.78	*0.50*	-	-	0.86	*0.47*	0.27	*0.77*

The analysis of variance failed to show any block or treatment effect at $P<0.05$ for all variables but the clay contents of the 5-15 cm, 50-100 cm, 100-200 cm and 200-300 cm layers. For these layers, the root mean square errors (RMSE) of the linear regressions were < 1.5 % which corresponded to the measurement accuracy (Table 14).

B.2.1.7 Variability within plot: data set SOIL$_{BCF}$-2

Figure 20 Linear regression of organic carbon C (%) as a function of the distance to the nearest trees (f coefficient of Figure 14) calculated for data set SOIL$_{BCF}$-2. f=0 corresponds to a maximum influence of the trees, and f=1 to a minimum influence of the trees. R-square, F value and P>F, together with the intercept and slope calculated for the regression are given (n=27).

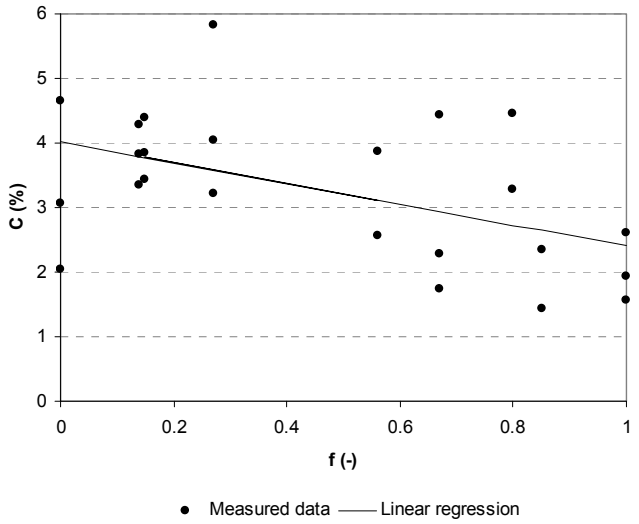

Dependant variable	Regressor	R-square	F value	P > F	*Intercept*	*Slope*
C (%)	f	0.25	7.42	0.0124	*4.014**	*-1.609**

* different from 0 at P < 0.05

Data set SOIL$_{BCF}$-2 confirmed the correlations already observed for data set SOIL$_{BCF}$-1a. Moreover, C and N contents, H_{water}, H_{KCl} and CEC were negatively correlated with f (data not shown). It showed that the OM content, the acidity and the CEC decreased with the distance from the trees in the upper soil layer (Figure 20).

B.2.1.8 Discussion and conclusions on soil basic characteristics and spatial heterogeneity

Pedological descriptions are in good agreement with the definition of Dystrophic Red-Yellow Latosol: (i) general hues yellow/red, (ii) upper soil horizon influenced by OM and horizon below a depth of 50-70 cm with an increase of 8 % in the clay content from the upper soil limit down to a depth of 1 m, and (iii) very low CEC and organic matter content (CEC < 1 cmolc kg^{-1}, C < 0.6 % and N < 0.05 % below a depth of 15 cm) (EMBRAPA, 1999; Fontes and Weed, 1991; Segalen, 1995).

The CEC was positively correlated with the gradient of OM, which confirmed that the CEC must be mainly hold by the organic matter and that the clay fraction may not participate much to it. Given the CEC values and the acidic soil pH (< 4.5 in upper soil layer and <5.5 deeper), the retention of cations at soil pH is expected to be limited and a great part of the CEC will be occupied by solubilized aluminium.

The pH in KCl was always less than the pH in water of about 0.5 unit pH, which is classical for soils for which the negative charge (CEC) prevails (Bolan et al., 1999; Uehara and Gillman, 1981). The non-specific retention of anions is thus expected to be limited. Below a depth of 3 m, pH in KCl almost equaled pH in water which meant that the soil in deeper layers is closed to its point of zero net charge and that the negative charge participates as much as positive charge to the soil surface charge.

Most of the variability was located in the upper soil layer (0-5 cm) and was the result of the heterogeneities in organic matter contents. On the contrary, soil deeper layers showed highly homogeneous physical and chemical properties. The variability among the sampled plots grouped by treatment or by block was of the same order of magnitude as the variability inside each plot. Only a small significant effect of the sampled block was observed for the clay content but the RMSE of the model was < 1.5 % which was in the order of magnitude of the measurement accuracy. Inside each plot, greatest OM contents were found in the 0-5 cm layer close to the trees where the soils were more acidic and the CEC greatest. This effect was significant ($P < 0.05$) but weak since the slopes of the regressions were close to zero. This meant that soils must be sampled from the stump to the inter-row of planting to integrate this intra-plot spatial pattern. Once sampled in this way, the changes which may be observed in the studied variables during the fertilization experiment may be attributed to the treatments established and not to a consequence of the location of the sampled plot.

B.2.2 Soil mineralogy

B.2.2.1 Aggregation

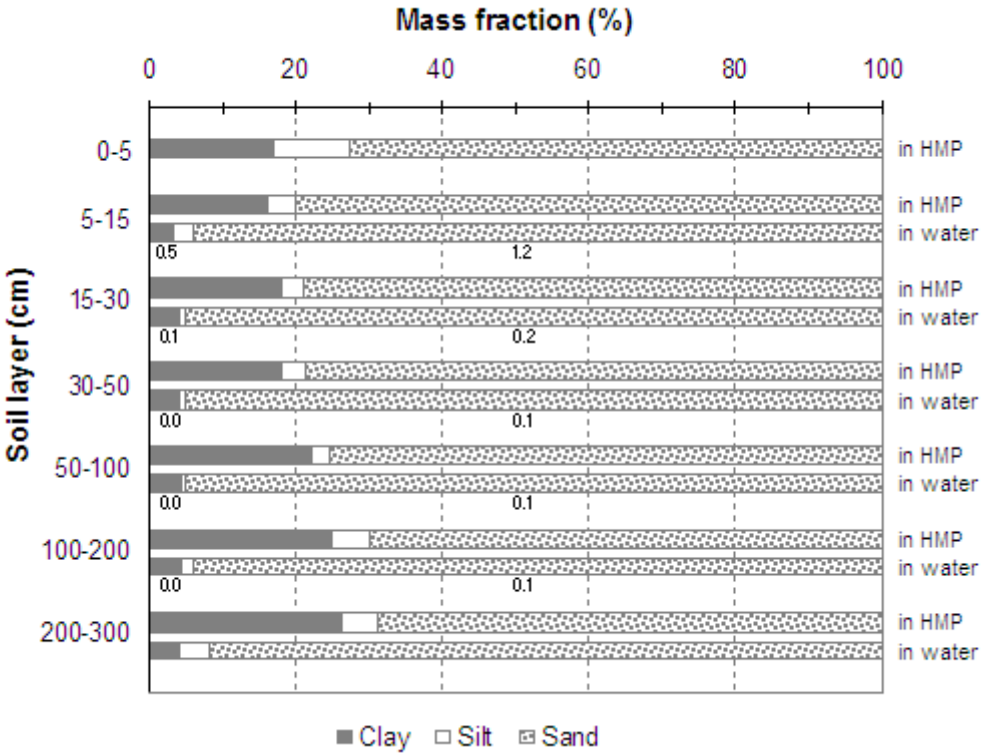

Figure 21 Particle-size analysis performed in hexametaphosphate (HMP) and in water for pit 3 of data set $SOIL_{AP11}$. Standard errors of the analytical repetitions are given for clay and sand fractions when n≥3.

The particle-size distribution for the 2004 sampling (data set $SOIL_{AP11}$) confirmed the results already presented in §B.2.1.2. When the particle-size analysis was performed in water (no dispersing agent), clay content decreased to about 4 % and sand content increased to 94 % independently of the soil layer (Figure 21) as was already observed in other studies (Igwe et al., 1999; Westerhof et al., 1999; Wohlenberg et al., 2004).

Particle-size analysis performed in water confirmed the importance of aggregation for these soils in which particles are naturally bound to form aggregates of the size of silts or sands (pseudo sands or silts). When the soil/solution suspension differs in its chemistry (pH, ionic strength, …), these aggregates may disperse into further subunits until finally into individual oxides and minerals (clay fraction obtained while using hexametaphosphate) (Pinheiro-Dick and Schwertmann, 1996). The aggregated fractions have thus different mineralogical compositions than the dispersed ones and may influenced

mineralogical studies. Here, we chose to disperse as much aggregates as possible in order to analyze all the mineralogical clays of the soil matrix even if those clays were hidden inside the aggregates.

B.2.2.2 Total chemical composition of bulk soil

Table 15 Mass proportion of total elements, amorphous (Ox) [b] and free (DCB) [c] Al and Fe contents in bulk soil for data sets $SOIL_{AP11}$ and $SOIL_{15m}$. Standard errors for n≥3 are given in italic.

Soil layer	N	C	SiO_2	Fe_2O_3	Al_2O_3	MnO	MgO	CaO	Na_2O	K_2O	TiO_2	P_2O_5	LI[a]	Fe_2O_3 Ox[b]	Fe_2O_3 DCB[c]	Al_2O_3 Ox	Al_2O_3 DCB	Al_{subs}[d]
cm										*%*								*mol mol^{-1}*
Data set $SOIL_{AP11}$																		
0-5	0.18 *0.05*	3.20 *1.03*	81.62 *1.43*	3.29 *0.11*	5.16 *0.31*	0.02 *0.00*	0.04 *0.00*				0.80 *0.02*	0.04 *0.01*	8.69 *1.99*	0.12 *0.01*	2.67 *0.08*	0.21 *0.03*	0.88 *0.01*	0.29 *0.01*
5-15	0.06 *0.00*	0.79 *0.01*	84.35 *0.05*	3.70 *0.12*	6.02 *0.31*	0.02 *0.00*	0.03 *0.00*				0.94 *0.05*	0.04 *0.00*	4.69 *0.09*	0.11 *0.00*	2.58 *0.02*	0.16 *0.00*	0.78 *0.01*	0.28 *0.00*
15-30	0.05 *0.00*	0.68 *0.04*	83.81 *0.71*	3.72 *0.12*	6.08 *0.34*	0.03 *0.00*	0.03 *0.00*	<0.02	<0.07	<0.05	0.93 *0.02*	0.04 *0.00*	4.55 *0.18*	0.10 *0.00*	2.63 *0.02*	0.15 *0.01*	0.77 *0.02*	0.28 *0.00*
30-50	0.04 *0.00*	0.55 *0.02*	83.07 *0.43*	3.87 *0.07*	6.41 *0.17*	0.03 *0.00*	0.03 *0.00*				1.00 *0.01*	0.03 *0.00*	4.58 *0.09*	0.09 *0.00*	2.99 *0.22*	0.14 *0.00*	0.86 *0.07*	0.28 *0.00*
50-100	0.03 *0.00*	0.47 *0.01*	81.71 *0.66*	4.49 *0.10*	7.79 *0.19*	0.03 *0.00*	0.03 *0.00*				1.16 *0.03*	0.04 *0.00*	4.95 *0.12*	0.08 *0.00*	3.59 *0.07*	0.16 *0.00*	1.04 *0.02*	0.28 *0.00*
200-300	0.02 *0.00*	0.22 *0.01*	79.04 *1.05*	4.95 *0.19*	8.62 *0.40*	0.04 *0.00*	0.04 *0.00*				1.32 *0.06*	0.04 *0.00*	4.84 *0.16*	0.05 *0.00*	3.48 *0.17*	0.14 *0.00*	0.85 *0.04*	0.25 *0.00*
Data set $SOIL_{15m}$																		
500	0.01	0.17	79.33	5.16	9.13	0.04	0.04				1.37	0.03	4.73	0.06	3.57	0.12	0.57	0.17
700	0.02	0.27	79.80	4.93	8.70	0.04	0.03				1.27	0.04	4.84	0.06	3.69	0.11	0.48	0.14
900	0.01	0.12	81.13	4.70	8.28	0.04	0.04	<0.02	<0.07	<0.05	1.24	0.03	3.99	0.05	3.90	0.08	0.30	0.08
1100	0.01	0.12	84.29	3.86	6.26	0.04	0.03				1.17	0.03	3.18		3.06		0.26	
1300	0.01	0.07	80.15	6.43	7.15	0.06	0.09				1.72	0.04	3.87	0.07	6.86	0.07	0.28	0.05
1500	0.00	0.04	82.41	5.89	5.15	0.10	0.10				2.17	0.06	2.70	0.07	3.61	0.04	0.12	0.03

[a] LI = Loss on Ignition 110-1000°C; [b] Tamm, 1922 ; [c] Mehra & Jackson, 1960 ; [d] $Al_{subs} = \frac{Al_{DCB} - Al_{Ox}}{\left(Al_{DCB} - Al_{Ox}\right) + \left(Fe_{DCB} - Fe_{Ox}\right)}$ where Al_{DCB}, Al_{Ox}, Fe_{DCB}, Fe_{Ox} are expressed in mole.

Total analysis of the bulk soil showed that it was constituted of about 80 % of SiO_2, from 5 to 10 % of Al_2O_3, from 3 to 6.5 % of Fe_2O_3 and from 0.8 to 2 % of TiO_2. MnO, MgO, K_2O and P_2O_5 total contents were < 0.05 %, CaO content was < 0.02 % and Na_2O content < 0.07 %. The spatial variability for a given soil layer was low with standard errors < 0.7 % for all the elements but SiO_2, and < 2.5 % for SiO_2 (Table 15). The bulk soil composition was homogeneous down to a depth of 15 m with a slight increase of Fe_2O_3, MnO, MgO and TiO_2 below a depth of 12 m.

Table 16 Pearson correlation coefficients between (i) total Al_2O_3, Fe_2O_3 and TiO_2 and clay contents, and (ii) total SiO_2 and sand contents calculated for data set $SOIL_{AP11}$, all soil layers taken altogether. Intercept and slope of the corresponding linear regressions are given for Fe_2O_3 and SiO_2. All slopes and intercepts were significantly different from zero at $P < 0.05$.

	Fe_2O_3 (%)	Al_2O_3 (%)	TiO_2 (%)	Clay (%)	SiO_2 (%)
Fe_2O_3 (%)	1				
Al_2O_3 (%)	0.997 *(Fe_2O_3=0.885+0.467 Al_2O_3)*	1			
TiO_2 (%)	0.989 *(Fe_2O_3=0.651+3.269 TiO_2)*	0.982	1		
Clay (%)	0.951 *(Fe_2O_3=0.990+0.149 Clay)*	0.950	0.947	1	
Sand (%)					0.919 *(SiO_2= 42.141+0.534 Sand)*

Number of observations = 18.

The analysis of correlations showed that the SiO_2 contents were highly correlated to the sand contents, and Fe_2O_3, Al_2O_3, and TiO_2 to the clay contents (Table 16). The corresponding linear regressions are easy tools to estimate total Fe, Al, Ti and Si contents for this soil type from simple clay and sand content measurements.

Total analysis performed on the soil fractions confirmed these correlations showing more silica (> 97 % of SiO_2) in the sand fraction than in the silt and clay fractions, and more Al, Fe and Ti in the clay fraction than in the sand and silt fractions (about a third of the clay fraction was made of Al_2O_3, about 15 % of Fe_2O_3 and about 2.7 % of TiO_2) (ANNEX 3).

The chemical compositions of the bulk soil and of the soil fractions are in good agreement with the literature (Alves and Lavorenti, 2004; Marques et al., 2004).

B.2.2.3 Identification of the minerals

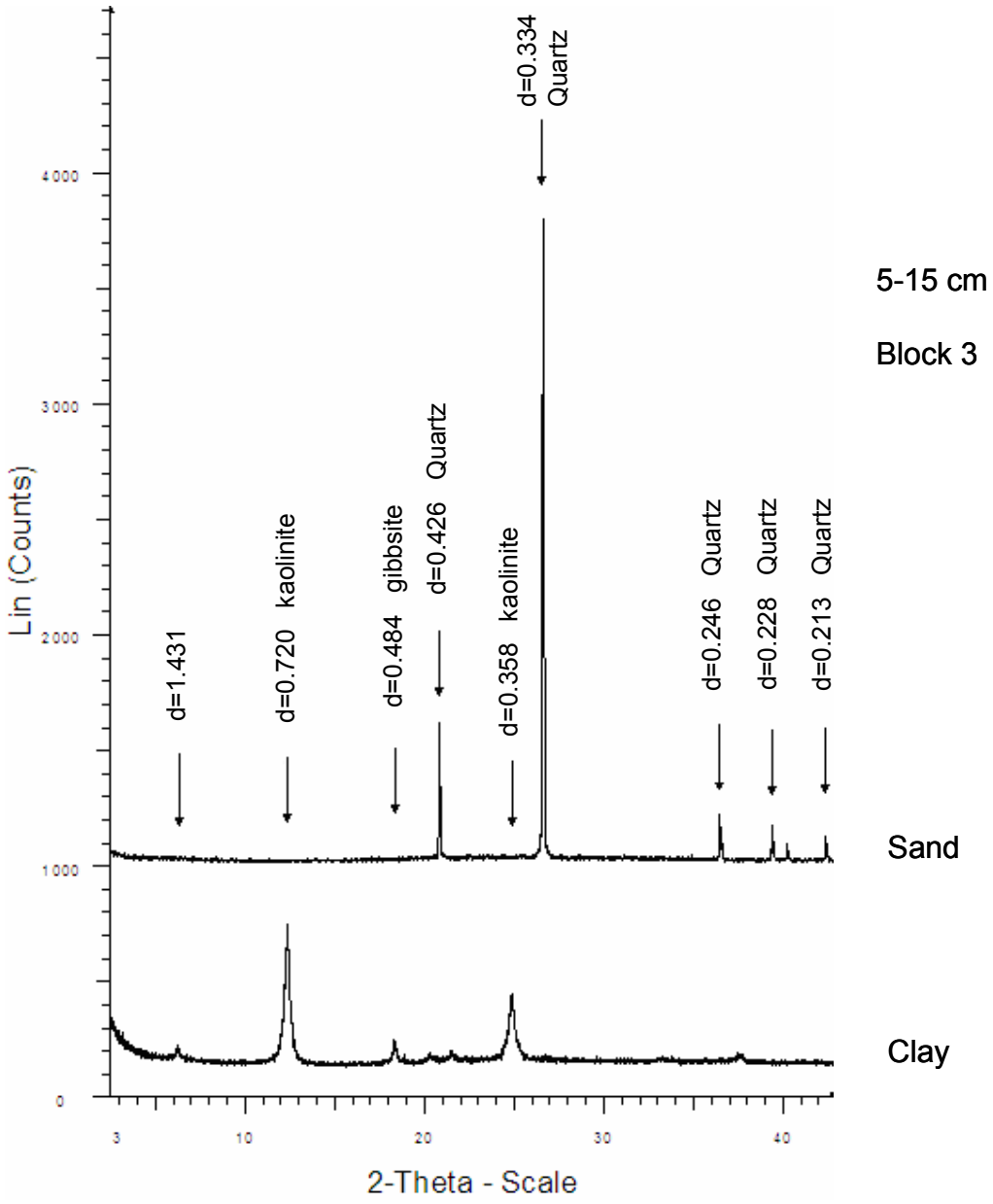

Figure 22 Mineralogy of the clay and sand fractions: XR diffractograms performed on oriented deposit of the clay fraction Mg^{2+} saturated and on raw powder of the sand fraction for block 3, layer 5-15 cm of data set $SOIL_{AP11}$. The main peaks are given in nm together with the mineral they identify.

X-rays performed on soil fractions confirmed that the sand fraction was almost only made of quartz and that the clay fraction was free of quartz (at a 5 % theoretical detection threshold for X-ray analysis) (Figure 22). The silt fraction presented intermediary features between sands and clays, but as it represented less than 5% of the particle-size distribution, less attention was put on this fraction.

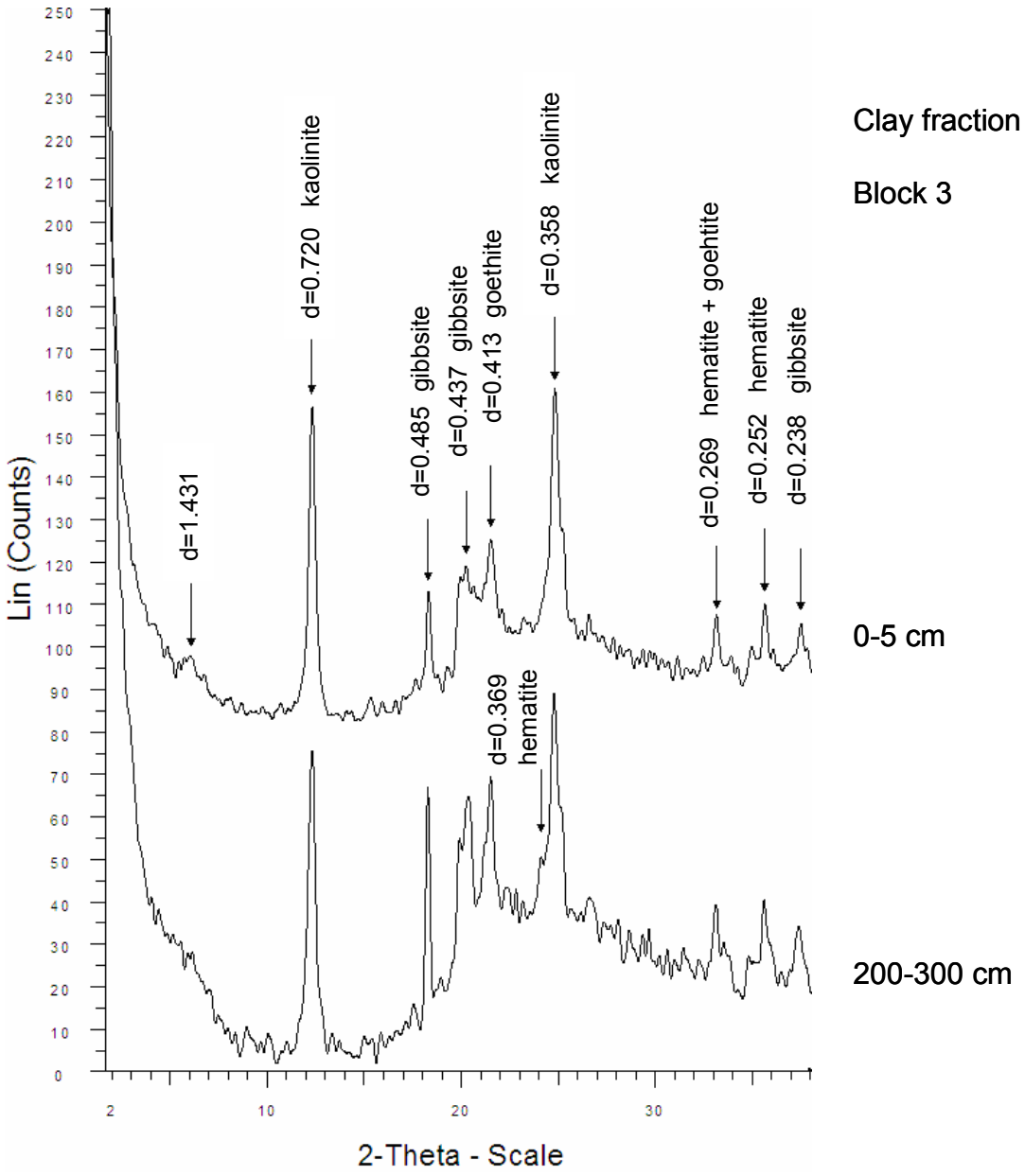

Figure 23 Homogeneity with depth of the mineralogy of the clay fraction: RX diffractograms performed on raw powder of the clay fraction Mg^{2+} saturated for block 3 of data set $SOIL_{AP11,}$ layers 0-5 cm and 200-300 cm. The main peaks are given in nm together with the mineral they identify.

The X-ray analysis performed on the oriented clay deposits and on raw powder of the clay fraction showed the characteristics reflections of kaolinite (0.72 and 0.357 nm), gibbsite (0.485 and 0.437 nm, reflexions at 0.431 and 0.238 nm), goethite (0.418, 0.269 nm) and hematite (0.270 and 0.252 nm) (Dixon and Weed, 1989). RX analysis showed that the clay mineralogy was highly homogeneous whatever the depth sampled. A slight increase in gibbsite and hematite contents in deeper soil layers is suggested (Figure 23).

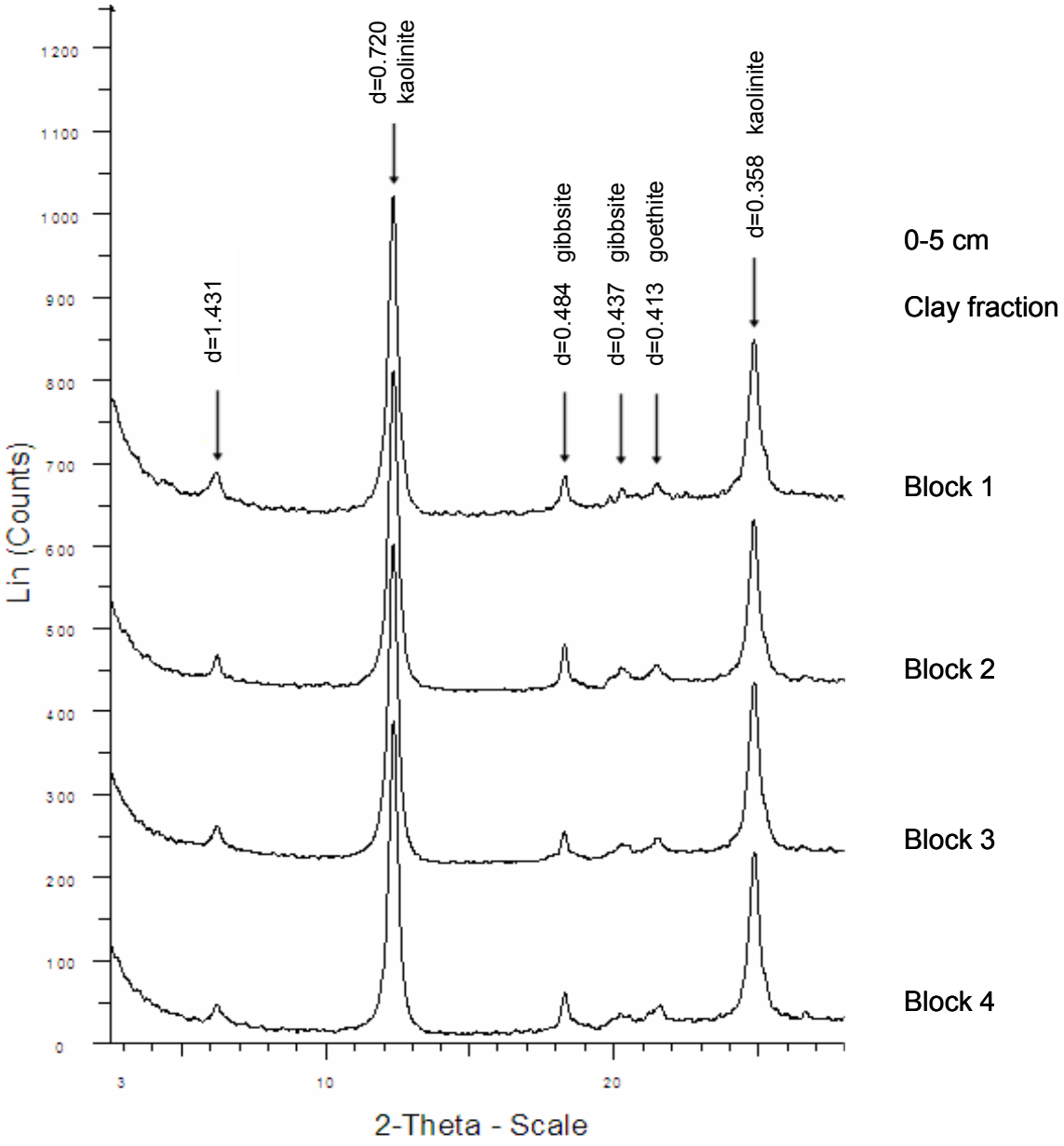

Figure 24 Spatial homogeneity of the mineralogy of the clay fraction: RX diffractograms performed on oriented deposit of the clay fraction Mg^{2+} saturated for all blocks of data set $SOIL_{AP11,}$ layer 0-5 cm. The main peaks are given in nm together with the mineral they identify.

RX spectra showed a great homogeneity according to blocks. Spectra are given for the clay fraction at depth 0-5 cm for which the maximum heterogeneity was expected (Figure 24).

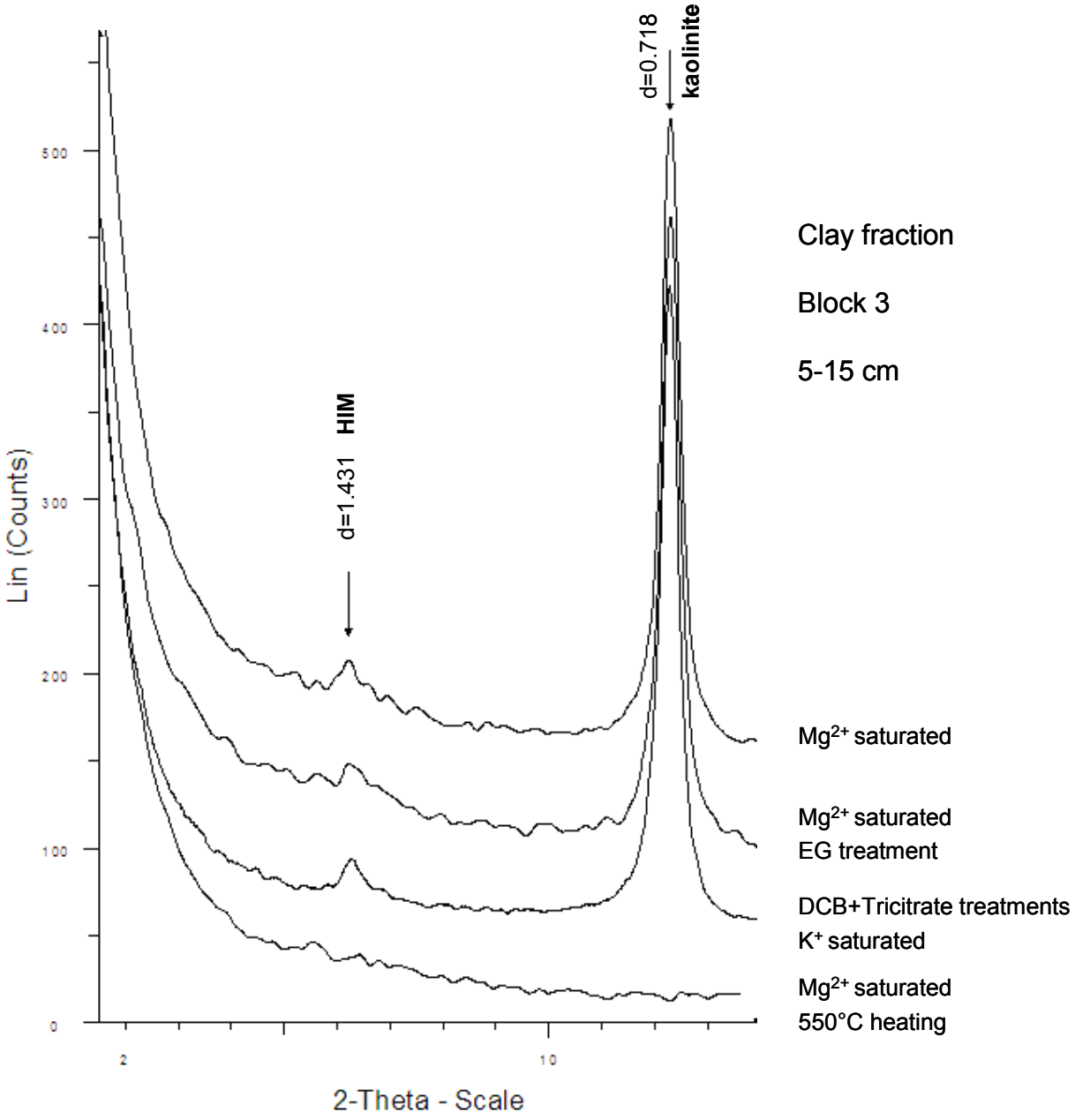

Figure 25 Identification of the peak at 1.431 nm: influence of treatments (Mg^{2+} saturation, ethylene glycol (EG) treatment, DCB followed by tricitrate extractions and saturation by K^+, heating at 550°C) on RX diffractograms performed on oriented deposits of the clay fraction for layer 5-15 cm block 3 of data set $SOIL_{AP11}$.

A peak at 1.4 nm indicated the presence of a 2:1 phyllosilicate visible for bulk soil samples as well as for oriented clay deposits. Its location changed neither after treatment with ethylene glycol nor after DCB+Tamura treatments and K^+ saturation, but the peak disappeared after heating at 550°C together with the kaolinite peaks, as classically observed (Bish and Duffy, 1990; Dejou et al., 1977). No peak appeared at 1.0 nm after heating at 550°C (Figure 25).

According to Table 9, the X-ray patterns of the 2:1 mineral corresponded to a hydroxylated interlayered mineral present in small amounts since it was not always visible on X-ray charts and since no peak appeared after heating at 1 nm (below the detection threshold of 5%). Such minerals have been observed in highly weathered tropical soils (Bryant and Macedo, 1990; Fontes and Weed, 1991; Kampf and Schwertmann, 1983; Olmos I. L et al., 1993) and their occurrence in tropical soils is not well understood. Hydroxy-Al interlayered smectite and vermiculite are thought to occur as either weathering products derived from chlorite weathering or more commonly from the deposition of hydroxy-Al polymeric components within the interlayer spaces of these expansible or limited expansible layer silicates (Barnhisel and Bertsch, 1989). It has been suggested that moderately acidic conditions, low organic matter content, oxidizing conditions, and frequent wetting and drying cycles are optimal environmental conditions for pedogenic hydroxy-Al interlayer formation. Other authors have also suggested that the interlayer component was a kaolin mineral and not a hydroxy-Al polymeric material. They proposed that the structure of the intergradient vermiculite-kaolin mineral consisted of vermiculite and vermiculite that had been transformed to double kaolin layers (Wada and Kakuto, 1983). This type of structure may explain the disappearance of all peaks after heating at 550°C without any newly formed peak at 10 nm, since kaolinite mineral structure is lost at such a temperature.

B.2.2.4 Fe and Al specific extractions

Al_2O_3 extracted by the oxalate treatment (Tamm) was about 0.15 % of the bulk soil mass. It was a little more in the 0-5 cm layer where it reached 0.21 %. DCB treatment (Mehra & Jackson) extracted about 0.8 % of aluminium (expressed in Al_2O_3) whatever the soil layer. Beyond a depth of 3 m, aluminium extracted by both treatments decreased gradually down to a depth of 15 m where it reached values < 0.04 % for the oxalate extraction and < 0.12 % for the DCB extraction (Table 15).

Iron extracted by the oxalate treatment decreased gradually with depth from 0.12 % of iron expressed in Fe_2O_3 in the 0-5 cm layer, to 0.05 % beyond a depth of 3 m. DCB treatment extracted about 2.6 % of iron expressed in Fe_2O_3 down to a depth of 50 cm, about 3.5 % beyond a depth of 50 cm, and about 7 % at depths 12, 13 and 14 m (Table 15).

The oxalate treatment extracted less than 4 % of total iron and less than 5 % of total aluminium. DCB treatment extracted about 75 % of total iron and less than 15 % of total

aluminium. Most standard deviations were quasi systematically < 10 % of the measured value.

The amounts of iron and aluminium extracted for the same soil type are generally larger in other studies (Alves and Lavorenti, 2004; Bryant and Macedo, 1990; Kampf and Schwertmann, 1983; Neufeldt et al., 1999; Olmos I. L et al., 1993). A one-hour single extraction was performed in the present work whereas other studies report that longer contact times or successive extractions are necessary to extract all free Al and Fe in these soils particularly rich in oxides (Fontes and Weed, 1991; Loeppert and Inskeep, 1996).

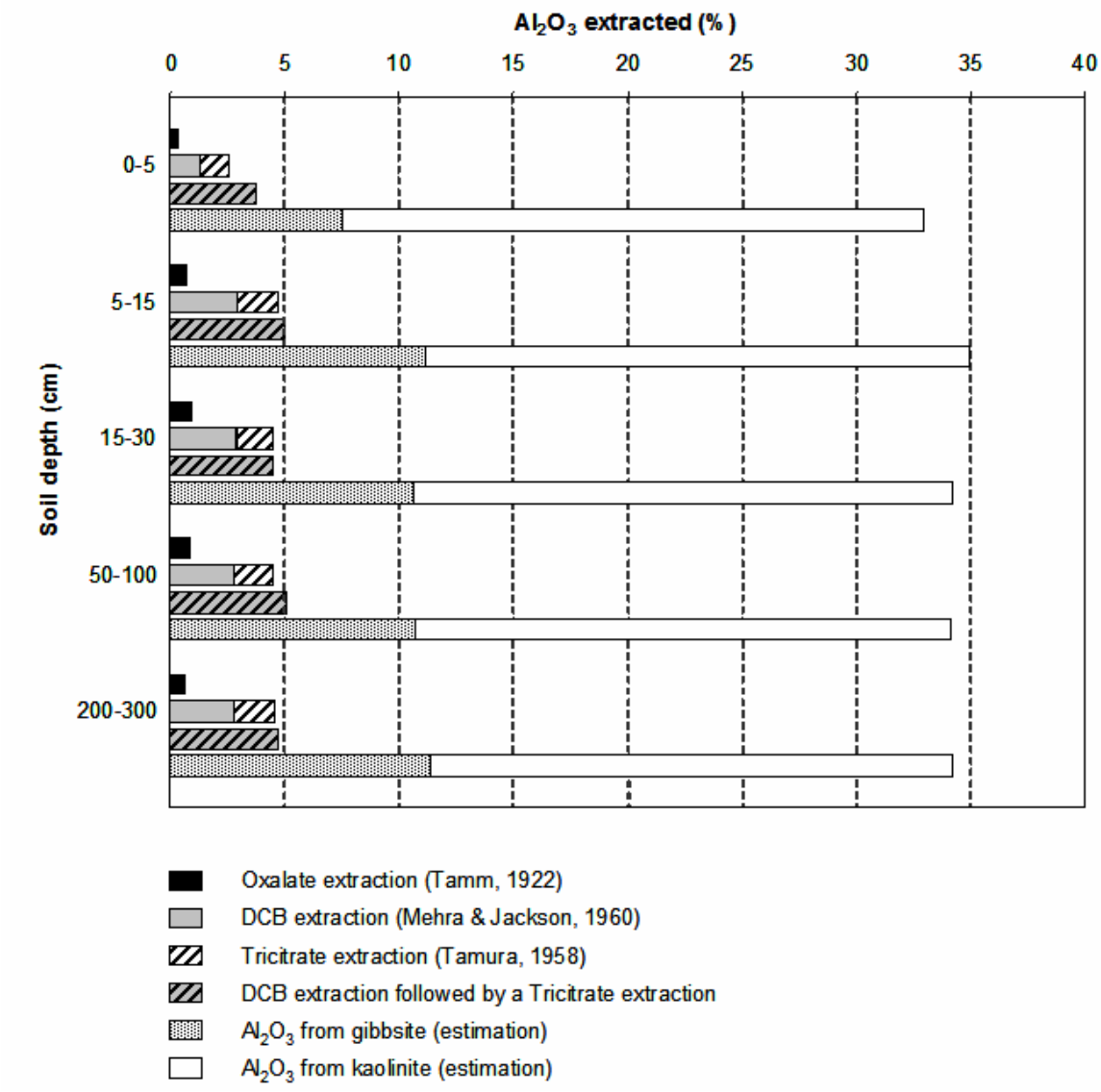

Figure 26 Al_2O_3 extracted (%) by different analytical methods (oxalate, DCB and tricitrate) from the clay fraction of pit 3 of data set $SOIL_{AP11}$. Al_2O_3 from gibbsite and kaolinite estimated from §B.2.2.5 are also represented.

These extractions were also performed on soil fractions. The results for the clay fraction are presented in figure Figure 26 for aluminium. Complete results are given in ANNEX 3 but will not be discussed here. Oxalate extracted less than 0.9 % of aluminium (expressed in Al_2O_3), DCB treatment extracted less than 3 % of Al_2O_3, and tricitrate treatment (Tamura) about 1.7 % of Al_2O_3. DCB treatment immediately followed by tricitrate treatment extracted about 4.7 % of aluminium which equals the sum of aluminium extracted independently by DCB treatment and tricitrate treatment.

B.2.2.5 Quantitative estimation of soil mineralogy

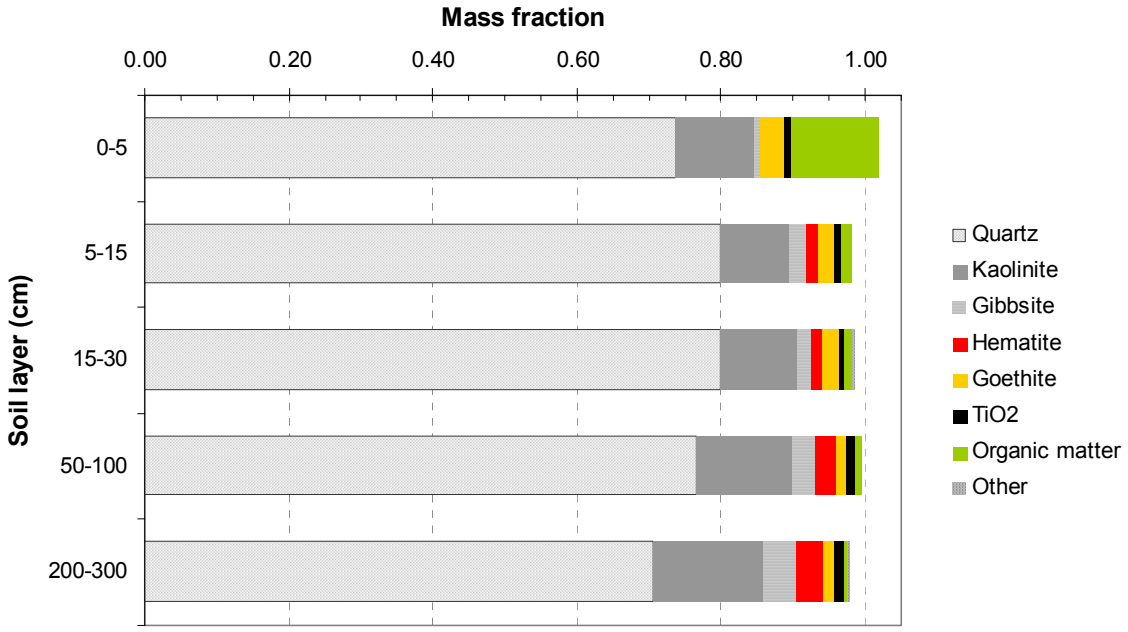

Figure 27 Estimated mineralogical composition of the bulk soil calculated from §B.1.2.6.4 for pit 3 of data set $SOIL_{AP11}$.

The clay fraction contained about 35 % of Al_2O_3. About 24 % were attributed to kaolinite and 11% to gibbsite (data not shown). The corresponding bulk soil composition was of about 70 to 80 % of quartz, 10 to 15 % of kaolinite, 0.5 to 4.5 % of gibbsite, 0 to 3.7 % of hematite and 1.3 to 3.5 % of goethite. The 0-5 cm layer was slightly depleted in quartz and gibbsite, but enriched in organic matter (Figure 27) in comparison to deeper layers. The sum of all estimated minerals reconstituted more than 98 % and less than 102 % of the total soil mass. It is reminded that Figure 27 represents the total composition of the soils of pit 3 which may differ slightly from the average bulk soil composition, particularly for organic matter in the 0-5 cm layer where the heterogeneity is greatest.

The estimated kaolinite and gibbsite compositions were checked thanks to TGA results. The weight losses recorded by TGA or estimated from the previous calculation are given for the clay fraction in Table 17. It confirmed the order of magnitude of the estimated kaolinite compositions. Results for gibbsite and goethite are less consistent but the TGA results for these two minerals are less reliable since they interfere with each other in the range 220-320°C (Bish and Duffy, 1990; Dejou et al., 1977).

Table 17 Weight losses (%) measured by thermogravimetry compared to weight losses from the normative calculation of the clay fraction for pit 3 of data set $SOIL_{AP11}$.

	Weight losses (%)			
	Simulated (normative calculation)		Thermogravimetry	
Soil layer (cm)	Kaolinite	Goethite+hematite	Kaolinite	Goethite+hematite
0-5	9.02	5.55	8.17	4.24
5-15	8.42	6.81	7.22	4.19
15-30	8.38	6.51	7.60	4.17
50-100	8.31	6.11	7.13	4.58
200-300	8.10	6.45	7.42	4.79

It is rather difficult to quantitatively differentiate goethite from hematite. Classically, such determinations are performed after isolating the oxide fractions by selective dissolutions of kaolinite and gibbsite by NaOH (Balwant and Gilkes, 1991; Cornell and Schwertmann, 2003), then by comparing the relative intensity of some specific reflections of the RX spectra. Goethite and hematite have also been quantified from the ratio of citrate extractable Fe and Al compared to DCB extractable Fe and Al at 20°C (Cornell and Schwertmann, 2003). Such analyses were not considered essential within the scope of this study since neither hematite nor goethite is likely to release nutrients by weathering. Goethite versus hematite ratios were taken from the literature on yellowing as already mentioned, but since they were not calculated from direct measurements, goethite and hematite contents must be handled cautiously and regarded much as an order of magnitude.

In the calculation, all the aluminium which was not attributed to kaolinite was attributed to gibbsite. However, there may be other minerals containing Al which were not taken into account (in particular phyllosilicate at 1.4 nm). Thermogravimetric analysis seemed to confirm the overestimation of gibbsite. Actually, Al may substitute Fe in goethite and hematite. For our soil types, rates of substitution < 10 % (mole) for hematite and between 15 and 25 % (mole) for goethite are frequently reported (Anand and Gilkes, 1987; Bryant and Macedo, 1990; Fontes and Weed, 1991). This substitution was not

considered in the calculations since the contents of hematite versus goethite were uncertain, but it can be estimated from the DCB and Tamura extractions performed on the clay fraction. For those samples, the aluminium extracted by the Tamura reactant seemed to be part of a mineral fraction different from that extracted by the DCB reactant since the Al extracted by the DCB treatment followed by the Tamura treatment equaled the sum of each extraction performed independently. Since the DCB extraction is reported to extract goethite + hematite oxides, one can suppose that the DCB extraction extracted the Al substituted in goethite and hematite. The ratio $Al_{DCB}/(Al_{DCB}+Fe_{DCB})$ was between 0.25 and 0.30 which actually corresponded to the substitution ratios given by the literature for goethite. Introducing Al-substitution in the calculations led to gibbsite contents for the clay fraction of 12 % which is close to the gibbsite contents calculated from the TGA analysis.

As titanium content was < 5% in bulk soil and in soil fractions, it was impossible to determine its mineralogical nature by X-ray diffraction. It was thus kept in calculations as TiO_2 (rutile) but it may exist in association with other elements in soils, especially iron to form ilmenite $FeTiO_3$. The occurrence of this mineral is frequently reported for tropical ferralsols (Cornell and Schwertmann, 2003; Nzila, 2001; Olmos I. L et al., 1993) and is generally found in association with magnetite Fe_3O_4 (Dixon and Weed, 1989; Pinheiro-Dick and Schwertmann, 1996). A black powder with magnetic properties was systematically found in all soil fractions. This powder was isolated and unsuccessfully analyzed by X-ray diffractometry but was very likely magnetite. The presence of ilmenite and magnetite may slightly decrease the calculated contents of hematite and goethite.

The resulting mineralogical composition for bulk soil and clay fraction was in good agreement with the literature (Costa et al., 2004; Fontes and Weed, 1991).

B.2.2.6 Conclusion: weathering potential and expected soil surface reactivity

The mineralogical composition obtained is typical of Dystrophic Red-Yellow Latosols which contains large quantities of well crystallized iron and aluminium oxides, few amorphous aluminium and iron, and mainly kaolinite in its clay fraction. The mineralogy of the bulk soil was highly homogeneous. All minerals were common to all soil layers and blocks sampled but were present in different amounts depending mainly on the soil layer. A slight change in the mineralogy is suggested below a depth of 12 m but further mineralogical analysis, including X-ray diffractions of the clay fraction would be necessary

to confirm this hypothesis. It was not regarded as a priority within the scope of this study. The identified 2:1 phyllosilicate is very stable since it remained unaffected by DCB or Tamura treatments and only lost its mineral structure after heating at 550°C. Together with total analyses which indicated total bulk soil contents of Mg, K, Na and Ca < 0.07 %, this meant that no significant amount of these elements may be released in soil solution by weathering.

As for surface reactivity, the mineralogical composition indicates that a general behavior of variable charge soil may be expected. Amorphous iron and aluminium are not present in large quantities so that the anion exchange capacity may be limited at soil pH and mainly hold by hematite, goethite and gibbsite. According to Table 8, kaolinite is expected to be little charged at soil pH and the CEC must be mainly carried by the organic matter. The HIM may exhibit a large capacity to retain cations since the permanent charge of the vermiculite is about 170 cmolc kg^{-1}. Even present in little quantity, such a mineral may greatly influence the CEC. Yet, the permanent charge of HIM is partly compensated by the interlayered aluminium so that the resulting charge is reduced (Dixon and Weed, 1989). The CEC of the clay fraction measured was about 6 cmolc kg^{-1} (Table 18) which is approximately the CEC of kaolinite at pH 5. Even if the HIM mineral participates to this CEC, the permanent charge of such a mineral seems to be limited.

Table 18 Cation exchange capacity of the clay fraction measured by Sr saturation in cmol/kg. Standard errors are given in brackets for n≥3.

Depth *cm*	CEC clay fraction *cmolc kg^{-1}*
0-5	8.10 *(1.045)*
5-15	6.16
15-30	5.69
30-50	
50-100	5.50
100-200	
200-300	6.49

B.2.3 Surface reactivity

B.2.3.1 CEC & pH: complement to § B.2.1

Table 19 pH in water and in KCl 1 mol L^{-1}, effective cation exchange capacity (CEC in cmolc kg^{-1}) and saturation in alkaline earth cations (Sat in cmolc kg^{-1}) measured every meter down to a depth of 15 m for data set $SOIL_{15m}$ (n=1).

Depth	pH H_2O	pH KCl	Sat	CEC	Sat/T
cm	-	-	*cmolc kg^{-1}*		*%*
100	5.9	4.5		0.58	1
200	6.0	5.4		0.25	1
300	5.9	5.3		0.08	8
400	6.1	5.2		0.02	42
500	5.9	5.6		0.06	9
600	6.1	5.1	<0.01	0.19	3
700	6.0	5.5		0.26	1
800	6.0	5.7		0.32	4
900	5.7	4.7		0.26	1
1000	6.0	4.9		0.52	1
1100	5.5	5.0		0.40	1
1200	5.1	4.0	0.02	1.33	1
1300	5.1	4.3	0.01	1.55	1
1400	4.8	4.1	<0.01	1.87	0
1500	4.8	4.2		2.09	0

No inversion between pH in water and in KCl occurred down to a depth of 15 m which meant that CEC always prevailed over AEC even in very deep soil layers. The change in soil mineralogy suggested in §B.2.2.2 seems to be confirmed by the CEC values which increased below a depth of 12 m to more than 1.5 cmolc kg^{-1} (Table 19). Nevertheless, the saturation in basic cations remained very low with almost 100% of the cation exchange capacity saturated by aluminium. These results suggest that the soil matrix holds a large capacity to retain cations and anions which might be leached below a depth of 3 m, especially through the large volume of exchanger available (soil profile deeper than 15 m…).

B.2.3.2 Change in AEC and CEC with pH

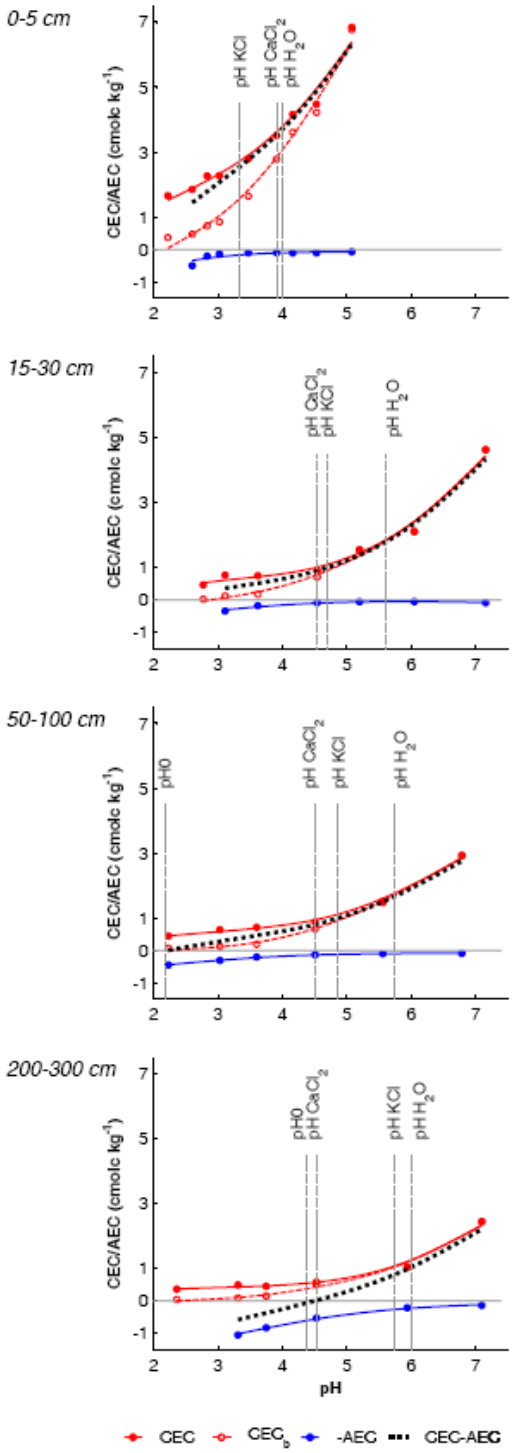

Figure 28 Change in cation exchange capacity (CEC), basic cation exchange capacity (CEC_b) and anion exchange capacity (AEC) with pH and depth for pit 3 of data set $SOIL_{AP11}$. The pH for which AEC equals CEC (point of zero net charge pH_0) together with the pH in $CaCl_2$ 0.002 mol L^{-1}, in KCl 1 mol L^{-1} and in water are also given.

As expected, the AEC and CEC varied with the pH of the contact solution (Figure 28): CEC increased and AEC decreased with pH. The CEC was almost constant below pH=4.5 and was saturated with aluminium. The basic cation exchange capacity (CEC_b) was null at about pH 2.5 which is the point of zero charge of quartz. The upper soil layer (0-5 cm) exhibited a greater CEC due to its high organic matter content. The AEC was null at pH 7-8 which is the point of zero charge of iron and aluminium oxides. AEC was greatest for the 200-300 cm layer.

The pH for which AEC equaled CEC (point of zero net charge pH_0) increased with depth. It was < 2 for the 0-5 cm layer, about 2 down to a depth of 1 m, 3.2 for the 100-200 cm layer and 4.4 for the 200-300 cm layer where it equaled soil pH. The pH in $CaCl_2$ 0.002 mol L^{-1} was 4.5 for all soil layers except for the 0-5 cm layer for which it was 3.9 (Figure 28 and Table 20).

CEC and AEC changes with pH as well as points of zero charge are in good agreement with the literature (Chorover and Sposito, 1995; Curtin and Syers, 1990a; Marcano-Martinez and McBride, 1989; Soares et al., 2005; Van Raij and Peech, 1972; Van Ranst et al., 1998).

Table 20 Cation exchange capacity (CEC), basic cation exchange capacity (CEC_b), and anion exchange capacity at soil pH measured in $CaCl_2$ 0.002 mol L^{-1} (no HCl or $CaOH_2$ addition) for pit 3 of data set $SOIL_{AP11}$. The pH for which AEC equals CEC (pH_0) together with the pH in KCl 1 mol L^{-1} and in water are also given.

Layer	CEC_b	CEC	AEC	pH_0	pH		
					$CaCl_2$ 0.002 mol L^{-1}	KCl 1 mol L^{-1}	water
cm		*cmolc kg^{-1}*			-		
0-5	2.78	3.50	0.10	-	3.9	3.3	4.0
5-15	0.85	1.21	0.08	1.7	4.5	4.5	5.6
15-30	0.70	0.89	0.09	2.0	4.5	4.7	5.6
30-50	0.75	0.97	0.13	2.1	4.5	4.7	5.0
50-100	0.66	0.87	0.14	2.2	4.5	4.9	5.7
100-200	0.56	0.71	0.30	3.2	4.5	4.9	5.8
200-300	0.51	0.58	0.53	4.4	4.5	5.7	6.0

B.2.3.3 Specific adsorption of nitrate, sulphate and phosphate

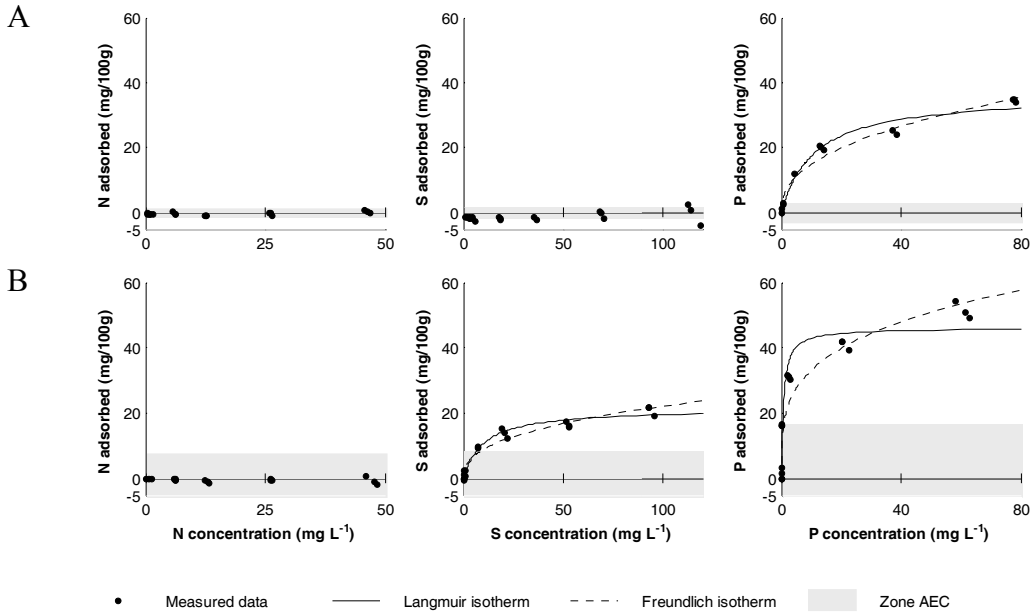

Figure 29 Isotherms of adsorption measured for the 0-5 cm layer (A) and the 200-300 cm layer (B) for nitrate, sulphate and phosphate. The Langmuir and Freundlich equations fitted on experimental data are represented. The grey zone on the graphics corresponds to the equivalent AEC (values of Table 20) for $N\text{-}NO_3^-$, $S\text{-}SO_4^{2-}$, and $H\text{-}H_2PO_4^-$.

The adsorption isotherms measured at pH 4 and for a ionic strength of 100 mmol L^{-1} (KCl as indifferent electrolyte) failed to show any specific adsorption of nitrates, but revealed the specific adsorption of sulphate for the 200-300 cm layer, and the increasing adsorption of phosphate with soil depth (Figure 29). The experimental reproducibility was good with standard errors < 1 mg/100g for q_{ads} and < 1 mg L^{-1} for $c_{solution}$ (n=3) except for the greatest concentration for which they were < 2.

The Langmuir equation fitted well the data (Table 21). The maximum adsorption is given by $q_{ads}^{\max}$ of the Langmuir equations (equation (26)) and was of 22 mg S / 100 g for the 200-300 cm layer, 37 mg P / 100 g for the 0-5 layer and 46 mg P / 100 g for the 200-300 cm layer. Such maximum values of adsorption are in good agreement with the literature for our soil type (Agbenin and Tiessen, 1994; Alves and Lavorenti, 2004; Couto et al., 1979; Gillman, 1984; Marcano-Martinez and McBride, 1989).

Table 21 Langmuir and Freundlich parameters fitted on the experimental data for the 0-5 cm layer (P) and the 200-300 cm layer (S and P). The sum of square errors (SSE) and the number of observations (n) are given.

Layer	Element	Langmuir [1]				Freundlich [2]			
		q_{ads}^{max}	K	SSE	n	k_f	n_f	SSE	n
cm		*mg/100g*	*L mol^{-1}*						
0-5	P	37	10	67	21	5.8	0.4	82	21
200-300	S	22	11	36	21	3.6	0.4	67	
	P	46	1	450	21	17.9	0.3	671	

[1] $q_{ads} = q_{ads}^{max} \frac{Kc_{solution}}{1 + Kc_{solution}}$ eq (26); [2] $q_{ads} = k_f c_{solution}^{1/n_f}$ eq (27), where q_{ads} is the quantity of N, S or P adsorbed on the soil surface (mg/100g) and $c_{solution}$ is the concentration of N, S or P in the contact solution (mg L^{-1})

B.2.3.4 Conclusion

The changes in CEC and AEC with the pH of the contact solution confirmed that the variable charges dominate in the soils of the experiment. Graphics are compatible with a small permanent charge of about -0.5 cmolc kg^{-1} but the experimental measurement of the permanent charge as explained by Chorover and Sposito (1995) or Gillman and Sumner (1987) would be necessary to rule on this point.

The upper soil layer (0-5 cm) is dominated by the CEC of the organic matter whereas AEC increased in deeper layers (200-300 cm) together with Fe and Al oxide contents of the clay fraction. The CEC and the AEC remained small at soil pH with mean values < ± 1 cmolc kg^{-1}. Cation retention may thus occur mainly in upper soil layers whereas anion retention may mainly occur in deeper soil layers below a depth of 50 cm. A change in pH would lead to a significant increase in CEC above pH 6, and a significant increase in AEC below pH 4 mainly in deep soil layers (below a depth of 50 cm).

Specific adsorption may occur for phosphate whatever the soil layer and for sulphate for soil layers which are not greatly influenced by organic matter. Such adsorptions were recorded at pH 4 but would change under different pH conditions, soil solution status (ionic strength, composition) and soil surface status (aggregation, previously adsorbed species).

B.3 GENERAL CONCLUSIONS

B.3.1 On soil general features

The soils of the experiment correspond to Dystrophic Red-Yellow Latosols and are characterized by (i) yellow/red hues, (ii) an upper soil horizon influenced by OM and a horizon below a depth of 50-70 cm with an increase of 8 % in the clay content compared to the upper soil layers, and (iii) very low CEC and organic matter content (CEC < 1 cmolc kg^{-1}, C < 0.6 % and N < 0.05 % below a depth of 15 cm). The soil surface behaviour is of a variable charge system (permanent charge < 0.5 cmolc kg^{-1}) for which CEC prevails in the upper soil layers and equals AEC in deep soil layers. Specific adsorptions of S and P occur.

B.3.2 On soil spatial heterogeneity

Most of the variability is localized in the upper soil layer (0-5 cm) and results from organic matter heterogeneities. In contrary, physical and chemical properties are highly homogeneous in deep soil layers. The variability among the sampled plots grouped by treatment or by block is of the same order of magnitude than the variability inside each plot, where a slight effect of the distance to the nearest trees was observed. This means that the changes which may be observed in the studied variables during the fertilization experiment may be attributed to the treatments established provided that the soils are sampled continuously from the stump to the inter-row.

B.3.3 On mineral weathering

The soils contain large quantities of quartz and well crystallized iron and aluminium oxides, few amorphous aluminium and iron, and mainly kaolinite in its clay fraction. The identified 2:1 phyllosilicate is very stable since it remained unaffected by DCB or Tamura treatments and only lost its mineral structure after heating at 550°C. Together with total analyses which indicated total bulk soil contents of Mg, K, Na and Ca < 0.07 %, this means that no significant amount of these elements may be released in soil solution by weathering. On the other hand, Al, Fe and Si may be released by the weathering of kaolinite and of more or less crystallized oxides.

B.3.4 On the expected soil response to the applied fertilizations

Table 22 Estimation of the capacity of the soil (in kg ha^{-1}) to retain cation or anion by non specific adsorption (CEC and AEC) or specific adsorption. For each element, the capacity is calculated for each soil layer from the bulk density of Table 11 and the CEC or AEC of Table 20 fully saturated with the studied element. The charge attributed to each element is +1 for Na, K and $N\text{-}NH_4$, +2 for Ca and Mg, +3 for Al, -1 for $N\text{-}NO_3$, Cl and $P\text{-}H_2PO_4$, and -2 for $S\text{-}SO_4$. Specific adsorptions are calculated from Table 21. n.d.=not determined.

	CEC					AEC					Specific adsorption	
	Na	K	Ca	Mg	Al	$N\text{-}NH_4$	$N\text{-}NO_3$	Cl	$S\text{-}SO_4$	$P\text{-}PO_4$	$S\text{-}SO_4$	$P\text{-}PO_4$
	kg ha^{-1}											
0-5 cm	511	869	446	270	200	311	9	23	10	20	0	232
5-15 cm	378	642	329	200	148	230	15	38	17	33	n.d.	n.d.
15-30 cm	443	753	386	234	173	270	27	69	31	61	n.d.	n.d.
30-50 cm	628	1067	547	332	246	382	53	134	61	117	n.d.	n.d.
50-100 cm	1394	2371	1215	737	545	849	132	334	151	292	n.d.	n.d.
100-200 cm	2270	3861	1979	1200	888	1382	578	1464	662	1279	n.d.	n.d.
200-300 cm	1852	3150	1614	979	725	1128	1031	2611	118	228	2996	6405

For cations, the fertilizers applied in treatments 1 and 3 brought about 400 kg ha^{-1} of Ca, 224 kg ha^{-1} of Mg, 107 kg ha^{-1} of K and 5 kg ha^{-1} of Na. Table 22 indicates that if Ca and Mg were preferentially adsorbed and if all the fertilizers were dissolved, the CEC of the 0-5 cm and 5-15 cm would be necessary to retain the Ca and Mg issued from the fertilizers. The other cations would then be leached down to 30 cm. As Al is preferentially adsorbed on CEC for acidic soil pH and as the CEC is already saturated by more than 80 % of aluminium, the negative sites effectively available for the adsorption of base cations may be highly reduced, and it is likely that some cations may be leached in deeper soil layers. If recalculating Table 22 from a reduced CEC (=20% of total measured CEC), the entire profile down to a depth of 3 m would be necessary to retain the cations contained in the fertilizers.

For anions, Cl is reported to be adsorbed preferentially over NO_3 by non specific adsorption. If all the Cl within the fertilizers was to be dissolved (95 kg ha^{-1}), the 0-5 cm, 5-15 cm and 15-30 cm would be necessary to adsorb it on their AEC. Nitrate would be leached in deeper horizons and all the soil layers down to 200 cm would be necessary to retain the $N\text{-}NO_3$ issued from the fertilizers (121 kg N ha^{-1} in T3 and 360 kg N ha^{-1} in T5) by adsorption. The $S\text{-}SO_4$ in fertilizers (141 kg ha^{-1} in T3 and 171 kg ha^{-1} in T5) may compete for these adsorption sites but the specific adsorption capacity of deeper soil layers

(probably below a depth of 30 cm) would be sufficient to adsorb it. The specific adsorption capacity of P in the 0-5 cm layer is sufficient to hold the P inputs by fertilization (35 kg ha^{-1} in T1 and T3, and 138 kg ha^{-1} in T5) so that P may not appear much in soil solutions.

Of course, all the fertilizers may not dissolve entirely at once and the immobilization in the soil organic matter and micro-organisms and in the vegetation biomass would considerably reduce the release of nutrients in soil solution. Moreover, specific interactions among nutrients such as Ca with SO_4 and PO_4 (as already mentioned in the introduction) may modify substantially this simplistic scheme. The clear felling would also release important quantities of $N\text{-}NO_3$ in soil solution by mineralization of the forest floor and of harvest residues, which may be adsorbed on AEC previously to the anions (in particular Cl and NO_3) brought by the fertilizers. Nitrogen may also be retained as $N\text{-}NH_4$ on the CEC.

CEC and AEC may also change with soil solution chemistry and pH. The mineralization of the soil organic matter after clear felling is expected to release protons in soil solution and thus to lead to more acidic pH and thus to enhance AEC over CEC. The fertilization on the other hand brought dolomitic limestone which may have the opposite effect. Phosphate, if specifically adsorbed, may also lower the PZC and thus increase cation retention. The adsorbed species may then reorganize slowly after the clear felling and the fertilization episodes, by immobilization, diffusion and occlusion into the aggregates and into minerals, desorption… While the time elapses, the soils may tend to return to their initial pH close to their PZNC (which is the thermodynamically stable state) if soil constituents have not been too much altered by the changes in pH and soil surface status.

In conclusion, the leaching of monovalent cations is expected down to a depth of 3 m, and of divalent cations down to 50-100 cm. P is expected to be quickly adsorbed in the upper soil layer (0-5 cm) and to appear little in soil solutions, especially in ZTL (zero tension lysimeter) which collects solutions in a narrow range of pressure heads. Sulphates are expected to be leached deeper down to a depth of 30-50 cm where they may be adsorbed on the soil surface. Cl may be adsorbed from the upper soil layer down to a depth of 30-50 cm, and NO_3 is expected to be leached down to 50-100 cm where it may be adsorbed on soil surface. Specific interactions between Ca and SO_4 or PO_4 suggest that these elements may appear concomitantly in soil solution.

B.3.5 On the methods used

Aggregation in our soil was highly dependant upon the soil solution chemisty. It would be interesting to further investigate (i) which surfaces (type and quantity) are available for adsorption depending on the soil aggregation status, and (ii) the nature of the organo-mineral associations constituting the aggregates.

Regarding the mineralogical study, further analysis would be needed to identify and quantify the oxides more precisely. Simple analyses which may be performed are for example (i) X-ray diffractions performed on the oxide fraction after removal of the other minerals (kaolinite), (ii) repeated extractions by dithionite-citrate-bicarbonate at 25°C compared to extractions with citrate-bicarbonate at 25°C, (iii) MEB observations, microprobe sampling and total analysis. Further analyses would also be needed to rule on the nature of the phyllosilicate at 1.4 nm, such as MEB observations, microprobe sampling and total analysis, progressive heating coupled to X-ray diffraction, …

Regarding the soil surface reactivity, adsorption isotherms were only performed at pH=4 for a given ionic strength and two soil layers (0-5 and 200-300 cm). Isotherms would be needed for the other soil layers, in particular for S which exhibited a broad gradient of maximum specific adorption from the upper soil layer down to a depth of 3m. Moreover, pH=4 corresponded to the lower values of pH observed in the experiment (soil pH and soil solution pH), but one more modality such as pH=6 would be needed to assess the range of variations of the S and P specific adsorptions within the range of variations of pH in the fertilization experiment. The desorption dynamics together with the possible interactions among other cations and anions would also need investigating.

Regarding the modelling of the soil/solution interactions, the calibration of the models requires precise knowledge of the soil mineralogy and surface reactivity. It is thus important to have reliable measurements of these characteristics for the studied soils within the range of variations expected for the control parameters (ionic strength, pH, …).

PART C

WATER FLUXES

INTRODUCTION

Soil water is a major component which integrates many physical, chemical and biological phenomena within forest ecosystems. While computing input-output budget of nutrients (Ranger and Turpault, 1999), precise knowledge of water fluxes in forest soils is needed to assess nutrient losses by drainage. As it is quite difficult to quantitatively measure soil water fluxes, modelling of water fluxes is classically used to compute soil water balance of the ecosystem (Beier, 1998; Granier et al., 1999a; Hornbeck et al., 1997; Ranger and Turpault, 1999; Ranger et al., 2002; Tsutsumi, 1969; Turpault et al., 1999; Williams, 1987). Nutrient balance will thus be highly dependant on the accuracy of such models especially for forest soils for which the hydrodynamic structures are highly heterogeneous (Fournier et al., 1994; Riha et al., 1986) and the collection of information (velocity, porosity) from field experiments, is a crucial step for precise calibration and setting up of deterministic flow or transport models (Ptak et al., 2004).

The water flow in soils is generally heterogeneous. As recalled by Dreuer et al. (2003), the causes of preferential or bypass flow are related to hydraulic characteristics such as the occurrence of macropores (Beven and Germann, 1982), dual or multimodal pore-size distributions (Gerke and van Genuchten, 1993; Zurmühl and Durner, 1996), discontinuities of texture (Kung, 1990) and the occurrence of biopores such as root channels (Bramley et al., 2003; Parsons et al., 2004). Many of the manifestations of preferential flow and transport have their genesis at the soil profile upper boundary (Clothier et al., 2008) through heterogeneous water inputs at the soil upper boundary or differences in infiltration resulting from heterogeneity of wettability of the soil surface. This is particularly true in forest ecosystems for which incident rainfall may be spatially distributed through stemflow and throughfall (Levia and Frost, 2003; Levia and Frost, 2006), and hydrophobic forest floor such as the *Eucalyptus* one may infiltrate water heterogeneously (Greiffenhagen et al., 2006; Laclau et al., 2004a).

Hydraulic properties of tropical ferralsols are reported to be highly homogeneous at a macroscopic scale (> 1 m) but to show random-like variations at a microscopic scale (Cichota et al., 2006). This heterogeneity is directly related to the microaggregated structure of ferralsols already presented in part B (Balbino et al., 2004; Pochet et al., 2007; Volland-Tuduri et al., 2004). The inter-aggregate porosity explains the high hydraulic

conductivity at saturation classically recorded for this type of soil of about 1-50 10^{-5} m s^{-1} (Balbino et al., 2004; Elsenbeer et al., 1999; Paiva et al., 2000; Pochet et al., 2007). This first type of porosity corresponds to pore diameters of 5 to 300 microns (pressure heads > -6m) which are extremely permeable to water (Cambier and Prost, 1981; Cornell and Schwertmann, 2003) and represent about half of total soil porosity (Balbino et al., 2002; Cambier and Prost, 1981; Neufeldt et al., 1999). The diameter of the second pore class associated to intra-aggregate porosity is about 20 nm (pressure head of about -1500m) (Balbino et al., 2002; Cambier and Prost, 1981; Neufeldt et al., 1999) and results in a high hydrodynamic dispersion (Cambier and Prost, 1981). Such pressure heads are hardly recorded experimentally in the field and a single pore distribution may be tested as a first modelling approach but a second class of porosity may be of crucial importance in terms of chemical reactivity.

The soil water fluxes are also highly dependant upon the transpiration of on-site vegetation and upon the evaporation of the upper soil layers. These two fluxes may take up a large amount of water (sink term) from the soil profile. The transpiration of fast-growing *Eucalyptus* trees is classically reported to be large (Almeida et al., 2007; Damman, 2001; Laclau, 2001; Soares and Almeida, 2001; Whitehead and Beadle, 2004). The supply of water seems to be the most limiting resource in Brazilian commercial plantations where large amounts of fertilizers are applied (Goncalves et al., 1997; Landsberg, 1999; Stape et al., 2004) and the canopy transpiration is limited by soil moisture and rainfall (David et al., 1997a; Mielke et al., 1999). It results in broad ranges of variations of soil water contents described in short time periods. Such conditions require robust algorithms of resolution from the models. Great care must be taken in the evapotranspiration flux input accuracy used as an input variable in the models.

Different types of water drainage models have been developed and used. The two main classes are (i) bucket models based on water balance which compute the differences in water content of the soil layers and compare them to the vegetation needs and (ii) mechanistic models derived from Darcy's law which mathematically describe the transient water flow in soils (Feyen et al., 1998; Samouëlian et al., 2007; Simunek et al., 2006). This second class of models requires more input parameters and careful calibration procedures but allows a dynamic description of the water flux and the coupling with chemical processes controlling the chemical composition of the soil solution. MIN3P (Mayer, 1999)

is one of these reactive transport models which showed a promising efficiency in modelling soil water and nutrients fluxes in forested ecosystems (Gerard et al., 2004).

Most studies on water fluxes in *Eucalyptus* plantations use water balance models (David et al., 1997a; Laclau, 2001; Langensiepen et al., 2006; Mielke et al., 1999; Soares and Almeida, 2001; Stape et al., 2004; Stape et al., 2008; White et al., 2000) but, to our knowledge, few mechanistic approaches have been tested up to date (Almeida et al., 2007; Bertolo et al., 2006; Damman, 2001; Klinge et al., 2001). However, the parameterization of mechanistic models are needed (i) to assess precise quantification of drainage budgets (nutrients and water) in fast-growing *Eucalyptus* plantations and (ii) to serve as water-flow model within reactive transport models.

The main goals of the present study were thus (i) to parameterize a water flux model which may serve as a basis for further chemical coupled modelling, (ii) to calculate the water fluxes at each depth where soil solutions were sampled throughout the experimental period and (iii) to assess the water balance of the stand during the experimental period by simulating the outflow leaving the soil profile by drainage and by evapo-transpiration (T_{eff} and EV_{eff}).

The chosen model was MIN3P. The working hypotheses were that (i) water was drained vertically in soils, homogeneously according to the horizontal plane (1-D simulations) through one single type of porosity, (ii) evapotranspiration rates could be optimized by minimizing the differences between the water contents measured in situ and the simulated ones. In situ calibrations were used as much as possible and the spatial heterogeneity of the input variables used in the model was discussed.

C.1 MATERIAL AND METHODS

C.1.1 MIN3P water balance module

C.1.1.1 General presentation of the model

MIN3P is a multicomponent-reactive transport model initially developed by U. Mayer (Mayer, 1999; Mayer et al., 2002) suitable for the simulation of physical and geochemical processes that control the evolution of pore water, pore gas and the mineralogical composition in variably-saturated porous media in one, two or three spatial dimensions. It considers advective-dispersive transport in the aqueous phase, as well as diffusive gas transport. Governing equations for multicomponent reactive transport in variably-saturated media consist of a mass conservation equation for water under variably-saturated conditions (Richard's equation), and a set of non linear transport equations coupled with geochemical reactions. The model formulation is based on the global implicit solution approach which considers reaction and transport processes simultaneously.

The governing equations are approximated by discretized equations (finite volume discretization and fully implicit time weighting) and global mass balance calculations. The equations are linearized using a modified Newton's method (Paniconi and Putti, 1994) and solved using a sparse iterative matrix solver (Vanderkwaak et al., 1997). The solution approach is based on the decoupling of groundwater flow and reaction-transport processes. It assumes that the movement of ground water is not affected by the presence of a gas phase and that geochemical reaction processes do not cause significant porosity changes, which could affect the medium's permeability. The solution of the system of equations consists of the solution of the variably-saturated flow problem and the subsequent solution of the reactive transport problem based on the fluxes and phase saturations obtained from the flow solution.

MIN3P performs 1 to 3-D simulations.

C.1.1.2 Variably saturated flow equations

The basic assumptions governing theoretical development of flow equations in MIN3P are: incompressible fluid, no hysteresis, and a passive air phase. Hydraulic head is taken as the primary dependent variable.

The saturation of the aqueous phase is used in the MIN3P code rather than the volumetric water content since it is a major control in the equilibrium between solute and gaseous species within a given pore. For practical purpose, the saturation will be kept in the theoretical presentation of MIN3P, whereas the output of the simulations will be analyzed using the volumetric water contents to match with the measured experimental data. Water content can be easily obtained from the saturation using:

$$S_a = \frac{\theta_a}{\theta_{sa}},\ S_{ra} = \frac{\theta_{ra}}{\theta_{sa}},\ \varphi = \theta_{sa}$$

where a identifies the aqueous phase, S_a is the saturation of the aqueous phase [m^3 water m^{-3} void], S_{ra} [m^3 water m^{-3} void] defines the residual saturation of the aqueous phase, θ_a is the volumetric water content [m^3 water m^{-3} bulk], θ_{sa} is the volumetric water content at saturation, θ_{ra} is the residual water content and φ stands for porosity [m^3 void m^{-3} bulk soil].

The mass conservation equation for the aqueous phase (Richards' equation) is given by (Neuman, 1973; Panday et al., 1993):

$$\varphi \frac{\partial S_a}{\partial t} - \nabla \cdot \left[k_{ra} \mathbf{K} \nabla h \right] - Q_a = 0 \tag{28}$$

where t[s] is time and k_{ra} is the relative permeability of the porous medium with respect to the aqueous phase [-]. h [m] is the hydraulic head, and Q_a is a source-sink term for the aqueous phase [s^{-1}], where a positive quantity defines the injection of water. $\mathbf{K}$ is the hydraulic conductivity tensor [m s^{-1}].

C.1.1.3 Soil hydraulic parameters

Since the saturation and the relative permeability are a function of the aqueous phase pressure, the equation mass is non linear. Relationships given by Mualem (1976) and Van Genuchten (1980) are used to describe these dependencies.

$$S_a = S_{ra} + \frac{1 - S_{ra}}{\left(1 + \left|\alpha \psi_a\right|^n\right)^m} \qquad (29)$$

$$k_{ra} = S_{ea}^l \left[1 - \left(1 - S_{ea}^{1/m}\right)^m\right]^2 \qquad (30)$$

with

$$m = 1 - \frac{1}{n} \qquad (31)$$

$$\psi_a = h - z \qquad (32)$$

$$S_{ea} = \frac{S_a - S_{ra}}{1 - S_{ra}} \qquad (33)$$

where α, n, m and l are the soil hydraulic function parameters, S_{ea} is the effective saturation of the aqueous phase, ψ_a [m] defines the pressure head of the aqueous phase and z [m] is the elevation with respect to a given datum. When the soil is saturated, $S_{ea} = 1$, $k_{ra} = 1$, and thus $\mathbf{K}$ defines the hydraulic conductivity tensor at saturation. l is an empirical pore tortuosity/connectivity parameter.

C.1.1.4 Evaporation and transpiration

The MIN3P evapotranspiration module was re-coded to ensure a better stability of the model under more drastic conditions (water content close to the residual, high evaporation or transpiration rates, high gradients of pressure head with rapid changes …) and to differentiate evaporation from transpiration. The transpiration and evaporation models already coded in MIN3P by F. Gerard and U. Mayer (Gerard et al., 2004) were kept and their choice will not be discussed here but their mathematical translation was adapted.

The rate of water uptake and loss is calculated at each time step by adopting a method similar to the one used in the soil water module SWIF of the FORHYD model (Tiktak and Bouten, 1992). The mass balance equation for water in the forest ecosystem can be expressed as:

$$ET_{\max} = T_{\max} + EV_{\max} + f_i I \qquad (34)$$

$$T_{\max} = T_{\max}^{input} - f_i I \qquad (35)$$

where ET_{max} is the maximum evapotranspiration [m s^{-1}], T_{max} is the maximum tree transpiration rate [m s^{-1}], EV_{max} corresponds to the sum of understorey plus soil evaporation [m s^{-1}], and I is the amount of intercepted water by the tree canopy [m]. The correction of T by the $f_i I$ term serves to take account of the tree transpiration reduction by the evaporative demand of a wet canopy on days with precipitation. T_{max}, EV_{max} and I are input data at each time step t, f_i is an input parameter specified for the whole simulation.

Both EV_{max} and T_{max} are thereafter reduced by the water availability in the soil profile at time t. Evaporation flux is calculated first considering that the trees may take up water deeper in the soil profile in case of water deficiency in the surface layers. Evaporation over bare ground involves very complex mechanisms of mass and heat exchanges at the interface soil/atmosphere. Their numerical simulation requires very detailed models using both a very short time step (namely of the order of 1 min) and large memory storage (Mahfouf and Noilhan, 1991). Consequently, simple parameterizations and an explicit formulation of the evaporation flux are required. Here, the effective evaporation rate EV_{eff} [m s^{-1}] is calculated as (Wu et al., 1999):

$$EV_{eff} = Min(\frac{AW_{ev}}{\Delta t}, EV_{max}) \tag{36}$$

$$AW_{ev} = \sum_{i_{ev}} vol(i) \cdot \varphi(i) \cdot R_{ev}(i) \cdot (S_a(i) - S_{a\_dry}(i)) \tag{37}$$

$$R_{ev}(i) = Min(\frac{S_a(i) - S_{a\_dry}(i)}{S_f(i) - S_{a\_dry}(i)}, 1) \tag{38}$$

where AW_{ev} [m^3] is the water available for evaporation in the soil profile, Δt is the time increment at time t of the simulation [s], i_{ev} indexes the soil profile cells which may evaporate, vol(i) [m^3] is the volume of cell i of the soil profile and $\varphi(i)$ [-] its porosity, $R_{ev}(i)$ [-] is a reduction factor which limits evaporation in cell i, $S_a(i)$ is the saturation in water of cell i, $S_{a\_dry}(i)$ its saturation for an air-dry pressure head (input parameter ψ_{dry}) and $S_f(i)$ its water saturation at a pressure head ψ_f (input parameter).

EV_{eff} is then distributed in each cell of the soil profile proportionally to its saturation in water:

$$EV_{eff}(i) = \frac{vol(i) \cdot \varphi(i) \cdot R_{ev}(i)}{AW_{ev}} \cdot (S_a(i) - S_{a\_dry}(i)) \cdot EV_{eff} \tag{39}$$

It can be checked that $\sum_{i_{ev}} EV_{eff}(i) = EV_{eff}$.

After evaporation occurred, the remaining water AW_{transp} [m^3] available for transpiration in the soil profile is calculated by:

$$AW_{transp} = \sum_{i_{transp}} vol(i) \cdot \varphi(i) \cdot rld(i) \cdot R_{transp}(i) \cdot (S_{a\_postev}(i) - S_{a\_\lim}(i)) \quad (40)$$

$$S_{a\_postev}(i) = S_a(i) - \frac{\Delta t \cdot EV_{eff}(i)}{\varphi(i)} \quad (41)$$

where i_{transp} indexes the profile cells where transpiration may occur, rld(i) is a reduction factor ≤ 1 which accounts for the root length density repartition in the soil profile, $R_{transp}(i)$ is a reduction factor which limits the transpiration rate in cell i, $S_{a\_postev}(i)$ is the water saturation in cell i once evaporation occurred, and $S_{a\_lim}(i)$ its water saturation for a given pressure head ψ_{lim} (input parameter).

The effective transpiration is then calculated as:

$$T_{eff} = Min(\frac{AW_{transp}}{\Delta t}, T_{\max}) \quad (42)$$

$R_{transp}(i)$ is calculated according to Battaglia & Sands (1997) and distributed in each cell using:

$$R_{transp}(i) = \frac{REW(i)^2 \cdot e^{p_1 \cdot REW(i)}}{REW_0^{\,2} \cdot e^{p_1 \cdot REW_0} + REW(i)^2 \cdot e^{p_1 \cdot REW(i)}} \quad (43)$$

$$REW(i) = Min(\frac{S_{a\_postev}(i) - S_{a\_\lim}(i)}{S_f(i) - S_{a\_\lim}(i)}, 1) \quad (44)$$

$$T_{eff}(i) = \frac{vol(i) \cdot \varphi(i) \cdot rld(i) \cdot R_{transp}(i)}{AW_{transp}} \cdot (S_{a\_postev}(i) - S_{a\_\lim}(i)) \cdot T_{eff} \quad (45)$$

where REW_i is the reserve of extractable water, REW_0 and p_1 are fitting parameters (Figure 30).

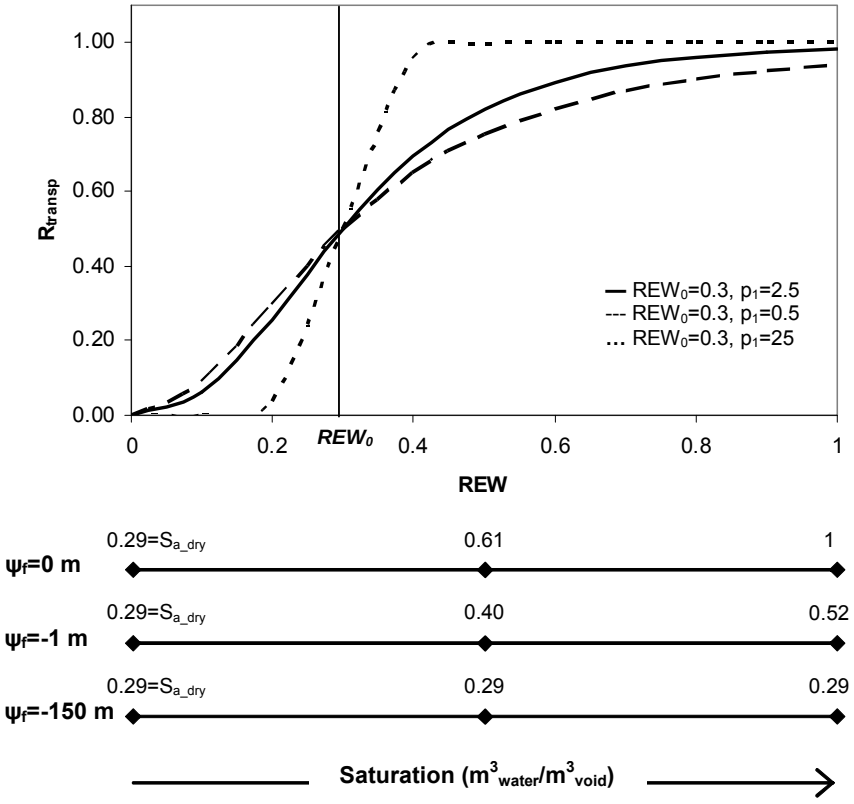

Figure 30 Influence of the transpiration parameters on the transpiration reduction factor R_{transp} (eq (43)). R_{transp} can be expressed as a function of the reserve of extractable water (REW) or as a function of the saturation in water S_a (eq (44)). S_a is controlled by ψ_f, the pressure head below which $R_{transp} \leq 1$, and by ψ_{lim}, the pressure head below which the transpiration stops (fixed at -150 m in the figure). The curve shape is controlled by REW_0 and p_1 (eq (43)).

C.1.1.5 Input and output

Table 23 MIN3P water balance module: inputs used in the simulations.

Input type		Input parameters or variables	Observations
Initial condition		Pressure head	Each soil layer (core file), or each cell (external file)
Boundary conditions	Upper	Flux (m s^{-1})	Time dependant, external file
	Lower	Pressure head (m^{-1})	
Soil hydraulic parameters	Retention curve	α, n, m S_{ra}, S_{sa}	Each soil layer, core file
	Hydraulic conductivity	Ks, l	
Source/sink term: evapotranspiration	Evaporation	EV_{max}	Time dependant, external file
		ψ_{dry}	Each soil layer
		Evaporation depth	Soil layers for which $\psi_{dry} \neq 0$
	Transpiration	T_{max}	Time dependant, external file
		p_1, REW_0 f_i	Core file common to all soil layers
		ψ_f, ψ_{lim}	Core file, each soil layer
		rld	Each cell (external file) or each soil layer (core file)

Boundaries may be specified in MIN3P in terms of specified head boundary (pressure head or hydraulic head), specified flux boundary or seepage face boundary, and can be constant or time dependant. The initial conditions, the soil hydraulic parameters and the controls for evapotranspiration must be specified as inputs in MIN3P (Table 23).

Table 24 MIN3P water balance module: outputs used in the simulations.

Output type		Output	Observation
Mass balance	Boundary fluxes	Total inflow Total outflow	At each time t from upper boundary to each observation node
	Evapotranspiration fluxes	Total evaporation Total transpiration	
	Change in soil water storage		
Soil profile snapshots	Soil water saturation, water content, pressure head, interfacial velocities		For each node (x,y,z) at a given t For each t at a given node (x,y,z)
	Evapotranspiration		For each node (x,y,z) at a given t

The main outputs of the water balance module of MIN3P are the water fluxes at the boundaries and the effective transpiration and evaporation (total for the soil profile) at each time step of the simulation. The model was also implemented to obtain these fluxes for each observation node of the soil profile. Snapshots of the soil profile are also available for some specified times t at each node of the soil profile (Table 24).

C.1.2 General characteristics of the performed simulations

C.1.2.1 Main goals

The main goals of the modelling were to assess the water balance throughout the experimental period, which meant to simulate daily outflow leaving the soil profile by drainage (depth of 3 m) and by evapotranspiration (T_{eff} and EV_{eff}). The water flux for each observation node also needed to be simulated to compute fluxes of nutrients in drainage water.

Simulations were also performed to adjust parameters of the model which were not experimentally acquired by optimizing the output of the simulations with the experimentally measured water contents.

C.1.2.2 Time step

As TDR measurements and climatic data were available at least at a daily time step (see § C.1.4 & C.1.3.2) and as our soil type is reported to drain very rapidly (Balbino et al., 2004; Elsenbeer et al., 1999; Libardi, 2005; Paiva et al., 2000; Pochet et al., 2007), the water drainage simulations were performed at a daily time step.

C.1.2.3 Monitoring period

The experimental period started in July 2003 and ended in April 2006 (7 months before clear felling until 24 months after planting), which corresponds to three distinct experimental periods : (i) before clear felling (BCF): from 09/07/2003 (N_{day}=1) to 14/02/2004 (N_{day}=221) included; (ii) after clear felling and before planting (CFP): from 20/02/2004 (N_{day}=227) to 22/04/2004 (N_{day}=289) included; (iii) after planting (AP): from 27/04/2004 (N_{day}=294) to 09/05/2006 (N_{day}=1036) (Figure 6). Data until 05/08/2006

(N_{day}=1124) were also used for the parameterization of the aboveground water fluxes (stemflow and throughfall) models in ANNEX 4.

The BCF period was sub-divided in two periods BCF1 (dry) and BCF2 (wet) and the CFP period was subdivided in CFP1 and CFP2. The AP period was divided in 6-month-long sub-periods (Figure 6).

C.1.2.4 Spatial unvariants: working hypotheses

Spatial heterogeneity of the transient water flow may result from heterogeneity of the water inflow at the upper boundary of the soil profile or of the water uptake by evapotranspiration, from spatial heterogeneity of the soil hydraulic properties, or from preferential flow paths in the soil (through bio-channels for example). These heterogeneities may occur at different scales and wide-range variability may be concealed by short-range variability (Legout et al., 2008; McBratney et al., 2003). Many of the manifestations of preferential flow and transport have their genesis at the upper boundary of the soil profile (Clothier et al., 2008).

In the studied experiment, the water inflow is expected to vary (i) at the tree scale, since the rainfall may be concentrated at the bottom of the tree stems by stemflow (Cattan et al., 2007; Chang and Matzner, 2000; Johnson and Lehmann, 2006; Levia and Frost, 2003) or differentially transmitted by throughfall (Delphis et al., 2006; Konishi et al., 2006; Levia and Frost, 2006), (ii) at the plot scale (intra plot, plot area = 600 m^2) since heterogeneities among the trees may modify these fluxes, and (iii) among the different plots (inter plot, stand area = 1.8 ha) since differences in growth and/or soil characteristics within the whole plot may also influence these fluxes. The spatial heterogeneity of rainfall may also influence the inflow more probably at the inter or intra plot scale, since tropical rain storms may occur locally (Levia and Frost, 2006). Differences in soil surface characteristics (wettability) may also induce spatial heterogeneity of the inflow at a < 1 m scale, especially for *Eucalyptus* forest floor which is well known for its hydrophobicity (Laclau et al., 2004a).

Water uptake by trees is expected to vary at the tree scale since the root system of the trees is spatially heterogeneous in the three dimensions of space, and at the intra-plot and inter-plot scale since these root systems may differ from one tree or plot to another, together with the water demand of the trees.

For the studied ferralsols, part B showed that there was no significant intra or inter-plot effect on major soil characteristics. The soil hydraulic properties are thus expected to be quite homogeneous from one tree or plot to another. On the other hand, the micro aggregation of this type of soil together with differences in the wettability of the soil surfaces may induce heterogeneities of the soil hydraulic properties at a scale < 1 m (Balbino et al., 2004; Cichota et al., 2006; Clothier et al., 2008; Elsenbeer et al., 1999; Greiffenhagen et al., 2006; Laclau et al., 2004a; Paiva et al., 2000; Pochet et al., 2007).

The main goal of the present study was to estimate the water drainage leaving the soil profile at a depth of 3 m at the plot scale. The working hypothesis was thus that the main heterogeneities of the soil hydraulic properties occurred at a scale < 1 m and that taking average soil hydraulic properties at this scale would allow a correct simulation of the soil moisture at this scale too. A single average porosity was thus hypothesized. Once this settled, heterogeneities of the water drainage due to heterogeneities of the inflow or of the uptake may be simulated by changing the upper boundary or the uptake on a 1-D profile under the hypothesis that lateral drainage is null. Such 1-D simulations do not allow the construction of spatial maps of water drainage but may allow qualitative studies of the different processes. 1-D simulations are easier to handle since they need less computing power and model inputs. They were regarded sufficient within the scope of this study, considering that the number of probes used to monitor soil water content was not sufficient to validate a 2-D hydrological model. Preferential flow paths were not studied.

The simulations are thus performed for a vertical profile invariant according to the horizontal plane, with a single average porosity. The water drainage only occurs vertically which means that the lateral water movements are neglected. Since the slopes of the experiment are flat and the soil quite homogeneous, the approximation seems reasonable.

C.1.2.5 Soil profile characteristics

The soil profile was deep of 3 m and composed of 4 layers:

- Layer 1: 0-30 cm observed at a depth of 15 cm
- Layer 2: 30-70 cm observed at a depth of 50 cm
- Layer 3: 70-230 cm observed at a depth of 150 cm
- Layer 4: 230-300 cm observed at a depth of 300 cm.

The soil layers were defined from the pedological layers presented in part B: layer 1 corresponds to the soil layers greatly influenced by organic matter, layer 2 is a transition layer between the soil layers influenced by organic matter and deeper soil layers for which clay contents increase, layers 3 and 4 correspond to an increasing gradient of clay content. As already mentioned in part B, the transitions between soil layers are gradual in this type of soil and the main difference lies between the surface layers influenced by OM and the deeper soil layers where clay contents are greatest (about 24%). Layer 4 was not included in layer 3 because TDR measurements indicated wetter conditions at a depth of 3 m than at a depth of 1.5 m (see § C.2.2). The observation nodes were located at the centre of the soil layers except for layer 4 for which the observation node corresponded to the lower boundary of the soil profile.

Although it has been shown that the *Eucalyptus* root structure develops deeper than 3 m (Knight, 1999; Laclau et al., 2001; Robinson et al., 2006), only a soil profile deep of 3 m was studied. Water content measurements were available down to a depth of 3 m and so were the soil solution samples. The stress was laid on evaluating with accuracy the water fluxes in the soil profile between the surface and a depth of 3 m where most of the nutrient uptake is expected to occur. It was thus considered essential to fix the lower boundary of the profile as a measured value and not to introduce unknown variability in the simulations from unknown and unobserved deeper soil layers.

In the model, the vertical profile was composed of 300 cells each one of dimension (1 m x 1 m x 0.01 m) in (x, y, z) from coordinates (1, 1, 0.01) to (1, 1, 3) and invariant according to the plane (x, y) (1-D simulations).

C.1.2.6 Methodology

The first step was to assess which data may be used to calculate the time-dependant inputs of the model, that is, data for the maximum evapotranspiration (outflow of the soil profile), for the upper boundary (inflow) and the lower one (outflow) (Table 23). The spatial heterogeneity of the inputs thus obtained was discussed (§ C.1.3 & C.2.1, ANNEX 4). As they will be used to assess the efficiency of the simulations, the water contents measured on-site were also analyzed and their spatial heterogeneity discussed (§ C.1.4 & C.2.2). Given the spatial heterogeneities observed, a general strategy was then decided whether to test or not the influence of some heterogeneity among plots or treatments on the model outputs (§ C.2.3).

The input parameters which were not time dependant also needed to be set (§ C.1.5 & C.2.4). The soil hydraulic properties were assessed for each soil layer. They were considered invariant according to the horizontal plane (working hypothesis). The parameterization of the input parameters driving the evapotranspiration was discussed.

The model was then used to adjust the evapotranspiration parameters which remained unknown (§ C.1.6 & C.2.5): the CFP period was used to adjust the evaporation parameters (no vegetation transpiration), the BCF period was used to adjust transpiration parameters (mature *Eucalyptus* stand with a closed canopy), the AP period was a mixed between the CFP and the BCF period and was used the check the validity of the model thus parameterized. The sensitivity of the model to soil hydraulic properties, boundaries and initial conditions was tested on the data from the CFP period.

Finally, the water fluxes leaving the soil profile at depths 15, 50, 100 and 300 cm were calculated by running the model thus parameterized over the whole period (§ C.2.6).

C.1.3 Time-dependant inputs of the model: daily maximum evaporation and transpiration, and daily water inflow at the soil surface

C.1.3.1 The transpiration term: evolution of the vegetation during the studied period

The transpiration flux is defined by the water taken up by the vegetation and may be influenced by changes in leaf area and stomatal regulation. The vegetation may also influence the evaporation flux by changing the soil coverage and thus the energy reaching the soil.

During the BCF1 and BCF2 period, the soil was covered by a mature stand of *Eucalyptus* trees with a closed canopy. During the CFP period, the soil was covered by the harvest residues of the clear felling of the BCF *Eucalyptus* stand and no vegetation was present (use of glyphosate). During the AP period, a new *Eucalyptus* stand was planted and managed according to 3 different silvicultures. This new stand grew rapidly and its canopy was closed after 12 months of growth. The growth of the different stands was not studied in the present work but some major data from Laclau *et al.* (2004b; 2005b; 2007) are presented in the preamble of the thesis (Part A).

In MIN3P, the transpiration is regulated by (i) the daily maximum transpiration, (ii) non-time dependant parameters regulating this maximum transpiration and (iii) the root length densities (rld(z) of eq. (40)) which distribute the water uptake all along the soil profile. The root length density profiles needed thus to be defined for the BCF and AP periods (*Eucalyptus* trees). A classic exponential decay equation was fitted on the experimental data already presented in part A and was used to compute root length densities all along the soil profile:

$$RLD(z) = A_{rld} + B_{rld} \ \exp\left(-C_{rld} z\right) \tag{46}$$

where RLD is the root length density, z the depth in cm and A_{rld}, B_{rld}, C_{rld} the parameters to be fitted. This root length density needed to be normalized to match the model input format, which was done by:

$$rld(i) = a_{rld} + b_{rld} \ \exp\left(-c_{rld} i\right)$$

$$a_{rld} = \frac{A_{rld}}{A_{rld} + B_{rld}} \ , \ b_{rld} = \frac{B_{rld}}{A_{rld} + B_{rld}} \ , \ c_{rld} = C_{rld} \qquad (47)$$

where rld(i) is the root length density input for cell i, and A_{rld}, B_{rld}, C_{rld} the fitted parameters of equation (46).

Using a continuous function was preferred to the discontinuous experimental data since: (i) gradual decrease of the root length density was observed during the pedological descriptions (part B), (ii) it allows simple comparisons among the root length density profiles by analyzing the fitted parameters, (iii) and such functions are necessary to implement the model with a root growth module if needed.

C.1.3.2 Meteorological data

The effective transpiration may be experimentally measured by monitoring xylem sap fluxes (Granier, 1987). Together with the monitoring of soil water content and of meteorological data, it allows the experimental calibration of the parameters controlling transpiration (reduction factor R_T) (Granier et al., 1999a). This study was at its beginning in the experimental area when the present work was realized so that the maxima plant uptake (transpiration) and soil evaporation needed to be estimated from meteorological data. The parameters driving the transpiration had to be either fixed using the literature or optimized by simulation.

Available meteorological data were weekly rainfall (Pi) in a 1 ha opened area next to the experimental site, daily rainfall (Pi_{ref}) and temperature (minimum, maximum, average) at 2 km from the experimental site (Itatinga, SP), global radiation, wind velocity, insolation and relative water content at about 20 km from the experimental site (meteorological station of UNESP, Botucatu, SP) (Table 25). On-site daily rainfall will thus have to be estimated from on-site weekly measurements and from the daily Pi_{ref}. The calculation is given in ANNEX 4. The maximum evaporation and transpiration will have to be estimated from the Botucatu data.

Table 25 Monitored fluxes: number of collectors and time steps of data acquisition.

	Type of collecting device	Location	Abbreviation	Number	Time step
Above ground fluxes	Rain Gauge	Open area next to experimental site	Pi	1	Weekly
		Itatinga (2 km)	Pi_{ref}	1	Daily
	Total depositions	Open area next to experimental site	Th_{ref}	1	Weekly
	Throughfall	On site	Th	9	Weekly
	Stemflow	On site	St	BCF 8	Weekly
				AP 27	Weekly
Soil water monitoring	TDR probes	On site, at depths of:			Every 12 hours
		15 cm		9	
		50 cm		9	
		150 cm		9	
		300 cm		9	
Meterological data	Global radiation, wind velocity, insolation and relative water content	Botucatu (20 km)			Daily
	Temperature (maximum, minimum, average)	Itatinga (2 km)			Daily

Penman Monteith equation (Monteith, 1981) is commonly used to calculate maximum evapotranspiration from weather data:

$$ET = \frac{1}{\lambda} \cdot \frac{\Delta\left(R_n - G\right) + \rho_a c_p \left(e_s - e_a\right) / r_a}{\Delta + \gamma\left(1 + r_s / r_a\right)} \tag{48}$$

where Rn is the net radiation, G is the soil heat flux, (e_s-e_a) represents the vapour pressure deficit of the air, ρ_a is the mean air density at constant pressure, c_p is the specific heat of the air, Δ represents the slope of the saturation vapour pressure temperature relationship, γ is the psychrometric constant, and r_s and r_a are the (bulk) surface and aerodynamic resistances. These resistances are vegetation specific. Aerodynamic resistance determines the transfer of heat and water vapour from the evaporation surface into the air above the canopy and is calculated from wind and water content measurements. 'Bulk' surface resistance describes the resistance of vapor flow through the transpiring vegetation and evaporating soil surface.

The surface resistance was undefined for the soils and the *Eucalyptus* vegetation of the experiment and the available meteorological data were obtained at 20 km far from the experimental site and in tropical climates, weather changes may occur at short range. The maximum evaporation and transpiration needed thus to be adjusted to on-site conditions. Two types of evapotranspiration were calculated for this purpose. The first one was the

reference FAO evapotranspiration (ET_{ref}) which is the evapotranspiration for a hypothetical reference crop of height 0.12 m, surface resistance 70 s m^{-1} and albedo 0.23. It closely resembles the evaporation of an extension surface of green grass of uniform height, actively growing and adequately watered. It was used to compare our results to a standard evapotranspiration and was computed thanks to the FAO Penman-Monteith method as (Allen et al., 1998):

$$ET_{ref} = \frac{0.408 \cdot \Delta \cdot (R_n - G) + \gamma \cdot 900 / (T + 273) \cdot u_2 (e_s - e_a)}{\Delta + \gamma (1 + 0.34 \cdot u_2)} \quad (49)$$

with ET_{ref} the reference evapotranspiration [mm day^{-1}], R_n the net radiation at the crop surface [MJ m^{-2} day^{-1}], G the soil heat flux density [MJ m^{-2} day^{-1}], T the mean daily air temperature at 2 m height [°C], u_2 the wind speed at 2 m height [m s^{-1}], e_s the saturation vapour pressure [kPa], e_a the actual vapour pressure [kPa], (e_s-e_a) the saturation vapour pressure deficit [kPa], Δ the slope of the saturation vapour pressure temperature relationship [kPa $°C^{-1}$] and γ the psychrometric constant [kPa $°C^{-1}$].

An evaluation of the maximum energy available for evapotranspiration (ET_{max}) was also performed using Penman Monteith equation with r_s set to its minimum (r_s=0 in eq (48)) and Rn maximum (albedo=0). ET_{ref} was used to test different levels of maxima evaporation (EV_{max}) and transpiration (T_{max}). Once limited by the water availability in the soil profile, EV_{max} and T_{max} constitute the effective transpiration (T_{eff}) and evaporation (EV_{eff}) computed as outputs by the water drainage model.

C.1.3.3 Inflow at the upper boundary of the soil profile: throughfall, stemflow and surface run-off

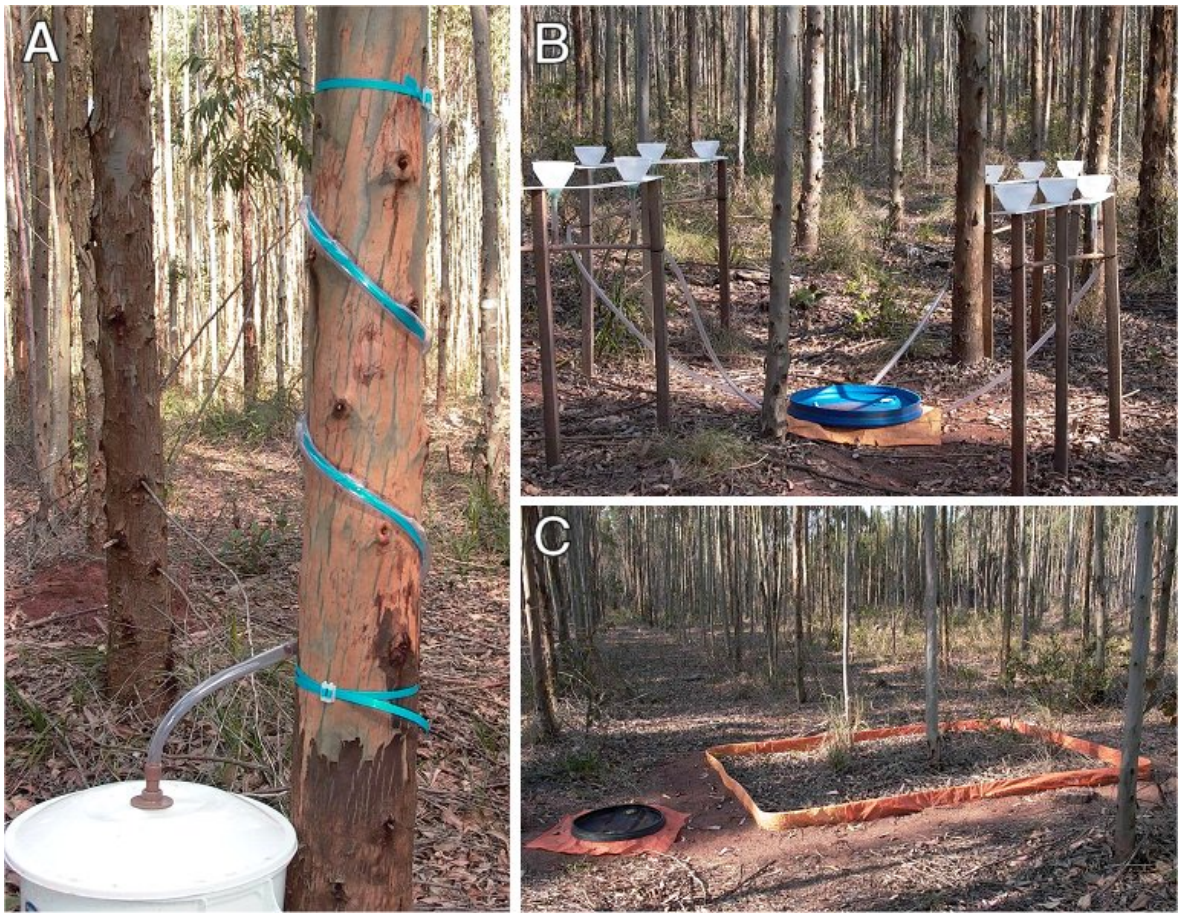

Figure 31 Aboveground water fluxes collectors: stemflow (A); throughfall (B) and surface run-off (C).

The water inflow at the upper boundary of the soil profile (P_{soil}) and the interception term (I) are inputs of the model. P_{soil} is the upper boundary and I participates in the transpiration calculation. For forest ecosystems, they are classically calculated as:

$$P_{soil} = Th + St - Ru \tag{50}$$

$$I = Pi - Th - St \tag{51}$$

where Th stands for throughfall, St for stemflow and Ru for surface run-off.

Throughfall solutions were measured weekly in collecting devices made of 12 funnels systematically distributed beneath the trees to integrate the heterogeneity at the tree scale (Figure 31). Nine replicates of collecting devices were monitored before clear-felling to check the inter plot spatial heterogeneity. Then, one collecting device per experimental plot

in treatment 1, 3 and 5 and blocks 1, 2 and 3 was monitored (total of 9 devices) after trees had reached a sufficient height (10 months after planting in block 1 and 14 months after planting in blocks 2 and 3).

Stem flows (St) were collected from helical collars installed on trees (Marques, 1996) and measured weekly in a collection bucket (St[mL]) (Figure 31). Before clear felling, eight of these collars were installed on trees representative of the stand. After clear felling, stem flow collecting devices were installed in January 2006 (20 months after planting) around 3 trees per experimental plot (blocks 1, 2 and 3 of treatments 1, 3 and 5 of the fertilization experiment).

Surface runoff was measured and collected weekly in each treatment from one 3x2 m collector.

Throughfall, stemflow and surface run-off were measured weekly. As the model operates at a daily time step, they needed to be estimated daily. This calculation together with the analysis of the spatial heterogeneity of these fluxes is detailed in ANNEX 4. It was placed in annex since material, methods and results were frequently inter-related in these calculations.

C.1.4 Data used to assess the simulations' efficiency: soil water monitoring

Soil moisture was measured every twelve hours (except in case of equipment failure) thanks to TDR probes (Time Domain Reflectometry) installed at the depths of 15, 50, 150 and 300 cm. The probes were installed at 3 distances from the planting row (close to an average tree, ¼ and ½ of the inter-row) at each depth in 3 plots. Before clear felling, these 3 plots were independent repetitions. After clear felling, the three plots corresponded to block 1 of treatments 1, 3 and 5, where the lysimetric design was installed (Figure 4 & Figure 5). Daily data were obtained by calculating the average water contents measured for the current day.

The water content measured by each probe was compared to the average value obtained for all TDR probes at a fixed depth by linear regression using proc GLM of SAS Software (www.sas.com). The linear regressions thus obtained were used to study the spatial heterogeneity of the measured water contents. In particular, the effects of block and treatment were tested on the intercepts by ANOVA analysis (proc GLM) to test the hypothesis of systematic wetter or dryer water contents in some block or treatment.

C.1.5 Non time-dependant inputs of the model

C.1.5.1 Parameters regulating transpiration

REW_0, p_1, ψ_{lim}, ψ_f, and f_l still remained to be set. Litterature reports values of REW_0 of 0.3 or 0.4 for other tree species (Battaglia and Sands, 1997; Granier et al., 2007; Kirschbaum et al., 2007) and p_1=2.5, ψ_f is classically set to -1 (field capacity) and ψ_{lim} to the wilting point (Battaglia and Sands, 1997). As *Eucalyptus* trees are reported to be highly efficient in their water consumption and as very low water contents were reached during the experimental period (down to residual water contents) suggesting that *Eucalyptus* trees could extract water down to very low absolute potentials, we chose to fix ψ_{lim} down to the residual water content and to optimize the others parameters together with T_{max} using the data of the very dry period BCF1.

The values of f_l used in the literature range from 0.14 to 0.2 (Gerard et al., 2004; Tiktak and Bouten, 1994). This parameter was not optimized since it affects the interception term which was low in the studied stand (cf C.2.1.3) and may thus not influence much the simulations. It was set to 0.2.

C.1.5.2 Soil hydraulic parameters: transient flow experiment

C.1.5.2.1 Transient flow experiment

Characterization of soils and the vadose zone includes the estimation of the soil water retention and unsaturated hydraulic conductivity relations for a wide range of volumetric water content values. Although laboratory experiments have the advantage of being quick and precise, they often lead to soil hydraulic properties that are not representative of the field. Among available field experimental procedures, transient experiment and inverse modelling approach allow the simultaneous estimation of both the soil water retention and the unsaturated hydraulic conductivity function (Hopmans et al., 2002; Vachaud and Dane, 2002). An inverse method includes three interrelated functional parts: (i) a controlled transient flow experiment for which boundary and initial conditions are prescribed and various flow variables are measured; (ii) a numerical flow model simulating the transient flow regime of this experiment; (iii) and an optimization algorithm, which estimates the unknown parameters through minimization of the difference between observed and

simulated flow variables. Among the benefits of inverse methods is the fact that they are equally applicable to field experiments, even under nontrivial boundary conditions. The difficulty of the inverse resolution is that the solution is generally non-unique and is highly dependant upon the initial set of parameters chosen (Hill, 1998). This approach was used here and adapted to the model requirements.

The transient flow experiment chosen was that of the instantaneous profile (also known as internal drainage method) which is considered a standard (Hopmans et al., 2002; Vachaud and Dane, 2002). It was conducted between clear felling and planting (from 20/04/2004 till 23/04/2004) on a 15 m^2 vegetation-free plot of block 1 of treatment 3. The area was set superior to 12 m^2 to limit the relative importance of lateral water movement at the plot boundary. Its centre was positioned above the 3 replicates of TDR probes installed 8-months earlier in this plot at depths 15 cm, 50 cm, 150 cm, 300 cm. The plot was further instrumented in its centre with tensiometers at depths 15 cm, 50 cm, 1 m, 1.50 m, 2 m, 2.50 m and 3 m.

The experiment was initiated by pounding water over the entire plot area until pressure head values were approximately zero or did not change with time down to a depth of 3m. After the water supply was stopped and the pounded water had infiltrated, the plot was covered with a plastic sheet and insulated to ensure a zero-flux top boundary condition and to reduce temperature variations (Figure 32). Subsequently, the soil was allowed to drain by gravity. The transient drainage process was monitored by simultaneous measurements of soil water content and pressure head every half hour in the first day of the experiment, and then daily until the end of the internal drainage experiment.

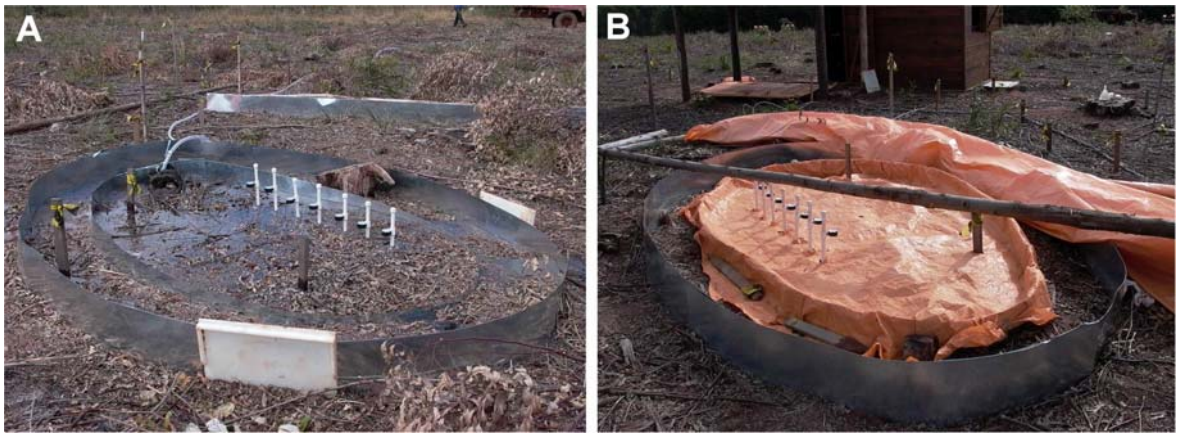

Figure 32 Interval drainage experiment (a) during pounding (b) during transient drainage (the plastic sheet ensures a zero-flux top boundary).

The estimation of the unknown soil hydraulic parameters was not performed thanks to an inversion procedure stricto senso because MIN3P did not have an inverse procedure. The inverse procedure of Hydrus 1D (www.pc-progress.cz/Pg_Hydrus_1D.htm) was tested but was unstable with our data set. The calculation of the water retention curve and the soil hydraulic conductivity parameters is explained thereafter.

C.1.5.2.2 Water retention curve parameters

Water retention curve parameters (α, n, m, θ_{ra} and θ_{sa}) were estimated for each soil layer from the water contents and the pressure heads experimentally acquired during the internal drainage experiment at depths 15 cm, 50 cm, 150 cm and 300 cm. As the experimental data at high absolute pressure heads were scarce, θ_{ra} ($\lim_{\psi_a \to \infty} \theta_a$) was set as the average of the driest water contents reached from July 2003 to September 2006 in each block and treatment for each depth. θ_{sa} was set as the volumetric water content measured at t=0 during the drainage experiment at each monitored depth. α, n, m were fitted using the software SWRC (Dourado-Neto et al., 2001).

C.1.5.2.3 Hydraulic conductivity parameters

Hydraulic conductivity parameters (Ks and l) were calculated to minimize the difference between simulated data by MIN3P and experimental records of the drainage experiment. The top boundary flux (z=0) was set to zero (no evapotranspiration, no rainfall), and the initial condition (t=0) taken as the soil profile fully saturated ($\psi_a(z) = 0 \ \forall \ 0 \le z \le 3m$). Ks and l were considered constant within a homogeneous soil layer. The studied soil layers were as presented in §C.1.2.5.

The numeric problem was complex. It was constituted of 8 parameters taken independently (Ks and l for each studied layer) but interactions between these parameters may influence each layer response. In order to estimate such influences, a statistical model based on Design Of Experiments (DOE) has been designed to determine the effects of the various factors. At a first level of modeling, DOE supposed linear influence of each parameter on each output. Deviations to linearity are taken into account by the introduction of interactions among the studied factors (Sabre, 2007; Taguchi, 1986).

For each time t and layer k, the simulated water content is supposed to be a linear response of the eight factors Ks_i l_i and without interaction:

$$\theta_{k,t}\left(Ks_{1\le i\le 4}, l_{1\le i\le 4}\right)=\theta_{k,t}^{average}+x_{k,t}^{1}Ks_1+x_{k,t}^{2}l_1+x_{k,t}^{3}Ks_2+x_{k,t}^{4}l_2+x_{k,t}^{5}Ks_3+x_{k,t}^{6}l_3+x_{k,t}^{7}Ks_4+x_{k,t}^{8}l_4 \quad (52)$$

Under some conditions of orthogonality, the $\left\{x_{k,t}^{i}\right\}_{1\le i\le 8}$ and $\theta_{k,t}^{average}$ may be calculated from a minimum set of simulations (experiment matrix) using combinations of extrema values of the eight factors $Ks_{1\le i\le 4}, l_{1\le i\le 4}$ (Taguchi, 1986). Then, eight observed values of $\theta_{k,t}$ allow the calculation of $\left\{Ks_i, l_i\right\}_{1\le i\le 4}$ by solving the matrix equation $\boldsymbol{\theta}_{k,t}=\boldsymbol{\theta}_{k,t}^{average}+\mathbf{x}_{k,t}^{i}\bullet\mathbf{Ks}_i,\mathbf{l}_i$. The difficult step is to establish the extrema values of the eight factors that will be used in the matrix of experiment due to the quasi linearity supposed by the DOE theory. Deviations to linearity are taken into account introducing interactions among the studied factors. The choice of the matrix depends on the complexity of the model supposed by the user. In this case, it can be shown that a 16x8 matrix enables the study of a model with 8 parameters and 4 independent interactions (Taguchi, 1986).

The matrix used comported 2 levels of factors (minimum, maximum), eight columns (8 factors) and 16 lines ($L_{16}(2^8)$) (Taguchi, 1986). In a second step of calculation, another table was used $L_8(2^7)$ which did not use the Ks_4 factor.

Preliminary studies (trial and error) helped us define the extrema:

- Ks_1^{min}=9 10^{-5} m s-1, Ks_1^{max}=15 10^{-5} m s^{-1}, l_1^{min}=3, l_1^{max}=5
- Ks_2^{min}=10 10^{-5} m s^{-1}, Ks_2^{max}=20 10^{-5} m s^{-1}, l_2^{min}=3, l_2^{max}=7
- Ks_3^{min}=5 10^{-5} m s^{-1}, Ks_3^{max}=10 10^{-5} m s^{-1}, l_3^{min}=2, l_3^{max}=4
- Ks_4^{min}=1.5 10^{-5} m s^{-1}, Ks_4^{max}=4 10^{-5} m s^{-1}, l_4^{min}=0.5, l_4^{max}=4

The simulated water contents were observed at t=1 hour and t=4.5 hours for layers 1 and 2, and at t=1.5 hour and t=4.5 hours for layer 3 and t=2.5 hour and t=4.5 hour for layer 4 (8 responses of water content). The first time of observation was different for layers 3 and 4 since a slight delay occurred before the discharge of these layers began.

C.1.6 Simulations

C.1.6.1 Efficiency of the simulations

For all simulations, the linear regressions of simulated against measured water contents were fitted at each observation depth. The efficiency of the simulation was evaluated through the sum of square of the simulated against the measured data. Two efficiency coefficients were defined:

$$EFF1_n = 1 - \frac{\sum_k \sum_t \left(\theta_{n,k,t}^{simulated} - \theta_{n,k,t}^{measured}\right)^2}{\underset{n}{Max}\left(\sum_k \sum_t \left(\theta_{n,k,t}^{simulated} - \theta_{n,k,t}^{measured}\right)^2\right)} \quad (53)$$

$$EFF2_n = 1 - \frac{\sum_k \sum_t \left(DM\theta_{n,k,t}^{simulated} - DM\theta_{n,k,t}^{measured}\right)^2}{\underset{n}{Max}\left(\sum_k \sum_t \left(DM\theta_{n,k,t}^{simulated} - DM\theta_{n,k,t}^{measured}\right)^2\right)} \quad (54)$$

with $DM\theta_{n,k,t} = \theta_{n,k,t} - \overline{\theta_{n,k}}$

where k are the monitored depths (15 cm, 50 cm, 150 cm, the 300 cm observation node is the lower boundary) and t the output times of the simulation, n indexes the performed simulation, $\theta_{n,k,t}$ are the measured and simulated water content for the simulation n, observation node k and time t and $\overline{\theta_{n,k}}$ is the average water content for all times t of the simulation n, observation node k. $\sum_k \sum_t \left(\theta_{n,k,t}^{simulated} - \theta_{n,k,t}^{measured}\right)^2$ is the sum of square errors for all layers k and times t of the simulation n. $\sum_k \sum_t \left(DM\theta_{n,k,t}^{simulated} - DM\theta_{n,k,t}^{measured}\right)^2$ is the sum of square errors of the deviation to the mean water content for all layers k and times t of the simulation n.

EFF1 and EFF2 were defined so that: $0 \leq EFF \leq 1$. A perfect fit is indicated by EFF1=EFF2=1, and the worst fit by EFF1=0 and/or EFF2=0. EFF2 was introduced to assess the efficiency of the fit regardless of the bias of the simulation. EFF1 and EFF2 were built as tools to help comparing the simulations within a given set of simulations (maxima defined within this simulation set) but do not allow comparing the simulations among different sets of simulations (different maxima).

C.1.6.2 CFP period: fit of the evaporation term

During this period, the transpiration term was null (no trees thus no uptake) and the water uptake from the soil profile by evapotranspiration was evaporation so. Evaporation parameters (EV_{max} and evaporation depth) were adjusted to optimize the simulations against the measured values on the first 33 days of the period (CFP1) when water content measurements were available.

Levels of maximum evaporation tested were $EV_{max} = f_{EV}\ ET_{max}$, with $f_{EV} \in \{0.1\ 0.2\ 0.3\ 0.4\ 0.5\ 0.6\ 0.7\ 0.8\ 0.9\ 1\}$. Evaporation depths tested were: $z_{EV} \in \{1\ 5\ 10\ 15\ 20\ 25\ 30\}$ in cm. All in all, 70 simulations were performed (Table 26).

C.1.6.3 BCF period: fit of the transpiration term

Table 26 Values tested for the input parameters regulating transpiration and evaporation fluxes in the model. Each parameter is presented in § C.1.1.

	Parameter	Tested values	Soil layer	Time period
Evaporation	f_{EV}	0.1 ; 0.2 ; 0.3 ; 0.4 ; 0.5 ; 0.6 ; 0.7 ; 0.8 ; 0.9 ; 1	common	CFP
	ψ_{dry}	-150 m	each	
	z_{EV} (cm)	1 ; 5 ; 10 ; 15 ; 20 ; 25 ; 30	common	
Transpiration	f_T	0.1 ; 0.2 ; 0.3 ; 0.4 ; 0.5 ; 0.6 ; 0.7 ; 0.8 ; 0.9 ; 1	common	BCF2
	p1	0.1 ; 2.5 ; 25	common	BCF1
	REW_0	0.1 ; 0.3 ; 0.5 ; 0.7 ; 0.9	common	
	f_i	0.8	common	
	ψ_f	0 m ; -1 m ; -150 m	each	
	ψ_{lim}	-150 m	each	
	rld	Eq 47	each cell	

The BCF period represents a pole of mature *Eucalyptus* with a closed canopy. Only a transpiration term was considered during this period, which was in fact the sum of an evaporative flux and a predominant transpiration flux. The level of maximum transpiration was adjusted during the BCF2 period when absolute pressure heads were < 1 m (rainy period, classically no regulation of the transpiration for these pressure heads). The maximum transpiration levels tested were of $T_{max} = f_T\ ET_{max}$, with $f_T \in \{0.1\ 0.2\ 0.3\ 0.4\ 0.5\ 0.6\ 0.7\ 0.8\ 0.9\ 1\}$ (Table 26).

The parameters regulating transpiration were subsequently optimized during the BCF1 period when few rainy events and very low pressure heads (drying) occurred, using the retained level of ET_{max}. The limit pressure head for which no more transpiration occur ψ_{lim}

was fixed at -150 m for all layers. Since the residual water content is reached for a pressure head of – 5 m, this means that the pressure head below which *Eucalyptus* uptake stops was entirely controlled by the reduction factor R_T and thus by the REW_0, p_1 and ψ_f parameters (Figure 30) and not by the ψ_{lim} parameter.

The parameters controlling the transpiration are more or less redundant and that is why ψ_{lim} was not optimized. Yet, altering ψ_f is the only way to introduce differences among soil layers in the regulation of the transpiration. ψ_f controls the threshold pressure head below which the transpiration is regulated by the R_T coefficient (Figure 30). ψ_f was optimized because *Eucalyptus* trees are reported to be very efficient in their water uptake and may uptake water down to very low pressure heads. Moreover, the retention curves for this soil type are steep and the classically used ψ_f=-1 m may underestimate the regulation threshold in terms of water contents (water content varying quickly with pressure head in this zone of the water retention curve).

Three values of ψ_f were tested: ψ_f [m] $\in$ {0 -1 -150} (Table 26). ψ_f=0 means that the transpiration is always regulated, ψ_f=-1 m corresponds to the soil field capacity and is the value classically used (Battaglia and Sands, 1997), and ψ_f=-150 m means that the transpiration is never regulated in the soil layer. ψ_f was also used to test the heterogeneity of the regulation among soil layers. This heterogeneity may result from an underestimation of the residual water content for deep soil layers which rarely dry, and/or from a preferential uptake in these deep and wet soil layers when the upper soil layers dry. The number of simulations was reduced considering that $|\psi_f|$ for a given soil layer was necessarily $\geq$ than $|\psi_f|$ of the soil layer right above.

The parameters controlling the regulation curve REW_0 and p_1 were also adjusted. The range of theoretical variations for REW_0 is [0 1] so that five evenly distributed values were tested: $REW_0 \in$ {0.1 0.3 0.5 0.7 0.9}. The theoretical range of variation of p_1 is [0 +∞[. 3 values were tested: $p_1 \in$ {0.5 2.5 25}, where 2.5 is the value used by Battaglia for other tree species (Battaglia and Sands, 1997) and 0.5 and 25 were used to test the effect of large modifications of this value (Table 26).

C.1.6.4 AP period: model validation

The AP period (after planting) was used to check the validity of the parameterization of both evaporation and transpiration parameters. This period corresponds to the first two years of growth of the newly planted *Eucalyptus* stand.

Since T_{max} for the 6-months-old *Eucalyptus* trees must be less than T_{max} after canopy closure at 12 months after planting, T_{max} needed to be reduced by a function of the stand growth. As transpiration is reported to vary with leaf area index (LAI) (Granier et al., 1999b; Stape et al., 2004; Whitehead and Beadle, 2004), LAI was used to reduce T_{max} input in the model.

Even if the mathematical dimension of leaf surface (from which LAI is derived) is an area (m^2), leaves grow on tree in the three dimensions of space. Supposing that the water uptake by the trees (and thus tree growth) may be modelled by a one-dimension function, LAI would then be related to the cube of this function. A simple reduction function of $(LAI)^{1/3}$ fitted on the data presented in part A was thus tested to reduce T_{max} during the AP period:

$$T_{\max}(t) = RF(LAI)\ T_{\max}^{AP} \tag{55}$$

$$RF\left(LAI\right) = \frac{LAI^{1/3}}{Max\left(LAI^{1/3}\right)} \tag{56}$$

where RF(LAI) ($0 \leq RF(LAI) \leq 1$) is the reduction function of the transpiration term (Figure 33) and $T_{\max}^{AP}$ the maximum level of transpiration for a reduction of factor of 1 during the AP period. The resulting function was in good agreement with similar observations made by Granier *et al.* (2007; 1999b).

Since the new stand was more efficiently fertilized than the BCF one, the LAI for the AP period were greater than that for the BCF one. The reduction curve of Figure 33 gives the RF factor corresponding to the LAI of the BCF period. $T_{\max}^{AP}$ was then calculated as:

$$T_{\max}^{AP} = \frac{RF(LAI_{BCF})}{T_{\max}^{BCF}} \tag{57}$$

The evaporation term was considered to decrease linearly from the planting (EV_{max} parameterized during the CFP period) to the canopy closure occurring at 12 months old ($EV_{max}=0$).

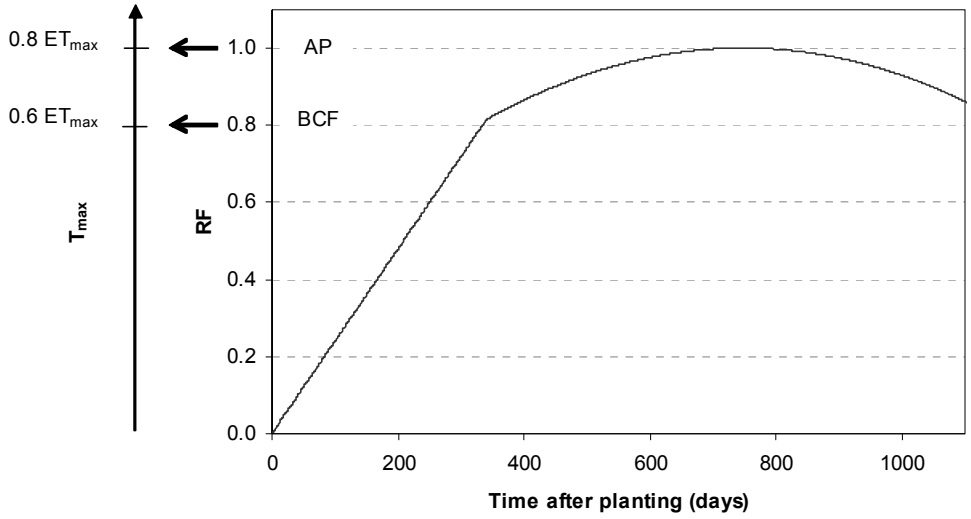

Figure 33 Time course of the RF factor (eq. (55) & (56)) reducing the maximum transpiration (T_{max}) over the AP period. The corresponding T_{max} for the BCF and the AP periods are given.

C.1.6.5 Sensitivity tests

The model sensitivity to soil hydraulic parameters, boundaries and initial conditions was tested on the CFP period (no *Eucalyptus*) with the evaporation term set to zero. Table 27 gives the values of each input parameter or variable. Each one of these values was tested with all other variables and parameters set to its average value. The range of variation of water contents (θ_a) (and of their derived pressure heads ψ_a) was set to $\theta_a \pm 1$ %. The rainfall (Pi) range of variation was set to Pi ± 0.25 Pi. The Ks range of variation for the 0-5 cm layer was Ks/2<Ks<2Ks. For all other soil hydraulic parameters, the range of variation was taken as ± 10% of the parameter value for the 0-5 cm layer.

For water content and rainfall, the range of variation corresponded to the average variability observed in the experimental data sets (C.2.2). For other parameters, it was difficult to assess the variability which may be expected and the range of variation of ± 10% was arbitrary tested. For Ks, the literature reports differences of up to ten times when measured by different experimental methods (Reynolds et al., 2002). The range of variation was thus broadened to [Ks/2 2 Ks].

Table 27 Parameter values used for the sensitivity tests. The parameters are explained in (§ C.1.1.4).

Studied parameters		Lower value	Average value	Upper value	Observations
Boundaries	Upper: inflow	0.75 Pi	Pi	1.25 Pi	0 cm
	Lower: pressure head	$\psi_a(\theta_a(300cm)-1)$	$\psi_a(\theta_a(300cm))$	$\psi_a(\theta_a(300cm)-1))$	300 cm
Initial condition	Pressure head	$\psi_a(\theta_a-1)$	$\psi_a(\theta_a)$	$\psi_a(\theta_a+1)$	All layers
Soil hydraulic parameters	Retention curve parameters	0.9 α	α	1.1 α	0-30 cm layer
		0.9 n	n	1.1 n	
		θ_{ra}-1	θ_{ra}	θ_{ra}+1	
		θ_{sa}-1	θ_{sa}	θ_{sa}+1	
	Velocity parameters	0.5 Ks	Ks	2 Ks	
		0.9 l	l	1.1 l	

C.2 RESULTS AND DISCUSSION

C.2.1 Time dependant inputs: inflow at the soil surface, maximum evaporation and maximum transpiration

C.2.1.1 Meteorological data

In total, 34 months were monitored during the studied period (8 months before clear felling, two years of growth after planting and 3 months between clear felling and planting). The annual mean temperature was about 19°C for years 2003, 2004 and 2005, which is the average temperature classically recorded since 1990 in the area. The annual precipitation was 1320 mm in year 2003, 1082 mm in year 2004, and 1400 mm during year 2005. In 2003 and 2004, the rainfall was about the same as classically recorded since 1990 (about 1370 mm) but year 2004 was dryer, especially during the winter (from June to September).

The average daily rainfall event was 7.64 mm but could reach up to 100 mm (Figure 34). The dry months presented colder temperature (average of 15°C and minimum below 5°C) in May, June, July and August. The rainy season presented greater rainfall (between 100 and 150 mm) and warmer temperature (average beyond 20°C) from October to February.

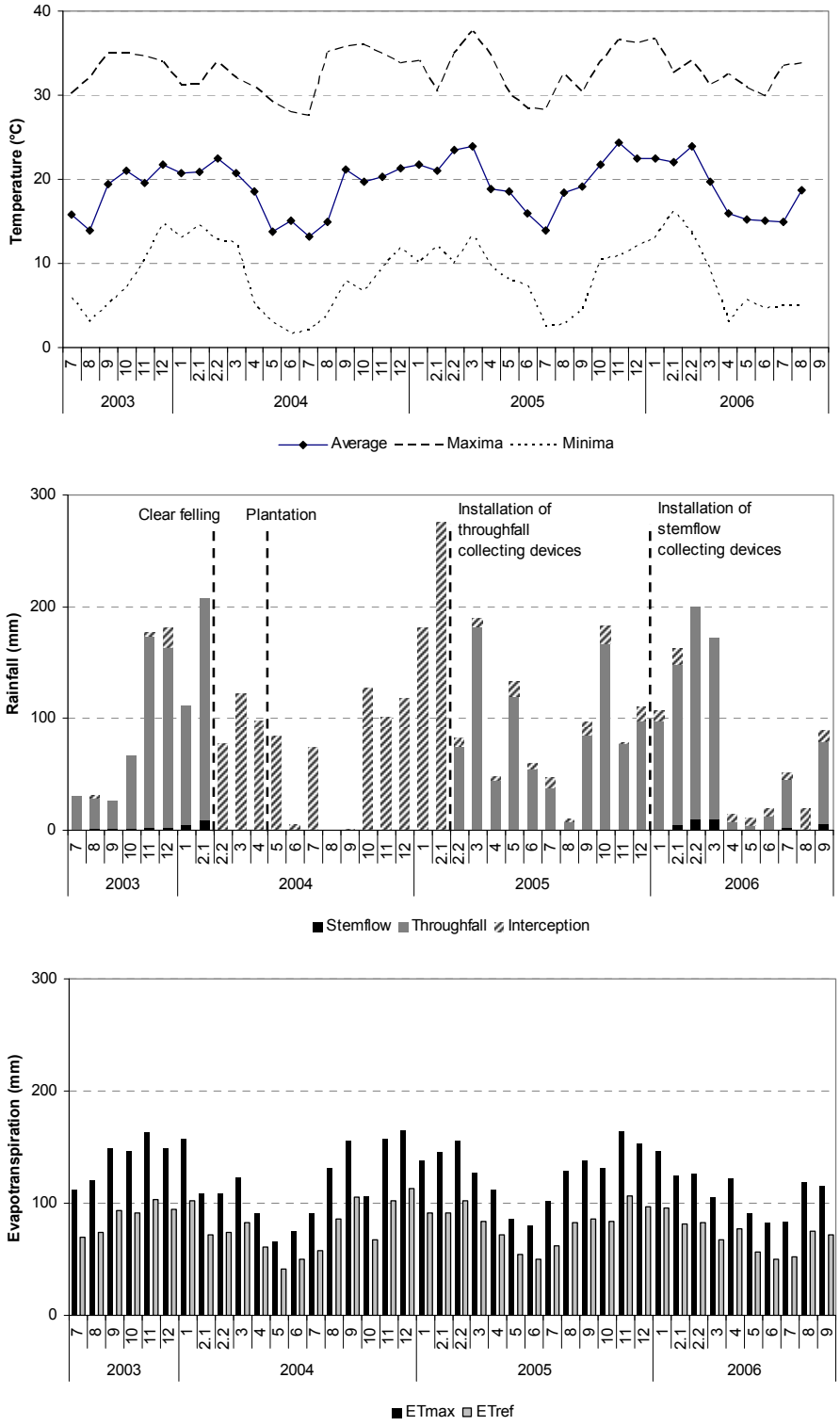

Figure 34 Time course of temperature, rainfall and evapotranspiration (ET) over the time of the experiment. The rainfall partition between stemflow, throughfall and interception is given. From 02/2004 to 02/2005, interception represents rainfall since throughfall was not monitored during this period (young *Eucalyptus* trees). The maximum evapotranspiration (ET_{max}) and the FAO reference evapotranspiration (ET_{ref}) are given.

The calculated evapotranspirations (ET_{max} and ET_{ref}) were minima in May and June during the dry and cold months with values of about 50 to 70 mm month^{-1} for ET_{ref} and ET_{max} (Figure 34). They were maxima during the wet and warm months with values reaching 110 mm month^{-1} for ET_{ref} and 170 mm month^{-1} for ET_{max}. Daily ET_{max} was in average 4.38 mm day^{-1} and ET_{ref} 2.81 mm day^{-1}. ET_{ref} was linearly correlated to ET_{max} (r^2 = 0.98) and was about 64 % of ET_{max}.

The calculated evapotranspirations were of the same order of magnitude than the rainfall during the wet months and largely greater than rainfall during the dry season. In the presence of vegetation, the drainage is thus expected to be limited, especially during the dry months when soil drying is to be expected.

C.2.1.2 Root length density

The fitted parameters for equation (47) describing the root length density repartition with depth for the different time periods are given in Table 28. Figure 35 shows the fitted function against the measured data at the end of the rotation of the old *Eucalyptus* stand (BCF period).

Table 28 Parameters of the root length density model over the studied period.

Period	age (months)	a_{rld}	b_{rld}	c_{rld}
BCF	72	0.018	0.982	0.054
AP	4	0.045	0.955	0.049
	6	0.044	0.956	0.054
	12	0.081	0.919	0.048
	22	0.051	0.948	0.058
	average	0.055	0.945	0.052

For the new stand planted in 2004 (AP period), the fitted curves once normalized were more or less the same for all ages so that only an average curve was used as input for the simulations.

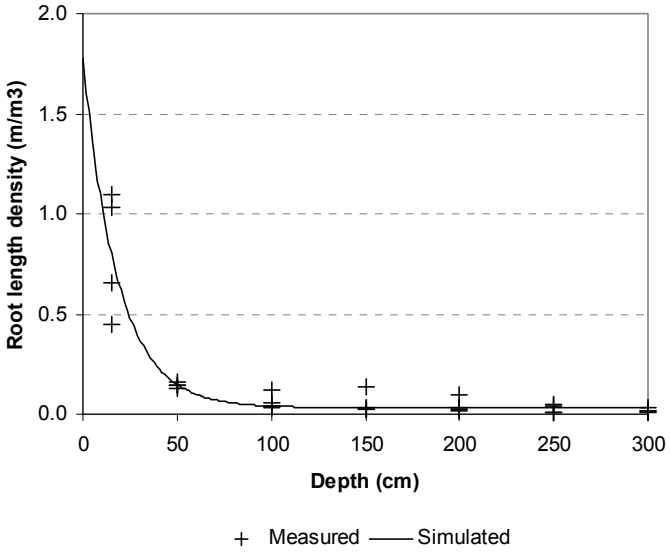

Figure 35 Root length density measured and simulated (eq. (47)) at the end of the previous stand rotation (BCF period, age 72 months).

C.2.1.3 Inflow at the upper boundary of the soil profile

The calculations of this section (material and methods and results) are detailed in ANNEX 4. Only the main conclusions are recalled here.

The linear regression simulated the on-site weekly rainfall from the reference rainfall located at 2 km of the experiment with a root mean square error (RMSE) of 7.36 mm. In average, the simulated Pi differed of about 25 % from the measured one for rainfall > 2 mm.

The rate of throughfall was constant above a threshold rainfall of 10 mm at about 98 % of rainfall before clear felling and 87 % of rainfall after planting. This decrease corresponds to greater LAI in the newly planted stand than in the old one before it was clear felled. Around the threshold of 10 mm, a few rates of throughfall > 100 % (up to 120-140 %) might result from the spatial variability between rainfall in the experiment and the adjacent open area where Pi was recorded (located about 300 m apart) and/or from a concentration of rainfall by tree foliage above the collectors. This pattern was already observed in forest ecosystems (Konishi et al., 2006) for which throughfall is classically reported to show a large degree of temporal and spatial variability generally greater within a particular vegetation than among different cover types (Levia and Frost, 2006). The root mean square errors of the regressions used to simulate the rate of throughfall from daily estimated rainfall were about 16 %. No significant difference among plots (before clear

felling) and among treatments (after planting) was observed. This is in good agreement with the homogeneity of the LAI observed among the different treatments once the canopy closed (about age 12 months, when the monitoring of throughfall started).

The stemflow volume collected on individual trees was less for small trees and low rainfall intensity and greatest at a constant value of about 37 L $week^{-1}$ for circumference at breast height (CBH) > 8 cm and rainfall > 50 mm. In-between, the stemflow increased together with CBH and rainfall intensity. Daily stemflow for each tree of the experiment was estimated from its CBH at the latest inventory and from the daily estimated rainfall using a mathematical function fitted on weekly stemflows and rainfall. This model presented root mean square error of 3.084 L and was more efficient to simulate the stemflows when they were > 10 L (average collected volume for all collectors during the studied period). If all trees in the stand collected the same volume of water, this would correspond to a threshold of 1.7 mm of water collected and to a RMSE of 0.514 mm. The stemflow in mm was obtained for each plot by summing daily stemflow estimated for each tree, divided by the plot area. A significant effect of the treatment was observed after clear felling but this effect was limited (the simulated stemflow differed less than 0.24 mm among treatments). The stemflow (in mm) was greater before clear felling (about 3.37 % of rainfall) than after planting between age 20 and 27 months (about 2.62% of rainfall).

Surface runoff was in average 0.16 % of rainfall and was neglected in the calculation of P_{soil}.

The rates of throughfall and stemflows are in good agreement with the literature for *Eucalyptus* plantations in tropical ecosystems (Crockford and Khanna, 1997; Johnson and Lehmann, 2006; Levia and Frost, 2003; Levia and Frost, 2006).

C.2.2 Soil water monitoring

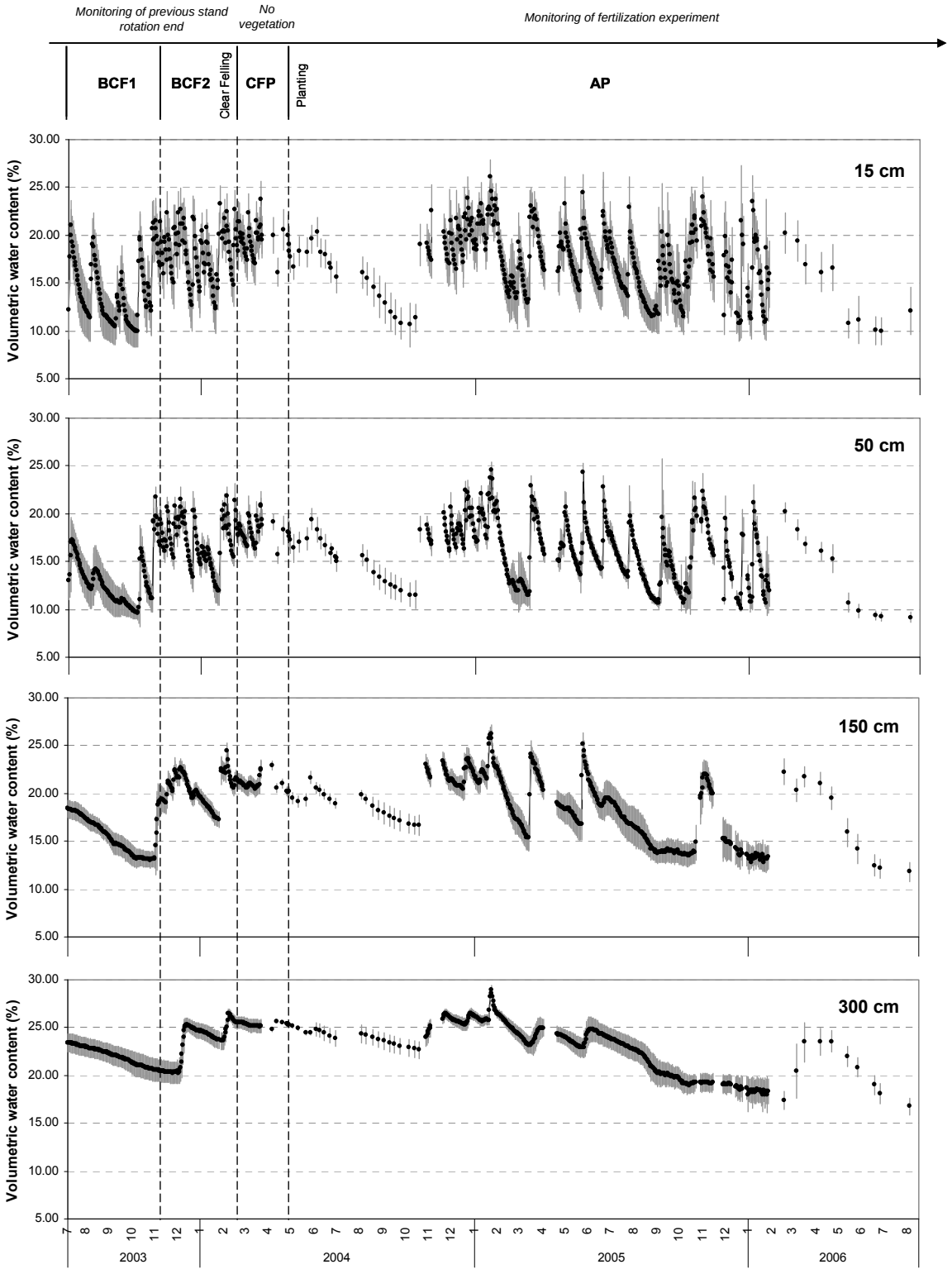

Figure 36 Time course of the volumetric water content (%) measured on-site at the depths of 15 cm, 50 cm, 150 cm and 300 cm over the studied period. The average value (black dots) and the standard deviation for n≥3 (grey lines) are represented.

The volumetric water content measured by the TDR equipment behaved distinctly depending on the studied period (Figure 36):

- Period BCF1: dry season (July 2003) characterized by few rainy events, a great transpiration of the Eucalyptus trees, and very low water contents (about 10% at the depths of 15 and 50 cm, about 13% at 150 cm and about 20% at 300 cm).
- Period BCF2: large tree transpiration together with large rainfall amount resulting in a broad range of volumetric water contents. At a depth of 300 cm, the water content increased from 20 % during the BCF1 period to 25 %. The maxima values observed were about 22 % at a depth of 50 cm and about 25 % at 15, 150 and 300 cm.
- Period CFP: no transpiring vegetation together with moderate rainfall and high soil evaporation resulting in a limited range of variations of the volumetric water contents (about 5% for layers 1, 2 and 3 and almost constant for layer 4) which remained close to the maxima values observed during the BCF2 period. The first 33 days (CFP1) were monitored daily in all treatments. The last 30 days (CFP2) were monitored weekly only in treatment 3 due a failure in the TDR system.
- Period AP: increasing transpiration of the fast growing Eucalyptus trees (newly planted stand), and successive dry and rainy season. During the first and last 6 months, the volumetric water contents were monitored weekly due to a failure in the TDR equipment. In between, the water contents were monitored daily and reached a broad range of water content values (about 15% for all soil layers). The maxima water contents were about the same as during the BCF1 period. Very dry values of water contents (about the minima reached during the BCF1 period, even drier values down to about 17% for layer 4) were observed from age 1 year to 2 years.

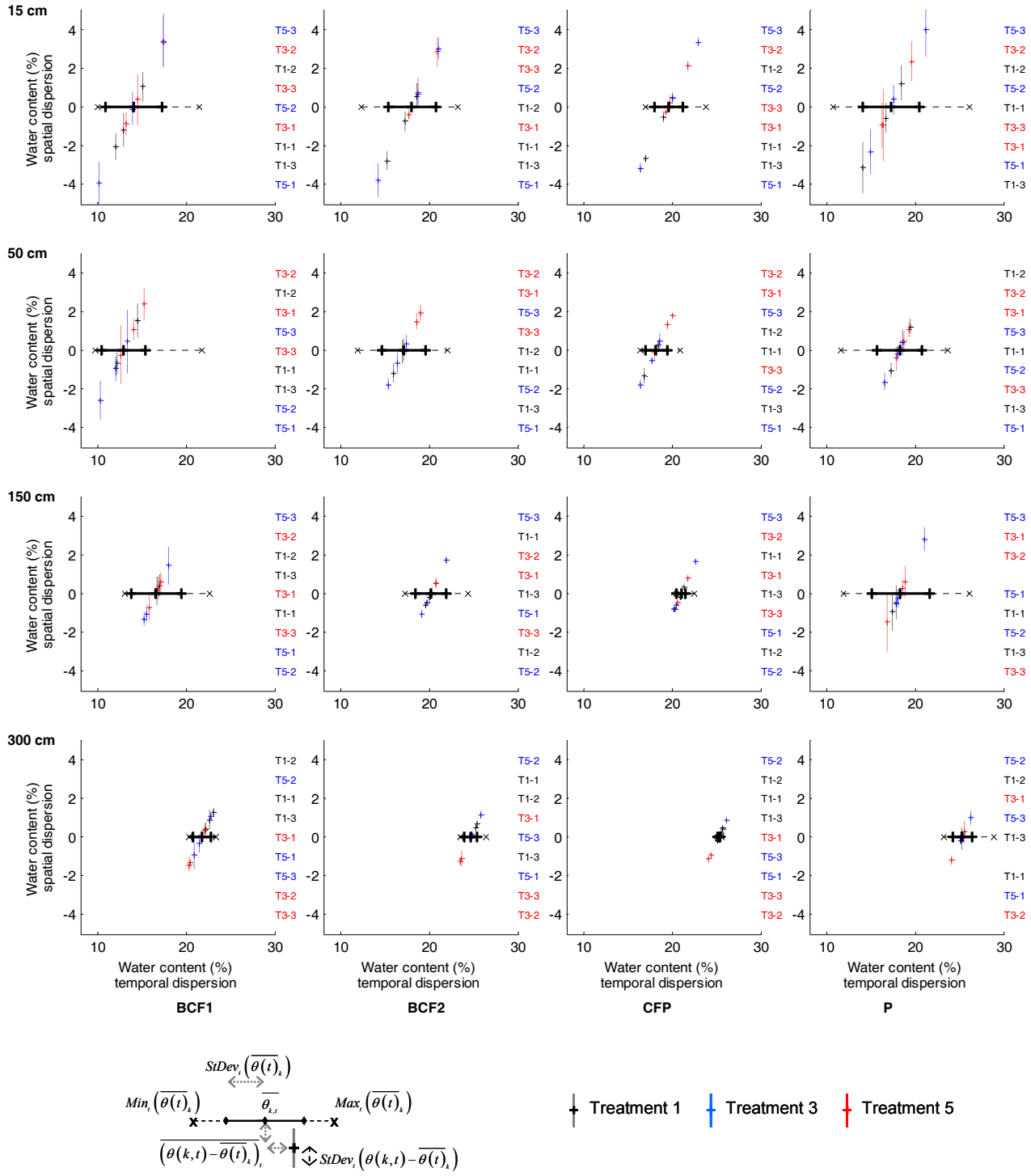

Figure 37 Dispersion in time and space of the volumetric water content (%) measured at the depths of 15 cm, 50 cm, 150 cm and 300 cm in treatments 1, 3 and 5. The dispersion in time is given by the time course of the average water content for all probes k ($\overline{\theta(t)_k}$): the maximum (Max), minimum (Min), and mean ($\overline{\theta_{k,t}}$) values are represented together with the standard deviation (StDev) in abscissa. The dispersion in space is given by the time course of the difference between the water content measured for a given probe k ($\theta_{k,t}$) and the average water content $\overline{\theta(t)_k}$ for all probes k: the mean value and the standard deviation are represented in ordinate. For better reading, the order of appearance of each probe k is indicated on the right of each plot: for example T1-1 indicates the probe located in treatment (T) 1 block 1.

Maxima, minima and average values reached during each period are represented on the temporal dispersion axis of Figure 37. Figure 37 shows that the range of variation of water contents (average for all TDR probes $\overline{\theta(t)_k}$) was broadest during the AP period and narrowest during the CFP one. The range of water contents reached during the experimental period changed to wetter water contents with increasing depth.

When the soil profile was wet and the transpiration low (CFP period more specifically), the water brought by rainfall was drained within 1 day down to a depth of 3 m. Water content peaks following rainfall were distinctly visible on Figure 36 at the depths of 15 cm and 50 cm. At a depth of 150 cm, some rainfall drainage events were no more visible especially when the layer was dry before the rainfall occurred and during periods of intensive transpiration. At a depth of 300 cm, few peaks of water content were observed following rainfall events. These peaks occurred mainly during the wet seasons. This pattern resulted in Figure 37 in narrower ranges of variation of water contents (average for all TDR probes $\overline{\theta(t)_k}$) with increasing depth (range of variation < 5% at a depth of 3 m).

The spatial dispersion of the measured water contents decreased with depth: the water content measured in average for the whole period for a given probe k ($\overline{\theta(k)_t}$) varied from its average ($\theta_{k,t}$) of about ± 4% at 15 cm, 2.6 % at 50 cm, 1.7 % at 150 cm and 1.5 % at 300 cm ($\overline{\left(\theta(k,t)-\overline{\theta(t)_k}\right)_t}$ on Figure 37). This spatial dispersion was more or less constant in time for a given probe k and is represented on Figure 37 by the vertical bars $StDev_t\left(\theta(k,t)-\overline{\theta(t)_k}\right)$. This difference between $\theta_{k,t}$ and $\overline{\theta(k)_t}$ (average for all probes) varied more in time when the temporal dispersion of θ was greatest, that is during the BCF1 and AP periods and for layers 1 and 2. Least variations were recorded when the temporal dispersion of θ was least, that is, during the CFP period and for layer 4. It is thus suggested that the water content measured by a given probe is more or less a translation of the average signal for all probes. The magnitude of the translation increased with decreasing depth. Slight distortion of the average signal for a given probe k occurs when the temporal dispersion of the water contents increases.

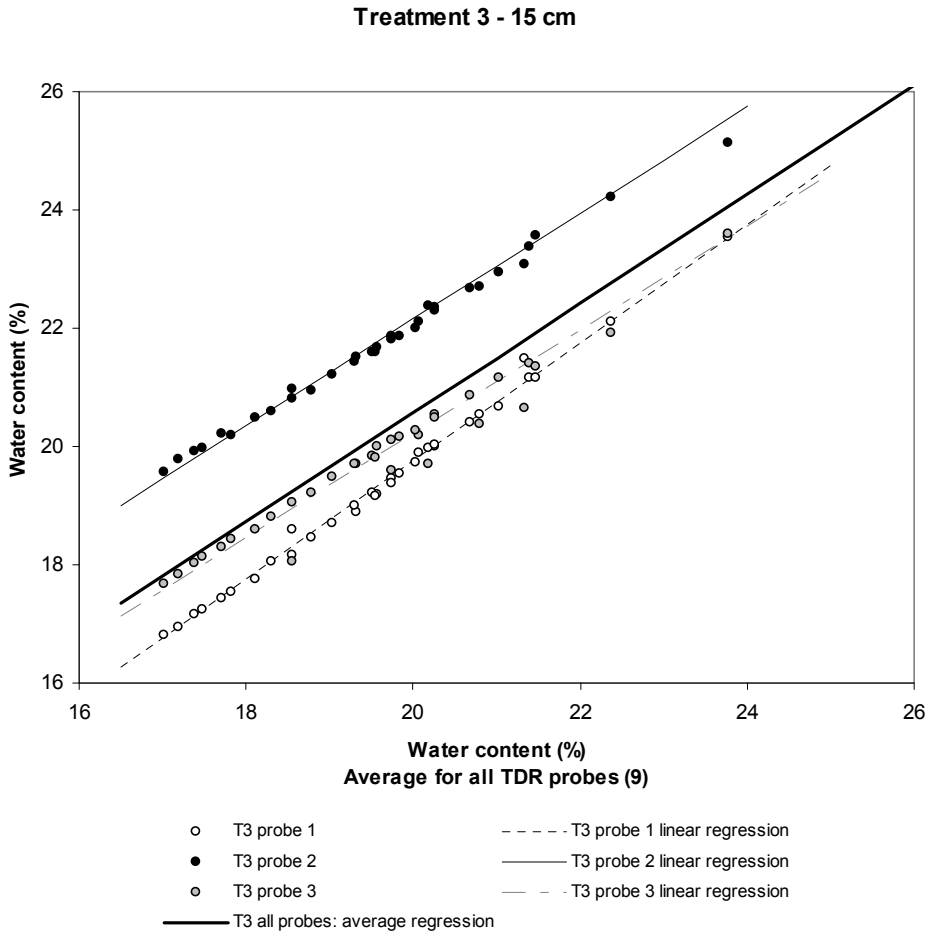

Figure 38 Volumetric water content (%) measured at a depth of 15 cm by the three TDR probes of treatment 3 as a function of the volumetric water content measured in average for all TDR probes of T3 at a depth of 15 cm. The fitted linear regressions are represented.

The water contents measured for a given probe k were linearly related to the average water content for all probes k (Figure 38 for treatment 3). The R-square of these regressions were > 0.95 in most cases (ANNEX 5). Their slope varied from 0.8 to 1.2 and could be set common to all periods for a given probe. The intercept for a given probe (magnitude of the translation) varied according to the time period but its order of magnitude remained the same. The effects of the probe location (treatment, replicate and depth) and of the time period tested by ANOVA analysis on the intercepts of the regressions were not significant at a 5% threshold.

Table 29 Volumetric water content measured by the TDR probes in treatment 3 and by soil sampling next to the TDR location.

Depth	Volumetric water content		
	TDR	Soil sampling	difference
		%	
15 cm	17.1	16.7	0.4
50 cm	15.5	15.7	-0.2
	15.2	17.2	-2.0
	12.5	12.9	-0.4
150 m	15.6	16.0	-0.4
	14.8	16.4	-1.6
	14.9	16.1	-1.2
300 cm	24.4	21.6	2.8
	24.7	19.5	5.3
	23.8	22.6	1.3

When the TDR system was installed, the water content measured by each probe in water and in air was checked. In treatment 3, soil was sampled next to each TDR probe and the water content of the soil sample was measured. The differences between the water content measured by the TDR probes and by direct sampling ranged from -1.6% to 5.3% and the mean absolute difference was in average 1.6% (Table 29). These ranges of variation are of the same order of magnitude as the biases observed in the water contents measured in situ and may be the result of spatial heterogeneity between the probe and the sampling location, of the bulk density measurement accuracy, and/or of the probe calibration.

Variations of the TDR signal are reported to be highly dependant on the contact surface between the soil matrix and the probe. In particular the air gaps around electrodes may cause serious errors while determining soil moisture (Noborio, 2001). This author reports a standard deviation of 2.5% in soil moisture measured at a depth of 2.5 cm. This may explain the observed heterogeneities in the measured water contents, in particular for the upper soil layers which are sandier than the deeper ones. The fact that the spatial dispersion decreases with depth whereas the differences observed in Table 29 tend to increase with depth (and thus with bulk density) would suggest that the observed translations are more the result of spatial heterogeneities than of calibration biases. Moreover, the spatial variability of fine root density in the studied stand was much greater in the upper layer than in deep soil layers (Jourdan et al., 2008). Tommaselli and Bachi (2001) also showed that the TRASE system calibration needed to be corrected for most

brazilian soils but that it was accurate for our soil type within the measured range of water contents (< 30 %).

C.2.3 Conclusions on the spatial heterogeneity of inputs and validation data sets used in the model

Aboveground water collectors seemed to work efficiently above a threshold of collected water of 2 mm. A good description of water fluxes for rainfall events < 2 mm may not be expected for the present model.

P_{soil} was mainly made of throughfall (98 % before clear felling and 87% after planting) for which the intra-plot variability was always superior to the inter-plot variability (block or treatment effect). The rate of throughfall varied of about 25% around its average from one collector to another. Little water reached the soil by stemflow (3.4% before clear felling and 2.62 % after planting) but this flux may induce great heterogeneity in the studied plot since it concentrates water next to tree stems. All these fluxes were estimated at a daily time step from a regression simulating on-site rainfall from rainfall recorded daily 2 km far from the experimental site. 25 % of error may be expected on average for this regression. A great heterogeneity of the water contents issued from an heterogeneity of the upper boundary flux is thus to be expected at the tree scale.

It is difficult to assess whether the transpiration flux may vary from one treatment to another. The dynamics of leaf area development suggest that trees may take up less water in T1 and T5 than in T3 during the first year of growth. However, belowground biomasses were not significantly different among the three treatments. The water contents measured on-site could have confirmed the hypothetical differences in water uptake among treatments, but once again, the intra-plot variability was far more than the inter-plot variability and no significant effect of treatments on water contents could be observed.

It was thus decided to focus our study on the parameterization of a single average model at the plot scale and to test the effect of the variability of the upper boundary inflow through sensitivity tests. To avoid the errors of parameterization due to differences in the water contents measured in one plot or another, all parameterizations were performed on the data of treatment 3 where soil hydraulic parameters were calculated (internal drainage experiment).

C.2.4 Soil hydraulic parameters

C.2.4.1 Retention curves

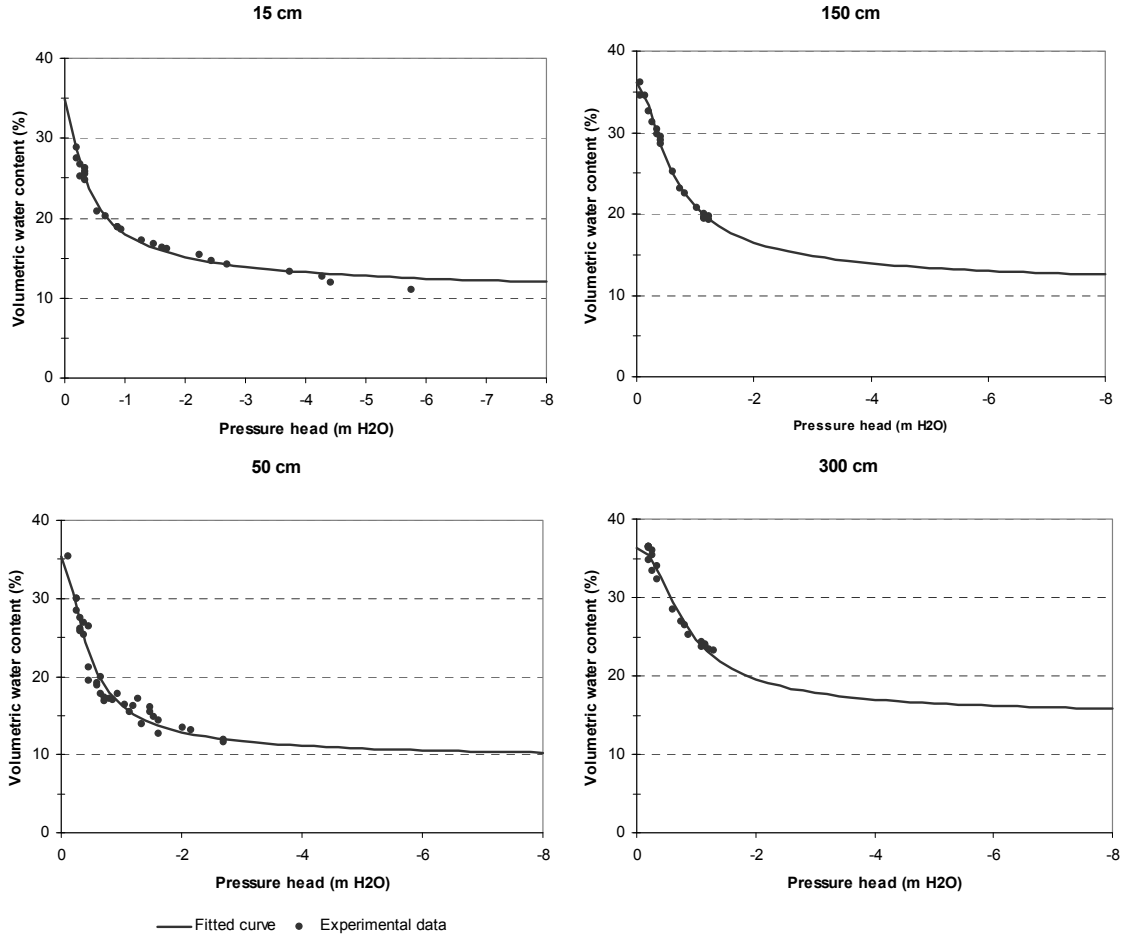

Figure 39 Volumetric water content (%) as a function of pressure head (m) at each monitored depth: the fitted retention curve (eq. (29)) and the experimental data recorded during the water drainage experiment are represented.

Table 30 Soil hydraulic parameters fitted from the water contents and the pressure heads experimentally recorded during the water drainage experiment. The parameters are explained in § C.1.1.3.

	Retention curve					Velocity parameters		
Depth	θ_r	θ_s	α	n	*R-square*	Ks	l	*R-square*
cm	*m^3 solution / m^3 sol*		*m^{-1}*	-		*m s^{-1}*	-	
0-30	0.099	0.349	5.38	1.6520	*0.987*	13.3 10^{-5}	4.28	*1.000*
30-70	0.094	0.354	3.50	2.0264	*0.953*	15.8 10^{-5}	5.34	*1.000*
70-230	0.117	0.362	2.62	1.9511	*0.995*	9.9 10^{-5}	3.37	*0.997*
230-300	0.167	0.363	1.76	2.3618	*0.979*	2.0 10^{-5}	2.25	*Lower boundary*

The retention curves showed a great homogeneity among soil layers. The calculated parameters progressively changed from the upper soil layer (0-30 cm) down to the deepest soil layer (230-300 cm) (Figure 39). The water content at saturation (θ_s) was more or less constant at about 35-36% whatever the soil layer (Table 30). The water content decrease with decreasing pressure head was slower with increasing depth (α and n of Table 30), except for the 30-70 cm for which the decrease was faster than for the 0-30 cm layer. The residual saturation (θ_r) increased with soil depth from 9.9 % for the 0-5 cm layer to 16.7 % at a depth of 300 cm.

The R-square of the water retention curve adjustments were > 0.95 (Table 30). The range of pressure heads reached during the water drainage experiment corresponds to the beginning of the retention curve where the curve is the sharpest (Figure 39) so that the parameters fitted for the deeper soil layers (100 cm and 300 cm) were highly dependant upon the residual water content θ_r. For this purpose, θ_r was not fitted together with the other parameters as explained in the material & methods section, but was calculated from the TDR measurements recorded all over the monitored period. Still, a doubt remains whether the lowest water contents reached during this period actually represents the residual water content, especially for deep soil layers.

C.2.4.2 Hydraulic conductivity

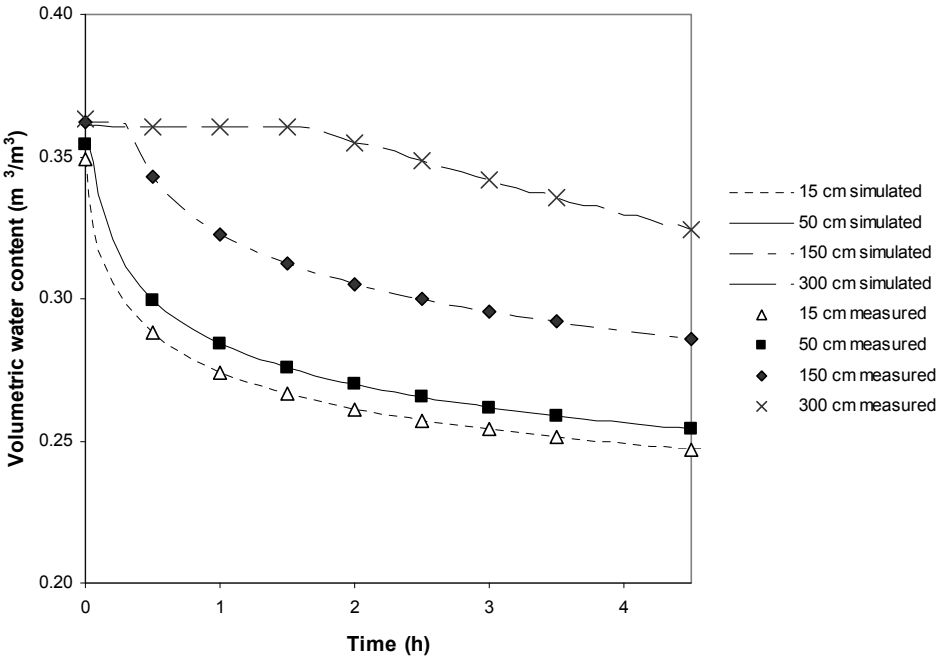

Figure 40 Volumetric water content in the first 4.5 hours of the water drainage experiment at each monitored depth: data measured during the experiment and simulated by MIN3P after DOE resolution of the Ks and l parameters for each monitored depth.

The resolution of the DOE matrix system needed to be performed in two steps. When fixing the pressure head at a depth of 3 m (lower boundary), the simulated water content at a depth of 3 m equaled the measured one and $\theta_{t,4}$ cannot be used in the resolution of the matrix problem. Tests were performed trying to replace $\theta_{t,4}$ by θ_t of layers 3 and 2 and revealed a high correlation between Ks_3 and Ks_4. Ks_4 actually controls the delay before layer 3 begins to discharge. This preliminary study also revealed that the l_4 parameter could not be determined with accuracy since it controls the convexity of the discharge curve and the time of the experiment was too short to observe it.

These two difficulties were overlapped by solving the matrix system with the lower boundary of layer 4 fixed at a depth of 6 m (more degree of freedom for layer 4). This resolution was not very efficient for layers 1, 2 and 3 but allowed the determination of Ks_4. It also confirmed the non-dependency of layers 1 and 2 to layer 4, and of layers 1, 2 and 3 to l_4. Thus, the independent determination of Ks_4 and l_4 may not affect much the determination of the other factors, providing the fact that the determined value of Ks_4

should allow a correct determination of Ks_3. l_4 was manually adjusted using t values > 4.5 hours recorded after the end of the experiment.

The resolution of the matrix for layers 1, 2 and 3 using pre-determined values of Ks_4 and l_4 was efficient in simulating the experimentally measured water contents of the drainage experiment (Figure 40). It also confirmed the independency of layers 1, 2 and 3, since no interactions needed to be introduced in the linear model. The correct discharge of layer 3 (Figure 40) validated the pre-determination of Ks_4.

The Ks and l thus calculated confirmed the trends observed for the retention curve parameters (Table 30). They indicated that the discharge of the soil layers was slower when the depth increased with Ks decreasing from 3.3 10^{-5} m s^{-1} for the 0-5 cm layer to 2 10^{-5} m s^{-1} for the 230-300 cm layer and l from 4.28 (0-5 cm) to 2.5 (230-300 cm). The 30-70 cm layer showed a particular behavior since its discharge was faster than the 0-30 cm layer with Ks of 15.8 10^{-5} m s^{-1} and l of 5.34. The resolution of the DOE matrix suggested that the problem was over parameterized since it was impossible to solve layer 4 together with the other layers. One possibility would have been to integrate layer 4 into layer 3 but as already mentioned before, the water contents experimentally measured indicated permanent wetter conditions at this depth. The Ks obtained after the DOE resolution would confirm that the hydraulic conductivity was slower in this deep soil layer compared to the other soil layers since Ks_4 was < 20 % of $Ks_{1, 2 \& 3}$.

C.2.5 Simulations

C.2.5.1 CFP simulations: fit of the evaporation parameters

The CFP simulation period was only 33 day-long so that the pool of simulated against measured data was small. The absence of water uptake by trees during this period led to a narrow range of water contents reached during the simulations.

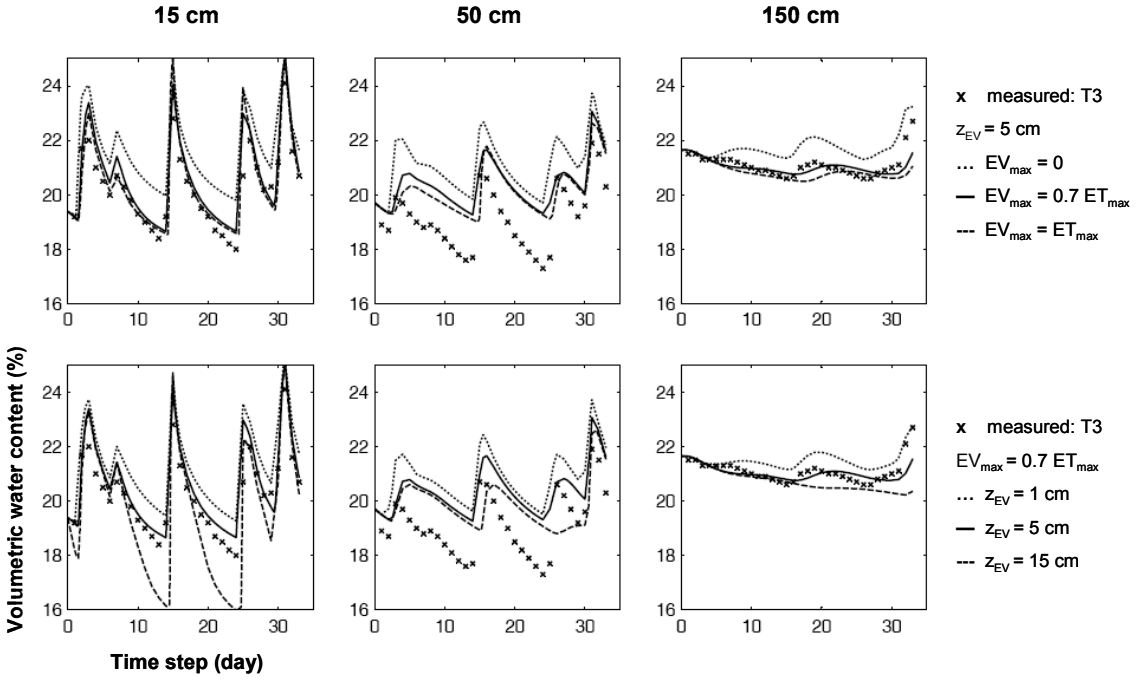

Figure 41 Influence of the evaporation maximum intensity EV_{max} (EV_{max}= f_{EV} ET_{max}) and depth (z_{EV}) on the simulated volumetric water content in treatment 3. The values kept for further simulations were f_{EV}=0.7 and z_{EV}=5 cm.

Optimizing the evaporation depth and level did improve the simulations of the CFP period. In particular, it translated the curve simulated at a depth 15 cm down to the measured one (Figure 41). At a depth of 50 cm, it was impossible to reduce the gap between simulated and measured data especially for low water content values (simulated value always greater of about 2 % than the measured one) without omitting peaks of water contents following rainfall or altering the efficiency of the simulation for the 0-30 cm layer. At a depth of 150 cm, the range of water contents reached during the simulations was narrow (< 2 %) so that the simulation efficiency was less dependant on the evaporation parameters for this soil layer. The delay of reload of this soil layer was directly the consequence of the behavior of the simulation at a depth of 50 cm.

Table 31 Efficiency of the simulations through EFF1 and EFF2 coefficients (eq (53) & (54)) for the CFP period. The best simulations are in bold. The simulation kept for the rest of the study is underlined. The maximum sum of square errors recorded for all simulations (SSEmax) and the duration of the simulations (t_{tot} in days) are indicated. f_{EV} defines the maximum evaporation EV_{max} (EV_{max}= f_{EV} ET_{max}) and z_{EV} the depth down to which evaporation occurs.

	EFF1								**EFF2**							
Reference data set = measured water content, t_{tot} = 33 days																
SSEmin				346								79				
SSEmax				2172								585				
z_{EV} (cm) / f_{EV}	**0**	**1**	**5**	**10**	**15**	**20**	**25**	**30**	**0**	**1**	**5**	**10**	**15**	**20**	**25**	**30**
0	0.62								**0.84**							
0.1		0.68	0.69	0.69	0.70	0.70	0.69	0.69		0.83	0.82	0.82	0.82	0.82	0.82	0.82
0.2		0.71	0.75	0.75	0.76	0.76	0.76	0.76		0.82	0.81	0.80	0.79	0.79	0.79	0.80
0.3		0.72	0.79	0.80	0.81	0.80	0.81	0.81		0.82	0.79	0.77	0.75	0.74	0.75	0.77
0.4		0.72	0.81	0.81	0.83	0.78	0.81	0.83		0.82	0.77	0.75	0.70	0.67	0.70	0.72
0.5		0.72	0.82	0.83	0.81	0.72	0.77	0.81		0.82	0.76	0.73	0.66	0.58	0.62	0.66
0.6		0.72	0.83	0.85	0.81	0.61	0.70	0.76		0.82	0.75	0.71	0.61	0.46	0.52	0.58
0.7		0.72	**0.86**	**0.86**	0.80	0.47	0.59	0.69		0.82	0.74	0.69	0.57	0.34	0.41	0.49
0.8		0.72	0.85	**0.86**	0.78	0.34	0.41	0.54		0.82	0.73	0.67	0.52	0.23	0.27	0.36
0.9		0.72	**0.86**	**0.86**	0.74	0.19	0.27	0.35		0.82	0.72	0.65	0.47	0.12	0.16	0.20
1		0.72	**0.87**	0.85	0.68	0.00	0.07	0.12		0.82	0.71	0.62	0.42	0.00	0.02	0.05

The most efficient simulations according to EFF1 were obtained for evaporation levels > 0.5 ET_{max} and evaporation depths of 5 or 10 cm (Table 31). The most efficient simulations according to EFF2 were obtained when the evaporation was minimum (z_{EV}=0 to 1 cm). The differences between EFF1 and EFF2 indicated that the simulation for which evaporation was null was mainly a translation of the experimentally measured data (best fit according to EFF2). Introducing evaporation in the simulations reduced this offset at the depths of 15 cm and 150 cm. When trying to reduce the offset at a depth of 50 cm by increasing the evaporation (best fit according to EFF1 for f_{EV}=1 and z_{EV}=5 cm), the shape of the simulated water content simulated was altered (mainly omission or delay of the peaks of water contents following rainfall) resulting in poorer EFF2 coefficients. The simulation performed with z_{EV}=5 cm and f_{EV}=0.7 was the one which maximized EFF1 and EFF2 and was thus kept as best fit. For this fit, the simulation reproduced fairly well the experimental data at the depths of 15 cm and 150 cm, but a bias of about 2 % remained at a depth of 50 cm (Figure 41).

The regressions of simulated against measured data for the BCF2 period are given in ANNEX 6.

C.2.5.2 BCF simulations: fit of transpiration parameters

C.2.5.2.1 Maximum transpiration

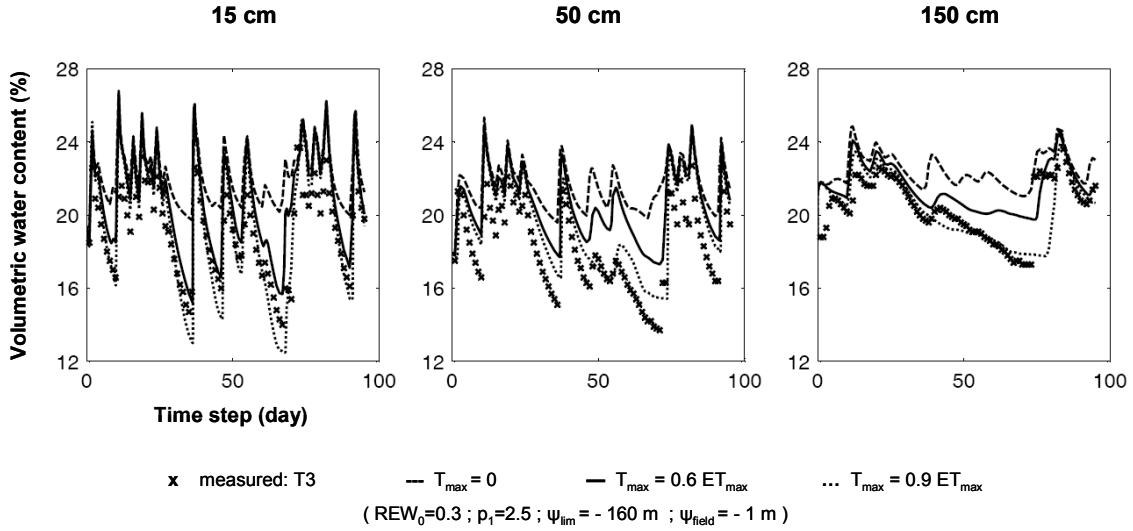

Figure 42 Influence of the maximum transpiration level T_{max} (T_{max}= f_T ET_{max}) on the simulated volumetric water content (%) during the BCF2 period. The level kept for further simulations was f_T=0.6.

The optimization of the maximum transpiration through the f_T parameter, revealed the same behavior as was observed for the evaporation term. It was actually impossible to reduce the bias observed at a depth of 50 cm without altering the curve shape at a depth of 15 cm or 150 cm, or omitting (or largely delay) peaks of water contents following rainfall events at the depths of 50 cm and 150 cm (Figure 42, for example peaks at t=50 days).

Table 32 Efficiency of the simulations measured by EFF1 and EFF2 (eq (53) & (54)) for different levels of maximum transpiration T_{max} (T_{max}= f_T ET_{max}) over the BCF2 period. SSEmax (min) is the maximum (minimum) sum of square errors (all layers k) of the set of simulations. t_{tot} is the duration of the simulation (days). The grey cells correspond to simulations for which a peak of water content experimentally measured was not simulated by the model for one of the observation nodes. The best simulations are in bold. The simulation kept for the rest of the study is underlined.

	EFF1	**EFF2**
Reference data set = measured water content, t_{tot}=95		
SSEmin	688	289
SSEmax	2823	818
f_T		
0	0.00	0.36
0.1	0.04	0.37
0.2	0.22	0.50
0.3	0.30	0.54
0.4	0.22	0.44
0.5	0.51	0.63
0.6	**0.61**	**0.65**
0.7	0.69	0.60
0.8	0.74	0.52
0.9	**0.76**	0.34
1	0.70	0.00

Among all levels of maximum transpiration tested during the BCF2 period, the most efficient fit was obtained for 0.9 ET_{max} according to EFF1 and for 0.6 ET_{max} according to EFF2 (Table 33). When discarding the simulations for which a drainage event was omitted for one of the observation node (grey cells in Table 33), the best fit was obtained for 0.6 ET_{max} according to EFF1 and EFF2. The level T_{max}=0.6 EP_{max} was thus kept as best fit. As a consequence, the simulated water content at a depth of 50 cm was systematically about 2% greater than the measured one.

For all simulations, keeping a bias at a depth 50 cm was preferred to omitting drainage events following rainfall since (i) bias were already observed in the TDR measurements whereas drainage events were rarely omitted, (ii) most of the water drainage occurred during these periods, (iii) the relative changes in water content influence more geochemical processes than a constant bias does.

C.2.5.2.2 Parameters regulating the transpiration

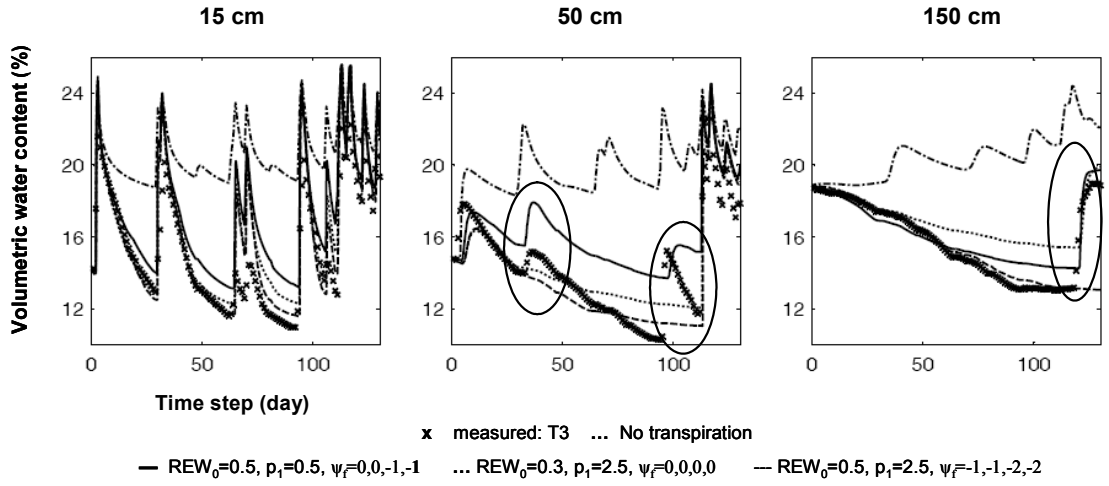

Figure 43 Influence of the transpiration parameters on the simulated volumetric water contents for the BCF1 period (T_{max}=0.6 ET_{max}). The circles focus on water content peaks omitted by some of the simulations. The parameters kept for further simulations were REW_0=0.5, p_1=0.5 and ψ_f=-1m. The parameters are explained in section (C.1.1.4).

Once more, the same behavior as during the CFP and BCF2 period was observed during the BCF1 period and it was impossible to reduce the bias at a depth of 50 cm without altering the water content dynamics (omission of drainage events) at the depths of 50 cm and 150 cm (Figure 43). Nevertheless, the optimization of the parameters regulating transpiration did succeed in improving the simulation efficiency at low water contents (< 16 %) at the depths of 15 and 150 cm (Figure 43).

Table 33 Efficiency of the simulations calculated as EFF1 and EFF2 (eq (53) & (54)) as a function of the transpiration parameters for the BCF1 period (T_{max}=0.6 ET_{max}). SSEmax (min) is the maximum (minimum) sum of square errors (all layers k) of the set of simulations. t_{tot} is the duration of the simulation (days). The grey cells correspond to simulations for which a peak of water content experimentally measured was not simulated by the model for one of the observation nodes. The best simulations are in bold. The simulation kept for the rest of the study is underlined. The simulations of Figure 43 are preceded by *.

			EFF1											**EFF2**									
Reference data set = measured water content, t_{tot}=130 days																							
SSEmin								917											5				
SSEmax								13351											22				
	$\|\psi_f\|$ of layer	**1**	**0**	**0**	**0**	**0**	**0**	**0**	**1**	**1**	**1**	**2**	**0**	**0**	**0**	**0**	**0**	**0**	**1**	**1**	**1**	**2**
		2	**0**	**0**	**0**	**1**	**1**	**2**	**1**	**1**	**2**	**2**	**0**	**0**	**0**	**1**	**1**	**2**	**1**	**1**	**2**	**2**
REW_0	**p1**	**3**	**0**	**1**	**2**	**1**	**2**	**2**	**1**	**2**	**2**	**2**	**0**	**1**	**2**	**1**	**2**	**2**	**1**	**2**	**2**	**2**
	0.5		0.93	0.93	0.93	0.91	0.91	0.91	0.90	0.91	0.90	0.89	0.70	0.69	0.68	0.67	0.66	0.66	0.62	0.63	0.61	0.58
0.1	**2.5**		0.93	0.93	0.93	0.91	0.91	0.91	0.90	0.91	0.90	0.89	0.70	0.69	0.68	0.67	0.67	0.66	0.61	0.64	0.61	0.58
	25		0.93	0.93	0.93	0.91	0.91	0.91	0.91	0.91	0.90	0.89	0.71	0.69	0.69	0.67	0.67	0.66	0.63	0.63	0.61	0.58
	0.5		0.93	0.93	0.91	0.91	0.90	0.89	0.93	0.92	0.91	0.89	0.76	0.75	0.72	0.70	0.69	0.66	0.69	0.68	0.66	0.58
0.3	**2.5**		* 0.93	0.92	0.90	0.90	0.90	0.88	0.93	0.92	0.91	0.89	* **0.77**	0.77	0.71	0.71	0.68	0.66	0.70	0.68	0.65	0.58
	25		0.79	0.83	0.82	0.88	0.87	0.85	0.93	0.92	0.91	0.89	0.63	0.73	0.71	0.71	0.67	0.60	0.71	0.69	0.65	0.58
	0.5		0.87	* **0.88**	0.85	0.89	0.88	0.87	0.93	0.93	0.91	0.89	0.71	* **0.77**	0.74	0.74	0.70	0.65	0.71	0.70	0.66	0.58
0.5	**2.5**		0.79	0.81	0.79	0.88	0.85	0.84	**0.93**	* 0.93	0.91	0.89	0.63	0.73	0.73	0.75	0.67	0.63	0.72	* 0.70	0.66	0.58
	25		0.24	0.39	0.42	0.69	0.69	0.69	0.93	0.92	0.89	0.89	0.06	0.24	0.31	0.56	0.58	0.53	0.74	0.68	0.63	0.58
	0.5		0.74	0.77	0.77	0.87	0.85	0.83	0.93	0.93	0.91	0.90	0.58	0.67	0.71	0.74	0.71	0.63	0.74	0.71	0.67	0.61
0.7	**2.5**		0.58	0.63	0.63	0.81	0.79	0.78	0.93	0.92	0.90	0.89	0.41	0.51	0.56	0.71	0.70	0.62	0.75	0.71	0.66	0.58
	25		0.01	0.19	0.25	0.59	0.62	0.64	0.86	0.88	0.87	0.89	0.00	0.13	0.17	0.45	0.58	0.52	0.68	0.69	0.61	0.58
	0.5		0.62	0.67	0.67	0.81	0.81	0.82	0.92	0.92	0.90	0.91	0.46	0.54	0.58	0.70	0.72	0.69	0.75	0.71	0.67	0.64
0.9	**2.5**		0.34	0.42	0.46	0.70	0.71	0.74	0.90	0.92	0.89	0.90	0.16	0.27	0.34	0.56	0.65	0.64	0.74	0.74	0.66	0.62
	25		0.00	0.09	0.24	0.50	0.58	0.64	0.72	0.80	0.83	0.89	0.03	0.11	0.15	0.34	0.55	0.52	0.53	0.67	0.57	0.58

EFF1 and EFF2 showed two poles of efficient simulations (Table 33). The first pole is obtained for ψ_f=-1 m (all soil layers), REW_0=0.5 and p_1=2.5. The corresponding simulations omitted water content peaks following rainfall events at the depths of 50 and 150 cm (grey cells in Table 33). The second pole was obtained for ψ_f=0 m down to a depth of 70 cm and ψ_f=-1 below, REW_0=0.5 and p_1=0.5. The corresponding simulation simulated fairly well the experimental data but, here again, with a bias of approximately 2 % (wet conditions) to 5 % (water contents close to the residual) at a depth of 50 cm. $|\psi_f|$ of layer 3 and 4 needed to be > $|\psi_f|$ of layer 1 and 2 to efficiently simulate the water contents at a depth of 150 cm, especially when the water contents were close to the residual (days 60 to 120 in Figure 43). This may be explained, as already mentioned, by a preferential uptake of *Eucalyptus* trees in wetter deep soil layers when the surface layers dry, but it may also be the result of the bias observed at a depth of 50 cm. The bias may result in transmitting too much water down to a depth of 150 m. As the lower boundary was fixed, the only way for the model not to transmit the bias at a depth of 150 m is then to transpire the water in excess between the depth of 50 and 150 cm.

The regressions of simulated against measured data for the BCF1 and BCF2 periods are given in ANNEX 6.

C.2.5.3 AP: verification of the parameterized model

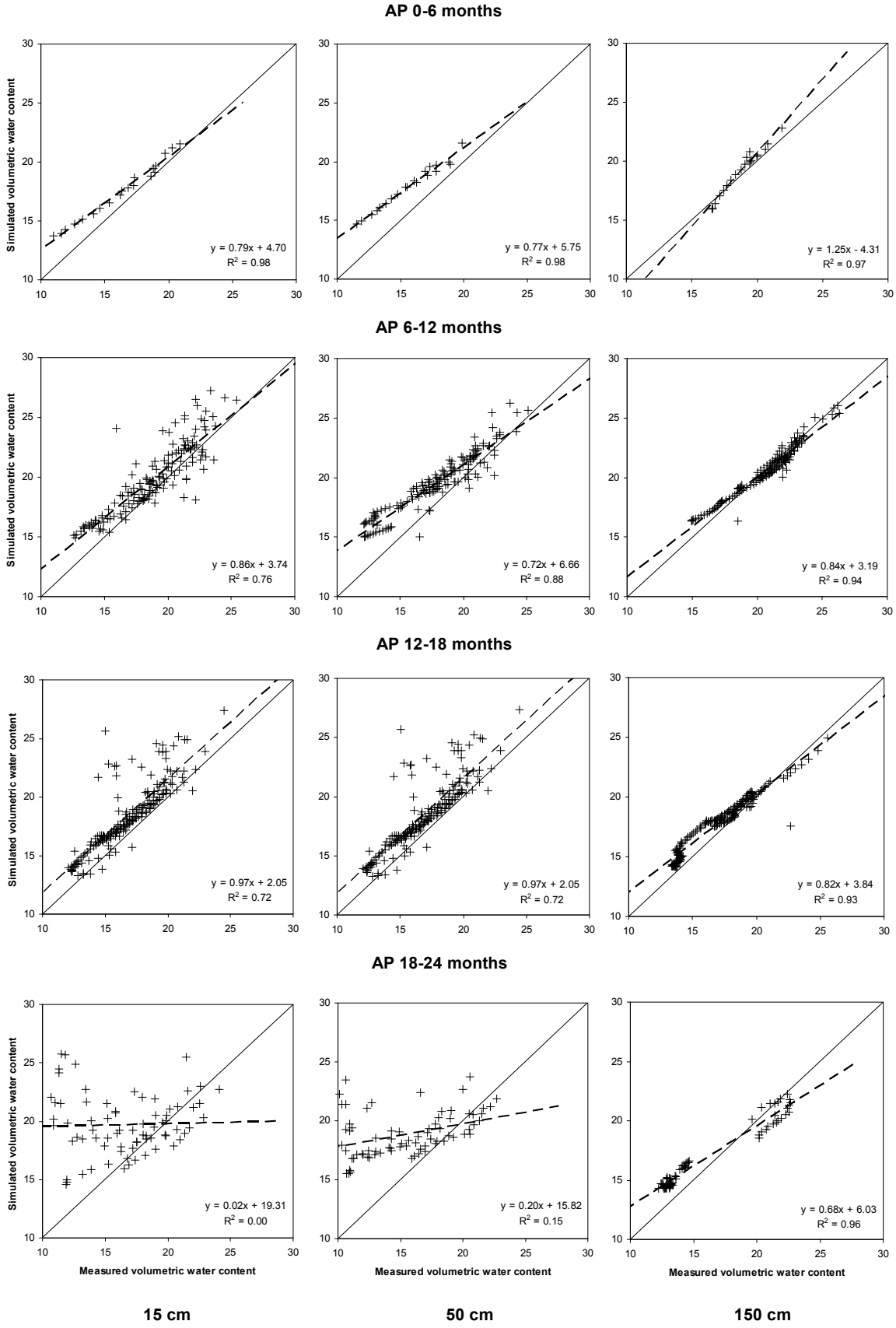

Figure 44 Simulated against measured volumetric water content for T3 and AP period.

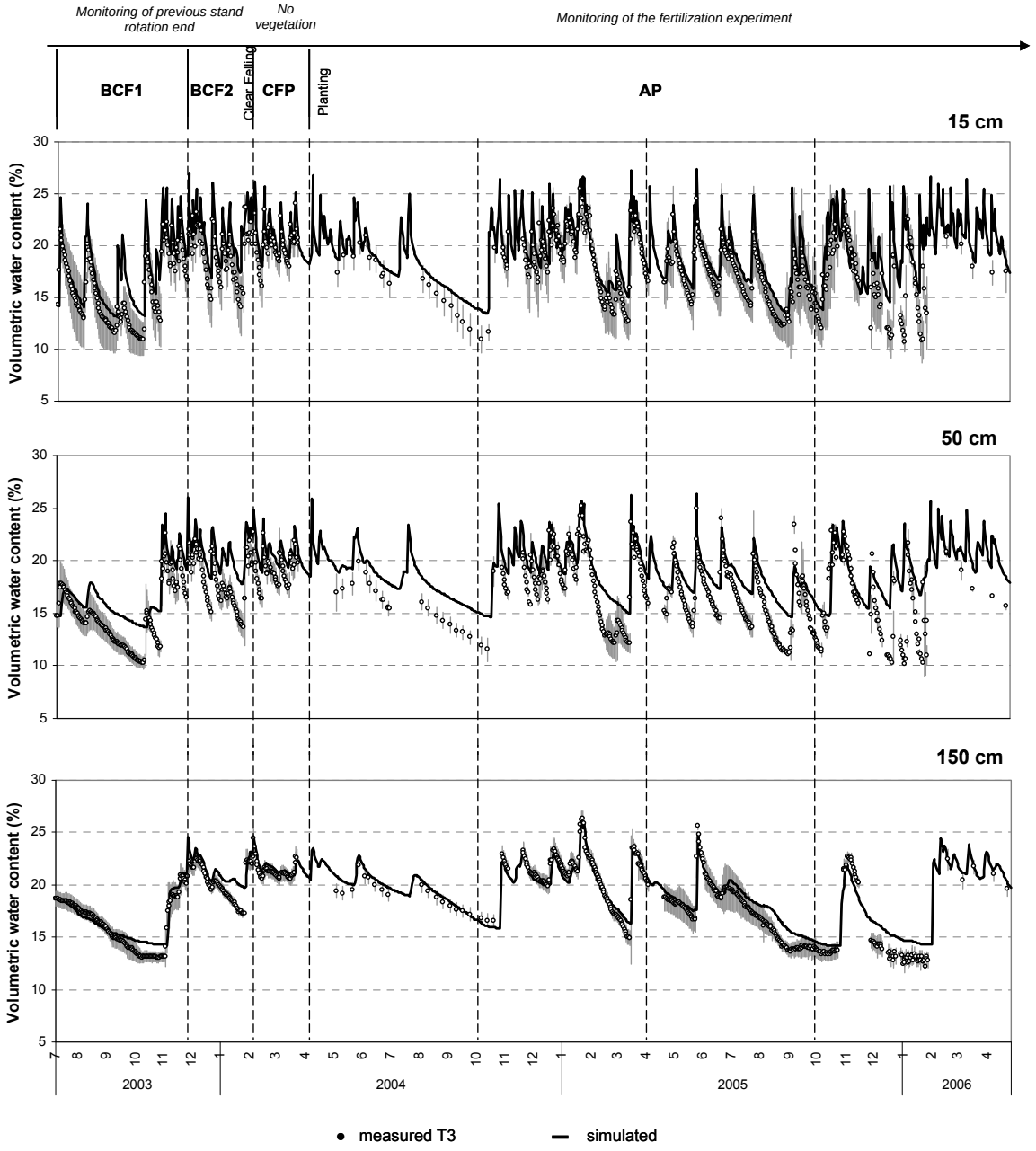

Figure 45 Time course of the volumetric water content measured in treatment 3 (T3) and simulated using MIN3P for each observation node over the studied period. The standard errors of the water content measured in T3 (n=3) are represented in grey.

Except during the last six months, the model simulated quite fairly the soil moisture in the experiment (Figure 44 & Figure 45). The R-square of the linear regressions of the simulated against measured water contents were > 0.7 at the depths of 15 cm and 50 cm, and > 0.9 at a depth of 150 cm. The intercepts of the linear regressions between simulated and measured soil water contents were between 2 and 7 % (period AP 0-6 months at a depth of 150 cm excluded), which confirms the general overestimation of the soil moisture especially at a depth of 50 cm, as already observed and discussed for the BCF and CFP

simulations (intercepts of about 2-4.5 % at 15 cm, 6-8 % at 50 cm and 4-9 % at 150 cm (ANNEX 6). The slopes of these linear regressions were between 0.75 and 1 (period AP 0-6 at a depth of 150 cm excluded) which confirms the correct simulation of the relative changes in water contents. Intercepts and slopes at the depth of 150 cm shows greater variations since the range of water contents reached at this depth is narrow and the data available for the regressions were grouped during the BCF1 and CFP periods. All major increases in water contents due to the drainage of a rainfall event were simulated by the model. Whether not, they would appear in the lower-right corner of the plots on Figure 44 (measured water content >> simulated water content). The water contents at a depth of 50 cm were always overestimated, especially for water contents < 16 % (Figure 45), as a direct consequence of the modelling choices made in §C.2.5.1 & C.2.5.2.

In the first six months of the AP period, few experimental data were available but the R-square of the regressions were all > 0.97. At the depths of 15 cm and 50 cm, the intercepts were about the same as during the BCF and CFP periods but the slope was 0.1 less at a depth of 15 cm. This suggests that the evaporation was slightly overestimated during the first 6 months of the experiment. At a depth of 150 cm, the negative intercept together with the slope > 1 suggests that the transpiration was overestimated in this soil layer. This is probably due to an overestimation of the root length density in deep soil layers during the first year of growth of the stand. During the root sampling which was used to fit the root length density profile at age 6 and 12 months, dead roots inherited from the previous stand were very likely mistaken with the roots of the newly planted stand. Counts of root impacts carried out lately in a *Eucalyptus* stand next to the experimental stand confirmed this feature.

The model simulated the experimental soil moisture of the 6-12 months period in the same way than it did for the BCF and CFP simulations.

The next six months of growth (12-18 months after planting) were particularly well simulated by the model. The intercepts were about 2 % at 15 cm and 50 cm, and < 4 % at a depth of 150 cm. The slopes were close to 1 (0.97 at 15 and 50 cm, and 0.82 at 150 cm).

At first sight, the last six months seemed poorly simulated, especially for the measured water contents < 16 % which were largely overestimated by the model. During this period, few continuous experimental data were available (TDR equipment failure). The transpiration was greatest and the interval of water contents simulated broadest, with

extreme changes occurring very quickly (within 2 months at the depths of 15 and 50 cm). The poor frequency of TDR records during this period (once every 15 days) may easily result in missing a peak of water content following rainfall. The close observation of water contents measured in other treatments and simulated during these problematic periods revealed that they always corresponded to very dry soil moistures followed by an increase in the soil moisture (rainfall drainage). This increase was more or less delayed or even did not appear depending on TDR probes. During these periods, T_{eff} was less than T_{max}, which means that the transpiration was limited by the soil water availability and that increasing the maximum transpiration would have no result on the simulated water contents unless the parameters regulating transpiration are changed. It is thus suggested that the re-humidification of the soil profile once the soil dried (soil moisture < 16 %) is heterogeneous in space and time. This heterogeneity is enhanced by the intensive transpiration of the *Eucalyptus* trees which is greatest at this stage of stand growth and the spatial heterogeneity of the root system. Moreover, such soil moisture conditions (dry soils and broad gradients of soil moisture changing quickly) put the TDR system under severe constraints. Some probes failed and the discrepancies due to problems of calibration (if existing) may be enhanced during this period.

Table 34 Number of days (t_{tot}) measured and simulated, sum of squares (SS), sum of square errors (SSE), root mean square error (RMSE) and mean error (ME) for each simulated period and observation node.

Period		**BCF1**	**BCF2**	**BCF**	**CFP1**	**CFP2**	**CFP**	**AP6**	**AP12**	**AP18**	**AP24**	**AP**	**TOT**
$\mathbf{N_{day}}$		1-130	131-225	1-225	226-259	260-291	226-291	292-476	477-658	659-841	842-1023	292-1023	**1-1023**
Date	*Start*	*09/07/2003*	*16/11/2003*	*09/07/2003*	*18/02/2004*	*24/03/2004*	*18/02/2004*	*25/04/2004*	*27/10/2004*	*27/04/2005*	*27/10/2005*	*25/04/2004*	*09/07/2003*
	End	*15/11/2003*	*18/02/2004*	*18/02/2004*	*23/03/2004*	*24/04/2004*	*24/04/2004*	*26/10/2004*	*26/04/2005*	*26/10/2005*	*26/04/2006*	*26/04/2006*	*26/04/2006*
$\mathbf{t_{tot}}$	Measured	130	95	225	34	0	34	20	148	180	74	422	**681**
	Simulated	130	95	225	34	32	66	185	182	183	182	732	**1023**
SS	15 cm	40438	43123	83560	14964		14964	6221	59926	62534	29203	157884	**256409**
	50 cm	35078	41436	76515	14571		14571	6460	57397	59359	26625	149841	**240927**
	150 cm	34249	43778	78028	15575		15575	7462	63785	56882	21362	149491	**243094**
SSE	15 cm	861	505	1366	24		24	41	486	899	2098	3524	**4913**
	50 cm	716	722	1437	85		85	103	644	1047	1715	3510	**5032**
	150 cm	84	164	248	6		6	8	59	226	199	491	**745**
RMSE	15 cm	2.57	2.31	2.46	0.84		0.84	1.43	1.81	2.23	5.32	2.89	**2.69**
	50 cm	2.35	2.76	2.53	1.58		1.58	2.27	2.09	2.41	4.81	2.88	**2.72**
	150 cm	0.81	1.31	1.05	0.42		0.42	0.63	0.63	1.12	1.64	1.08	**1.05**
ME	15 cm	1.96	2.02	1.99	0.67		0.67	1.24	1.05	1.59	3.11	1.65	**1.71**
	50 cm	1.93	2.57	2.20	1.53		1.53	2.19	1.67	1.81	3.39	2.06	**2.08**
	150 cm	0.35	1.00	0.62	0.26		0.26	0.39	-0.09	0.80	0.93	0.49	**0.52**

All in all, the root mean square errors and mean errors were of the same order of magnitude for all the studied period, except the last six months of the AP as already discussed (Table 34). Mean errors (ME) were > 0 for all the simulated periods which confirms a general overestimation of water contents in average < 2 % at a depth of 15 cm, < 2.5 % at 50 cm and < 1 % at 150 cm. The root mean square errors (RMSE) were < 2.7 % at the depths of 15 and 50 cm, and < 1.5 % at a depth of 150 cm. RMSE were about the same as ME which confirms that most of the error is due to the bias in the simulations.

C.2.5.4 Sensitivity tests

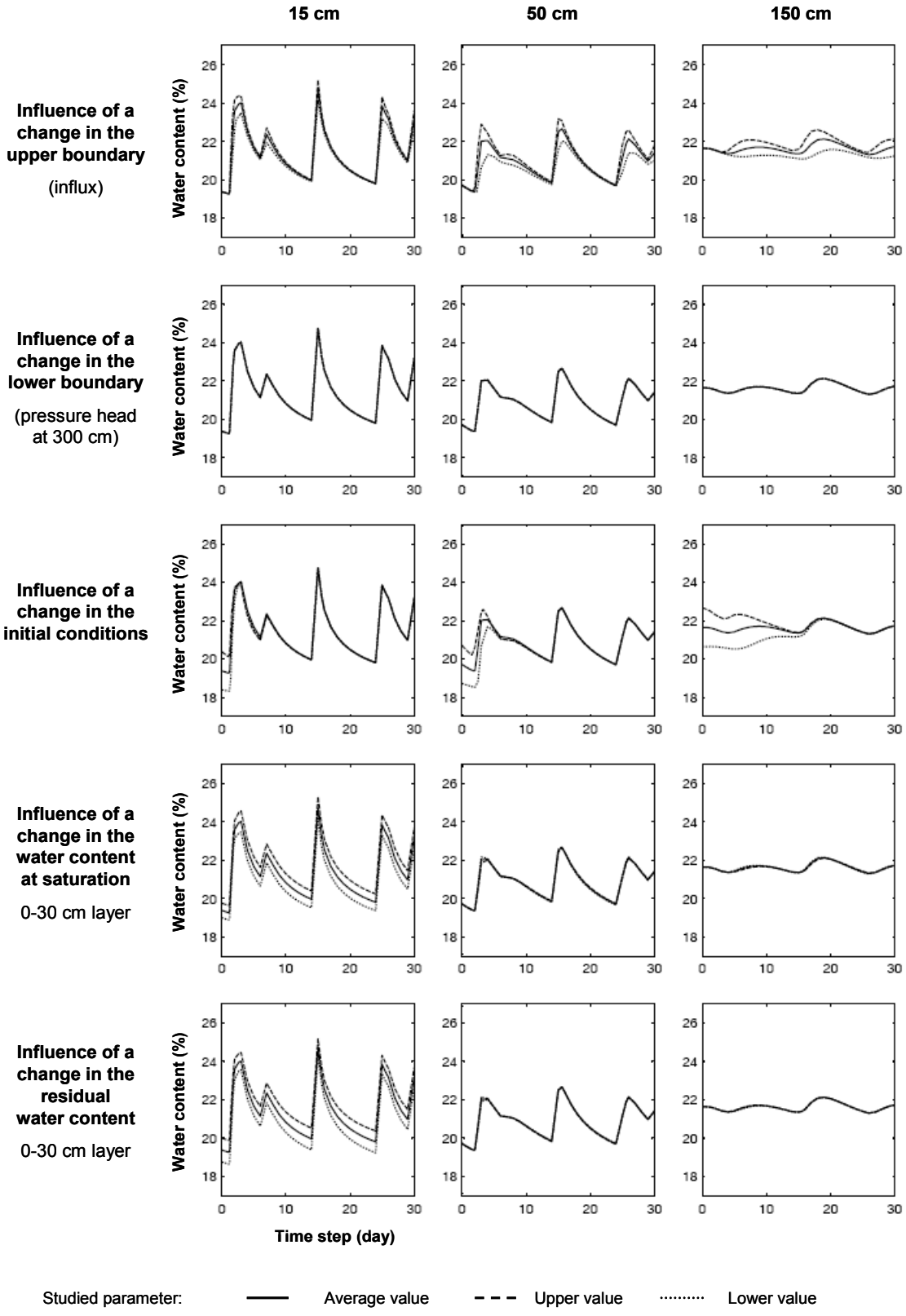

Figure 46 Sensitivity of the simulations to a change in the boundary conditions, in the initial condition or in the soil hydraulic parameters at each monitored node during the CFP period (EV_{max}=0, T_{max}=0). The average, upper and lower value taken for the simulations are given in Table 27. The initial conditions were changed for all layers whereas only the water content of the 0-30 cm (residual and at saturation) was changed.

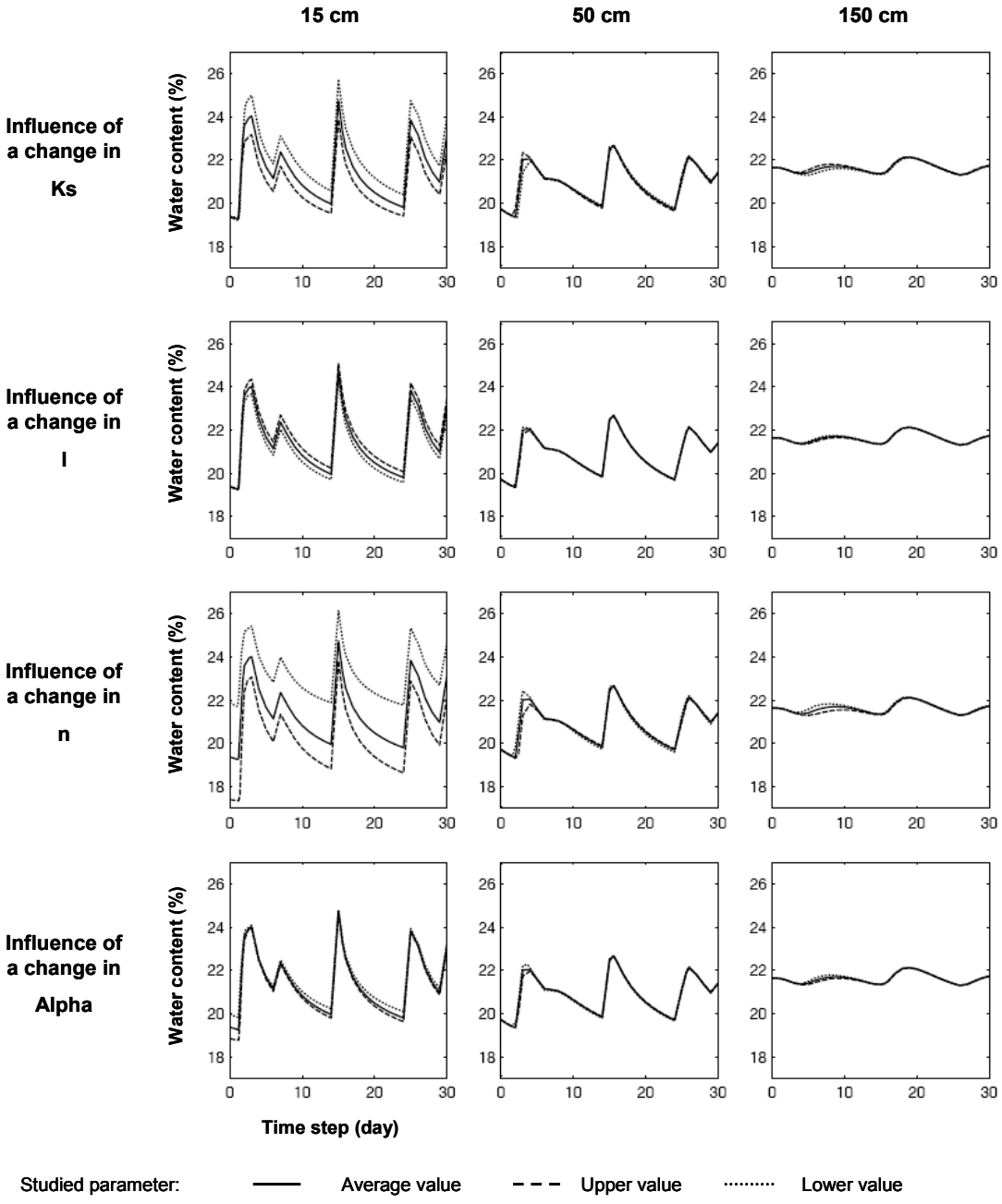

Figure 47 Sensitivity of the simulations to a change in the soil hydraulic parameters of the 0-30 cm layer during the CFP period (EV_{max}=0, T_{max}=0). The average, upper and lower value taken for the simulations are given in Table 27.

Table 35 Changes in the simulation efficiency (EFF1 and EFF2 coefficients eq (53) & (54)) with changes in the input parameters (Table 27) during the CFP period (EV_{max}=0, T_{max}=0). The reference simulation is taken as the average parameter values of Table 27. SSEmax (min) is the maximum (minimum) sum of square errors (all layers k) of the set of simulations. t_{tot} is the duration of the simulation (days).

			Parameter value	EFF1	EFF2
Characteristics of the set of simulations	Reference data set		-	average values of all parameters (table)	
	t_{tot}		-	33	
	SSEmin		-	0.09	0.09
	SSEmax		-	99.42	10.84
Initial condition			Lower	0.84	0.00
			Upper	0.89	0.15
Boundaries	Lower		Lower	1.00	0.99
			Upper	1.00	0.99
	Upper		Lower	0.83	0.27
			Upper	0.91	0.63
Soil hydraulic parameters	α		Lower	0.98	0.94
			Upper	0.99	0.95
	n		Lower	0.00	0.51
			Upper	0.61	0.72
	θ_{ra}		Lower	0.91	0.95
			Upper	0.91	0.96
	θ_{sa}		Lower	0.92	0.96
			Upper	0.92	0.96
	Ks		Lower	0.79	0.77
			Upper	0.87	0.81
	l		Lower	0.97	0.97
			Upper	0.97	0.97

The sensitivity tests performed for the CFP period shows that a small change in the initial condition (±1% in water content for all layers) influences the simulations until the next rainfall event. For all simulations performed in part C.2.5, the rainfall event preceding the studied period was simulated and its output served as initial condition for the simulation.

Changing the lower boundary little influences the simulations (Figure 46), as shown by the efficiency coefficients which are greatest (EFF1=1 and EFF2=0.99) and the SSE < 0.1 of Table 35. This means that an error of ±1 % in the water content of the lower boundary (heterogeneity observed in situ) is not likely to explain the bias observed at 50 cm. The same is observed for the l and α parameters for which EFF1 > 0.97.

EFF2 > EFF1 indicates that the parameter change partially translates the simulation (bias). This can be obtained by changing the residual water content, the water content at saturation or the n parameter of the water retention curve (Figure 46 & Figure 47). A change in the Ks parameter also results in a general translation of the simulated curve but as it also delays the peaks of water contents, EFF2 and EFF1 are similar.

Poor EFF2 and EFF1, with EFF2 ≥ EFF1 indicates a distortion of the simulated curve compared to the reference one. This occurs when changing the upper boundary (inflow). A higher inflow on the soil surface actually increases the water content peaks but has no influence on the water content once the water brought by the inflow peak is drained. As our soil type drains very quickly, a change in the upper water inflow at the top of the soil profile influences the simulated water contents for all soil layers of the profile (Figure 46).

Figure 47 confirmed that the soil layers are quite independent one with another as was already shown by the DOE resolution of Ks and l. Indeed, a change in the soil hydraulic parameters of the 0-30 cm layer does not influence the water content simulated at deeper observation nodes. This means that changing the soil hydraulic parameters of the 30-70 cm or of the 70-230 cm layers would influence the water content observed at the depths of 50 cm or 150 cm in the same way as a change in the 0-30 cm layer influences the water content observed at a depth of 15 cm. This was checked by running the corresponding simulations (data not shown).

The sensitivity tests suggests that the water content dynamics observed at a depth of 50 cm in the CFP and BCF simulations may result from heterogeneities (or errors of parameterization) of the soil hydraulic parameters of the 30-70 cm layer (mainly Ks, n, θ_r and θ_s) or of the upper boundary (inflow). During the BCF1 period, the best unbiased simulation was obtained for ψ_f=-1 m for layers 1 and 2, ψ_f=-2 m for layers 3 and 4, REW_0=0.5 and p_1=2.5. Still, this set of transpiration parameters did not simulate all the water content peaks experimentally observed at the depths of 50 cm and 150 cm. To check whether the suggested changes in Ks, n, θ_r or θ_s of the 30-70 cm layer or in the upper boundary might improve the simulation, sensitivity tests were repeated for the BCF1 period with this set of transpiration parameters, and changing Ks, n, θ_r and θ_s of the 30-70 cm layer and the upper boundary according to Table 35 .

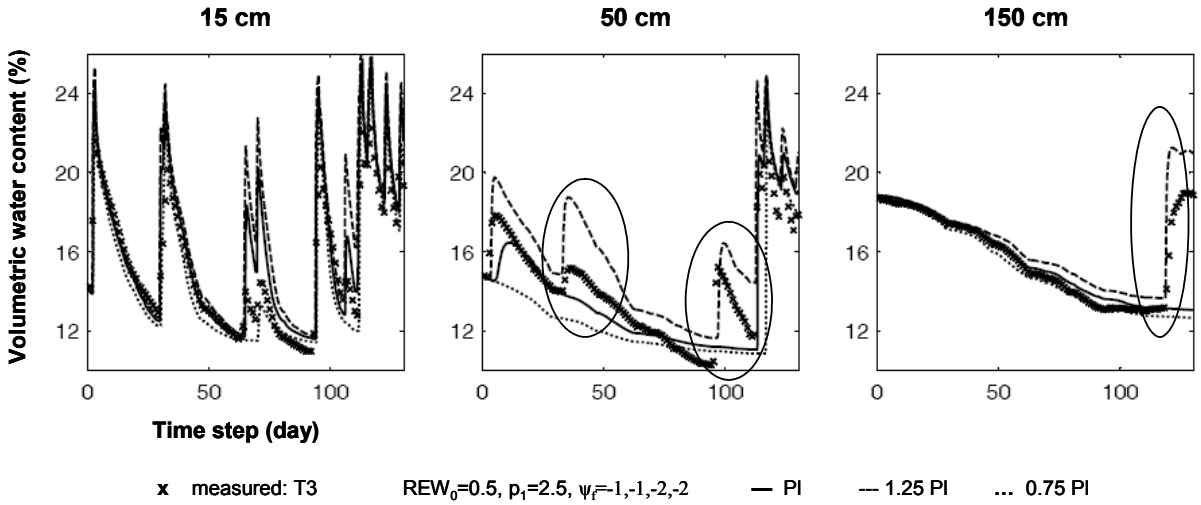

Figure 48 Influence of the rainfall intensity (upper boundary condition) on the simulated water contents for the BCF1 period (T_{max}=0.6 ET_{max}). The circles focus on the water content peaks which were not simulated using the experimentally measured rainfall.

None of the changes of the soil hydraulic parameters of the 30-70 cm layer succeeded in simulating correctly all the water content peaks experimentally observed at the depths of 50 cm and 150 cm. On the contrary, an increase of 25 % in the rainfall did allow the simulation of those water content peaks (Figure 48).

Only the effect of a change in one single parameter on the simulated water contents was analyzed. Interactions among parameters are likely to exist but were not tested here.

C.2.6 Water fluxes budget

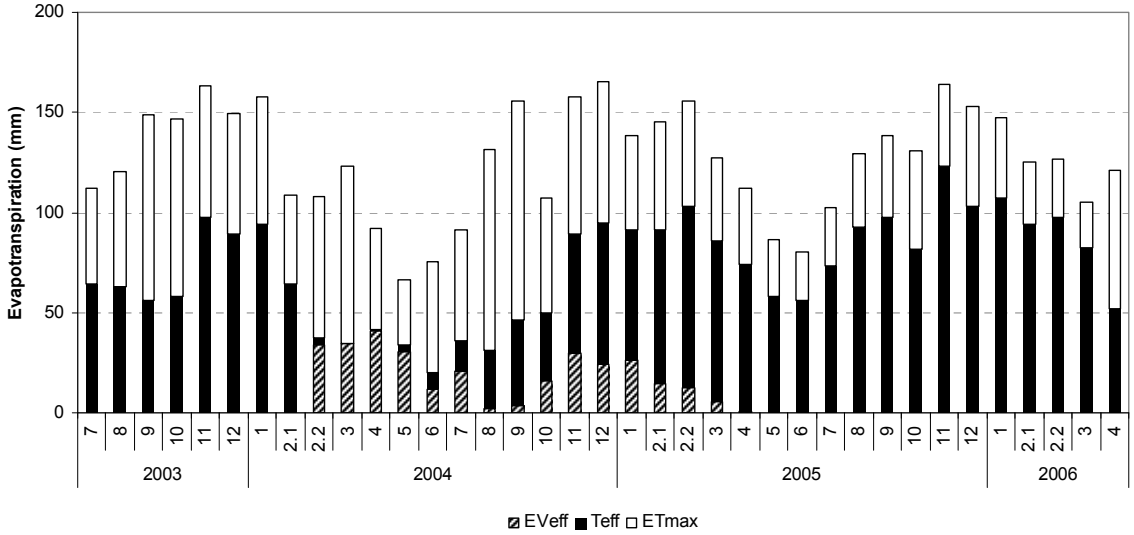

Figure 49 Amount of water effectively evaporated (EV_{eff}) and tranpirated (T_{eff}) and maximum amount of water potentially evaporated or transpirated (ET_{max}, §C.1.1.4) in mm. EV_{eff} and T_{eff} are output of the MIN3P simulations.

During the CFP period, the effective evaporation was in average 68 % of EV_{max}: 100% .(EV_{max}=0.7 ET_{max}) during the rainy days and about 10 to 20 % when the soil was dry, which was more or less the level of evaporation 0.1 ET_{max}. (Figure 49). During the BCF period, 90% of T_{max} was, in average, effectively transpirated, 100% (T_{max}=0.6 ET_{max}) when the soil was wet and down to 23% under water stress conditions. During the AP period, 90% of the maximum transpiration was in average effectively taken up, up to 100% the rainy days and down to 0% during the first 6 months of growth, when evaporation dried the soil down to its residual saturation.

Table 36 Water balance (mm) for each monitoring depth over each simulated period. The proportion of the studied flux relatively to the cumulated rainfall during the studied period is given in italic.

			BCF1		BCF2		**BCF**		CFP1		CFP2		**CFP**		AP 0-6		AP 6-12		AP 12-18		AP 18-24		**AP**	
0-15 cm	Inflow	Psoil	324	*100%*	593	*100%*	**917**	***100%***	126	*100%*	148	*100%*	**275**	***100%***	349	*100%*	932	*100%*	512	*100%*	876	*100%*	**2669**	***100%***
		Upward flow	1	*0%*	0	*0%*	**1**	***0%***	1	*0%*	1	*1%*	**2**	***1%***	3	*1%*	3	*0%*	1	*0%*	0	*0%*	**7**	***0%***
	Outflow	Evaporation	0	*0%*	0	*0%*	**0**	***0%***	-49	*-39%*	-41	*-27%*	**-89**	***-33%***	-105	*-30%*	-113	*-12%*	0	*0%*	0	*0%*	**-217**	***-8%***
		Transpiration	-119	*-37%*	-98	*-17%*	**-217**	***-24%***	0	*0%*	0	*0%*	**0**	***0%***	-15	*-4%*	-93	*-10%*	-145	*-28%*	-203	*-23%*	**-457**	***-17%***
		Downward flow	-195	*-60%*	-497	*-84%*	**-692**	***-75%***	-80	*-63%*	-105	*-71%*	**-185**	***-67%***	-227	*-65%*	-734	*-79%*	-369	*-72%*	-678	*-77%*	**-2008**	***-75%***
	Difference in water storage		-11	*-3%*	3	*0%*	**-9**	***-1%***	2	*2%*	-4	*-3%*	**-2**	***-1%***	-5	*-2%*	6	*1%*	2	*0%*	5	*1%*	**6**	***0%***
0-50 cm	Inflow	Psoil	324	*100%*	593	*100%*	**917**	***100%***	126	*100%*	148	*100%*	**275**	***100%***	349	*100%*	932	*100%*	512	*100%*	876	*100%*	**2669**	***100%***
		Upward flow	0	*0%*	0	*0%*	**0**	***0%***	0	*0%*	0	*0%*	**0**	***0%***	0	*0%*	0	*0%*	0	*0%*	0	*0%*	**0**	***0%***
	Outflow	Evaporation	0	*0%*	0	*0%*	**0**	***0%***	-49	*-39%*	-41	*-27%*	**-89**	***-33%***	-105	*-30%*	-113	*-12%*	0	*0%*	0	*0%*	**-217**	***-8%***
		Transpiration	-205	*-63%*	-173	*-29%*	**-378**	***-41%***	0	*0%*	0	*0%*	**0**	***0%***	-37	*-11%*	-184	*-20%*	-254	*-50%*	-366	*-42%*	**-842**	***-32%***
		Downward flow	-85	*-26%*	-423	*-71%*	**-508**	***-55%***	-79	*-63%*	-105	*-71%*	**-184**	***-67%***	-189	*-54%*	-659	*-71%*	-253	*-49%*	-525	*-60%*	**-1626**	***-61%***
	Difference in water storage		-34	*-10%*	4	*1%*	**-30**	***-3%***	2	*1%*	-3	*-2%*	**-1**	***0%***	-17	*-5%*	24	*3%*	-5	*-1%*	15	*2%*	**16**	***1%***
0-150 cm	Inflow	Psoil	324	*100%*	593	*100%*	**917**	***100%***	126	*100%*	148	*100%*	**275**	***100%***	349	*100%*	932	*100%*	512	*100%*	876	*100%*	**2669**	***100%***
		Upward flow	0	*0%*	0	*0%*	**0**	***0%***	0	*0%*	0	*0%*	**0**	***0%***	0	*0%*	0	*0%*	0	*0%*	0	*0%*	**0**	***0%***
	Outflow	Evaporation	0	*0%*	0	*0%*	**0**	***0%***	-49	*-39%*	-41	*-27%*	**-89**	***-33%***	-105	*-30%*	-113	*-12%*	0	*0%*	0	*0%*	**-217**	***-8%***
		Transpiration	-259	*-80%*	-237	*-40%*	**-496**	***-54%***	0	*0%*	0	*0%*	**0**	***0%***	-78	*-22%*	-317	*-34%*	-374	*-73%*	-543	*-62%*	**-1311**	***-49%***
		Downward flow	-14	*-4%*	-341	*-58%*	**-356**	***-39%***	-77	*-61%*	-112	*-76%*	**-190**	***-69%***	-139	*-40%*	-564	*-60%*	-107	*-21%*	-368	*-42%*	**-1179**	***-44%***
	Difference in water storage		-51	*-16%*	-14	*-2%*	**-65**	***-7%***	0	*0%*	5	*3%*	**5**	***2%***	-27	*-8%*	61	*7%*	-31	*-6%*	35	*4%*	**38**	***1%***
0-300 cm	Inflow	Psoil	324	*100%*	593	*100%*	**917**	***100%***	126	*100%*	148	*100%*	**275**	***100%***	349	*100%*	932	*100%*	512	*100%*	876	*100%*	**2669**	***100%***
		Upward flow	0	*0%*	0	*0%*	**0**	***0%***	0	*0%*	0	*0%*	**0**	***0%***	4	*1%*	19	*2%*	5	*1%*	0	*0%*	**29**	***1%***
	Outflow	Evaporation	0	*0%*	0	*0%*	**0**	***0%***	-49	*-39%*	-41	*-27%*	**-89**	***-33%***	-105	*-30%*	-113	*-12%*	0	*0%*	0	*0%*	**-217**	***-8%***
		Transpiration	-306	*-95%*	-284	*-48%*	**-590**	***-64%***	0	*0%*	0	*0%*	**0**	***0%***	-134	*-38%*	-482	*-52%*	-497	*-97%*	-656	*-75%*	**-1769**	***-66%***
		Downward flow	-9	*-3%*	-219	*-37%*	**-228**	***-25%***	-78	*-62%*	-105	*-70%*	**-183**	***-67%***	-159	*-46%*	-383	*-41%*	-53	*-10%*	-185	*-21%*	**-781**	***-29%***
	Difference in water storage		-8	*-3%*	-90	*-15%*	**-98**	***-11%***	1	*1%*	-3	*-2%*	**-2**	***-1%***	45	*13%*	26	*3%*	31	*6%*	-35	*-4%*	**68**	***3%***

Compared to the water inflow at the soil surface (P_{soil}), the evaporation represented 33% of P_{soil} during the CFP period and during the first 6 months of growth of the newly planted *Eucalyptus* stand (AP 0-6 period), and 12 % of P_{soil} for the next six months (AP 6-12) (Table 36). All this flux was taken up in the upper 5 cm (z_{EV}) of the soil profile. The evaporation flux was null during the other periods (BCF and AP 12-24).

During the dry winters, almost 100 % of the incoming rainfall was transpired by the *Eucalyptus* trees (periods BCF1 and AP 12-18) which confirms that during these periods, the tree transpiration is controlled by the water availability in the soil. During the wet months, the rate of tree uptake relatively to the amount of incoming rainfall was less. It was about 50 % when the transpiration of the *Eucalyptus* trees was moderate (periods BCF2 and AP 0-12) and reached 75 % when the transpiration of the *Eucalyptus* trees was greatest (AP 12-24). During these wet periods, the transpiration was more limited by the stand requirements and the available energy than by the water availability in soils. As a result, the transpiration rates were lower in the less productive stand of the BCF period (about 64 % from 0 to 300 cm) than in the fast-growing newly planted one (about 75 % during the AP 18-24 period). Almost 50 % of the water taken up by the vegetation occurs in the deeper soil layers between a depth of 50 cm and 300 cm.

As a consequence, little water relatively to P_{soil} was drained at a depth of 300 cm during the winters (< 10 % during the BCF1 and AP 12-18 periods). During the wet summers, less water was drained in the fast-growing stand of the AP 18-24 period (21 % of P_{soil}) than in the less productive one during the BCF period (37 % of P_{soil}). Between 40 % and 50 % of the incoming water at the soil surface was drained during the first year of growth of the new planted *Eucalyptus* stand (period 0-12). When only evaporation occurs (CFP period), all the water which was not evaporated in the upper 5 cm of the soil profile (about 65-70 % of P_{soil}) is drained down to a depth of 3m. In most studied periods, differences in soil water storage were less than ± 3 % of P_{soil} at all observation nodes.

Upward flow was simulated at all monitored depths. This flow was significant (about 1-2 % of P_{soil}) at the depth of 15 cm during the whole simulated period, and at a depth of 300 cm during the AP period.

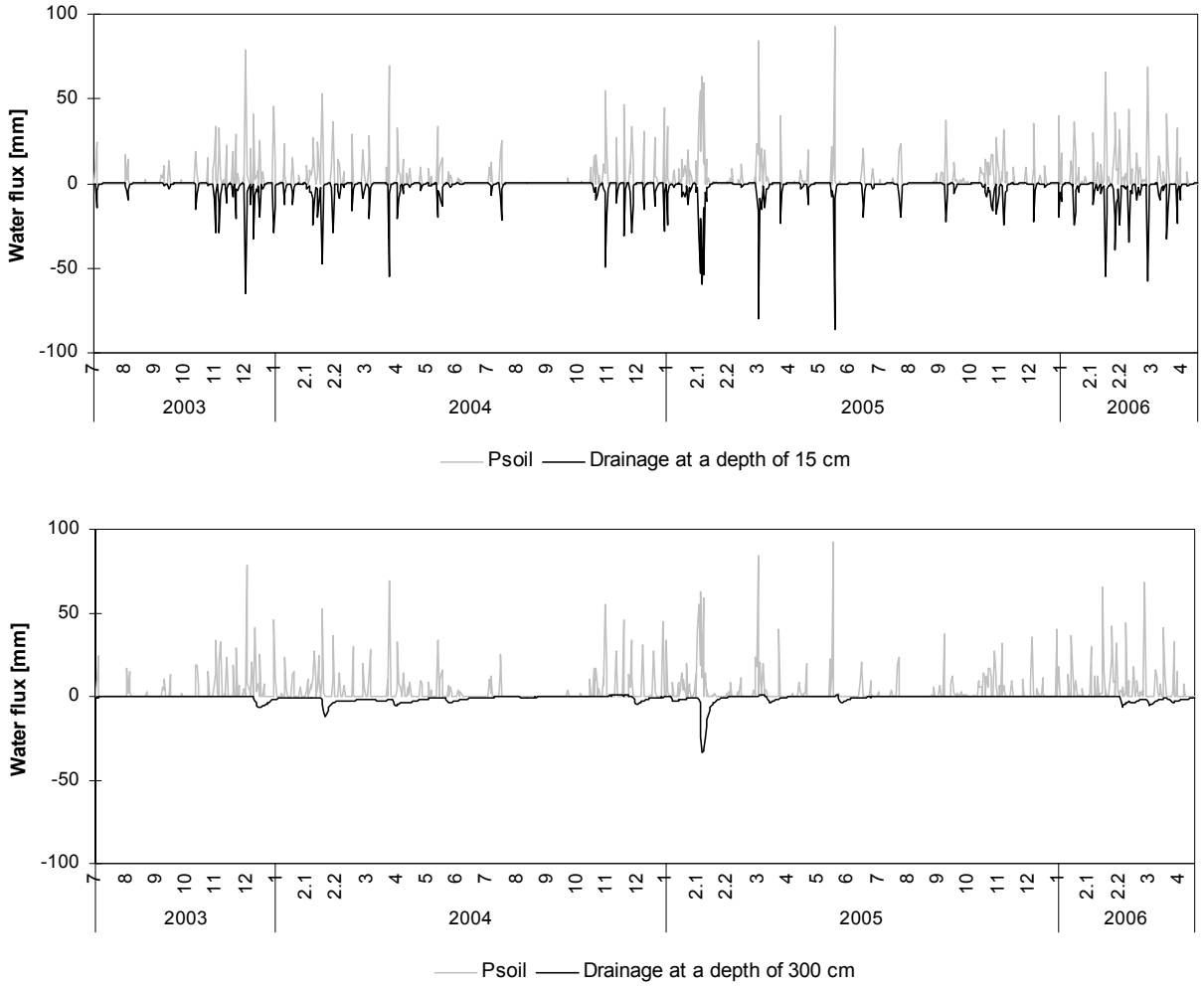

Figure 50 Time course of daily water fluxes (mm) entering the soil profile by throughfall + stemflow (P_{soil}) and leaving the soil profile by drainage at the depths of 15 cm and 300 cm (output of MIN3P simulations) over the studied period. The drainage is positive when upward water flux occurs.

P_{soil} is actually drained almost instantaneously at a depth of 15 cm (Figure 50) and upward flux occurs between rainfall events when the soil evaporation and/or the stand transpiration dry the upper soil layer (0-15 cm). At a depth of 300 cm, most of the water drainage occurs at a more or less small constant flux (average of 1 mm day^{-1} over the studied period) (Figure 50). During the wet summers (December till February), episodes of larger drainage may occur (summers 2003-2004 and 2004-2005) unless the water uptake by the vegetation is too great (summer of late 2004 when the water uptake by the fast-growing young *Eucalyptus* stand is greatest). Upward flow occurs at a depth of 300 cm when there is almost no rainfall whereas transpiration is great: from September to November 2004 and in February-March 2005 (average rate of 0.3 mm day^{-1} and up to 1.3 mm day^{-1}), and from August 2005 until February 2006 (average rate of 0.1 mm day^{-1}).

C.3 GENERAL DISCUSSION AND CONCLUSIONS

C.3.1 On soil hydraulic properties

The soil hydraulic properties estimated from field measurements were of the same order of magnitude as those reported by the literature for this soil type (Elsenbeer et al., 1999; Paiva et al., 2000). The trend of increasing Ks with increasing soil depth observed in our study seems a controversial point in the literature for Brazilian ferralsols since authors also report the inverse trend (Balbino et al., 2004). However, in all studies hydraulic conductivity is reported to be highly dependant on the soil aggregation status and on the bulk soil density (Balbino et al., 2004; Elsenbeer et al., 1999; Paiva et al., 2000; Pochet et al., 2007). Since a more developed micro-aggregation was observed in part B for upper soil layers (down to a depth of 50 cm) and since the bulk density increased both with depth and increasing clay content, the decrease of Ks with depth does not seem surprising. The faster hydraulic conductivity observed for layer 2 (30-50 cm) compared to layer 1 (0-30 cm) can be either attributed to the bump of the bulk density observed above a depth of 30 cm or to a more developed aggregation in this soil layer less influenced by silvicultural management and pH changes over the studied period. The same observations were made by Paiva *et al.* (2000).

The retention curves showed the same characteristics as those measured for the same soil type in Brazil (Balbino et al., 2004; Cichota et al., 2008; Elsenbeer et al., 1999; Klinge et al., 2001). The range of pressure heads reached in situ during the water drainage experiment was too narrow to rule upon the existence of a second type of porosity at very low pressure heads. Specific analysis of the pore size distribution (such as mercury porosimetry) would be needed to rule on this point.

The soil hydraulic parameters calculated in this study may not be the unique set of parameters which correctly simulates soil water fluxes. The very principle of inverse resolution means that the calculated parameters may be a virtual set of parameters which mathematically enable a good simulation of experimental data. The non uniqueness of the solution and its dependency on the initial conditions used for the inverse simulation are classically observed (Bertolo et al., 2006; Hill, 1998; Madsen, 2000). In the present study, the water retention curves were not included in the inverse resolution, which means that they most likely approximate field characteristics. For hydraulic conductivities, the method

adopted here guarantees the uniqueness of the solution but solely within the range of variations chosen for Ks and l.

C.3.2 On the validity of the simulations

The parameterized model fitted fairly well the experimental data. Still, the model did not succeed in correctly simulating the soil moisture at a depth of 50 cm. Sensitivity tests and simulations of the AP 18-24 months period suggest that differences in infiltrations at the upper boundary of the soil profile and hysteresis in the profile humectation may explain this difficulty. The hydrophobicity of *Eucalyptus* litter is reported to induce heterogeneous water infiltration at the soil surface (Laclau et al., 2004a) and water repellency occurring in the forest floor and the soil profile below a water content of 14-16 % (threshold actually observed in the present study) was already observed (Greiffenhagen et al., 2006). Moreover, heterogeneities due to preferential flows along the stem and the root system (Cattan et al., 2007; Johnson and Lehmann, 2006; Levia and Frost, 2003), and heterogeneous water uptake depending on the spatial organization of this root system may also result in larger amounts of water transported quicker at a depth of 50 cm.

The heterogeneities observed in the TDR measurements can be explained by the heterogeneities mentioned above. Such random-like micro-variations were already observed by (Cichota et al., 2006) and may as well result from the microaggregated structure of these ferralsols. At deeper depths, these heterogeneities may be homogenized while the increasing clay content slows the hydraulic conductivity. The sandy nature of the soil and its high degree of micro aggregation may also result in a non uniform contact between the TDR probes and the soil matrix which may explain the heterogeneity of the soil moisture measurements (Noborio, 2001). Since the clay content increases with depth, the contact between TDR probes and the soil matrix may improve with soil depth and thus lead to narrower ranges of variations of soil moisture. The soil/probe contact may also be altered by the growth of *Eucalyptus* root systems and may deteriorate with time. A degradation of the TDR system after 2 years of installation was already observed in brazilian ferralsols (Cichota et al., 2008). The generalized use of tensiometers together with soil moisture equipments may be useful to hep understanding spatial heterogeneities of water flow in soils.

Daily on-site measurements of the aboveground fluxes would be needed to more precisely study the spatial heterogeneity of the water inflow at the upper boundary of the

soil profile. Moreover, infiltration studies may inform on the heterogeneity of the water infiltration within the forest floor and the soil profile, and on the hysteresis of the soaking of the soil profile. If the observed heterogeneities are created by heterogeneities of the influx at the upper boundary of the soil profile, the inclusion of additional dimensions in the simulations may allow a simple verification of these assumptions. If hysteresis actually occurs, further implementation of the MIN3P code would be needed.

C.3.3 On the evapotranspiration of the *Eucalyptus* stands and on the water balance

The optimized levels of maximum transpiration for both *Eucalyptus* stands correspond to high rates of transpiration (0.6 ET_{max} before clear felling and 0.8 ET_{max} one year after planting) and reflect the difference of productivity between the old *Eucalyptus* stand of the BCF period and the well managed one of the fertilization experiment (AP period). They are in good agreement with the potential evapotranpirations measured for *Eucalyptus* stands in other studies (Almeida et al., 2007; Damman, 2001; Landsberg, 1999; Soares and Almeida, 2001; Stape et al., 2004; Whitehead and Beadle, 2004). These studies also recorded similar ranges of variation between effective evapotranspiration and potential evapotranspiration depending on the water availability in the soil profile.

Deep root systems enable *Eucalyptus* trees to access water not available to shallow rooted trees down to a depth > 10 m, and thus to maintain their relatively high transpiration rates over dry summer periods (Klinge et al., 2001; Knight, 1999; Robinson et al., 2006). Even if root density is reduced below a depth of 50 cm, deeper soil layers represent about 50 % of the water uptake during the wet periods and up to 75 % during the dry ones and are thus essential in the computation of the water balance of such ecosystems. In the present study, only the upper 3m of the soil profile were studied which means that the water uptake by the *Eucalyptus* trees may be underestimated particularly the second year after planting when the water requirements are greatest. Since the transpiration was adjusted to soil moisture measurements, the effective transpiration simulated by the model actually represents the transpiration of the *Eucalyptus* trees from the soil surface down to a depth of 3 m but it does not include the trees water uptake from deeper soil layers. TDR measurements at deeper depths are being conducted in the experimental site and will inform on this point.

As a consequence of the intensive uptake of the fast growing *Eucalyptus* stands, the average water drainage was < 5 % of the incoming rainfall at a depth of 3 m from 6 months after planting onwards. Drainage occurs at this depth during the wet season at a small constant rate (1 mm day^{-1}) or after large rainfall events. Deep soil layers also act as a water storage compartment for upper soil layers when drying occurs. Indeed, upward flow of about 1 mm day^{-1} occurs during the dry periods at a depth of 3 m and confirms the observations made for similar plantations by (Almeida et al., 2007; Soares and Almeida, 2001).

The optimization of the parameters regulating the *Eucalyptus* tree transpiration confirms its ability to take up water down to very low pressure heads. The regulation of the transpiration begins below a pressure head of -1 m but the smaller value of the p_1 parameter (0.5) compared to the literature (2.5) (Battaglia and Sands, 1997; Granier et al., 2007; Kirschbaum et al., 2007) implies that the transpiration is not severely regulated down to low pressure heads.

The heterogeneity among TDR probe measurements did not allow the estimation of differences in water consumption among the fertilization treatments. Direct measurements of the transpiration flux by sap flow monitoring are being conducted in the experimental stand and will inform on this point. They will also validate (or not) the effective transpiration simulated by the model.

Once the *Eucalyptus* stand was clear felled, drainage occured quickly in deeper soil layers as classically observed in *Eucalyptus* plantations (Goncalves et al., 1997). The fitted maximum evaporation was high (0.7 ET_{max}) but the effective evaporation flux was less since it was largely limited by the water availability of the upper soil layers. In average it represented 33 % of the incoming rainfall. The simulation of the evaporative flux was highly influenced by the depth down to which evaporation occurs as suggested by (Klinge et al., 2001; Mahfouf and Noilhan, 1991; Wu et al., 1999).

C.3.4 On the validity of the model to compute nutrient fluxes and to perform reactive transport modelling

The water fluxes were computed in average for treatment 3 which means that it did not simulate the heterogeneities of the water flux at the tree scale and among treatments. The present study showed that most of the heterogeneity is to be expected at the tree scale. The use of an average water flux to compute soil nutrient fluxes will thus necessarily induce large uncertainties in these calculations. Since soil solution collectors integrate spatial heterogeneity at the tree scale, we may nevertheless hypothesize that at the stand scale, the order of magnitude of the nutrient fluxes will be accurate. The largest errors are expected for solutions collected close to the tree stems, below the buried fertilization pocket.

Since the lower boundary of the soil profile was set at a depth of 3m and since the water contents showed little spatial heterogeneities at this depth, the nutrient flux leaving the soil profile is most likely accurate. However, the nutrient fluxes at the depths of 15 cm, 50 cm and 150 cm are likely to be overestimated. Of course, such nutrient fluxes will be highly dependant on the representativeness of the solutions collected by soil solution sampling devices.

In terms of chemical reactive transport, the major problems which need resolving are (i) the occurrence of a second type of porosity in which kinetically controlled reactions (slow) may prevail in opposition to larger pores where faster thermodynamically controlled reactions are expected, (ii) the spatial heterogeneity of the inflow at the soil upper boundary which may induce preferential dissolutions of fertilizers or faster nutrient transports within the soil profile, (iii) a wettability heterogeneity within the soil matrix which may systematically modify the water transport and the gas/solution equilibrium within certain pores of the soil profile.

PART D

SOIL SOLUTIONS

INTRODUCTION

Whereas soil properties may be slow to respond to a chronic stress, soil solution chemistry may provide an early indication of the long term changes in soils associated with a chronic stress (McDowell et al., 2004). The concentrations of a nutrient in soil solution may also be a useful indicator of nutrient limitation because these concentrations are an integral part of the mechanisms of nutrient supply and uptake and they are highly correlated with growth and yield of a range of plant species (Smethurst, 2000). Soil solution chemistry can have a large influence on the nutrient budgets of the ecosystem as losses of nutrients by deep drainage can be a major output for forest ecosystems (Marques, 1996). In this way, soil solution is a precursor of the groundwater and stream qualities (Stumm and Morgan, 1996). It is thus important (i) to monitor qualitatively the soil solution composition in particular after major disturbances of the ecosystem (clear felling and fertilizations) and (ii) to compute accurate nutrient fluxes leaving the system by deep drainage.

The effect of clear felling on soil solution composition has been widely studied in temperate as well as in tropical forests and plantations. After clear-felling, the mineralization of the forest floor and of the harvest residues and the nitrification of ammonium occur differently depending on vegetation and local conditions (Vitousek and Melillo, 1979). Increases of H^+ and NO_3^- in soil solutions released from the nitrification of ammonium (from the mineralization of the forest floor) have been observed in temperate ecosystems (Baeumler and Zech, 1998; Carnol et al., 1997; Iseman et al., 1999; Strahm et al., 2005; Zhang and Justice, 2001) as well as in Amazonia (Neill et al., 2006) or under *Eucalyptus* plantations in Australia (Smethurst et al., 2001). This increase in nitrate concentrations in soil solutions is particularly large when herbicide is applied (thus preventing the N uptake by the re-growing vegetation) or when the plant cover is not yet active (Duwig et al., 1998; Likens et al., 1978). For example, concentrations of NO_3 of up to 60 mg L^{-1} were observed at a depth of 10 cm after clear felling an *Eucalyptus* stand in Australia (Weston and Attiwill, 1996). On the other hand, clear felling may also stop the stimulating effect of the vegetation on soil nitrifyers thus leading to increases in ammonium concentrations in soil solutions after clear felling (Ranger et al., 2007; Titus et al., 1997).

Processes driving the composition and dynamics of soil organic matter are generally similar in temperate and tropical soils except that the turnover rates in tropical ecosystems are usually higher. The rates of transformations are controlled primarily by climatic factors and only to a lesser extent by chemical factors such as pH, C/N or litter quality (Zech et al., 1997). Generally, mineralization and nitrification are reported to occur at highest rates during late winter and spring when microbial activity is not limited by soil moisture deficits and soil temperatures are rising, and at lowest rates when the upper soil layers dry to below wilting point (Abbadie et al., 2000; Bustamante et al., 2006; Lilienfein et al., 2000; Moldan and Wright, 1998; O'Connell and Rance, 1999; Stuanes et al., 1995).

The nitrification process is particularly important for soil sustainability because it affects soil acidification in two principal ways: firstly the process of nitrification results in the net release of H^+ ions, 2nd, leaching of the highly mobile product NO_3, when it is not taken up by the vegetation, leads to an associated loss of soil cations (Julien et al., 2005; Reuss and Johnson, 1986; Van Miegroet and Johnson, 1993). The pH, the mineralogy and the exchange capacity of a soil dictate whether NO_3 leaching is balanced by H, Ca, Mg, Al or other cations. NO_3 leaching is generally correlated with Al release in acidic soils (pH<4.5) whereas base cations are released in less acidic soils (de Vries et al., 2003). The release of Al in soil solution may be toxic for plant growth and natural water biota and is thus of high importance. The most toxic forms of Al are Al^{3+}, hydroxyl-Al and $AlSO_4$ (Boudot et al., 2000). Enhanced acidification was already observed under *Pinus* in Brazil (Lilienfein et al., 2000), under *Eucalyptus* in Australia (Prosser et al., 1993) and in Hawaï (Rhoades and Binkley, 1996). The study of the fluxes of nitrates, Al, H and basic cations in soil solution after clear felling and planting is thus of great importance for (i) groundwater quality (pollution by NO_3 or Al in particular), (ii) soil sustainability (acidification and loss of nutrients reserves) and (iii) stand nutrition (loss of base cations by leaching). Regarding this last point, *Eucalyptus* plantations are reported to be highly dependant on the recycling of nutrients from the mineralization of the forest floor (Laclau et al., 2003c) and of the harvest residues after clear-felling (Deleporte et al., 2004-2006; Nambiar, 1996). The needs in fertilizers may be highly dependant upon this recycling and it is important to assess the forms and quantities of N in excess released in soil solution and its fate over the whole stand rotation.

Fertilizers are also major drivers of soil solution composition. Sulphate brought by fertilization is reported to enhance the mobility of Ca and Mg and to increase exchangeable

Mg and Ca contents (Adams et al., 1997; Carnol et al., 1997; Ponette et al., 1997) which may be provided by the dissolution of dolomitic limestone (Ponette et al., 1996). Mg and Ca released by the dissolution of fertilizers may also displace H and Al from exchange sites which then move down with the mobile SO_4 anions (Ponette et al., 1997). Seemingly, liming is reported to increase SO_4 and H_2PO_4 leaching in tropical ferralsols because more S and P are released from (i) the mineralization of organic matter (OM) by microorganisms growing in more favourable pH environment (ii) the chemical hydrolysis of OM, (iii) the desorption of previously adsorbed P and S and (iv) sparingly soluble Fe and Al hydroxyl sulphates and phosphates which become more soluble at higher pH values (Bolan et al., 1999; Mare and Leon, 1989). The consequences of N-fertilizer applications are mainly the same than after clear felling and are linked to the nitrification (or denitrification) of the applied ammonium (or nitrate) and its further leaching if it is not taken up by plants. N-fertilizers effects have been widely studied in northern temperate forests when increasing N-atmospheric depositions increased the scientific concern about possible N-saturation of the ecosystems and risks of forest dieback and groundwater pollution by nitrates (Aber et al., 1989; Aber et al., 1991; Emmett et al., 1995; Gundersen, 1998; Magill et al., 2000; Moldan and Wright, 1998; Stuanes and Kjonaas, 1998). Effects of N fertilizer applications has been studied in the tropics for crops (Duwig et al., 1998; Lehmann et al., 2004) or under coffee trees (Harmand et al., 2007) but few studies have been conducted under *Eucalyptus* plantations.

One major difficulty in soil solution studies is the experimental sampling of soil solutions. Various methods exist: destructive soil sampling combined to sequential extractions using centrifugation or not (not adequate for continuous monitoring), or on-site continuous sampling using various types of lysimeters or capillary wick samplers (Titus and Mahendrappa, 1996). Classically the joint use of zero tension lysimeters (ZTL) and tension lysimeters (TL) gives indications on the chemistry of the gravitational (ZTL) and of the weakly retained solutions (TL) and the chemical composition usually differs in solutions collected by ZTL from those collected by TL (Jaffrain, 2006; Marques et al., 1996; Ranger et al., 1993). The major difficulties associated to the use of ZTL or TL regards (Corwin, 2002; Ploeg and Beese, 1977; Titus and Mahendrappa, 1996): (i) the disruption of soil environment and soil solution natural flow, (ii) the volume of soil sampled, (iii) the range of pressure head effectively collected depending on the soil water regime at the time of sampling, (iv) the flow properties of the sampler which can be time

variant if the vacuum is unstable (TL) or if pores become clogged with fine material or microorganisms (TL), (v) the representativeness of the solution sampled as preferential channelling of soil solution through macropores may bypass TL samplers, (vi) the retention of ions on the lysimeter, (vii) the loss of volatile compounds and redox-dependent ions (TL) , and (viii) pH changes due to CO_2 degassing (TL).

Nevertheless, the sampled solutions provide relevant information about the changes occurring within the ecosystem, even though a real difficulty remains when trying to calculate nutrient fluxes. The flux of a solvated nutrient generally differs from the flux of the mobile phase in which it is solvated (mostly aqueous) due to chemical interactions, surface adsorptions with the soil matrix, diffusion phenomena, etc … One way to quantify nutrient fluxes would be to model them as classically done for water fluxes thanks to a multicomponent-reactive transport model such as MIN3P, but two difficulties are encountered to do so: the theoretical difficulty to model the nutrient flux (far more difficult than the water flux) and the experimental difficulty to sample soil water solutions to parameterize the models (as already explained). One classical approach to roughly estimate these fluxes is to multiply water fluxes simulated by the water flow model (part C) to the concentrations in nutrients measured in the sampled soil solutions. This method has been adopted in the present study.

The main goals of the soil solution study were (i) to identify the major processes governing soil solution dynamics and chemistry (vector ions and interactions), in particular after major ecosystem perturbations (clear felling and fertilizer application), and (ii) to estimate nutrient losses by drainage at a depth of 3m (output in the nutrient budget of the studied system). Nutrient fluxes at intermediary depths (15 cm, 50 cm and 150 cm) were also computed to help understanding the mineral functioning of the *Eucalyptus* stand together with the adsorption/desorption dynamics within the soil profile.

D.1 MATERIAL AND METHODS

D.1.1 Available data

D.1.1.1 Aboveground solutions

Aboveground solution collectors were those described in the water fluxes section. Briefly, rainfall (Pi) was collected in a 1 ha opened area adjacent to the experimental design (same devices as throughfall solutions), throughfall solutions (Th) were collected from devices made of 12 funnels located at different distances from the trees (nine repetitions before clear-felling, then one collecting device per experimental plot –$treatment_{1,3,5}$ x $block_{1,2,3}$-, 10 months after planting in block 1, and 14 months after planting in blocks 2 and 3). Stem flows (St) were collected before clear felling from eight helical collars installed on trees representative of the stand, then 20 months after planting, from helical collars installed on three trees per experimental plot ($treatment_{1,3,5}$ x $block_{1,2,3}$) (one composite sample per plot for chemical analyses) (Table 37). As it was shown in the water flux section that surface runoff (Ru) was less than 1% of rainfall, it was neglected in the soil solution study.

Table 37 Solutions collected and analyzed by ion chromatogry (IC), inductively coupled plasma (ICP) and dissolved organic carbon analyzer (DOC) over the experimental period in each treatment (T), block (B) and collector (C). The table indicates the combinations of T x B x C collected and analyzed. Superscript f stands for composites collected altogether in the field, whereas superscript l stands for composites prepared in laboratory. Unless mentioned in brackets, all analyses were performed (ICP/IC/DOC). 1:i stands for 1,2,…,i. ZTL=zero-tension lysimeter, TL=tension lysimeter.

Examples: T ={1+3+5}^{l} B={1:3}^{l} C={1:9}^{f} means that one single combination is possible: in the field, one sample was collected from nine collecting devices (superscript f), then one composite sample of all collected blocks and treatments was prepared in the laboratory (superscript l) and analyzed. T∈{1,3,5} B∈{1,2,3} C={1} means that one single collector was available in each treatment and block and that all samples were analyzed for each block and treatment independently.

		Year	2003		2004	Clear Felling		Planting		2005				2006	
		Month	7		1	2.2	3	4	12	1	5	6	12	1	4
		N_{month}	*1*		*8*	*9*	*10*	*11*	*19*	*20*	*25*	*26*	*32*	*33*	*37*
T	Stream, Rainfall														
	Stemflow													T∈{1,3,5}	
	Throughfall		T={1+3+5}^{l}							T∈{1,3,5}					
	ZTL, TL					T∈{1,3,5}									
B	Stream, Rainfall														
	Stemflow													B∈{1,2,3} (IC), B={1:3}^{l} (ICP/DOC)	
	Throughfall		B∈{1,2,3}							B∈{1}		B∈{1,2,3} (IC), B={1:3}^{l} (ICP/DOC)			
	ZTL, TL					B∈{1,2,3} (IC), B={1:3}^{l} (ICP/DOC)									
C	Stream, Rainfall		C={1}												
	Stemflow		C={1:8}^{l}											C={1:3}^{c}	
	Throughfall		C={1}							C={1}					
	ZTL	0 cm	C={1:9}^{f}												
		15 cm	C={1:5}^{f}												
		50 cm													
		100 cm	C={1:4}^{f}												
	TL	15 cm				C={1:4}^{f}		C={1:4}^{f}							
		50 cm						C∈{1:4} if T∈{3,5} & B=1 (IC), else C={1:4}^{f}							
		100 cm						C={1:4}^{f}		C∈{1:4} if T=3 (IC), else C={1:4}^{f}					
		300 cm						C∈{1:4} if T∈{3,5} & B=1 (IC), else C={1:4}^{f}		C∈{1:4} if T=3 or (T=5 & B=1) (IC), else C={1:4}^{f}					

D.1.1.2 Soil solution sampling equipment

Figure 51 Soil solution sampling equipments: zero-tension lysimeters in soils (A) and under the forest floor (C), pit where soil solutions were kept in the field (B) and pump used to maintain vacuum in tension lysimeters (D).

The soil solution sampling equipment was installed at the beginning of 2003 in delimited plots corresponding to blocks 1, 2 and 3 of treatments T1, T3 and T5 of the fertilization experiment planned on the same site after harvesting the 5.5-year-old *E. saligna* stand. The equipments were not moved after clear felling so that their distance to the nearest tree differed before clear felling and after planting as defined in Figure 4.

In each plot, 3 sets of 9 narrow zero-tension lysimeters (40 x 2.5 cm) (ZTL) were installed beneath the forest floor, five replicates of zero-tension plate lysimeters (50 x 40 cm) (ZTL) were introduced at the depths of 15, 50 and 100 cm, and four replicates of tension lysimeters (TL) (Soil Moisture, product n°1911, bubbling pressure of 100 kPa) were installed horizontally at the depths of 15 cm, 50 cm, 1 m, and 3 m. Tension lysimeters were maintained at a constant suction of –60 kPa thanks to a manual pump until May 2004 and to an automatic vacuum pump thereafter. Forest floor and ZTL solutions were collected in polyethylene containers located downhill (depth of 2 m) in closed pits. TL solutions were collected downhill in glass bottles (depth of 1 m for 15, 50 and 100 cm TL, and depth of 2 m for 300 cm TL). All lysimeters were introduced from pits backfilled after installation with the soil horizons in their natural arrangement and were set up representatively near and between the trees (Figure 51).

For each plot and collection depth, ZTL and TL replicates were collected in the same container (composite sample of nine lysimeters for the forest floor, of five lysimeters for ZTL and of four lysimeters for TL). After April 2004, TL replicates of treatments 3 and 5 were collected separately at the depths of 50 cm and 300 cm in block 1. After January 2005, TL replicates of treatment 3 were also collected individually at a depth of 100 cm in blocks 1, 2 and 3 and at a depth of 300 cm in blocks 2 and 3 (Table 37). Difficulties were encountered to maintain vacuum in tension lysimeters during the first months so that the data acquisition for TL actually began on 02/2004 (month 2.1 of Figure 6).

D.1.1.3 Chemical analyses

A 3-month period was left for soil stabilization. Then, solutions were collected weekly from the experimental catchment's area and kept in cooler. One composite sample was made every four weeks from the weekly collected samples, proportionally to their weekly collected volumes. The monthly composites were then filtered (0.45 µm) and their pH was measured. SO_4^{2-}, NO_3^-, NH_4^+, Cl^-, $H_2PO_4^-$, K^+, Ca^{2+}, Mg^{2+}, Na^+ were analysed by ion chromatography (IC) (Dionex) (CENA, Laboratorio de Ecologia Isotopica). Al, Fe, Si were determined by inductively coupled plasma (ICP) (CENA, Laboratorio de Química Analítica) and dissolved organic carbon (DOC) by Shimadzu equipment (CENA, Laboratorio de Biogeoquímica Ambiental).

The pH was measured for each monthly sample. ICP measurements were performed for one composite sample per collector type and depth until 04/2004 included, then for one

composite sample per treatment, collector type, and depth. DOC measurements were performed monthly for one composite sample per block, collector type and depth until 04/2004 included (except for stemflow solutions for which one composite sample of all treatments and blocks was analyzed), then for one composite sample per treatment, collector type, and depth. Dionex measurements were performed for one composite per block, collector type and depth until 01/2004 included (except stemflow for which one single composite of all blocks was analyzed), and for each sample individually thereafter (Table 37).

D.1.2 Data analysis

D.1.2.1 Time periods, time step, and fertilization dates

The studied periods were those of the water fluxes study and lasted from July 2003 to April 2006 (7 months before clear felling until 24 months after planting). Whereas the water flux study was made on a daily time step basis, the chemistry of the solutions was studied on a 4-week-time basis to reduce analytical cost. The four-week frequency of chemical analysis divided the year in 13 months. The 13th month was reported in February so that February 1 and 2 will be encountered in figures and tables. The number of analytical months elapsed since the beginning of the study (N_{month}) will be frequently used to simplify the data analysis (see Figure 6 for date correspondence).

The overall monitoring period was subdivided in three periods:

- before clear felling (BCF): 07/2003 (N_{month}=1) to 02(1)/2004 (N_{month}=8) included,
- after clear felling and before planting (CFP): 02(2)/2004 (N_{month}=9) to 03/2004 included (N_{month}=10),
- after planting (AP) (first two years of growth): 04/2004 (N_{month}=11) to 04/2006 included (N_{month}=37).

The last period (AP) was punctuated with fertilization events differing from one treatment to another (Table 1). The first event of fertilization occurred at planting (04/2004, N_{month}=11). In treatments 1 and 3, fertilizers were buried at a depth of 5 cm at both sides of each *Eucalyptus* seedling (half dose uphill, half dose downhill). For treatment 5, the sewage sludge was applied in two lines right uphill and downhill the planting row. The next fertilizations were spread on the whole surface area in 12/2004 & 01/2005

(N_{month}=19 & 20), then in 05/2005 (N_{month}=25), and finally in 11/2005 (N_{month}=31) (Table 1 & Figure 6).

The soil solution data analysis mainly aimed at studying the dynamics of nutrient concentrations and fluxes and in particular, the dynamics of exceptional events (particularly large concentrations and fluxes resulting from the silvicultural practices (clear felling, planting, fertilizations…). The data continuity was thus favored as much as possible to better identify and differentiate exceptional events from the baseline and the ecosystem background signals. The 37 months of monitoring were studied continuously for the whole period and were not grouped into different sub-periods as in the water fluxes study to preserve data continuity.

D.1.2.2 Nutrient fluxes calculation

D.1.2.2.1 Water fluxes in lysimeters

The soil solution compositions available to compute nutrient fluxes are those of the solutions collected by ZTL and TL. In this study, TL and ZTL were considered as collecting the soil water flux in different ranges of pressure heads, that is, as collecting part of the soil solution. The main consequence is that in the present study the nutrient fluxes calculated are those potentially collected by ZTL or TL, that is, a fraction of the whole nutrient fluxes and a fraction of the water fluxes simulated in part C. Their representativenes regarding the whole nutrient flux in soils is discussed.

The best way to estimate water fluxes in ZTL and TL collectors would be to model them as sinks directly into the MIN3P simulations. This would require (i) at least 2-D simulations, and (ii) the knowledge of the effective potential at the captor end. In the present study, we simplified the problem by considering that the water fluxes in the lysimeters corresponded to the simulated fluxes of part C, integrated over the range of pressure heads collected by the lysimeters. The main difficulty was thus to set these ranges of pressure heads.

For ZTL, we observed experimentally that ZTL collected soil solution mainly at a depth of 15 cm when the soil was wet and stopped below a pressure head of -0.5 m. This value was thus kept to estimate water fluxes in ZTL at a depth of 15 cm. ZTL at deeper depths were not studied since they collected very low amounts of water. For TL, the average of the dry and wet thresholds for each depth was used to estimate water fluxes in collectors.

For TL, we used rough theoretical calculations to estimate the ranges of pressure heads sampled by the ceramic cups, as calculated in Figure 52 when the collecting tube is full of water (wet conditions) or full of air (dry period).

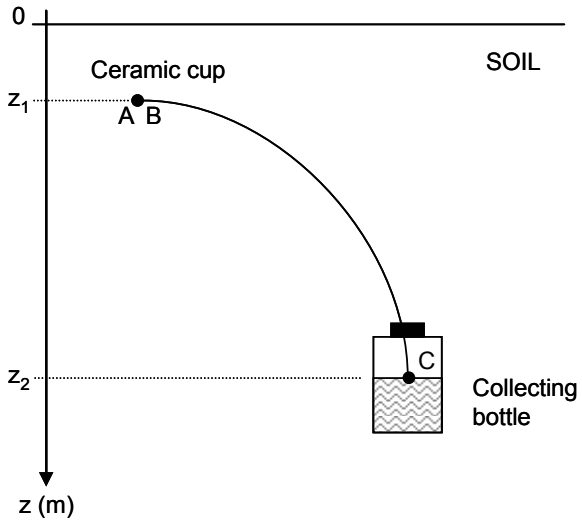

$h_A=h_{atm}+h_m-z_1$ (h_m = pressure head in m)

$h_B=h_C$ (collecting tube full of air)

$h_B=h_C-(z_2-z_1)$ (collecting tube full of water)

$h_C=h_{atm}-6$ (TL)

Water movement for $h_A > h_B$

	full of air	full of water
TL	$h_m > z_1-6$	$h_m > 2\,z_1-z_2-6$

Lower theoretical limit for h_m for samplers of the experiment

		Full of air	Full of water
TL	15 cm	-5.85	-6.30
	50 cm	-5.50	-5.50
	100 cm	-5	-5
	300 cm	-3	-2

Figure 52 Theoretical conditions for soil solution collection in tension lysimeters (TL). Pressures and potentials (h) are given in m of water. H_{atm}=10 m=100 kPa. Collection containers were placed at a depth of 1 m for TL collecting water at the depths of 15, 50 and 100 cm and at a depth of 2 m for TL collecting water at a depth of 3 m.

The ceramic cups were considered as ideal and punctual samplers. Actually, the samplers are not ideals (porosity and wettability of ceramic cups, dimension of the collecting pipe…) and the collection tubes are neither full of air nor full water but generally constituted of a succession of complex biphasic water / gaz bubble systems. The calculated ranges of pressure for ZTL used for further calculations are thus theoretical and may differ from the ranges of pressure truly collected in the field.

Only drainage fluxes were taken into account since it was impossible to differentiate soil solution due to upward fluxes from soil solution due to downward fluxes in the solutions collected by the lysimeters.

D.1.2.2.2 Calculation of nutrient fluxes

Nutrient fluxes were obtained by multiplying the nutrient concentration measured in the soil solution by the water flux estimated from the above paragraph for the collecting lysimeter.

As already mentioned in the water fluxes section, the water flux was considered invariant in the horizontal plane. For a given observation date and depth, the differences between two nutrient fluxes in two different treatments, blocks, or collectors, were thus the result of differences in the nutrient concentrations.

D.1.2.3 Missing data and aberrant data tracking

Missing data occurred when (i) no water was collected by the collecting device because the pressure head was below the pressure head threshold of the device, or for TL in case of vacuum drop, (ii) the collected volume was insufficient to perform chemical analyses, (iii) the analysis was missing (hardly ever).

Missing data are classically estimated from other collectors and sampling times. This was not performed here since the fertilization events resulted in localized (time and space) very high peaks of concentration, and since there were few records left uninfluenced by these events (management practices). Missing data were thus considered as “not a number” (NaN) for concentrations and nutrient fluxes (integrated as spatial heterogeneity). Average fluxes were always calculated from an average concentration multiplied by the water flux so that an average flux was null only when all fluxes composing the average were null.

For the same reasons than for missing analysis, no efficient aberrant data tracking could be reliably performed. For a given sample, it was impossible to differentiate sample pollution during the analytical process from a fertilization peak. Ionic balances were checked but pollution often occurs as a cation-anion pair. Moreover, organic charges (DOC and DON) contributed quite largely to the ionic balance for some samples but their charge could not be determined. The analytical process was carefully checked. Data were kept un-modified and the analytical risk of pollution was integrated as spatial variability.

D.1.2.4 Analysis of the concentrations and cumulative fluxes signals

D.1.2.4.1 General strategy

The time-course of concentrations and cumulative fluxes can be analyzed as spectra (same as a chromatogram spectrum for concentrations and same as a pH-titration for cumulative fluxes). In this study, an equivalent chromatogram was considered constituted of three parts: the baseline, the background signal, and the exceptional events:

- the baseline contains the analysis uncertainty and the average minimum signal,
- the background signal (above the baseline) reflects the mean specific signal of the ecosystem without exceptional perturbations, spatial variability among collectors and analysis uncertainty,
- and the exceptional events (major peaks) represent flushes of nutrients in solutions due to specific processes (high atmospheric deposits, fertilization, microbial activity …).

Baseline and background signals depend on collector type, collection depth and mineral element analyzed. Exceptional events depend mainly on changes in the entry signal (rainfall) and on silvicultural practices. The main difficulty in such an analysis is to define the baseline, the ecosystem background signal and the threshold above which a peak is regarded exceptional.

D.1.2.4.2 Baseline, background signal and thresholds

Our main goal was to study the exceptional events, that is, the clear felling and the fertilization effects. Usually, the baseline and background signals are estimated from a time-period poor in exceptional event and long enough to include seasonal variations.

Consequently, the exceptional events are those concentration peaks greater than the average variations around the background signal. Our study period was too short to do so, particularly for tension lysimeters for which almost no data were available before clear felling.

The baseline was thus estimated from concentration spectra for each mineral element, as the first quartile of all measured data (3 blocks x 3 treatments x 37 months) for each collector type and depth. The first quartile was chosen since it favors the lower values and minimizes the effect of exceptional events on the result. This baseline was subtracted to cumulative fluxes to better analyze the effect of exceptional events on the nutrient flux dynamics.

Background signal was defined only for aboveground collectors (for which few exceptional events occurred) as the median of the population for each collector type and mineral element analyzed.

The threshold for exceptional events was not calculated from the background signal but from the maximum signal resulting from exceptional events (CF_{max}). This maximum was calculated as the maximum of all final (N_{month}=37) cumulative fluxes after baseline subtraction (average per treatment, collector type and collection depth). The average cumulative flux was chosen for minimizing the influence of localized (time and space) large concentration peaks and for integrating the whole period of the experiment. CF_{max} was taken as the maximum for all collector types, collecting depths, treatments and mineral elements (expressed in mmol) in order to have a common reference for all collectors, that is, (i) to identify the maximum response of the ecosystem to a given perturbation, (ii) to observe its attenuation with depth and its dispersion in time and space, and (iii) to compare its intensity according to the mineral element observed. For DOC which could not be expressed in mmol, CF_{max} was taken as the greatest cumulative flux recorded.

The threshold above which a final cumulative flux is considered to have experienced an exceptional event (CF_t) was then taken as $CF_t=CF_{max}/50$, which is approximately one tenth of the CF_{max} transmitted at a depth of 3 m given the attenuation of the water flux at this depth. The threshold for nutrient fluxes CF'_t was taken as $CF'_t=CF_t/12$, where $CF_t/12$ represents the average monthly ionic flux of CF_t spread over 12 months (actually observed for the present study). The threshold for concentrations (C_t) was then CF'_t divided by the average monthly water flux.

D.1.2.4.3 Spectra analysis

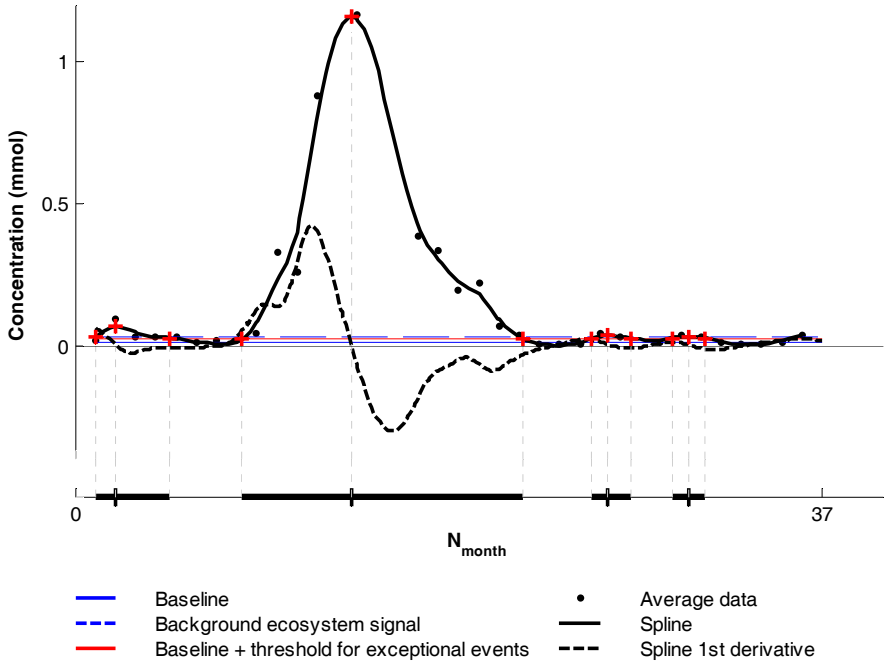

Figure 53 Example of spectrum analysis for concentrations.

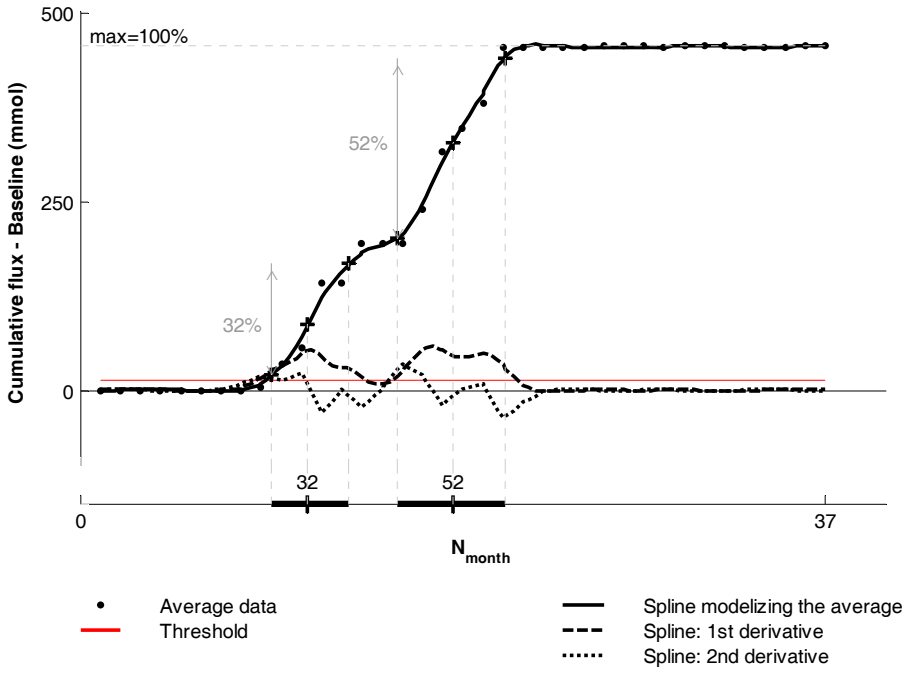

Figure 54 Example of spectrum analysis for cumulative flux.

Spectra analysis had to be performed on a continuous function whereas experimental data were discontinuous at a monthly time step. The concentration spectra were thus simulated continuously thanks to a slightly smoothed spline using Matlab software (www.mathworks.fr). The peaks of the spectra were then calculated as the zeros of the spline 1st derivative for which the concentration was above baseline+C_t (Figure 53).

For cumulative fluxes, only the spectra for which the final cumulative flux was above CF_t were analyzed. The data were also simulated thanks to a slightly smoothed spline. The equivalences between two plateaus (time and intensity) were given by the zero of the second derivative of the spline (Figure 54).

The concentration spectra were mainly used qualitatively to localize exceptional events and to compare the dynamics of one nutrient in respect to the others. Cumulative fluxes were used for all quantitative studies.

D.1.2.5 Ionic strength

The ionic strength (IS) in mol was calculated as:

$$IS = \frac{1}{2}\sum_i z_i^2 C_i \qquad (58)$$

where i are the mineral elements in solution, z_i is the charge of each element and C_i its concentration in mol L^{-1}. The charge attributed to each element was +1 for K, Na and NH_4, +2 for Ca and Mg, +3 for Al and Fe, -1 for Cl, NO_2, NO_3 and H_2PO_4, and -2 for SO_4.

Ionic strength was calculated as an indicator of the status of the sampled solution but since no speciation study was performed (especially for Al), it must be handled cautiously. The pKe of the first acidity of Al is 5 (Stumm and Morgan, 1996) and soil solution pH were mainly < 5 so that Al was considered as 3+ in the ionic strength calculation. It is obviously a rough approximation since organic ligands and locally basic pH may reduce the positive charge of Al (Driscoll and Schecher, 1990).

D.1.2.6 Statistical analyses

The effect of treatment on cumulative fluxes (from the clear felling until the end of the experimental period) was tested for each collector type and depth, and for each element thanks to one-way ANOVA analyses and t-tests using proc GLM of SAS Software. Differences among treatments were considered significant at $P < 0.05$.

D.1.2.7 Sequence of data analysis adopted

Finally the data analysis was performed in the following way:

- All mass data were converted to moles to enable direct comparisons among elements.
- Baselines and thresholds were first calculated on concentration spectra and cumulative flux spectra respectively.
- Aboveground fluxes were studied mainly on the basis of their concentration spectra. Baseline and background signal (median) were quantified and exceptional events localized to identify whether atmospheric events may interfere with clear felling and fertilization events in soil solution signals.
- Soil solutions were then studied considering ZTL only at a depth of 15 cm (since deeper ZTL collected almost no water), and TL only after February 2004 (since vacuum difficulties did not allow continuous sampling before). Cumulative fluxes were studied, once their baseline subtracted, for the whole period continuously so that, unless mentioned, an offset must be considered between ZTL and TL. It was done so in order to better visualize the ecosystem background signal from exceptional events when those signals were both available (ZTL).
- Nitrate and sulphate were analyzed in detail as case studies. For these two elements, the average concentration and the average cumulative flux spectra were first studied for each collector type, collection depth and treatment. The spatial variability of the signal among the three blocks was studied qualitatively reporting the data of each block on the studied average spectra. The spatial variability among individual collectors was also studied on cumulative fluxes by qualitatively comparing the spectrum analysis of each individual collector (available for TL at depths 50 cm, 100 cm and 300 cm in treatments 3 and 5). Concentrations in solutions collected by ZTL and TL were qualitatively compared at a depth of 15 cm.
- Differences in nutrient dynamics were finally studied by comparing the average spectra analysis for each nutrient (concentrations and cumulative fluxes). Total cumulative fluxes (including baseline) from the clear felling to the end of the

experiment (no more offset between ZTL and TL) were finally given with their standard errors (variability among blocks and collectors).

To better visualize the differences among collectors or elements, the projections of the concentration and cumulative spectras on the time axis were generally preferred to their corresponding 2D-plots which are space consuming (Figure 53 & Figure 54).

D.2 RESULTS AND DISCUSSION

D.2.1 Water fluxes collected by the lysimeters calculated from the MIN3P simulations

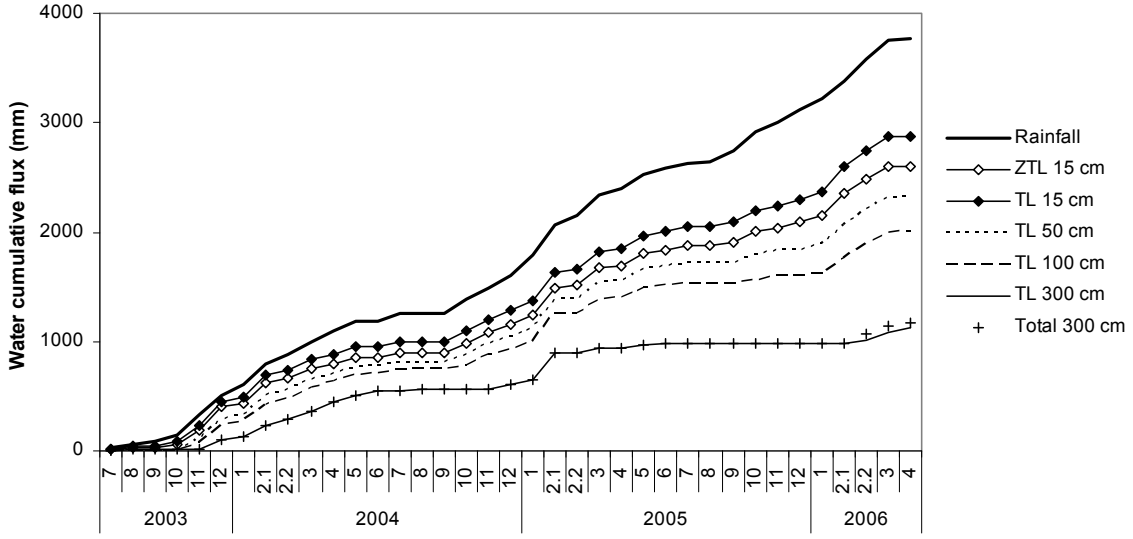

Figure 55 Estimated cumulative water fluxes (mm) drained in the soil profile (total) and collected by the lysimeters (ZTL=zero-tension lysimeter, TL= tension lysimeter) at a given depth (estimation from the water flux model of part C and from the pressure head ranges of D.1.2.2). The cumulative flux measured for rainfall is also represented.

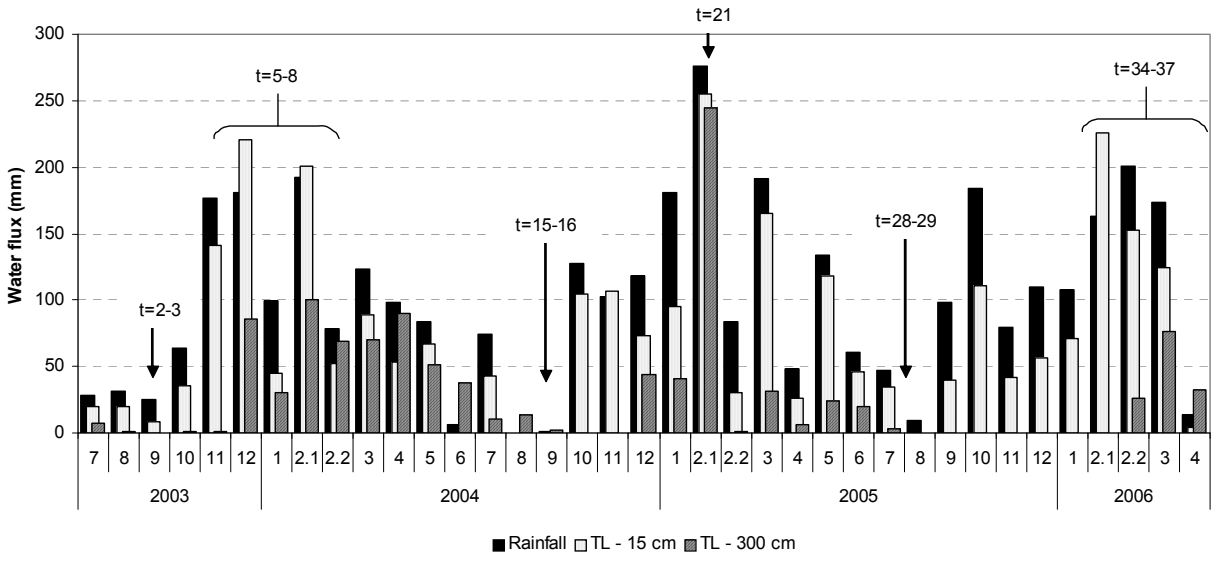

Figure 56 Water fluxes (mm) measured for rainfall (Pi) and calculated from the soil water flux model for tension lysimeters (TL) at the depths of 15 cm and 300 cm, over the studied period. The most pronounced wet and drought events are indicated in total months elapsed since the beginning of the study ($t=N_{month}$).

At the depths of 15 cm, 50 cm and 150 cm, the calculations show that tension lysimeters may collect the whole soil water flux simulated by the water drainage module of MIN3P (part C). Indeed, the pressure head theoretically collected by TL at these depths ranged from less than -5 m to 0 m (Table 37) which corresponded to the whole retention curve of Figure 39, that is, to the entire water flux simulated at these depths. As the lower boundary -5 m is located on a plateau of the retention curve, a slight change in this lower boundary will not influence much the water flux collected. These calculations were confirmed by field observations: TL always collected water at these depths during the periods of drainage indicated by the model. TL water fluxes thus calculated are likely to approximate the water fluxes effectively collected at these depths as far as (i) the water flux model is accurate, (ii) TL do not deviate too much from their ideal behavior, and (iii) a constant vacuum is guaranteed.

At a depth of 300 cm, calculations show that TL may collect the whole soil water flux when the soil is wet but barely any flux during the very dry period of February 2006. Indeed, the pressure head theoretically collected by TL at a depth of 3 m ranged from about -2.5 m to 0 m. The lower boundary -2.5 m is located on the far end of the steep decreasing part of the retention curve which meant that (i) the collected water flux represents almost the whole water flux except a residual part moving very slowly in the soil profile, and (ii) a small change or error of determination in the lower boundary may influence greatly the water flux fraction collected. These calculations were confirmed on field: TL at a depth of 300 cm showed a greater heterogeneity in their ability to collect water during the dry periods and were very sensitive to slight drops of the vacuum applied. The model used to compute the water flux collected in TL at a depth of 300 cm is thus submitted to the same restrictions as mentioned for TL at depths of 15, 50 and 150 cm, and is likely to overestimate the water flux effectively collected during the dry periods. As a direct consequence, TL at a depth of 300 cm may not sample the whole soil water flux during the dry periods.

The model estimated that the proportion of the whole drainage sampled by ZTL was in average 80% at a depth of 15 cm (Figure 55 & Figure 56) which, once more, corresponded to the steep part of the retention curves of Figure 39. This means that ZTL are expected to collect the major part of the water collected by TL at a depth of 15 cm especially in periods of large drainage (high pressure heads). On the other hand, the solutions collected by TL and ZTL are expected to differ when drainage occurs at lower pressure heads. Moreover,

as TL collect water down to lower pressure heads, TL may collect chemical species in a lower state of potential than does ZTL, that is, species moving in soil solution closer to the soil surface than does ZTL (due to specific adsorption or in smaller pores for example).

The fact that almost no water was collected in ZTL at the depths of 50 cm and 100 cm confirms that no major preferential flow occurred in the studied soils. As mentioned in section 5 (water flux model), intensive water drainage occurred down to a depth of 3 m from November 2003 to February 1 2004 (N_{month}=5 to 8), in February 1 2005 (N_{month}=21), and from February 1 to March 2006 (N_{month}=34 to 37). Periods of drought occurred in August and September of each year (N_{month}=2-3, 15-16, and 28-29). At a depth of 300 cm, the 2005-2006 drought lasted from 07/2005 until 02-2/2006.

D.2.2 Median and quartile, aboveground solutions

D.2.2.1 Baselines

Table 38 Concentration baselines (µmol L^{-1} and mg L^{-1} for DOC) calculated for each element and collector type as the 1st quartile of all blocks and treatments data for the studied period and background ecosystem signal calculated for aboveground collector as the medians of all blocks and treatments data.

Collector type	Depth (cm)	Element concentration														
		H	Cl	NO_2	SO_4	NO_3	H_2PO_4	Na	NH_4	K	Mg	Ca	Fe	Al	Si	DOC
		µmol L^{-1}														*mg L^{-1}*
1st quartile = baseline																
Aboveground and stream collectors																
S		1	9		0	0		17	0	3	11	10	1		170	1
Pi		2	9	0	3	7	0	4	4	3	2	6		0	1	1
Th		3	13		3	7		6	5	10	4	7	0		0	2
St		7	32		3	5		23	2	26	10	14			0	15
Soil and forest floor solution collectors																
ZTL	**0**	2	33		5	7		17	3	30	23	29	2	6	7	19
	15	43	30		7	9		15	1	8	16	10	1	11	33	8
TL	**15**	25	37	0	6	7	0	18	0	8	15	15		19	121	4
	50	28	34		1	16		14	1	6	8	13	0	23	129	2
	100	28	35		0	44		13	0	3	6	8		17	99	1
	300	4	10		0	26		10	0	3	4	9		0	80	1
Median = ecosystem background																
Aboveground and stream collectors																
S		2	15	0	0	0		19	0	5	15	15	2	1	190	2
Pi		4	11	1	5	12	0	6	16	6	4	9		0	1	1
Th		5	20	1	6	14		10	10	14	7	13	0	0	1	4
St		16	48	0	4	9		42	9	43	21	28		1	1	26

S=Stream, Pi=rainfall, Th=Throughfall, St=Stemflow, ZTL=zero tension lysimeter, TL=tension lysimeter

All baselines except Si (< 170 µmol L^{-1}) and DOC (DOC < 19 mg L^{-1}) were < 50 µmol L^{-1} (Table 38). For NO_2, PO_4 and Fe the baselines and medians were very low (< 2 µmol L^{-1}) whatever the collector. The analytical "noise" was thus generally < 0.5 ppm whatever the element analyzed so that the concentrations above this threshold can be reliably attributed to the ecosystem. It also indicates that no major continuous pollution occurred for all the collecting devices.

Al and Si baselines were respectively 2 and 4 times as much in TL as in ZTL at a depth of 15 cm. This behavior could be explained by the influence of the high concentration peaks occurring after clear felling and fertilizing on the baseline calculation for TL (contrary to ZTL, no before-clear-felling data were used to calculate TL baseline),

or to a slight contamination of the soil extracts by the porous cup material as classically observed (Titus and Mahendrappa, 1996). In contrast, H and DOC baselines were two times as much in ZTL as in TL. The filtration of large organic molecules through the poral network of the ceramic cups (TL) is also classically observed (Corwin, 2002; Titus and Mahendrappa, 1996).

Stream baselines (but Si) were < 20 μmol L^{-1} and equaled 1 mg L^{-1} for DOC. The ecosystem background was less than two times its corresponding baseline. This average signal is far less than the legislation of drinkable water of the European Union for all elements (UE, 1998) and indicates high quality water regarding the measured elements.

Aboveground solutions contained very small amounts of NO_2, H_2PO_4, Fe, Al and Si (baselines and medians < 2 μmol L^{-1}). The stemflow ecosystem background was about twice the throughfall one, and four times the rainfall one for Cl, K, Mg and Ca (rainfall medians of 5 μmol L^{-1} for Mg, 6 μmol L^{-1} for Na and K, 9 μmol L^{-1} for Ca and of 11 μmol L^{-1} for Cl). SO_4 ecosystem background was more or less the same for all collectors (median of about 6 μmol L^{-1}). H and DOC ecosystem backgrounds were low in rainfall and throughfall (medians < 5 μmol L^{-1} and mg L^{-1}) but increased in stemflow (medians of 16 μmol L^{-1} for H and 26 mg L^{-1} for DOC). The opposite behaviour was observed for NO_3 (medians of about 13 μmol L^{-1} in rainfall and throughfall, and of 9 μmol L^{-1} in stemflow) and NH_4 (medians of 16, 10 and 9 μmol L^{-1} in rainfall, throughfall and stemflow respectively). The baseline pH decreased in the following order: stream (5.7) > Rainfall (5.4) > Throughfall (5.3) > Stemflow (4.8). The ecosystem backgrounds ranged between once to twice their corresponding baselines.

The overall pattern for above ground solutions is thus that an increase in H, Cl, K, Mg, Ca and DOC occurs while passing through the *Eucalyptus* crown (throughfall) or when running off the *Eucalyptus* stem. On the contrary, uptake of nitrogen through its nitrate or ammoniacal form occurred during the transfer of the solution from the canopy to the soil. This pattern is classically observed in tropical forests (Xu et al., 2005) and plantations (Laclau et al., 2003a) as well as in temperate forests on N deficient soils (Gonzalez-Arias et al., 2006; Klopatek et al., 2006). Stemflow do not represent much of the water flux entering the soil, but as its input is localized at the stem basis and its solutions are particularly concentrated, they may induce a heterogeneous pattern in soil solutions along main roots (Beier, 1998; Cattan et al., 2007; Levia and Frost, 2003).

The corresponding baselines in term of cumulative fluxes are given in Table 39.

D.2.2.2 Thresholds

Table 39 Baseline cumulative flux (mmol L^{-1} and mg L^{-1} for DOC) for each element, collector type and collection depth (all blocks and treatments taken altogether for the studied period), and cumulative flux minus baseline cumulative flux for each element, collector type, collection depth and treatment (all blocks taken altogether for the studied period). The maximum cumulative flux is given in bold.

Collector type	Depth (cm)	Tr	Element cumulative flux over the 37 months of the studied period														
			H	Cl	NO_2	SO_4	NO_3	PO_4	Na	NH_4	K	Mg	Ca	Fe	Al	Si	DOC
			mmol														*g*
Baseline cumulative flux																	
Pi			*8*	*36*	*1*	*12*	*28*	*0*	*17*	*17*	*14*	*9*	*26*	*0*	*0*	*2*	*4*
ZTL	**0**		7	129	0	19	27	0	66	12	115	90	113	9	24	25	72
	15		112	78	0	18	24	0	38	2	21	40	27	3	29	87	21
TL	**15**	**Average**	55	80	0	13	16	0	39	0	18	32	33	0	42	264	9
	50		54	66	0	2	31	0	28	1	11	17	26	0	45	254	5
	100		48	61	0	0	76	0	22	0	6	10	15	0	29	172	2
	300		4	10	0	0	26	0	10	0	3	4	9	0	0	80	1
Cumulative flux – Baseline cumulative flux																	
Pi			*22*	*36*	*3*	*6*	*20*	*1*	*12*	*41*	*8*	*6*	*9*	*0*	*0*	*6*	*2*
ZTL	**0**	**1**	58	149	15	9	37	2	39	43	97	168	88	1	2	10	25
		3	91	249	13	196	36	7	78	376	156	159	98	8	11	13	37
		5	118	257	17	218	84	10	103	346	155	18	53	24	18	22	25
	15	**1**	104	70	2	4	181	1	32	25	32	24	17	1	43	27	8
		3	193	151	6	303	254	19	71	187	86	65	75	1	79	54	15
		5	244	227	7	276	588	1	40	364	83	29	80	2	240	94	6
TL	**15**	**1**	30	275	4	29	325	1	120	20	90	49	34	0	69	53	6
		3	63	80	3	320	456	96	119	131	63	94	235	0	108	66	9
		5	78	323	5	75	572	3	54	28	191	19	37	0	189	12	2
	50	**1**	35	335	1	11	328	0	139	104	101	23	8	0	109	9	3
		3	23	99	2	83	428	2	109	94	46	39	45	0	102	11	4
		5	46	300	2	6	624	0	54	8	200	17	10	0	203	65	1
	100	**1**	32	592	1	2	211	0	78	97	211	17	15	0	130	54	3
		3	1	70	1	3	316	0	146	53	21	21	17	0	51	0	3
		5	32	105	5	1	355	0	51	5	35	16	15	0	130	0	2
	300	**1**	5	8	0	0	16	0	12	5	2	6	12	0	15	15	3
		3	2	2	1	0	3	0	4	4	1	1	1	0	1	0	1
		5	11	6	0	0	22	0	34	4	1	3	7	0	3	0	1
		Maxima	244	592	17	320	**624**	96	146	376	211	168	235	24	240	94	37

As mentioned in the material and methods sections, the thresholds were calculated from the cumulative flux for each element, treatment, collector type and collection depth, once the baseline subtracted (Table 39). The greatest cumulative flux (624 mmol) was obtained

for nitrate, in TL of treatment 3 at a depth of 50 cm. The threshold for cumulative fluxes was then of SC_t=12.5 mmol (734 mg for DOC), which was of the same order of magnitude than Pi cumulative fluxes. The threshold for ion flux was then SC'_t=1.04 mmol month^{-1} (61 mg month^{-1} for DOC). The average water flux for TL at 50 cm was of 66 mm month^{-1}, which gave a threshold for concentrations of C_t=16 µmol L^{-1} (1 mg L^{-1} for DOC).

ANOVA analysis were not performed for the data of Table 39 since such an analysis will be finally performed on cumulative fluxes from the clear felling until the end of the experimental period to conclude the soil solution chapter in §D.2.5.4.

D.2.2.3 Exceptional events for aboveground solutions

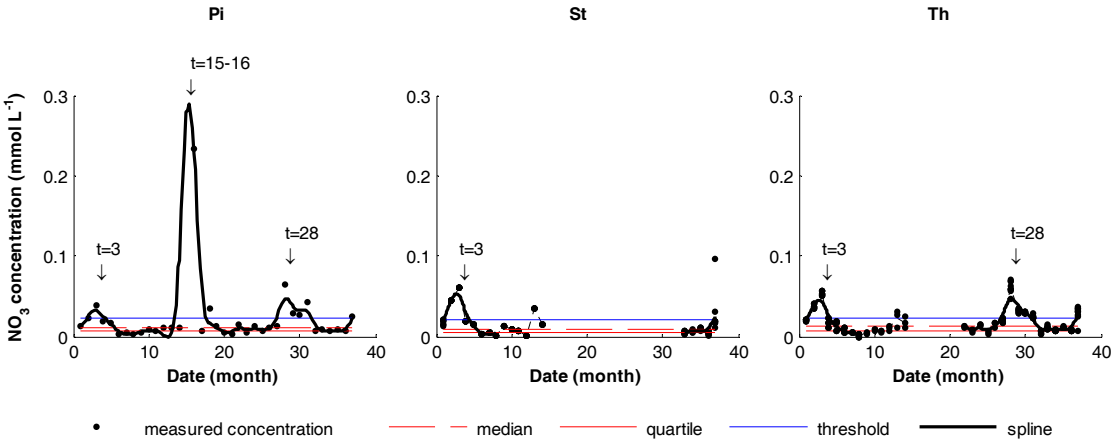

Figure 57 Time-course (t=N_{month}) of nitrate concentrations (mmol L^{-1}) in aboveground collectors (Pi=Rainfall, Th=Throughfall, St=Stemflow). The first quartile (baseline) and the medians (ecosystem background) of the populations are given, together with the concentration threshold (Ct=16 µmol L^{-1}) and the spline modelizing the average.

Aboveground solution concentrations were homogeneously dispersed around the median concentration (Figure 57 for nitrates). Baselines and medians were below C_t except for Cl, Na, K, Mg and Ca in stemflow collectors which were in the range [threshold, threshold*3]. Once more, it is suggested that even if stemflows represent a small part of the total inflow at the upper boundary of the soil profile it can induce patterns of spatial heterogeneities in nutrients fluxes (Beier, 1998; Cattan et al., 2007; Levia and Frost, 2003).

Table 40 Time (t=N_{month}) and intensity (mmol L^{-1}) of exceptional events in aboveground solutions collectors (Pi=Rainfall, Th=Throughfall, St=Stemflow).

N_{month}	Collector type	H	Cl	NO_2	SO_4	NO_3	PO_4	Na	NH_4	K	Mg	Ca	Fe	Al	Si	DOC
		mmol L^{-1}														*mg L^{-1}*
3	Pi	-	-	-	-	0.03	-	-	0.05	-	-	0.04	-	-	-	2.94
	St	-	-	-	-	0.05	-	0.55	0.07	0.26	0.19	0.22	-	-	-	-
	Th	-	-	-	0.03	0.04	-	0.03	0.05	0.04	0.02	0.05	-	-	-	6.21
15-16	**Pi**	**-**	**0.19**	**-**	**0.08**	**0.29**	**-**	**0.07**	**0.19**	**0.09**	**0.09**	**0.15**	**-**	**-**	**-**	**22.11**
28	Pi	-	0.04	-	-	0.05	-	-	0.07	0.02	-	0.03	-	-	-	3.93
	Th	-	0.12	-	0.02	0.05	-	0.03	0.05	0.06	0.04	0.06	-	-	-	12.21

The concentration spectra analysis for aboveground collectors outlined three events above C_t for N_{month}=3, 15-16, and 28 (Table 40 and Figure 57) for all elements but Fe, Al, Si, H, NO_2 and PO_4 which were always very low for aboveground collectors. The main peak occurred at N_{month}=15-16 for which rainfall concentrations reached 0.29 mmol L^{-1} for NO_3, 0.19 mmol L^{-1} for Cl and NH_4, 0.15 mmol L^{-1} for Ca and 22.11 mg L^{-1} for DOC. Exceptional events could not be seen in stemflow at N_{month}=15-16 and N_{month}=28, and in throughfall at N_{month}=15-16, since these collectors were disabled at these dates. These three concentration peaks corresponded to the dryer months of years 2003, 2004 and 2005 during which rainfall was < 30 mm $month^{-1}$. They may be attributed to the leaching by small amounts of water of dry depositions accumulated during the droughts, as classically observed (Laclau et al., 2003a).

As a conclusion, the large concentrations which may be observed in the forest floor and soil solutions may not result from the average input of throughfall. Concentration peaks up to 0.05 mmol L^{-1} may locally (at the stem basis) result from the average stemflow input. Concentration peaks up to 0.3 mmol L^{-1} may result from exceptionally concentrated stemflow and throughfall inputs during the dry periods. Figure 58 summaries the chronology of events related to high concentrations in aboveground collectors or to the ecosystem management.

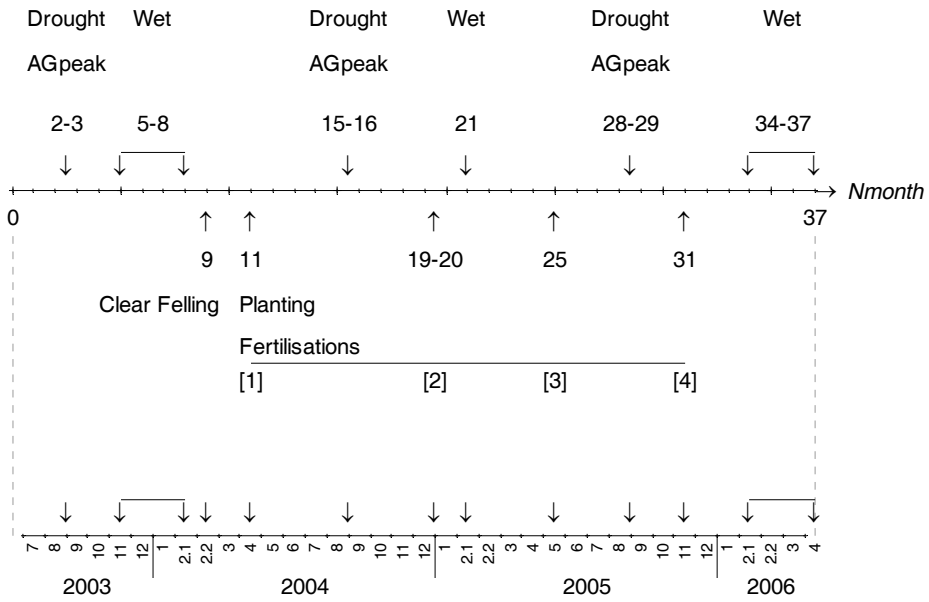

Figure 58 Chronology of events related to high concentrations in aboveground collectors (AGpeak), to the weather (wet or drought) or to the ecosystem management (mainly silviculture) in the experiment.

D.2.3 Soil solutions, case study 1: nitrate

D.2.3.1 Concentrations

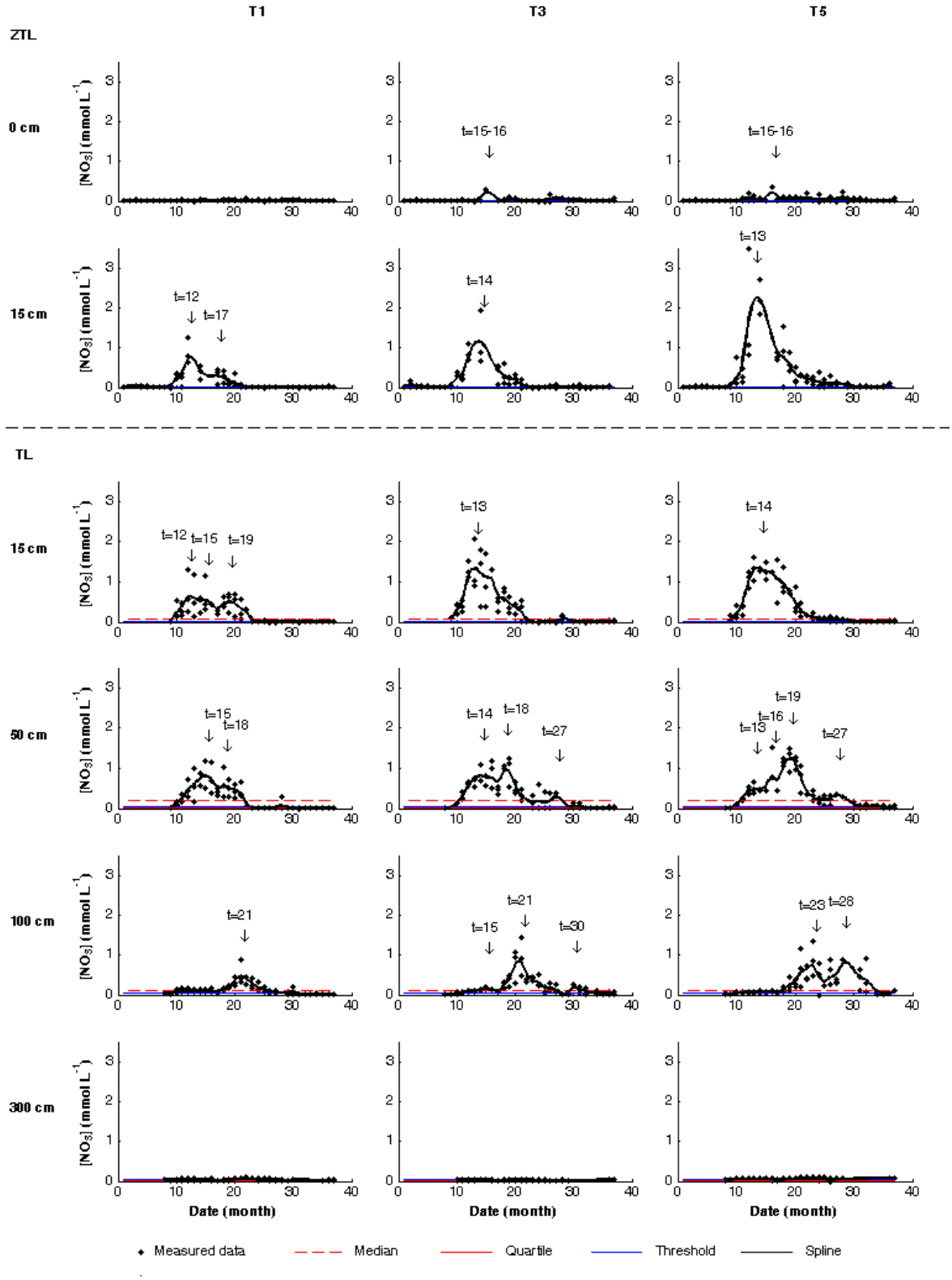

Figure 59 Time course of the concentration in nitrate (mmol L^{-1}) measured in each treatment and soil solution collector (ZTL=zero tension lysimeter, TL=Tension lysimeter) over the 37 months of monitoring. The quartile and median of the populations (all treatments taken altogether) are represented. The main peaks localized above the threshold of § D.2.2.2 are indicated together with the spline modelizing the average concentration.

Forest floor solutions showed a nitrate concentration peak in T3 and T5 at N_{month}=15-16 (Clear Felling (CF) + 6 months), which corresponded to a drought period and consequently to a nitrate concentration peak in solutions collected above ground (Figure 59).

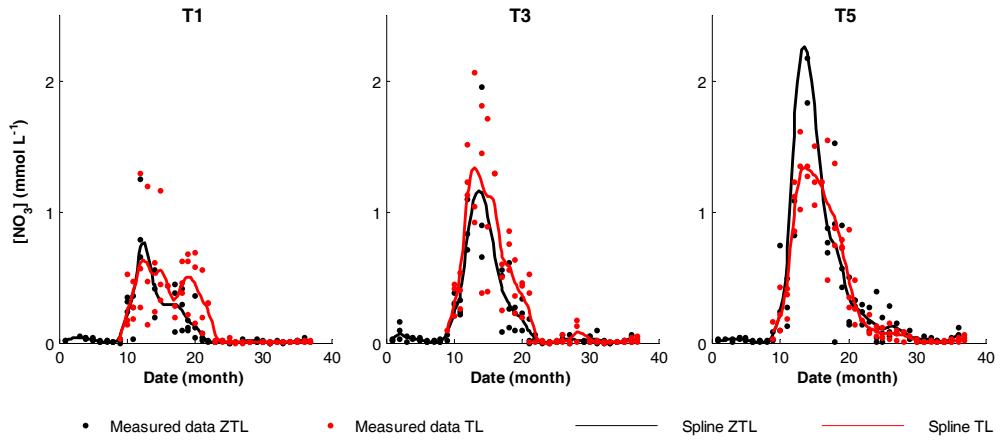

Figure 60 Nitrate concentrations in mmol L^{-1} measured in zero tension lysimeter (ZTL) and tension lysimeter (TL) at a depth of 15 cm. The spline modelizing the average concentration is also represented.

At a depth of 15 cm, the dynamics of nitrate concentrations were equivalent in ZTL and TL (Figure 60) as was suggested by the water fluxes study (§D.2.1). Three major concentration peaks occurred in T1 at N_{month}=12 (CF+2), N_{month}=15-16 (CF+5, drought and AG peak), and N_{month}=19 (CF+10, Fertilisation 2 with KCl (F2)). Concentrations peaks were greater in T3 and T5 than in T1 so that one single peak at N_{month}=13-14 (CF+4) could be distinguished.

The concentration peaks were transmitted at a depth of 50 cm at N_{month}=14-15 (CF+5), 18-19 (CF+9) and 27 (CF+18, F2+8). The delay between concentration peaks at 15 cm and at 50 cm ranged from 3-4 months to 8 months in case of drought periods.

At a depth of 100 cm, the concentration peaks appeared at N_{month}=15 (CF+6), 21-23 (CF+12, large drainage period after drought) and N_{month}=30 (CF+21, F2+11, large drainage period after drought). The delay between concentration peaks at 50 cm and at 100 cm was thus of about 3 months.

At a depth of 300 cm, no significantly large nitrate peak was observed.

NO_3 concentrations reached up to 3, 1.5, 1 and < 0.2 mmol L^{-1} at the depths of 15, 50, 150 and 300 cm respectively, which corresponded to 217, 93, 62, and 12 mg L^{-1} respectively.

The projection of each plot of Figure 60 on the time axis informs more in detail on the onset and ends of the peaks (Figure 61).

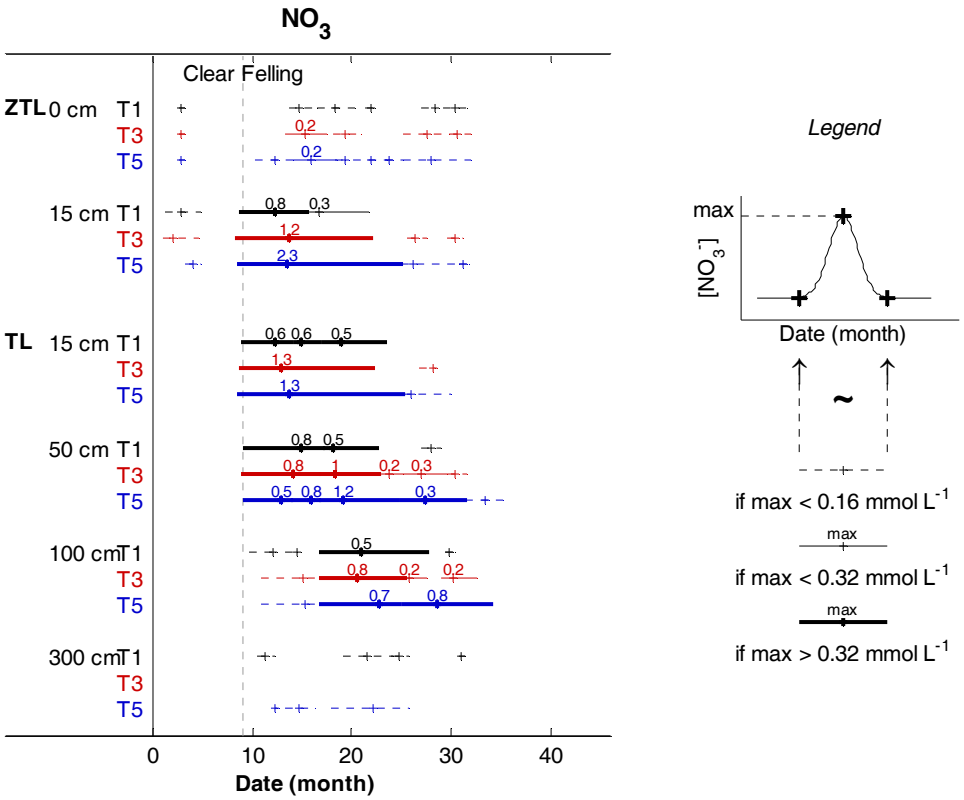

Figure 61 Projection of the average concentration in nitrate (mmol L^{-1}) measured in each treatment (T1, T3 and T5) and soil solution collector (ZTL=zero tension lysimeter, TL=Tension lysimeter) on the time axis (month). Only concentration peaks above the threshold Ct are represented. The value of 0.16 mmol L^{-1} was chosen as ten times the threshold defined for concentrations (§ D.1.2.4.2).

Figure 61 confirms that all peaks were weak in the forest floor solutions. They occurred after droughts (N_{month}=3, 16-19, 30-31), high rainy events (N_{month}=22) and after N fertilizer was spread on soil (N_{month}=12 (F1) in T5 and 19-22 (F2) in T3 and T5). The main peak started at N_{month}=14 (CF+5) in all treatments and lasted 3 months in T1, 4 months in T3 and 5 months in T5.

The main concentration peak started at clear felling (N_{month}=9) at a depth of 15 cm (TL and ZTL) and at 50 cm. At a depth of 100 cm, it started weakly at N_{month}=11 (CF+2) then

markedly at N_{month}=17 (CF+8, first large drainage period after drought). At a depth of 300 cm, concentration peaks appeared very weakly (max<0.16 mmol L^{-1}).

Main peaks lasted longer in T5 (16 months at 15 cm, 21 months at 50 cm and 17 months at 100 cm) than in T3 (13 months at 15 cm, 19 months at 50 cm and 16 months at 100 cm) and in T1 (13 months at 15 cm, 14 months at 50 cm and 11 months at 100 cm). Greatest peak intensities were always observed in T3 or T5.

D.2.3.2 Cumulative fluxes

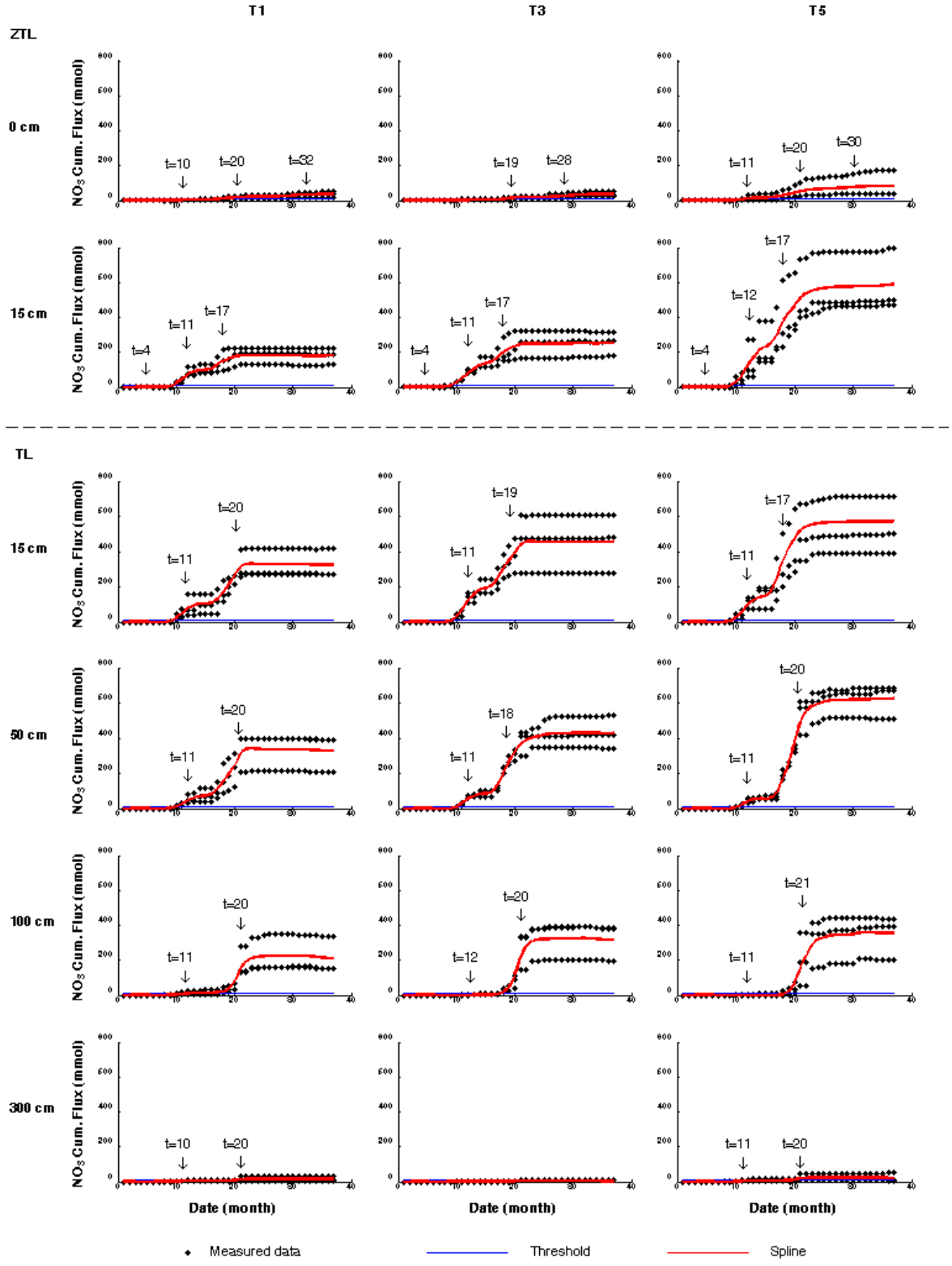

Figure 62 Cumulative fluxes (minus baseline) of nitrates (mmol) calculated for each soil solution collector (ZTL=zero-tension lysimeter, TL=tension lysimeter) in each treatment (T1, T3 & T5) over the 37 months of the studied period. The threshold for cumulative fluxes SC_t is represented, together with the spline modelizing the average cumulative flux for all blocks (n=3). The main steps are indicated.

Events appear far more homogeneously for cumulative nitrate fluxes than for concentrations. Four nitrate flushes occurred at N_{month}=4 (after 1st drought) in ZTL at 15 cm, N_{month}=10-11 (CFP period) and N_{month}=17-21 (F2, intensive drainage period after drought) for all collectors and depths, and N_{month}=30-32 (F4, intensive drainage period after drought) in the forest floor.

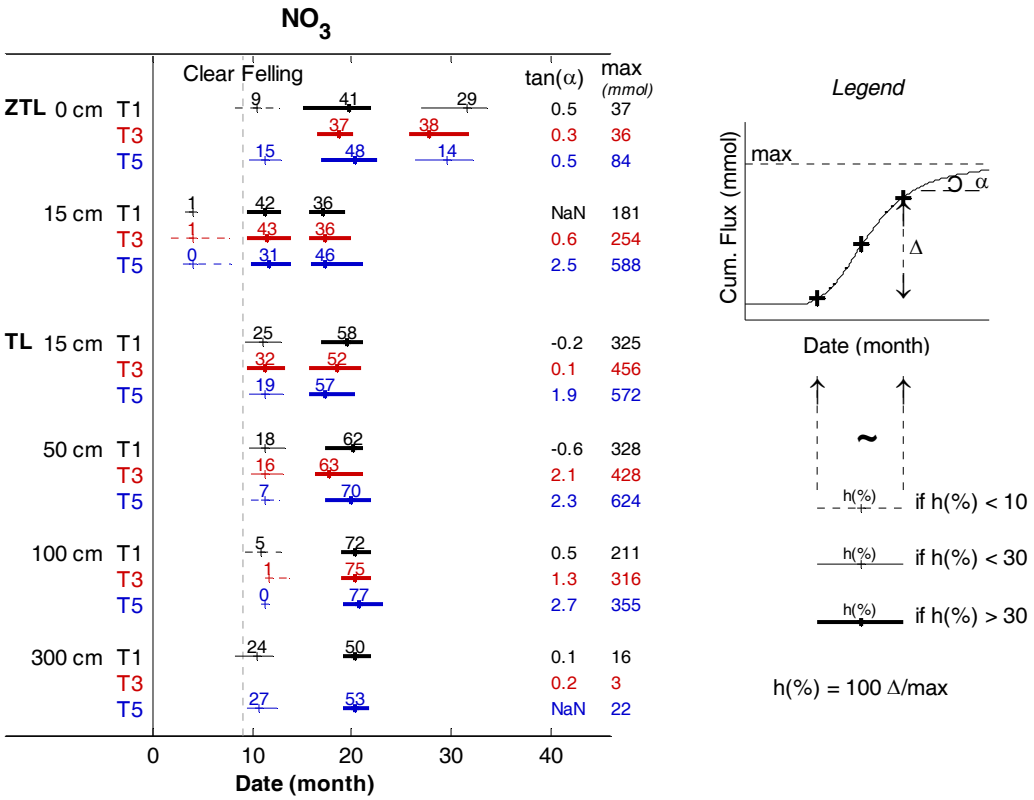

Figure 63 Projection of the average cumulative nitrate fluxes (mmol) (minus baseline) calculated for each soil solution collector (ZTL=zero-tension lysimeter, TL=tension lysimeter) in each treatment (T1, T3 & T5) on the time axis (month). The cumulative flux (max) and the slope of the curve tangent (tan α) at the end of the experimental period are indicated. The contribution of each step to the final cumulative flux is also given (h(%)). Steps were calculated only when max > SC_t (§ D.2.2.2). NaN stands for non calculable (tangent close to zero or step still running at the end of the studied period).

The projection of the average cumulative nitrate fluxes on the time axis (Figure 63) shows that the flushes last in average four months. At a depth of 15 cm, two concentration flushes contribute to final cumulative fluxes in equal proportion for ZTL (40 % each). In TL, whilst the contribution of the 1st flush decreases with depth (30% at 15 cm, 20% at 50 cm and less than 5% at 100 cm), the contribution of the second flush increases (55% at 15 cm, 65% at 50 cm and 75 % at 100 cm).

Final cumulative fluxes were very small at a depth of 300 cm (< 21 mmol). They were always in the following order: T5 > T3 > T1. Quasi no attenuation of the total nitrate flux was observed between TL at 15 cm and TL at 50 cm (max≈325 mmol in T1, max≈440 mmol in T3, max≈500 mmol in T5). About 2/3 of the 15 and 50 cm fluxes reached a depth of 100 cm (max=211 mmol in T1, max=316 mmol in T3, max=355 mmol in T5). In the forest floor, cumulated fluxes over the whole period were about 10 % of the fluxes estimated from TL collectors (max=37 mmol in T1 and T3, max=84 mmol in T5).

The slope of the curve tangent at the end of the experiment (tanα) showed that a plateau was reached in T1 and T3 at the depths of 0 cm and 15 cm (tanα close to zero), but that nitrates fluxes are still increasing for T5 at a depth of 15 cm and in T3 and T5 at the depths of 50 and 100 cm (tanα between 1.3 and 2.7).

D.2.3.3 Spatial variability

Qualitatively, Figure 60 and Figure 62 showed that the dynamics of nitrate concentrations and fluxes did not differ among the three blocks measured, but that the final cumulative flux of nitrates varied up to 50 % around its average among the three blocks.

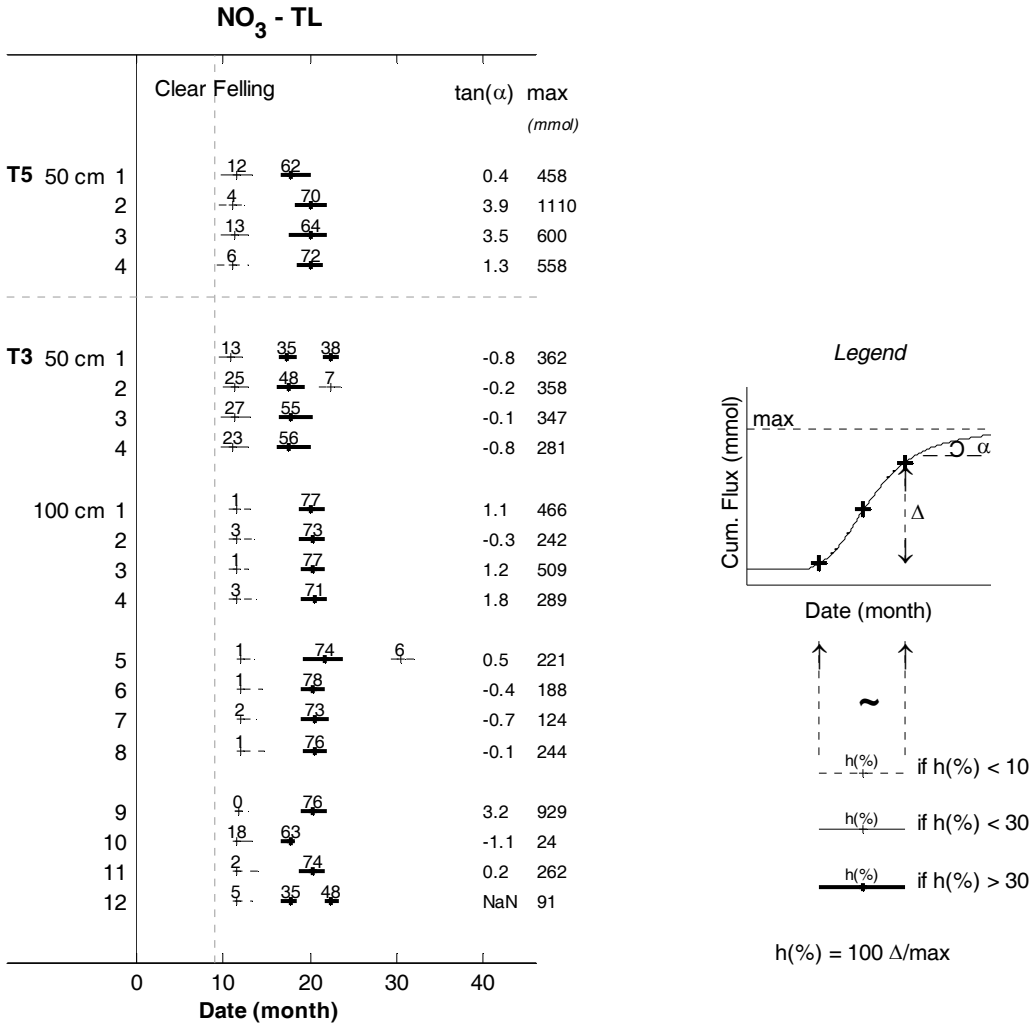

Figure 64 Projection of the nitrate cumulative flux (minus baseline) on the time axis (month) for each tension lysimeter (TL) collected independently at 50 cm in block 1 treatments 3 and 5 (collectors 1 to 4), and at 100 cm in block 1, 2 and 3 of treatment 3 (collectors 1 to 12). The cumulative flux (max) and the slope of the curve tangent (tan α) at the end of the experiment are indicated. The contribution of each step to the final cumulative flux is also given (h(%)). Steps were calculated when max > SCt of § D.2.2.2.

The main differences among individual TL were in the final cumulative flux (at a depth of 50 cm, max=682 ± 292 mmol (average ± standard deviation) in T5 and max=337 ± 38 mmol in T3, and at a depth of 100 cm, max=299 ± 242 mmol in T3). In T5, the largest cumulative flux measured by TL 2 can be explained by its location below the fertilization line of the sewage sludge. In T3, the different TL were located at different distances from the planting row: TL 1, 5, 9 under the stem basis (M1 of Figure 14), TL 2, 6, 10 (M3) and TL 4, 8, 12 (M7) in the inter-rows, and TL 3, 7, 11 in-between (M6). No clear spatial trend could be observed in Figure 64. This may be explained by (i) the

homogeneization of the water flux between the depths of 15 cm and 100 cm observed in part C, (ii) the 1-D horizontally invariant simulated water flux which may underestimate, for example, the flux at the stem basis, or plainly by (iii) the spatial homogeneity of nitrate production and leaching.

D.2.3.4 Conclusions and discussion

Nitrates were mainly released in soil solutions in the upper 15 cm of the soil profile after clear felling (main peak) and after N fertilizing and may be explained by (i) the mineralization and nitrification of the harvest residues and of the soil organic matter after clear felling which released large quantities of nitrates in soil solution which were no more taken up by the vegetation, and (ii) the mineralization of the sewage sludge in T5 and the dissolution+nitrification of the ammonium sulphate in T3. These patterns were classically observed in temperate as well as in tropical eco-systems (Gundersen, 1998; Harmand et al., 2007; Neill et al., 2006; Smethurst et al., 2001; Vitousek and Melillo, 1979) As the use of glyphosate prevented the vegetation re-growth and thus the nitrate uptake, the concentration peaks were particularly high. This pattern was classically observed in plantations using chemical weedings after logging (Duwig et al., 1998; Weston and Attiwill, 1996).

Nitrogen fertilizations enhanced nitrate production and its subsequent release in soil solutions which lasted from 13 to 16 months at a depth of 15 cm. In particular in T5, the continuous mineralization of the sewage sludge led to a greater leaching of nitrate which lasted more than in T1 and T3. The high solubility of ammonium sulphate led to shorter times of nitrate release in T3 than in T5.

Nitrate production was enhanced during the periods of large drainage just following droughts which is not surprising since the most favorable conditions for nitrifying populations are reported to occur during the wet periods of moderate temperatures (Bustamante et al., 2006; Lilienfein et al., 2000; Moldan and Wright, 1998; O'Connell and Rance, 1999; Stuanes et al., 1995; Zech et al., 1997). As the clear felling and the first N-fertilization occurred during a well drained period with warm temperature (end of summer), almost no-delay occurred between the clear felling and the beginning of the nitrate production and its subsequent leaching.

Nitrates were leached to deeper soil layers in periods of large drainage quasi instantaneously down to a depth of 1 m whereas the concentration peaks were delayed between 3 to 8 months from a 15 to 50 cm and from 50 to 100 cm. This suggests two different behaviors for nitrates in soil solutions: (i) a rapid leaching in periods of large drainage, and (ii) a slow diffusion in drier periods. The first large nitrate leaching occurred after the clear felling and the 1st fertilization. Its intensity decreased slightly between the depths of 15 cm and 50 cm, and then nitrates disappeared from the soil solution between the depths of 50 and 100 cm. The second large nitrate leaching occurred 6 months later, and its intensity only began to decrease below a depth of 50 cm. This behavior suggests a progressive saturation of the soil adsorption capacity from the soil surface down to a depth of 1 m. Both flushes did not reach the depth of 300 cm, which suggests that the main soil adsorption capacity for nitrates lies between the depths of 100 and 300 cm, as was measured in part B. However, this pattern might also reflect N uptake by trees which increased greatly from age 6 months onwards. Even if very large nitrate concentrations were reached at the depths of 15, 50 and 100 cm (> 100 mg L^{-1}), nitrate concentrations at a depth of 300 cm was always < 50 mg L^{-1} (Figure 60) which is the legal threshold in Brazil and in Europe for drinkable sub-surface waters.

Since the simulated water flux was horizontally invariant, it was quite difficult to assess the spatial heterogeneity of the nitrate flux. Still, nitrate concentrations were quite homogeneous among treatments. At the tree scale, T5 showed a well defined pattern of increasing nitrate concentration below the sewage sludge fertilization line at a depth of 50 cm.

D.2.4 Soil solutions, case study 2: sulphate

D.2.4.1 Concentrations

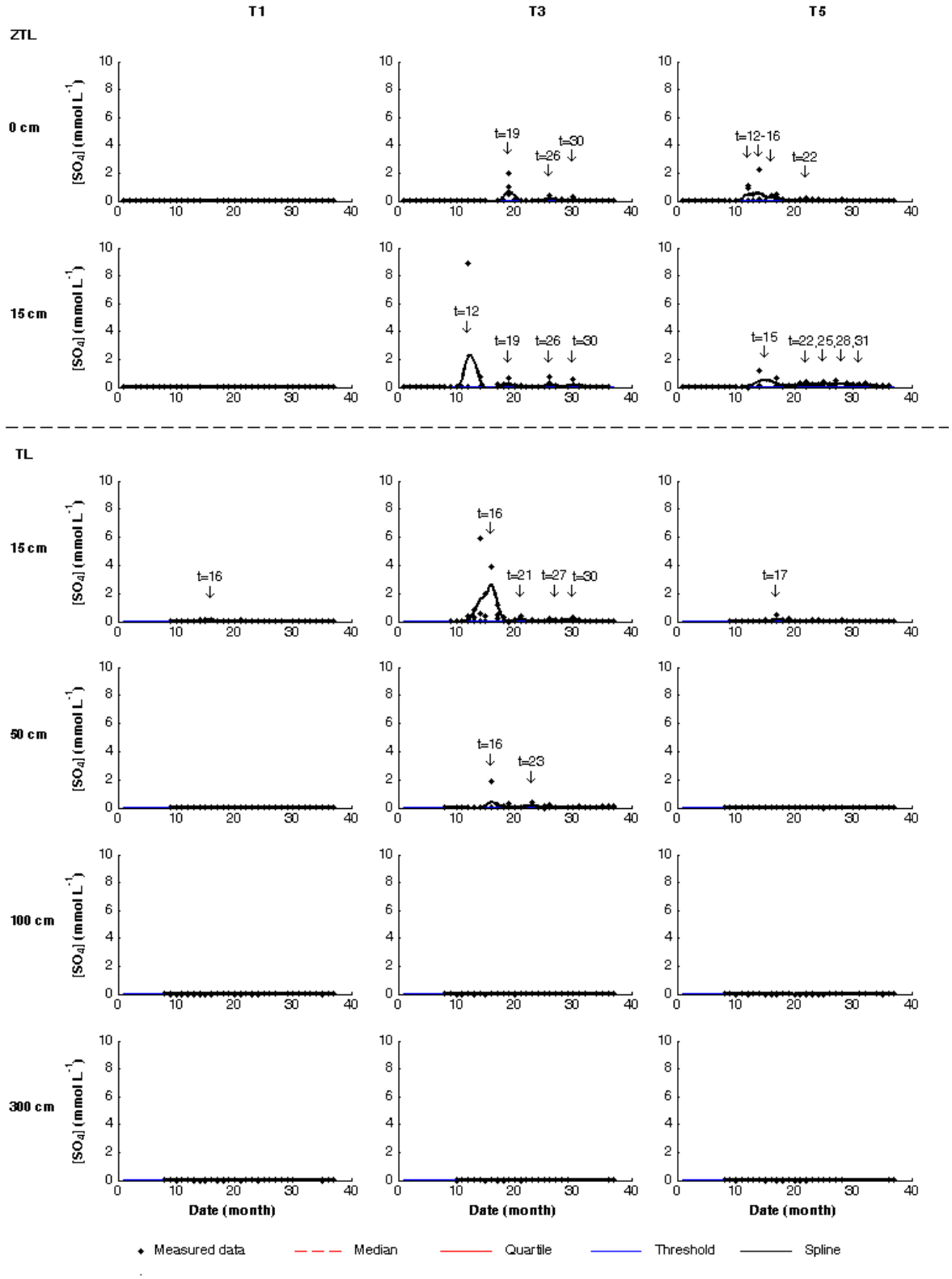

Figure 65 Time course of sulphate concentrations (mmol L^{-1}) measured in each treatment and soil solution collector (ZTL=zero tension lysimeter, TL=Tension lysimeter) over the 37 months of monitoring. The quartile and median of the populations (average for all treatments) together with the spline modelizing the average concentration in each treatment are represented. The main peaks above Ct (threshold for concentrations) are given.

Concentration peaks above C_t for sulphate occurred almost only in treatments 3 and 5 (Figure 65), down to a depth of 50 cm in T3, and down to a depth of 15 cm in T5.

In T3, concentration peaks occurred in TL and ZTL down to a depth of 15 cm when fertilizers were applied on soils, that is, at N_{month}=19-21 (F2), 26-27 (F3) and 30-31 (F4). The first fertilization (buried at a depth of 5 cm) was detected only at a depth of 15 cm. The related peak started at N_{month}=11 (F1) in TL and ZTL, but reached its maxima later in TL than in ZTL (N_{month}=12 (F1+1) in ZTL, N_{month}=16 (F1+4, large drainage after drought) in TL) (Figure 65). At a depth of 50 cm, concentration peaks occurred at N_{month}=16 (F1+4, intensive drainage after drought) and N_{month}=23 (F2+4, wet period).

In T5, concentration peaks occurred in TL at N_{month}=17 (F1+6, intensive drainage after drought), and in ZTL from N_{month}=12 to 16 (F1-F1+5), then from N_{month}=22 (F2+2, wet period) to N_{month}=30 quite continuously.

Except for solutions collected in the forest floor in T3, the first peak was always the main peak in terms of maximum concentration (Figure 66).

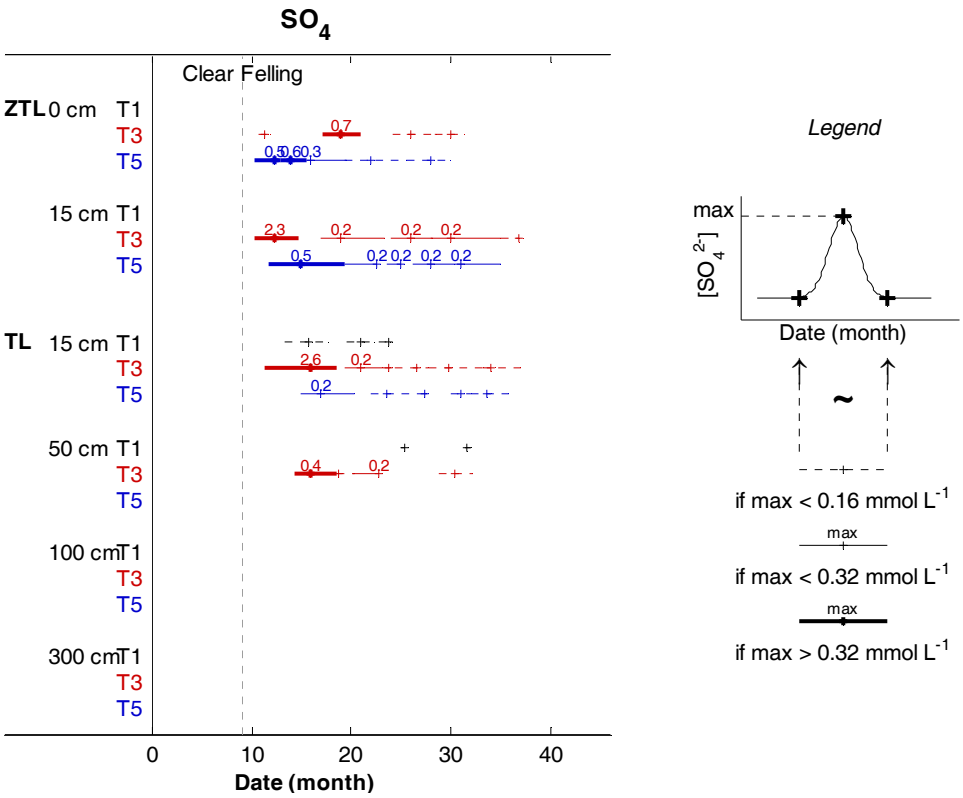

Figure 66 Projection on the time axis (month) of the average concentration in sulphate (mmol L^{-1}) measured in each treatment (T1, T3 and T5) by each collector type (ZTL=zero tension lysimeter, TL=Tension lysimeter). Only concentration peaks above the threshold are represented. The value of 0.16 mmol L^{-1} was chosen as ten times the threshold defined for concentrations.

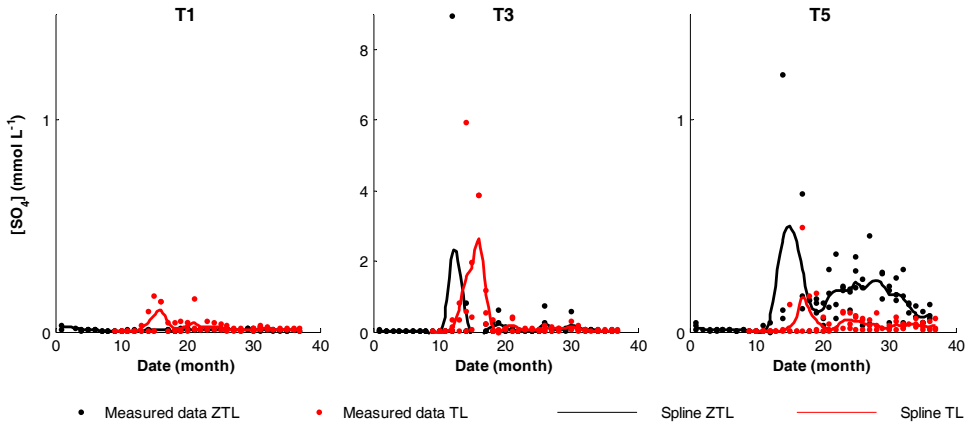

Figure 67 Sulphate concentrations in mmol L^{-1} measured in zero tension lysimeter (ZTL) and in tension lysimeter (TL) at a depth of 15 cm. The spline modelizing the average concentration is also represented.

More differences were observed between TL and ZTL at a depth of 15 cm for sulphate than for nitrate (Figure 67). The dynamics of sulphate were comparable in both sampler types but TL seems to register the sulphate concentration peaks later than does ZTL. In T5, ZTL collected more sulphate than TL.

D.2.4.2 Cumulative fluxes

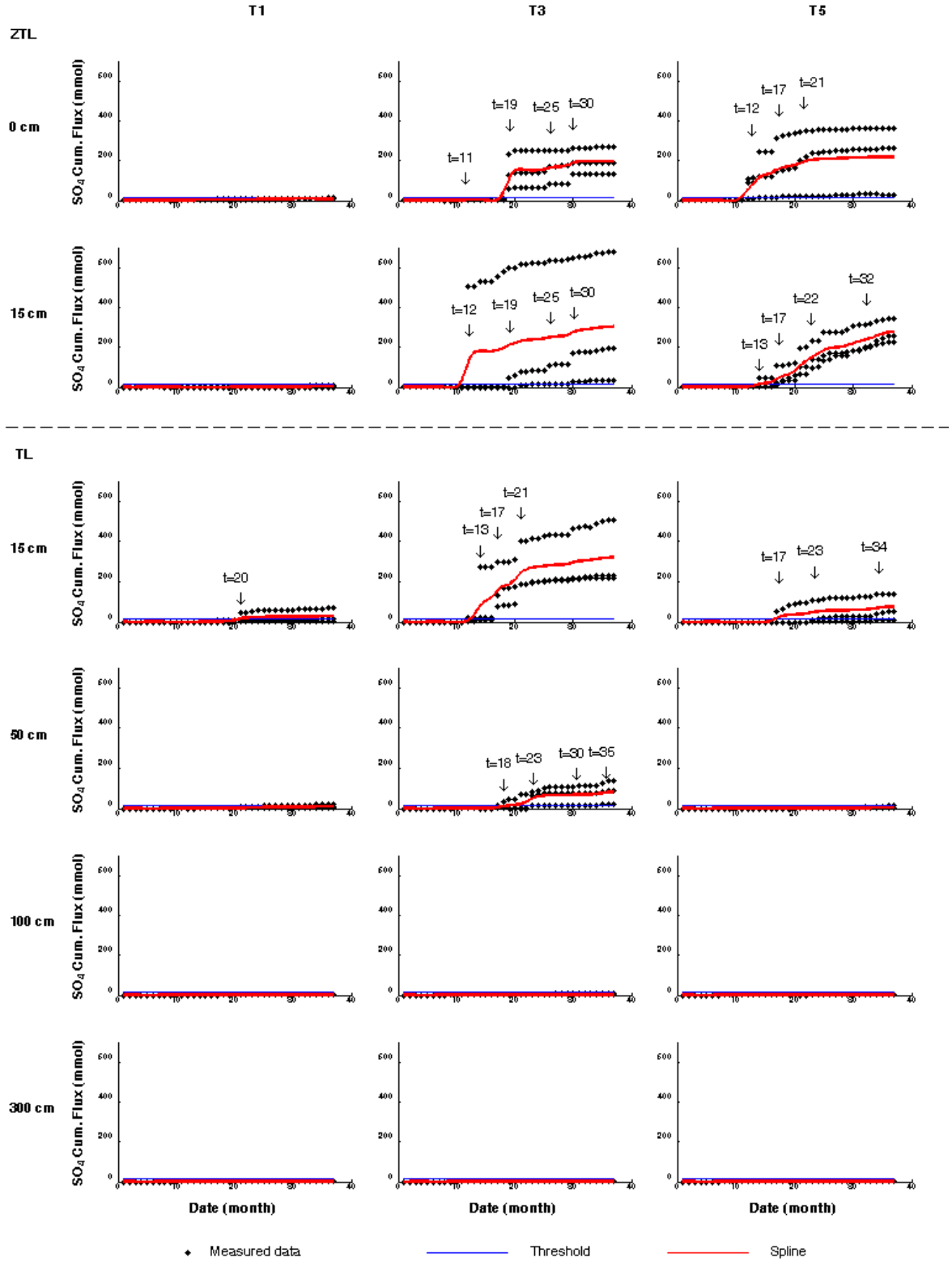

Figure 68 Cumulative fluxes (minus baseline) of sulphate (mmol) calculated for each soil solution collector (ZTL=zero-tension lysimeter, TL=tension lysimeter) in each treatment (T1, T3 & T5) for the 37 months of the experiment. The CFt threshold of § D.2.2.2 is represented, together with the spline modelizing the average cumulative flux. The main steps of the curve are indicated.

In T3, a step in the cumulative flux curve occurred at each date of ammonium sulphate application for ZTL (N_{month}=11-12 (F1) only at a depth of 15 cm, N_{month}=19 (F2), N_{month}=25 (F3) and N_{month}=30 (F4)) (Figure 68). The first step was always the main step (Figure 69). Three steps were observed for TL at a depth of 15 cm at N_{month}=13 (F1+2), N_{month}=17 (F1+6, intensive drainage after drought) and N_{month}=21 (F2+2, large drainage). All steps were equivalent in intensity (about 25% each of the final cumulative flux). The four events of fertilization observed at a depth of 15 cm in ZTL appeared at a depth of 50 cm with a 4 to 7 months delay in periods of large drainage (N_{month}=18 (F1+7), 23 (F2+4), 30 (F3+5) and 36 (F4+5).

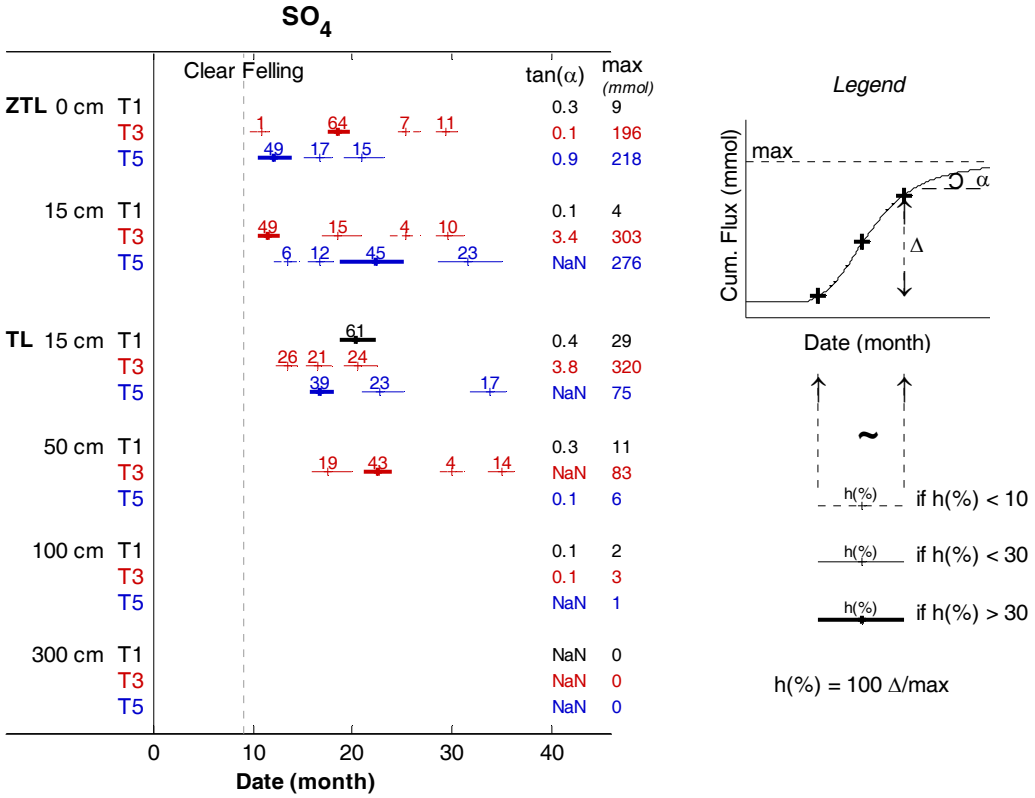

Figure 69 Projection on the time axis (month) of the average cumulative sulphate fluxes (mmol) (minus baseline) calculated for each soil solution collector (ZTL=zero-tension lysimeter, TL=tension lysimeter) in each treatment (T1, T3 & T5). The cumulative flux (max) and the slope of the curve tangent (tan α) at the end of the experiment are indicated. The contribution of each step to the final cumulative flux is also given (h(%)). Steps were calculated when max > CFt (threshold for cumulative fluxes).

In T5, a step in the cumulative flux curve appeared within two months after each application of sewage sludge (N_{month}=12-13 (F1+1) and N_{month}=21-22 (F2+1 to F2+2)). Both fertilizations occurred in periods of large water drainage. A supplementary step

appeared at N_{month}=17 (F1+6) intensive drainage after drought) in TL and ZTL solutions, as was observed in T3 for TL at a depth of 15 cm. Another step occurred at a depth of 15 cm for TL and ZTL at N_{month}=32-34 (F4+1 to F4+3, intensive drainage). Main steps came always later in T5 than in T3, except for ZTL in the forest floor since the first fertilization (F1) was buried in T3 and not in T5.

The tangent to the curve at the end of the experiment indicated an increasing function for T3 at the depths of 15 cm (tanα≈3.5) and 50 cm, and for T5 at a depth of 15 cm in ZTL and TL (tanα=NaN since a step in the curve was still occurring at the end of the experiment) (Figure 69).

The final cumulative flux was maxima in T3 at a depth of 15 cm (max≈310 mmol in TL and ZTL) and was attenuated to about 1/4 of this value at a depth of 50 cm (max=83 mmol). The final cumulative flux in the forest floor was in-between (max≈200 mmol). In T5, the maximum cumulative flux occurred in ZTL (max≈250 mmol in the forest floor and at 15 cm), and was attenuated to about 1/3 of this value in TL at a depth of 15 cm (max=75 mmol).

D.2.4.3 Spatial variability

Figure 65, Figure 68 showed a great heterogeneity among blocks and collectors for sulphate concentrations and cumulative fluxes which was more pronounced in treatment 3 than in treatment 5. Concentration peaks and cumulative fluxes steps were localized in time and space. The heterogeneity among the different collectors could only be observed in treatment 3 at a depth of 50 cm since no sulphate peaks were recorded in T5 at a depth of 50 cm and in T3 at a depth of 100 cm. At a depth of 50 cm in block 1 treatment 3, only the collector located at the stem basis detected the fertilization event (Figure 70).

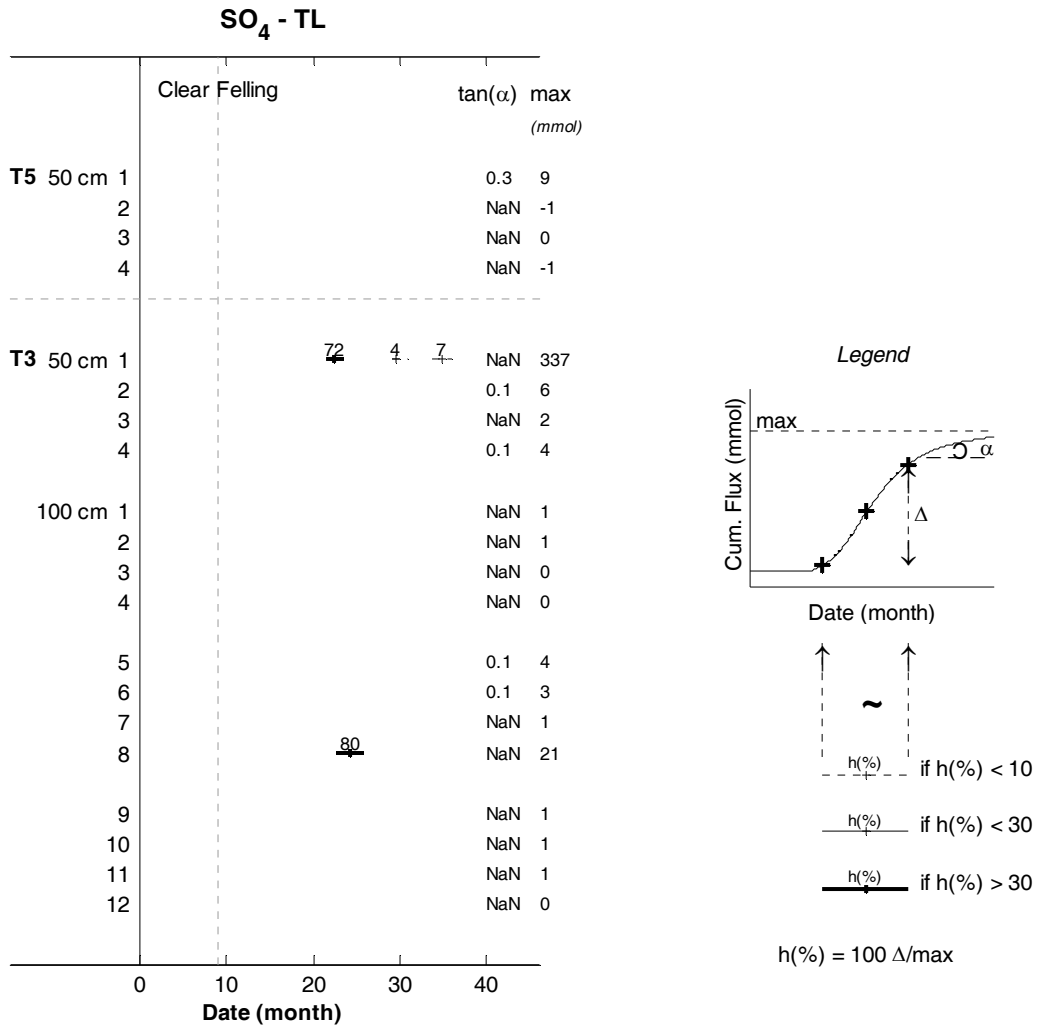

Figure 70 Projection of the sulphate cumulative flux (minus baseline) on the time axis (month) for each tension lysimeter (TL) collected independently at a depth of 50 cm in block 1, treatments 3 and 5 (collectors 1 to 4), and at a depth of 100 cm in block 1, 2 and 3 of treatment 3 (collectors 1 to 12). The cumulative flux (max) and the slope of the curve tangent (tan α) at the end of the experiment are indicated. The contribution of each step to the final cumulative flux is also given (h(%)). Steps were calculated when max > CFt.

D.2.4.4 Conclusion

In treatment 3, the sulphate concentration peaks occurred at the same time as the periods of sulphate leaching: just following fertilizations in ZTL and at the first wet period following the fertilization for TL. These peaks were spatially heterogeneous and localized in time (one month) and resulted, in wet periods, from local dissolution of the ammonium sulphate applied, in particular under the pocket of fertilizers buried at the stem basis. The peaks appeared sooner in ZTL than in TL which may be explained by two different collection modes: (i) particles of fertilizers may be transported by the water flux and collected by ZTL whereas filtered by the TL ceramic cups and (ii) sulphate may be present in soil solution in a plane closer to the soil surface than the nitrate was. Since TL collects soil solution at lower pressure heads than ZTL, they may collect this sulphate whereas ZTL do not.

In T5, the sulphate peaks appeared more continuously than in T3. They occurred within the first large drainage periods after both applications of sewage sludge and were still running at the end of the experimental period. Here again, ZTL peaks appeared sooner than TL peaks just after the fertilizations. This pattern suggests (i) a particulate transport of SO_4 in TL just after the fertilizations, (ii) a slow release of SO_4 as the sewage sludge is mineralized, and (iii) a remaining stock of sewage sludge still un-mineralized at the end of the experimental period.

In both T3 and T5, the main peaks were the first peaks, which suggest better rates of sulphate dissolution or solvatation after the first fertilizer application. The hypothesis are that (i) the external conditions were more favorable to sulphate dissolution during the first fertilization (drainage, temperature, microbial activity…), (ii) less sulphate uptake occurred after the first fertilization since the trees were small at this time, (iii) other chemical species dissolved at the same time as ammonium sulphate (ionic strength was greatest after the first fertilization since other fertilizers were concentrated at the stem basis together with ammonium sulphate and KCl in T3) may have competed for adsorption sites, and (iv) the water flux was larger after the first fertilizer application (young *Eucalyptus* trees) than after the next fertilizer applications (high transpiration rates of the fast growing *Eucalyptus* trees) and more sulphate may have been dissolved and leached during this early growth period.

No sulphate peak was ever observed at depths > 50 cm which suggests that sulphate was strongly adsorbed on soil surface below this depth. This tends to confirm the potential specific adsorption measured for sulphate in part B. In T5, sulphate never appeared at a depth of 50 cm which may result from (i) less SO_4 released in soil solutions by the sewage sludge mineralization than by the dissolution of ammonium sulphate, (ii) a reduced mobility of SO_4 in soil solution due to fewer preferred pair-cations available in soil solutions or to higher competition of other anions for adsorption sites.

D.2.5 Joint dynamics of the measured mineral elements

D.2.5.1 Preamble

Case studies 1 and 2 showed that two different behaviors were observed for nitrates and sulphates. Nitrates were produced in upper soil layers by the mineralization of the harvest residues and of the soil organic matter after clear felling when no vegetation uptake occurred, and by the nitrification of the fertilizers applied (ammonium sulphate in T3 and sewage sludge in T5). This production was particularly high during the wet periods following droughts. During these periods, nitrates were leached down to deep soil layers. Nitrate dynamics were spatially homogeneous but differed in intensity. The nitrate release was more continuous and lasted more in T5 than in T3 and T1.

Sulphates were mainly transported just after the fertilizer applications or dissolved in periods of intensive drainage just following the fertilizations in T3 and T5. These flushes were localized in upper soil layers (down to a depth of 50 cm in T3, 15 cm in T5). Their dynamics were highly heterogeneous and flushes were localized temporally and spatially. Sulphate release was more continuous in T5 than in T3. It was still running in T5 at the end of the experimental period.

For both anions, adsorption on soil surface is thought to happen in the upper soil layer for sulphate and down to a depth of 300 cm for nitrate. Competition with other anions for adsorption sites and association with mobile cations is suggested for sulphate in treatment 3.

Two behaviors can thus be expected for cations and anions others than nitrate and sulphate: (i) release in soil solutions of mineral elements due to the mineralization of organic matter (in particular harvest residues and forest floor after clear felling), or due to the mineralization of the sewage sludge in T5: direct release is expected for NH_4 and H and for Na, K, Ca, Mg just below the forest floor, and direct and/or indirect release for Al and Si; (ii) transport or release in soil solutions of partially dissolved or solvated fertilizers after the fertilizer applications and/or the periods of large drainage: K, Cl, Ca, Mg and Si in all treatments, and NH4, SO4 in T3. The analysis of the joint dynamics of these elements in soil solution will inform on the accuracy of this scheme and on the interactions occurring among mineral elements, as well as on the roles of the soil matrix and of the fast growing *Eucalyptus* tree in these dynamics.

D.2.5.2 pH and ionic strength

pH was in average 4.4 for all soil solution collectors. Soil solutions were more acidic when collected by ZTL at a depth of 15 cm (average pH of 4) and more basic when collected by ZTL in the forest floor or by TL at a depth of 300 cm (average pH of 4.7). Very acidic pH values (minimum of 2.9) were recorded in the forest floor and in soil solutions, especially in T3. They probably correspond to local reorganizations of the dissolved fertilizers or of the nitrates leached with the available protons (H_2SO_4 or HNO_3 for example). The range of pH variations for a given collector type, collection depth and treatment was < 3.5. The pH dynamics will be more thoroughly studied together with the other mineral elements through H^+ concentrations and fluxes.

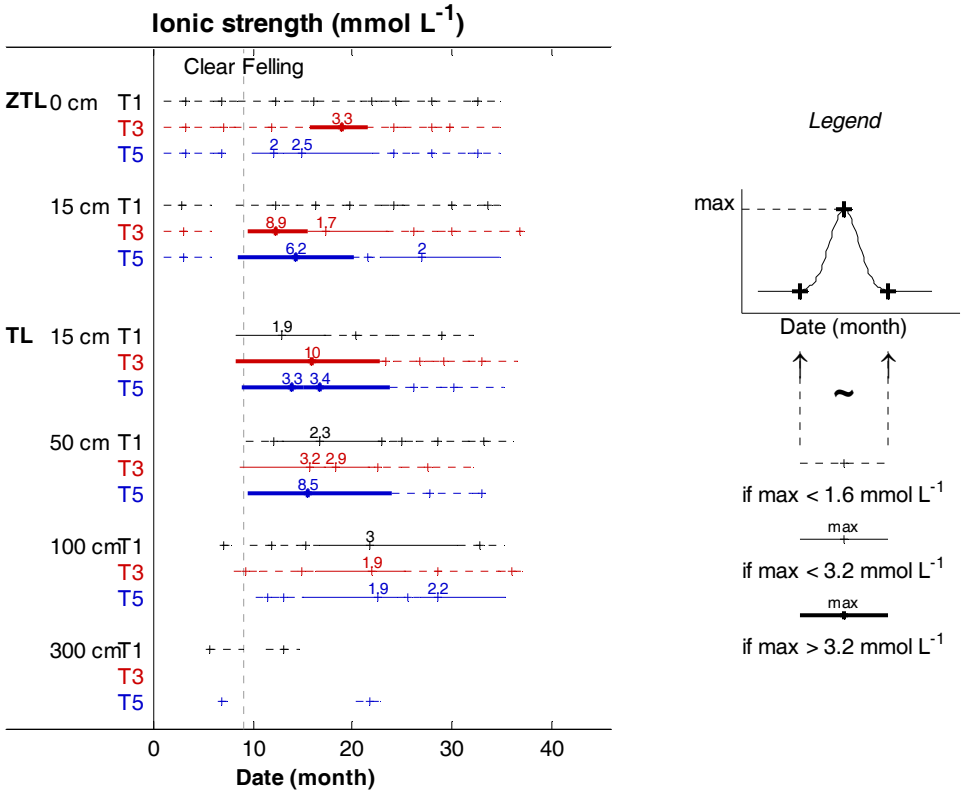

Figure 71 Projection of the average ionic strength (mmol L^{-1}) estimated in each treatment (T1, T3 and T5) and soil solution collector (ZTL=zero tension lysimeter, TL=Tension lysimeter) on the time axis (month). Only ionic strength peaks above 10*Ct=0.16 mmol L^{-1} are represented.

The average ionic strength estimated for all TL and ZTL was 0.80 mmol L^{-1}. A minimum of 0.02 mmol L^{-1} was recorded in TL at a depth of 300 cm and a maximum of 29.60 mmol L^{-1} in ZTL at a depth of 15 cm in T3. Ionic strength was in average about 0.4

mmol L^{-1} in ZTL in the forest floor and at a depth of 15 cm. In TL, the average ionic strength decreased with depth in T3 and T5 from about 1.78 mmol L^{-1} at a depth of 50 cm, to 0.59 mmol L^{-1} at a depth of 1 m. At a depth of 300 cm, ionic strength was <0.13 mmol L^{-1} in all treatments.

Ionic strength peaks (Figure 71) occurred in TL (except at a depth of 300 cm) and ZTL (except in the forest floor) with a higher intensity in T3 and T5 than in T1. Peaks started after clear felling at the depths of 15 cm and 50 cm, and at N_{month}=15 at a depth of 100 cm. Ionic strength dynamics showed the features of both nitrate and sulphate dynamics: large ionic strength resulted from the mineralization of the forest floor or fertilizers after clear felling and during the drainage periods following droughts, as well as from the transport and dissolution of fertilizers following their applications.

D.2.5.3 Concentrations

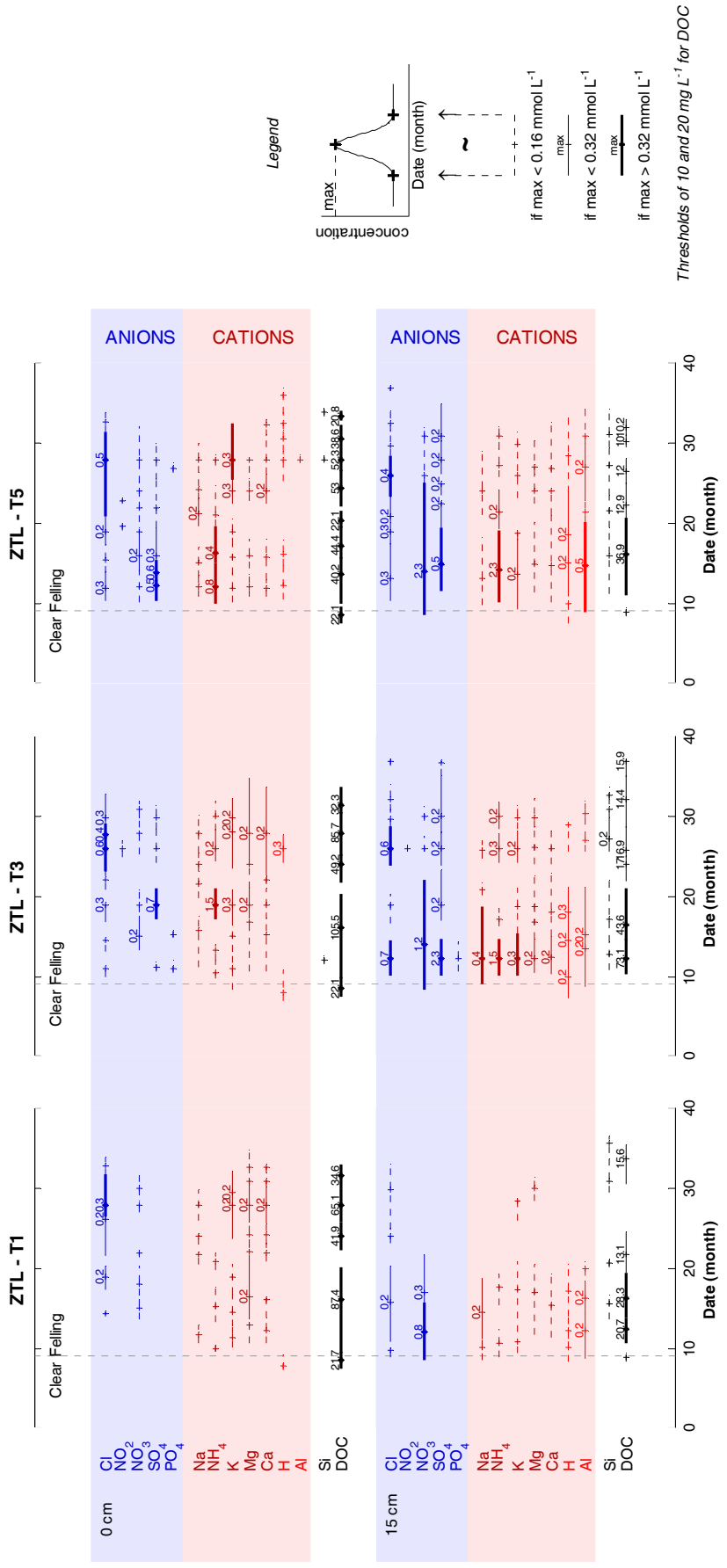

Figure 72 Projection on the time axis (N_{month}) of the average concentration in cations and anions (mmol L^{-1}, DOC in mg L^{-1}) measured in soil solutions collected by zero tension lysimeters (ZTL) in treatment 1, 3 and 5 at the depths of 15, 50 and 100 cm. Only peaks above the threshold for concentrations C_t=0.016 mmol L^{-1} (1 mg L^{-1} for DOC) are represented.

D.2.5.3.1 Chemical composition below the forest floor

Results

Beneath the forest floor, the time course of Cl concentrations exhibited concentration peaks in all treatments at each drought period (N_{month}=15-16 and N_{month}=28-29), and at each KCl fertilizer application (N_{month}=19, 25 & 31 + N_{month}=11 in T5) (Figure 72). The concentration peaks were more continuous in T5. K presented the same behaviour as Cl. Ammonium followed the same dynamics as sulphate. Mg and Ca concentrations peaks were spread over the whole period; their main peaks were centred on exceptional events (AG peak, droughts, fertilizations and intensive drainage periods). Na concentrations remained low over the whole experimental period. H peaks occurred only after clear felling in T1 and T3, but over the whole experimental period after clear felling in T5. DOC concentration peaks were spread over the whole period. Its main peaks occurred just after droughts (N_{month}=17 and 29-30). The solutions were poor in Al.

Discussion

The major concentration peaks thus resulted from:

- the fertilizer dissolution: the cation-anion pair of the fertilizer was kept in the forest floor solutions and K appeared together with Cl after fertilizations 1, 2, 3 and 4 in T5 and after fertilizations 2, 3 and 4 in T1 and T3 (the 1st fertilization was buried), and ammonium appeared together with sulphate after fertilizations 2, 3 and 4 in T3,
- the organic matter mineralization (harvest residues, forest floor and soil organic matter) and the nitrification of ammonium in nitrates: it occurred more strongly after clear felling and after drought periods and released directly or indirectly H, NH_4, NO_3, DOC, Ca, Mg, K and Cl in the forest floor solution.

Some secondary concentration peaks could be encountered especially for K and Cl as a result of large dry depositions during the dry periods.

D.2.5.3.2 Soil solutions at a depth of 15 cm

Results

ZTL solutions at a depth of 15 cm presented less Ca, Mg and DOC peaks but more Al and Si peaks compared to the forest floor solutions. The first fertilization, which was

buried in T1 and T3, led to high concentrations of Cl, NO_3, Na, NH_4, K, H and Al at N_{month}=11-12 (F1) in all treatments. This peak was more intense in T3 and T5 than in T1. Concentration peaks were also observed after the first fertilizer application for SO_4, Ca and Mg in T3 and T5, and for H_2PO_4 in T3.

Two zones of concentration peaks could be distinguished on the whole spectra for all elements. The first one occurred from N_{month}=10 to N_{month}=20 for all treatments and all elements but SO_4 in T1, and PO_4 in T1 and T5. The 2nd occurred from N_{month}=23 to 31 with a weaker intensity and was not seen in T1. Both zones were contiguous in T5. Each one of these periods experienced fertilization during its first months followed by a period of moderate drainage, and then, by a period of drought followed by drainage again. Both periods ended with large drainage episodes.

In general, (i) K behaved as Cl, (ii) NH_4, Mg, Ca and to a lesser extent Si behaved as SO_4, and (iii) H and Al behaved as nitrate. DOC concentration peaks at a depth of 15 cm were lower than in the forest floor and were delayed of about 2 months (N_{month}=11=F1=CF+2).

TL solutions at a depth of 15 cm showed the same general dynamics than ZTL solutions (Figure 73). Both zones of concentration peaks appeared in the same way for solutions collected by TL as for solutions collected by ZTL, except that the 2nd zone became visible in T1 for all cations plus Cl. More SO_4 (all treatments), Ca and H_2PO_4 (in T3) were observed in TL than in ZTL. These peaks corresponded to a change in the drainage regime or to fertilization events. Except at N_{month}=12, NH_4 and Si peaks were not observed anymore in T5. DOC peaks were weaker and centred at N_{month}=15-18, 21 and 32 (droughts and intensive drainage following droughts).

Discussion

Soil solutions at a depth of 15 cm are greatly influenced by the first buried fertilizers in T1 and T3. As observed in the forest floor, mineral elements are found in soil solution in their original pairs within the fertilizers: K and Cl, NH_4 and SO_4 (only in T3), Ca and H_2PO_4. Such dissolutions of buried fertilizers are likely to have occurred all over the studied period until complete dissolution of the fertilizers and made it difficult to observe specifically the transfer of the elements leached below the forest floor.

NO_3 peaks are associated to H and Al peaks, as classically observed after clear felling in acidic soils: harvest residues are first mineralized in ammonium which is then nitrified

(if not immobilized or taken up) releasing protons in soil solutions (Julien et al., 2005; Lilienfein et al., 2000; Prosser et al., 1993; Reuss and Johnson, 1986; Rhoades and Binkley, 1996). The pH decreases and consequently the CEC (variable charge soil). Since Al is present at > 90 % on the CEC and is labile at such pH, Al is released in soil solutions. Silica peaks are also observed concomitantly in soil solutions which suggests that the proton release may also have induced dissolution of soil constituants (especially organic matter and amorphous), and/or dissolution of the dolomitic limestone and/or of the superphosphate fertilizer in T1 and T3.

More NO_3 is observed in T3 and T5 than in T1 which suggests that part of the nitrate released in soil solution comes from the nitrification of the fertilizers (ammonium sulphate and sewage sludge). An increasing release of protons in soil solution may thus be expected in T3 and T5 compared to T1. On the other hand, the adsorption in the upper soil layer of phosphate issued from the fertilizers may decrease the point of zero charge, thus increasing CEC and impeding Al release (Uehara and Gillman, 1981). Specific adsorption of sulphate release by the fertilizers may act in the same way, but the high affinity of sulphate for H may also induce H_2SO_4 leaching, in particular if the sulphate paired cation (ammonium in T3) in the fertilizers is nitrified (Ponette et al., 1997). As a conclusion, even if nitrification is higher in T3 and T5, this may not necessarily result in a decrease of soil pH and in an increase of Al leaching in soil solution. On the contrary, it may induce a higher mobility of sulphate through the soil profile. Cumulative fluxes will help ruling on these hypotheses.

The leaching of Ca and Mg is only observed at a depth of 15 cm when associated to sulphate or phosphate. This pattern is consistent with the nitrification of the ammonium (paired cation of sulphate in the fertilizer) and the reorganization of sulphate with the available cations, with a preference for divalent cations Ca and Mg as classically observed (Adams et al., 1997; Carnol et al., 1997; Ponette et al., 1997). This observation also works successfully with a preferential co-adsorption (and desorption) of calcium and sulphate (or phosphate) on the soil surface as already observed in the literature (Bolan et al., 1999) and suggested in part B.

Differences observed between TL and ZTL suggest that TL succeeds in collecting chemical species of lower potential status (either because they are solvated in a plane closer to the soil surface -for example sulphates or phosphates- or because they are located in a smaller porosity) than does ZTL.

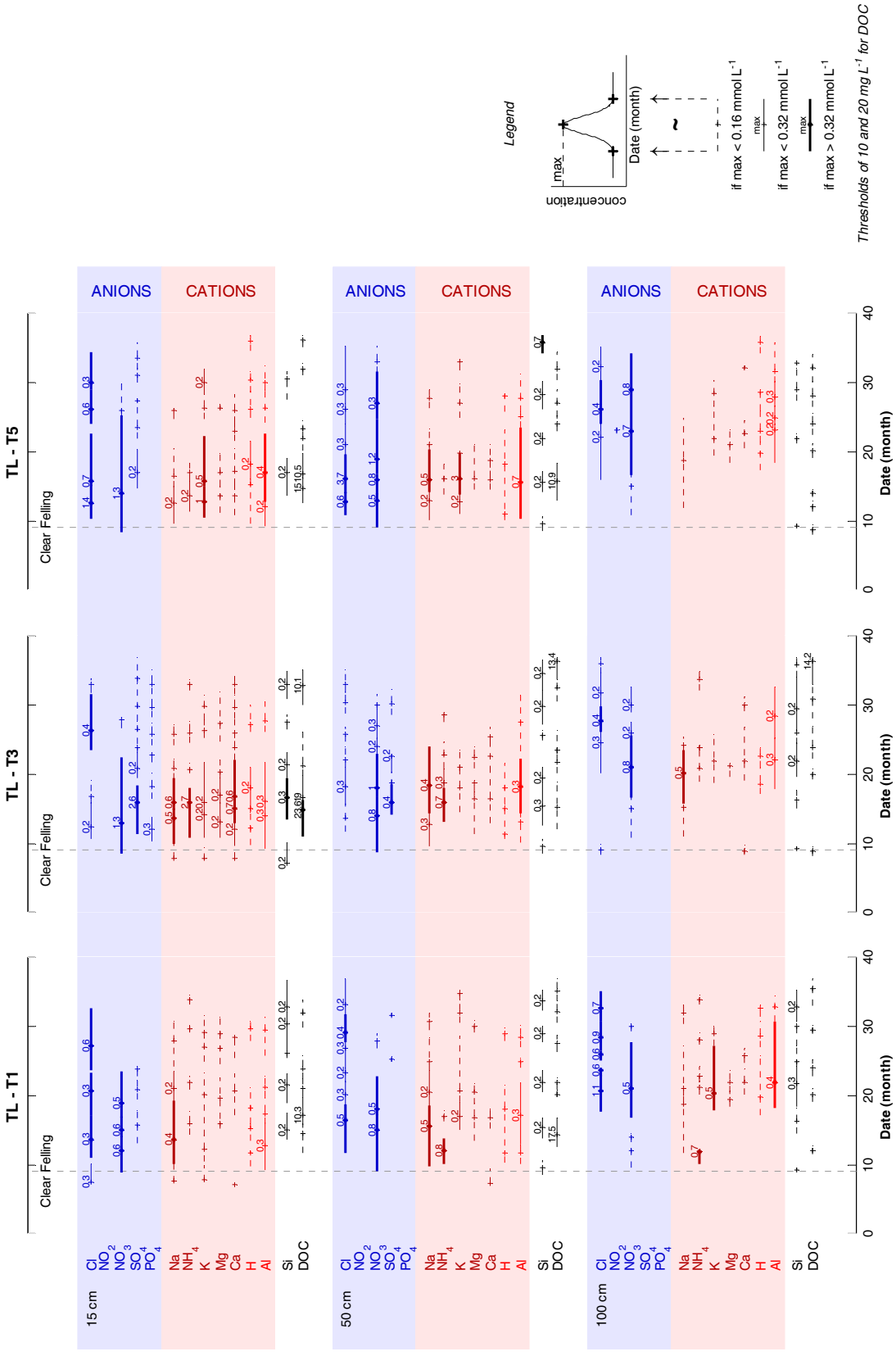

Figure 73 Projection on the time axis (N_{month}) of the average concentration in cations and anions (mmol L^{-1}, DOC in mg L^{-1}) measured in soil solutions for tension lysimeters (TL) in treatment 1, 3 and 5 at the depths of 15, 50 and 100 cm. Only peaks above the threshold for concentrations Ct=0.016 mmol L^{-1} (1 mg L^{-1} for DOC) are represented.

D.2.5.3.3 Soil solutions in deep soil layers

Results

Concentration peaks observed at a depth of 15 cm appeared in soil solutions collected by TL at a depth of 50 cm with almost no delay. The dynamics of mineral elements were the same as at a depth of 15 cm but occurred with less intensity. Phosphate was no more detected in T3. Sulphate was no more visible in T5 and only 3 peaks remained in T3 at N_{month}=17, 22 and 30 (intensive drainage periods following droughts). At the same time, concentration peaks were weaker for Ca and Mg in all treatments, for K and Na in T3, and for NH_4 in T1 and T5. Only the first peak of DOC at N_{month}=15 in T1 and T5 was above 10 mg L^{-1}.

At a depth of 100 cm, the 1st period of peaks was translated of about 6 months and occurred from N_{month}=16 to 25, except a first weak peak of Na (and NH_4 in T1) and NO_3 beginning rapidly after clear felling at N_{month}=11. The second period of concentration peaks was almost not visible. Peaks of SO_4 and PO_4 did not occur anymore, and Ca and Mg peaks were seen weakly only during the first peak period. Peaks of Na did not occur anymore in T1 and T5, the same for NH_4 in T5. K and Cl peaks were more intense in T1 than in T3 and T5.

At a depth of 300 cm, almost all peaks were below the thresholds for concentrations (C_t), so that they were not represented in Figure 73 and Figure 74.

Discussion

As a conclusion, the influence of the fertilizers observed at a depth of 15 cm is less in deeper soil layers. In particular, S and P disappear of the soil solution between the depths of 15 and 100 cm. The dynamics of the soil solution chemistry suggest a strong adsorption of (i) P from the soil surface down to a depth of 15 cm in T5 and down to a depth of 50 cm in T3, and (ii) S from the soil surface down to a depth of 50 cm in T5 and down to a depth of 100 cm in T3. These anions (especially S) brought by the fertilizers are vectors for Ca and Mg in soil solutions as already explained.

The influence of clear felling and of the nitrification is observed down to a depth of 1 m: H, Al, NO_3 and DOC are leached together as already observed at a depth of 15 cm. Concentration peaks associated to nitrification do not seem to increase during their transfer in soils which may indicate that nitrification mainly occurs in the upper 15 cm of the soil profile. On the contrary, peak intensities are slightly less at a depth of 100 cm than at a

depth of 50 cm which suggests that nitrate adsorption, aluminium adsorption or precipitation and pH buffering occur below a depth of 50 cm. The analysis of cumulative fluxes may help ruling on this point.

Fertilizers in their original pairs (anions/cations) are observed down to a depth of 1 m, in particular K/Cl, and SO_4/NH_4. More generally, NH_4 is only observed in T3 in association with SO_4 and in T5 below the forest floor and at a depth of 15 cm, that is, occurs in soil solution during the periods of large and rapid dissolution (or mineralization) and leaching of the fertilizers applied. This would suggest that ammonium is either immobilized by the soil microbial populations, or quickly transformed in nitrates and organic forms (DON or SOM), or taken up preferentially by the trees.

Concentration peaks are delayed of about six months between the depths of 50 cm and 300 cm. This suggests that absorption by trees and slow transformations and reorganizations (adsorption, occlusion, diffusion, immobilization…) of the elements dissolved in the soil solution have time to occur during their transfer throughout the soil profile.

D.2.5.4 Cumulative fluxes

D.2.5.4.1 Dynamics

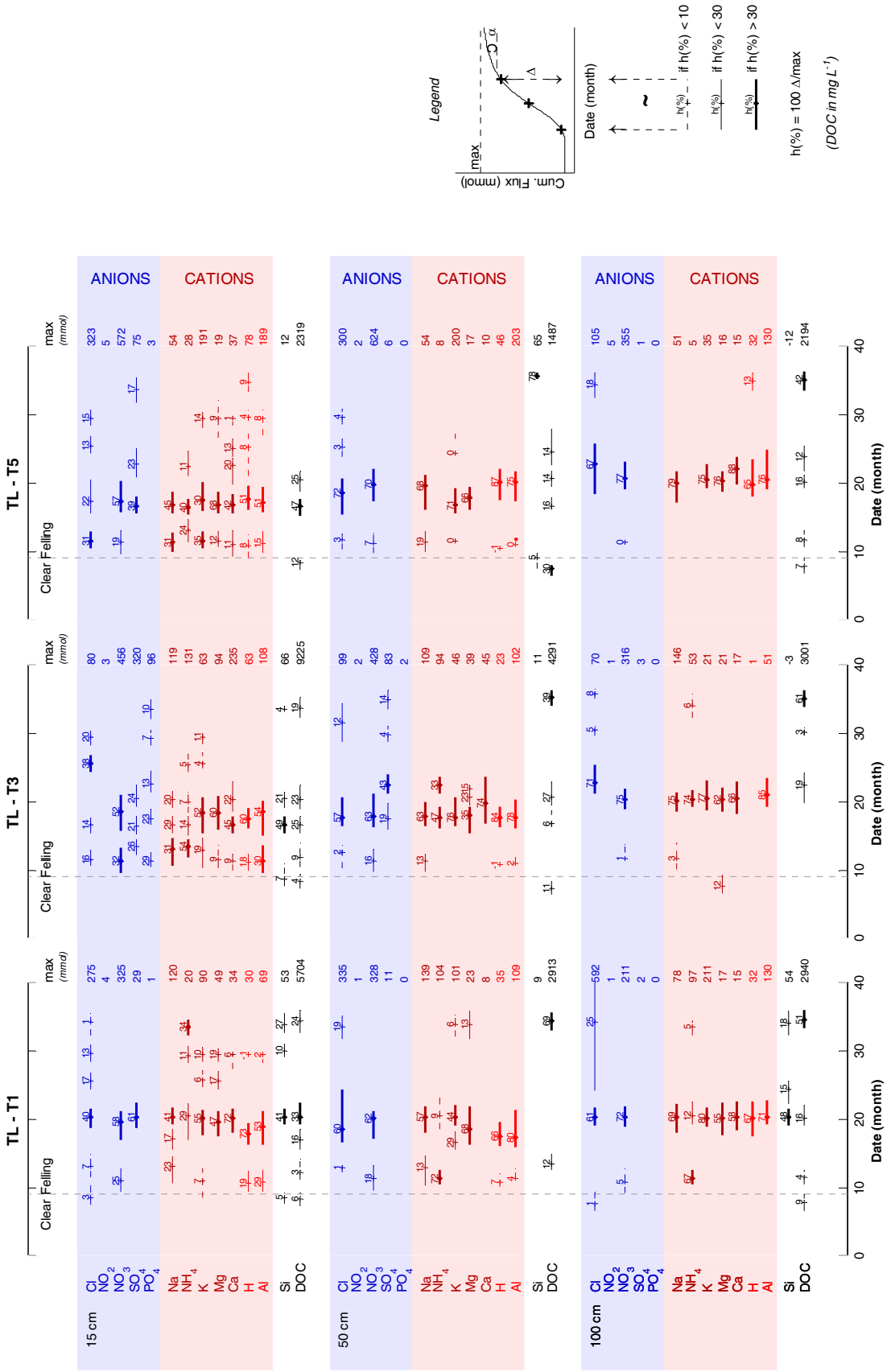

Figure 74 Projection on the time axis (N_{month}) of the average cumulative flux of cations and anions (mmol, DOC in mg) calculated in soil solutions for tension lysimeters (TL) in treatment 1, 3 and 5 at the depths of 15, 50 and 100 cm. The steps of the cumulative flux curve were not calculated when the final cumulative flux (max) was below the threshold (CFt= 12.5 mmol, 735 mg for DOC).

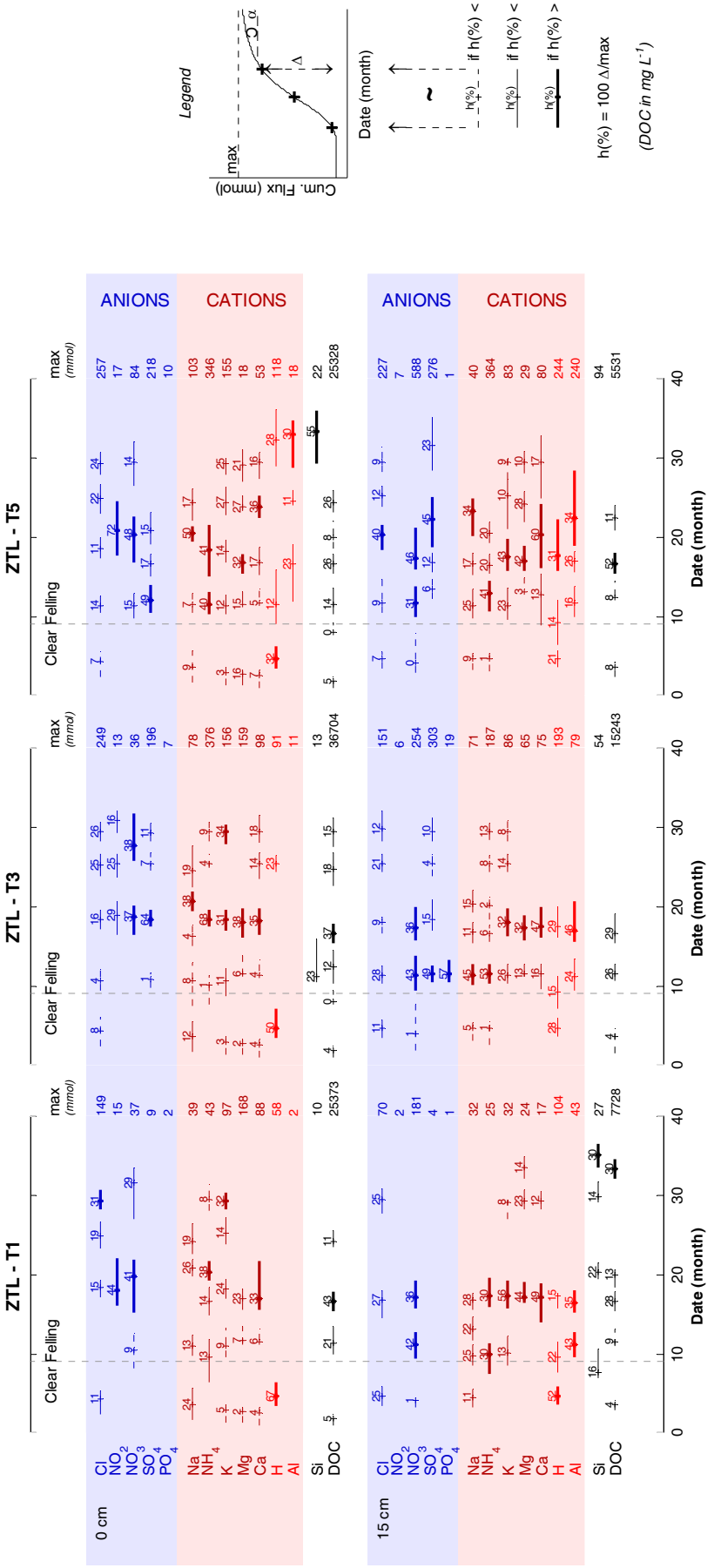

Figure 75 Projection on the time axis (N_{month}) of the average cumulative flux of cations and anions (mmol, DOC in mg) calculated in soil solutions for zero tension lysimeters (ZTL) in treatment 1, 3 and 5 at the depths of 15, 50 and 100 cm. The steps of the cumulative flux curve were not calculated when the final cumulative flux (max) was below the threshold (CF_t= 12.5 mmol, 735 mg for DOC).

The curves of cumulative fluxes are composed of five main steps (Figure 74 & Figure 75), which occurrences depend on the element analyzed, the collector type, the collection depth, and the treatment:

- The 1st step occurs before CF just after the 1st drought at N_{month}=4 and can be observed in all treatments, but only in ZTL since no data were available for TL before CF.
- The second step occurs for solutions collected by TL and ZTL at planting at N_{month}=11 (fertilization 1, CF+2) and corresponds to the end of the rainy season. Leaching of all elements occurs down to a depth of 50 cm.
- The third step occurs from N_{month}=17 to N_{month}=20 and corresponds to a period of intensive drainage after the winter drought, followed by the second fertilization. Leaching of all elements occurs down to a depth of 1 m within 1 to 2 months.
- The last two steps occur at N_{months}=25 and 30-31. They correspond to the end of the 2005 summer and to the end of the winter (intensive drainage after drought) respectively, and to the 3rd and 4th fertilization respectively. Leaching occurs for only small contents of mobile anions and cations down to a depth of 15 cm.

The first step of nutrient fluxes corresponds to the mineralization of the forest floor in the old *E. saligna* stand before it was clear felled and is interesting to observe since it is not polluted by nutrients released by the fertilizers. Although it can only be studied in ZTL, it suggests a strong recycling of Ca, Mg and K in the upper soil layers by the *Eucalyptus* trees. NO_3 appears in soil solutions at a depth of 15 cm. Since no NH_4 is observed in the solutions, we can assume that NH_4 is preferentially taken up by plants, immobilized by micro-organisms or very quickly nitrified. *Eucalyptus* trees are known to take up NH_4 or NO_3 or both chemical forms depending on the species and the geographical site (Smethurst, 2000) so that this result is not surprising. A preferential uptake of NH_4 over NO_3 has already been observed for *Eucalyptus* in Brazil (Vale et al., 1984).

The nutrients released by the mineralization of the organic matter (harvest residues, forest floor and soil organic matter) and of the sewage sludge, and by the dissolution of the first fertilization are firstly leached just after planting down to a depth of 15-50 cm (2nd step), but the main leaching occurs with the first heavy rainfall after the winter drought and reaches a depth of 1 m within two months (3rd step). This suggests that, after planting, either the drainage is not large enough to transport the solutes in deeper soil layers, or the dissolved nutrients are adsorbed and/or immobilized and/or taken up in the upper soil

layers. The limited rainfall of the winter period together with the transpiration of the *Eucalyptus* trees allow a slow transfer of the concentration front to deeper soil layers which may explain that it takes six months for the concentrations to reach a depth of 100 cm whereas the nutrient fluxes are not delayed. The first heavy rainfall washes the soil profile and pushes the elements down to deeper soil layers where free exchanger surfaces are available. This nutrient leaching is increased by the dissolution and mineralization of the 2nd fertilization and the activation of the mineralization of the forest floor. Ionic strengths are greater and so is the competition of anions and cations for exchange sites, which participates in leaching nutrients deeper in the soil profile.

The last two periods of leaching (3rd and 4th steps) correspond to the mineralization of the forest floor and/or to the dissolution of the next two fertilizations (KCl in all treatments and ammonium sulphate in T3) and remain localized in the upper 15 cm of the soil profile.

The chemical associations observed for concentrations were confirmed by the observation of the nutrient fluxes.

D.2.5.4.2 Total cumulative fluxes from the clear felling until two years after planting

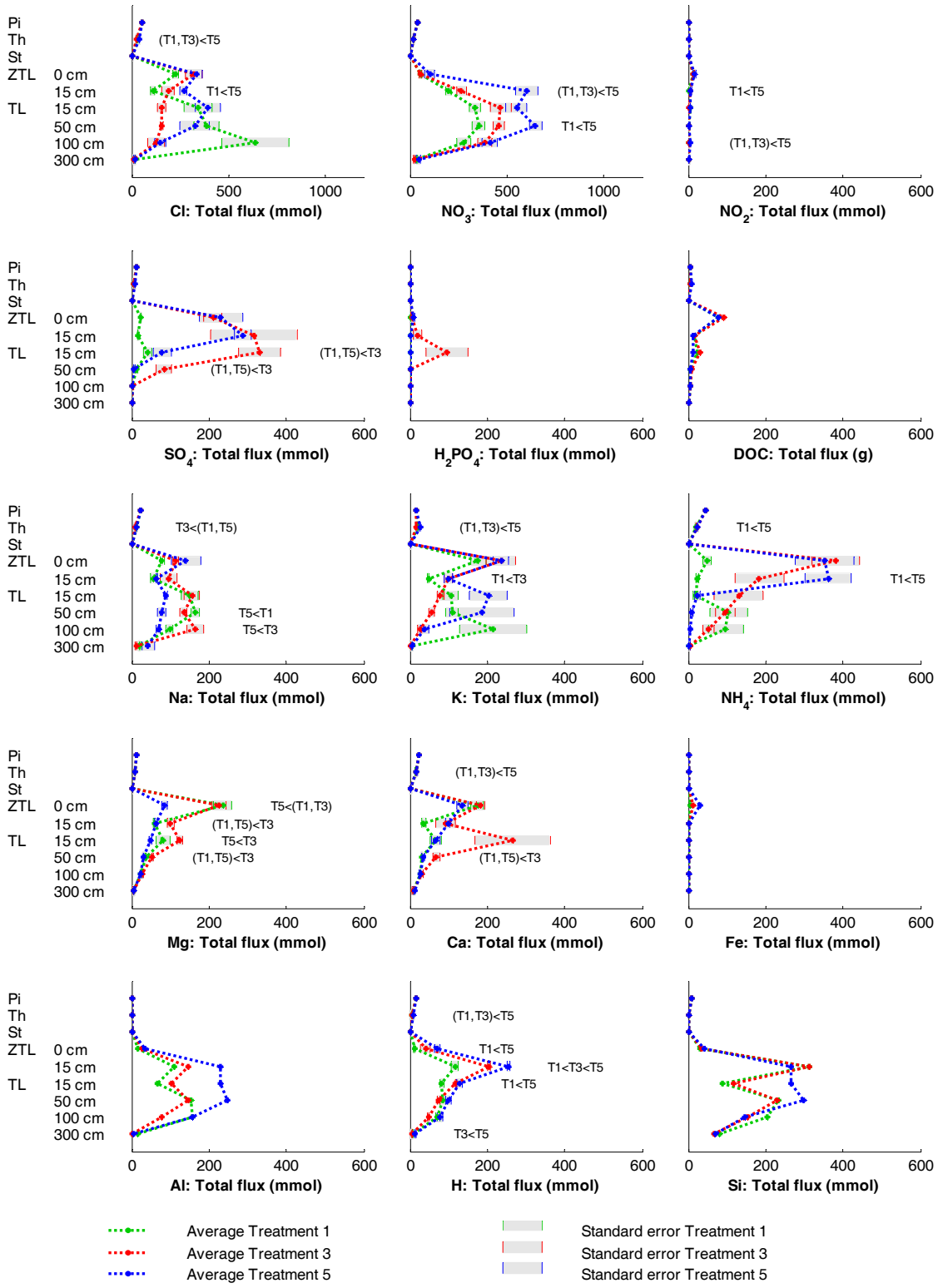

Figure 76 Mean cumulative fluxes and standard errors (when n=3) calculated from the clear felling (N_{month}=9) to the end of the experimental period (N_{month}=37) for cations and anions measured in soil solutions for each collector type (Pi=Rainfall, Th=Throughfall, St=Stemflow, ZTL=zero tension lysimeter, TL=tension lysimeter), collection depth and treatment. Differences among treatments are indicated when significant at P<0.05.

The greatest total cumulative fluxes (from the clear felling until the end of the experimental period) were found for NO_3 (about 500 mmol from a depth of 15 cm down to a depth of 100 cm in all treatments), then for Cl (about 300 mmol from the forest floor down to a depth of 100 cm), SO_4 and NH_4 in T3 and T5 (about 300 mmol from the forest floor down to a depth of 15 cm, except in TL for NH_4). Total cumulative fluxes for H, Al, K, Mg and Ca came next with greatest total fluxes from 100 and 200 mmol (Figure 76).

Standard errors were large in particular for Cl, SO_4, H_2PO_4, NH_4, Ca and K, so that few significant differences could be observed. Qualitatively, the order of decreasing total flux for NO_3, H and Al was T5 > T3 > T1 whatever the depth. SO_4 fluxes were large only in T3 and T5 and found deeper in T3 (down to a depth of 50 cm) than in T5 (down to a depth of 15 cm). Mg total fluxes were less in T5 (where dolomitic lime was not applied) than in T1 and T3 and reached deeper soil layers in T3 (down to a depth of 50 cm) than in T1 and T5. In general, the largest values were reached in the forest floor or at a depth of 15 cm then total fluxes decreased with depth. More NH_4 was leached in the forest floor and at a depth of 15 cm in T3 and T5 than in T1. The main significant differences showed:

- larger cumulative fluxes of nitrates, H and NH_4 in T5 than in other treatments at the depths of 15 and 50 cm for nitrates, and in the forest floor and at a depth of 15 cm for H and NH_4
- smaller cumulative fluxes of Na and Mg in T5 than in other treatments at depths of 50 cm (T1) and 100 cm (T3) for Na, and in the forest floor for Mg,
- larger cumulative fluxes of sulphates, Ca and Mg in T3 than in other treatments at the depths of 15 (sulphate and Mg only) and 50 cm,

Differences among treatments could not be studied for Al, Fe, Si and DOC since one single composite sample per treatment was analyzed.

This quantitative analysis confirms that ammonium and nitrates are released together with H and Al in the upper soil 15 cm of the soil profile (no increase of total flux below this depth). The ammonium cumulative flux is large only in the forest floor and in the upper soil layers (15 cm) which suggests that an excess of NH_4 is quickly released in soil solution before nitrification occurs or that NH_4 is only partly nitrified. It also confirms that ammonium, nitrate and aluminium releases are in the following order: T5 > T3 > T1. The same quantitave trends among treatments are observed for H but only in the upper soil layer (15 cm) which would confirm an increase in the system buffering capacity when

fertilizers are applied as already suggested in § D.2.5.3. On the contrary, aluminium began to decrease only below a depth of 50 cm together with nitrate.

The depths of presumed adsorptions for anions are also confirmed: NO_3 mainly from 100 cm down to 300 cm, SO_4 from a depth of 15 cm down to a depth of 50-100 cm in T3 and of 50 cm in T5, and H_2PO_4 from the soil surface down to a depth of 50 cm in T3 and of 15 cm in T5. Immobilization in the organic matter and/or microbial biomass and uptake by the fast growing *Eucalyptus* trees may also have occurred at the same depths, especially for NO_3. In T5, smaller cumulative fluxes of Mg confirm the results of the vegetation dynamics which showed smaller Mg contents in the *Eucalyptus* of T5 than of T1 and T3.

D.2.5.4.3 Dynamics at the end of the experimental period

Table 41 Slope (mmol L^{-1} or g L^{-1} for DOC) of the tangent to the cumulative flux curve at the end of the experimental period for each collector type (ZTL=zero tension lysimeter, TL=tension lysimeter), collection depth and treatment (T). The slopes are given in bold when there value was above the threshold for nutrient flux SC'_t=1 mmol $month^{-1}$ (0.06 g $month^{-1}$ for DOC).

			H	Cl	NO_2	NO_3	SO_4	PO_4	Na	NH_4	K	Mg	Ca	Fe	Al	Si	DOC
		T							*mmol*								*g*
ZTL	**0 cm**	**1**	<0.5	2.0		<0.5				<0.5		**5.8**	**3.2**		<0.5	<0.5	**0.1**
		3		<0.5						0.9		**5.2**	1.0				<0.03
		5	**5.3**	**2.4**		0.9	<0.5			1.0		<0.5	<0.5		**1.1**	**4.0**	**0.2**
	15 cm	**1**	<0.5	<0.5		<0.5				<0.5		**1.6**			<0.5	**3.2**	**1.2**
		3	**1.6**			**3.4**	0.6				<0.5	**1.7**	1.0		**1.1**	**1.7**	**0.3**
		5	**3.8**	0.6		**11.0**	**2.5**			0.6		<0.5	<0.5		**4.4**	**2.7**	<0.03
TL	**15 cm**	**1**	<0.5	**1.2**		<0.5	<0.5			**3.6**						**5.9**	**0.5**
		3		<0.5		**3.8**						**1.1**	**1.7**			<0.5	**0.7**
		5	**2.8**	**1.1**	<0.5	**4.8**	**1.9**	<0.5	<0.5	<0.5		<0.5		<0.5	<0.5	0.6	<0.03
	50 cm	**1**				<0.5	<0.5				**2.4**	**1.1**				<0.5	**0.9**
		3		<0.5		**4.9**	**2.1**				<0.5						**0.8**
		5	<0.5				**2.3**								0.8	**47.0**	<0.03
	100 cm	**1**		**11.0**			0.5			**2.4**	0.9		<0.5		**1.5**	**3.6**	**0.7**
		3		**4.1**			**1.3**			**1.1**		<0.5			<0.5		**0.8**
		5	**1.9**	**6.1**		<0.5	**2.7**								**1.8**		**0.4**
	300 cm	**1**								<0.5	<0.5					<0.5	**0.9**
		3	<0.5	<0.5			<0.5								<0.5		<0.03
		5															**0.1**

The increasing trends for H, Cl, Al, NO_3 and SO_4 observed at the end of the experimental period in T5 in the forest floor and at a depth of 15 cm (Table 41) suggest that the sewage sludge is not completely mineralized in T5, as confirmed on field by visual observations of remaining sludge.

The increasing trends observed at the depth of 1 m for H, NH_4, Al, Cl and SO_4 suggest that the dynamics of downward transfer of the mineral elements issued from the clear felling and the fertilizer applications are still running at a depth of 1 m. At a depth of 300 cm, no increasing trend above the thresholds is recorded, which means that this downward transfer did not reach a depth of 3 m yet. The increasing trends of Mg and Ca beneath the forest floor, and of NO_3, NH_4, H and Al in the upper soil layers may be explained by the mineralization of the forest floor which occurs continuously all over the stand rotation, first from the harvest residues left on floor after clear felling, then from the litterfall of the new stand which started after about one year of growth.

D.3 CONCLUSIONS

D.3.1 On the dynamics of nutrients in soils

Concentration and fluxes of nutrients in the soil solution were thus driven by two main processes:

- The mineralization of the harvest residues, of the forest floor and of the soil organic matter followed by the nitrification of the ammonium, released H, Al and NO_3 in the upper layers of the soil profile (0-15 cm). This release was enhanced by the nitrification of the fertilizers in particular in T5 (sewage sludge). Dissolution of other fertilizers together with specific adsorption of S and P probably buffered the protons release in all treatments and more particularly in T3,
- The dissolution of the fertilizers released nutrients in soil solutions in their original chemical association (K/Cl and NH4/SO4 in T3), but SO4 was quickly reorganized with Mg and Ca, enhancing Mg and Ca mobility. Mg and Ca came from the mineralization of the forest floor, the dissolution of the dolomitic limestone in T1 and T3, and the mineralization of the sewage sludge in T5 (mainly Ca since the sewage sludge was Mg-poor). These dissolutions were highly heterogeneous in time and space (localized under the fertilizer pocket buried at the tree stem in T1 and T3, and below the sewage sludge line in T5). Mineralization of the sewage sludge and dissolution of the mineral fertilizers were still running at the end of the experimental period but with a weak intensity.

Nutrients released in soil solution were quickly transported to deeper soil layers first after clear felling and planting, and mainly with the first heavy rainfall following the dry period after planting. Between the periods of large drainage, slower diffusion processes and chemical reorganizations occurred within the soil profile. The nutrient front reached the depth of 1 m but was never observed at a depth of 3 m so that even if very large concentrations of all elements were observed in upper soil layers the concentrations at the outlet of the studied soil profile always remained below the thresholds of groundwater quality. The doubt remained whether the nutrient flux was stopped because nutrients were adsorbed, immobilized or taken up between the depths of 1 to 3 m or simply because there

was no water enough to transport them due to the high transpiration of the *Eucalyptus* trees.

The soil solution study suggested that, once released in soil solutions, NO_3 was adsorbed on soil surface (or immobilized or taken up) between the depths of 1 to 3 m together with Al, SO_4 was adsorbed from a depth of 15 to 100 cm in T3 and to 50 cm in T5, and H_2PO_4 from a depth of 15 to 50 cm in T3. These hypotheses are in good agreement with the potential adsorptions capacity measured in part B but are to be checked.

As ammonium was never observed in soil solutions except when quickly dissolved from the fertilizer together with sulphate, it is suggested that *Eucalyptus* trees preferred ammonium to nitrate, but ammonium may also have been quickly nitrified.

D.3.2 On the methods used

In part C, it was shown that the water drainage model systematically overestimated the water fluxes in the plantation especially at a depth of 50 cm, but that the flux at the outlet of the soil profile was accurate since it was fixed as the lower boundary of the soil profile. The same trends are thus to be expected for nutrient fluxes. Moreover, the spatial heterogeneity at the tree scale was not accounted for in the water drainage model but spatial patterns of nutrient concentrations were observed in soil solutions in particular near the tree stem where the water drainage is thought to be heterogeneous (stemflow input and higher fine root density than in the inter-row). Spatial heterogeneity of the water flux should be integrated in the model to compute more accurately nutrient fluxes. The spatial heterogeneity of the nutrient input by stemflow and by localized application of fertilizers is also essential in case of geochemical modelling, together with the knowledge of the rates of dissolution and/or mineralization of the fertilizers.

The type of data analysis enabled to study the nutrient dynamics in its continuity with simple analytical tools. Compared to discontinuous analysis, this method allows an easier comparison of the concentration events from one treatment or collector to another (onset, intensity, delay of maximum intensity, end). This first approach may be completed by the use of more powerful softwares of spectra analysis which would enable more sensitive calculations of the peaks characteristics and quantitative calculations of the peak areas. Statistical analysis may then be performed on these characteristics to study more precisely the effect of spatial heterogeneities or treatments on the soil solution chemistry and the

correlations among mineral elements. This method would be quite useful since statistical analysis usually performed on soil solution concentrations do not respect independency hypotheses.

The thresholds used in the present study were defined as to observe the appearance and attenuation of the main concentration peaks issued from the clear felling and from the fertilizer applications. As the influence of these ecosystem perturbations will decrease with time, lower thresholds will have to be defined, for example using the major concentration peaks observed in aboveground solution collectors.

PART E

NUTRIENT BUDGETS

INTRODUCTION

Over the studied period, the soil solution chemistry experienced changes under the influence of the silviculture (clear felling and fertilizing) and of the stand development. Large contents of mineral elements were leached down to the depth of 1 m, but the question remains about what happened of these elements between the depths of 1 to 3 m, and which part of the fertilizers (in particular K, Ca, Mg and P) has been dissolved or mineralized and subsequently taken up by the fast growing *Eucalyptus* trees since they did not appear in large quantities in soil solution. The system D of Figure 2 shows that the interactions of the soil solution with i) the vegetation, (ii) the soil surface and the soil matrix, and (iii) the soil organic matter and microbial biomass, account for the differences between the amounts of mineral elements released in the soil solution (from the mineralization of the forest floor and of the sewage sludge in T5 and from the dissolution of the fertilizers in T1 and T3) and the mineral elements leaving the soil solution system by leaching at a depth of 3 m.

The vegetation monitoring showed, as reminded in part A, a strong recycling of mineral elements in the forest floor and in the upper soil layers as already observed in others *Eucalyptus* plantations (Laclau et al., 2003c). This pattern suggests that a great part of the fertilizers were directly taken up by the trees without being observed in the soil solutions experimentally collected.

The soil study of part B showed that the soil mineral constituents could mainly released Fe, Al, Si and H in the soil solution. The potential for adsorption of cations on the soil surface was < 1 cmolc kg^{-1} but was highly pH dependant. The CEC was mainly saturated with Al so that basic cations may be adsorbed on the CEC provided the fact that either the CEC increases or Al is released in soil solution. The anion exchange capacity may lead to an adsorbption of anions especially below a depth of 1 m. Specific adsorptions may result in large retention of S and P in soils from the upper soil boundary down to a depth of 3 m. This seems in good agreement with the observations of the soil solution chemistry but mineral elements actually adsorbed on the soil surface remain to be checked.

Water drainage is essential in the computation of mineral element fluxes. Part C showed that (i) even if the water flux is probably overestimated at the depths of 15, 50 and 100 cm, the water flux at a depth of 3 m is likely to be accurate since it was fixed as the

lower boundary of the studied profile (provided the fact that the hypothesis of a single porosity is accurate), and (ii) a large water uptake of the fast growing *Eucalyptus* stand which limited the water drainage at a depth of 3 m to less than 5% of the incoming rainfall (in average) from six months after planting onwards. Drainage occurs at this depth during the wet season at a small constant rate (1 mm day^{-1}) or after large rainfall events (N_{month}=21 & 36) and upward flow (about 1 mm day^{-1}) occurs during the dry periods. In part D, it was shown that nutrients realeased in soil solutions after clear felling and fertilizing were mainly transported in deep soil layers with the first heavy rainfall following the dry period after planting at N_{month}=17-18. The nutrient flux reached a depth of 1 m within 2 months so that we can assume that it would have reached a depth of 3 m within, at least, 2 to 4 more months, that is, at N_{month}=22-24. Since water drainage at a depth of 3 m decreased sharply after N_{month}=21 (Figure 50), a doubt remains whether the mineral elements transported in the soil solution at a depth of 1 m did not leave the soil profile because they had been taken up, adsorbed or immobilized in the soil organic matter and microbial biomass, or simply because there was no water enough to transport them.

Quantitative study of the global budget of the system may help rule on the hypotheses formulated. As already mentioned in the general introduction of this thesis, system D (soil solution) will not serve to compute nutrient mass budgets because two many fluxes are impossible to measure and to compute. System A (tree+soil+soil solution) will thus be preferred to compute mass budgets as all major fluxes of this system were experimentally measured. The main goal of this part is to check by simple mass budget wether the hypotheses formulated in parts A, B, C and D are consistant with the mass transfers among storage compartments occurring during the experimental period. The computed budgets are not fertility budgets of the plantation.

The nutrient budgets are established for K, Ca, Mg, P and N in priority since these elements were quantified in the trees. The organic part of the soil system was not studied in this thesis but its influence on the mass budget is discussed.

E.1 MATERIAL AND METHODS

E.1.1.1 Studied system and times of observations

The studied system was the system A of Figure 2 already presented in the general introduction of this thesis, that is, the whole stand plus the soil and the soil solution down to a depth of 3 m. The system was observed from the clear felling until 24 months after planting.

We already mentioned that the *Eucalyptus* root system reaches soil depths > 3 m within 1 year of growth. As the studied systems stops at a depth of 3 m, a supplementary flux should be added on Figure 2-A: the root uptake and exudates occurring below a depth of 3 m. Here, we suppose that all nutrients are taken up in the 0-3 m soil layer and that these fluxes, although substantial for water uptake, are insignificant for nutrient uptake. The very low contents of available nutrients measured in soils below a depth of 3 m in part A would confirm this hypothesis but it remains to be checked.

It has to be reminded that the water uptake (evapotranspiration) estimated in part C was optimized by comparing the simulated water contents to the measured soil moistures down to a depth of 3 m, with the lower boundary of the soil profile fixed as the measured soil moisture at a depth of 3 m. The evapotranspiration thus estimated corresponded to the effective uptake within the upper 3 m of the soil profile and did not account for the *Eucalyptus* uptake from deeper soil layers, so that the water budget performed in part C was accurate.

E.1.1.2 In and out fluxes

Table 42 Fluxes entering or leaving the studied system (system A of Figure 2).

		Calculation	**Abbreviation**
Deposits	Bulk	Measured (Rainfall)	$\mathbf{F_{Pi}}$
	Dry	Estimated and neglected	**0**
Gazeous exchanges		Not calculated	$\mathbf{F_{GE}}$
Soil solution flow at a depth of 3 m	Downward	Calculated from the simulated water flow (MIN3P) and the soil solution extracts analysis	$\mathbf{F_{SoilWDown}}$
	Upward	Not calculated	$\mathbf{F_{SoilWUp}}$
Diffusion		Not calculated	$\mathbf{F_{Diff}}$
Fertilizers		Measured (total analysis)	$\mathbf{F_{Ferti}}$

The sum of fluxes entering and leaving the system may be written as (see Table 42 for abbreviations):

$$\Sigma F = F_{Pi}+F_{GE}+F_{SoilWDown}+F_{SoilWUp}+F_{Diff}+F_{Ferti} \quad (59)$$

$\Sigma F > 0$ means that nutrients were stocked within the studied system whereas $\Sigma F < 0$ means that nutrients were lost from the studied system. Under the hypothesis that $F_{SoilWUp}+F_{Diff}+F_{GE} << F_{Pi}+F_{SoilWDown}+F_{Ferti}$, ΣF can be written:

$$\Sigma F \sim F_{Pi}+F_{SoilWDown}+F_{Ferti} \quad (60)$$

Gazeous fluxes for N are reported to be limited after clear felling in Brazil (Neill et al., 2006) and K, Ca, Mg and P do not normally participate to F_{GE}. Diffusion and upward fluxes may account for large nutrient fluxes but such processes are very slow. Moreover, soil solutions are diluted at a depth of 3 m which may suggest that even if upward movement of solution occurred at this depth, little amount of nutrients may have been entering the system from deeper soil layers. We thus assumed that these fluxes were insignificant at a two-year scale compared to the fertilizer input. Nevertheless, such fluxes may be quite important in natural ecosystems to restore the equilibrium gradient of nutrients in soil after a perturbation occurred (Grigal and Ohmann, 2005).

Dry depositions are difficult to measure experimentally so that they were calculated as the difference between nutrient fluxes in throughfall and bulk precipitations. This difference was insignificant compared to the rainfall nutrient fluxes, which may be explained (i) by the limited foliage of the *Eucalyptus* trees during the first year of growth,

and/or (ii) by the fact that bulk deposition collectors already collected a great part of the dry depositions. It was further neglected in ΣF.

The fluxes were calculated from the results of part D which means that losses of organic N were not accounted for in the nitrogen budget since DON was not measured in soil solutions.

E.1.1.3 Changes in nutrient stocks

E.1.1.3.1 Stocks of the studied system

The main compartments of the studied system are detailed in Table 43.

Differences in stocks from clear felling to two years after planting can be written as (see Table 43 for abbreviations):

$$\mathbf{\Delta S = \Delta S_{St1} + \Delta S_{AB2} + \Delta S_{FF1} + \Delta S_{Rem} + \Delta S_{FF2} + \Delta S_{R1} + \Delta S_{R2}} + \Delta S_{Ferti} + \mathbf{\Delta S_{SoilS}} + \Delta S_{SoilM} + \Delta S_{SoilW} + \Delta S_{SoilMB} \quad (61)$$

$\Delta S > 0$ means that nutrients were stocked within the system whereas $\Delta S < 0$ means that nutrients were lost from the system. Only the terms in bold were measured and calculated in the present budget:

$$\Delta S_{measured} = \Delta S_{AB1} + \Delta S_{AB2} + \Delta S_{FF1} + \Delta S_{Rem} + \Delta S_{FF2} + \Delta S_{R1} + \Delta S_{R2} + \Delta S_{SoilS} \quad (62)$$

The mass conservation implies that:

$$\Delta S = \Sigma F \quad (63)$$

or equally:

$$\Sigma F - \Delta S_{measured} = \Delta S_{Ferti} + \Delta S_{SoilM} + \Delta S_{SoilW} + \Delta S_{SoilMB} \quad (64)$$

Equation (64) shows that the differences between the measured fluxes and the measured changes in stocks may be explained by changes in stocks of fertilizers (ΔS_{Ferti}), soil solution (ΔS_{SoilW}), soil mineral matrix and soil organic matter (ΔS_{SoilM}), or soil microbial biomass (ΔS_{SoilMB}).

The stocks in the soil mineral matrix may be considered invariants for Ca, Mg and K ($\Delta S_{SoilM}=0$) since no mineral which may release such elements were found in the mineralogical study of part B, but differences in soil mineral stocks of S, P and Al may have occurred.

Soil organic stocks (soil and microbial biomass) were neither measured nor calculated but they may account for a great part of the observed differences in ΣF in particular for N. In this thesis, we focused on mineral elements but specific studies of the organic part of the system are currently being carried out in the experiment.

The fraction of the fertilizers (ΔS_{Ferti}) which remained at the end of the experiment may be large for low solubility fertilizers such as dolomitic limestone, as well as for the sewage sludge which may last to mineralize. On the contrary, KCl and $(NH_4)_2SO_4$ may dissolve quickly and ΔS_{Ferti} may be insignificant for these minerals.

Table 43 Stocks of the studied system at clear felling (T0) and two years after planting (Tf).

		T0 (N_{month}=9)	Tf (N_{month}=37)	Calculation	Abbreviation
Aboveground biomass	From the previous rotation	Stump	Remaining unmineralized	Considered invariant	ΔS_{St1}
	From the new planted stand	0	Bark, leaves, branches stem, stump	Direct measurement at Tf	ΔS_{AB2}
Forest floor and remnants	From the previous rotation	Left on floor	Remaining unmineralized	Direct measurement on site at T0, and from an adjacent plot kept free from remnants and vegetation at Tf	ΔS_{FF1}
		Bark, leaves, branches Left on site as remnants	Remaining unmineralized	Direct measurement at T0 and estimated from decomposition rates measured in litter bags	ΔS_{Rem}
	From the new planted stand	0	Fallen minus mineralized during the period	Direct measurement at Tf	ΔS_{FF2}
Belowground (roots)	From the previous rotation	Remaining at the end of the rotation	Remaining unmineralized	Direct measurement at T0 and estimated from decomposition rates measured in litter bags	ΔS_{R1}
	From the new planted stand	0	2 years-old	Direct measurement at Tf	ΔS_{R2}
Fertilizers	Forest floor + soil (T1, T3)	0	Remaining undissolved or unmineralized	Not calculated	ΔS_{Ferti}
Soil	Surface of soil constituents			Estimated from soil specific extractions	ΔS_{SoilS}
	Matrix (minerals + soil organic matter)			Not calculated	ΔS_{SoilM}
	Solution			Not calculated	ΔS_{SoilW}
	Microbial biomass			Not calculated	ΔS_{SoilMB}

E.1.1.3.2 Measurements and calculations

The main terms of eq (61) represent (i) the changes in stocks of nutrients in the *Eucalyptus* trees and (ii) the changes in stocks of nutrients adsorbed (more or less specifically) on the soil constituents surface. The vegetation stocks were taken from Laclau *et al* (2004b; 2005b; 2007) as presented in part A. Specific extractions were performed on soils to quantify the elements effectively adsorbed and are described thereafter.

For the quantification of adsorbed elements, a new soil sampling was performed 2 years after planting (AP_{24}). In May 2006, soil samples were collected for one pit per block and treatment, in treatments 1, 3 and 5, blocks 1, 2 and 3, and from three pits excavated in part of the former stand kept uncut (named reference – R). In each pit, soils were sampled at the depths of 0-5 cm, 5-15 cm, 15-30 cm, 30-50 cm, and 50-100 cm. In block 1 and all blocks of treatment 3 and reference, supplementary samples were collected at the depths of 50-100 cm, 100-200 cm, and 200-300 cm. Samples were taken continuously from the tree stem to the inter-row to integrate the soil spatial heterogeneity at the tree scale.

The soils of the reference plot were considered to be equivalent to the soils of the experiment at clear felling. In fact, the soils thus sampled had experienced more two years of growth of the *E. saligna* stand, but as this stand was more than 6 years-old, it may be considered at a steady-state compared to the major perturbations occurring at clear felling, fertilizing, and re-planting. The soil status after two years of growth was compared to this reference preferentially than to the soils sampled before clear-felling (data set $SOIL_{BCF}$ of part B) because (i) extractions on fresh soils for nitrates and ammonium were needed but had not been performed on the $SOIL_{BCF}$ sampling, and (ii) the concentrations measured in the soil extracts are generally very small for such soil type (CEC & AEC < 1 cmolc kg^{-1}, saturations in basic cations < 0.1 cmolc kg^{-1}) and analytical series are very sensitive to the experimental conditions at the time of the extraction (deionized water, ambient conditions, equipment calibration, …). We preferred comparing samples from the same experimental series than risking an analytical bias when using data of the $SOIL_{BCF}$ analytical series.

Once collected, fresh soils were immediately extracted with (i) distilled water, and (ii) KCl 2 mol L^{-1} using a soil-solution ratio of 1/10 (Mulvaney, 1996). After a 1-hour shaking, the soil suspensions were filtered and kept at 4°C. In the water extracts, Ca, Mg, Na, NH_4, NO_3, SO_4 and H_2PO_4 concentrations were measured by ion chromatography (CENA, Laboratorio de Ecologia Isotopica) and Al by ICP (CENA, Laboratorio de Química

Analítica). K and Cl were also measured in the water extracts but the results were discarded since contamination of KCl occurred during the extractions performed in the field. In the KCl extracts, NH_4 and NO_3 concentrations were measured by colourimetry (CENA, Laboratorio de Biogeoquímica Ambiental).

The soils were subsequently air-dried. The CEC was measured following the same protocol than in the soil section (§ B.1.1.2). Sulphates were extracted by H_2PO_4 (ratio 2/5) and measured by turbidimetry (Cantarella and Prochnow, 2001). Phosphates were extracted by the Mehlich 1 protocol (ratio 1/10) and measured by colourimetry (da Silva et al., 1999). The extractions were performed at ESALQ, Departamento de Ciências do Solo, Laboratorio de Analises Químicas-Pesquisa.

Classically, successive extractions are recommended to extract the whole pool of adsorbed sulphate (Delfosse, 2005; Prietzel et al., 2001) but the available photocolourimeter was not sensitive enough to small concentrations. KH_2PO_4 is also reported to extract about 50 % of the S pool in acidic forest soils that received much S from the atmosphere or from gypsum or ammonium sulphate fertilizations (Prietzel and Hirsch, 2000). In the same way, the Mehlich method is reported to extract available P (Kuo, 1996), which means that a great part of the adsorbed P may not have been extracted by this method. These extractions give a good idea of the relative distribution of the S and P adsorbed at clear felling and two years after planting according to the soil layer sampled. Nevertheless, their absolute values must be handled cautiously since they are likely to underestimate the whole pool of adsorbed S and P.

Computing differences in stocks in the soil is highly problematic: little changes in the studied variable may be confounded with spatial heterogeneity or analytical variations and when integrated over the entire soil mass these tiny values may represent very large amounts. To preclude summing non significant differences over the whole soil profile, two thresholds were defined

- a threshold of analytical determination estimated by diluting standards until the measured data differed > 10 % from the theoretical one,
- a threshold of analytical repeatability: 3 replicate analysis were performed for one sample per depth, and differences between two samples for a given depth were considered significant when larger than twice the standard error of the 3 replicate analyses.

Differences in stocks of adsorbed nutrients were computed for all cations (except NH_4) from the CEC measurements, for NO_3 and NH_4 from the KCl extractions performed on soils at field moisture, and for S and P from extractions by KH_2PO_4 and by the Mehlich protocol, respectively.

E.2 RESULTS AND DISCUSSION

E.2.1 Nutrient fluxes entering and leaving the studied system

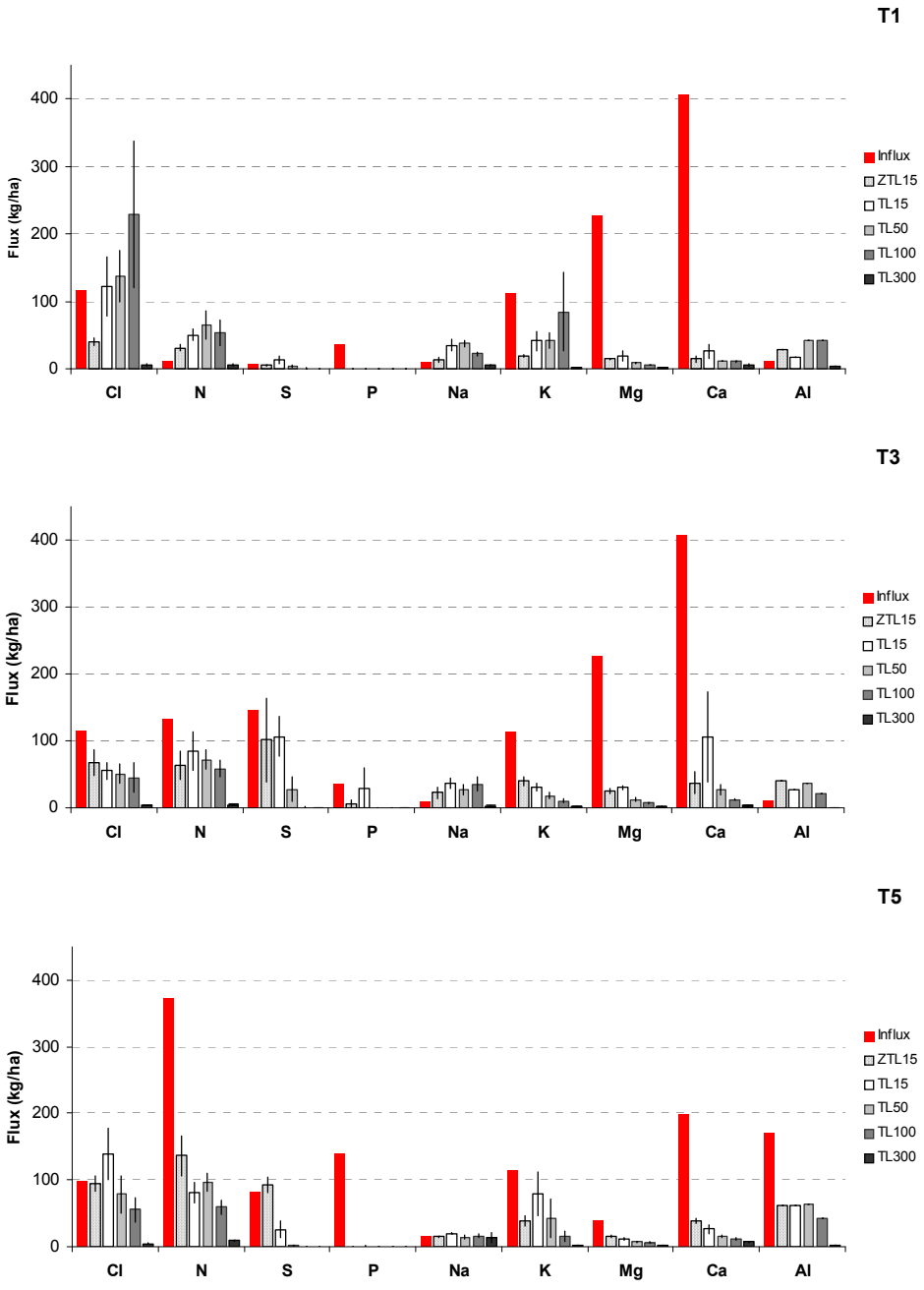

Figure 77 Total nutrient influx (fertilizer + total atmospheric deposits) and amounts of nutrients leached in soil solutions (estimated from part D) at the depths of 15, 50, 150 and 300 cm from the clear felling until age two years in the fertilization experiment for treatments 1 (T1), 3 (T3) and 5 (T5). Vertical bars stand for standard errors (in T3 at 50 cm and in T5 at 100 cm and 300 cm, n=6; in T3 at 100 cm and 300 cm n=12; n=3 elsewhere). TL=Tension lysimeter, ZTL= Zero tension lysimeter.

As already mentioned in part D, almost no nutrient was leached at a depth of 3 m. To help understanding the nutrient dynamics within the studied system, nutrients fluxes at depths < 300 cm will be compared to nutrient inputs, but total budgets should not be performed at these depths since other fluxes such as tree uptake in deeper soil layers should be accounted for.

About 50 to 100 % of the chloride entering the system was leached down to a depth of 100 cm (Figure 77). This flux was poorly attenuated between the depths of 15 to 100 cm. In T1, a release of chloride in soil solution seemed to occur between the depths of 50 to 100 cm but the spatial heterogeneity associated to this flux was high.

The sulphate fluxes confirmed the observations made in part D. In T1 almost no S entered or left the studied system. Almost all the S applied was leached at a depth of 15 cm in T3 and in ZTL of T5. S fluxes were rapidly attenuated in deeper soil layers. The amounts of S leached were of the same order of magnitude as measured in European soils which received 75 kg N ha^{-1} $year^{-1}$ through $(NH_4)_2SO_4$ fertilizers (Carnol et al., 1997).

Almost none of the P applied was leached at a depth of 15 cm in T1 and T5. In T3, the P fluxes at a depth of 15 cm equaled the P influx. The spatial heterogeneity associated to this flux was very high so that it may correspond to localized dissolutions of P.

When no N was applied (T1), N leaching was greater than the N influx down to a depth of 50 cm which confirmed that nitrate and ammonium were released in the soil solution in the upper layers of the soil profile (about 65 kg ha^{-1}). Larger amounts of N were leached in T3 and T5 than in T1 as already mentioned in part D, but these amounts were far less than the N brought by the fertilizers. If we attribute 65 kg N ha^{-1} of these amounts to the mineralization of the harvest residues and of the organic matter as in T1 (part A), then about 10 % of the N from the fertilizers were leached in T3 (25 kg N ha^{-1}) and in T5 (35 kg N ha^{-1}) at the depth of 50 cm. Comparatively in the forests of England, 77 and 113 kg ha^{-1} of $N\text{-}NO_3$ where leached after clear felling and clear felling + fertilizing with 75 kg N ha^{-1} of $(NH_4)_2SO_4$, respectively (Carnol et al., 1997). In the US forests, 60-90 kg $N\text{-}NO_3$ ha^{-1} $year^{-1}$ were leached down to a depth of 1 m after bole-only harvesting (Strahm et al., 2005). This pattern would confirm, as reviewed by Zech *et al.* (1997), that the dynamics of soil organic matter share common features in temperate and tropical soils.

In T1 and T3, no significant amount of aluminium entered the system but Al was released in soil solution between the depths of 0 to 15 cm (about 25-50 kg ha^{-1}). It was

subsequently transported down to a depth of 1 m with almost no attenuation. This Al release occurred simultaneously to the NO_3 release and was the direct consequence of soil organic matter and harvest residues mineralizations as already explained. The amount of Al leached in T5 was about 25 kg ha^{-1} larger than in T1 and T3, which represents about 10 % of the amount of Al in the sewage sludge. Once more, these values are very close from the 29 kg ha^{-1} of Al leaching measured by Carnol *et al.* (1997) after clear felling and 54 kg ha^{-1} after clear felling plus fertilizing.

All the sodium entering the system was leached down to a depth of 100 cm without attenuation which suggests that Na was little taken up by the *Eucalyptus* trees in these plots where large amounts of K was applied. However, an adjacent trial showed that *Eucalyptus* trees take up large amounts of Na when K is highly deficient. A slight release of Na in the soil solutions in the upper soil layers (0-15 cm) in T1 and T3 suggests that Ca and Mg (from the dolomitic limestone) may have replaced Na on the soil exchange capacity.

In T1 and T3, about 40 % of the K entering the system was leached at a depth of 15 cm. This flux was gradually attenuated as the depth increased. In T1, K was released together with Cl below a depth of 50 cm which may correspond to KCl from the fertilizer locally leached in deep soil layers. Fluxes of dissolved K in deep soil layers in T1 may also result from a lower K demand of the *Eucalyptus* trees in T1 compared to T3 and T5 (where the stand early development was greatest).

Even though Mg and Ca fluxes in soil solutions were slightly larger in T3 (dolomitic limestone dissolution and sulphate as vector anion) than in T1 and T5, they represented less than 10-25 % of the influx in all treatments. Other studies showed that most Ca cycling and vegetation uptake occurs in the upper soil layers (Dambrine et al., 1997; Poszwa et al., 2002). This may explain why very little Ca and Mg were observed in soil solutions at a depth of 15 cm even if it had been dissolved from the fertilizers.

In conclusion, questions remain about the fate of the mineral elements which were observed in soil solutions but were not leached at a depth of 3 m. Are concerned:

- 25-65 kg ha^{-1} of Al and 50-75 kg ha^{-1} of $N\text{-}NO_3$ below a depth of 1 m,
- 100 kg S ha^{-1} between the depths of 15 to 100 cm in T3 and T5,
- 35 kg P ha^{-1} in T3 between the depths of 15 to 50 cm,
- 20-40 kg ha^{-1} of Ca and Mg and about 70-90 kg ha^{-1} of K below a depth of 15 cm.

These elements may have either been adsorbed on the soil surface, immobilized in the soil organic matter or soil microbial biomass, taken up by the *Eucalyptus* trees, or may be still present in the soil solution.

A large part of the nutrients which entered the system never appeared in soil solutions:

- 60 to 90 % of the K, Ca and Mg influx,
- 90 % of the N fertilizer in T3 and T5,
- 100 % of the P influx in T1 and T5.

These nutrients may have either been adsorbed or immobilized in the soil organic matter and soil microbial biomass in the upper 15 cm of the soil profile, may have been taken up by the *Eucalyptus* trees, or may be still undissolved or unmineralized (N in T5, Ca, Mg, and P in all treatments).

Paragraphs E.2.2 and E.2.3 present the results of the extractions performed on the soils two years after planting. Their purpose is to check qualitatively the hypotheses regarding the nutrients adsorbed on the soil surface or still present in soil solutions, and in particular the depth limits presented in the conclusions of this paragraph. Quantitative study for the whole system (whole soil profile integrated) are presented in § E.2.4. The values in kg ha^{-1} corresponding to the charts of § E.2.2 and E.2.3 are given in ANNEX 1.

E.2.2 Soil water extracts composition at 2 years after planting

To help understanding whether nutrients were stopped in soil solutions between the depths of 1 to 3 m, water extractions were performed on fresh soils at the end of the experimental period. Water extractions extract (i) soil solution, (ii) soluble salts or hydrophilic OM of bulk soil and (iii) weakly adsorbed species.

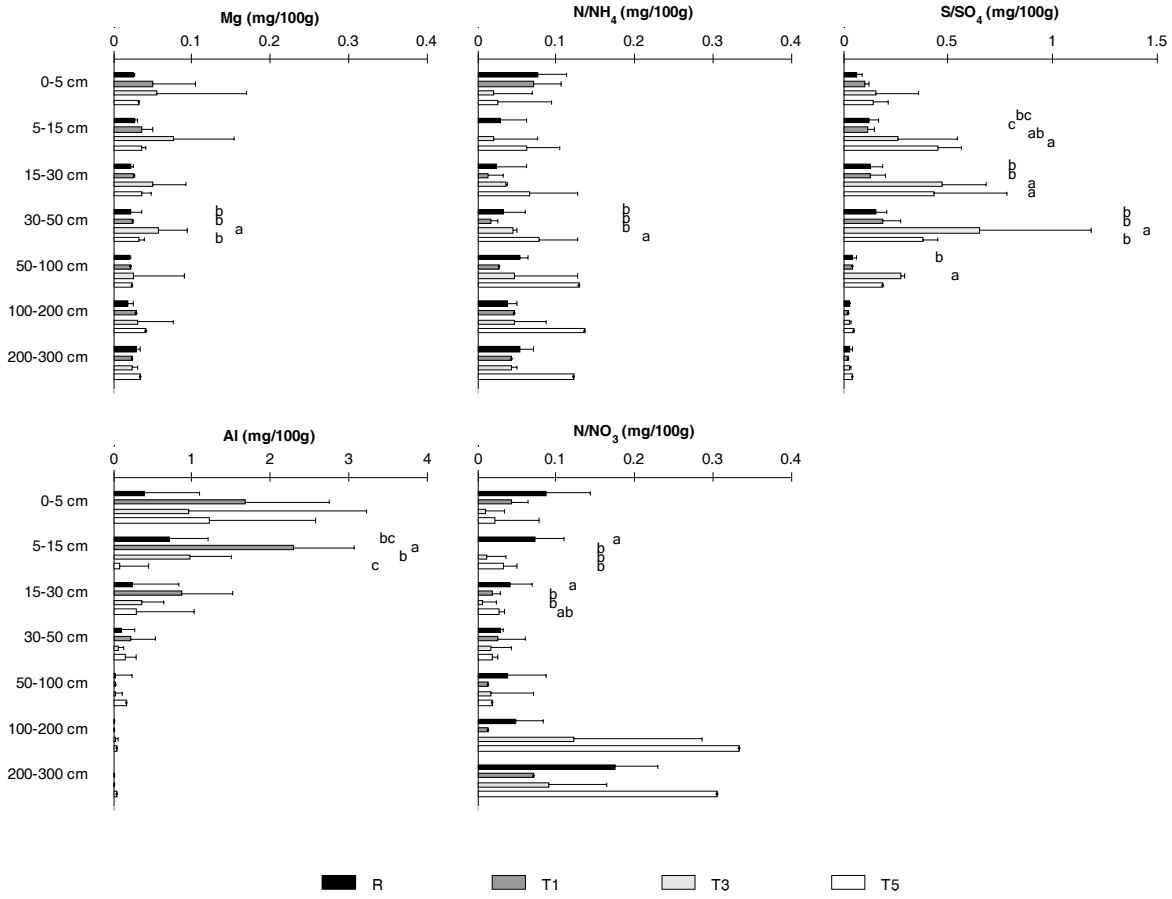

Figure 78 Composition in Mg, Al, N-NH_4, N-NO_3, and S-SO_4 of soil water extracts at age two years (AP24) (mg/100g) in treatments 1 (T1), 3 (T3) and 5 (T5) compared to the reference treatment R (part of the previous stand (BCF) kept uncut). Horizontal bars stand for standard errors (n=3 for all treatments down to a depth of 50 cm, n=3 for R and T3 and n=1 for T1 and T5 from a depth of 50 cm down to a depth of 3 m). Different letters indicate differences when significant at $P<0.05$. Soils were extracted just after sampling, at field moisture.

The pH of the water extracts were in average 4.4 which is close to the soil pH (4.5) measured in $CaCl_2$ 0.002 mol L^{-1} (part B). We may thus assume that the extraction by

deionized water did not influence much the soil equilibrium (surface charge, adsorbed species, speciations, …) prior to the extraction.

Mg concentrations in water extracts were greater in T3 than in the reference (R), in T1 and in T5 down to a depth of 50 cm (Figure 78). This pattern suggests that (i) there is still soluble Mg in the upper soil horizons either weekly adsorbed on the soil surface or coming from the dolomitic limestone still not dissolved (ii) Mg is leached more deeply in the soil profile in a soluble way when associated to sulphate (T3).

The amount of SO_4 extracted by water was greater in T3 and T5 than in the reference and in T1. Greatest concentrations were reached between the depths of 15 to 30 cm in T5 and deeper between the depths of 30 to 50 cm in T3. Greater concentrations of sulphates in T3 and T5 compared to the reference were still found below these concentration peaks. It is suggested that (i) most of the SO_4 release already occurred (concentrations in surface less than in deeper soil layers) (ii) a great part of the sulphate observed in the soil solution monitoring is under a soluble form (iii) SO_4 leaching may still occur 2 years after planting since high concentrations seem to be transmitted to deeper soil layers.

Most of the Al in water extracts was located above a depth of 30 cm in the reference as well as in all treatments. It thus seems to be linked to the mineralization of the forest floor still running at the date of the sampling. Al concentrations in water extracts were higher in T1 than in the other treatments, which suggest that the protons released by nitrification were mainly buffered by the Al release in this treatment compared to the N-fertilized ones. As 25-65 kg ha^{-1} of Al were leached down to a depth of 1 m, greatest concentrations in soil extracts were expected below a depth of 1 m in all treatments compared to the reference but this was not the case. It can be supposed that in these oxidic soils, Al was quickly immobilized and/or precipitated when reaching less acidic soil layers.

NO_3 was effectively found in soil water extracts between the depths of 1 to 3 m in the expected order T1 < T3 < T5. The surprising observation was that the same nitrate dynamics were observed in the reference treatment which was neither clear felled nor fertilized in 2004. Nitrate concentrations were not significantly less in the reference compared to all treatments two years after planting, which suggests that nitrate had already been leached in these deep soil layers before the clear felling and the fertilization experiment occurred. This nitrate probably came from the previous harvests of the stand managed in short rotation coppice since 1945 and may have been adsorbed on the anion

exchange capacity increasing below a depth of 1 m (part B). Since below a depth of 50 cm only one soil pit in T1 and T5 was extracted, it is difficult to status upon the significance of the larger nitrate concentrations observed in T5 below a depth of 1m, and in T3 between the depths of 1 to 2 m, compared to R and T1.

Table 44 Pearson coefficients of correlation calculated for fresh soil water extracts at age two years (AP24) in treatments 1 (T1), 3 (T3) and 5 (T5) compared to the reference treatment R (part of the previous stand (BCF) kept uncut). Only the coefficients corresponding to $P<0.05$ are given.

Reference

	Mg	Ca	Al	Na	N-NO_3	S-SO_4	N-NH_4	H
Mg	1							
Ca		1						
Al			1					
Na		0.52		1				
N-NO_3				0.64	1			
S-SO_4						1		
N-NH_4							1	
H	0.48	0.47	0.59	0.62	0.46			1

Treatment 1

	Mg	Ca	Al	Na	N-NO_3	S-SO_4	N-NH_4	H
Mg	1							
Ca	0.85	1						
Al	0.64	0.58	1					
Na				1				
N-NO_3					1			
S-SO_4						1		
N-NH_4	0.70	0.60					1	
H								1

Treatment 3

	Mg	Ca	Al	Na	N-NO_3	S-SO_4	N-NH_4	H
Mg	1							
Ca	0.81	1						
Al	0.65	0.45	1					
Na	0.66	0.78	0.43	1				
N-NO_3					1			
S-SO_4	0.45	0.59			-0.44	1		
N-NH_4	0.48						1	
H						0.67		1

Treatment 5

	Mg	Ca	Al	Na	N-NO_3	S-SO_4	N-NH_4	H
Mg	1							
Ca	0.54	1						
Al			1					
Na		0.72		1				
N-NO_3					1			
S-SO_4	0.71				-0.55	1		
N-NH_4		-0.68		-0.58			1	
H	0.82	0.65				0.67		1

The main chemical associations occurring in the soil water extracts are given by the correlations of Table 44. In the reference plot, protons were associated to all other cations and NO_3 in the water extracts. In T1, Ca, Mg, Al and NH_4 were positively correlated. In T3, SO_4 was positively correlated with Mg, Ca and H and negatively correlated with NO_3, and NH_4 was positively correlated with Mg. T5 followed more or less the same scheme than T3 except that NH_4 was negatively correlated with Ca and Na.

These results suggest that in the reference plot and in T1, the mineralization of the forest floor and of the organic matter is the main process driving the composition of the water extracts: the mineralization of the forest floor releases NH_4 and nutrients in soil solution, then the nitrification releases NO_3 and H which is next buffered by the release of

Al from the cation exchange capacity and the dissolution of minerals (in particular the dolomitic limestone in T1).

In T3 and T5, sulphate seems to be the main driver to the soil solution composition. It is solvated in the water extracts with Ca and Mg as observed in part D. Its positive correlation with H may result from desorption of weekly adsorbed sulphate. The negative correlation between sulphate and nitrate confirms that sulphates are preferentially retained on the soil surface over nitrates.

As already explained, K and Cl could not be analyzed in the water extracts.

E.2.3 Changes in adsorbed nutrients from the clear-felling until two years after planting

E.2.3.1 Cations

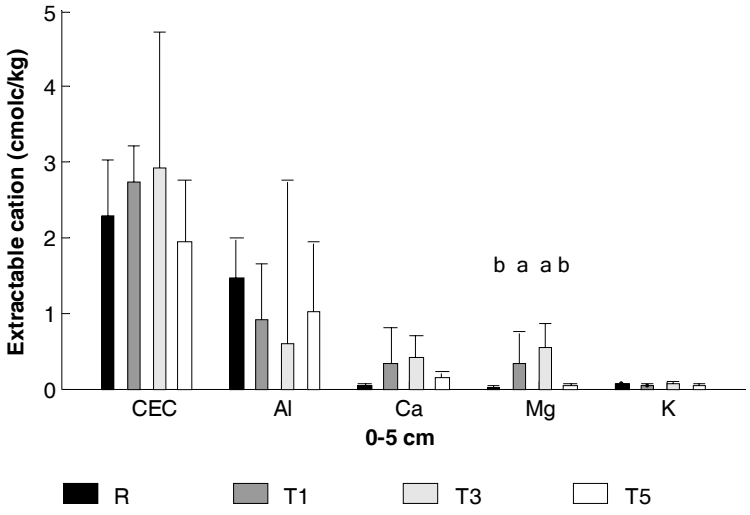

Figure 79 Effective cation exchange capacity and exchangeable Al, Ca and Mg contents (cmolc kg^{-1}) in the 0-5 cm soil layer at age two years (AP24) in treatments 1 (T1), 3 (T3) and 5 (T5) and in the reference treatment R (part of the previous stand (BCF) kept uncut). Horizontal bars stand for standard errors (n=3). Different letters indicate significant differences at $P<0.05$.

The main differences in the amounts of cations adsorbed were observed for the upper soil layer (0-5 cm) (Figure 79). It confirms that more Ca and Mg were adsorbed on the soil surface in T1 and T3 (where dolomitic limestone was applied) compared to the reference plot and T5, but this trend was only significant for Mg. No significant difference was observed for the effective cation exchange capacity and Al.

It seems that cations were neither leached nor retained in great quantities on the soil surface. The main hypothesis is that they were mainly taken up by trees, or immobilized in the soil biomass, or still not dissolved (T1 and T3) or mineralized (T5).

E.2.3.2 N/NO_3, N/NH_4

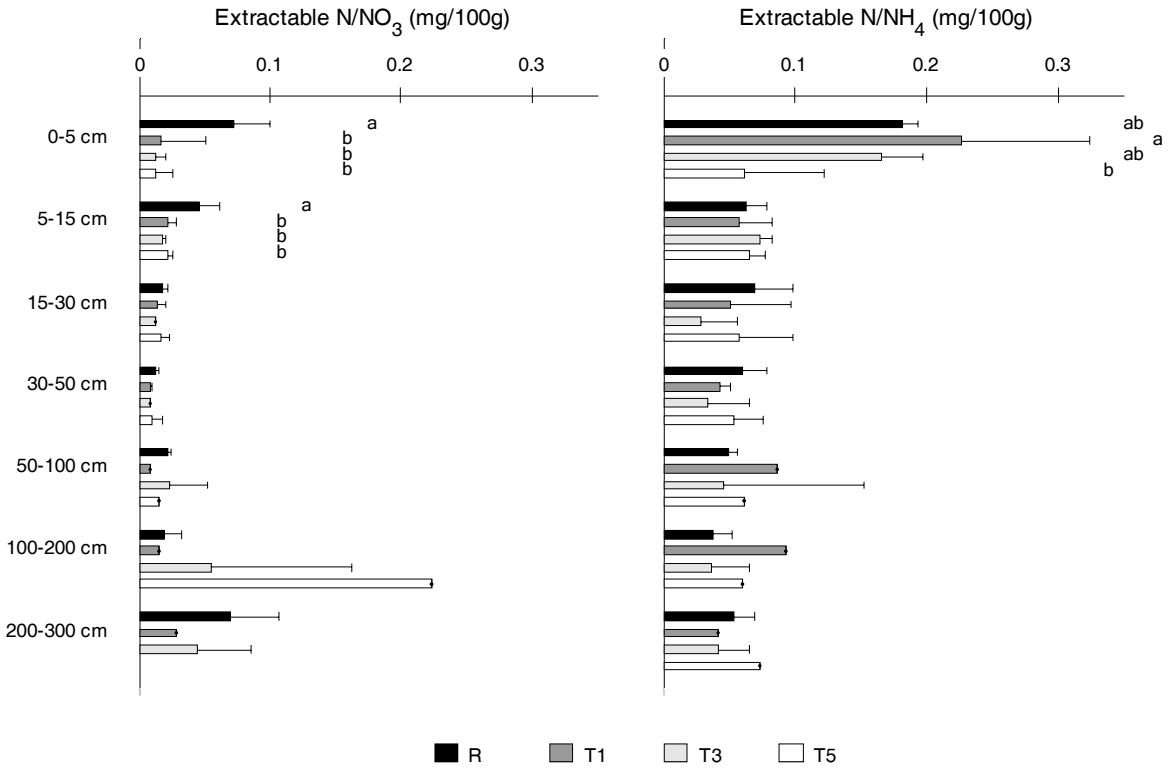

Figure 80 Composition in $N\text{-}NO_3$ and $N\text{-}NH_4$ of fresh soil KCl (1 mol L^{-1}) extracts at age two years (AP_{24}) (mg/100g) in treatments 1 (T1), 3 (T3) and 5 (T5) compared to the reference treatment R (part of the previous stand (BCF) kept uncut). Horizontal bars stand for standard errors (n=3 for all treatments down to a depth of 50 cm, n=3 for R and T3 and n=1 for T1 and T5 from a depth of 50 cm down to a depth of 3 m). Different letters indicate significant differences at $P<0.05$.

KCl extractions performed on fresh soils classically extract the same fraction of nutrients as water plus chemical species adsorbed non-specifically on the soil surface. NO_3 and NH_4 concentrations are thus usually greater in KCl extracts than in water extracts. However, water extracts were dosed by ion chromatography and KCl extracts by photo-colourimetry. As the concentrations in the extracts (about 0.1 mol L^{-1}) were close to the detection limits of the analysers, biases between both methods of measurement may exist and it is thus difficult to compare absolute values of KCl extracts to those of the water ones. Nevertheless, small difference between both extractions indicates that non-specific adsorption is limited in the studied soils, which was the case here (Figure 78 & Figure 80).

KCl extracts showed the same dynamics as water extracts (Figure 80). Nitrate concentrations were highest in T5 in the 100-200 cm soil layer (> 0.2 mg $N\text{-}NO_3$ / 100 g). The anion exchange capacity (AEC) measured in part B corresponded to about 1.2, 2, 4.2 and 7.4 mg $N\text{-}NO_3$ / 100 g for the 0-30 cm, 30-100 cm, 100-200 cm, and 200-300 cm layers, respectively. The amount of nitrates extracted by KCl thus corresponded to less than 10 % of the AEC. In comparison, about 0.5 mg/100 g of $N\text{-}NH_4$ and 4 mg/100 g of $N\text{-}NO_3$ were adsorbed on the soil surface below a depth of 60 cm in Costa Rica under coffee trees (Harmand et al., 2007). Such adsorption explained the difference between the 90 kg N ha^{-1} $year^{-1}$ leached at a depth of 60 cm and the 16-27 kg N ha^{-1} $year^{-1}$ leached at a depth of 2 m. In contrary to the soil of the present study, the soil pH in Costa Rica was more basic in KCl than in water indicating a large anion exchange capacity. Our soils exhibit lower AEC and thus fewer nitrates were desorbed from the soil surface.

More nitrates were extracted in the upper soil layer (0-5 cm) in the reference plot compared to all treatments. When soil sampling occurred, N requirements in the old *Eucalyptus* stand were much lower than in the young fast growing plantation and less nitrate and/or ammonium are likely to be taken up from the soil solutions.

E.2.3.3 Sulphate and phosphate

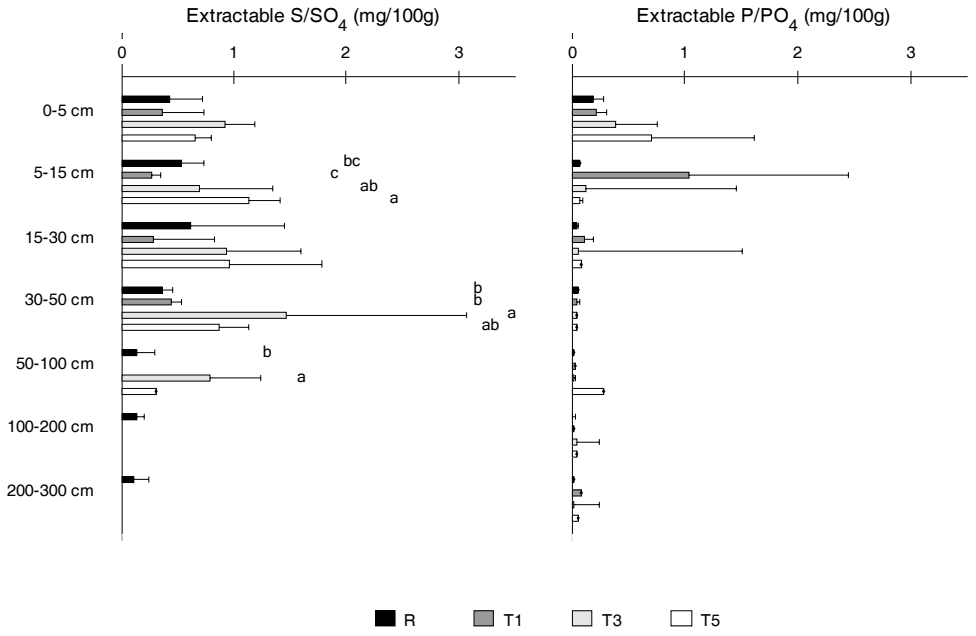

Figure 81 S-SO_4 extracted by KH_2PO_4 and P-PO_4 extracted by the Mehlich protocol at age two years (AP24) (mg/100g) in treatments 1 (T1), 3 (T3) and 5 (T5) compared to the reference treatment R (part of the previous stand (BCF) kept uncut). Horizontal bars stand for standard errors (n=3 for all treatments down to a depth of 50 cm, n=3 for R and T3 and n=1 for T1 and T5 from a depth of 50 cm down to a depth of 3 m). Different letters indicate significant differences at $P<0.05$.

The specific extractions of P and S confirmed their depths of adsorption. P was mainly adsorbed in the 0-5 cm layer in T1 and T5 and in the 0-15 cm upper soil layer in T3, which confirms a higher mobility of P in T3 than in T1 and T5. This is probably the result of the competition with sulphate for sorption sites. Sulphate extracted by H_2PO_4 showed the same dynamics as when extracted by water but the quantities desorbed were three times greater.

The specific adsorption measured for S in part B was null in the upper soil layer (0-5 cm) and of about 20 mg/100g at a depth of 3 m. Assuming that this specific adsorption was proportional to the AEC, then, it would be of about 3 and 5 mg/100g in the 5-30 cm and 30-50 cm soil layers, respectively. S desorbed by H_2PO_4 accounted for about one third of these specific adsorption capacities. However, the soil pH at field conditions may be more basic than pH=4 at which the isotherms were performed, so that the specific adsorption at field conditions may be slightly less than the measured one. Furthermore, we may not have

extracted the whole fraction of adsorbed S as already mentioned in the material and methods section. The amount of sulphate extracted was more or less constant from the upper boundary of the soil profile down to a depth of 30 cm which may suggest that the adsorption capacities of the upper soil layers are saturated.

The specific adsorption capacity for P was measured in part B at 37 mg/100 g in the 0-5 cm layer. The amount of P extracted accounted for about 2.5 % of this value.

For the same soil type without fertilizer applications, adsorptions of 0.2 to 0.4 mg/100g were recorded for S and P under *Eucalyptus* (Neufeldt et al., 1999) or other vegetation types (Alves and Lavorenti, 2004). This suggests that the larger values measured in the present study resulted from the fertilizer applications. The amount of S extracted was within the range of 0.3 to 30 mmol kg^{-1} of S extracted in andosols which received dry inputs of about 2-800 mg S m^{-3} day^{-1} (Delmelle et al., 2003).

E.2.3.4 Conclusions

Qualitatively, § E.2.3 showed that the hypotheses formulated about the adsorption and desorption processes on the soil surfaces were correct. It was shown that nitrate was effectively present between the depths of 1 to 3 m and was weekly adsorbed on the soil surfaces, that S was adsorbed weakly (1/3) and more specifically (2/3) between the depths of 5 to 100 cm, and that P was specifically adsorbed in the upper soil layers (0-50 cm). Ca and Mg were adsorbed on the CEC in the upper soil layers (0-15 cm). Non specific and specific adsorptions are likely to have been underestimated since successive extractions would have been necessary but could not be performed.

E.2.4 Global budgets

Table 45 Input and output budgets calculated from the clear felling (CF) until age two year (AP_{24}) for N, P, K, Mg and Ca, and partially for Al and S in treatments 1, 3 and 5. Total inflow entering the system (by fertilization and bulk deposits) and total outflow leaving the system by drainage at a depth of 3 m are given, together with changes in stocks measured after clear felling and at age two years. The stem is the biomass fraction which may be exported at clear felling. Abbreviations are detailed in Table 43.

				N	P	K	Mg	Ca	Al	S
				kg ha^{-1}						
Treatment 1	**Fluxes**	Inflow	Fertilizer	0	35	107	224	398	12	2
			Dry & wet deposits	12	0	7	3	9	0	5
			Total Inflow	12	36	113	226	407	12	7
		Outflow	TL at a depth of 3m	6	0	2	2	5	4	0
		Inflow-Outflow (ΣF)		**6**	**36**	**112**	**224**	**401**	**8**	**7**
	Changes in stocks	Adsorbed on soil constituents		1	23	51	46	66	-509	-10
		Forest floor and harvest residues		-175	-7	-20	-7	-48		
		Aboveground and belowground biomass		116	9	77	24	62		
			stem	*30*	*3*	*23*	*9*	*3*		
		$Stock_{CF}$-$Stock_{AP24}$ total ($\Delta S_{measured}$)		**-59**	**24**	**107**	**63**	**80**		
		$\Delta S_{Ferti}+\Delta S_{SoilM}+\Delta S_{SoilW}+\Delta S_{SoilMB}$ ($\Sigma F-\Delta S_{measured}$)		**65**	**12**	**5**	**161**	**321**		
Treatment 3	**Fluxes**	Inflow	Fertilizer	121	36	107	224	399	12	141
			Dry & wet deposits	12	0	7	3	9	0	5
			Total Inflow	133	36	114	227	407	12	145
		Outflow	TL at a depth of 3m	4	0	1	1	3	0	0
		Inflow-Outflow (ΣF)		**129**	**36**	**113**	**226**	**404**	**12**	**145**
	Changes in stocks	Adsorbed on soil constituents		11	28	105	64	64	-156	121
		Forest floor and harvest residues		-156	-7	-20	-6	-47		
		Aboveground and belowground biomass		154	10	88	30	78		
			stem	*46*	*3*	*31*	*10*	*4*		
		$Stock_{CF}$-$Stock_{AP24}$ total ($\Delta S_{measured}$)		**9**	**30**	**172**	**89**	**94**		
		$\Delta S_{Ferti}+\Delta S_{SoilM}+\Delta S_{SoilW}+\Delta S_{SoilMB}$ ($\Sigma F-\Delta S_{measured}$)		**120**	**6**	**-59**	**137**	**310**		
Treatment 5	**Fluxes**	Inflow	Fertilizer	360	138	107	36	191	171	77
			Dry & wet deposits	12	0	7	3	9	0	5
			Total Inflow	373	138	114	39	200	171	82
		Outflow	TL at a depth of 3m	9	0	2	1	7	1	0
		Inflow-Outflow (ΣF)		**364**	**138**	**100**	**38**	**193**	**170**	**82**
	Changes in stocks	Adsorbed on soil constituents		28	24	-27	3	58	-213	34
		Forest floor and harvest residues		-174	-7	-21	-13	-54		
		Aboveground and belowground biomass		148	13	82	13	71		
			stem	*43*	*5*	*31*	*10*	*2*		
		$Stock_{CF}$-$Stock_{AP24}$ total ($\Delta S_{measured}$)		**1**	**30**	**34**	**3**	**75**		
		$\Delta S_{Ferti}+\Delta S_{SoilM}+\Delta S_{SoilW}+\Delta S_{SoilMB}$ ($\Sigma F-\Delta S_{measured}$)		**363**	**108**	**66**	**35**	**118**		

The difference between input and output fluxes gives the amounts of nutrients which were stocked or released in/from the ecosystem. We already said that almost no nutrient left the system by deep drainage so that the general feature here was that the whole input (major part made of fertilizers) was stocked within the system. The study of changes in stocks will help understanding which ecosystem compartments experienced mass changes and may thus hold these inputs. Table 45 gives the global budget of the system.

E.2.4.1 Nitrogen

In T1, the nitrogen input was very low. Over the first two years of growth of the *Eucalyptus* stand, the forest floor lost part of its mass whereas the tree biomass stocked nutrients (Table 45). The pool of adsorbed N did not experience large mass changes. For the budget to be balanced, 65 kg ha^{-1} must have been stocked within the soil organic matter and/or soil microbial biomass. This amount of N equals (i) the amount of nitrates which were leached in soil solutions down to a depth of 1 m, and (ii) the absolute difference between the mass loss of the forest floor and the mass increase of the vegetation. If we suppose that all the mass increase of the vegetation came from the mass loss of the forest floor, then 65 kg ha^{-1} of the mass loss of the forest floor must have been transferred to other stocking compartments, and we may suppose that this mass was leached in soil solutions and accumulated in deep soil layers. Of course this hypothesis is not accurate since part of the mass gain of the vegetation may have come from the mobilization of the soil organic matter and microbial biomass. Only mass changes over the whole experimental period are studied here but absolute N cumulative fluxes among the system compartments may have been far greater.

In T3 and T5, large inputs of nitrogen came from the fertilizer applications and we may wonder in which compartments this nitrogen was stocked. If we suppose that the mass balances observed in T1 equally occurred in T3 and T5, then the mass of fertilizer entering the system must be split, in T3 and T5 respectively, in: (i) 38 and 32 kg N ha^{-1} allocated to a mass increase in the tree biomass, (ii) 19 and 1 kg N ha^{-1} allocated to a mass increase in the forest floor, (iii) 10 and 27 kg N ha^{-1} allocated to a mass increase in the pool of adsorbed species and (iv) 55 and 298 kg N ha^{-1} allocated to a mass increase in the soil organic matter and microbial biomass and/or to the pool of fertilizers still unmineralized in T5. The mass increase of the pool of adsorbed N is of the same order of magnitude as the amounts of nitrates attributed to fertilizer leaching in § E.2.1 (about 25-35 kg ha^{-1}).

Soil organic matter and microbial biomass pools seem to be essential in the N budget of the ecosystem and their mass changes would be needed to check the validity of the present budget. Fluxes of N leaving the studied system may also have been underestimated since dissolved organic nitrogen (DON) was not quantified in the soil solutions collected on-field. DON is considered the most active and mobile SOM pool (Zech et al., 1997) and may contribute largely to total N leaching (Lehmann et al., 2004; Qualls et al., 2000; Vestgarden et al., 2001). N-containing organic molecules of light molecular weight (amines I, II and III) were observed while analyzing cations by ion chromatography in the soil solutions of the experiment. Tentative were made to quantify the DON fraction of these solutions but they failed due to experimental problems. Total dissolved organic carbon (DOC) fluxes over the studied period were about 50 kg ha^{-1} at the depths of 50 and 100 cm, and of about 30 kg ha^{-1} at a depth of 3 m. If we assume that the C/N of the dissolved organic matter was about the same as the vegetation present aboveground (about 20 for *Eucalyptus* according to the results of part B), then DON fluxes would be < 3 kg ha^{-1} below a depth of 50 cm and may not influence much the N budget. If the C/N of the soil solutions were lower then DON may represent a significant part of the N budget.

Under the hypothesis that (i) SOM was not mobilized in T1, and (ii) that the mass transfer which occurred in T1 equally occurred in T3 and T5, the nitrogen issued from the fertilizers served to increase the N stocks of more or less all compartments of the studied system (tree, soil and solution). The use of N fertilizers would thus serve to maintain high levels of all types of N sources, thus furnishing N supply for (i) microbial and fungal biomasses (mineralization of soil organic matter and forest floor), (ii) soil organic matter, and (iii) tree uptake. In this way, Zeller *et al.* (2000) measured by ^{15}N labelling that the soluble N (DON) was the main source for soil microbial biomass, whereas the N accumulated in tree storage compounds was the main source of nitrogen in leaves, and soil organic nitrogen (SON) the main source of mycorrhizal N. Even if this study was conducted for European beech, the rough budget established here would tend to confirm that the system is more efficient (at least regarding tree growth) when high levels of all N pools in the ecosystem are maintained, which may be completed by fertilizer applications.

The analysis of N fluxes in soil solutions showed that a nitrogen transfer of about 100 kg ha^{-1} occurred from the forest floor down to a depth of 1 m. This pattern suggests that the mass transfers observed among the system compartments certainly not occurred homogeneously within the 3 m of the soil profile. For example, the pool of adsorbed N and

the soil organic matter are likely to have gained part of their mass deeper than 1 m. The validity of the hypothesis that SOM was not mobilized in T1 is also highly dependant of the distribution of mass losses and gains all along the soil profile: SOM mobilization may have occurred in upper soil layers but may have been compensated by mass increases in deeper soil layers. ^{15}N labelling studies would be needed to rule on (i) the origin of the mass transfers observed, (ii) the reorganization of the N pools along the soil profile, (iii) the fate of the nitrate leached, and (iv) the nature of N sources for tree uptake and the real N requirements in fertilizers of the stand.

E.2.4.2 P, K, Ca and Mg

Regarding phosphorus, 24 and 30 kg ha^{-1} out of the 36 kg P ha^{-1} which entered the system were recovered in the measured stock changes (tree biomass, forest floor, and P adsorbed pool) in T1 and T3 respectively. In all treatments, the pool of adsorbed P increased of about 25 kg ha^{-1}. This pool was greatest in T3, which confirms an enhanced availability of phosphate in T3 when competing anions such as sulphates are present. In T5, 108 kg P ha^{-1} were attributed either to changes in the organic P pools or in the mineral phases (or strongly adsorbed P which was not experimentally extracted), or to a pool of P still unmineralized in the sewage sludge.

Almost all the K which entered the system was recovered in the measured stock changes. The pool of adsorbed K increased between 50 to 100 kg ha^{-1} in T1 and T3 but decreased in T5. This result was rather surprising since almost all the K from the fertilizers was leached at a depth of 15 cm and an increase in the pool of adsorbed K may thus have been expected below this depth.

The pool of adsorbed Ca and Mg also increased during the first 2 years of growth (50-60 kg ha^{-1} except for Mg in T5). Still, about two thirds of the Ca and Mg which entered the system were not recovered in the measured stock changes. The dolomitic limestone may not have completely dissolved and the mineral sludge mineralized. Ca and Mg may also participate in precipitation or adsorption of S and P chemical species.

In all treatments, if we assume that, at the very most, all the mass of nutrients lost by the forest floor was transferred to the tree biomass, then about ¼ (P and Ca) and ¾ (K and Mg – except in T5) of the tree biomass increases would still have to be explained by mass transfers among the other system compartments (OM, pools of adsorbed nutrients) or from

the influx (fertilizer). This pattern highlights the role of the fertilizers K, Ca, Mg and P in the tree nutrient supply. Of course all the mass loss of the forest floor was not necessarily transferred to the tree biomass increase. Even if a strong re-cycling occurs in the upper soil layers, *Eucalyptus* requirements may punctually be higher than the nutrient supply. Fertilizers are then useful buffers to maintain high nutrient concentrations in soil solution, higher saturations in basic cations on the soil surface and better conditions for the microbial biomass activity.

E.2.4.3 S and Al

Only part of the budgets was performed for S and Al.

More than 100 kg ha^{-1} of Al was desorbed from the soil surface (> 500 kg ha^{-1} in T1), of which only 25 to 75 kg ha^{-1} were leached in soil solution. This suggests that the major part of the aluminium desorbed was quickly re-adsorbed or precipitated in deeper soil layers. In treatment 1, the greater amount of Al desorbed from the soil surface may suggest that the soil buffering capacity mainly occurs in T1 through Al desorption whereas in T3 and T5 other processes such as the release and adsorption of specifically adsorbed anions (SO_4 and H_2PO_4) may contribute to H buffering. However, the differences among treatments were not significant in the KCl extracts and the large amounts of Al present in the mineral phases of these soils may contribute to systematic large values of Al in soil solutions and in soil extracts.

The sulphate extracted from the soil surface confirmed that almost all the S from the fertilizers was dissolved (or mineralized), leached and adsorbed in the upper 1 m of the soil profile, without being taken up by the *Eucalyptus* trees. Still, we already mentioned that the amounts of S extracted may have been underestimated and successive soil extractions would be needed to check the accurary of the calculated budget. Moreover, organic S and mineral phases may also participate largely to S cycling (Edwards, 1998).

E.3 CONCLUSIONS

E.3.1 On the use of fertilizers

As part of the system budget, fertilizers held different roles:

- once dissolved in soil solution, S was mainly retained on the soil surface. It participated in pH buffering and enhanced P, Ca and Mg solubilities and availabilities,
- K, Ca, Mg, and P are likely to have participated in tree nutrition. They may also have contributed to maintain a pool of adsorbed nutrients on the soil surface and favourable conditions for microbial populations, and may have participated in pH buffering,
- under the hypotheses that (i) SOM was not mobilized in T1, (ii) mass transfer occurred in the same way in T1 as in T3 and T5, N fertilizations may have participated in tree nutrition and in maintaining high levels of N in all compartments of the studied system (pool of adsorbed nitrate, forest floor, SOM, SON and microbial biomass).

Smethurst (2000) reviewed that the *Eucalyptus* trees responded to fertilizers when the concentrations of N in soil solutions were < 50 μmol N L^{-1}, and when the available P extracted by the Mehlich protocol was < 0.5 mg P/100g. Fertilizer applications helped maintaining concentrations in soil solution above these thresholds throughout the early growth of the stand. The response to the N fertilizers observed during the first year of growth may thus result from positive effects of (i) the NH_4 brought by the fertilizers compared to the NO_3 available in soils, (ii) the fertilizer concentration at the stem basis of the tree which leaded to high nutrient concentrations in soil solution, next to the root tips.

Nitrate leaching is likely to have been enhanced by the fertilizer applications by about 35 kg N ha^{-1}. This nitrate leaching may suggest that about one (38 kg ha^{-1}) out of the four mineral fertilizations in ammonium sulfate may have been in excess during the first year of growth, when most of the nitrate leaching occurred. Still, this amount of nitrogen in excess should be reduced in case the *Eucalyptus* stand took up part of the nitrates leached in deeper soil layers. On the other hand, the vegetation monitoring showed that the trees responsed to N fertilizers during the first year of growth but that the biomasses were of the

same order of magnitude in all treatments during the second year of growth. This pattern may suggest that the last two N-fertilizer applications were unnecessary in T3 during the second year of growth (2*38 kg ha^{-1}). The system N budget also indicated a mass increase in the vegetation biomass larger of about 38 kg N ha^{-1} in T3 and T5 than in T1 over the first two years of growth. This pattern may suggest that up to three mineral fertilizer applications may have been in excess in T3 compared to T1 (3*38 kg ha^{-1}). However, it is difficult to rule on the amount of N fertilization which may have been brought in excess since: (i) nitrogen may be needed in other compartments of the ecosystem to maintain high tree uptake, in particular in the soil organic matter and microbial pools, (ii) changes in stocks do not represent total tree requirements (fluxes) over the whole period, (iii) the synchronism between tree requirements, lack of available N, and N supply by the fertilizers is important but was not assessed here. In conclusion, it may be suggested that 38-76 kg ha^{-1} are likely to have been in excess in the studied system. The synthesis of the different studies conducted in the experiment will help ruling on this point.

E.3.2 On the sustainability of the plantation regarding soils and waters

Leaching of nutrients is important regarding the sustainability of the studied system because nutrients may be lost from the ecosystem by deep drainage, and may eventually lead to groundwater pollution (by nitrates for example). Upper soil layers may also be impoverished by nutrient leaching and their transfer to deep soil layers. The first period of nutrient leaching occurred just after planting and fertilizing (parts C and D): 159 mm (46 % of the incoming rainfall) of water was drained at a depth of 3 m, but the nutrient front stopped at a depth of 50 cm at the beginning of the dry winter 4 months after planting. During the following six months, 383 mm (41% of the incoming rainfall) of water was drained at a depth of 3 m mainly during the 11th month after planting (N_{month}=21). This drainage period corresponded to the most intense nutrient leaching period, but this nutrient leaching stopped at a depth of 1m. During the second year of growth, the high transpiration of the fast growing *Eucalyptus* trees reduced greatly water drainage and nutrient leaching at a depth of 3 m: 53 and 185 mm (10 and 21% of the incoming rainfall) were drained at a depth of 3 m during the 12-18 and 18-24 months of growth, respectively. Drainage occurred at this depth during the wet season at a small constant rate (1 mm day^{-1}) or after

large rainfall events (N_{month}=36), and upward flow (about 1 mm day^{-1}) occurred during the dry periods.

It is thus difficult to assess whether the mineral elements leached in soil solution at a depth of 1 m did not leave the soil profile because they had been taken up, adsorbed or immobilized in the soil organic matter and microbial biomass, or because there was no water enough to transport them. If this was the case, then a risk would exist that they should leave the soil profile as the *Eucalyptus* uptake decreases and more intense drainage is restablished. It was shown that part of the nitrate leached at a depth of 1 m was effectively present between the depths of 1 to 3 m and was weekly adsorbed on the soil surfaces but about 65 kg ha^{-1} of the nitrate leached may have been uptaken or immobilized in the soil organic matter or microbial biomass (if KCl extractions did not underestimate the pool of adsorbed N). However, even if these nitrates were still present between the depths of 1 to 3 m, the large volume of soil available down to a depth of 10 m together with the increasing anion exchange capacity below a depth of 1 m, suggest that they are not a great threat to groundwater quality.

Among the other nutrients which were leached in soil solutions, S was adsorbed weakly (1/3) and more specifically (2/3) between the depths of 5 to 100 cm, and P was specifically adsorbed in the upper soil layers (0-50 cm). Ca and Mg were adsorbed on the CEC in the upper soil layers (0-15 cm). We may thus conclude that S, P, Ca and Mg are not likely to leave the studied soil profile even if quantitative water drainage at a depth of 3 m is re-established.

Nutrient leaching may be problematic mainly during the first two years of growth when (i) stand requirements are high and losses of nutrients by drainage may decrease the nutrients amounts available for the trees, (ii) large amounts of nutrients are present in soils under a soluble form and may be leached in deeper soil layers and subsequently threaten water quality. Other studies showed that, after this period of early growth, the nutrient concentrations in soil solution return to low levels (Laclau et al., 2003b). During this period of early growth, it thus seems that nutrient leaching results from an equilibrium (or disequilibrium) between (i) the quantity of water drained and the succession of periods of high and low drainage, (ii) the amounts of nutrients concentrated in soils in a soluble form, (iii) the capacity of the soil to retain these nutrients by adsorption or immobilization in soil organic matter and microbial biomass, and (iv) the tree uptake. Nutrient leaching is highly dependant on the kinetics of each process, but fluxes of nutrients in soil solution are likely

to be largest when large quantities of nutrients are present in soils under a soluble form during periods of large water drainage. In our soil type, the water and nutrient fluxes were greatly homogeneized below a depth of 1 m as the clay content increased (part C) which contributed to slow down the nutrient front below a depth of 1 m. The nutrient leaching following the clear felling and the fertilizer applications would have reached deeper soil layers in less homogeneous soils.

We already mentionned that large amounts of sulfate from the ammonium sulfate fertilizers had been stocked on the soil surface in a more or less strongly adsorbed way down to a depth of 1 m and that the adsorption capacity of sulphate was probably saturated above this depth. Further fertilizations with ammonium sulphate may thus participate in deeper leaching of Ca and Mg, unless this S is reorganized or transformed before the next *Eucalyptus* rotation (for example within the mineral phase or immobilized in the soil organic matter). This pool of adsorbed sulphate may be slowly desorbed as the concentrations in soil solutions decrease, and a joint release of protons may then be expected which may participate to soil acidification. Such pattern was already observed in Europe during ecosystem recovery once enhanced sulphate depositions had stopped (Folster et al., 2003).

After clear felling and planting, the large amounts of nitrates leached in soil solutions down to a depth of 1 m were accompanied by Al and proton leaching from the upper soil layers down to deep soil layers. Such pattern of enhanced acidification was already observed in Brazil under *Pinus* compared to cerrado (Lilienfein et al., 2000) and in Australia under *Eucalyptus* compared to pastures (Prosser et al., 1993). In Hawaii, a decline in soil pH from 5.9 to 5 was observed under *Eucalyptus* plantations in 8 years (Rhoades and Binkley, 1996). However, high concentrations of aluminium in soil solutions may not influence *Eucalyptus* growth since *Eucalytpus* are not greatly sensitive to Al toxicity (IPEF, 2004). High reserves of aluminium in these oxidic soils may suggest that the pH-buffering by Al release may still exist for long, and that Al may be quickly reprecipitated in these soils.

E.3.3 On the method used

Nutrient fluxes within the vegetation were not studied here, but a more thorough synthesis of the different studies conducted in the experiment may help understanding nutrient dynamics in the *Eucalyptus* stand. In particular, nutrient budgets calculated for shorter periods are needed to understand the synchronism between stand requirements and nutrient supply. Nutrient budgets calculated for different sub-systems (in particular at intermediary depths in soils and in the forest floor), are also needed to localize the different zones where nutrients are lost or gained. However, such budgets may be difficult to establish accurately since (i) the dynamics of fertilizer dissolution and/or sewage sludge mineralization in the forest floor and in the upper soil layers are unknown, and (ii) the nutrient uptake by the *Eucalyptus* root system is difficult to split over the soil profile.

We already mentioned that soil extractions were likely to have underestimated the amounts of nutrients adsorbed on soil surface. Moreover, very low concentrations in the soil extracts make the results highly dependant on the experimental conditions during the extractions (water quality, ambient conditions, etc…) and on the analytical equipment used to measure these concentrations. Successive extractions measured independently would be needed to (i) measure accurately the first extract (most concentrated), (ii) check that the whole pool of adsorbed nutrients was extracted.

Nutrient budgets showed that the organic part of the system was essential to explain N dynamics within the ecosystem. Organic pools may be important also for S, P and Al budgets. The pools of adsorbed nutrients were important in the system budgets for S, P and all cations. The pool of fertilizers still not dissolved or not mineralized was supposed to participate largely in nutrient budgets for Ca and Mg in T1 and T3, and for all nutrients in T5. Sulphur, P and Al may also have interacted with more or less crystallized soil fractions but this hypothesis needs further investigation. Regarding reactive transport modeling, it thus seems important to further investigate (i) the interactions between the soil solution and the soil organic pools, (ii) the adsorption and desorption processes, and (iii) the dynamics of fertilizer dissolution and sewage sludge mineralization. If using MIN3P, the adsorption module is already coded for cations but needs to be implemented for anions. The nutrients release by mineral fertilizer dissolution may be simulated from theoretical constants, but the case of sewage sludge mineralization needs to be investigated.

GENERAL CONCLUSIONS AND PERSPECTIVES

Over the studied period, the soil solution chemistry (part D) experienced changes under the influence of the silviculture (clear felling and fertilizing): (i) large contents of mineral elements were released in the upper soil layers and leached down to the depth of 1 m, in particular NO_3 and Al following clear felling and fertilizing, but never appeared at a depth of 3 m, (ii) part of the fertilizers (in particular K, Ca, Mg and P) was dissolved or mineralized and taken up by the fast growing *Eucalyptus* trees without appearing in soil solution, (iii) S present in the nitrogen fertilizers increased Ca, Mg and P mobilities, and decreased the H and Al release in soil solution.

Water drainage is essential in the computation of mineral element fluxes. Part C showed that (i) even if the water flux is probably overestimated at the depths of 15, 50 and 100 cm, the water flux at a depth of 3 m is likely to be accurate since it was fixed as the lower boundary of the studied profile (provided the fact that the hypothesis of a single porosity is accurate), (ii) a large uptake of water by the *Eucalyptus* trees occurred as soon as six months after planting; it reduced largely the water drainage at a depth of 3 m and resulted in periods of upward flow from one year after planting until the end of the experimental period, (iii) the water flux was slowed down and homogeneized below a depth of 1m.

The soil study of part B showed that the soil mineral constituents could mainly release Fe, Al, Si and H in the soil solution. The potential for adsorption of cations on the soil surface was < 1 cmolc kg^{-1} but was highly pH-dependant. The CEC was mainly saturated with Al so that basic cations may be adsorbed on the CEC provided the fact that either the CEC increases or Al is released in soil solution. The anion exchange capacity may adsorb anions in particular below a depth of 1 m. Specific adsorptions may result in large retention of S and P in soils down to a depth of 3 m. This was in good agreement with the observations of the soil solution chemistry. Analysis of the soil surface at the end of the experimental period showed: (i) an increase in Mg on the CEC in the upper soil layers (0-15 cm) in particular in T3, (ii) a trend to Al desorption from the CEC in the upper soil layers, (iii) adsorption of sulphate in T3 and T5 down to a depth of 50-100 cm, the soil adsorption capacity seems to be saturated down to a depth of 50-100 cm and signs of leaching down to deeper soil layers were observed, however the major part of the

fertilizers seems to have been already dissolved and leached, (iv) adsorption of phosphate in the upper soil layers (0-15 cm) with increased P availability in T3, and (v) weak adsorption of nitrates between the depths of 1 to 3 m. A great part of the adsorbed NO_3 and S were extractable by water and may be remobilized in soil solution as large drainage periods should occur.

Nutrient budgets together with the conclusions from the vegetation monitoring realized independently of this thesis helped understanding the role of the vegetation in the chemical composition of the soil solution. A strong recycling of mineral elements in the forest floor and in the upper soil layers occurred. The major part of the nutrients supporting the initial growth of the stand was issued from the mineralization of the harvest residues and of the forest floor, and by the dissolution (or mineralization) of the fertilizers (sewage sludge in T5) which were taken up before being leached to deeper soil layers. About 65 kg ha^{-1} of nitrate was realeased in soil solutions from the mineralization of the soil organic matter, forest floor and harvest residues, this leaching may have been increased of about 35 kg ha^{-1} by the fertilizer applications. As differences of growth among treatments were observed during the first year after planting but as these differences disappeared during the second year of growth, it is suggested that the starter fertilization is important to maintain the global equilibrium of the soil nutritional status. Fertilizations may guaranty better conditions for microbial activity, better nutrient availability and may constitute a buffer pool of available nutrients when the requirements of the *Eucalyptus* stand exceed the releases by mineralization. It thus seems that the N fertilizations made after one year of growth may be reduced without altering the stand productivity, but the study of the organic part of the system is needed to check that this will not be to the detriment of the SON storage.

In terms of ecosystem sustainability, it is shown that (i) the high water uptake of the fast growing *Eucalyptus* trees reduced the water drainage at a depth of 3 m during the second year of growth, (ii) almost no nutrient left the studied system at a depth of 3 m by leaching in deep soil layers. Even if the nitrates leached down to a depth of 1 m (65-100 kg ha^{-1}) were to be leached below a depth of 3 m, they may not threaten ground water quality since a large volume of soil is available down a depth of 15 m, anion exchange capacity increases below a depth of 1m and tree roots constitute a safety net in deep soil layers (fine roots were found down to a depth of 10 m in T3 after 3.5 years of growth), (iii) large amounts of S were adsorbed on the soil surface in the treatments where sewage sludge or

ammonium sulphate were applied. This adsorption buffered the acidification in soil surface, but if this sulphate happens to be desorbed, greater soil acidification is to be expected, (iv) acidification occurred in the upper soil layers after clear felling: Al and H were displaced together with nitrates down to deeper soil layers. However, in these ferralsols containing large amounts of oxides and kaolinite, the soil Al reserve and buffering capacity are still large, and (v) the sewage sludge seemed to be efficient as a fertilizer but it enhanced the acidification process since its mineralization leaded to a nitrate production higher than tree requirements. Adverse effects of heavy metal toxicity on trees and on microbial communities were not studied in this thesis.

In terms of scientific perspectives, it seems that the study of the spatial heterogeneity at the tree scale is of great importance in the accurate calculation of nutrients and water fluxes. This heterogeneity may come from heterogeneous patterns in soil solution entering the soil profile by stemflow or throughfall, as well as from differences in infiltration due to the microtopography, the spatial heterogeneity of the soil hydraulic properties and the soil surface wettability, or from spatial heterogeneity of fine root densities. These patterns are especially important when the soil is dry (soil moisture < 16 %). The hypothesis of a second type of porosity was not excluded, in particular at the outlet of the soil profile (depth of 3m) where the measured water contents did not allow an accurate determination of the water retention curve at low pressure heads. This should be checked since water may have left the soil profile by drainage or by diffusion at lower pressure heads. Regarding the overall functioning of the ecosystem, a large part of the dynamics of the ecosystem could only be hypothesized since it was impossible to differentiate nutrient fluxes from the fertilizers and nutrient fluxes from the organic matter mineralization. Isotopic labeling such as ^{15}N coupled to reactive transport geochemical modelling may be powerful tools to go further in the understanding of nutrient fluxes in tropical soils. Regarding reactive transport modeling, it seems important to further investigate (i) the interactions between soil solutions and the soil organic pool in particular for N, S, P and Al, (ii) adsorption processes and desorption processes (if using MIN3P, the model needs implementing for the anionic part) (iii) the dynamics of fertilizer dissolution and sewage sludge mineralization, (iv) the interactions with the more or less cristallized phases for S, P and Al.

Long-term monitoring of the ecosystem is needed to assess changes in nutrient dynamics throughout the stand rotation.

ANNEXES

ANNEX 1 TOTAL ANALYSIS OF THE FERTILIZERS APPLIED

Table A-1 Total analysis of the sewage sludge applied in the experiment (ND = Not Detected).

	1st application	**2nd application**
pH (5% in water)	8.79	8.57
Water content (mass %)	80.5	81.6
Content (110°C dry basis) (mg kg^{-1})		
Al	12535	21624
As	ND	< 0.5
B	10	16
Organic C	302227	302600
Ca	16376	21804
Cd	11	7
Cu	621	1476
Cr	497	1009
Fe	17289	27840
Hg	ND	ND
K	1193	913
Mg	3294	3982
Mn	119	369
N/NH_4	3980	504
N/NO_2	136	4
N total	35195	36900
Na	602	1108
Ni	175	389
P	13700	13900
Pb	68	220
S	8929	6500
Zn	1895	3626

Table A-2 Total analyses of the mineral fertilizers (na= not analyzed)

A) analyzed in the CIRAD laboratory

	Trace elements	Borogran	$(NH_4)_2SO_4$	KCl
		g/100g		
Fe	22.53	2.28	0.03	0.00
Cu	1.004	0.04	0.00	
Zn	12.83	0.48	0.00	0.00
Mn	3.59	1.46	0.00	0.00
B	1.77	na	na	na
B_2O_3	na	33.07	na	na
Ca	3.84	14.12	0.12	0.08
Mg	2.38	1.32	0.06	0.03
K	1.35	0.55	0.10	na
K_2O	na	na	na	62.04
Na	0.93	0.78	0.01	1.03
Al	1.68	1.09	0.01	0.01
S	1.72	2.98	na	0.07
SO_3	na	na	60.50	na
P	0.19	0.04	0.03	0.04
Pb	1.32	0	na	na
Cr	0.11	na	na	na
Mo	0.08	na	na	na
Ni	0.02	na	na	na
As	na	0.03	na	na
Sr	na	1.05	na	na
N total	na	na	21.11	na
Cl	na	na	na	47.64
Total	*55*	*59*	*82*	*111*

B) analyzed at the CRPG (Nancy)

	Dolomitic Limestone	Triple Superphosphate
	g/100g	
SiO_2	11.92	0.74
Al_2O_3	1.01	0.30
Fe_2O_3	0.54	2.18
MnO	0.13	0.07
MgO	18.33	0.73
CaO	25.61	19.85
Na_2O	0.15	0.13
K_2O	0.16	0.10
TiO_2	0.05	0.62
P_2O_5	0.06	47.60
Loss on ignition (110°C-1000°C)	40.81	27.66
Total	*98.74*	*99.97*

ANNEX 2 COMPLEMENTS TO STAND GROWTH DATA AND DECOMPOSITION RATES OVER THE EXPERIMENTAL PERIOD

Table A-3 Time course of the nutrient accumulation in aboveground biomass at the end of the rotation of the *E. saligna* stand.

		Average	St Dev	Jan-2003	Dec-2003	Annual increment
		kg tree^{-1}			*kg ha^{-1}*	
Dry matter	Wood	15.81	12.90	24302	35566	12288
	Bark	2.25	2.47	3459	5297	2005
	Leaves	1.54	1.63	2365	3331	1053
	Coarse branches	2.60	1.10	4003	4010	8
	Twigs	0.73	0.95	1122	1685	615
	Dead branches	0.36	0.00	548	548	0
	Total (aboveground)	***23.29***	***18.55***	***35800***	***50438***	***15969***
N content	Wood	0.0150	0.0144	23	33	11
	Bark	0.0059	0.0093	9	16	8
	Leaves	0.0235	0.0270	36	52	17
	Coarse branches	0.0070	0.0034	11	11	1
	Twigs	0.0023	0.0032	4	5	2
	Dead branches	0.0007	0.0000	1	1	0
	Total (aboveground)	***0.0543***	***0.0557***	***84***	***119***	***39***
P content	Wood	0.0053	0.0051	8	12	4
	Bark	0.0009	0.0010	1	2	1
	Leaves	0.0011	0.0012	2	2	1
	Coarse branches	0.0004	0.0002	1	1	0
	Twigs	0.0002	0.0002	0	0	0
	Dead branches	0.0001	0.0000	0	0	0
	Total (aboveground)	***0.0080***	***0.0077***	***12***	***18***	***6***
K content	Wood	0.0040	0.0098	6	13	8
	Bark	0.0052	0.0032	8	11	3
	Leaves	0.0042	0.0042	7	9	3
	Coarse branches	0.0010	0.0006	2	2	0
	Twigs	0.0004	0.0006	1	1	0
	Dead branches	0.0001	0.0000	0	0	0
	Total (aboveground)	***0.0150***	***0.0182***	***23***	***37***	***15***
Ca content	Wood	0.0049	0.0043	8	11	4
	Bark	0.0067	0.0100	10	16	6
	Leaves	0.0052	0.0108	8	12	4
	Coarse branches	0.0034	0.0012	5	6	1
	Twigs	0.0012	0.0014	2	3	1
	Dead branches	0.0003	0.0000	1	1	0
	Total (aboveground)	***0.0217***	***0.0275***	***33***	***48***	***16***
Mg content	Wood	0.0016	0.0013	2	4	1
	Bark	0.0020	0.0028	3	5	2
	Leaves	0.0024	0.0027	4	5	2
	Coarse branches	0.0010	0.0006	2	2	0
	Twigs	0.0003	0.0004	1	1	0
	Dead branches	0.0001	0.0000	0	0	0
	Total (aboveground)	***0.0075***	***0.0077***	***11***	***16***	***5***

Table A-4 Biomass and nutrients accumulation in *E. grandis* trees in T1, T3 and T5 from age 6 months to age 2 years.

		T1					T3					T5				
		N	**P**	**K**	**Ca**	**Mg**	**N**	**P**	**K**	**Ca**	**Mg**	**N**	**P**	**K**	**Ca**	**Mg**
		kg ha^{-1}														
Age 6 months	Leaves	5.2	0.3	0.9	1.0	0.5	10.8	0.5	2.7	2.0	0.9	6.0	0.3	2.6	1.3	0.5
	Branches + stem	1.7	0.1	0.9	0.8	0.2	1.7	0.1	1.5	1.6	0.4	1.1	0.1	0.7	0.7	0.2
	Stump + coarse roots	0.2	0.0	0.2	0.1	0.0	0.4	0.0	0.3	0.2	0.1	0.1	0.0	0.1	0.1	0.0
	Medium-size roots	0.1	0.0	0.1	0.1	0.0	0.2	0.0	0.2	0.1	0.1	0.1	0.0	0.1	0.1	0.0
	Total (aboveground)	**6.9**	**0.4**	**1.8**	**1.8**	**0.7**	**12.5**	**0.6**	**4.2**	**3.6**	**1.3**	**7.1**	**0.4**	**3.3**	**2.0**	**0.7**
Age 12 months	Wood	2.8	0.3	2.8	0.8	0.3	5.1	0.6	3.5	1.2	0.5	4.2	0.5	2.8	1.0	0.3
	Bark	0.9	0.1	1.1	2.0	0.5	2.0	0.2	1.9	2.4	0.8	2.1	0.2	1.4	1.9	0.7
	Leaves	27.8	1.2	9.3	10.0	4.0	51.0	2.1	13.6	14.3	5.5	42.0	3.9	11.7	12.3	4.8
	Branches	8.0	0.4	4.5	5.1	1.1	12.0	0.5	6.6	10.9	1.6	10.2	0.8	5.6	8.8	1.3
	Stump + Coarse roots	3.9	0.2	2.2	2.8	0.4	5.6	0.3	3.4	4.0	0.6	4.8	0.3	2.9	3.5	0.5
	Medium-size roots	5.1	0.2	3.3	2.7	1.2	2.6	0.1	1.3	1.4	0.7	3.9	0.2	1.4	1.7	0.4
	Fine roots	18.3	0.7	5.3	6.1	3.6	16.4	1.1	3.7	5.2	3.4	20.3	1.3	3.2	5.6	1.7
	Total (aboveground)	**39.5**	**2.0**	**17.7**	**17.9**	**5.9**	**70.1**	**3.4**	**25.6**	**28.8**	**8.4**	**58.5**	**5.4**	**21.5**	**24.0**	**7.1**
	Total (roots)	**27.3**	**1.1**	**10.8**	**11.6**	**5.2**	**24.6**	**1.5**	**8.4**	**10.6**	**4.7**	**29**	**1.8**	**7.5**	**10.8**	**2.6**
	Total	**66.8**	**3.1**	**28.5**	**29.5**	**11.1**	**94.7**	**4.9**	**34.0**	**39.4**	**13.1**	**87.5**	**7.2**	**29**	**34.8**	**9.7**
Age 24 months	Wood	29.6	2.5	22.7	8.8	3.5	45.8	3.0	30.5	10.4	4.1	43.5	4.8	30.8	9.9	2.3
	Bark	9.1	0.6	7.6	16.1	6.2	10.9	0.9	8.9	28.0	7.4	10.3	1.0	8.5	18.1	3.3
	Leaves	83.0	4.9	27.5	26.6	13.0	94.6	4.9	26.1	24.6	15.4	90.4	5.1	22.1	23.8	8.2
	Branches	19.7	0.8	7.9	17.4	5.3	23.1	0.9	9.1	21.3	6.2	24.4	1.5	8.7	23.2	3.3
	Stump + Coarse roots	12.9	2.1	9.8	9.3	1.9	15.2	2.5	11.6	10.9	2.2	14.5	2.4	11.0	10.4	2.1
	Medium-size roots	3.1	0.1	1.8	1.9	0.9	3.7	0.3	1.6	2.1	0.8	5.9	0.3	2.5	4.1	1.0
	Fine roots	15.6	0.5	5.8	3.8	3.5	17.4	0.7	6.2	2.4	3.8	16.0	0.7	5.1	3.8	2.7
	Total (aboveground)	**141.4**	**8.8**	**65.7**	**68.9**	**28**	**174.4**	**9.7**	**74.6**	**84.3**	**33.1**	**168.6**	**12.4**	**70.1**	**75.0**	**17.1**
	Total (roots)	**31.6**	**2.7**	**17.4**	**15**	**6.3**	**36.3**	**3.5**	**19.4**	**15.4**	**6.8**	**36.4**	**3.4**	**18.6**	**18.3**	**5.8**
Total		**173.0**	**11.5**	**83.1**	**83.9**	**34.3**	**210.7**	**13.2**	**94**	**99.7**	**39.9**	**205.0**	**15.8**	**88.7**	**93.3**	**22.9**

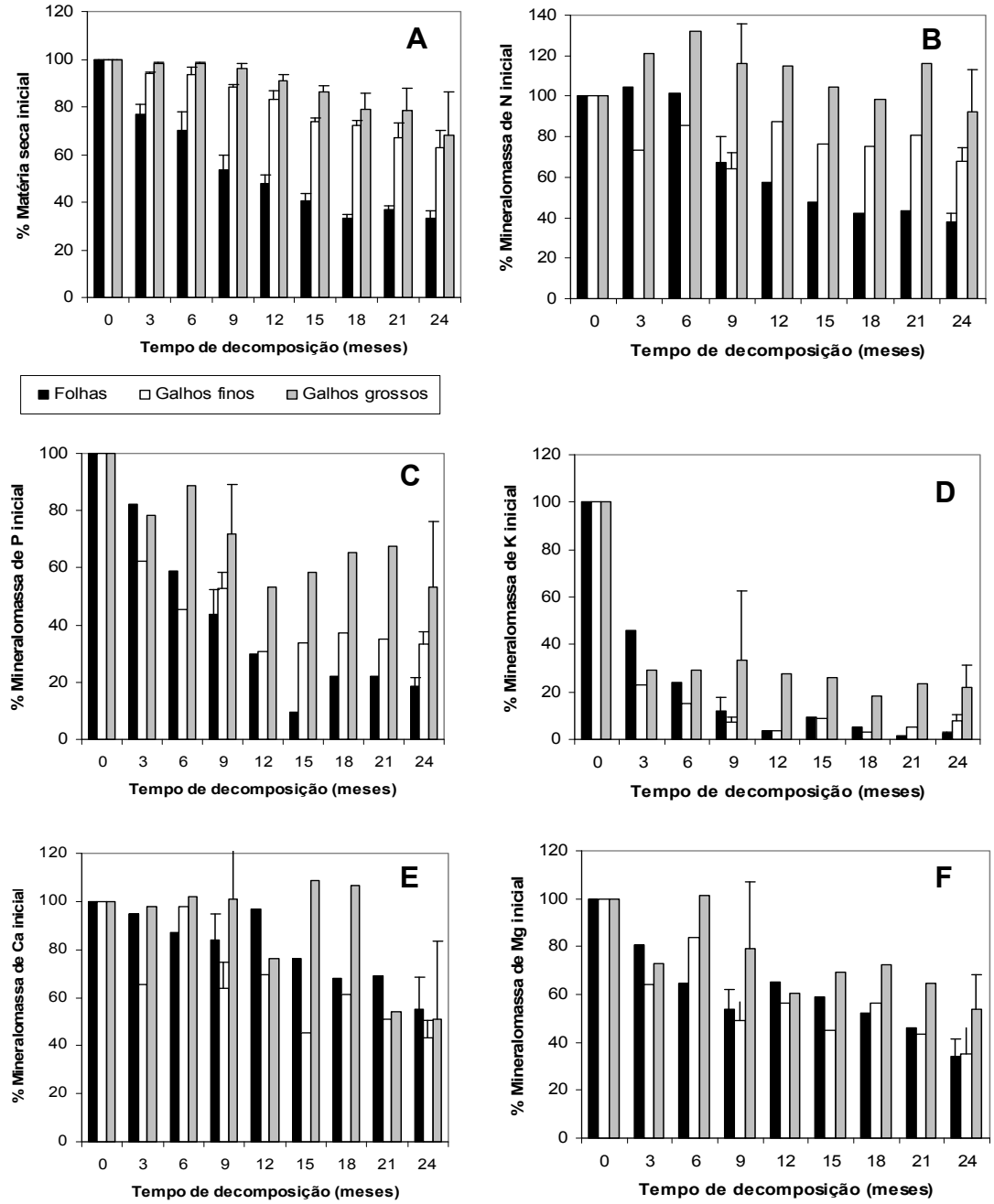

Figure A-1. Harvest residues decomposition over the first 2 years following the clear felling of the *E. saligna* stand: dry matter of harvest residues (leaves, coarse and medium-size branches) (A), N content (B), P content (C), K content (D), Ca content (E) and Mg content (F).

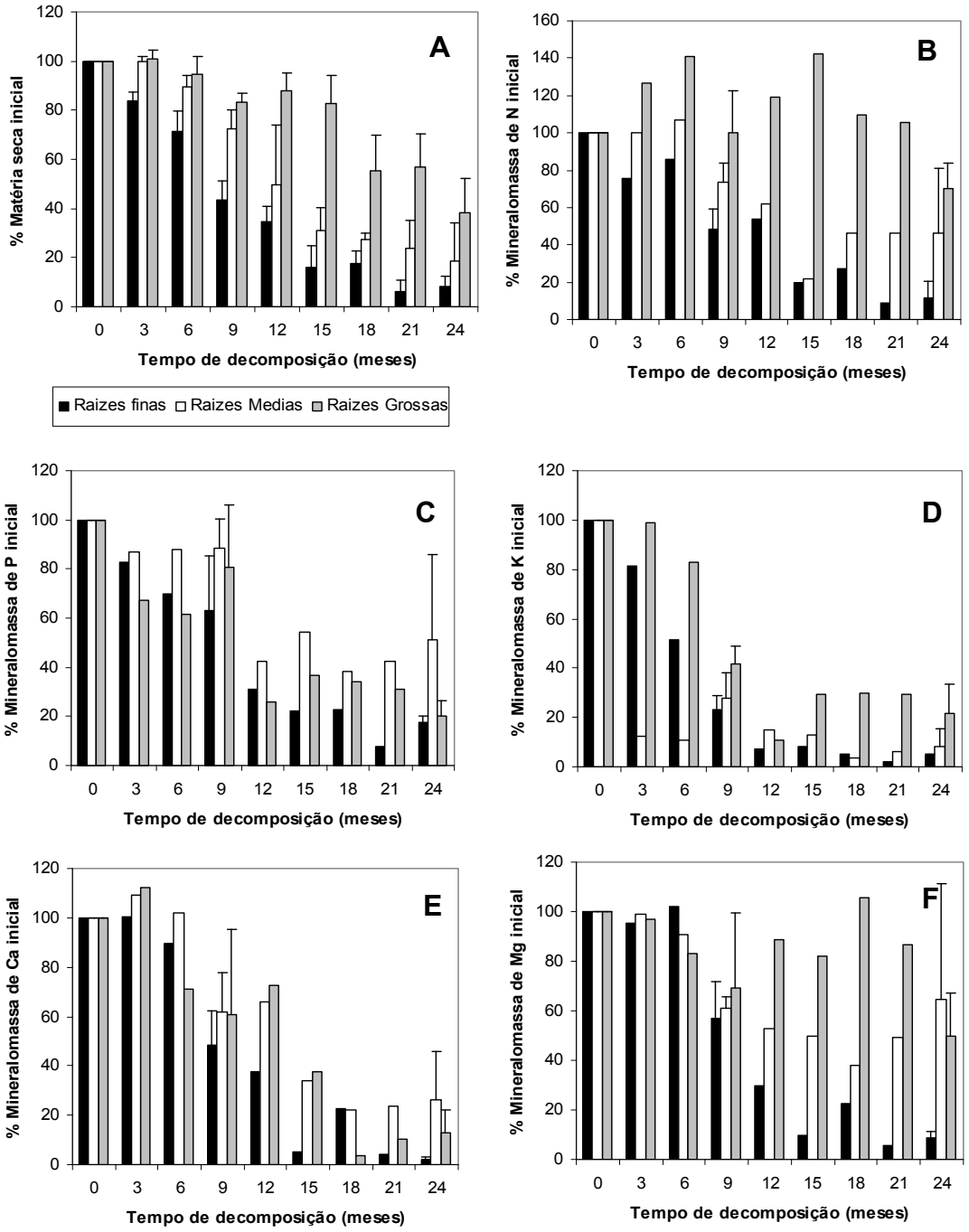

Figure A-2. Root decomposition over the first 2 years following the clear felling of the *E. saligna* stand: dry matter of residues (A), N content (B), P content (C), K content (D), Ca content (E) and Mg content (F).

ANNEX 3 DATA SETS $SOIL_{BCF}$ AND $SOIL_{AP11}$: SOIL CHEMICAL AND PHYSICAL CARACTERISTICS

Table A-5 Chemical and physical characteristics of data set $SOIL_{BCF}$

		Depth (cm)								
		0-5	5-15	15-50	50-100	100-200	200-300	300-400	400-500	500-600
pH and CEC										
pH H_2O	-	4.2	5.1	5.2	5.4	5.6	5.7	5.3	5.7	5.8
pH KCl	-	3.6	4.3	4.6	4.6	5.0	5.2	5.1	5.4	5.6
K	*cmolc/kg*	0.02 (0.001)	<0.01							
Ca		0.05 (0.006)		<0.01	<0.01	<0.01				
Mg		0.06 (0.004)	0.01 (0.001)				<0.01	<0.01	<0.01	<0.01
Na		0.02 (0.002)	<0.01							
H		0.73 (0.055)	0.22 (0.007)	0.19 (0.003)	0.16 (0.006)	0.12 (0.003)				
Al		1.95 (0.103)	0.94 (0.044)	0.69 (0.019)	0.48 (0.019)	0.27 (0.013)	0.08 (0.012)	0.03 (0.004)	0.00 (0.002)	0.01 (0.004)
CEC		2.95 (0.173)	1.20 (0.052)	0.89 (0.017)	0.65 (0.021)	0.41 (0.014)	0.09 (0.013)	0.04 (0.004)	0.02 (0.003)	0.02 (0.006)
SatCEC	%	9	2	1	1	3	18	36	79	56
n	-	36	9	9	9	9	9	9	9	9
Particle-size distribution										
Clay	%	14 (0.3)	16 (0.8)	15 (0.3)	20 (0.6)	22 (0.5)	23 (0.5)			
Silt		8 (1.1)	5 (0.4)	7 (0.5)	5 (0.5)	7 (0.5)	7 (0.4)			
Sand		78 (1.1)	79 (0.5)	78 (0.6)	74 (0.6)	71 (0.6)	70 (0.7)			
n	-	36	9	9	9	9	9			
Bulk density										
		1.12 (0.027)	1.38 (0.009)	1.38 (0.011)	1.35 (0.010)	1.37 (0.010)	1.40 (0.008)			
n	-	27	27	27	27	27	27			
Organic C and N content										
N	%	0.19 (0.016)	0.06 (0.003)	0.04 (0.005)	0.03 (0.001)	0.02 (0.005)	0.02 (0.000)	0.01 (0.005)	0.01 (0.004)	0.01 (0.003)
C		3.57 (0.318)	0.80 (0.035)	0.59 (0.012)	0.45 (0.010)	0.31 (0.010)	0.21 (0.002)	0.18 (0.020)	0.13 (0.008)	0.12 (0.012)
n	-	36	9	9	9	3	2	3	3	3

Table A-6 Chemical and physical characteristics of data set $SOIL_{AP11}$: C & N contents, pH and CEC, and particle-size distribution

		Depth (cm)											
		0-5	5-15	15-30	30-50	50-100	100-200	200-300	500	700	900	1300	1500
Organic C and N content													
N	%	0.18 (0.051)	0.06 (0.002)	0.05 (0.003)	0.04 (0.001)	0.03 (0.001)	0.02 (0.001)	0.02 (0.001)	0.01	0.02	0.01	0.01	0.00
C	%	3.15 (1.001)	0.78 (0.011)	0.67 (0.038)	0.55 (0.015)	0.47 (0.011)	0.34 (0.015)	0.22 (0.009)	0.17	0.27	0.12	0.07	0.04
n	-	4	4	4	4	4	4	4	1	1	1	1	1
pH and CEC													
pH H_2O	-	4.5	5.7	5.6	5.4	5.7	5.7	6.0	5.9	6.0	5.7	5.1	4.8
pH KCl	-	3.8	4.6	4.7	4.8	4.8	5.1	5.6	5.6	5.5	4.7	4.3	4.2
K	*cmolc kg*$^{-1}$	0.01 (0.002)	<0.01	<0.01	<0.01	<0.01	<0.01	<0.01			<0.01		
Ca	*cmolc kg*$^{-1}$	0.25 (0.108)											
Mg	*cmolc kg*$^{-1}$	0.40 (0.110)	0.06 (0.009)	0.02 (0.003)									
Na	*cmolc kg*$^{-1}$	<0.01	<0.01	<0.01									
H	*cmolc kg*$^{-1}$	0.61 (0.205)	0.21 (0.002)	0.19 (0.003)	0.14 (0.027)	0.16 (0.002)	0.14 (0.010)	0.02 (0.024)	<0.01	0.12	0.12	0.15	0.13
Al	*cmolc kg*$^{-1}$	1.53 (0.413)	0.90 (0.034)	0.75 (0.017)	0.69 (0.026)	0.53 (0.022)	0.30 (0.017)	0.08 (0.028)	0.06	0.13	0.14	1.39	0.92
CEC	*cmolc kg*$^{-1}$	2.87 (0.654)	1.19 (0.026)	0.96 (0.020)	0.84 (0.016)	0.70 (0.024)	0.44 (0.021)	0.11 (0.004)	0.06	0.26	0.26	1.55	1.06
Sat/CEC	%	28	7	3	2	1	2	2	9	1	1	1	0
n	-	4	4	4	4	4	4	4	1	1	1	1	1
Particle-size distribution													
Clay	%	17 (1.0)	18 (1.0)	19 (0.5)	19 (0.6)	23 (0.6)	25 (0.5)	26 (0.1)	26	26	24	24	16
Silt	%	7 (1.4)	4 (0.6)	3 (0.6)	4 (0.6)	4 (0.4)	5 (0.4)	4 (0.8)	6	5	8	8	6
Sand	%	76 (1.1)	79 (0.6)	78 (0.4)	77 (0.7)	73 (0.7)	70 (0.2)	69 (0.8)	68	69	67	68	78
n	-	4	4	4	4	4	4	4	1	1	1	1	1

Table A-7 Chemical and physical characteristics of data set $SOIL_{AP11}$: Al an Fe extractions and total analysis

		Depth (cm)										
		0-5	5-15	15-30	30-50	50-100	100-200	200-300	500	700	900	1300	1500
Fe, Si and Al specific extractions													
Fe Ox[a]	mg/100g	0.08 (0.006)	0.07 (0.002)	0.07 (0.003)	0.06 (0.002)	0.06 (0.001)		0.04 (0.001)	0.04	0.04	0.04	0.05	0.05
Si Ox[a]		0.01 (0.003)	0.00 (0.000)	0.00 (0.000)	0.00 (0.000)	0.00 (0.000)		0.01 (0.000)	0.01	0.01	0.01	0.01	0.00
Al Ox[a]		0.11 (0.017)	0.08 (0.002)	0.08 (0.003)	0.08 (0.002)	0.09 (0.001)		0.07 (0.001)	0.06	0.06	0.04	0.04	0.02
Fe DCB[b]		1.84 (0.058)	1.79 (0.017)	1.82 (0.015)	2.07 (0.156)	2.49 (0.051)		2.41 (0.118)	2.47	2.56	2.71	4.76	2.51
Si DCB[b]		0.05 (0.011)	0.02 (0.001)	0.02 (0.000)	0.02 (0.001)	0.01 (0.001)		0.01 (0.001)	0.02	0.02	0.03	0.10	0.05
Al DCB[b]		0.46 (0.005)	0.41 (0.006)	0.41 (0.008)	0.45 (0.037)	0.55 (0.010)		0.45 (0.022)	0.30	0.25	0.16	0.14	0.06
n	-	4	4	4	4	4	0	4	1	1	1	1	1
Total analyse													
SiO_2	%	81.62 (1.433)	84.35 (0.046)	83.81 (0.709)	83.07 (0.429)	81.71 (0.657)		79.04 (1.049)	79.33	79.80	81.13	80.15	82.41
Al_2O_3		5.16 (0.313)	6.02 (0.309)	6.08 (0.336)	6.41 (0.174)	7.79 (0.190)		8.62 (0.398)	9.13	8.70	8.28	7.15	5.15
Fe_2O_3		3.29 (0.106)	3.70 (0.124)	3.72 (0.117)	3.87 (0.065)	4.49 (0.098)		4.95 (0.195)	5.16	4.93	4.70	6.43	5.89
MnO		0.02 (0.001)	0.02 (0.001)	0.03 (0.001)	0.03 (0.001)	0.03 (0.001)		0.04 (0.002)	0.04	0.04	0.04	0.06	0.10
MgO		0.04 (0.003)	0.03 (0.002)	0.03 (0.003)	0.03 (0.003)	0.03 (0.002)		0.04 (0.003)	0.04	0.03	0.04	0.09	0.10
CaO		<0.2						<0.2	<0.2	<0.2	<0.2	< 0.2	< 0.2
Na_2O		<0.07						<0.07	<0.07	<0.07	<0.07	< 0.07	< 0.07
K_2O		<0.05						<0.05	<0.05	<0.05	<0.05	< 0.05	< 0.05
TiO_2		0.80 (0.021)	0.94 (0.047)	0.93 (0.018)	1.00 (0.005)	1.16 (0.034)		1.32 (0.056)	1.37	1.27	1.24	1.72	2.17
P_2O_5		0.04 (0.005)	0.04 (0.002)	0.04 (0.002)	0.03 (0.002)	0.04 (0.002)		0.04 (0.002)	0.03	0.04	0.03	0.04	0.06
LI[c]		8.69 (1.985)	4.69 (0.089)	4.55 (0.181)	4.58 (0.088)	4.95 (0.121)		4.84 (0.163)	4.73	4.84	3.99	3.87	2.70
n	-	3	3	3	3	3	0	3	1	1	1	1	1

[a] Tamm, 1922 ; [b] Mehra & Jackson, 1960; [c] LI = Loss on Ignition 110-1000°C.

Table A-8 Al an Fe extractions and total analysis of soil fractions of data set $SOIL_{AP11}$

		Clay fraction, Mg saturated										Silt fraction					Sand fraction				
		0-5 cm		5-15 cm		15-30 cm		50-100 cm		200-300 cm		0-5	5-15	15-30	50-100	200-300	0-5	5-15	15-30	50-100	200-300
Fe, Si and Al specific extractions																					
Fe Ox[a]		202	(20.5)	230	(6.4)	236	(5.8)	231	(6.2)	138	(4.3)	57	(12.4)	67	101	100	99	18	17	18	18	9
Si Ox[a]		103	(20.4)	176	(34.2)	209	(9.0)	211	(11.5)	204	(12.7)	18	(7.2)	35	61	67	83	0	1	1	1	1
Al Ox[a]		313	(48.7)	417	(18.6)	429	(23.1)	417	(18.3)	383	(20.4)	33	(8.8)	51	85	93	145	1	2	3	4	3
Fe DCB[b]	mg/100g	6036	(601.7)	7128	(224.0)	7338	(153.1)	7066	(97.4)	7250	(130.5)	2535	(329.1)	3118	3604	3960	5427	537	605	585	587	520
Si DCB[b]		325	(16.4)	400	(33.5)	442	(12.9)	445	(7.4)	452	(10.8)	220	(20.9)	189	212	211	226	4	6	5	8	7
Al DCB[b]		1109	(167.9)	1536	(42.8)	1579	(39.1)	1519	(24.8)	1399	(17.9)	247	(72.4)	393	543	585	803	25	33	34	40	32
Fe TC[c]		197	(19.6)	230	(11.8)	256	(8.4)	267	(12.5)	253	(67.8)	71	(23.2)	109	171	166	127	4	7	6	9	6
Si TC[c]		392	(34.9)	412	(29.9)	438	(19.8)	457	(20.0)	465	(6.8)	878	(120.1)	627	478	365	334	15	16	16	23	32
Al TC[c]		758	(69.5)	840	(44.5)	865	(3.6)	925	(15.0)	935	(23.4)	139	(53.6)	273	443	520	758	3	8	9	16	12
Al DCB+TC		2252	(109.8)	2596	(58.5)	2685	(106.8)	2676	(4.3)	2498	(22.6)	521	(115.3)	981	623	1065	1313					
n	-					4						4			2					1		
Total analysis																					
Sr	mg/100g	355	(45.8)	270		249		241		284							3	1	1	1	1
SiO_2		29	(0.4)	28		28		28		27							98	97	98	97	98
Al_2O_3		34	(0.4)	36		35		35		35							0	0	0	0	0
Fe_2O_3		14	(0.0)	14		14		14		15							1	1	1	1	1
MnO		0	(0.0)	0		0		0		0							0	0	0	0	0
MgO		1	(0.2)	1		1		1		1							0	0	0	0	0
CaO	%	0	(0.2)	0		0		0		1									<0.01		
Na_2O		0	(0.0)	0		0		0		0							0	0	0	0	0
K_2O		0	(0.0)	0		0		0		0									<0.01		
TiO_2		3	(0.0)	3		3		3		3							0	0	0	0	0
P_2O_5		0	(0.0)	0		0		0		0									<0.015		
LI [d]		18	(0.3)	18		18		18		19							0	0	0	0	0
Total		100	(0.1)	100		100		100		100							100	99	100	99	100
n	-	4				1						0					1				

[a] Tamm, 1922 ; [b] Mehra & Jackson, 1960; [d] LI = Loss on Ignition 110-1000°C.

ANNEX 4 ABOVEGROUND SOLUTIONS MONITORING

1 Rainfall

1.1 Experimental design

Rainfall (Pi) was measured weekly in a 1 ha opened area next to the experimental plots (Pi[mm]) and daily in the experimental station located at 2 km used as a reference rainfall (Pi_{ref}[mm]).

1.2 Estimation of daily data from weekly measurements

As the water flux model operates at a daily time step, weekly data needed to be estimated at a daily time step too. Daily rainfall (Pi_{daily}) in the experimental site was simulated from the measured rainfall in the experimental station (Pi_{ref}) thanks to the regression:

$$Pi_{daily}\left[mm\right] = 0 \quad \text{if} \quad Pi_{ref} = 0 \tag{A-1}$$

$$Pi_{daily}\left[mm\right] = a_{Pl} \cdot Pi_{ref}\left[mm\right] + Pi_{0,Pl} \tag{A-2}$$

$Pi_{0,Pl} \neq 0$ means that there can be a systematic offset between both sites and/or rain gauges. a_{Pl} and $Pl_{0,Pl}$ parameters were fitted on weekly measured rainfall using proc GLM of SAS Software (www.sas.com).

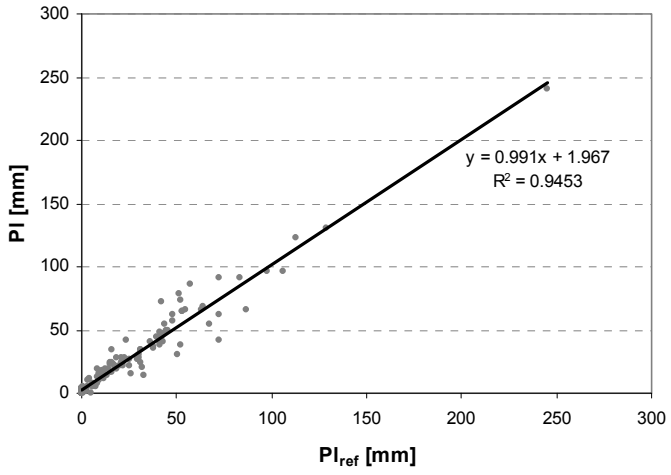

Figure A-3. Correlation between weekly rainfall measured on-site (Pi) and at 2 km in Itatinga experimental station (Pi_{ref})

On-site weekly rainfall (Pi[mm]) was linearly correlated to weekly rainfall measured at Itatinga experimental station. The regression was good with a R^2 of 0.95. On-site rainfall differed very little from Itatinga rainfall with a fitted slope close to 1 (0.99) and a small

intercept of 1.97 mm (Figure A-3). The root mean square error of the regression (RMSE) was of 7.36 mm and in average, the simulated Pi differed of about 42 % from the measured one. This deviation was reduced at about 25% when considering only Pi>2 mm.

The regression was used to estimate daily rainfall from the Itatinga daily measurements.

2 Throughfall

2.1 Experimental design

Throughfall solutions (Th) were measured weekly in collecting devices made of 12 funnels (Th[mL]) systematically distributed beneath the trees to integrate the heterogeneity at the tree scale. Nine repetitions of collecting devices were monitored before clear-felling to check the inter plot spatial heterogeneity. Then, one collecting device per experimental plot in treatment 1, 3 and 5 and blocks 1, 2 and 3 was monitored (total of 9 devices) after trees had reached a sufficient height (10 months after planting in block 1 and 14 months after planting in blocks 2 and 3). The same sampling device was also installed in the same opened area next to the experimental plot (Th_0[mL]) and was used as a reference for throughfall sampling (rainfall collection = throughfall when no tree is present).

2.2 Calculation of weekly throughfall in mm

Throughfall in mm were obtained thanks to:

$$\mathrm{Th}\left[\mathrm{mm}\right] = \frac{1}{S} \cdot \mathrm{Th}\left[\mathrm{mL}\right] \tag{A-3}$$

where S is the total collecting surface of one collecting device made of 12 funnels. $\frac{1}{S}$ was experimentally fitted thanks to the regression:

$$\mathrm{Pi}\left[\mathrm{mm}\right] = \frac{1}{S} \cdot \mathrm{Th}_0\left[\mathrm{mL}\right] \tag{A-4}$$

as Th_0 collected rainfall from the same sampling device as used for throughfall collection (Th). The fitted surface was preferred to the theoretically calculated one to check the homogeneity of sampling device installation and to integrate the non horizontality of the installation.

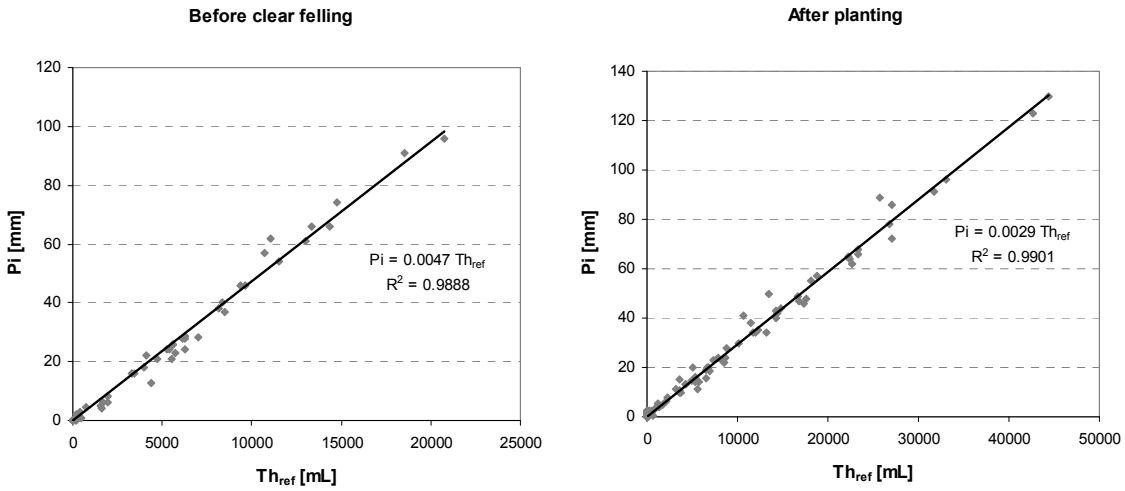

Figure A-4. Regressions of on-site rainfall (Pi) as a function of total depositions (Ps_{ref}) before clear felling and after planting. The slope of the linear regressions gives the total surface of throughfall collecting devices.

Linear regressions of on site rainfall (Pi) as a function of total depositions (Th_{ref}) are given in Figure A-4. The total surface of throughfall collecting devices was given by the slope of these regressions and was of 0.21 cm^2 before clear felling and 0.34 m^2 after planting (replacement of the collecting devices). Throughfall in mm were then calculated from eq (A-3) and the corresponding fitted S.

2.3 Estimation of daily throughfall from weekly measurements

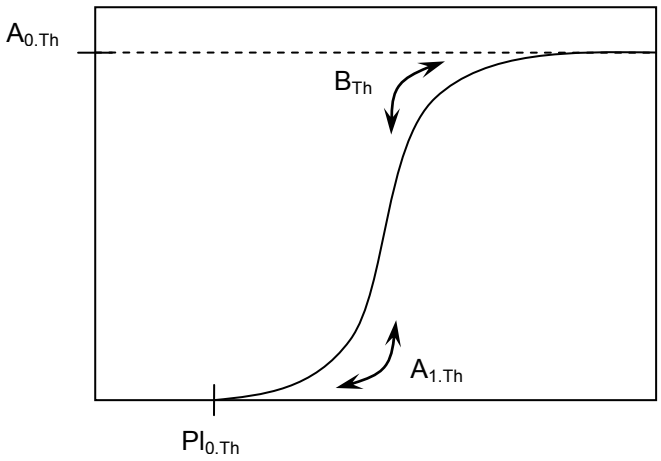

Figure A-5. Non linear function used for relating throughfall to rainfall: parameters explanation.

Daily throughfall (Th_{daily}) were obtained thanks to the non linear regression:

$$\frac{\mathrm{Th}_{\mathrm{daily}}\left[mm\right]}{\mathrm{Pi}_{\mathrm{daily}}\left[mm\right]} = \frac{A_{0,Th}\cdot\left(\mathrm{Pi}_{\mathrm{daily}}\left[mm\right]-\mathrm{Pi}_{0,\mathrm{Th}}\right)^{b_{Th}}}{A_{1,Th}+\left(\mathrm{Pi}_{\mathrm{daily}}\left[mm\right]-\mathrm{Pi}_{0,\mathrm{Th}}\right)^{b_{Th}}} \qquad \text{(A-5)}$$

$$\mathrm{Pi}_{0,\mathrm{Th}} = 0$$

The $Pi_{0,Th}$ threshold for which Th is non null was not used here, since preliminary studies showed that it did not differ significantly from zero. $A_{0,Th}$ is the maximum ratio ($\lim_{\mathrm{Th}_{\mathrm{daily}}[mm]\to\infty}\left(\frac{\mathrm{Th}_{\mathrm{daily}}\left[mm\right]}{\mathrm{Pi}_{\mathrm{daily}}\left[mm\right]}\right)$), b_{Th} and $A_{1,Th}$ are curvature parameters (Figure A-5).

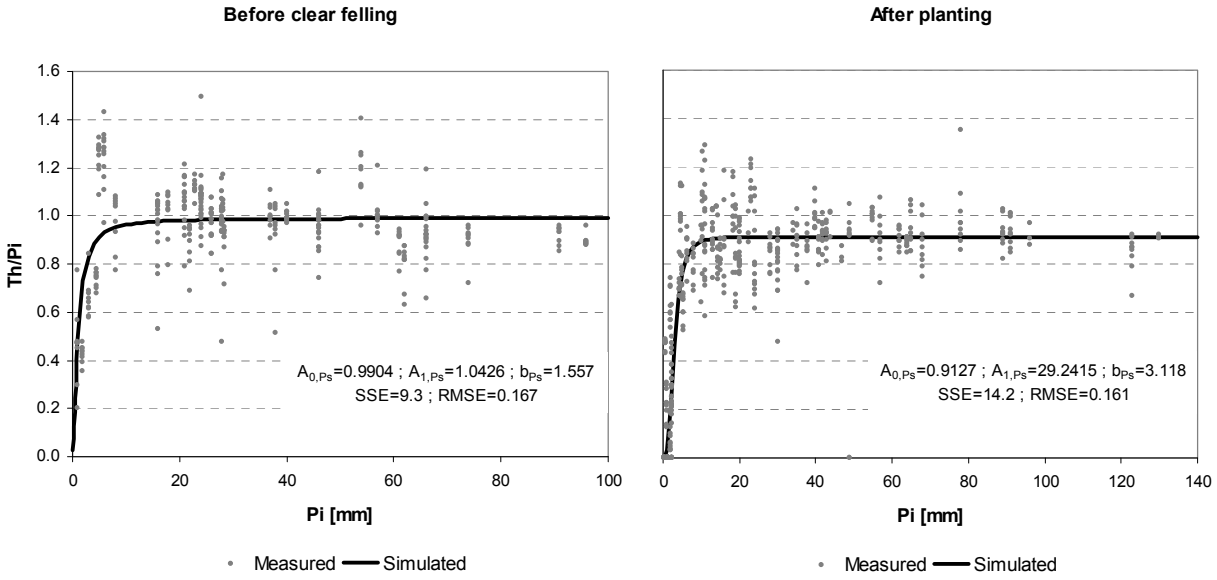

Figure A-6. Non linear regressions relating the rate of weekly throughfall (Th) to on-site weekly rainfall (Pi) before clear felling and after planting. The weekly experimental data and the simulated ones (eq A-5) are represented. The parameters, the sum of squares errors (SSE) and the root mean square errors (RMSE) of the fitted functions are given.

The relationship between throughfall and on site rainfall was not obvious. The fitted curve and the estimated parameters are given in Figure A-6. The limit parameter ($\lim_{\mathrm{Pi}[mm]\to\infty}\left(\frac{\mathrm{Th}\left[mm\right]}{\mathrm{Pi}\left[mm\right]}\right)$) was less after planting ($A_{0,Th}$=0.91) than before clear felling ($A_{0,Th}$=0.99), which corresponds to the smallest interception recorded. The overall curves showed a quasi constant interception above a threshold rainfall of 10 mm, and a steep slope below 10 mm. Around the threshold of 10 mm, a few data > 1 (up to 1.2-1.4 mm) might be

a result of the spatial variability between rainfall in the experiment and the adjacent open area where Pi was recorded (located about 300 m apart) and/or a concentration of rainfall by tree foliage above the collectors. The root mean square errors (RMSE) were about 0.16. These fits were used to estimate daily Th from the daily simulated rainfall Pi_{daily}.

2.4 Temporal and spatial heterogeneity of weekly measured throughfall

Temporal and spatial heterogeneity was studied thanks to function A-5. Function A-5 was fitted for each collector individually or grouped by block or treatment, and for all collectors altogether using PROC NLIN of SAS software (www.sas.com). The effect of clear felling was also tested by fitting the models independently before and after clear felling.

Differences among the models were evaluated from *F* tests calculated on the residual. This test is based on the sums of squares of errors (SSE) and the total number of parameters involved in the models. It compares F_{obs} and F_{tab} calculated as:

$$F_{obs} = \frac{\left(SSE_2 - SSE_1\right)/\left(p_1 - p_2\right)}{SSE_1/\left(n - p_1\right)} \quad \text{(A-6)}$$

where p_1 is the number of parameters for the more complete model (for example the sum of the collector specific models), p_2 is the number of parameters for the global model ($p_2<p_1$) (for example, all collectors fitted altogether), SSE_1 is the sum of square errors for the complete model, SSE_2 is the sum of square errors for the global model, and n is the number of observations. F_{tab} is the theoretical value given in the Fischer's table $F_{tab}=F(p_1-p_2,n-p_1)$. If $F_{obs}>F_{tab}$ then the local model describes the data set better than the global model and there is a significant effect of the studied variable on the fitted function (ref Brown & Rothery, 1993). All differences were considered significant at a 5% threshold. The effects tested are given in Table A-9.

Table A-9 Effects tested on model A-5 and results of the F-tests. p_1 and p_2 are the number of parameters of the models, n the number of observations. F_{obs} calculation is given in eq. A-6 and F_{tab} is the theoretical value given in the Fischer's table.

Data set	Effect tested	p_1	p_2	n	F_{obs}	F_{calc}
BCF	Collector	3	27	335	1.47	1.55
AP	Collector	3	27	540	0.97	1.54
	Treatment	3	9	540	0.78	2.12
BCF+AP	Clear felling	3	6	875	58.06	2.62

The analysis of throughfall data (expressed in [mm]) showed that there was no significant effect of the treatment or block before and after planting, but that there was a significant effect of the clear felling (Table A-9). Indeed, the interception was greater after planting (average throughfall = 87 % of rainfall) than at the end of the previous rotation (average throughfall = 98 % of rainfall). This greater interception corresponded to greater leaf area index (LAI) after planting than at the end of the previous rotation. Since the canopy closure occurred after 12 months of stand growth and since the throughfall collecting devices were installed 10 months after planting, no time differentiation was made during the AP period.

This study validates the use of two single models (before and after clear felling) to simulate daily throughfall from daily rainfall.

3 Stemflow

3.1 Experimental design

Stem flows (St) were collected from helical collars installed on trees and measured weekly in the collection bucket (St[mL]). Before clear felling, eight of these collars were installed on trees representative of the stand according to four basal area classes (January 2003 inventory) (Table A-10).

Table A-10 Repartition of the stand and stem flow sampling devices into basal area classes before clear felling.

	Stem flow : basal area classes			
Class number	1	2	3	4
Basal area (cm^2)	0-20	20-30	30-40	40-60
Number of trees	144	342	370	154
Number of trees sampled for St	1	3	3	1

After clear felling, stem flow collecting devices were installed in January 2006 (20 months after planting). In each experimental plot of treatment 1, 3 and 5 and blocks 1, 2 and 3, three trees (small, medium, and big according to age 18.5 months inventory) were equipped with helical collars. As it was impossible to measure girth breast height (CBH) for these monitoring trees once equipped, CBH was estimated thanks to the growth equations:

$$CBH(t) = CBH(18.5) + a_{CBH} \cdot t^2 + b_{CBH} \cdot t + c_{CBH} \quad \text{(A-7)}$$

where CBH(18.5) is the girth breast height in meter measured for the considered monitoring tree at age 18.5 months, t is the time in months,, a_{CBH}, b_{CBH}, and c_{CBH} are the parameters fitted for each treatment thanks to stand inventories available at ages 9.5, 11.5, 18.5, 23.5, 30, and 36 months (Table A-11).

Table A-11 Growth parameters (eq. A-7) used to estimate the girth breast height (CBH) of the trees equipped with stemflow monitoring devices after clear felling.

Treatment	a_{CBH}	b_{CBH}	c_{CBH}	r2
Tr1	-0.0114	0.8488	-11.751	0.81
Tr3	-0.0113	0.8141	-11.152	0.76
Tr5	-0.0106	0.7587	-10.388	0.71

3.2 Calculation of weekly stemflow in mm (stand scale)

Before clear felling, stem flow in mm (St[mm]) was obtained thanks to:

$$St[mm] = 1000 \frac{1}{S_s} \sum_{1 \le i \le 4} St_{i,t} n_i \quad \text{(A-8)}$$

where $St_{i,t}$ is the average stem flow within class i measured at week t, n_i is the number of trees of class i, and S_s is the total area of the stand (6480 m^2). This simple equation was used since the stand

before clear felling was considered at a steady-state (growth very slow so that the inventory of Table A-10 can be regarded as constant).

After clear felling, stemflows were installed at age 20 months and the tree growth was not achieved. As the relationship between St and rainfall had to be studied to estimate daily data from weekly data, we tried to study more thoroughly the relationships between the stemflow collected volumes, the amount of rainfall and the diameter of the tree. All data from age 20 months after planting to age 27 months were used, under the hypothesis that the relationship was independent of the stand age (no interactions between adjacent trees).

After preliminary study of the surface representing stemflow in mL as a function of rainfall and girst breast height, a mathematical function describing the stemflow volume $St_{k,t}$[mL] (measured for each collecting tree k at time t) as a function of the rainfall intensity and the girth breast height was tested:

$$St_{k_{i,j},t}\left[\text{mL}\right]\left(Pi_t, GBH_{k_{i,j},t}\right) = A_{0,St} \cdot \frac{\left[\frac{Pi_t}{120}\cdot\left(\frac{GBH_{k_{i,j},t}}{11.4}\right)^{c_{St}}\right]^{b_{St}}}{A_{1,St}+\left[\frac{Pi_t}{120}\cdot\left(\frac{GBH_{k_{i,j},t}}{11.4}\right)^{c_{St}}\right]^{b_{St}}} \quad \text{(A-9)}$$

where $St_{k_{i,j},t}\left[\text{mL}\right]$ is the stem flow volume measured for tree $k_{i,j}$ at time t in mL, $Pi_t\left[\text{mm}\right]$ is the rainfall intensity in mm measured at time t, $GBH_{k_{i,j},t}$ is the girth breast height estimated for collecting tree k at time t, $A_{0,St}$, $A_{1,St}$, c_{St} and b_{St} are parameters fitted from the pool of all available data (times t and trees k). $A_{0,St}$ is the maximum stemflow ($\lim_{Pi_t, GBH_{k_{i,j},t}\to\infty}\left(St_{k_{i,j},t}\right)$), $A_{1,St}$ and b_{St} are curvature parameters, c_{St} is a weight between $Pi_t\left[\text{mm}\right]$ and $GBH_{k_{i,j},t}$, 120 and 11.4 are constants used to help the model converge.

This function was inspired from the stemflow one (eq. A-5) given the facts that: (i) it mathematically describes the type of surface experimentally measured, (ii) it corresponds to a joint increase of stemflow, Pi and CBH (c_{EC} weights this increase between rainfall and CBH), (iii) the function reaches a limit when the rainfall increases which means that the stemflow process is limited by the surface of stem available for the stemflow to drain. It is reminded that this model was tested for our experimental site conditions and studied stand

ages. Its validity was not checked for other ages, locations, and tree species. Parameters were fitted thanks to the NLIN procedure of SAS Software.

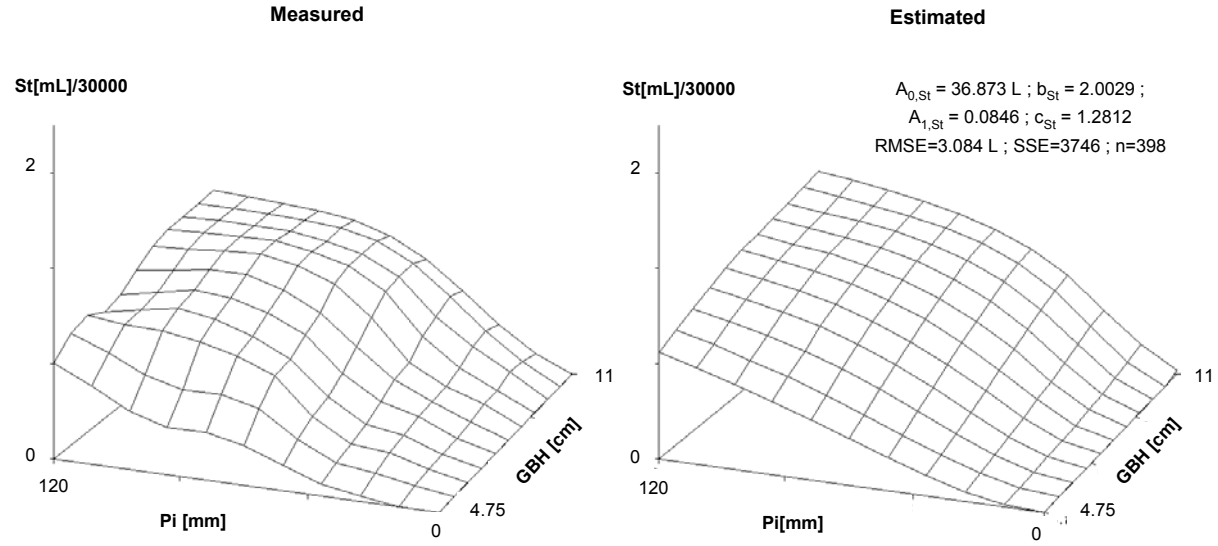

Figure A-7. Volumes of stemflow (St) in mL as a function of girth breast height (CBH) and rainfall (Pi): data measured after planting in treatments 1, 3 and 5, blocks 1, 2 and 3, and simulated using eq. A-9.

Two plateaus can be observed (Figure A-9): for small trees and low rainfall intensity the stemflow was quasi null; above a threshold of 8 cm of CBH and of 50 mm of rainfall intensity, the stemflow was maximum and quasi constant ($A_{0,EC}$=36.873 L). In-between, the stemflow increased together with CBH and rainfall intensity. The function of eq A-9 simulated the surface with a root mean square error of 3.084 L. The simulated volume differed in average of 84% from the measured one, but this value decreases down to 30 % if considering only the collected volumes > 10 L (average collected volume for all collectors during the studied period). This means that the model was more efficient to simulate the stemflows when the volume of water collected weekly was > 10 L. If all trees in the stand collected the same volume of water, this would correspond to a threshold of 1.7 mm of water collected and to a RMSE of 0.514 mm.

This relationship can give for each weekly volume of rainfall recorded and tree k of CBH the volume of stemflow corresponding. Stemflow in mm are the sum of each volume collected for each tree of the plot divided by the surface of the plot so that stemflow $St_{i,j,t}$[mm] of treatment i and block j can be obtained thanks to:

$$St_{i,j,t}[mm] = \frac{1}{1000 \cdot S} \cdot \sum_{1 \le k_{i,j} \le 36} St_{k_{i,j},t}[mL] \qquad \text{(A-10)}$$

where $St_{i,j,t}\,[mm]$ is the stemflow in treatment i and block j at time t, S is the area of the experimental plot in m^2 (216 m^2) and $k_{i,j}$ one of the 36 trees of treatment i and block j, $St_{k_{i,j},t}\,[mL]$ is the steamflow estimated from equation 8 with $CBH_{k_{i,j},t}$ measured for tree $k_{i,j}$ at the latest inventory and $Pi_t\,[mm]$ measured at time t.

3.3 Estimation of daily stemflow from weekly data

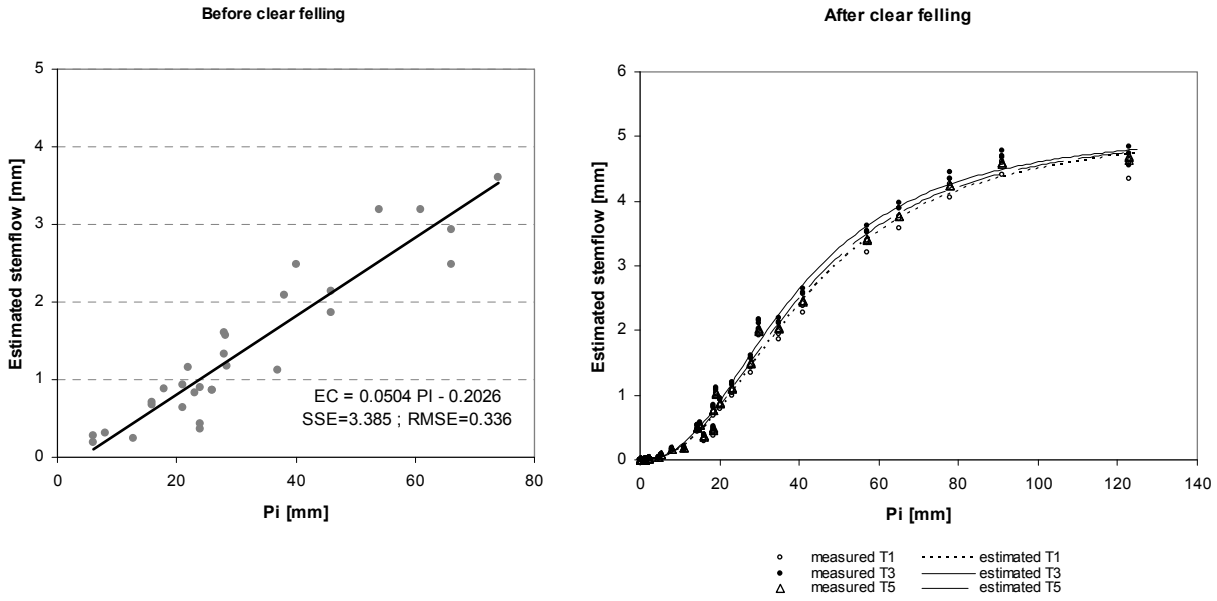

Figure A-8. Weekly stemflow (in mm) estimated at the stand scale from eq. A-8 before clear felling and at the plot scale from eq. A-9 and eq A-10 after planting as a function of weekly rainfall (Pi) recorded on site.

Before clear felling, daily stemflow (St_{daily}) can be estimated from daily rainfall thanks to a linear regression:

$$St_{daily}\,[mm] = 0 \quad \text{if} \quad St_{daily}\,[mm] < Pi_{0,EC}$$

$$St_{daily}\,[mm] = a_{St} \cdot Pi_{daily}\,[mm] + b_{St} \quad \text{otherwise} \qquad \text{(A-11)}$$

A simple linear regression was used since there were two little data to fit a more complicate function (for example of the type of the throughfall one). The root mean square error of the regression was of 0.336 mm.

After clear felling, daily stemflow ($St_{daily(i,j)}$) may be calculated directly from Pi_{daily}[mm] and $CBH_{k_{i,j},t}$ measured at the latest inventory for all trees $k_{i,j}$ of $plot_{i,j,}$ using

equations A-9 and A-10, provided that daily rainfall follow the same relationship as weekly rainfall in eq. A-9.

Figure A-8 represents the weekly measured stemflow (once estimated at the plot scale) as a function of the weekly measured rainfall for treatments 1, 3 and 5. For each rainfall recorded, a data on Figure A-8 is the average projection of Figure A-7 on the rainfall axis for each CBH of the corresponding plot. This projection differed very little among the fertilization treatments, which indicates that the plots followed more or less the same growth between age 20 months and age 28 months in the 3 treatments. The spatial heterogeneity between treatments can be analyzed in the same way as the throughfall spatial heterogeneity by fitting equation A-5 on the data of Figure A-8 for each treatment and for all treatments altogether and by performing *F* tests calculated on the residual. Ideally, this type of study would better be done directly on the parameters of the fitted surface of equation A-9 but two little data were available to do so. The F-tests showed a slight effect of the treatment on the fitted function (F_{obs}=7.70 > F_{calc}=2.13). This effect is a consequence of differences of growth among treatments. The stemflows estimated by these functions differed less than 0.24 mm among treatments which was less than the RMSE calculated for function 8 (0.514 mm) which shows that the effect of treatment is weak.

The stemflow (in mm) was greater before clear felling (about 3.37 % of rainfall) than after planting between age 20 and 27 months (about 2.62% of rainfall).

4 Surface runoff

4.1 Experimental design

Surface runoff (Ru) was measured and collected weekly in one block for each treatment from one 3x2 m collector (Thomas et al., 2000).

4.2 Weekly run-off in mm

The volume of surface run-off collected was converted to mm by dividing it by its surface:

$$Ru[mm]=Ru[mL]/6000 \quad \text{(A-12)}$$

Surface runoff was in average 0.16 % of rainfall and in maximum of 1.39 % of rainfall. These very small values are the direct consequence of the flat slopes of the experiment (< 6°).

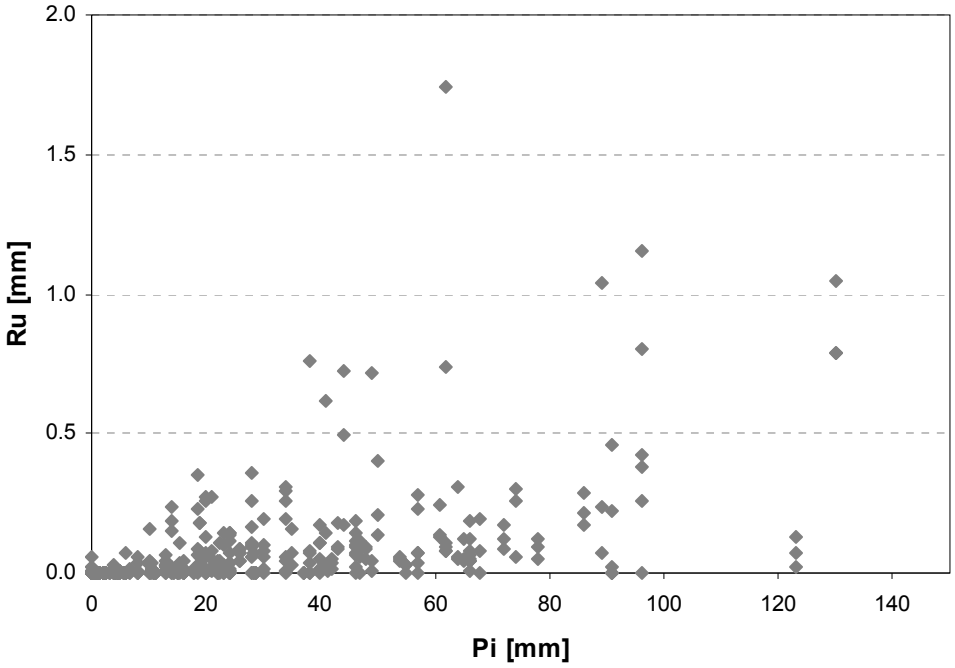

Figure A-9. Surface run-off (Ru) as a function of rainfall (Pi) over the studied period.

No clear correlation between surface run-off and the weekly measured rainfall was observed (Figure A-9).

ANNEX 5 LINEAR REGRESSIONS AMONG THE MEASURED SOIL MOISTURES

Table A-12 Intercepts, slopes and R-square of the linear regressions relating the water contents measured for a given TDR probe to the average water content for all probes of the experiment.

Treatment		Repetition	Intercept (%)				Slope	R-square
			BCF1	*BCF2*	*CFP*	*AP*		
15 cm	1	1	-1.98	-1.74	-1.58	-1.51	1.05	0.96
		2	-0.22	-1.07	-1.26	-0.33	1.09	0.96
		3	-0.83	-1.19	-0.93	-1.63	0.91	0.90
		All	*-1.01*	*-1.33*	*-1.26*	*-1.16*	*1.02*	*0.99*
	3	1	-0.83	-0.34	-0.23	-0.92	1.00	0.93
		2	4.78	4.68	4.15	4.12	0.90	0.90
		3	2.11	2.93	2.62	1.21	0.88	0.80
		All	*2.02*	*2.42*	*2.18*	*1.47*	*0.92*	*0.97*
	5	1	-4.81	-4.95	-4.44	-3.40	1.06	0.93
		2	-1.54	-1.20	-1.56	-1.40	1.10	0.97
		3	3.34	2.89	3.23	3.87	1.01	0.89
		All	*-1.01*	*-1.09*	*-0.92*	*-0.31*	*1.06*	*0.98*
50 cm	1	1	-1.20	-0.74	-0.75	-0.59	1.04	0.98
		2	0.62	-1.27	-0.98	-0.05	1.07	0.96
		3	-0.35	-0.45	-0.55	-0.24	0.96	0.98
		All	*-0.31*	*-0.82*	*-0.76*	*-0.29*	*1.02*	*0.99*
	3	1	1.97	2.67	2.56	1.73	0.93	0.98
		2	2.06	1.53	1.37	0.62	1.02	0.97
		3	1.00	1.68	1.60	1.35	0.90	0.91
		All	*1.68*	*1.96*	*1.84*	*1.23*	*0.95*	*0.98*
	5	1	-2.33	-1.39	-1.37	-1.25	0.98	0.97
		2	-1.21	-0.98	-0.88	-0.52	1.02	0.98
		3	-0.57	-1.05	-1.00	-1.05	1.08	0.92
		All	*-1.37*	*-1.14*	*-1.08*	*-0.94*	*1.03*	*0.99*
150 cm	1	1	-2.07	-2.16	-2.49	-2.88	1.13	0.97
		2	2.40	1.83	1.75	0.10	0.88	0.98
		3	-0.45	-1.10	-1.12	-1.74	1.04	0.94
		All	*-1.03*	*-1.68*	*-1.87*	*-2.13*	*1.08*	*0.98*
	3	1	1.17	1.13	1.13	1.58	0.95	0.95
		2	-0.76	-1.09	-0.85	-1.18	1.08	0.99
		3	1.06	1.73	1.82	0.51	0.89	0.87
		All	*0.49*	*0.59*	*0.70*	*0.30*	*0.97*	*0.99*
	5	1	-0.63	0.05	-0.05	0.19	0.97	0.98
		2	-0.94	-0.59	-0.33	-0.09	0.98	0.99
		3	1.71	2.02	2.02	3.06	0.98	0.96
		All	*0.04*	*0.49*	*0.55*	*1.06*	*0.98*	*0.99*
300 cm	1	1	-0.55	-1.00	-1.25	-1.74	1.07	0.93
		2	1.45	0.68	0.67	0.46	0.99	0.98
		3	-0.51	-1.02	-0.88	-1.10	1.04	0.98
		All	*0.13*	*-0.45*	*-0.49*	*-0.79*	*1.03*	*0.98*
	3	1	5.28	5.75	5.91	5.99	0.77	0.97
		2	-3.47	-3.69	-3.62	-3.71	1.10	0.99
		3	-3.67	-3.66	-3.49	0.10	1.10	0.97
		All	*-0.13*	*0.01*	*0.16*	*0.30*	*0.97*	*0.99*
	5	1	2.59	3.24	3.17	3.19	0.87	0.98
		2	3.91	4.33	4.19	4.27	0.87	0.99
		3	-6.12	-5.83	-5.95	-6.03	1.24	0.97
		All	*0.13*	*0.58*	*0.47*	*0.48*	*0.99*	*0.99*

ANNEX 6 SIMULATED AGAINST MEASURED WATER CONTENTS FOR THE BCF AND CFP PERIODS

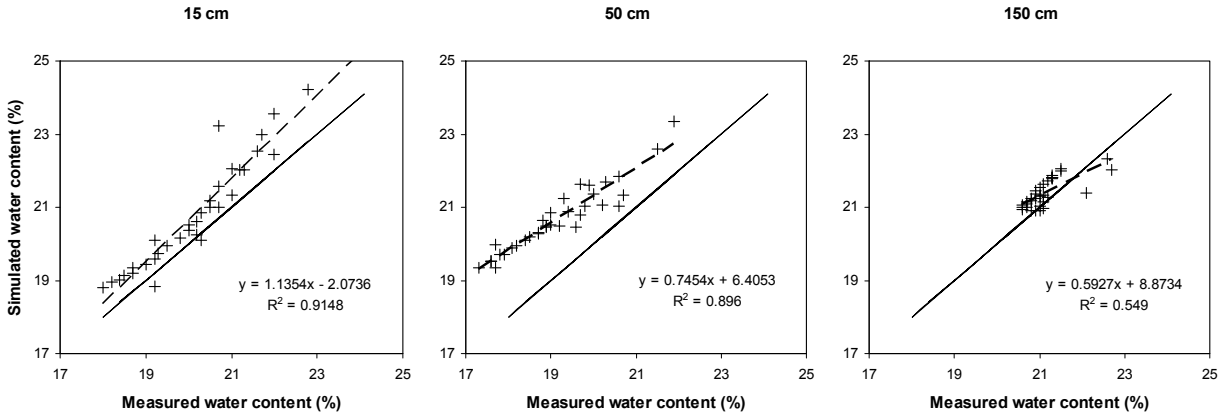

Figure A-10. Simulated against measured volumetric water contents for the CFP period in treatment 3. The intercept, slopes and R-square of the regressions are indicated.

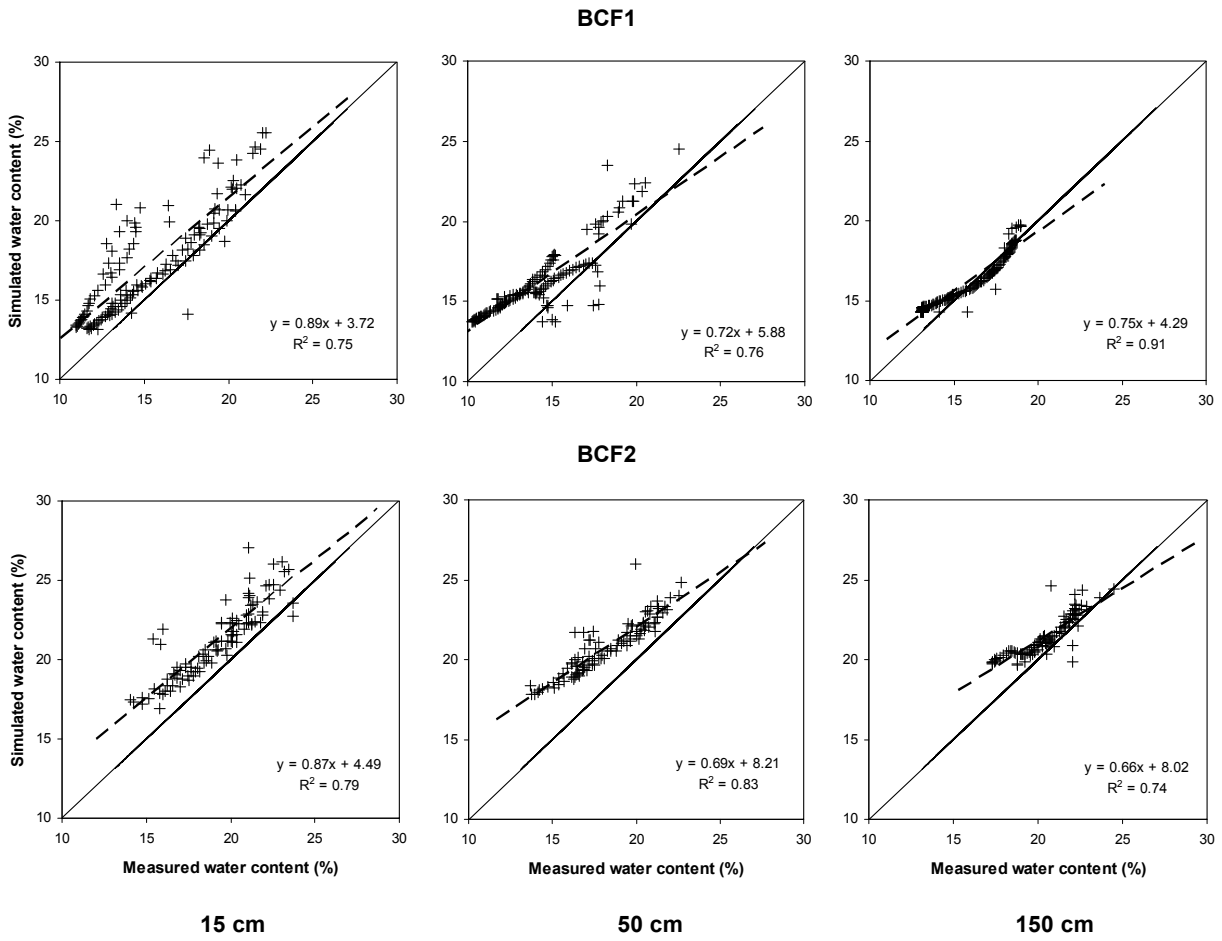

Figure A-11. Simulated against measured volumetric water contents for the BCF period in treatment 3. The intercept, slopes and R-square of the regressions are indicated.

ANNEX 7 CUMULATIVE FLUXES FROM CLEAR FELLING UNTIL THE END OF THE EXPERIMENTAL PERIOD

Table A-13 Average cumulative fluxes and standard deviations (when n≥3) calculated from the clear felling (N_{month}=9) to the end of the experimental period (N_{month}=37) for cations and anions measured in soil solutions for each collector type, collection depth and treatment.

	Treatment	Cl	NO_3	NO_2	NH_4	SO_4	PO_4	H	Na	K	Mg	Ca	n_{obs}	Fe	Al	Si	DOC
		mmol m^{-2}												*mmol m^{-2}*			*g m^{-2}*
Rainfall		57	39	3	45	14	1	18	23	17	11	22	1	0	0	8	4
Throughfall	1	29 *(4)*	21 *(0)*	2 *(0)*	20 *(2)*	7 *(0)*	0 *(0)*	7 *(0)*	13 *(1)*	19 *(2)*	9 *(1)*	15 *(2)*	3	0	1	2	7
	3	24 *(2)*	21 *(1)*	2 *(0)*	22 *(1)*	7 *(1)*	1 *(0)*	7 *(0)*	10 *(1)*	15 *(1)*	9 *(0)*	15 *(1)*	3	0	1	2	7
	5	40 *(6)*	20 *(0)*	2 *(0)*	23 *(1)*	8 *(0)*	1 *(0)*	9 *(1)*	13 *(1)*	26 *(6)*	9 *(0)*	18 *(1)*	3	0	1	3	8
Stemflow	1	3 *(1)*	0 *(0)*	0 *(0)*	0 *(0)*	0 *(0)*	0 *(0)*	0 *(0)*	1 *(0)*	1 *(1)*	1 *(0)*	0 *(0)*	3	0	0	0	0
	3	2 *(1)*	0 *(0)*	0 *(0)*	0 *(0)*	0 *(0)*	0 *(0)*	0 *(0)*	1 *(0)*	1 *(0)*	0 *(0)*	0 *(0)*	3	0	0	0	0
	5	3 *(1)*	0 *(0)*	0 *(0)*	0 *(0)*	0 *(0)*	0 *(0)*	0 *(0)*	1 *(0)*	1 *(1)*	0 *(0)*	0 *(0)*	3	0	0	0	0
Zero-tension lysimeter																	
0 cm	1	227 *(50)*	56 *(15)*	14 *(3)*	49 *(34)*	23 *(3)*	2 *(1)*	11 *(10)*	78 *(16)*	177 *(56)*	235 *(75)*	174 *(52)*	3	7	18	30	79
	3	321 *(130)*	55 *(14)*	13 *(6)*	382 *(182)*	210 *(69)*	7 *(6)*	40 *(42)*	114 *(21)*	235 *(113)*	225 *(52)*	182 *(35)*	3	14	27	33	91
	5	334 *(91)*	103 *(77)*	16 *(9)*	352 *(224)*	231 *(169)*	10 *(6)*	72 *(22)*	140 *(115)*	235 *(59)*	84 *(22)*	136 *(42)*	3	29	34	43	76
15 cm	1	111 *(30)*	197 *(46)*	2 *(0)*	23 *(9)*	16 *(4)*	1 *(0)*	117 *(28)*	57 *(25)*	47 *(8)*	59 *(7)*	36 *(18)*	3	3	67	90	24
	3	191 *(97)*	267 *(70)*	6 *(3)*	184 *(187)*	315 *(335)*	19 *(31)*	204 *(14)*	96 *(61)*	101 *(33)*	100 *(26)*	93 *(73)*	3	3	103	117	31
	5	268 *(55)*	604 *(181)*	7 *(2)*	362 *(178)*	288 *(62)*	1 *(0)*	255 *(8)*	65 *(8)*	98 *(32)*	64 *(9)*	98 *(17)*	3	4	264	157	21
Tension lysimeter																	
15 cm	1	343 *(214)*	334 *(84)*	4 *(3)*	19 *(16)*	41 *(34)*	1 *(1)*	83 *(16)*	150 *(66)*	106 *(61)*	81 *(55)*	66 *(45)*	3	0	109	311	15
	3	155 *(64)*	468 *(166)*	3 *(2)*	131 *(187)*	331 *(162)*	96 *(164)*	118 *(5)*	156 *(59)*	79 *(26)*	125 *(22)*	265 *(290)*	3	0	147	313	18
	5	393 *(191)*	550 *(165)*	5 *(2)*	24 *(25)*	79 *(67)*	2 *(2)*	128 *(25)*	87 *(11)*	203 *(145)*	48 *(13)*	66 *(30)*	3	0	229	267	11
50 cm	1	387 *(190)*	355 *(105)*	1 *(1)*	104 *(147)*	13 *(10)*	0 *(0)*	85 *(23)*	164 *(35)*	109 *(50)*	37 *(3)*	30 *(1)*	3	0	153	240	7
	3	142 *(100)*	410 *(84)*	2 *(1)*	101 *(159)*	87 *(134)*	1 *(2)*	69 *(13)*	117 *(82)*	45 *(31)*	51 *(26)*	67 *(49)*	6	0	136	220	8
	5	221 *(195)*	679 *(236)*	2 *(1)*	8 *(6)*	6 *(6)*	0 *(0)*	108 *(37)*	60 *(31)*	111 *(180)*	30 *(7)*	38 *(12)*	6	0	238	294	5
100 cm	1	645 *(528)*	281 *(104)*	1 *(0)*	97 *(136)*	2 *(1)*	0 *(0)*	74 *(19)*	98 *(24)*	216 *(257)*	25 *(3)*	28 *(4)*	3	0	157	208	5
	3	126 *(213)*	368 *(242)*	1 *(1)*	45 *(74)*	3 *(6)*	0 *(0)*	46 *(13)*	154 *(164)*	26 *(27)*	28 *(13)*	30 *(10)*	12	0	79	158	5
	5	156 *(91)*	416 *(124)*	5 *(2)*	5 *(3)*	1 *(0)*	0 *(0)*	80 *(24)*	71 *(17)*	39 *(33)*	26 *(8)*	28 *(8)*	3	0	159	160	4
300 cm	1	17 *(7)*	38 *(21)*	0 *(0)*	4 *(3)*	0 *(0)*	0 *(0)*	8 *(4)*	21 *(4)*	5 *(1)*	7 *(2)*	13 *(7)*	3	0	15	83	3
	3	10 *(4)*	24 *(12)*	1 *(0)*	4 *(8)*	0 *(0)*	0 *(0)*	5 *(2)*	12 *(6)*	3 *(1)*	4 *(2)*	8 *(3)*	12	0	1	66	1
	5	13 *(5)*	56 *(23)*	1 *(0)*	6 *(4)*	0 *(0)*	0 *(0)*	15 *(3)*	56 *(85)*	4 *(1)*	6 *(1)*	17 *(9)*	6	0	4	84	2

ANNEX 8 SPECIFIC EXTRACTIONS PERFORMED ON SOILS AT AGE 2 YEARS AFTER PLANTING

Table A-14 Specific extractions performed on soils at age 2 years after planting: reference stand kept uncut. Mean and standard errors (when n≥3) are given.

		Reference						
		0-5 cm	5-15 cm	15-30 cm	30-50 cm	50-100 cm	100-200 cm	200-300 cm
Water extraction on fresh soil								
Ca	kg ha^{-1}	1 *0.2*	1 *0.0*	1 *0.1*	2 *0.2*	5 *1.3*	9 *1.1*	11 *0.4*
Mg		0 *0.0*	0 *0.0*	1 *0.0*	1 *0.2*	1 *0.1*	3 *0.6*	4 *0.4*
Na		1 *0.0*	2 *0.3*	3 *0.2*	3 *0.2*	11 *0.8*	17 *3.9*	25 *0.8*
H		0 *0.0*	1 *0.0*	1 *0.0*	1 *0.1*	2 *0.2*	5 *0.7*	6 *0.3*
Al		5 *2.3*	13 *3.4*	12 *6.5*	5 *2.5*	9 *7.4*	1 *0.4*	1 *0.7*
N/NH_4		1 *0.1*	1 *0.2*	1 *0.4*	1 *0.4*	4 *0.3*	6 *0.8*	9 *1.3*
N/NO_3		1 *0.2*	1 *0.3*	1 *0.3*	1 *0.1*	4 *1.7*	9 *2.4*	28 *3.8*
S/SO_4		0 *0.1*	2 *0.3*	3 *0.6*	5 *0.7*	4 *0.7*	4 *0.3*	5 *0.6*
KCl extraction on fresh soil								
N/NO_3	kg ha^{-1}	1 *0.1*	1 *0.1*	0 *0.0*	0 *0.0*	2 *0.1*	4 *1.0*	12 *2.6*
N/NH_4		1 *0.0*	1 *0.1*	2 *0.3*	2 *0.3*	4 *0.2*	6 *1.0*	8 *1.1*
KCl extractions (except for K, NH_4Cl extraction) (air-dry soil)								
K	kg ha^{-1}	15 *1.5*	15 *1.1*	13 *0.8*	13 *3.0*	22 *4.5*	32 *3.3*	34 *4.0*
Ca		7 *2.0*	14 *2.3*	17 *7.5*	9 *8.8*	44 *12.6*	144 *41.2*	145 *49.2*
Mg		2 *0.5*	3 *0.3*	2 *0.5*	0 *0.5*	5 *4.9*	15 *8.8*	8 *4.6*
Na		0 *0.0*	0 *0.0*	0 *0.0*	0 *0.0*	93 *93.1*	328 *167.7*	74 *74.3*
H		4 *1.1*	1 *0.0*	2 *0.1*	1 *0.7*	2 *0.9*	6 *0.1*	0 *0.0*
Al		159 *23.5*	167 *6.7*	226 *7.7*	229 *5.7*	420 *21.8*	628 *23.8*	169 *7.4*
Saturation	cmolc/kg	0.3 *0.05*	0.1 *0.01*	0.1 *0.02*	0.1 *0.02*	0.1 *0.01*	0.1 *0.02*	0.1 *0.02*
CEC	cmolc/kg	2.7 *0.37*	1.2 *0.01*	1.0 *0.01*	0.5 *0.22*	0.4 *0.18*	0.5 *0.02*	0.1 *0.01*
N/NO_3	kg ha^{-1}	2 *0.6*	3 *1.6*	3 *0.2*	4 *0.9*	15 *3.7*	30 *11.8*	87 *28.1*
S (total)		49 *10.1*	88 *4.3*	170 *13.0*	210 *8.0*	349 *77.1*	786 *101.8*	451 *99.4*
P (total)		5 *0.5*	10 *1.5*	17 *3.0*	17 *0.1*	45 *8.3*	99 *7.2*	90 *0.3*
Specific extractions								
S/SO_4	kg ha^{-1}	4 *0.9*	9 *1.4*	22 *9.1*	12 *1.2*	15 *5.5*	24 *5.0*	24 *9.0*
P/PO_4		2 *0.3*	1 *0.0*	1 *0.1*	2 *0.1*	1 *0.3*	3 *1.0*	3 *0.0*

Table A-15 Specific extractions performed on soils at age 2 years after planting: Treatment 1. Mean and standard errors (when n≥3) are given.

		Treatment 1							
		0-5 cm	5-15 cm	15-30 cm	30-50 cm	50-100 cm	100-200 cm	200-300 cm	
Water extraction on fresh soil									
Ca	kg ha^{-1}	1 *0.3*	2 *0.3*	2 *0.1*	3 *0.7*	5	12	10	1
Mg		0 *0.2*	1 *0.1*	1 *0.0*	1 *0.0*	2	4	3	0
Na		2 *0.1*	4 *0.5*	5 *0.9*	6 *0.5*	17	32	34	2
H		0 *0.0*	0 *0.1*	1 *0.2*	1 *0.1*	1	4	2	0
Al		14 *3.4*	37 *5.2*	26 *6.9*	10 *4.4*	2	2	1	14
N/NH_4		1 *0.1*	0 *0.2*	0 *0.2*	1 *0.1*	2	7	6	1
N/NO_3		0 *0.1*	0 *0.2*	1 *0.1*	1 *0.5*	1	2	10	0
S/SO_4		1 *0.1*	2 *0.2*	4 *0.7*	6 *1.2*	3	3	3	1
KCl extraction on fresh soil									
N/NO_3	kg ha^{-1}	0 *0.1*	0 *0.0*	0 *0.1*	0 *0.0*	1	2	4	0
N/NH_4		2 *0.3*	1 *0.2*	2 *0.5*	1 *0.1*	6	13	6	2
KCl extractions (except for K, NH_4Cl extraction) (air-dry soil)									
K	kg ha^{-1}	14 *1.2*	13 *0.8*	13 *1.5*	11 *1.2*	15	114	15	14
Ca		73 *29.9*	13 *8.3*	4 *4.3*	9 *8.6*	0	0	65	73
Mg		42 *15.7*	9 *2.6*	5 *2.3*	5 *2.4*	9	20	31	42
Na		0 *0.0*	0 *0.0*	0 *0.0*	10 *9.9*	0	0	86	0
H		2 *0.9*	2 *0.4*	2 *0.3*	2 *0.1*	2	4	0	2
Al		92 *25.6*	127 *9.6*	174 *10.4*	206 *9.8*	321	400	81	92
Saturation	cmolc/kg	1.3 *0.45*	0.2 *0.06*	0.1 *0.03*	0.1 *0.02*	0.0	0.0	0.1	
CEC	cmolc/kg	3.0 *0.24*	1.2 *0.15*	1.0 *0.08*	0.9 *0.02*	0.6	0.4	0.2	
N/NO_3	kg ha^{-1}	2 *0.3*	2 *0.7*	2 *1.6*	4 *0.8*	12	3	47	2
S (total)		23 *4.4*	41 *6.2*	68 *10.1*	122 *4.3*	122	163	209	23
P (total)		2 *0.6*	5 *1.5*	8 *2.7*	12 *4.8*	8	19	20	2
Specific extractions									
S/SO_4	kg ha^{-1}	3 *1.2*	4 *0.5*	12 *5.9*	14 *1.4*	0	0	0	3
P/PO_4		2 *0.3*	24 *9.7*	3 *0.8*	2 *0.4*	2	4	13	2

Table A-16 Specific extractions performed on soils at age 2 years after planting: Treatment 3. Mean and standard errors (when n≥3) are given.

		Treatment 3						
		0-5 cm	5-15 cm	15-30 cm	30-50 cm	50-100 cm	100-200 cm	200-300 cm
Water extraction on fresh soil								
Ca	kg ha^{-1}	1 *0.2*	2 *0.3*	3 *0.7*	3 *0.8*	7 *2.1*	13 *2.4*	10 *1.4*
Mg		1 *0.4*	2 *0.5*	2 *0.5*	2 *0.5*	4 *2.2*	7 *3.2*	4 *0.6*
Na		2 *0.2*	4 *0.5*	5 *0.8*	6 *1.3*	14 *1.2*	29 *3.8*	24 *2.6*
H		0 *0.0*	1 *0.1*	1 *0.1*	2 *0.2*	3 *0.3*	7 *0.6*	4 *1.0*
Al		13 *7.2*	17 *3.7*	11 *3.1*	3 *1.0*	5 *2.9*	5 *2.1*	2 *0.3*
N/NH_4		0 *0.2*	1 *0.4*	1 *0.0*	1 *0.1*	6 *2.8*	9 *2.9*	7 *0.6*
N/NO_3		0 *0.1*	0 *0.2*	0 *0.2*	1 *0.4*	3 *1.9*	29 *11.4*	18 *5.1*
S/SO_4		2 *0.6*	6 *1.9*	13 *2.3*	26 *7.6*	20 *0.7*	5 *0.7*	5 *0.6*
KCl extraction on fresh soil								
N/NO_3	kg ha^{-1}	0 *0.0*	0 *0.0*	0 *0.0*	0 *0.0*	3 *1.0*	15 *7.5*	9 *2.9*
N/NH_4		1 *0.1*	1 *0.1*	1 *0.3*	1 *0.5*	7 *3.7*	7 *2.1*	7 *1.7*
KCl extractions (except for K, NH_4Cl extraction) (air-dry soil)								
K	kg ha^{-1}	19 *4.9*	77 *63.5*	12 *2.2*	12 *1.9*	60 *39.8*	35 *28.7*	10 *6.3*
Ca		71 *19.0*	8 *1.9*	19 *18.3*	3 *2.3*	4 *4.4*	16 *16.4*	55 *32.0*
Mg		55 *12.3*	14 *1.7*	8 *1.6*	6 *1.5*	10 *10.2*	12 *12.2*	4 *4.3*
Na		1 *1.0*	0 *0.0*	2 *2.2*	0 *0.0*	0 *0.0*	0 *0.0*	12 *12.2*
H		4 *1.9*	2 *0.2*	3 *0.2*	2 *0.1*	3 *0.1*	5 *0.8*	0 *0.0*
Al		121 *45.4*	143 *20.1*	207 *15.9*	251 *12.1*	423 *27.1*	531 *54.8*	148 *36.3*
Saturation	cmolc/kg	1.5 *0.31*	0.3 *0.12*	0.1 *0.04*	0.1 *0.01*	0.1 *0.01*	0.0 *0.01*	0.0 *0.01*
CEC	cmolc/kg	3.8 *0.90*	1.4 *0.15*	1.1 *0.10*	0.9 *0.07*	0.7 *0.02*	0.4 *0.03*	0.0 *0.01*
N/NO_3	kg ha^{-1}	1 *0.3*	1 *0.1*	1 *0.3*	3 *1.0*	11 *3.5*	81 *32.4*	62 *18.2*
S (total)		37 *3.0*	77 *14.2*	195 *12.6*	402 *84.4*	546 *14.3*	298 *57.9*	262 *65.8*
P (total)		4 *1.4*	7 *2.4*	7 *2.8*	9 *3.5*	23 *10.8*	44 *22.0*	47 *27.7*
Specific extractions								
S/SO_4	kg ha^{-1}	7 *0.8*	14 *4.4*	27 *7.1*	64 *22.5*	71 *15.9*	6 *5.6*	0 *0.0*
P/PO_4		4 *1.2*	11 *9.1*	17 *15.6*	1 *0.1*	2 *0.6*	20 *14.3*	19 *15.4*

Table A-17 Specific extractions performed on soils at age 2 years after planting: Treatment 5. Mean and standard errors (when n≥3) are given.

		Treatment 5											
		0-5 cm		5-15 cm		15-30 cm		30-50 cm		50-100 cm	100-200 cm	200-300 cm	
Water extraction on fresh soil													
Ca	kg ha^{-1}	1	*0.1*	2	*0.2*	3	*0.6*	3	*0.1*	5	14	12	
Mg		0	*0.0*	1	*0.0*	1	*0.1*	1	*0.1*	2	6	5	
Na		2	*0.2*	3	*0.4*	6	*2.1*	5	*1.1*	15	24	29	
H		0	*0.1*	1	*0.0*	2	*0.4*	1	*0.1*	2	8	6	
Al		12	*4.3*	4	*2.5*	14	*8.0*	6	*2.1*	11	5	5	
N/NH_4		0	*0.2*	1	*0.3*	2	*0.7*	3	*0.7*	9	19	17	
N/NO_3		0	*0.2*	1	*0.1*	1	*0.1*	1	*0.1*	1	46	43	
S/SO_4		1	*0.2*	7	*0.8*	13	*3.8*	12	*1.0*	13	7	6	
KCl extraction on fresh soil													
N/NO_3	kg ha^{-1}	0	*0.0*	0	*0.0*	0	*0.1*	0	*0.1*	1	31	0	0
N/NH_4		1	*0.2*	1	*0.1*	2	*0.4*	2	*0.3*	4	8	10	1
KCl extractions (except for K, NH_4Cl extraction) (air-dry soil)													
K	kg ha^{-1}	15	*1.9*	13	*0.5*	11	*0.6*	8	*1.4*	17	21	8	15
Ca		23	*3.6*	1	*0.6*	3	*3.1*	4	*2.1*	86	0	3	23
Mg		5	*1.0*	1	*0.1*	3	*2.0*	2	*1.7*	36	9	19	5
Na		0	*0.0*	0	*0.0*	0	*0.0*	0	*0.0*	448	0	0	0
H		3	*0.7*	2	*0.2*	8	*5.3*	2	*0.8*	5	6	0	3
Al		118	*31.0*	167	*1.0*	227	*3.9*	226	*5.4*	377	500	137	118
Saturation	cmolc/kg	0.4	*0.03*	0.1	*0.01*	0.1	*0.02*	0.2	*0.13*	0.1	0.0	0.0	
CEC	cmolc/kg	2.4	*0.41*	1.2	*0.02*	1.1	*0.06*	1.0	*0.20*	0.8	0.5	0.0	
N/NO_3	kg ha^{-1}	2	*0.3*	2	*0.2*	3	*1.0*	4	*1.3*	24	66	92	2
S (total)		42	*9.7*	141	*26.7*	238	*71.3*	221	*38.9*	281	21	0	42
P (total)		3	*1.5*	8	*2.9*	9	*3.9*	11	*6.7*	11	23	40	3
Specific extractions													
S/SO_4	kg ha^{-1}	5	*0.4*	17	*1.8*	30	*9.0*	28	*3.9*	22	0	0	5
P/PO_4		7	*2.9*	1	*0.1*	2	*0.0*	1	*0.1*	20	6	9	7

ARTICLE

European Journal of Soil Science, October 2008, **59,** 863–877 doi: 10.1111/j.1365-2389.2008.01059.x

Influence of land use (savanna, pasture, *Eucalyptus* plantations) on soil carbon and nitrogen stocks in Brazil

V. MAQUERE[a,b], J. P. LACLAU[b,d], M. BERNOUX[c], L. SAINT-ANDRE[b], J. L. M. GONÇALVES[d], C. C. CERRI[e], M. C. PICCOLO[e] & J. RANGER[f]

[a]*ENGREF, 19 av. du Maine, 75732 Paris Cedex 15, France*, [b]*CIRAD, UPR80, TA 10/D, 34398 Montpellier Cedex 5, France*, [c]*IRD, UR SeqBio, SupAgro – Bâtiment 12, 2 place Viala, 34060 Montpellier Cedex 1, France*, [d]*Department of Forest Sciences, ESALQ/USP, Piracicaba, SP, Brazil*, [e]*Laboratório de Biogeoquímica Ambiental, CENA/USP, Piracicaba, SP, Brazil, and* [f]*INRA Centre de Nancy, Biogéochimie des Ecosystèmes Forestiers, 54280 Champenoux, France*

Summary

In Brazil, most *Eucalyptus* stands have been planted on Cerrado (shrubby savanna) or on Cerrado converted into pasture. Case studies are needed to assess the effect of such land use changes on soil fertility and C sequestration. In this study, the influence of Cerrado land development (pasture and *Eucalyptus* plantations) on soil organic carbon (SOC) and nitrogen (SON) stocks were quantified in southern Brazil. Two contrasted silvicultural practices were also compared: 60 years of short-rotation silviculture (EUC_{SR}) versus 60 years of continuous growth (EUC_{HF}). C and N soil concentrations and bulk densities were measured and modelled for each vegetation type, and SOC and SON stocks were calculated down to a depth of 1 m by a continuous function.

Changes in SOC and SON stocks mainly occurred in the forest floor (no litter in pasture and up to 0.87 kg C m^{-2} and 0.01 kg N m^{-2} in EUC_{SR}) and upper soil horizons. C and N stocks and their confidence intervals were greatly influenced by the methodology used to compute these layers. C/N ratio and ^{13}C analysis showed that down to a depth of 30 cm, the Cerrado organic matter was replaced by organic matter from newly introduced vegetation by as much as 75–100% for pasture and about 50% for EUC_{HF}, poorer in N for *Eucalyptus* stands (C/N larger than 18 for *Eucalyptus* stands). Under pasture, 0–30 cm SON stocks (0.25 kg N m^{-2}) were between 10 and 20% greater than those of the Cerrado (0.21 kg N m^{-2}), partly due to soil compaction (limit bulk density at soil surface from 1.23 for the Cerrado to 1.34 for pasture). Land development on the Cerrado increased SOC stocks in the 0–30 cm layer by between 15 and 25% (from 2.99 (Cerrado) to 3.86 (EUC_{SR}) kg C m^{-2}). When including litter layers, total 0–30 cm carbon stocks increased by 35% for EUC_{HF} (4.50 kg C m^{-2}) and 53% for EUC_{SR} (5.08 kg C m^{-2}), compared with the Cerrado (3.28 kg C m^{-2}), independently of soil compaction.

Introduction

Organic matter (OM) is an essential component for soil fertility: it is a direct source of nutrients and contributes to cation retention, soil structure and biological activity. Soil organic nitrogen (SON) is essential because nitrogen is involved in numerous physiological functions and is the most abundantly accumulated nutrient in plant biomass (Marschner, 1995). As for soil organic carbon (SOC), the present debate on climate change has highlighted the importance of high soil C storage capacity that is still poorly quantified at this time (Intergovernmental Panel on Climate Change, 2001). Organic matter is essential in tropical soils where primary minerals have generally been totally depleted (Feller & Beare, 1997). To exemplify this, wood production in tropical *Eucalyptus* plantations planted on poor soils has been shown to be dependent on the amount of organic matter left on-site when the former stand was harvested (Nambiar *et al*., 2004).

In Brazil, *Eucalyptus* plantations have been introduced since the beginning of the 20th century on more than three million hectares and obtain high yields (typically, 40–50 m^3 ha^{-1} $year^{-1}$). Their management can greatly modify soil chemical and physical properties (Gonçalves *et al*., 2004). It was observed in the Congo that long-term silviculture of *Eucalyptus* led to

Correspondence: V. Maquère. E-mail: valerie.maquere@m4x.org
Received 4 May 2007; revised version accepted 29 May 2008

imbalanced N budgets (Laclau *et al*., 2005), which can result in SON impoverishment. The quantification of SOC and SON changes is thus essential to assess the long-term impact of *Eucalyptus* plantations on soil fertility compared with more traditional land uses (Cerrado and pasture in Brazil).

In the Amazon, SOC stocks were estimated in primitive forest on the regional scale (Moraes *et al*., 1995; Bernoux *et al*., 1998a, 2002). Other studies were conducted in Brazil on the plot scale when native vegetation (Cerrado or primitive forest) was converted to pasture or crops (Moraes *et al*., 1996; Bernoux *et al*., 1998c; De Freitas, 2000; Cerri *et al*., 2004; Corbeels *et al*., 2006). However, little information is available concerning the impact of pine (Smith *et al*., 2002; Lilienfein & Wilcke, 2003) and *Eucalyptus* plantations (Lepsch, 1980; Zinn *et al*., 2002; Lima *et al*., 2006) on SOC and SON stocks. Moreover, one possible option for increasing carbon sequestration in tropical forest plantations (clean development mechanisms) discussed in post-Kyoto meetings would be to lengthen rotation time. The influence of this silvicultural scenario on SOC and SON stocks has not yet been studied in Brazilian *Eucalyptus* plantations.

This study aimed at: (i) quantifying, on a hectare basis, the influence of different Cerrado land developments (pasture versus *Eucalyptus* plantations) on SOC and SON stocks, 20 and 60 years after land use change; (ii) assessing the influence of contrasted silvicultural practices (60 years of continuous growth versus short-rotation silviculture over 60 years) on SOC and SON storage; (iii) quantifying the effect of soil compaction on SOC and SON stocks; and (iv) modelling SOC and SON stocks down to a depth of 1 m using a continuous function for each land use.

Material and methods

Experimental area

The study was conducted at the experimental station of São Paulo University, Itatinga, Brazil (23°02′S, 48°38′W). The climate is *Cfa* according to the Köppen classification. The average annual precipitation was 1370 mm and the average annual temperature was 19.2°C from 1990 to 2004.

The relief is typical of the São Paulo Western Plateau, with topography varying from flat to hilly (FAO, 1977). The maximum altitude is 860 m. The lithology is a Cretaceous sandstone belonging to the Marília formation and the Bauru group.

Soil spatial distribution is organized according to altitude and slope. Sampled plant communities are located on 'latosolos vermelhos amarelos distroficos typicos A', according to the Brazilian classification (EMBRAPA, Centro Nacional de Pesquisa de Solos, 1999), and Ferralsols, according to the FAO classification. Preliminary geomorphological studies showed that their occurrence at the Itatinga Experimental Station corresponded to altitudes > 800 m and slopes $< 10\%$.

Sampled vegetation types (VT)

Soils were sampled under five plant communities: a prevailing shrub and tree savanna known as Cerrado (CER) in Brazil, a pasture established on this Cerrado 20 years ago (PAS_{20}), a pasture established on this Cerrado 80 years ago (PAS_{80}), a 60-year-old *Eucalyptus saligna* Smith stand managed in short rotations of 6–10 years (EUC_{SR}), and a 60-year-old *Eucalyptus saligna* high forest (EUC_{HF}). The dominant species of both pastures is *Brachiaria*. The dominant species of the plant communities sampled are given in Maquère, 2004. Both *Eucalyptus* stands were planted between 1941 and 1944 on 20-year-old pastures, previously established on the same Cerrado. For all vegetation types (VT), the slope was less than 10% (Table 1).

Emphasis was placed on choosing sites whose history was well known (from 60 years ago to today), that presented homogenous ecological conditions (soil, geology, topography). Such sites were scarce because 60-year-old *Eucalyptus* high forests are quite exceptional in Brazil. One site for each vegetation type was found within a 2-km-radius area (Figure 1). The soil spatial heterogeneity within and between vegetation types was then carefully studied (see below) to make sure that SOC and SON stock variations resulted from land use change and not from differences in ecological conditions.

Table 1 Characteristics of the five studied vegetation types

Vegetation type (VT)	Abbreviation	Vegetation	Slope/°	Management
Cerrado	CER	*Shrubs and Graminaceae*	4	Casual extensive pasture
20-year-old pasture	PAS_{20}	*Brachiaria*	7	Extensive pasture
80-year-old pasture	PAS_{80}	*Brachiaria*	6	Extensive pasture
Eucalyptus short-rotation management since 1944	EUC_{SR}	*Eucalyptus saligna*	1	Coppice management from 1944 to 1997: 6–10 year-long rotations, no fertiliser input Site replanted in 1998 with 1667 trees ha^{-1} density. Fertilisation at planting: 300 kg ha^{-1} NPK 10:20:10 Chemical weeding (glyphosate) the first year after planting
Eucalyptus high forest planted in 1944	EUC_{HF}	*Eucalyptus saligna*	1	Casual local thinning

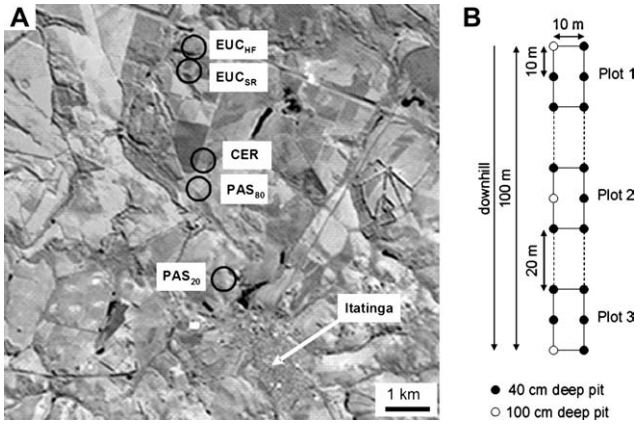

Figure 1 Localization of each sampled vegetation type (a) and sampling design used in each one of them (b) CER = Cerrado; EUC_{SR} = 60-year-old *Eucalyptus saligna* Smith stand managed in short rotations; EUC_{HF} = 60-year-old *Eucalyptus saligna* high forest; PAS_{20} = pasture installed on the Cerrado 20 years ago; PAS_{80} = pasture installed on the Cerrado 80 years ago.

Sampling

In each VT, three plots were positioned along a 100-m long transect going down the slope. Each plot was composed of five 40-cm deep pits, plus one 100-cm deep soil pit. All in all, 18 pits were sampled in each vegetation type (Figure 1). Soils were sampled with a 10-cm diameter corer at depths of 0–5 cm, 5–10 cm, 10–20 cm, 20–30 cm and 30–40 cm, plus 40–60 cm, 60–80 cm and 80–100 cm for the 100–cm deep soil pits. Sampling was performed at a fixed depth since no clear limit between soil horizons could be observed.

Soils were oven dried at 40°C, passed through a 2-mm mesh, and an aliquot was ground to 150 μm for carbon and nitrogen determination (LECO analyser). Individual analyses were performed for each sample collected. A soil aliquot was dried at 105°C for residual humidity and bulk density determinations. Individual bulk density was measured for each sample in order to avoid any systematic error due to the use of an average bulk density (Arrouays *et al*., 2003).

Litter (L1) was sampled in each vegetation type with a 30-cm diameter metal ring at 1 m from each pit. For EUC_{HF}, the litter sampling scheme needed to be adapted: a supplementary layer (L2) made of charcoal, sand and a dense root material that adhered to decomposed OM was observed between the fresh litter layer and the mineral soil. Such a litter structure had already been observed in Congolese *Eucalyptus* plantations (Laclau *et al*., 2004). This layer was sampled for each pit, whenever present, using a 225-cm^2 frame, and its thickness was measured. Litter and roots were dried at 65°C. L1 litter was divided into four fractions (bark, branch, leaf and miscellaneous), each fraction was weighed, and one composite sample per fraction and per plot was ground for C and N determination. L2 litter was divided into three fractions: charcoal, roots and pieces of vegetal matter > 2mm, and mineral and organic particles < 2 mm. Each fraction was weighed and then ground for C and N determination.

Soil parent material homogeneity between and within vegetation types

Preliminary studies showed that the soils of the sampled region were spatially distributed according to topography and differed by their particle size distribution and mineralogy (EMBRAPA, Centro Nacional de Pesquisa de Solos, 1999). These characteristics, little affected by land use in deep soil horizons, were chosen to check the homogeneity of the soil parent material.

A particle-size analysis and a pedological description were performed in each vegetation type for a whole profile down to a depth of 1 m. For particle size distribution, differences among VT were expected to occur in the accumulation horizon, i.e. beyond a depth of 40 cm (EMBRAPA, Centro Nacional de Pesquisa de Solos, 1999). Soil layers deeper than 40 cm were thus considered as a unique layer, and their corresponding particle size distribution values were taken as a unique data set for each VT.

For three pits per vegetation type, a mineralogical analysis was performed by X-ray diffraction on soil samples collected in the 80–100 cm layer. The X-ray diffractometer was a Siemens D5000 (Siemens AG, Munich, Germany) equipped with a Cu anticathode and a graphite monochromator (30 mA and 40 KeV). The rotation speed was 0.02° s^{-1} (absolute). The diffractograms were performed on powder made from the whole soil.

^{13}C measurements

In each vegetation type, $\delta^{13}C$ was measured down to a depth of 1 m for one soil profile and its corresponding L1 and/or L2 litter samples. One composite sample consisting of ground roots dried at 65°C was also analysed for each VT. The isotopic composition of soil organic matter closely resembles the isotopic composition of the vegetation from which it is derived because the fractionation during decomposition is small relative to the original fractionation during C fixation (Peterson & Fry, 1987; Nadelhoffer & Fry, 1988; Bernoux *et al*., 1998c). When one type of vegetation is replaced by another, $\delta^{13}C$ values can be used to identify soil OM derived from the original vegetation residues (Cerrado) or from the new vegetation residues. The C content of each component is given by Cerri *et al*. (1985), Bernoux *et al*. (1998c) and Wilcke & Lilienfein (2004):

$$C_{VT}(x) = C_{Original}(x) + C_{Veg}(x), \quad (1)$$

$$C_{Veg}(x) = Q_{Veg}(x) \times C_{VT}(x), \quad (2)$$

$$\begin{aligned} C_{Original}(x) &= Q_{Original}(x) \times C_{VT}(x) \\ &= (1 - Q_{Veg}(x)) \times C_{VT}(x), \end{aligned} \quad (3)$$

$$Q_{\mathrm{Veg}}(x) = \frac{\delta^{13}C_{\mathrm{VT}}(x) - \delta^{13}C_{\mathrm{CER}}}{\delta^{13}C_{\mathrm{Veg}}(x) - \delta^{13}C_{\mathrm{CER}}}, \quad (4)$$

where $C_{\mathrm{VT}}(x)$ is the C concentration function in % measured at depth x in vegetation type VT. $Q_{\mathrm{Original}}(x)$ and $C_{\mathrm{Original}}(x)$ are the C fraction and the C concentration in % taken from the C pool before the land use change, and $Q_{\mathrm{Veg}}(x)$ and $C_{\mathrm{Veg}}(x)$ are the C fraction and the C concentration in % taken from the present vegetation type at depth x. $\delta^{13}C_{\mathrm{VT}}(x)$ is the $\delta^{13}C$ measured at depth x in the vegetation type VT, $\delta^{13}C_{\mathrm{CER}}(x)$ is the $\delta^{13}C$ measured in the Cerrado at the same depth x, and $\delta^{13}C_{\mathrm{Veg}}$ is the $\delta^{13}C$ signature of the fresh organic matter input of the present vegetation and was taken as the average litter and root $\delta^{13}C$ values for each vegetation type (Bernoux *et al.*, 1998c). Differences in the $\delta^{13}C$ signature were considered significant if greater than 1‰.

Calculations

Carbon and nitrogen concentration profiles. A preliminary analysis showed that C and N concentrations were quite similar for all VT beyond a depth of 40 cm. An adaptation of the classical exponential decay type equation was thus chosen to model C and N vertical distribution, inspired from the model used by Arrouays and Pélissier (1994) and Bernoux *et al.* (1998b).

$$\text{Model 1} \qquad f_{\mathrm{VT}}(x) = a + b_{\mathrm{VT}} \exp(-c_{\mathrm{VT}}x), \quad (5)$$

$$b_{\mathrm{VT}} = \frac{a - \overline{f_{\mathrm{VT}}(x<5)}}{\exp(-\overline{(x<5)}c_{\mathrm{VT}})} \quad (6)$$

where f is the C or N concentration function in %, and x is the depth in cm. VT is a label for the vegetation type. The a parameter is the asymptotic depth limit concentration ($x \to \infty$) fitted in common to all vegetation types, in other words, it is constant within a given ecological region (global), $a + b_{\mathrm{VT}}$ is the concentration on the surface ($x = 0$), b_{VT} is an input variable obtained from solving Equation 2 for the limit condition on the surface $x \in \{x<5\}$, $\overline{(x<5)}$ is the average $x \in \{x<5\}$, and $\overline{f_{\mathrm{VT}}(x<5)}$ is the average $f_{\mathrm{VT}}(x) \in \{f_{\mathrm{VT}}(x<5)\}$ (for each VT), b_{VT} is vegetation type-dependent within a given ecological region (local) and can be easily obtained from soil measurements, and c_{VT} is the exponential decrease rate for each VT and is the only parameter dependent of vegetation type to be fitted.

Bulk density profiles. Preliminary studies showed that bulk densities were quite similar for all VT beyond a depth of 40 cm. Bulk density profiles were thus modelled using a quadratic polynomial equation whose depth limit value was the same for all vegetation types:

$$\text{Model 2} \quad d_{\mathrm{VT}}(x) = \alpha_{\mathrm{VT}} + \beta_{\mathrm{VT}}x - \gamma_{\mathrm{VT}}^2x^2, \quad \text{if } x < 40 \text{ cm} \quad (7)$$

$$d_{\mathrm{VT}}(x) = \delta, \quad \text{if } x \geq 40 \text{ cm} \quad (8)$$

$$\beta_{\mathrm{VT}} = \frac{\delta - \alpha_{\mathrm{VT}}}{40} + 40\,\gamma_{\mathrm{VT}}^2, \quad (9)$$

where d_{VT} is the bulk density, x the depth in cm, β_{VT} is derived from $d_{\mathrm{VT}}(40)$ to complete the model continuity for $x = 40$ cm ($d_{\mathrm{VT}}(40) = \delta$), and α_{VT} and γ_{VT} are the parameters to be fitted, α_{VT} is the bulk density on the surface ($x \to 0$). The maximum bulk density is $d_{\max}$ and is reached for a depth $x_{\max}$, α_{VT} and γ_{VT} are local parameters, whereas δ is a global parameter.

Comparison between local and global fits

After building and simplifying, Models 1 and 2 were fitted for each vegetation type (local models) and for the whole set of data (global models) using PROC MODEL of SAS software (www.sas.com). Differences among local and global models were evaluated from F-tests calculated on the residual. This test is based on the sums of squares of errors (SSE) and the total number of parameters involved in the models. It compares F_{obs} and F_{tab} calculated as:

$$F_{\mathrm{obs}} = \frac{(SSE_2 - SSE_1)/(p_1 - p_2)}{SSE_1/(n - p_1)}, \quad (10)$$

where p_1 is the number of parameters for the local model, p_2 is the number of parameters for the global model ($p_2 < p_1$), SSE_1 is the sum of square errors for the local model, SSE_2 is the sum of square errors for the global model, and n is the number of observations. F_{tab} is the theoretical value given in the Fischer's table $F_{\mathrm{tab}} = F(p_1{-}p_2, n{-}p_1)$. If $F_{\mathrm{obs}} > F_{\mathrm{tab}}$ then the local model described the data set better than the global model and there was a significant effect of the vegetation type on the studied function (Brown & Rothery, 1993). All differences were considered significant at a 5% threshold.

Soil C and N stocks as a function of depth

SOC and SON stocks were calculated by multiplying the C or N model by the bulk density model and integrating it from 0 to a fixed depth.

$$\text{Model 3} \quad S_{\mathrm{VT}}(x) = \int_0^x f_{\mathrm{VT}}(\mu)d_{\mathrm{VT}}(\mu)d\mu, \quad (11)$$

where S_{VT} is the C or N stock function in kg m^{-2}, x the depth in m, f_{VT} the C or N concentration function in % obtained from Model 1 (Equations 5 and 6), and d_{VT} the bulk density function obtained from Model 2 (Equations 7–9).

C and N stocks were then computed continuously from the soil mineral surface down to a depth of 1 m. Confidence intervals (CI) were calculated for these stocks from the following equation (Parresol, 1999):

$$\hat{S} \pm t_{\left(\frac{\alpha}{2}\right)} \sqrt{Var_{\hat{S}}^2 + \frac{\hat{\sigma}^2 x^{\hat{k}}}{18}}, \qquad (12)$$

where $\hat{S}$ is the estimated C or N stock, x is the depth in cm, and

$$Var_{\hat{S}}^2 = \left(\frac{\partial S}{\partial \beta}\right)' \hat{\Sigma}_\beta \left(\frac{\partial S}{\partial \beta}\right). \qquad (13)$$

$Var_{\hat{S}}^2$ is the variance of $\hat{S}$ with $\partial S/\partial\beta$ the derivative matrix of S with respect to the matrix set of parameters β, $(\partial S/\partial\beta)'$ the transpose matrix of $\partial S/\partial\beta$, and $\hat{\Sigma}_\beta$ the covariance matrix of the model parameter (delta method; Serfling, 1980), $\hat{\sigma}^2$ is the estimated variance of the model and $x^{\hat{k}}$ the estimated weighted function with k being the optimal exponent for correcting the data heteroscedasticity. The second term under the square root $\hat{\sigma}^2 X^{\hat{k}}/18$ stands for the residual variability of the model spread over the 18 pits considered independently. It contains the $\overline{f_{VT}(x<5)}$ surface parameter contribution to the model variability.

In order to minimize the influence of localized, large C or N surface concentrations in the 0–5 cm bulk soil layer or the L2 litter layer for EUC_{HF} (due to charcoal, OM fragments, etc.) on the model parameters, Model 3 was fitted without these localized C or N concentration points. A stock profile was then considered to be the sum of two components (Figure 2): (i) a main component computed from Model 3 and the $f_{VT}(x<5)$ value of the profile studied as an input parameter; and (ii) a second component computed as the measured stock minus its estimated main component resulting from (i). The average stock for each VT was obtained by taking the main component from Model 3 with $\overline{f_{VT}(x<5)}$ as an input parameter, and the second component as the average of the second component for all 18 pits. For EUC_{HF}, because there was no clear limit between the L2 litter layer and the mineral soil itself, the L2 layer (root fraction excluded) was included in the soil profile and was computed, whenever present, as the particular points mentioned above (Figure 2).

SOC and SON stocks as a function of soil mass

SOC and SON stock changes can also be assessed independently of soil compaction. The common stock calculation (Intergovernmental Panel on Climate Change, 1997) integrates soil stocks down to a fixed depth, that is, it calculates the stocks contained in a fixed volume. Changes in stocks may then result from a soil mass increase (or decrease) in this fixed volume, as well as from an absolute C or N enrichment (or depletion) of the volume solid phase itself. This effect can be avoided by integrating the stocks down to a fixed soil mass instead of to a fixed soil depth (Ellert *et al*., 2002).

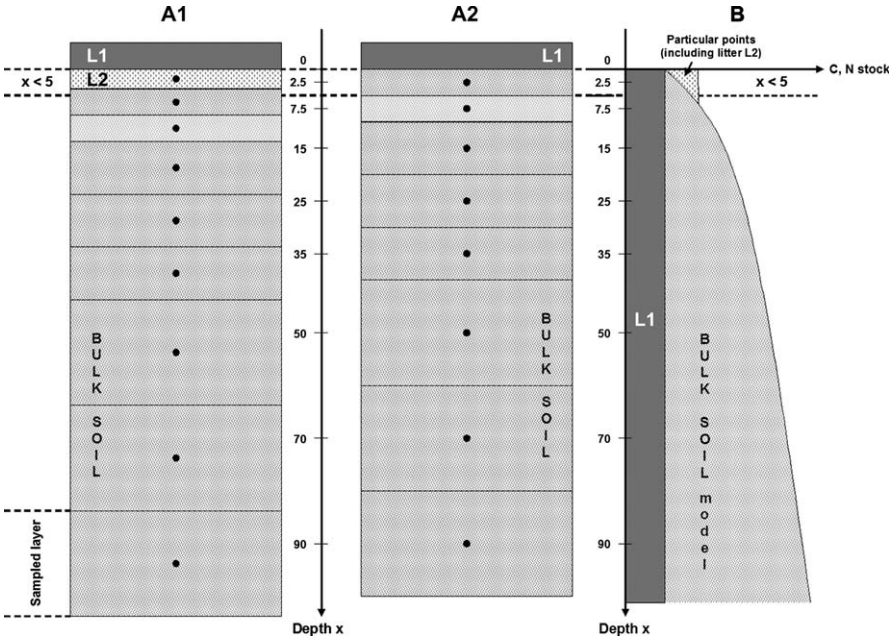

Figure 2 Organization of litter layers and soil profile whenever litter L2 is present (EUC_{HF}) (A1) or not (A2). Conceptual distribution of total C and N stock between L1 litter, particular points (L2 litter included), and the bulk soil component of the model (Model 3) for a sampled pit (B) Note that $\overline{(x<5)} = 2.5$ whenever L2 is not present (soil layers are sampled at fixed depths). In EUC_{HF}, $\overline{(x<5)} \neq 2.5$ because L2 is considered part of the soil profile and its thickness is not necessarily 5.

For all vegetation types, the depth intervals were converted to soil mass based on the bulk density measurements per soil sample. C and N profiles were modelled as a function of soil mass using the same exponential decay-type function as in Model 1.

Soil C and N profiles were then:

$$\text{Model 4} \quad f_{VT}(m) = a + b_{VT} \exp(-c_{VT} m), \qquad (14)$$

$$b_{VT} = \frac{a - \overline{f_{VT}(m < 62)}}{\exp(-\overline{(m < 62)} c_{VT})}, \qquad (15)$$

where f_{VT} is the C or N concentration function in %, m is the soil mass in kg m^{-2}, and a and c_{VT} are the parameters to be fitted. The average soil mass per unit area of the Cerrado 0–5 cm bulk soil layer is 62 kg m^{-2}.

The resulting stocks were then calculated as:

$$\text{Model 5} \; S_{VT}(m) = \int_0^m (a + b_{VT} \exp(-c_{VT} \mu)) d\mu. \qquad (16)$$

This model is simple to integrate and to fit, and avoids the use of a complex bulk density model. The confidence intervals were obtained using the method described above.

Results

Soil parent material homogeneity between and within vegetation types

For particle-size analysis, differences in clay contents among vegetation types were less than 5% (Figure 3). They were not significant at a 5% threshold except for PAS_{20} and EUC_{SR}, for which the average clay contents differed by 4%. These differences were close to the measurement accuracy.

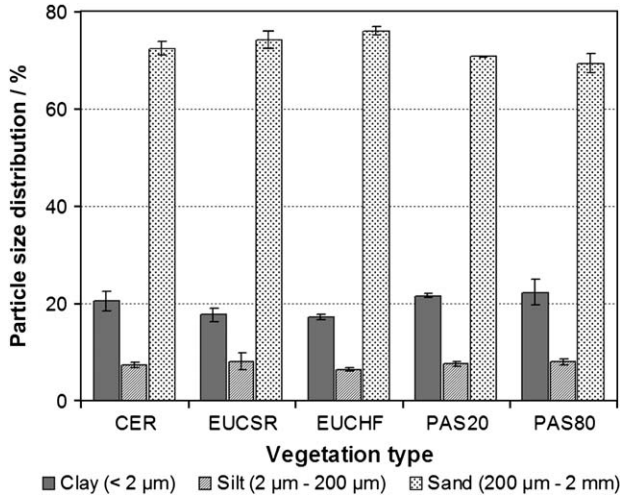

Figure 3 Homogeneity of soil parent material of the five studied vegetation types checked by particle size analysis of the 40–100 cm soil layer. Vertical bars represent the standard error ($n = 5$); CER, EUC_{SR}, EUC_{HF}, PAS_{20}, PAS_{80}: see Table 1.

All vegetation types presented a quasi-identical mineralogical X-ray signature in their 80–100-cm layer. X-ray spectra showed the presence of quartz, kaolinite, hematite, goethite and gibbsite. A non-attributed silicate layer (probably vermiculite) was suggested by a peak that occurred between 2 and 6 degrees 2 θ. Its identification would have required further analysis. As this silicate was rather scarce, it was not considered within the scope of this study. It was thus concluded that all vegetation types shared the same parent material, and that selected sites met the requirements for the study.

Litter layers and particular points

Some surface samples (0–5 cm bulk soil layer and the L2 litter layer) had large C and N concentrations and low bulk densities, which corresponded to local specificities such as litter remains, charcoal, pieces of termite mound or ant-hill, and localized OM accumulation. Such samples were considered as outliers and were found in EUC_{SR} (seven pits), EUC_{HF} (L2 litter present for 13 pits), and PAS_{20} (six pits). For EUC_{HF}, the thickness of the L2 layer ranged from one to 10 cm, with an average of 3.6 cm. Approximately 90% of its biomass consisted of finely divided OM ($\leq$ 1 mm). The C stocks of the second component of particular points were 0.36 kg C m^{-2} for EUC_{HF}, 0.35 kg C m^{-2} for EUC_{SR}, and 0.03 kg C m^{-2} for PAS_{20}. These points accounted for N stocks less than 0.05 kg N m^{-2} (Table 2).

L1 biomass was greatest for EUC_{SR} and negligible for both pastures. C litter stocks were greatest for EUC_{SR} (0.87 kg C m^{-2}), followed by EUC_{HF} (0.46 kg C m^{-2}) and CER (0.29 kg C m^{-2}). Nitrogen amounts within the forest floor were less than 0.01 kg N m^{-2} for all vegetation types (Table 2).

Bulk density

Bulk densities ranged from an average of 1.28 kg dm^{-3} for the 0–5 cm layer, to an average of 1.38 kg dm^{-3} for the 80–100 cm layer. Their depth profiles presented a bump between a depth of 0 and 40 cm, and remained constant below 40 cm (Figure 4). F tests showed that Model 2 could be simplified by fixing the α parameter common to all arboreal formations ($\alpha_{CER} = \alpha_{EUCHF} = \alpha_{EUCSR}$) and to both pastures ($\alpha_{PAS20} = \alpha_{PAS80}$), as well as by fixing the γ parameter common to all situations except for EUC_{HF} (Table 3). As a result, the CER and EUC_{SR} situations shared common bulk density profiles, as did both pastures. EUC_{HF} presented a single bulk density profile (Figure 4). The bulk density at the surface (α parameter) was greater under pastures ($\alpha = 1.34$ kg dm^{-3}) than under arboreal vegetation types ($\alpha = 1.23$ kg dm^{-3}). The maximum bulk density, d_{max}, was greater under pastures ($d_{max} = 1.49$) than under CER and EUC_{SR} ($d_{max} = 1.45$ kg dm^{-3}), and least for EUC_{HF} ($d_{max} = 1.39$ kg dm^{-3}). This maximum bulk density

Table 2 Biomass of litter layers and distribution of C and N stocks between the different components of the model. Confidence intervals at 95% are indicated, and the contribution of the surface parameter ($\overline{f_{VT}(x<5)}$) to stock CI is given between parenthesis

	CER[a]		EUC_{SR}[a]		EUC_{HF}[a]		PAS_{20}[a]		PAS_{80}[a]	
Carbon stocks/kg C m^{-2}										
Litter L1	0.29 ± *0.048*		0.87 ± *0.142*		0.46 ± *0.106*		0.00 ± *0.000*		0.00 ± *0.000*	
Particular points[b]	0.00 ± *0.000*		0.35 ± *0.270*		0.36 ± *0.333*		0.03 ± *0.028*		0.00 ± *0.000*	
Bulk soil[c]										
0–30 cm	2.99 ± *0.207*	(50%)	3.86 ± *0.243*	(50%)	3.68 ± *0.284*	(53%)	3.46 ± *0.181*	(64%)	3.72 ± *0.179*	(59%)
0–100 cm	7.27 ± *0.524*	(27%)	8.08 ± *0.489*	(18%)	8.11 ± *0.606*	(42%)	8.19 ± *0.534*	(23%)	8.56 ± *0.630*	(28%)
Total										
0–30 cm	3.28 ± *0.212*		5.08 ± *0.390*		4.50 ± *0.450*		3.50 ± *0.183*		3.72 ± *0.179*	
0–100 cm	7.56 ± *0.526*		9.31 ± *0.580*		8.93 ± *0.699*		8.22 ± *0.535*		8.56 ± *0.630*	
Nitrogen stocks/kg N m^{-2}										
Litter L1	0.09 ± *0.001*		0.01 ± *0.002*		0.01 ± *0.001*		0.00 ± *0.000*		0.00 ± *0.000*	
Particular points[b]	0.00 ± *0.000*		0.01 ± *0.009*		0.00 ± *0.021*		0.00 ± *0.002*		0.00 ± *0.000*	
Bulk soil[c]										
0–30 cm	0.21 ± *0.010*	(91%)	0.22 ± *0.007*	(65%)	0.20 ± *0.016*	(84%)	0.25 ± *0.009*	(54%)	0.24 ± *0.009*	(54%)
0–100 cm	0.51 ± *0.029*	(29%)	0.48 ± *0.032*	(50%)	0.45 ± *0.055*	(9%)	0.56 ± *0.033*	(18%)	0.55 ± *0.031*	(17%)
Total										
0–30 cm	0.22 ± *0.010*		0.24 ± *0.011*		0.20 ± *0.022*		0.25 ± *0.009*		0.24 ± *0.009*	
0–100 cm	0.52 ± *0.029*		0.50 ± *0.033*		0.46 ± *0.057*		0.56 ± *0.033*		0.55 ± *0.031*	
Biomass/kg m^{-2}										
Litter L1	0.86 ± *0.136*		1.92 ± *0.313*		1.04 ± *0.237*		0.00 ± *0.000*		0.00 ± *0.000*	
Litter L2					11.86 ± *4.809*					
Particular point frequency[d]										
	0		7		13		6		0	

[a]CER, EUC_{SR}, EUC_{HF}, PAS_{20}, PAS_{80}: see Table 1.
[b]Outliers of the 0–5 cm bulk soil layer and L2 litter.
[c]First component of the model (Model 3).
[d]Number of pits out of 18 pits per vegetation type presenting particular points in its 0–5 cm bulk soil layer or L2 litter layer, whenever present (EUC_{HF}).

was reached closer to the surface for pastures (x_{max} = 22.14 cm) than for CER and EUC_{SR} (x_{max} = 26.43 cm) and corresponded to a bump in the bulk density profile. Under EUC_{HF}, this bump disappeared so that d_{max} was confounded with δ (depth limit parameter) and was thus reached for x_{max} = 40 cm.

All root mean square errors (RMSE) obtained using Model 2 were less than 0.1 (Table 4), that is, of the same order of magnitude as the estimated accuracy of the measurement. Heterogeneity was greatest under arboreal VT and least under pastures. *F*-tests showed that the effect of vegetation type on Model 2 was significant (Table 4).

Carbon and nitrogen contents

C and N contents decreased with soil depth from an average of 1.25% C and 0.07% N for the 0–5 cm layer, to an average of 0.42% C and 0.03% N for the 80–100 cm layer (Figure 5). Surface C and N contents for $x = 0$ ($a + b$ calculated variable in model 1, Equations 5 and 6) were greatest for both *Eucalyptus* stands (Table 3). For C profiles, *F* tests showed that the decay rate (c_{VT} parameter of model 1, Equations 5 and 6) could be established at the same value for CER and EUC_{HF} (c_{CER} = c_{EUCHF}) and for both pastures ($c_{PAS20} = c_{PAS80}$). This decay rate was slowest for pastures and fastest for EUC_{SR}. For N profiles, *F*-tests showed that the c_{VT} parameter could be established at the same value for both *Eucalyptus* stands ($c_{EUCSR} = c_{EUCHF}$), and for Cerrado and both pastures ($c_{PAS20} = c_{PAS80} = c_{CER}$). It was fastest for *Eucalyptus* stands.

Carbon and nitrogen model RMSEs were less than 0.220% C and 0.013% N, respectively (Table 4). The largest RMSEs were found under both *Eucalyptus* stands as a result of the greatest variability in C and N contents. *F*-tests performed on the local models and the global one (common to all vegetation types) showed a significant effect of the vegetation type on Model 1.

SOC and SON origin

C/N ratios ranged from 23.6 (EUC_{SR} and EUC_{HF}) to 15.1 (PAS_{20}). They decreased with depth down to 25 cm, where they reached their smallest values (13 to 15). On the surface, C/N ratios were greatest under *Eucalyptus* stands (Figure 6).

The $\delta^{13}C$ values ranged from −16‰ to −29‰. For all vegetation types except EUC_{HF}, $\delta^{13}C$ presented a common,

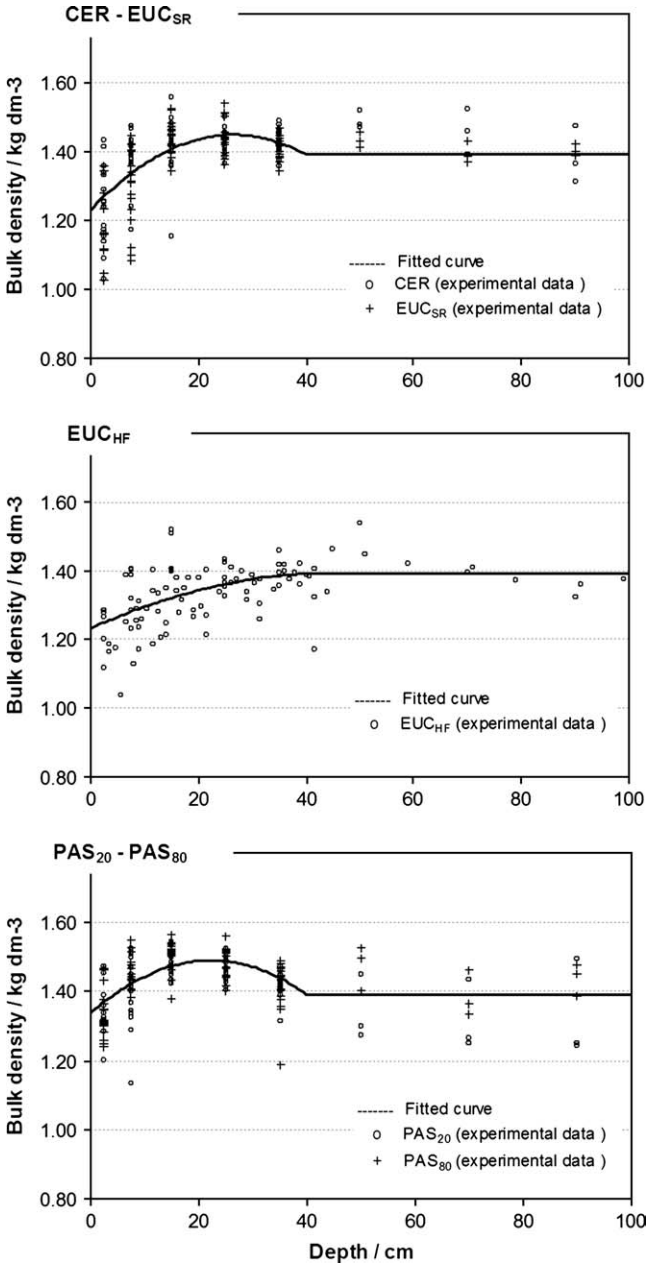

Figure 4 Measured and predicted (Model 2) bulk density as a function of depth and vegetation type. CER, EUC_{SR}, EUC_{HF}, PAS_{20}, PAS_{80}: see Table 1.

constant value of $-17‰$ beyond a depth of 30 cm (Table 5). Both pasture profiles were similar. The $\delta^{13}C$ signature of pasture litter and roots was $-16‰$. The C fraction from the pasture (Q_{veg} in Table 5; see Equation 4) was 100% in the 0–5 cm layer, and decreased with depth down to 30 cm, where it reached a value close to zero. The C fraction originating from *Eucalyptus* in EUC_{HF} decreased from 50% on the surface to about 20% at a depth of 1 m. *Eucalyptus* and Cerrado litter and roots presented an identical $\delta^{13}C$ signature of $-29‰$, which made it impossible to distinguish OM origin in the 0−5 cm layer of these vegetation types.

Stocks

Soil C and N stocks were first calculated for bulk soil, excluding litter layers and outliers in order to later assess the impact of these components on stock calculation.

The smallest soil organic carbon (SOC) stock values were found in the Cerrado and the largest values in EUC_{SR} (Table 2, Figure 7). Integrating C stocks as a function of soil mass mainly led to smaller differences between vegetation types and distinctly wider confidence intervals in EUC_{HF}. For the 0−30 cm layer, EUC_{SR} and PAS_{80} presented significant increases in SOC stocks of about 25% compared with the Cerrado, regardless of the type of integration. SOC stock under PAS_{20} and EUC_{HF} increased by 15% in relation to the Cerrado, but this result was significant only when integration took place according to depth. Introducing litter layers and outliers in the stock calculations led to increasing stocks for all arboreal VT. *Eucalyptus* stands presented an increase of about 35% for EUC_{HF} and 53% for EUC_{SR} of their total C stocks in relation to the Cerrado, regardless of the type of integration. For pastures, only the PAS_{80} total C stock was significantly greater than that of the Cerrado (+ 14%). This result was significant only when integrating depth-wise, that is, it was partly the result of soil compaction. At a depth of 1 m, increasing CI tended to decrease these differences so that only the PAS_{80} for SOC stocks (+ 18%) and EUC_{SR} for total stocks (about + 20%) were significantly greater than the Cerrado stocks (Table 2).

The smallest soil organic nitrogen (SON) stock values were found for EUC_{HF}, and the largest values for pastures. Integrating SON stocks as a function of soil mass mainly led to switching the order between the pastures, making the PAS_{80} stock consistently greater than the PAS_{20} stock and strongly increasing EUC_{HF} confidence intervals. For 0–30 cm SON stocks, both pastures presented stocks that were 20% greater than all arboreal VT stocks. This increase was reduced to 10% when integrating on the basis of mass. Introduction of litter layers and outliers led to a decrease in these differences (about 10% increase in relation to the Cerrado, regardless of the type of integration) and to increasing total N stock in EUC_{SR} up to the level of total N stocks of both pastures. At a depth of 1 m, differences almost disappeared so that only PAS_{80} SON and total stocks were greater than those of the Cerrado when integrating according to mass (Table 2).

CI were minimal for both pastures and maximal for EUC_{HF}. For 0–30 cm SOC stocks, the residual variability (second term under the root square of Equation 12, containing the $\overline{f_{VT}(x<5)}$ surface parameter contribution to the model variability) accounted for between 50% of total CI for all arboreal VT and about 60% for both pastures. For 0–30 cm SON stocks, the residual variability accounted for 54% of total CI

Table 3 C, N, and bulk density model parameters

			CER[a]	EUC_{SR}[a]	EUC_{HF}[a]	PAS_{20}[a]	PAS_{80}[a]
C/% as a function of depth/cm *Model 1*[b]	Fitted parameters	a_{VT}	0.4150				
		c_{VT}	0.0666	0.0850	0.0666	0.0467	0.0467
	Input variables	$\overline{f_{VT}(x<5)}$	1.0952	1.7361	1.4492	1.0501	1.1471
		$\overline{(x<5)}$	2.5	2.5	3	2.5	2.5
	Calculated variable	$a+b$	1.2185	2.0488	1.6781	1.1288	1.2379
N % as a function of depth/cm *Model 1*[b]	Fitted parameters	a_{VT}	0.0227				
		c_{VT}	0.0330	0.0511	0.0511	0.0330	0.0330
	Input variables	$\overline{f_{VT}(x<5)}$	0.0643	0.0796	0.0740	0.0705	0.0686
		$\overline{(x<5)}$	2.5	2.5	3	2.5	2.5
	Calculated variable	$a+b$	0.0679	0.0873	0.0825	0.0746	0.0726
Bulk density /kg dm^{-3} as a function of depth/cm *Model 2*[c]	Fitted parameters	α_{VT}	1.2313		1.2313	1.3378	
		γ_{VT}	0.0176		0.0088	0.0176	
		δ_{VT}	1.3909				
	Calculated parameter	β_{VT}	0.0164		0.0071	0.0137	
	Calculated variable	x_{max}[d]	26.43		40.00	22.14	
		d_{max}[e]	1.45		1.39	1.49	
		$d_{max}-d_0$[f]	0.22		0.16	0.15	

[a]CER, EUC_{SR}, EUC_{HF}, PAS_{20}, PAS_{80}: see Table 1.
[b]Model 1, Equations 5 and 6 in text.
[c]Model 2, Equations 7–9 in text.
[d]x_{max} = depth of maximum bulk density.
[e]d_{max} = maximum bulk density.
[f]$d_{max}-d_0$ = bump amplitude.

for pastures and between 65 and 91% for arboreal vegetation types. When simulating soil C and N stocks for each pit by means of their corresponding measured $f(x < 5)$ values as an input variable, the regressions of predicted against measured stocks led to R^2 values greater than 0.95, regardless of the vegetation type.

Changes in C and N stock values when integrated according to mass and not to depth, were less than 6%.

Discussion

Litter layers (Table 2)

Litter layer mass was negligible under both pastures as generally observed. Under Cerrado, C and N litter stock values were greater than the values measured by Lilienfein *et al.* (2001) and less than those measured by Zinn *et al.* (2002), as the result of the great heterogeneity of Brazilian Cerrados (more or less arboreal according to the site).

Forest floor mass in EUC_{HF} was of the same order of magnitude as those measured by Zinn *et al.* (2002) in 7-year old Brazilian *Eucalyptus grandis* plantations. Carbon and nitrogen stocks in L1 were greater in EUC_{SR} than in EUC_{HF}. This pattern might result from smaller litter falls in the old stand where tree density was less. L2 litter in the old stand may also account for a part of these differences. Both *Eucalyptus* stands experienced wildfires some 30 years ago.

Bulk density, C and N profiles (Figures 4, 5, Table 3)

Bulk densities matched those already observed under pasture (Szakács, 2003), *Eucalyptus* plantations and Cerrado (Zinn *et al.*, 2002) of the region in this type of soil. The bulk density curve analysis suggested soil compaction under pasture as a result of cattle trampling, as already observed by Feigl *et al.* (1995) and Moraes *et al.* (1995). Soil decompaction was also observed for the old *Eucalyptus* stand (EUC_{HF}), where the whole profile down to a depth of 40 cm was affected. This may be attributed to root development and macrobiotic activity that homogenized the densities throughout the profile. The short-rotation *Eucalyptus* stand (EUC_{SR}) seemed less affected by these phenomena because its bulk density profile was not significantly different from that of the Cerrado.

The C and N contents were characteristic of tropical sandy Ferralsols which are generally poor in organic matter, and corresponded to those measured for Brazilian Ferralsols by Kanda *et al.* (2002) under pastures, by Zinn *et al.* (2002) and Lima *et al.* (2006) under *Eucalyptus* and Cerrado, and by Lilienfein *et al.* (2001) under *Pinus* and Cerrado. The C and N profiles were influenced by the vegetation in the upper 10 cm soil layer, under root and litter influence. Greater heterogeneity observed in C and N contents for all arboreal VT was mainly the result of these influences.

Changes due to land use may not yet have influenced the deeper layers of the profile, as suggested by the model depth limit

Table 4 Sums of squares errors (SSE), root mean square errors (RMSE) and *F*-tests at $P = 0.05$ of the different bulk densities, C and N models

			Local models			Global model		
			CER[a]	EUC_{SR}[a]	EUC_{HF}[a]	PAS_{20}[a]	PAS_{80}[a]	All vegetation types
C content/%	Model 1[b]	RMSE	0.1631	0.2182	0.2110	0.1170	0.1200	0.2085
		SSE	2.606	4.382	4.361	1.259	1.396	20.564
	Global versus local	F_{obs}[d]				55.17		
		F_{tab}[e]				2.39		
N content/%	Model 1[b]	RMSE	0.0087	0.0101	0.0122	0.0076	0.0071	0.0098
		SSE	0.007	0.009	0.015	0.005	0.005	0.046
	Global versus local	F_{obs}[d]				11.89		
		F_{tab}[e]				2.39		
Bulk density/g m^{-3}	Model 2[c]	RMSE	0.0766	0.0805	0.0742	0.0631	0.0693	0.0876
		SSE	0.574	0.596	0.540	0.387	0.442	3.622
	Global versus local	F_{obs}[d]				24.71		
		F_{tab}[e]				1.96		

[a]CER, EUC_{SR}, EUC_{HF}, PAS_{20}, PAS_{80}: see Table 1.
[b]Model 1, Equations 5 and 6 in text.
[c]Model 2, Equations 7–9 in text.
[d]$F_{obs} = \dfrac{(SSE_2 - SSE_1)/(p_1 - p_2)}{SSE_1/(n - p_1)}$ (Equation 10 in text) with p_1 = number of parameters for the local model, p_2 = number of parameters for the global model ($p_2 < p_1$), SSE_1 = SSE for the local model, SSE_2 = SSE for the global model, and n = number of observations.
[e]F_{tab} is the theoretical value $F(p_1-p_2,n-p_1)$ given in the Fisher's table.

parameters, which could be established at the same value for all vegetation types without significant loss of information. The C/N ratios tend to confirm this hypothesis, showing no differentiation in OM beyond a depth of 30 cm (Figure 6). Still, the small number of data per VT and their great variability beyond a depth of 40 cm led to wide confidence intervals for the depth limit parameters, a_{VT}. When fitting the same value of a to all VT, 45 data items were then available instead of nine for each a_{VT}, and the confidence interval for a was thus narrower. This gain in CI overlapped differences between vegetation types in terms of depth.

SOC and SON stocks (Figure 7, Table 2)

SOC and SON stocks were of the same order of magnitude as those reported in the same vegetation types by other Brazilian studies (Bernoux *et al*., 1998a; Lilienfein *et al*., 2001; Bernoux *et al*., 2002; Szakacs, 2003). The great variability observed for all arboreal vegetation types was mainly due to the surface input variable of Model 1 (Table 2). Intensive surface sampling is thus essential to detect accurately the effect of land use changes on SOC and SON stocks, even for the more arboreal vegetation types.

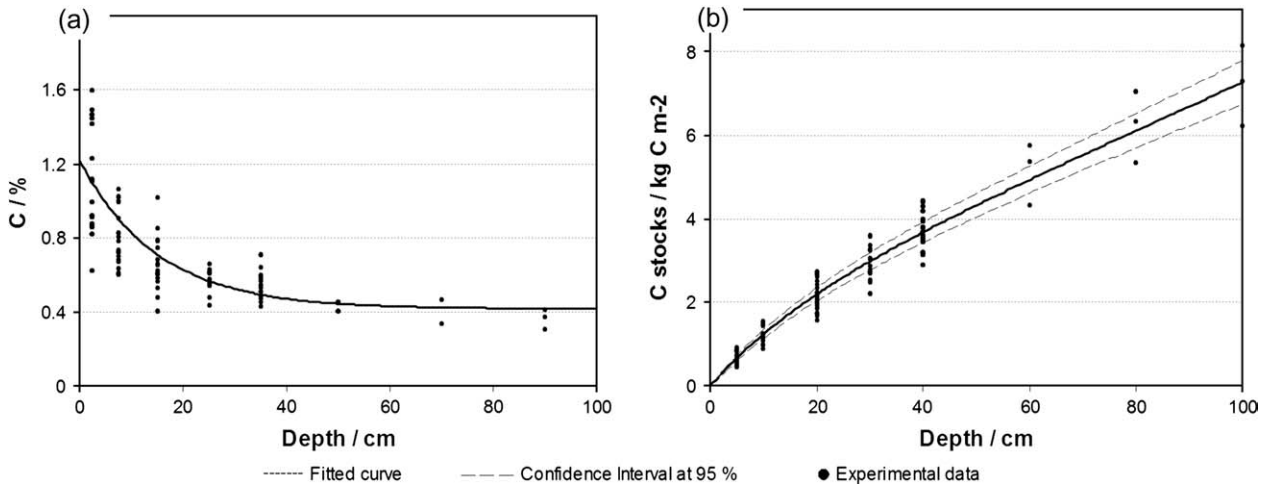

Figure 5 Models of C concentrations (Model 1) (a) and C stocks (Model 3) (b) the Cerrado example.

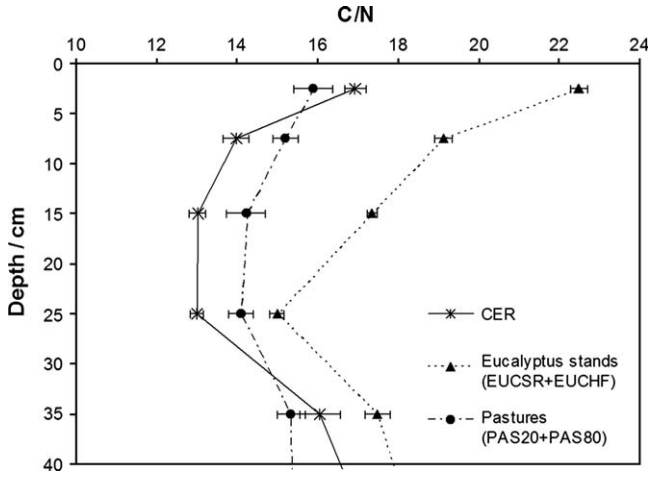

Figure 6 Soil C/N profiles of the studied vegetation types grouped as: Cerrado (native vegetation type – CER); pastures (PAS_{20} and PAS_{80}); *Eucalyptus* stands (EUC_{SR} and EUC_{HF}). Horizontal bars represent the standard errors ($18 < n < 41$). CER, EUC_{SR}, EUC_{HF}, PAS_{20}, PAS_{80}: see Table 1.

Transformation of a native arboreal vegetation to pasture or short-rotation forest plantation is often reported to decrease SOC and SON stocks (Desjardins *et al*., 1994; Jolivet, 2000; Paul *et al*., 2002; Zinn *et al*., 2002). This decrease can be offset by a return to the initial stocks 20 or 30 years after land-use change (Bashkin & Binkley, 1998; Binkley & Resh, 1999; Turner & Lambert, 2000; Paul *et al*., 2002).

Table 5 ^{13}C signatures of the soil carbon of each vegetation type (VT) and fraction of C taken from the vegetation present aboveground down to a depth of 1 m

	$\delta^{13}C_{VT}$[b] ‰			Q_{Veg}[c]		
	CER[a], EUC_{SR}[a]	EUC_{HF}[a]	PAS_{20}[a], PAS_{80}[a]	EUC_{SR}[a]	EUC_{HF}[a]	PAS_{20}[a], PAS_{80}[a]
Input[d]	−29	−29	−16			
0–5 cm	−27	−27	−16	NS[e]	NS	1.00
5–10 cm	−24	−26	−17	NS	0.40	0.88
10–20 cm	−20	−25	−17	NS	0.56	0.75
20–30 cm	−18	−23	−17	NS	0.48	NS
30–40 cm	−17	−22	−17	NS	0.42	NS
40–60 cm	−17	−21	−17	NS	0.36	NS
60–80 cm	−17	−19	−17	NS	0.20	NS
80–100 cm	−17	−20	−17	NS	0.28	NS

[a]CER, EUC_{SR}, EUC_{HF}, PAS_{20}, PAS_{80}: see Table 1.
[b]$\delta^{13}C_{VT}$ is the $\delta^{13}C$ value measured at a given depth in the vegetation type VT.
[c]Q_{Veg} is the C fraction taken from the present vegetation. The Cerrado profile is taken as a reference.
[d]Input = average litter and root $\delta^{13}C$ values.
[e]n.s. = The difference between $\delta^{13}C_{VT}$ and $\delta^{13}C_{CER}$ is < 1‰, which makes Q_{Veg} calculation irrelevant.

For Brazilian pastures more specifically, an increase in SOC and SON stocks was observed 20 years after conversion of primary forest to pasture by Moraes *et al*. (1996) and by Feigl *et al*. (1995). These results corroborate the meta-analysis made from 74 publications by Guo & Gifford (2002), who reported an average increase of 8% in SOC stocks when switching from native forest to pasture. However, this general increase was not significant in sites where annual precipitation was < 2000 mm $year^{-1}$ (present experimental site conditions). Our study actually showed that, compared with the native arboreal vegetation (Cerrado), the longer the pasture had existed, the more SOC and SON stocks increased. This phenomenon was amplified by soil compaction due to cattle trampling when not calculating stocks according to the equivalent mass method (Figure 7). Changes observed in SOC and SON storage among vegetation types were accompanied by changes in the C and N origin, as shown by C/N ratios and $\delta^{13}C$ profiles (Figure 6, Table 5), which can be explained by a progressive replacement of SOC and SON at the surface under litter and root influences (Trouvé, 1992; Moraes *et al*., 1996; Bashkin & Binkley, 1998; Bernoux *et al*., 1998c; Binkley & Resh, 1999; Lima *et al*., 2006).

In the old *Eucalyptus* stand, the observed trend was of greater SOC stocks and smaller SON stocks compared with those of the Cerrado, which would confirm data found in the literature supporting unchanged SOC stocks when broad leaf tree plantations replace native forests (Guo & Gifford, 2002) or native herbaceous savannah (Landais, 2003). However, greater spatial variability (common to all high forests) made part of the results non-significant. The progressive replacement of SOC and SON at the surface already observed under pastures was confirmed by the large C/N ratios characteristic of soils planted with *Eucalyptus* (Bernhard-Reversat, 1993, 1999; Chapuis-Lardy *et al*., 2002). Even if ^{13}C determinations were only performed in one profile per situation, $\delta^{13}C$ profiles suggest that SOC and SON changes in EUC_{HF} did not only occur down to a depth of 30 cm, as observed for all other vegetation types, but down to a depth of 1 m (Table 5). This pattern might be the result of a greater and deeper soil bioturbation and macrofaunal activity observed from the pedological descriptions (great worm and termite activities in particular). However, ^{13}C determinations were only performed in one pit per VT, and a spatial variability of $\delta^{13}C$ profiles within the study area might account for some of the differences observed among VT.

The old *Eucalyptus* stand (EUC_{HF}) can be seen as a secondary forest close to equilibrium, and thus be taken as a reference for the vegetation dynamics in the short-rotation *Eucalyptus* stand (EUC_{SR}) if the clear cuts had not occurred. In comparison with EUC_{HF}, the short-rotation *Eucalyptus* stand also showed the large C/N values typical of *Eucalyptus* stands. However, in contrast to EUC_{HF}, the ^{13}C profile of EUC_{SR} was similar to that of the Cerrado. This would suggest that the short-rotation process limited deep input of *Eucalyptus* C and N into the soil. Because *Eucalyptus* organic matter

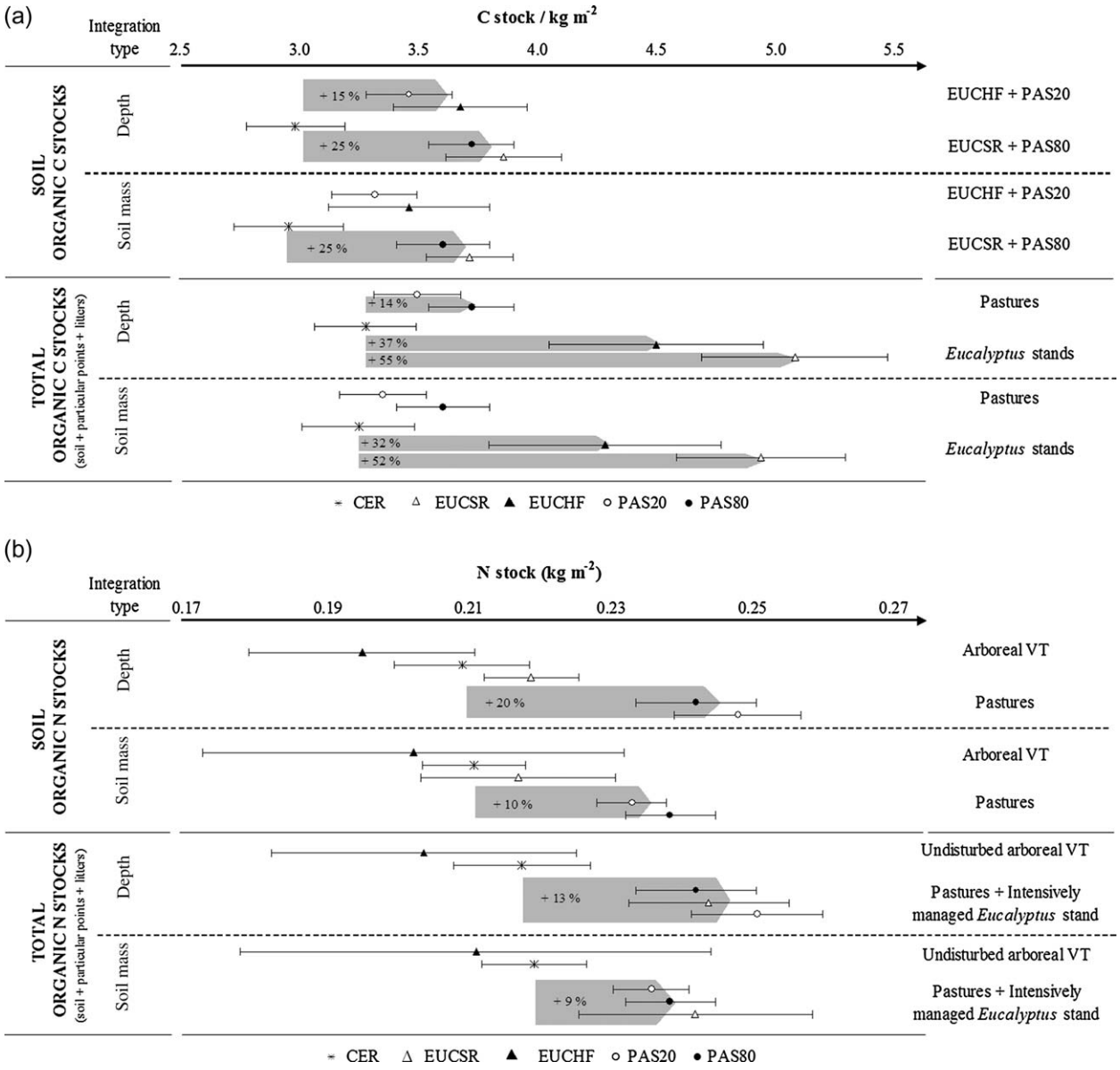

Figure 7 Changes in carbon (a) and nitrogen (b) 0–30 cm stocks of each vegetation type (VT) according to integration type (depth or soil mass). Bulk soil stocks and total stocks (bulk soil + particular points + litter layers) are represented. Horizontal bars represent confidence intervals at 95%. CER, EUC_{SR}, EUC_{HF}, PAS_{20}, PAS_{80}: see Table 1.

input is poorer in N than that of the Cerrado, this could partly account for the greater N stocks observed for EUC_{SR} compared with EUC_{HF}. As C stocks are reported to increase with lengthened rotation (Guo & Gifford, 2002; Paul *et al*., 2002), smaller C stocks for EUC_{SR} compared with EUC_{HF} could have been expected, but no significant difference between both *Eucalyptus* stands was observed.

Compared with the Cerrado, N stocks under EUC_{SR} were not significantly modified in relation to those of the Cerrado. These results were unexpected because the lack of N fertilization together with biomass export (short-rotation management) might have led to negative budgets and, therefore, to a decrease in soil N stocks. Considerable atmospheric inputs in the area (sugar cane burning) might help to limit the N deficit in this system, as well as the small amounts of biomass removed during the 1940–1998 period from these relatively unproductive, non-fertilized coppices. Input-output budgets based on biogeochemical cycle studies are usually more sensitive than soil analysis for detecting long-term changes in soil nutrient availability (Ranger & Turpault, 1999). A comprehensive study of nutrient cycling is in progress in the EUC_{SR} stand.

Soil organic C and N storage in the 0–30 cm layer accounted for 40–50% of the 0–100 cm storage, and for 13–18% of the 0–600 cm stocks estimated by Maquère (2004). In these deep tropical soils, even if land use influenced SOC and SON stocks in the upper soil layers, such surface layers only contain a tiny part of total SOC and SON stocks. The major part of the deep C and N is often stable and very old (Trouvé, 1992; Nepstad *et al*., 1994; Poirier *et al*., 2002).

Influence of litter and localized specificities (Tables 2, 6)

As reported by Guo & Gifford (2002), carbon and nitrogen stocks are greatly influenced by the methodology used for stock computation, which makes it more difficult to compare the results of various studies. In the present study, stock calculation for EUC_{HF} was greatly dependent on the L2 layer computation methodology (Table 6). The L2 layer was a mixed soil/litter layer, which could be seen as an independent litter layer added to bulk soil, or as a part of the bulk soil profile. Our model assumed that the L2 layer was part of the soil profile because it was the most coherent in terms of data set homogeneity. Computing this layer as an independent litter layer resulted in increasing C and N stocks for EUC_{HF}, which, in our view, overestimated the C and N stocks.

Litter layers and charcoal influence greatly C and N storage, especially in afforested sites. In such poor tropical soils, the density of fine roots, charcoal and decomposing organic material in upper soil layers is high and is recognized as being responsible for most SOC and SON changes on the surface (Guo & Gifford, 2002; Hopmans *et al*., 2005). In the present study, it was shown that *Eucalyptus* plantations stored large amounts of carbon at the soil/atmosphere interface in these intermediary layers (L1 + L2 + 0–5 cm bulk soil layer). The influence of the forest floors on 0–30 cm N stocks was less because the concentration of N in *Eucalyptus* litter layers is small (Judd, 1996).

Table 6 Influence of the computation method on C and N stocks for the 60-year-old *Eucalyptus saligna* high forest (EUC_{HF}). Confidence intervals (CI) at 95% are indicated

	C		N	
Computation type	Stock/ kg C m^{-2}	CI 95%	Stock/ kg N m^{-2}	CI 95%
Bulk soil + L2 as an additional litter layer	4.32	± 0.334	0.24	± 0.016
Bulk soil including L2 as first soil layer	3.99	± 0.337	0.28	± 0.034
Model used in the present study (first component = bulk soil and L2 computed as particular points)	4.04	± 0.437	0.20	± 0.022

Consequences of afforestation with Eucalyptus on C sequestration

Brazilian soils roughly correspond to 5% of the world's C stock, estimated to be 684 Pg C in the upper 30-cm soil layer (Batjes, 1996). Total Brazilian CO_2 emissions, as reported by the first National Communication, amounted to 1030 Tg for the year 1994. Seventy-five per cent of these emissions were attributed to the agriculture and forestry sector, and 23% to the energy sector. C emissions associated with changes in soil C stocks following soil management and land use changes indicated a net annual atmospheric emission of CO_2 of 46.4 Tg CO_2 (or 12.65 Tg C) for the period 1975–1995 (Bernoux *et al*., 2001). As most *Eucalyptus* plantations in Brazil have been established on degraded pastures and cover about 3 million hectares, this land use change may contribute noticeably to Brazilian CO_2 emission changes. A chronosequence approach in two Brazilian regions of contrasted productivity confirmed a substantial accretion in SOC storage after afforestation of former degraded pasturelands (Lima *et al*., 2006). However, other studies showed that pasture afforestation with *Eucalyptus* can lead to different SOC changes according to management practices, climate and soil types (Turner & Lambert, 2000; Mendham *et al*., 2002; Sicardi *et al*., 2004). Great caution should then be taken before generalizing locally drawn conclusions to large tropical areas. The overall trend in the increase in SOC storage after afforestation with *Eucalyptus* in a widespread soil type under the tropics may nevertheless be of importance, considering the recent worldwide development of forest plantations, whose area increased from about 100 million hectares in 1990 to 140 million hectares in 2005 (FAO, 2006).

Conclusions

In this study, C and N stocks were computed for five different vegetation types from the soil surface down to a depth of 1 m on a continuous basis. Emphasis was placed on evaluating the influence of soil surface layers (litter layers and the first 0–5 cm of the bulk soil layer) and soil compaction on these computations. For pastures, the observed trend was of increasing C and N stocks and soil compaction with increasing pasture time. As there was no litter layer, there was no major influence of surface layer computation on C and N stock results. Both *Eucalyptus* stands significantly increased C storage in comparison with the Cerrado and both pastures. Short-rotation forestry has not significantly impoverished SON stocks yet, but is actually slowly replacing the Cerrado organic matter by *Eucalyptus* organic matter that is poorer in N. These changes occurred mainly in soil/litter interface layers and were not greatly affected by soil compaction or decompaction. C and N stocks and their confidence intervals were greatly influenced by the methodology used to compute litter/soil interface layers. No significant difference could be observed between the C and N stocks of both *Eucalyptus* stands, which was partly due to large CI for C and N stocks in the high forest stand down to a depth of 40 cm.

Using modelling tools helped us to understand whether stock differences between VT were the result of bulk density effects or of C and N concentration changes, and to localize these changes along the soil profile. It also made it possible to carry out continuous C and N stock simulations from 0 to 100 cm in depth, which is particularly useful when comparing data from various studies. It greatly reduced stock confidence intervals beyond a depth of 40 cm and allowed more sensitive stock changes to be detected.

Acknowledgements

We would like to thank the entire staff of the Itatinga Experimental Station for field assistance, Estevão Araújo (ESALQ) for sample collection, Dr Sandra Maria Oliveira Sa and Pr Marcelo Zacharias Moreira (CENA) for chemical and isotopic analysis. This study was funded by FAPESP (No. 2002/11827-9), USP/COFECUB (No. 2003.1.10895.1.3.), the French Ministry of Foreign Affairs, the European Ultra Low CO2 Steelmaking project (ULCOS - Contract n°515960) and the French Ministry of Agriculture and Fishing (GREF).

References

Arrouays, D. & Pélissier, P. 1994. Modeling carbon storage profiles in temperate forest humic loamy soils of France. *Soil Science*, **157,** 185–192.

Arrouays, D., Feller, C., Jolivet, C., Saby, N., Andreux, F., Bernoux, M. *et al*. 2003. Estimation de stocks de carbone organique des sols à différentes échelles d'espace et de temps. *Etude et Gestion des Sols*, **10,** 347–354.

Bashkin, M.A. & Binkley, D. 1998. Changes in soil carbon following afforestation in Hawaï. *Ecology*, **79,** 828–833.

Batjes, N.H. 1996. Total carbon and nitrogen in the soils of the world. *European Journal of Soil Science*, **47,** 151–163.

Bernhard-Reversat, F. 1993. Dynamics of litter and organic matter at the soil-litter interface in fast-growing tree plantations on sandy ferrallitic soils (Congo). *Acta Oecologica*, **14,** 179–195.

Bernhard-Reversat, F. 1999. The leaching of Eucalyptus hybrids and *Acacia auriculiformis* leaf litter: laboratory experiments on early decomposition and ecological implications in congolese tree plantations. *Applied Soil Ecology*, **12,** 251–261.

Bernoux, M., Arrouays, D., Cerri, C.C., de Alencastro Graça, P.M., Volkoff, B. & Trichet, J. 1998a. Estimation des stocks de carbone des sols du Rondônia (Amazonie brésilienne). *Etude et Gestion des Sols*, **5,** 1–38.

Bernoux, M., Arrouays, D., Cerri, C.C. & Bourennane, H. 1998b. Modeling vertical distribution of carbon in oxisols of the western Brazilian Amazon (Rondonia). *Soil Science*, **163,** 941–951.

Bernoux, M., Cerri, C.C., Neill, C. & de Moraes, J.F.L. 1998c. The use of stable carbon isotopes for estimating soil organic matter turnover rates. *Geoderma*, **82,** 43–58.

Bernoux, M., Carvalho, M.D.S., Volkoff, B. & Cerri, C.C. 2001. CO_2 emission from mineral soils following land-cover change in Brazil. *Global Change Biology*, **7,** 779–787.

Bernoux, M., Carvalho, M.D.S., Volkoff, B. & Cerri, C.C. 2002. Brazil's soil carbon stocks. *Soil Science Society of America Journal*, **66,** 888–896.

Binkley, D. & Resh, S.C. 1999. Rapid changes in soils following *Eucalyptus* afforestation in Hawaii. *Soil Science Society of America Journal*, **63,** 222–225.

Brown, D. & Rothery, P. 1993. *Models in Biology: Mathematics, Statistics and Computing*. John Wiley & Sons, Chichester.

Cerri, C., Feller, C., Balesdent, J., Victoria, R. & Plenecassagne, A. 1985. Application du traçage isotopique naturel en ^{13}C à l'étude de la dynamique de la matière organique dans les sols. *Comptes-rendus de l'Académie des Sciences, Paris*, **300,** 423–428.

Cerri, C.E.P., Paustian, K., Bernoux, M., Victoria, R.L., Melillo, J.M. & Cerri, C.C. 2004. Modeling changes in soil organic matter in Amazon forest to pasture conversion with the Century model. *Global Change Biology*, **10,** 815–832.

Chapuis-Lardy, L., Contour-Ansel, D. & Bernhard-Reversat, F. 2002. High-performance liquid chromatography of water-soluble phenolics in leaf litter of three *Eucalyptus* hybrids (Congo). *Plant Science*, **163,** 217–222.

Corbeels, M., Scopel, E., Cardoso, A., Bernoux, M., Douzet, J.M. & Neto, M.S. 2006. Soil carbon storage potential of direct seeding mulch-based cropping systems in the Cerrados of Brazil. *Global Change Biology*, **12,** 1773–1787.

De Freitas, P.L., Blancaneaux, P., Gavinelli, E., Larré-Larrouy, M.C. & Feller, C. 2000. Nível e natureza do estoque orgânico de latossolos sob diferentes sistemas de uso e manejo. *Pesquisa Agropecuaria Brasileira*, **35,** 157–170.

Desjardins, T., Andreux, F., Volkoff, B. & Cerri, C.C. 1994. Organic carbon and ^{13}C contents in soils and soil size-fractions, and their changes due to deforestation and pasture installation in eastern Amazonia. *Geoderma*, **61,** 103–118.

Ellert, B.H., Janzen, H.H. & Entz, T. 2002. Assessment of a method to measure temporal change in soil carbon storage. *Soil Science Society of America Journal*, **66,** 1687–1695.

EMBRAPA, Centro Nacional de Pesquisa de Solos 1999. *Sistema brasileiro de classificação de solos*. Embrapa Solos, Rio de Janeiro.

FAO 1977. *Directives pour la description des sols*, 2nd edn. FAO, Rome.

FAO 2006. *Global Forest Resources Assessment 2005, Main Report. Progress Towards Sustainable Forest Management*. FAO Forestry Paper 147. FAO, Rome.

Feigl, B.J., Melillo, J. & Cerri, C.C. 1995. Changes in the origin and quality of soil organic matter after pasture introduction in Rondônia (Brazil). *Plant and Soil*, **175,** 21–29.

Feller, C. & Beare, M.H. 1997. Physical control of soil organic matter dynamics in the tropics. *Geoderma*, **79,** 69–116.

Gonçalves, J.L.M., Stape, J.L., Laclau, J.P., Smethurst, P. & Gava, J.L. 2004. Silvicultural effects on the productivity and wood quality of eucalypt plantations. *Forest Ecology and Management*, **193,** 45–61.

Guo, L.B. & Gifford, R.M. 2002. Soil carbon stocks and land use change: a meta analysis. *Global Change Biology*, **8,** 345–360.

Hopmans, P., Bauhus, J., Khanna, P.K. & Weston, C. 2005. Carbon and nitrogen in forest soils: potential indicators for sustainable management of eucalypt forests in south-eastern Australia. *Forest Ecology and Management*, **220,** 75–87.

Intergovernmental Panel on Climate Change (IPCC) 1997. *Revised 1996 IPCC Guidelines for National Greenhouse Gas Inventories*. IPCC, Bracknell, UK.

Intergovernmental Panel on Climate Change 2001. *Climate Change 2001: The Scientific Basis. Contribution of Working Group I to the*

Third Assessment Report of the Intergovernmental Panel on Climate Change. Cambridge University Press, Cambridge.

Jolivet, C. 2000. *Le carbone organique des sols des Landes de Gascogne. Variabilité spatiale et effets des pratiques sylvicoles et agricoles*. Doctoral dissertation, Université de Bourgogne, Dijon, France.

Judd, T.S. 1996. Simulated nutrient losses due to timber harvesting in highly productive Eucalypt forests and plantations. In: *Nutrition of Eucalypts* (eds P.M. Attiwill & M.A. Adams), pp. 249–258. CSIRO Publishing, Collingwood, Victoria, Australia.

Kanda, K., Miranda, C.H.B. & Macedo, M.C.M. 2002. Carbon and nitrogen mineralization in soils under agro-pastoral systems in subtropical Central Brazil. *Soil Science and Plant Nutrition*, **48,** 179–184.

Laclau, J.P., Toutain, F., M'Bou, A.T., Arnaud, M., Joffre, R. & Ranger, J. 2004. The function of the superficial root mat in the biogeochemical cycles of nutrients in Congolese *Eucalyptus* plantations. *Annals of Botany*, **93,** 249–261.

Laclau, J.P., Ranger, J., Deleporte, P., Nouvellon, Y., Saint-André, L., Marlet, S. *et al*. 2005. Nutrient cycling in a clonal stand of *Eucalyptus* and an adjacent savanna ecosystem in Congo 3. Input–output budgets and consequences for the sustainability of the plantations. *Forest Ecology and Management*, **210,** 375–391.

Landais, D. 2003. *Etude quantitative et qualitative du carbone séquestré dans le sol après afforestation au Congo Brazzaville*. DESS dissertation, Université Louis Pasteur, Strasbourg, France.

Lepsch, I.F. 1980. Influencia do cultivo de *Eucalyptus* e *Pinus* nas propriedades quimicas de solos sob Cerrado. *Revista Brasileira de Ciência do Solo*, **4,** 103–107.

Lilienfein, J. & Wilcke, W. 2003. Element storage in native, agri-, and silvicultural ecosystems of the Brazilian savanna. *Plant and Soil*, **254,** 425–442.

Lilienfein, J., Wilcke, W., Thomas, R., Vilela, L., Lima, S.D. & Zech, W. 2001. Effects of *Pinus caribaea* forests on the C, N, P, and S status of Brazilian savanna Oxisols. *Forest Ecology and Management*, **147,** 171–182.

Lima, A.M.N., Silva, I.R., Neves, J.C.L., Novais, R.F., Barros, N.F., Mendonça, E.S. *et al*. 2006. Soil organic carbon dynamics following afforestation of degraded pastures with eucalyptus in southeastern Brazil. *Forest Ecology and Management*, **235,** 219–231.

Maquère, V. 2004. *Utilisation des terres (Cerrado, pâturages, eucalyptus) et stockage de matière organique dans les sols du Brésil*. MSc dissertation, Université Henri Poincaré, Nancy, France.

Marschner, H. 1995. *Mineral Nutrition of Higher Plants*, 2nd edn. Academic Press, London.

Mendham, D.S., O' Connell, A.M. & Grove, T.S. 2002. Organic matter characteristics under native forest, long-term pasture, and recent conversion to *Eucalyptus* plantations in Western Australia: microbial biomass, soil respiration, and permanganate oxidation. *Australian Journal of Soil Research*, **40,** 859–872.

Moraes, J.L., Cerri, C.C., Melillo, J.M., Kicklighter, D., Neill, C., Skole, D.L. *et al*. 1995. Soil carbon stocks of the Brazilian Amazon Basin. *Soil Science Society of America Journal*, **59,** 244–247.

Moraes, J.L., Volkoff, B., Cerri, C.C. & Bernoux, M. 1996. Soil properties under Amazon forest and changes due to pasture installation in Rondônia, Brazil. *Geoderma*, **70,** 63–81.

Nadelhoffer, K.J. & Fry, B. 1988. Controls on natural nitrogen-15 and carbon-13 abundances in forest soil organic matter. *Soil Science Society of America Journal*, **52,** 1633–1640.

Nambiar, E.K.S., Ranger, J., Tiarks, A. & Toma, T. 2004. *Site Management and Productivity in Tropical Plantation Forests*: Proceedings of Workshops in Congo, July 2001 and China, February 2003. CIFOR, Jakarta.

Nepstad, D.C., De Carvalho, C.R., Davidson, E.A., Jipp, P.H., Lefebvre, P.A. Negreiros, G.H. *et al*. 1994. The role of deep roots in the hydrological and carbon cycles of Amazonian forests and pastures. *Nature*, **372,** 666–669.

Parresol, B.R. 1999. Assessing tree and stand biomass: a review with examples and critical comparisons. *Forest Science*, **45,** 573–593.

Paul, K.I., Polglase, P.J., Nyakuengama, J.G. & Khanna, P.K. 2002. Change in soil carbon following afforestation. *Forest Ecology and Management*, **168,** 241–257.

Peterson, B.J. & Fry, B. 1987. Stable isotopes in ecosystem studies. *Annual Review of Ecology and Systematics*, **18,** 293–320.

Poirier, N., Derenne, S., Balesdent, J., Rouzaud, J.N., Mariotti, A. & Largeau, C. 2002. Abundance and composition of the refractory organic fraction of an ancient, tropical soil (Pointe Noire, Congo). *Organic Geochemistry*, **33,** 383–391.

Ranger, J. & Turpault, M.-P. 1999. Input-output nutrient budgets as a diagnostic tool for sustainable forest management. *Forest Ecology and Management*, **122,** 139–154.

Serfling, R.J. 1980. *Approximation Theorems of Mathematical Statistics. Wiley Series in Probability and Mathematical Statistics*. John Wiley & Sons, New York.

Sicardi, M., Garcia-Préchac, F. & Frioni, L. 2004. Soil microbial indicators sensitive to land use conversion from pastures to commercial *Eucalyptus* grandis (Hill ex Maiden) plantations in Uruguay. *Applied Soil Ecology*, **27,** 125–133.

Smith, C.K., De Assis Oliveira, F., Gholz, H.L. & Baima, A. 2002. Soil carbon stocks after forest conversion to tree plantations in lowland Amazonia, Brazil. *Forest Ecology and Management*, **164,** 257–263.

Szakács, G.G.J. 2003. *Seqüestro de carbono nos solos. Avaliação das potencialidades dos solos arenosos sob pastagens, Anhembi – Piracicaba/SP*. MSc dissertation, CENA/USP, Piracicaba, Brazil.

Trouvé, C. 1992. *Apport de la géochimie isotopique ($\delta^{13}C$) à l'étude du renouvellement des matières organiques et des sucres neutres dans les sols tropicaux soumis à des changements d'écosystèmes. Cas des aménagements forestiers sur les savanes de Pointe-Noire au Congo*. Doctoral dissertation, Université d'Orléans, France.

Turner, J. & Lambert, M. 2000. Change in organic carbon in forest plantation soil in eastern Australia. *Forest Ecology & Management*, **133,** 231–247.

Wilcke, W. & Lilienfein, J. 2004. Soil carbon-13 natural abundance under native and managed vegetation in Brazil. *Soil Science Society of America Journal*, **68,** 827–832.

Zinn, Y.L., Resck, D.V.S. & Da Silva, J.E. 2002. Soil organic carbon as affected by afforestation with Eucalyptus and Pinus in the Cerrado region of Brazil. *Forest Ecology and Management*, **166,** 285–294.

BIBLIOGRAPHICAL REFERENCES

Abbadie, L., J.C. Lata, and V. Tavernier. 2000. Impact des graminées pérennes sur une ressource rare: l'azote, p. 189-193, *In* C. Floret and R. Pontanier, eds. La jachère en Afrique Tropicale. John Libbey Eurotext, Paris.

Aber, J.D., K.J. Nadelhoffer, P. Steudler, and J.M. Melillo. 1989. Nitrogen saturation in northern forest ecosystems. BioScience 39.

Aber, J.D., J.M. Melillo, K.J. Nadelhoffer, J. Pastor, and R.D. Boone. 1991. Factors controlling nitrogen cycling and nitrogen saturation in northern temperate forest ecosystems. Ecological Applications 1.

Adams, M.B., T.R. Angradi, and J.N. Kochenderfer. 1997. Stream water and soil solution responses to 5 years of nitrogen and sulfur additions at the Frenow Experimental Forest, West Virginia. Forest Ecology and Management 95:79-91.

Agbenin, J.O., and H. Tiessen. 1994. The Effects of Soil Properties on the Differential Phosphate Sorption by Semiarid Soils from Northeast Brazil. Soil Science 157:36-45.

Allen, R.G., L.S. Pereira, D. Raes, and M. Smith. 1998. Crop evapotranspiration - Guidelines for computing crop water requirements. FAO, Rome.

Almeida, A.C., J.V. Soares, J.J. Landsberg, and G.D. Rezende. 2007. Growth and water balance of Eucalyptus grandis hybrid plantations in Brazil during a rotation for pulp production. Forest Ecology and Management 251:10-21.

Alves, M.E., and A. Lavorenti. 2004. Sulfate adsorption and its relationships with properties of representative soils of the Sao Paulo State, Brazil. Geoderma 118:89-99.

Anand, R.R., and R.J. Gilkes. 1987. Iron oxides in lateritic soils from Western Australia. Journal of Soil Science, UK 38:607-622.

Axe, L., and P.R. Anderson. 1999. Adsorption onto Oxides: The Role of Diffusion, p. 199-210, *In* J. A. Schwarz and C. I. Contescu, eds. Surfaces of Nanoparticles and Porous Materials. Marcel Dekker, New York.

Baeumler, R., and W. Zech. 1998. Soil solution chemistry and impact of forest thinning in mountain forests in the Bavarian Alps. Forest Ecology and Management 108:231-238.

Balbino, L.C., A. Bruand, M. Brossard, M. Grimaldi, M. Hajnos, and M.F. Guimaraes. 2002. Changes in porosity and microaggregation in clayey Ferralsols of the Brazilian Cerrado on clearing for pasture. European Journal of Soil Science 53:219-230.

Balbino, L.C., A. Bruand, I. Cousin, M. Brossard, P. Quetin, and M. Grimaldi. 2004. Change in the hydraulic properties of a Brazilian clay Ferralsol on clearing for pasture. Geoderma 120:297-307.

Balwant, S., and R.J. Gilkes. 1991. Concentration of iron oxides from soil clays by 5M NaOH treatment: the complete removal of sodalite and kaolin. Clay Minerals 26:463-472.

Barnhisel, R.I., and P.M. Bertsch. 1989. Chlorites and Hydroxy-Interlayared Vermiculites and Smectites, p. 729-788 SSSA Book Serie, Minerals in soil environments (2nd Edition).

Barrow, N.J. 1983. A mechanistic model for describing the sorption and desorption of phosphate by soil. Journal of Soil Science 34.

Bartoli, F., G. Burtin, and A.J. Herbillon. 1991. Disaggregation and clay dispersion of Oxisols: Na resin, a recommended methodology. Geoderma 49:301-317.

Bartoli, F., R. Philippy, and G. Burtin. 1992a. Influence of Organic-Matter on Aggregation in Oxisols Rich in Gibbsite or in Goethite .1. Structures - the Fractal Approach. Geoderma 54:231-257.

Bartoli, F., G. Burtin, and J. Guerif. 1992b. Influence of Organic-Matter on Aggregation in Oxisols Rich in Gibbsite or in Goethite .2. Clay Dispersion, Aggregate Strength and Water-Stability. Geoderma 54:259-274.

Battaglia, M., and P. Sands. 1997. Modelling site productivity of Eucalyptus globulus in response to climatic and site factors. Australian Journal of Plant Physiology 24:831-850.

Beier, C. 1998. Water and element fluxes calculated in a sandy forest soil taking spatial variability into account. Forest Ecology and Management 101:269-280.

Benyon, R. 1999. Nighttime water use in an irrigated Eucalyptus grandis plantation. Tree Physiol 19:853-859.

Bertolo, R., R. Hirata, and O. Sracek. 2006. Geochemistry and geochemical modeling of unsaturated zone in a tropical region in Urania, Sao Paulo state, Brazil. Journal of Hydrology 329:49-62.

Beven, K., and P. Germann. 1982. Macropores and water flows in soil. Water Resources Research 18:1311-1325.

Bevilacqua, E., T.J. Blake, and W.S. Filho. 1997. Modelling growth and ecophysiological responses of Eucalyptus grandis clones in Minas Gerais, Brazil. Journal of Tropical Forest Science 9:505-513.

Bish, D.L., and C.J. Duffy. 1990. Thermal Analysis in Clay Science CMS Workshop, Vol. 3. The Clay Minerals Society, Boulder, Colorado.

Bolan, N.S., R. Naidu, J.K. Syers, and R.W. Tillman. 1999. Surface charge and solute interactions in soils, p. 87-140 Advances in Agronomy, Vol 67, Vol. 67. ACADEMIC PRESS INC, San Diego.

Bosch, J.M., and R.E. Smith. 1989. The effect of afforestation of indigenous scrub forest with Eucalyptus on streamflow from a small catchment in the Transvaal, South Africa. Afrikaanse Bosboutydskrif 150:7-17.

Boudot, J.P., O. Maitat, D. Merlet, and J. Rouiller. 2000. Soil solutions and surface water analysis in two contrasted watersheds impacted by acid deposition, Vosges mountains, NE France: interpretation in terms of Al impact and nutrient imbalance. Chemosphere 41:1419-1429.

Bramley, H., J. Hutson, and S.D. Tyerman. 2003. Floodwater infiltration through root channels on a sodic clay floodplain and the influence on a local tree species Eucalyptus largiflorens. Plant and Soil 253:275-286.

Bryant, R.B., and J. Macedo. 1990. Differential chemoreductive dissolution of iron oxides in a Brazilian Oxisol. Soil Science Society of America Journal 54:819-821.

Bustamante, M.M.C., E. Medina, G.P. Asner, G.B. Nardoto, and D.C. Garcia-Montiel. 2006. Nitrogen cycling in tropical and temperate savannas. Biogeochemistry 79:209-237.

Camara, C.D., and W.P. Lima. 1999. Clearcutting of a 50 years old growth Eucalyptus saligna plantation: impacts on water balance and water quality in an experimental catchment. Scientia Florestalis 56.

Cambier, P., and R. Prost. 1981. Study of clay oxide associations: fabric of a ferrallitic material. Agronomie 1:713-722.

Cantarella, H., and L.I. Prochnow. 2001. Determinação de sulfato em solos., p. 285 Analise Quimica para Avaliação da Fertilidade de Solos Tropicais. Instituto Agronômico, Campinas, Brazil.

Carnol, M., P. Ineson, and A.L. Dickinson. 1997. Soil solution nitrogen and cations influenced by (NH4)(2)SO4 deposition in a coniferous forest. Environmental Pollution 97:1-10.

Cattan, P., M. Voltz, Y.M. Cabidoche, J.G. Lacas, and J. Sansoulet. 2007. Spatial and temporal variations in percolation fluxes in a tropical Andosol influenced by banana cropping patterns. Journal of Hydrology 335:157-169.

Chang, S.C., and E. Matzner. 2000. The effect of beech stemflow on spatial patterns of soil solution chemistry and seepage fluxes in a mixed beech-oak stand. Hydrological processes 14:135-144.

Chorover, J., and G. Sposito. 1995. Surface-Charge Characteristics of Kaolinitic Tropical Soils. Geochimica Et Cosmochimica Acta 59:875-884.

Churchman, G.J. 1997. Comparison of methods for the size fractionation of soils. 11th International Clay Conference. ICC97 Organizing committee, Ottawa, Canada.

Cichota, R., A.L.B. Hurtado, and Q.D. van Lier. 2006. Spatio-temporal variability of soil water tension in a tropical soil in Brazil. Geoderma 133:231-243.

Cichota, R., A.L.B. Hurtado, and Q.D. van Lier. 2008. Performance of a multi-level TDR system exposed to tropical field conditions - A time-space comparison with tensiometry. Journal of Hydrology 352:181-190.

Clothier, B.E., S.R. Green, and M. Deurer. 2008. Preferential flow and transport in soil: progress and prognosis. European Journal of Soil Science 59:2-13.

Corbeels, M., R.E. McMurtrie, D.A. Pepper, D.S. Mendham, T.S. Grovet, and A.M. O'Connell. 2005. Long-term changes in productivity of eucalypt plantations under different harvest residue and nitrogen management practices: a modelling analysis. For. Ecol. Manage. 217:1-18.

Cornell, R.M., and U. Schwertmann. 2003. The iron oxides: structure, properties, reactions, occurrences and uses The iron oxides: structure, properties, reactions, occurrences and uses. WILEY-VCH Verlag GMBH & Co. KGaA, Weinheim Germany.

Corwin, D.L. 2002. Suction Cups, p. 1261-1265, *In* J. H. Dane and G. C. Topp, eds. Methods of Soil Analysis. Part 4 - Physical Methods. Soil Science Society of America, Inc., Madison, Wisconsin, USA.

Cossalter, C., and C. Pye-Smith. 2003. Fast-Wood Forestry. Myths and Realities. CIFOR, Jakarta, Indonesia.

Costa, A.C.S., J.M. Bigham, C.A. Tormena, and J.C. Pintro. 2004. Clay mineralogy and cation exchange capacity of Brazilian soils from water contents determined by thermal analysis. Thermochimica Acta 413:73-79.

Couto, W., D.J. Lathwell, and D.R. Bouldin. 1979. Sulfate sorption by two oxisols and an alfisol of the Tropics. Soil Science 127.

Crockford, R.H., and P.K. Khanna. 1997. Chemistry of throughfall, stemflow and litterfall in fertilized and irrigated Pinus radiata. Hydrological Processes 11:1493-1507.

Curtin, D., and J.K. Syers. 1990a. Extractability and adsorption of sulphate in soils. Journal of Soil Science 41.

Curtin, D., and J.K. Syers. 1990b. Mechanism of sulphate adsorption by two tropical soils. Journal of Soil Science 41.

da Silva, F.C., P.A. da Eira, B. van Raij, C.A. Silva, C.A. de Abreu, C. Gianello, D.V. Perez, J.A. Quaggio, M.J. Tedesco, M.F. de Abreu, and W.d.O. Barreto. 1999. Analises quimicas para avaliação da fertilidade do solo. Embrapa Solos, Rio de Janeiro.

Dambrine, E., M. Loubet, J.A. Vega, and A. Lissarague. 1997. Localisation of mineral uptake by roots using Sr isotopes. Plant and Soil 192:129-132.

Damman, G. 2001. Etude et modélisation du fonctionnement hydrique de plantations d'eucalyptus au Congo. DAA Dissertation, Ecole Nationale Supérieure Agronomique, Montpellier, France.

David, T.S., M.I. Ferreira, J.S. David, and J.S. Pereira. 1997a. Transpiration from a mature Eucalyptus globulus plantation in Portugal during a spring-summer period of progressively higher water deficit. Oecologia 110:153-159.

David, T.S., M.I. Ferreira, J.S. David, and J.S. Pereira. 1997b. Transpiration from a mature Eucalyptus globulus plantation in Portugal during a spring-summer period of progressively higher water deficit. Oecologia 110:153-159.

de Vries, W., G.J. Reinds, and E. Vel. 2003. Intensive monitoring of forest ecosystems in Europe 2: Atmospheric deposition and its impacts on soil solution chemistry. Forest Ecology and Management 174:97-115.

Dejou, J., J. Guyot, M. Robert, and J. Pedro. 1977. Evolution superficielle des roches cristallines et cristallophyliennes dans les régions tempérées INRA.

Deleporte, P., J.P. Laclau, J.D. Nzila, G. Kazotti, J.N. Marien, J.P. Bouillet, M. Szwarc, R. D'Annunzio, and R. Ranger. 2004-2006. Effect of Slash and Litter Management Practises on Soil Chemical Properties and Growth of Second Rotation Eucalypts in the Congo, p. 5-22, *In* E. K. S. Nambiar, ed. Site Management and Productivity in Tropical Plantation Forests. CIFOR, Piracicaba, Brasil - Bogor, Indonesia.

Delfosse, T. 2005. Acid Neutralisation And Sulphur Retention in S-Impacted Andosols. Ph.D. Thesis, Université Catholique de Louvain, Louvain-la-Neuve, Belgium.

Delfosse, T., P. Delmelle, C. Givron, and B. Delvaux. 2005. Inorganic sulphate extraction from SO2-impacted andosols. European Journal of Soil Science 56:127-133.

Delmelle, P., T. Delfosse, and B. Delvaux. 2003. Sulfate, chloride and fluoride retention in Andosols exposed to volcanic acid emissions. Environmental Pollution 126:445-457.

Delphis, F., J. Levia, and E. Frost. 2006. Variability of throughfall volume and solute inputs in wooded ecosystems. Progress in Physical Geography 30:605-632.

Dixon, J.B., and S.B. Weed. 1989. Minerals in soil environments Minerals in soil environments. Soil Science Society of America Inc. (SSSA). Madison USA.

ESALQ, University of São Paulo. 2001. Soil Water Retention Curve. Release 3. ESALQ, University of São Paulo, Piracicaba, Brazil.

Driscoll, C.T., and W.D. Schecher. 1990. The chemistry of aluminum in the environment. Environmental Geochemistry and Health 12.

Duwig, C., T. Becquer, B.E. Clothier, and M. Vauclin. 1998. Nitrate leaching through oxisols of the Loyalty Islands (New Caledonia) under intensified agricultural practices. Geoderma 84:29-43.

Dye, P.J. 1996. Climate, forest and streamflow relationships in South African afforested catchments. Commonwealth Forestry Review 75:31-38.

Edwards, P.J. 1998. Sulfur cycling, retention, and mobility in soils: a review General Technical Report - Northeastern Research Station, USDA Forest Service. USDA Forest Service, Newtown Square USA.

Elsenbeer, H., B.E. Newton, T. Dunne, and J.M. de Moraes. 1999. Soil hydraulic conductivities of latosols under pasture, forest and teak in Rondonia, Brazil. Hydrological Processes 13:1417-1422.

EMBRAPA, C.N.d.P.d.S. 1999. Sistema brasileiro de classificação de solos. Embrapa Solos, Rio de Janeiro.

Emmett, B.A., S.A. Brittain, S. Hughes, J. Gorres, V. Kennedy, D. Norris, R. Rafarel, B. Reynolds, and P.A. Stevens. 1995. Nitrogen Additions (Nano3 and Nh4no3) at Aber Forest, Wales .1. Response of Throughfall and Soil-Water Chemistry. Forest Ecology and Management 71:45-59.

Ezzaim, A. 1997. Interêt de la mesure du flux d'éléments issu de l'altération des minéraux des sols dans le calcul des bilans miénraux d'un écosystème forestier. Thèse, Nancy I, Nancy.

FAO. 1998. World reference base for soil resources FAO, ISRIC and ISSS, Rome.

FAO. 2006. Global Forest Resources Assessment 2005, Main Report. Progress Reports Sustainable Forest Management. FAO, Rome.

Feller, C. 1991. Utilisation des résines sodiques et des ultrasons dans le fractionnement granulométrique de la matière organique des sols. Intérêt et limites. Science du sol 29:77-93.

Feyen, J., D. Jacques, A. Timmermann, and J. Vanderborght. 1998. Modelling water flow and solute transport in heterogeneous soils: a review of recent approaches. Journal of Agricultural Engineering Research 70:231-256.

Fichter, J. 1997. Minéralogie quantitative et flux d'éléments minéraux libéré par altération des minéraux des sols dans deux écosystèmes sur granite (bassin du Strengbach, Vosges). Thèse, Nancy I, Nancy.

Folster, J., L. Bringmark, and L. Lundin. 2003. Temporal and spatial variations in soilwater chemistry at three acid forest sites. Water Air and Soil Pollution 146:171-195.

Fontes, M.P.F., and S.B. Weed. 1991. Iron oxides in selected Brazilian Oxisols: I Mineralogy. Soil Science Society of America Journal 55:1143-1149.

Fournier, R.E., I.K. Morrison, and A.A. Hopkin. 1994. Short range variability of soil chemistry in three acid soils in Ontario, Canada. Communications in Soil Science and Plant Analysis 25:3069-3082.

Fuller, R.D., M.B. David, and C.T. Driscoll. 1985. Sulfate adsorption relationships in forested spodosols of the northeastern USA. Soil Science Society of America Journal 49.

Furian, S., L. Barbiero, R. Boulet, P. Curmi, M. Grimaldi, and C. Grimaldi. 2002. Distribution and dynamics of gibbsite and kaolinite in an oxisol of Serra do Mar, southeastern Brazil. Geoderma 106:83-100.

Gee, G.W., and J.W. Bauder. 1986. Particle-size analysis Methods of soil analysis. Part 1. Physical and mineralogical methods. American Society of Agronomy Inc., Madison, Wisconsin USA.

Geelhoed, J.S., T. Hiemstra, and W.H. VanRiemsdijk. 1997. Phosphate and sulfate adsorption on goethite: Single anion and competitive adsorption. Geochimica Et Cosmochimica Acta 61:2389-2396.

Gerard, F., M. Tinsley, and K.U. Mayer. 2004. Preferential flow revealed by hydrologic modeling based on predicted hydraulic properties. Soil Science Society of America Journal 68:1526-1538.

Gerke, H.H., and M.T. van Genuchten. 1993. A dual-porosity model for simulating preferential movement of water and solutes in structured porous media. Water Resources Research 29:305-319.

Gillman, G.P. 1984. Using variable charge characteristics to understand the exchangeable cation status of oxic soils. Australian Journal of Soil Research 22.

Gillman, G.P., and M.E. Sumner. 1987. Surface charge characterization and soil solution composition of four soils from the Southern Piedmont in Georgia. Soil Science Society of America Journal 51.

Goncalves, J.F.D., J.L. Stape, J.P. Laclau, P. Smethurst, and J.L. Gava. 2004. Silvicultural effects on the productivity and wood quality of eucalipts plantations. Forest Ecology and Management 193:45-61.

Goncalves, J.L.M., N.F. Barros, E.K.S. Nambiar, and R.F. Novais. 1997. Soil and stand management for short-rotation plantations Management of soil, nutrients and water in tropical plantation forests. Australian Centre for International Agricultural Research (ACIAR), Canberra Australia.

Gonçalves, T.D. 2003. Mapeamento de solos e de produtividade em plantações de Eucalyptus grandis na Estação Experimental de Itatinga, ESALQ, com uso de geoprocessamento. Master dissertation. ESALQ, Piracicaba.

Gonzalez-Arias, A., I.M. de Arano, M.J. Barcena-Ruiz, G. Besga, and M. Onaindia. 2006. Origin of atmospheric deposition and canopy buffering capacity in stands of radiata pine and pedunculate oak in the Basque Country. Forest Ecology and Management 229:268-284.

Granier, A. 1987. Mesure du flux de sève brute dans le tronc du Douglas par une nouvelle méthode thermique. Annals of Forest Science 44:1-14.

Granier, A., N. Breda, P. Biron, and S. Villette. 1999a. A lumped water balance model to evaluate duration and intensity of drought constraints in forest stands. Ecological Modelling 116:269-283.

Granier, A., N. Breda, P. Biron, and S. Villette. 1999b. A lumped water balance model to evaluate duration and intensity of drought constraints in forest stands. Ecological Modelling 116:269-283.

Granier, A., M. Reichstein, N. Breda, I.A. Janssens, E. Falge, P. Ciais, T. Grunwald, M. Aubinet, P. Berbigier, C. Bernhofer, N. Buchmann, O. Facini, G. Grassi, B. Heinesch, H. Ilvesniemi, P. Keronen, A. Knohl, B. Kostner, F. Lagergren, A. Lindroth, B. Longdoz, D. Loustau, J. Mateus, L. Montagnani, C. Nys, E. Moors, D. Papale, M. Peiffer, K. Pilegaard, G. Pita, J. Pumpanen, S. Rambal, C. Rebmann, A. Rodrigues, G. Seufert, J. Tenhunen, I. Vesala, and Q. Wang. 2007. Evidence for soil water control on carbon and water dynamics in European forests during the extremely dry year: 2003. Agricultural and Forest Meteorology 143:123-145.

Greiffenhagen, A., G. Wessolek, M. Facklam, M. Renger, and H. Stoffregen. 2006. Hydraulic functions and water repellency of forest floor horizons on sandy soils. Geoderma 132:182-195.

Grigal, D.F., and P.R. Ohmann. 2005. Calcium ans forest systems : diffusion from deep sources. Soil Science 170:129-136.

Gundersen, P. 1998. Effects of enhanced nitrogen deposition in a spruce forest at Klosterhede, Denmark, examined by moderate NH4NO3 addition. Forest Ecology and Management 101:251-268.

Harmand, J.M., H. Avila, E. Dambrine, U. Skiba, S. de Miguel, R.V. Renderos, R. Oliver, F. Jimenez, and J. Beer. 2007. Nitrogen dynamics and soil nitrate retention in a Coffea arabica-Eucalyptus deglupta agroforestry system in Southern Costa Rica. Biogeochemistry 85:125-139.

Hiemstra, T., and W.H. Van Riemsdijk. 2006. On the relationship between charge distribution, surface hydration, and the structure of the interface of metal hydroxides. Journal of Colloid and Interface Science 301:1-18.

Hill, M.C. 1998. Methods and guidelines for effective model calibration 98-4005. U.S. Geological Survey, Denver, Colorado.

Hingston, F.J., R.J. Atkinson, A.M. Posner, and J.P. Quirk. 1967. Specific Adsorption of Anions. Nature 215:1459-1461.

Hopmans, J.W., J. Simunek, N. Romano, and W. Durner. 2002. Inverse Methods, p. 963-1008, *In* J. H. Dane and G. C. Topp, eds. Methods of Soil Analysis. Part 4 - Physical Methods. Soil Science Society of America, Inc, Madison, Wisconsin, USA.

Hornbeck, J.W., S.W. Bailey, D.C. Buso, and J.B. Shanley. 1997. Streamwater chemistry and nutrient budgets for forested watersheds in New England: variability and manadgment implications. Forest Ecology and Management 93:73-89.

Igwe, C.A., F.O.R. Akamigbo, and J.S.C. Mbagwu. 1999. Chemical and mineralogical properties of soils in southeastern Nigeria in relation to aggregate stability. Geoderma 92:111-123.

IPEF. 2004. Forest Nutrition and Fertilization IPEF, Piracicaba.

IPT. 1981. Mapa Geomorfològico do Estado de São Paulo Instituto de Pesquisas Tecnologicas do Estado de São Paulo, São Paulo.

Iseman, T.M., D.R. Zak, W.E. Holmes, and A.G. Merrill. 1999. Revegetation and nitrate leaching from Lake States northern hardwood forests following harvest. Soil Science Society of America Journal 63:1424-1429.

Jaffrain, J. 2006. Effet des essences forestières sur le fonctionnement organo-minéral d'un sol acide: observations et modélisations. PhD Thesis, Université Henri Poincaré, Nancy, France.

Jeanroy, E. 1983. Diagnostics des formes du fer dans les pédogénèses tempérées. Evaluation par des réactifs chimiques d'extraction et apport de la spectrométrie Mossbauer., Université de Nancy 1, Nancy.

Johnson, M.S., and J. Lehmann. 2006. Double-funneling of trees: Stemflow and root-induced preferential flow. Ecoscience 13:324-333.

Jourdan, C., E.V. Silva, J.L.M. Gonçalves, J. Ranger, R.M. Moreira, and J.P. Laclau. 2008. Annual fine root production and turnover in Brazilian *Eucalyptus* plantations under contrasting nitrogen fertilization regimes.

Julien, J.L., L. Charlet, E. Dambrine, B. Delvaux, J.E. Dufey, J.C. Fardeau, E. Le Cadre, and D. Tessier. 2005. L'acidification des sols, p. 516-537 Sols et environnement. Dunod, Paris.

Kaiser, K., and W. Zech. 1996. Nitrate, sulfate, and biphosphate retention in acid forest soils affected by natural dissolved organic carbon. Journal of Environmental Quality 25:1325-1331.

Kallarackal, J., and C.K. Somen. 1997. An ecophysiological evaluation of the sustainability of Eucalyptus grandis for planting in the tropics. Forest Ecology and Management 95.

Kampf, N., and U. Schwertmann. 1983. Relations between iron oxides and soil colour in kaolinitic soils of southern Brazil. Revista Brasileira de Ciencia do Solo 7:27-31.

Kirschbaum, M.U.F., H. Keith, R. Leuning, H.A. Cleugh, K.L. Jacobsen, E. van Gorsel, and R.J. Raison. 2007. Modelling net ecosystem carbon and water exchange of a temperate Eucalyptus delegatensis forest using multiple constraints. Agricultural and Forest Meteorology 145:48-68.

Klinge, R., J. Schmidt, and H. Folster. 2001. Simulation of water drainage of a rain forest and forest conversion plots using a soil water model. Journal of Hydrology 246:82-95.

Klopatek, J.M., M.J. Barry, and D.W. Johnson. 2006. Potential canopy interception of nitrogen in the Pacific Northwest, USA. Forest Ecology and Management 234:344-354.

Knight, J. 1999. Root Distribution and Water Uptake Patterns in Eucalypts and Other Species, p. 55-78, *In* J. Landsberg, ed. The Ways Trees Use Water. Rural Industries Research and Development Corporation, Kingston.

Konishi, S., M. Tani, Y. Kosugi, S. Takanashi, M.M. Sahat, A.R. Nik, K. Niiyama, and T. Okuda. 2006. Characteristics of spatial distribution of throughfall in a lowland tropical rainforest, Peninsular Malaysia. Forest Ecology and Management 224:19-25.

Kung, K.J.S. 1990. Preferential flow in a sandy vadose zone: 1. Field observation. Geoderma 46:51-58.

Kuo, S. 1996. Phosphorus Methods of soil analysis. Part 3 - chemical methods. Soil Science Society of America Inc., Madison USA.

Laclau, J.P. 2001. Dynamique du fonctionnement minéral d'une plantation d'eucalyptus. Effets du reboisement sur un sol de savane du littoral congolais; conséquences pour la gestion des plantations industrielles., Institut National Agronomique, Paris-Grignon, France.

Laclau, J.P., M. Arnaud, J.P. Bouillet, and J. Ranger. 2001. Spatial distribution of Eucalyptus roots in a deep sandy soil in the Congo: relationships with the ability of the stand to take up water and nutrients (vol 21, pg 129, 2001). Tree Physiology 21:631-632.

Laclau, J.P., J. Ranger, J.P. Bouillet, J.D. Nzila, and P. Deleporte. 2003a. Nutrient cycling in a clonal stand of Eucalyptus and an adjacent savanna ecosystem in Congo - 1. Chemical composition of rainfall, throughfall and stemflow solutions. Forest Ecology and Management 176:105-119.

Laclau, J.P., J. Ranger, J.D. Nzila, J.P. Bouillet, and P. Deleporte. 2003b. Nutrient cycling in a clonal stand of Eucalyptus and an adjacent savanna ecosystem in Congo 2. Chemical composition of soil solutions. Forest Ecology and Management 180:527-544.

Laclau, J.P., P. Deleporte, J. Ranger, J.P. Bouilleti, and G. Kazotti. 2003c. Nutrient dynamics throughout the rotation of Eucalyptus clonal stands in Congo. Annals of Botany 91:879-892.

Laclau, J.P., F. Toutain, A.T. M'Bou, M. Arnaud, R. Joffre, and J. Ranger. 2004a. The function of the superficial root mat in the biogeochemical cycles of nutrients in Congolese Eucalyptus plantations. Annals of Botany 93:249-261.

Laclau, J.P., J. Ranger, P. Deleporte, Y. Nouvellon, L. Saint-Andre, S. Marlet, and J.P. Bouillet. 2005a. Nutrient cycling in a clonal stand of Eucalyptus and an adjacent savanna ecosystem

in Congo 3. Input-output budgets and consequences for the sustainability of the plantations. Forest Ecology and Management 210:375-391.

Laclau, J.P., J.C.R. Almeida, J.L.M. Gonçalves, L. Saint-André, M. Ventura, J. Ranger, R.M. Moreira, and Y. Nouvellon. 2008. Influence of nitrogen and potassium fertilizations on leaf lifespan and allocation of above-ground growth in *Eucalyptus* plantations. Tree Physiol:In press.

Laclau, J.P., J.L.M. Gonçalves, A.V. Krusche, F. Poggiani, J.L. Stape, M.C. Piccolo, R.M. Moreira, V. Maquere, W.P. Lima, and J. Ranger. 2004b. Processos de transfêrencia e balanço de agua e de nutrientes em povoamentos de Eucalyptus que receberam aplicações de nitrogênio e de biossolido: reflexos sobre a sustentabilidade. Relatorio Cientifico 1. FAPESP, São Paulo.

Laclau, J.P., J.L.M. Gonçalves, A.V. Krusche, F. Poggiani, J.L. Stape, M.C. Piccolo, R.M. Moreira, V. Maquere, W.P. Lima, and J. Ranger. 2005b. Processos de transfêrencia e balanço de agua e de nutrientes em povoamentos de Eucalyptus que receberam aplicações de nitrogênio e de biossolido: reflexos sobre a sustentabilidade. Relatorio Cientifico 2. FAPESP, São Paulo.

Laclau, J.P., J.L.M. Gonçalves, A.V. Krusche, F. Poggiani, J.L. Stape, M.C. Piccolo, R.M. Moreira, V. Maquere, W.P. Lima, and J. Ranger. 2007. Processos de transfêrencia e balanço de agua e de nutrientes em povoamentos de Eucalyptus que receberam aplicações de nitrogênio e de biossolido: reflexos sobre a sustentabilidade. 3. FAPESP, São Paulo.

Landsberg, J. 1999. Relationships between water use efficiency and tree production, p. 45-54, *In* J. Landsberg, ed. The Ways Trees Use Water. Rural Industries Research and Development Corporation, Kingston.

Langensiepen, M., S. Burgess, H. Lambers, P. Mitchell, and E. Veneklaas. 2006. A model for simulating transpiration of Eucalyptus salmonophloia trees. Physiologia Plantarum 127:465-477.

Legout, A., C. Walter, and C. Nys. 2008. Spatial variability of nutrient stocks in the humus and soils of a forest massif (Fougères, France). Annals of Forest Science 65:108-118.

Lehmann, J., J. Lilienfein, K. Rebel, S.D. Lima, and W. Wilcke. 2004. Subsoil retention of organic and inorganic nitrogen in a Brazilian savanna Oxisol. Soil Use and Management 20:163-172.

LeMaitre, D.C., and D.B. Versfeld. 1997. Forest evaporation models: Relationships between stand growth and evaporation. Journal of Hydrology 193:240-257.

Levia, D.F., and E.E. Frost. 2003. A review and evaluation of stemflow literature in the hydrologic and biogeochemical cycles of forested and agricultural ecosystems. Journal of Hydrology 274:1-29.

Levia, D.F., and E.E. Frost. 2006. Variability of throughfall volume and solute inputs in wooded ecosystems. Progress in Physical Geography 30:605-632.

Libardi, P.L. 2005. Dinâmica da Agua no Solo Editora da Universidade de São Paulo, São Paulo.

Likens, G.E., F.H. Bormann, R.S. Pierce, and W.A. Reiners. 1978. Recovery of a deforested ecosystem replacing biomass and nutrients lost in harvesting northern hardwoods may take 60 to 80 years. Science 199:492-496.

Lilienfein, J., W. Wilcke, M.A. Ayarza, L. Vilela, S.D. Lima, and W. Zech. 2000. Soil acidification in Pinus caribaea forests on Brazilian savanna Oxisols. Forest Ecology and Management 128:145-157.

Lima, W.P. 1996. Impacto ambiental do eucalipto. Universidade de São Paulo, São Paulo.

Lima, W.P., R.M. Moreira, F.P. Scardua, and A.V. Masetto. 1996. The hydrology of a small catchment covered with 50-year-old eucaliptus plantation in the Itatinga forest experimental station, State of São Paulo. Scientia Florestalis 50:11-19.

Loeppert, R.H., and W.P. Inskeep. 1996. Iron Methods of soil analysis. Part 3 - chemical methods. Soil Science Society of America Inc., Madison USA.

Madsen, H. 2000. Automatic calibration of a conceptual rainfall-runoff model using multiple objectives. Journal of Hydrology 235:276-288.

Magill, A.H., J.D. Aber, G.M. Berntson, W.H. McDowell, K.J. Nadelhoffer, J.M. Melillo, and P. Steudler. 2000. Long-term nitrogen additions and nitrogen saturation in two temperate forests. Ecosystems 3.

Mahfouf, J.F., and J. Noilhan. 1991. Comparative study of various formulations of evaporation from bare soil using in situ data. Journal of Applied Meteorology 30.

Maquere, V. 2004. Utilisation des terres (Cerrado, pâturages, *Eucalyptus*) et stockage de matière organique dans les sols du Brésil. MSc Dissertation, Université Henri Poincaré, Nancy, France.

Maquere, V., J.P. Laclau, M. Bernoux, L. Saint-André, J.L.M. Gonçalves, C.C. Cerri, M.C. Piccolo, and J. Ranger. 2008. Influence of land use (savanna, pastures, *Eucalyptus* plantations) on soil carbon and nitrogen stocks in Brazil. European Journal of Soil Science 59:863-878.

Marcano-Martinez, E., and M.B. McBride. 1989. Comparison of the titration and ion adsorption methods for surface charge measurement in Oxisols. Soil Science Society of America Journal 53.

Mare, P.H.l., and L.A. Leon. 1989. The effects of lime on adsorption and desorption of phosphate in five Colombian soils. Journal of Soil Science, UK 40.

Mareschal, L. 2008. Effet des substitutions d'essences forestières sur l'évolution des sols et de leur minéralogie: bilan après 28 ans dans le site expérimental de Breuil (Morvan). PhD Thesis, Université Henri Poincaré, Nancy, France.

Marques, J.J., D.G. Schulze, N. Curi, and S.A. Mertzman. 2004. Major element geochemistry and geomorphic relationships in Brazilian Cerrado soils. Geoderma 119:179-195.

Marques, R. 1996. Dynamique du fonctionnement minérale d'une plantation de Daouglas (Pseudotsuga menziesii (Mirb.) Franco) dans les monts du Beaujolais (France). Thèse, Nancy 1, Nancy.

Marques, R., J. Ranger, D. Gelhaye, B. Pollier, Q. Ponette, and O. Gobert. 1996. Comparison of chemical composition of soil solutions collected by zero-tension plate lysimeters with those from ceramic cup lysimeters in a forest soil. European Journal of Soil Science 47:407-417.

Mayer, K.U. 1999. A numerical model for multicomponent reactive transport in variably saturated porous media, University of Waterloo, Waterloo.

Mayer, K.U., E.O. Frind, and D.W. Blowes. 2002. Multicomponent reactive transport modeling in variably saturated porous media using a generalized formulation for kinetically controlled reactions. Water Resources Research 38.

McBratney, A.B., M.L. Mendonça Santos, and B. Minasny. 2003. On digital soil mapping. Geoderma 117:3-52.

McDowell, W.H., A.H. Magill, J.A. Aitkenhead-Peterson, J.D. Aber, J.L. Merriam, and S.S. Kaushal. 2004. Effects of chronic nitrogen amendment on dissolved organic matter and inorganic nitrogen in soil solution. Forest Ecology and Management 196:29-41.

Mehra, O.P., and M.L. Jackson. 1960. Iron oxide removal from soils and clays by a dithionite-citrate system buffered with sodium bicarbonate. Clays and Clay Minerals 7:317-327.

Meunier, A. 2003. Argiles GB Science, Paris.

Mielke, M.S., M.A. Oliva, N.F. de Barros, R.M. Penchel, C.A. Martinez, and A.C. de Almeida. 1999. Stomatal control of transpiration in the canopy of a clonal Eucalyptus grandis plantation. Trees-Structure and Function 13:152-160.

Moldan, F., and R.F. Wright. 1998. Changes in runoff chemistry after five years of N addition to a forested catchment at Gardsjon, Sweden. Forest Ecology and Management 101:187-197.

Monteith, J.L. 1981. Evaporation and surface temperature. Quart. J. Roy. Meteorol. Soc. 107.

Mualem, Y. 1976. A new model predicting the hydraulic conductivity of unsaturated porous media. Water Resour. Res. 25:513-522.

Mulvaney, R.L. 1996. Nitrogen - inorganic forms Methods of soil analysis. Part 3 - chemical methods. Soil Science Society of America Inc., Madison USA.

Nambiar, E.K.S. 1996. Sustained productivity of forests is a continuing challenge to soil science. Soil Science Society of America Journal 60:1629-1642.

Nambiar, E.K.S., J. Ranger, A. Tiarks, and T. Tomas. 2004. Site management and productivity in tropical plantation forests. CIFOR, Congo July 2001, China February 2003.

Neill, C., M.C. Piccolo, C.C. Cerri, P.A. Steudler, and J.M. Melillo. 2006. Soil solution nitrogen losses during clearing of lowland Amazon forest for pasture. Plant and Soil 281:233-245.

Nelson, D.W., and L.E. Sommers. 1996. Total carbon, organic carbon, and organic matter Methods of soil analysis. Part 3 - chemical methods. Soil Science Society of America Inc., Madison USA.

Neufeldt, H., M.A. Ayarza, D.V.S. Resck, and W. Zech. 1999. Distribution of water-stable aggregates and aggregating agents in Cerrado Oxisols. Geoderma 93:85-99.

Neuman, S.P. 1973. Saturated-unsaturated seepage by finite elements. ASCE, Journal of the Hydraulics Division 99:2233-2250.

Nimmo, J.R., and K.S. Perkins. 2002. Aggregate Stability and Size Distribution Methods of soil analysis. Part 4. Physical Methods. Soil Science Society of America, Inc, Madison, Wisconsin USA.

Noborio, K. 2001. Measurement of soil water content and electrical conductivity by time domain reflectometry: a review. Computers and Electronics in Agriculture 31:213-237.

Nzila, J.D. 2001. Caractérisation minéralogique des sols ferrallitiques sableux sous plantations d'*Eucalyptus* et sous savane naturelle de la région de Pointe-Noire (Congo). CIFOR, INRA, CIRAD, UR2PI.

O'Connell, A.M., and S.J. Rance. 1999. Predicting nitrogen supply in plantation eucalypt forests. Soil Biology and Biochemistry 31:1943-1951.

Olmos I. L, J., F.C.S. Amaral, and N.C. Sousa Neto. 1993. Relationship between content of dithionite-extractable free iron and sulfuric acid extractable Fe2O3-TiO2 in soils with Ki lower than 2.2. Revista Brasileira de Ciencia do Solo 17:315-317.

Paiva, A.D., L.D. Souza, A.C. Ribeiro, and L.M. Da Costa. 2000. Soil physical and hydraulic properties of a toposequence tableland in Bahia State, Brazil. Pesquisa Agropecuaria Brasileira 35:2295-2302.

Panday, S., P.S. Huyacorn, R. Therrien, and R.L. Nichols. 1993. Improved three-dimensional finite-element techniques for field simulation of variably saturated flow and transport. Journal of Contaminant Hydrology 12:3-33.

Paniconi, C., and M. Putti. 1994. A comparison of Picard and Newton iteration in the numerical solution of multidimensional variably saturated flow problems. Water Resources Research 30:3357-3374.

Parsons, D.F., M. Hayashi, and G.v.d. Kamp. 2004. Infiltration and solute transport under a seasonal wetland: bromide tracer experiments in Saskatoon, Canada. Hydrological Processes 18.

Pinheiro-Dick, D., and U. Schwertmann. 1996. Microaggregates from Oxisols and Inceptisols: dispersion through selective dissolutions and physicochemical treatments. Geoderma 74:49-63.

Ploeg, R.R.V.d., and F. Beese. 1977. Model calculations for the extraction of soil water by ceramic cups and plates. Soil Science Society of America Journal 41.

Pochet, G., M. Van der Velde, M. Vanclooster, and B. Delvaux. 2007. Hydric properties of high charge, halloysitic clay soils from the tropical South Pacific region. Geoderma 138:96-109.

Ponette, Q., S. Belkacem, and C. Nys. 1996. Ion dynamics in acid forest soils as affected by addition of Ca fertilizers. Geoderma 71:53-76.

Ponette, Q., J.E. Dufey, and F. Weissen. 1997. Downward movement of dolomite, kieserite or a mixture of CaCO3 and kieserite through the upper layers of an acid forest soil. Water Air and Soil Pollution 95:353-379.

Poszwa, A., E. Dambrine, B. Ferry, B. Pollier, and M. Loubet. 2002. Do deep tree roots provide nutrients to the tropical rainforest ? Biogeochemistry 60:97-118.

Prietzel, J., and C. Hirsch. 2000. Ammonium fluoride extraction for determining inorganic sulphur in acid forest soils. European Journal of Soil Science 51:323-333.

Prietzel, J., C. Weick, J. Korintenberg, G. Seybold, T. Thumerer, and B. Treml. 2001. Effects of repeated (NH4)(2)SO4 application on sulfur pools in soil, soil microbial biomass, and ground vegetation of two watersheds in the Black Forest/Germany. Plant and Soil 230:287-305.

Prinsloo, F.W., and D.F. Scott. 1999. Streamflow responses to the clearing of alien invasive trees from riparian zones at three sites in the Western Cape Province. Southern African Forestry Journal 185:1-7.

Prosser, I.P., K.J. Hailes, M.D. Melville, R.P. Avery, and C.J. Slade. 1993. A Comparison of Soil Acidification and Aluminum under Eucalyptus Forest and Unimproved Pasture. Australian Journal of Soil Research 31:245-254.

Ptak, T., M. Piepenbrink, and E. Martac. 2004. Tracer tests for the investigation of heterogeneous porous media and stochastic modelling of flow and transport - a review of some recent developments. Journal of Hydrology 294:122-163.

Qualls, R.G., B.L. Haines, W.T. Swank, and S.W. Tyler. 2000. Soluble organic and inorganic nutrient fluxes in clearcut and mature deciduous forests. Soil Science Society of America Journal 64:1068-1077.

Rahnemaie, R., T. Hiemstra, and W.H. van Riemsdijk. 2007a. Carbonate adsorption on goethite in competition with phosphate. Journal of Colloid and Interface Science 315:415-425.

Rahnemaie, R., T. Hiemstra, and W.H. van Riemsdijk. 2007b. Geometry, charge distribution, and surface speciation of phosphate on goethite. Langmuir 23:3680-3689.

Ranger, J., and M.P. Turpault. 1999. Input-output nutrient budgets as a diagnostic-tool for the sustainability of forest management. Forest Ecology and Management 122:7-16.

Ranger, J., S. Loyer, D. Gelhaye, B. Pollier, and P. Bonnaud. 2007. Effects of the clear-cutting of a Douglas-fir plantation (Pseudotsuga menziesii F.) on the chemical composition of soil solutions and on the leaching of DOC and ions in drainage waters. Annals of Forest Science 64:183-200.

Ranger, J., S. Allie, D. Gelhaye, B. Pollier, M.-P. Turpault, and A. Granier. 2002. Nutrient budgets for a rotation of a Douglas-fir plantation in the Beaujolais (France) based on a chronosequence study. Forest Ecology and Management 171:3-16.

Ranger, J., D. Discours, D. Mohamed Ahamed, C. Moares, E. Dambrine, D. Merlet, and J. Rouiller. 1993. Comparaison des eaux liées et des eaux libres des sols de trois peuplements d'épicéa (Picea abies Karst) des Vosges. Application à l'étude du fonctionnement actuel des sols et conséquences pour l'état sanitaire des peuplements. Annales des Sciences Forestiéres 50:425-444.

Rasiah, V., J.D. Armour, N.W. Menzies, D.H. Heiner, and M.J. Donn. 2004. Impact of pre-existing sulphate on retention of imported chloride and nitrate in variable charge soil profiles. Geoderma 123:205-218.

Reis, M.G.F., J.P. Kimmins, G.C. Rezende, and N.F. Barros. 1985. Acumulo de biomass em uma sequéncia de idade de Eucalyptus grandis plantado no cerrado em duas areas com diferentes produtividades. Revista Arvore 9:149-162.

Reuss, J.O., and D.W. Johnson. 1986. Acid deposition and the acidification of soils and waters. Springer-Verlag, New York.

Reynolds, W.D., D.E. Elrick, E.G. Youngs, A. Amoozegar, H.W.G. Booltink, and J. Bouma. 2002. Saturated and Field-Saturated Water Flow Parameters, p. 797-878, *In* J. H. Dane and G. C. Topp, eds. Methods of Soil Analysis. Part 4 - Physical Methods. Soil Science Society of America, Inc., Madison, Wisconsin, USA.

Rhoades, C., and D. Binkley. 1996. Factors influencing decline in soil pH in Hawaiian Eucalyptus and Albizia plantations. Forest Ecology and Management 80:47-56.

Rietra, R., T. Hiemstra, and W.H. van Riemsdijk. 1999. Sulfate adsorption on goethite. Journal of Colloid and Interface Science 218:511-521.

Rietra, R., T. Hiemstra, and W.H. Van Riemsdijk. 2001. Interaction between calcium and phosphate adsorption on goethite. Environmental Science & Technology 35:3369-3374.

Riha, S.J., B.R. James, G.P. Senesac, and E. Pallant. 1986. Spatial variability of soil pH and organic matter in forest plantations. Soil Science Society of America Journal 50:1347-1352.

Robinson, N., R.J. Harper, and K.R.J. Smettem. 2006. Soil water depletion by Eucalyptus spp. integrated into dryland agricultural systems. Plant and Soil 286:141-151.

Rouiller, J., B. Guillet, and S. Bruckert. 1980. Cations acides échangeables et acidité de surface. Approche analytique et incidences pédogénétiques. Science du Sol. Bulletin de l'Association Française de l'Etude des Sols 2:161-175.

Sabre, R. 2007. Plans d'expériences. Méthode de Taguchi Techniques de l'ingénieur. Base agroalimentaire, Vol. F-1006. Editions T.I. Techniques de l'Ingénieur, Paris, France.

Saint-Andre, L., A.T. M'Bou, A. Mabiala, W. Mouvondy, C. Jourdan, O. Roupsard, P. Deleporte, O. Hamel, and Y. Nouvellon. 2005. Age-related equations for above- and below-ground biomass of a Eucalyptus hybrid in Congo. Forest Ecology and Management 205:199-214.

Samouëlian, A., S. Cornu, A. Bruand, and G. Richard. 2007. Modélisation de l'évolution des sols liée à des processus hydrologiques et géochimiques. Etude et gestion des sols 14:195-204.

SBS. 2007. Fatos e Numeros do Brasil Florestal. Sociedade Brasileira de Silvicultura, São Paulo.

Schaefer, C.E.G.R., R.J. Gilkes, and R.B.A. Fernandes. 2004. EDS/SEM study on microaggregates of Brazilian Latosols, in relation to P adsorption and clay fraction attributes. Geoderma 123:69-81.

Scott, D., and Smith. 1997. Preliminary empirical models to predict reductions in total and low flows resulting from afforestation. Water SA 23:135-140.

Segalen, P. 1995. Ferrallitic soils and their geographical distribution. Volume 2. Ferrallitic soils: factors governing their formation, and ferrallitic soils in America Les sols ferrallitiques et leur repartition geographique. Tome 2: les sols ferrallitiques: les facteurs de formation et les sols ferrallitiques en Amerique. Office de la Recherche Scientifique et Technique Outre-Mer (ORSTOM), Paris France.

Simunek, J., C. He, L. Pang, and S.A. Bradford. 2006. Colloid-Facilitated Solute Tranporte in Variably Saturated Porous Media: Numerical Model and Experimental Verification. Vadose Zone J. 5:1035-1047.

Smethurst, P.J. 2000. Soil solution and other soil analyses as indicators of nutrient supply: a review. Forest Ecology and Management 138:397-411.

Smethurst, P.J., A.M. Herbert, and L.M. Ballard. 2001. Fertilization effects on soil solution chemistry in three eucalypt plantations. Soil Science Society of America Journal 65:795-804.

Soares, J.V., and A.C. Almeida. 2001. Modeling the water balance and soil water fluxes in a fast growing Eucalyptus plantation in Brazil. Journal of Hydrology 253:130-147.

Soares, M.R., L.R.F. Alleoni, P. Vidal-Torrado, and M. Cooper. 2005. Mineralogy and ion exchange properties of the particle size fractions of some Brazilian soils in tropical humid areas. Geoderma 125:355-367.

Soon, Y.K. 1993. Fractionation of Extractable Aluminum in Acid Soils - a Review and a Proposed Procedure. Communications in Soil Science and Plant Analysis 24:1683-1708.

Stape, J.L., D. Binkley, and M.G. Ryan. 2004. Eucalyptus production and the supply, use and efficiency of use of water, light and nitrogen across a geographic gradient in Brazil. Forest Ecology and Management 193:17-31.

Stape, J.L., D. Binkley, and M.G. Ryan. 2008. Production and carbon allocation in a clonal Eucalyptus plantation with water and nutrient manipulations. Forest Ecology and Management 255:920-930.

Stoop, W.A. 1980. Ion adsorption mechanisms in oxidic soils; implications for point of zero charge determinations. Geoderma 23.

Strahm, B.D., R.B. Harrison, T.A. Terry, B.L. Flaming, C.W. Licata, and K.S. Petersen. 2005. Soil solution nitrogen concentrations and leaching rates as influenced by organic matter retention on a highly productive Douglas-fir site. Forest Ecology and Management 218:74-88.

Stuanes, A.O., and O.J. Kjonaas. 1998. Soil solution chemistry during four years of NH4NO3 addition to a forested catchment at Gardsjon, Sweden. Forest Ecology and Management 101:215-226.

Stuanes, A.O., O.J. Kjonaas, and H. Vanmiegroet. 1995. Soil Solution Response to Experimental Addition of Nitrogen to a Forested Catchment at Gardsjon, Sweden. Forest Ecology and Management 71:99-110.

Stumm, W., and J.J. Morgan. 1996. Aquatic Chemistry. Chemical Equilibria and Rates in Natural Waters. 3 ed. Wiley-Interscience, New York.

Taguchi, G. 1986. Introduction to quality engineering. Designing quality into products and processes. Kraus International Publication, White Plains, New-York.

Tamm, O. 1922. Um best ämning ow de oorganiska komponenterna i markens gelcomplex. Medd. Statens Skogsförsökanst 19:385-404.

Tamura, T. 1958. Identification of clay minerals from acid soils. Journal of Soil Science 9:141-147.

Tiktak, A., and W. Bouten. 1992. Modeling Soil-Water Dynamics in a Forested Ecosystem .3. Model Description and Evaluation of Discretization. Hydrological Processes 6:455-465.

Tiktak, A., and W. Bouten. 1994. Soil-Water Dynamics and Long-Term Water Balances of a Douglas-Fir Stand in the Netherlands. Journal of Hydrology 156:265-283.

Titus, B.D., and M.K. Mahendrappa. 1996. Lysimeter system designs used in soils research: a review. Information Report - Newfoundland and Labrador Region, Canadian Forest Service.

Titus, B.D., B.A. Roberts, and K.W. Deering. 1997. Soil solution concentrations on three white birch sites in central Newfoundland following different harvesting intensities. Biomass & Bioenergy 13:313-330.

Tommaselli, J.T.G., and O.O.S. Bacchi. 2001. Calibration of a TDR equipment to moisture measurement in soils. Pesquisa Agropecuaria Brasileira 36:1145-1154.

Torrent, J., U. Schwertmann, H. Fechter, and F. Alferez. 1983. Quantitative relationships between soil color and hematite content. Soil Science 136:354-358.

Tsutsumi, T. 1969. Accumulation and circumation of nutrient elements in forest ecosystems, p. 543-552 Proc. Brussels Symp. Ecology and Conservation, 4, 1971.

Turpault, M.P., J. Ranger, R. Marques, and A. Ezzaïm. 1999. Les bilans entrées-sorties, indicateurs de gestion durable des écosystèmes forestiers : cas des plantations de douglas des monts du Beaujolais. Revue Forestière Française 2:184-196.

UE. 1998. Council Directive 98/83/EC of 3 November 1998 on the quality of water intended for human consumption.

Uehara, G., and G. Gillman. 1981. The mineralogy, chemistry, and physics of tropical soils with variable charge clays. Westview Press Inc., Boulder, Colorado USA.

USDA. 1999. Soil Taxonomy. A Basic System of Soil Classification for Making and Interpreting Soil Surveys. 2nd ed. USDA, Washington.

Vachaud, G., and J.H. Dane. 2002. Instantaneous Profile, p. 937-944, *In* J. H. Dane and G. C. Topp, eds. Methods of Soil Analysis. Part 4 - Physical Methods. Soil Science Sociey of America, Inc., Madison, Wisconsin, USA.

Vale, F.R., R.F. Novais, N.F. Barros, and R. Sant'ana. 1984. Efeito do aluminio sobre a cinética de absorção de amônio e nitrato em raizes intactas de Eucalyptus alba. Revista Arvore 8:123-132.

van Genuchten, M.T. 1980. A closed-form equation for predicting the hydraulic properties of unsaturated soils. Soil Science Society of America Journal 44:892-898.

Van Miegroet, H., and D.W. Johnson. 1993. Nitrate dynamics in forest soils., p. 75-97, *In* T. P. Burt, et al., eds. Nitrate: Processes, Patterns and Management. John Wiley & Sons, Chichester, England.

Van Raij, B., and M.V. Peech. 1972. Electrochemical properties of some oxisols and alfisols of the tropics. Soil Science Society of America Journal 36:587-593.

Van Ranst, E., J. Shamshuddin, G. Baert, and P.K. Dzwowa. 1998. Charge characteristics in relation to free iron and organic matter of soils from Bambouto mountains, western Cameroon. European Journal of Soil Science 49:243-252.

Vanderkwaak, J.E., P.A. Forsyth, K.T.B. MacQuarrie, and E.A. Sudicky. 1997. WatSolv sparse matrix iterative solver, user's guide for version 2.16. University of Waterloo, Waterloo, Canada.

Vestgarden, L.S., G. Abrahamsen, and A.O. Stuanes. 2001. Soil solution response to nitrogen and magnesium application in a Scots pine forest. Soil Science Society of America Journal 65:1812-1823.

Vitousek, P.M., and J.M. Melillo. 1979. Nitrate losses from disturbed forests: patterns and mechanisms. Forest Science 25.

Volland-Tuduri, N., M. Brossard, A. Bruand, and H. Garreau. 2004. Direct analysis of microaggregates shrinkage for drying: Application to microaggregates from a Brasilian clayey Ferralsol. C.R. Geoscience 336:1017-1024.

Volland-Tuduri, N., A. Bruand, M. Brossard, L.C. Balbino, M.I.L.d. Oliveira, and E.d.S. Martins. 2005. Mass proportion of microaggregates and bulk density in a Brazilian clayey oxisol. Soil Science Society of America Journal 69:1559-1564.

Wada, K., and Y. Kakuto. 1983. Intergradient vermiculite-kaolin mineral in a Korean Ultisol. Clays and Clay Minerals 31.

Westerhof, R., P. Buurman, C.v. Griethuysen, M. Ayarza, L. Vilela, and W. Zech. 1999. Aggregation studied by laser diffraction in relation to plowing and liming in the Cerrado region in Brazil. Geoderma 90:277-290.

Weston, C.J., and P.M. Attiwill. 1996. Clearfelling and burning effects on nitrogen mineralization and leaching in soils of old-age Eucalyptus regnans forests. Forest Ecology and Management 89:13-24.

White, D.A., C.L. Beadle, and D. Worledge. 2000. Control of transpiration in an irrigated Eucalyptus globulus Labill. plantation. Plant Cell and Environment 23:123-134.

Whitehead, D., and C.L. Beadle. 2004. Physiological regulation of productivity and water use in Eucalyptus: a review. Forest Ecology and Management 193:113-140.

Williams, G.R. 1987. The coupling of biogeochemical cycles of nutrients. Biogeochemistry 4:61-75.

Wohlenberg, E.V., J.M. Reichert, D.J. Reinert, and E. Blume. 2004. Aggregation dynamics of a sandy soil under five cropping systems in rotation and in succession. Revista Brasileira de Ciencia do Solo 28:891-900.

Wu, J.Q., R.D. Zhang, and S.X. Gui. 1999. Modeling soil water movement with water uptake by roots. Plant and Soil 215:7-17.

Xu, X.N., Q. Wang, and E. Hirata. 2005. Precipitation partitioning and related nutrient fluxes in a subtropical forest in Okinawa, Japan. Annals of Forest Science 62:245-252.

Zech, W., N. Senesi, G. Guggenberger, K. Kaiser, J. Lehmann, T.M. Miano, A. Miltner, and G. Schroth. 1997. Factors controlling humification and mineralization of soil organic matter in the tropics. Geoderma 79:117-161.

Zelazny, L.W., L. He, and A. Vanwormhoudt. 1996. Charge analysis of soils and anion exchange Methods of soil analysis. Part 3 - chemical methods. Soil Science Society of America Inc., Madison USA.

Zeller, B., M. Colin-Belgrand, E. Dambrine, F. Martin, and P. Bottner. 2000. Decomposition of N-15-labelled beech litter and fate of nitrogen derived from litter in a beech forest. Oecologia 123:550-559.

Zhang, Q., and C.O. Justice. 2001. Carbon emissions and sequestration potential of central african ecosystems. Ambio 30:351-355.

Zurmühl, T., and W. Durner. 1996. Modeling transient water and solute transport in biporous soil. Water Resources Research 32:819-829.

../..
Des gerçures crues l'ont balafrée de part en part,
une étiquette fanée rappelle son premier départ."

La Rumeur, *L'ombre sur la mesure,* 2002